

Engineering Design for Wear

Second Edition, Revised and Expanded

Raymond G. Bayer

Tribology Consultant

Vestal, New York, U.S.A.



MARCEL DEKKER, INC.

NEW YORK · BASEL

This edition is expanded and updated from a portion of the first edition, *Mechanical Wear Prediction and Prevention* (Marcel Dekker, 1994). The remaining material in the first edition has been expanded and updated for *Mechanical Wear Fundamentals and Testing: Second Edition, Revised and Expanded* (Marcel Dekker, 2004).

Although great care has been taken to provide accurate and current information, neither the author(s) nor the publisher, nor anyone else associated with this publication, shall be liable for any loss, damage, or liability directly or indirectly caused or alleged to be caused by this book. The material contained herein is not intended to provide specific advice or recommendations for any specific situation.

Trademark notice: Product or corporate names may be trademarks or registered trademarks and are used only for identification and explanation without intent to infringe.

Library of Congress Cataloging-in-Publication Data

A catalog record for this book is available from the Library of Congress.

ISBN: 0-8247-4772-0

This book is printed on acid-free paper.

Headquarters

Marcel Dekker, Inc.,
270 Madison Avenue, New York, NY 10016, U.S.A.
tel: 212-696-9000; fax: 212-685-4540

Distribution and Customer Service

Marcel Dekker, Inc.,
Cimarron Road, Monticello, New York 12701, U.S.A.
tel: 800-228-1160; fax: 845-796-1772

Eastern Hemisphere Distribution

Marcel Dekker AG,
Hutgasse 4, Postfach 812, CH-4001 Basel, Switzerland
tel: 41-61-260-6300; fax: 41-61-260-6333

World Wide Web

<http://www.dekker.com>

The publisher offers discounts on this book when ordered in bulk quantities. For more information, write to Special Sales / Professional Marketing at the headquarters address above.

Copyright © 2004 by Marcel Dekker, Inc. All Rights Reserved.

Neither this book nor any part may be reproduced or transmitted in any form or by any means, electronic or mechanical, including photocopying, microfilming, and recording, or by any information storage and retrieval system, without permission in writing from the publisher.

Current printing (last digit):

10 9 8 7 6 5 4 3 2 1

PRINTED IN THE UNITED STATES OF AMERICA

To my wife, Barbara

Preface

It has been a decade since the first edition of this book was published. During that period important changes in the field of tribology have occurred. As a consultant I have also gained additional tribological experience in a wide range of industrial applications. It was thus decided to develop a second edition with the goal of incorporating this new information and additional experience into a more useful and current book, as well as clarifying and enhancing the original material. The purpose and perspectives of the first edition were to be maintained, namely, “to provide a general understanding . . . for the practicing engineer and designer [and an] engineering perspective . . .”. As rewriting progressed it became clear that the greatly expanded text would develop into a much larger volume than the first. We therefore decided to divide the material into two volumes, while keeping the basic format and style. Essentially the first two parts of the original edition on the fundamentals of wear and wear testing are combined into a single volume, *Mechanical Wear Fundamentals and Testing* (Marcel Dekker, 2004). The remaining two parts of the first edition, which focus on design approaches to wear and the resolution of wear problems, are the basis for this second volume, *Engineering Design for Wear*.

While a good deal of background material is the same as in the first edition, significant changes have been made. The most pervasive is the use of a new way of classifying wear mechanisms, which I have found to be useful in formulating approaches to industrial wear situations. As a result, Part A, Fundamentals, has been reorganized and rewritten to accommodate this new classification and to include additional material on wear mechanisms. Additional wear tests are described in Part B, Testing, which has been expanded to include friction tests. These first two parts are discussed in *Mechanical Wear Fundamentals and Testing*. Part A, *Design, of Engineering Design for Wear* has been modified by expanding several sections, as well as adding a section on a design methodology, design triage, that has been found to be useful. Among the expanded treatments is the consideration of material aspects and the treatment of rolling bearing wear and rolling wear, as well as impact wear. An additional case study has been added to the Problem Solving section, Part B, which illustrates the use of analytical modeling for resolving wear problems. Additional appendixes have been added, providing further information for use in engineering situations. These additional appendixes include tables on threshold stress for galling and sliding wear relationships for different contact situations. A glossary of wear mechanisms has also been added.

This book demonstrates the feasibility of designing for wear and using analytical approaches to describe wear in engineering situations, based on my experience over the last 40 years.

Raymond G. Bayer

Contents

<i>Preface</i>	<i>v</i>
1 Design Perspective of Wear Behavior	1
1.1 Introduction	1
1.2 System Nature of Wear	2
1.3 Basic Mechanisms of Wear	3
1.4 Mild and Severe Wear Behavior	5
1.5 Operational Categories of Tribosystems	5
1.6 Two-Body Tribosystems	6
1.7 One-Body Tribosystems	17
1.8 Materials and Wear Behavior	17
2 Engineering Models for Wear	45
2.1 Introduction	45
2.2 Wear and Wear Rate Relationships for Sliding Wear	49
2.3 Wear and Wear Rate Relationships for Abrasive Wear	55
2.4 Zero Wear and Measurable Wear Models for Sliding	56
2.5 Percussive Impact Wear Models	75
2.6 Model for Rolling Wear	89
2.7 Model for Ball and Roller Bearing Wear	96
2.8 Models for Journal Bearing Wear	104
2.9 Models for Erosive Wear	123
2.10 Models for Tool Wear	127
3 Wear Design	137
3.1 General	137
3.2 System Analysis	140
	vii

3.3 Model Selection and Development	142
3.4 Database Identification and Development	147
3.5 Verification	147
3.6 Design Triage	148
4 Design Guidelines	151
4.1 Introduction	151
4.2 Guidelines	151
4.2.1 Reliance on Analytical Design Methods Increases the Degree of Conservatism Required	151
4.2.2 Wear is a System Property; Utilize All Design Parameters That Can Influence Wear	151
4.2.3 Approach Extrapolation of Data and Extension of Designs Cautiously	152
4.2.4 Design with Limits and Characteristics of Materials in Mind	152
4.2.5 Metals and Polymers Tend to Require Different Designs	152
4.2.6 Design So That a Mild Wear Condition Exists	153
4.2.7 A Minimum Requirement for Material Selection is That the Material Should be Stable in the Operating Environment	153
4.2.8 While Fluid or EHD Lubrication is very Effective for Reducing Wear, Specific Designs are Required to Insure this Form of Lubrication	153
4.2.9 Minimize Exposure to Abrasive Particles	154
4.2.10 In Abrasive Situations Make the Wear Surfaces Harder than the Abrasives	154
4.2.11 Optimize Contact Geometry to Minimize Stresses	154
4.2.12 Use a Lubricant Whenever Possible	155
4.2.13 Use Dissimilar Materials	155
4.2.14 Increasing Hardness Tends to Reduce Wear	155
4.2.15 To Increase System Life (Reduce System Wear), It is Sometimes Necessary to Increase the Hardness of Both Members	155
4.2.16 Rolling is Preferred Over Sliding	155
4.2.17 Sliding or Fretting Motions Should be Eliminated in Impact Wear Situations	156

4.2.18 Compound Impact Situations Can Often be Treated as a Sliding Wear Situation in Which the Loads (Stresses) are Determined by the Impact	156
4.2.19 Impacts Should be Avoided in Sliding and Rolling Contacts	156
4.2.20 Elastomers Frequently Outperform Harder Materials and Reduce Counterface Wear in Impact Situations	156
4.2.21 Thicknesses of Conventional Coatings Generally Should be Greater than 100 μm	156
4.2.22 Use Moderate Surface Roughnesses	157
4.2.23 Avoid the Use of Stainless Steel Shafting with Impregnated Sintered Bronze Bearings	157
4.2.24 When Molded Filled Plastics Tend to Exhibit Significantly Different Initial and Long-Term Wear Behavior	157
4.2.25 When Glass or Other Hard Fillers are Used, the Hardness of the Counterface Should be Equal to or Greater than that of the Filler	157
4.2.26 The Tendency for Galling to Occur can be Reduced by Using Dissimilar and Hard Materials of Low Ductility, Lubrication, and Rougher Surfaces	158
4.2.27 Avoid the Use of Designs in Which Fretting Motions Can Occur	158
4.2.28 When Fretting Motions are Present, Design to Optimize Sliding Wear Life and to Minimize Abrasive Wear	158
4.2.29 Sacrificial Wear Design Should be Considered an Option When Satisfactory Life Cannot be Achieved with Available Materials	158
4.2.30 Conform to Vendor Recommendations Regarding Optimum Wear Performance	159
4.2.31 Changes Associated with Design Modifications or New Applications Should be Reviewed Carefully with Respect to their Potential Effect on Wear Behavior	159
4.2.32 Provide Adequate Clearance in Journal Bearings	159
4.2.33 The Severity of the Wear (Wear Rate) in Rolling, Sliding, and Impact Wear Situations can Generally be Correlated to the Ratio of Operating Stress Over Yield Stress (Stress Ratio)	159
4.2.34 Design so that Severe Wear Mechanisms Associated with Adhesion and Single-Cycle Deformation do not Occur	160
5 Design Examples	161
5.1 Introduction	161
5.2 Printer Cartridge	161

5.3 Vacuum Probe	169
5.4 Forms Thickness Control	173
5.5 Plastic Gears	177
5.6 Type Carrier Backstop	179
5.7 Thermal Conduction Module	187
5.8 Hammer Pivot	202
5.9 Band–Platen Interface	216
5.10 Push Rod Tip	230
5.11 Band–Ribbon Interface	237
5.12 Magnetic Read Head	255
5.13 Erosion Applications	269
5.14 Abrasion Applications	283
5.15 Nuclear Valve	292
5.16 Plug Valve	300
5.17 Screwnut–Spindle	304
5.18 Cardan Joint	307
5.19 Electromagnetic Clutch	313
6 Problem Solving Methodology	325
6.1 General	325
6.2 Failure Analysis	326
6.3 Hypothesis Development	327
6.4 Testing	328
7 Problem Solving Case Studies	329
7.1 Introduction	329
7.2 Card Edge Connector Fretting	329
7.3 Excessive Carrier Backstop Wear	336
7.4 Push Rod Tip Failure	339
7.5 Separator Roll	345
7.6 Motor Brush Life	349
7.7 Memory Disk Drive Failures	353
7.8 Erosion in Fans and Blowers	354

7.9 Hydraulic Structure Wear	355
7.10 Teeter Bearing Wear	358
<i>Glossary of Wear Mechanisms, Related Terms, and Phenomena</i>	367
<i>Appendix I: Values of m and n for Use with the Hertz Contact Stress Equations</i>	375
<i>Appendix II: Zero Wear Factors and Coefficients of Friction for Sliding</i>	376
<i>Appendix III: Wear and Friction Data</i>	384
<i>Appendix IV: Approximate Relationship Between Vickers Hardness and Yield Point in Shear</i>	395
<i>Appendix V: Galling Threshold Stress</i>	396
<i>Appendix VI: Wear Relationships for Sliding Wear Based on the Zero and Measurable Wear Models for Sliding</i>	403
<i>Appendix VII: Model for the Effect of Fluid Lubrication on Zero Wear Factors</i>	410

1

Design Perspective of Wear Behavior

1.1. INTRODUCTION

General wear behavior was treated in Part A of *Mechanical Wear Fundamentals and Testing: Second Edition, Revised and Expanded* (MWFT2E); however, the focus of that treatment was primarily on wear mechanisms and wear phenomena. While such a focus provides an overview of wear and its complexity that is generally quite valuable to the designer, it is an approach that is more in line with the perspective and concerns of the physical scientist and materials engineer rather than those of the designer. The scientist is directly concerned with the identification and understanding of the mechanisms involved. The materials engineer or scientist is concerned with the relationship of material properties to these mechanisms, so that materials can be selected and developed to resist these mechanisms. On the other hand, the designer tends to view the wear situation in terms of operational parameters and has the goal to select or develop a design that has the desired wear life. Consequently, a treatment of wear behavior in terms of operational parameters would be more directly useful to the designer. This can be developed by considering the relationships of three major operational aspects to wear behavior, namely: the nature of the contact; the type of motion associated with the contact; and the environment surrounding the contact.

In terms of the nature of the contact, it is useful to consider two broad categories. One is two-body contact, such as between gear teeth, a ball and a race in a ball bearing, a cam and a follower, a magnetic tape and a recording head, etc.; in short, this category covers the contact between two solid bodies. The other general category is a single body in contact with a fluid or stream of particles. The contact situation associated with a ship propeller and water would be an example of this category. Other examples of this type of contact are an air frame moving through a rain or dust field and the interior of pipelines involved in the transmission of fluids or slurries. It is also useful to identify and define several broad categories of motion that can be associated with these two types of contact. For the two-body contact situation, there are rolling, sliding, and impact motions. For the contact between a fluid and a single body, typical categories are cavitating or non-cavitating flow, streamline or turbulent flow, and high angle or low angle particle impingement. There are several major environmental categories, which are useful to consider for general design purposes. Among these are environments with and without hard particles (abrasive and non-abrasive environments), lubricated and non-lubricated environments, and hostile or non-hostile ambient environments. The last category would include temperature as well as gaseous elements.

Before considering wear behavior in terms of these categories, it is worthwhile to consider some of the more general aspects of wear behavior in relationship to design and design practices. Design approaches to wear must recognize the following characteristics of wear:

1. Wear is a system property, not a material property.
2. Materials can wear by a variety of mechanisms and combinations of mechanisms, depending on the tribosystem in which it is used.
3. Wear behavior is frequently nonlinear.
4. Transitions can occur in wear behavior as a function of a wide variety of parameters.

As will be shown, the complexity of this situation can be reduced to a significant degree by categorizing wear situations according to operational characteristics.

1.2. SYSTEM NATURE OF WEAR

Wear is not a material property nor is it a unique physical mechanism. It is best thought of as a system response. Materials can wear by a variety of mechanisms and material properties and operational parameters jointly influence wear behavior. This general nature of wear is significant to the designer, as can be seen in the following considerations of some design practices.

A common and useful practice in design is to study the performance of an existing design and to look for correlation between various performance elements and design parameters. As will be brought out in this section on wear design and in the following one on problem solving, such an activity is a very valuable one for wear performance. However, the correlations sought and the considerations that must go along with the development of these correlations must take into account the nature of wear behavior and wear phenomena. This point can be illustrated by considering two errors frequently made in design situations. One is to attempt to use device wear performance to establish an intrinsic wear resistance or relative wear resistance for a material. The tendency in this case is to think of a material as a good or bad wearing material, in general, or as being a better or poorer wearing material than another, again in general. This violates one of the fundamental aspects of wear, namely that wear is a system property and not a material property. Consequently, rankings or assessments that can be made are relative to the conditions of that application. For different conditions, the wear performance of a material can change and different rankings can result. The second error is to use the wear behavior of a material observed in an application to infer a universal mode of wear for either that material or that situation. This second error is similar to the first in that it violates a fundamental aspect of wear behavior. Namely, materials can wear by several mechanisms, which are dependent not only on material properties but also on conditions surrounding the contact (i.e., the overall wear situation).

There is another general characteristic of wear that is significant in design. In development engineering or design, there is frequently the need to extrapolate performance characteristics of an existing mechanism from one application to another. In the case of wear, this might be the extension of a design to a higher load situation, faster speed, a different environment, or different life requirements. Particularly, with the latter, there is a tendency to assume a linear relationship for such extrapolations. However, because of the transitions in wear behavior that are possible and the complex nature of wear phenomena, such relationships are frequently nonlinear and can vary with the

wear situation or system. Therefore, it is not possible to identify a universal relationship or set of relationships that can be used for all cases. To the designer, this means that without the existence of supporting data such extrapolations can be erroneous and arbitrary. However, with the proper consideration of the tribosystem and supportive data, appropriate relationships can be selected and used to provide these types of extrapolations. Approaches of this type will be presented later in the section on design.

1.3. BASIC MECHANISMS OF WEAR

Several general mechanisms for wear were discussed in Part A of MWFT2E and were grouped into seven major categories: adhesive wear, single-cycle deformation wear, repeated-cycle deformation wear, oxidative wear, tribofilm wear, thermal wear, and abrasive wear. In design, a simplistic view of these basic categories for wear mechanisms is quite often useful and can aid in the identification of significant parameters and in the selection and formulation of engineering models for wear. Fundamental to adhesive wear is bonding between the two surfaces at the points of real contact. Consequently, surface properties of materials, cleanliness of the surfaces, and other parameters related to adhesion become significant for this mode of wear. Lubrication is a prime way of inhibiting this type of wear.

Single-cycle deformation wear is the result of a harder object deforming, cutting, or fracturing as a result of relative motion. A single engagement is all that is required for this type of wear. With this type of wear, the concern is with the presence of hard particles and sharp profiles. Consequently, shape, hardness, surface roughness, and number of particles are significant to wear behavior, as well as the mechanical properties of the material being worn. Lubrication has little effect on this type of wear and may increase wear under certain conditions.

Repeated-cycle deformation wear results from the accumulation of deformation as a result of repeated contact. This accumulation of deformation, caused by repeated cycles of stress and strain, lead to the formation and propagation of cracks. As discussed in Sec. 3.4 of MWFT2E, there are a number of different mechanisms of this type, for example, surface fatigue, delamination, and ratcheting. However, for engineering purposes, it is useful and generally sufficient to think of these as simply as fatigue or fatigue-like wear processes. Such processes can occur on a macro- or micro-scale in two-body contact situations, with particles in abrasive wear situations, and in one-body wear situations with particles and fluid flow. Mechanical properties of the wearing material and stress levels are primary factors in this mode. Since lubrication can reduce shear on the surface, it can reduce fatigue wear, however, it is usually more significant in terms of adhesive wear.

These three mechanisms, adhesion, single-cycle deformation, and repeated-cycle deformation (fatigue), directly result in material loss from a surface or deformation of a surface. Oxidative, tribofilm, and thermal wear processes are different. Oxidation, tribofilm formation, and thermal effects do not directly lead to material loss or damage. Oxidative, tribofilm, and thermal wear involve a combination of these effects with one of the other three mechanical wear processes, which do directly result in loss of material from a surface. A useful way of thinking about oxidative, tribofilm, and thermal wear mechanisms is as modifiers of the mechanical wear processes. It is also important to recognize that oxidation, tribofilm, and thermal processes can indirectly affect wear through their effect on friction, since wear processes can be sensitive to surface shear and traction.

With oxidative wear, the chemical reactivity of the surface is important, as well as the chemical environment and temperature of the application. Lubrication can be very

significant with relationship to oxidative wear, particularly if the lubricant contains surface-active elements which result in the formation of oxide layers. There are two other ways a lubricant can influence oxidative wear; it can provide a barrier to chemical attack from the environment and it can reduce surface temperatures by reducing friction and conducting heat away from the contact. Break-in or run-in can be an important factor in terms of oxidative wear as well.

For transfer and third-body film formation such aspects as roughness, motion, geometry, and composition (chemical aspects) are factors. The use of lubricant with material pairs that rely on the formation of physical films for good wear behavior can result in increased, rather than decreased wear. This is particularly true in the case of many situations involving the use of self-lubricating plastics, where good wear behavior is frequently associated with the formation of transfer films. As with oxidative wear, break-in can be an important factor in terms of the formation of these physical films and tribofilm wear.

The thermal properties of the materials, frictional heating, conduction of heat away from the interface, and the thermal characteristics of the materials affect thermal wear processes.

While abrasion is wear caused by hard particles or protuberances, it is generally only significant in situations that involve hard particles, either loose or attached to a surface. The size, shape, hardness, and number of particles are significant parameters in this type of wear, as well as their friability. When the wearing surfaces are softer than the particles, the dominant mechanisms for wear are single-cycle deformation processes, e.g., cutting and plowing. When the surface is harder, repeated-cycle deformation processes become dominant. In either case, oxidative wear processes can be involved and be significant, particularly in situations where there are liquids or hostile gaseous environments involved.

It is important in design to recognize that the composition and make-up of wear surfaces, as well as mechanical properties, can change during the wear process because of the formation of oxide and transfer films and work or strain hardening effects. As a result, the properties of those surfaces may be unique to the wear situation and may be significantly different than those of the original materials. It is also important to recognize that in most wear situations, it is possible and likely that more than one of the mechanisms may be present. As was discussed in Part A of MWFT2E these mechanisms can interact and combine, but one will frequently predominate as the controlling factor. The dominant mechanism can vary with different tribosystems.

The mildest forms of wear tend to be associated with repeated-cycle deformation mechanisms, either by themselves or in conjunction with tribofilm and oxidative wear mechanisms. (See Figure 4.14 in MWFT2E.) Repeated-cycle deformation mechanisms are generally the dominant wear mechanism associated with long-term behavior. Adhesion and single-cycle deformation mechanisms tend to be significant in initial wear behavior and can be much more severe than repeated-cycle deformation mechanisms. Abrasive wear can be the dominant form of wear, when there are sufficient particles present, and can be more severe than adhesive wear. The effect of single-cycle deformation wear can be eliminated and reduced in most cases by using smooth surfaces, appropriate shapes (e.g. well-rounded corners and edges), and keeping abrasive particles out of the wear zone. Similarly, the effects of adhesive wear can be minimized principally by the use of lubrication and also by the appropriate choice of materials. In general, it is desirable to select design parameters, which reduce the tendency toward the potentially more severe forms of wear, that is, adhesive, single-cycle deformation, thermal, and adhesive mechanisms, as well as the more severe forms of repeated-cycle deformation mechanisms.

1.4. MILD AND SEVERE WEAR BEHAVIOR

Among the many types of transitions that can occur in wear behavior, the transition from mild to severe wear is of singular importance in design. In order to achieve the lifetimes or reliability desired for most devices or machines, wear behavior must be in the mild regime. Wear rates associated with severe wear behavior generally are too high to provide long component life and low maintenance. In certain applications, severe wear behavior cannot be avoided, such as in ore processing or earth moving equipment. In these cases, routine maintenance is high.

Generally speaking, all materials can and do undergo transitions from mild to severe wear. Such transitions can occur for a variety of reasons. For example, many plastics undergo a transition from mild to severe wear as a function of sliding speed or the combination of sliding speed and pressure (1). This is associated with temperature increases at the interface that occurs with higher speeds and pressures. A metal in an abrasive wear situation might experience a transition as a function of the size and hardness of the abrasives encountered. If the abrasives are fine and are softer than the metal, polishing will occur; if coarser and harder than the metal, then a coarse, rough wear scar with many grooves will result (2,3). Changes in the angle of impingement of a fluid or slurry stream can also result in a transition from mild to severe wear, as can the introduction of slip in a rolling situation or sliding in an impact situation. An example of the latter is that of wear behavior of elastomers under nominal impact conditions. If there is little or no sliding associated with the impact, wear behavior can be mild. However, with the introduction of sliding or slip, wear rates increase dramatically and severe wear occurs (4). Also in impact situations, an over-stressed condition can occur for elastomers. At impact conditions below a critical stress, wear behavior is mild; while above the critical level (over-stressed), it is severe (5). From these examples it can be seen that the transition from mild to severe behavior for materials can involve any or all of the elements involved in a tribosystem, involving not only the chemical and physical elements, but also the mechanical elements as well.

During the development and the evaluation of a design, it is important to recognize the possibility of such transitions. From a design standpoint, it is obvious that it is desirable to select designs and design parameters that foster mild wear behavior and avoid those elements which tend to result in severe wear behavior. Consequently, an awareness of those elements, which control mild–severe wear transitions in an application, is important. These elements are addressed further in the sections on operational categories of tribosystems (1.5–1.7) and materials (1.8). Also, it should be kept in mind that while severe wear behavior is generally unacceptable, there is generally a considerable range for wear rates in the mild wear regime. As a result, simply insuring that mild wear behavior occurs is generally not adequate to insure adequate life. Because of the desirability to have long life with low maintenance, the designer is generally more concerned with the characteristics of mild wear behavior than severe wear behavior.

1.5. OPERATIONAL CATEGORIES OF TRIBOSYSTEMS

Since the designer can usually describe the tribosystem in terms of operational parameters, it would be useful to correlate wear mechanisms with these operational parameters. In this way the designer can understand the relationship of physical and material parameters with his design parameters and their influences on performance. Unfortunately, a general

correlation to specific mechanisms cannot be done at the present time; however, some general trends can be developed that relate broad categories of tribosystems and generic wear mechanisms. While there can be exceptions to such trends, they do provide useful information and guidance in design. One useful way of relating general trends of wear behavior to operational characteristics of tribosystems is shown in [Table 1.1](#). This scheme is based on three major attributes of the tribosystem, which were identified previously, namely the nature of the wear interface, the type of motion at that interface, and environment of that interface.

Two general types of wear interfaces are considered in this approach; one is an interface involving two solid surfaces, two-body, and the second involves a single solid surface interacting with a fluid or particle stream, one-body. For the two-body contact, three major types of relative motion are identified, rolling, impact, and sliding, along with some significant sub-categories. In the case of one-body contact, two major categories, impingement and flow, along with some sub-categories, replace these. The environment is broken down into lubricated or not, with and without particles, and normal and hostile ambient conditions. These operational characteristics are then related to the generic wear categories of abrasion and adhesive, single-cycle deformation, repeated-cycle deformation (fatigue), oxidative, tribofilm, and thermal wear mechanisms.

There are some general aspects that need to be considered in relationship to [Table 1.1](#). One of these is associated with the fact that different areas of or locations on a component may have different operational parameters associated with their wear. For example, at the pitch line of a gear tooth the motion may be pure rolling, while at the tip, it is mostly sliding. Similarly in a pump, different regions might be characterized as wearing by impingement and others by flow across the surface. Consequently, [Table 1.1](#) should be interpreted in terms of individual wear points or sites rather than in terms of a part or device. A second aspect is that the mechanisms identified are the most common ones not necessarily the only ones that may occur in these situations. For example, cutting tool wear, which can be considered sliding wear situation, can involve atomic wear processes (diffusion) in addition to those indicated in the table. Finally, chemically and physically formed layers may occur and frequently do when a lubricant is used. Such effects are considered as part of the lubrication processes, not as oxidative or tribofilm wear.

1.6. TWO-BODY TRIBOSYSTEMS

While all major categories of wear mechanisms can occur with two-body tribosystems, the nature of the relative motion between the surfaces, as well as the presence or absence of particles at the interface, is important in terms of their relative significance to long-term wear behavior. (See [Chapter 3](#) of *MWFT2E*). In the case of pure rolling and impact, repeated-cycle deformation, or more specifically, fatigue is the predominant mechanism. While with sliding, repeated-cycle deformation mechanisms, like fatigue and other fatigue-like mechanisms, and adhesive wear mechanisms are likely. Single-cycle deformation can also be significant and even dominate the wear behavior in these situations. However, their significance in typical engineering situations is typically limited to initial wear behavior and can be minimized and eliminated by the selection of appropriate shapes and roughness conditions. Under mild sliding conditions in such situations, repeated-cycle deformation tends to predominate; under severe conditions, adhesion predominates. With sliding or rolling, the presence of hard particles at the interface can introduce abrasive

Table 1.1 Operational Classification of Wear Situations

		Contact Type: Two-Body			Significant mechanisms ^b
Motion		Environment ^a			
		Lubrication	Particulates	Ambient	
Rolling	Without slip	None	None	Normal	SCD (if beyond elastic limit) RCD TH (with plastics)
				Hostile	SCD (if beyond elastic limit) RCD OX TH
				Hard particles	Normal
		Lubricated	None	Normal	SCD (if beyond elastic limit) RCD
				Hostile	SCD (if beyond elastic limit) RCD
				Hard particles	Normal
	With slip	None	None	Normal	AD SCD (if beyond elastic limit) RCD OX (with metals and ceramics) TH (with plastics) TF (with plastics, composites and ceramics)
				Hostile	AD SCD (if beyond elastic limit) RCD OX (with metals and ceramics) TH (with plastics) TF (with plastics, composites and ceramics)
				Hard particles	Normal

(continued)

Table 1 (Continued)

Motion	Environment ^a			Significant mechanisms ^b
	Lubrication	Particulates	Ambient	
			Normal	TF (with plastics, composites and ceramics) AB
			Hostile	AD SCD (if beyond elastic limit) RCD OX (with metals and ceramics) TH (with plastics) TF (with plastics, composites and ceramics) AB
	Lubricated	None	Normal	SCD (if beyond elastic limit) RCD
			Hostile	SCD (if beyond elastic limit) RCD
		Hard particles	Normal	SCD (if beyond elastic limit) RCD AB
			Hostile	SCD (if beyond elastic limit) RCD AB
Trends: wear increases with slip and presence of hard particles. RCD mechanisms tend to be the dominant and limiting mechanisms; abrasion can dominate, generally, mildest wear situation.				
Impact	With stationary body, without slip	None	None	Normal
				SCD (if beyond elastic limit)
				RCD TH (with polymers)
			Hostile	SCD (if beyond elastic limit) RCD OX (with metals and ceramics) TH
		Hard particles	Normal	SCD (if beyond elastic limit) RCD TH (with polymers) AB
			Hostile	SCD (if beyond elastic limit) RCD OX (with metals and ceramics) TH AB
	Lubricated	None	Normal	SCD (if beyond elastic limit) RCD

(continued)

Table 1 (Continued)

Motion	Environment ^a			Significant mechanisms ^b		
	Lubrication	Particulates	Ambient			
With stationary body, with slip	None	None	Hostile	SCD (if beyond elastic limit) RCD		
			Hard particles	Normal	SCD (if beyond elastic limit) RCD AB	
				Hostile	SCD (if beyond elastic limit) RCD AB	
			Hard particles	Normal	AD	
				Hostile	SCD (if beyond elastic limit) RCD OX (with metals and ceramics) TH (with polymers) TF (with plastics, composites and ceramics) AD	
			Hard particles	Normal	Normal	SCD (if beyond elastic limit) RCD OX (with metals and ceramics) TH (with polymers) TF (with plastics, composites and ceramics) AD
		Hostile			AD SCD (if beyond elastic limit) RCD OX (with metals and ceramics) TH (with polymers) TF (with plastics, composites and ceramics)	
		Hostile			AD SCD (if beyond elastic limit) RCD OX (with metals and ceramics) TH (with polymers) TF (with plastics, composites and ceramics) AB	
		None		None	Normal	SCD (if beyond elastic limit) RCD
					Hostile	SCD (if beyond elastic limit) RCD

(continued)

Table 1 (Continued)

Motion	Environment ^a			Significant mechanisms ^b
	Lubrication	Particulates	Ambient	
With moving body	None	Hard particles	Normal	SCD (if beyond elastic limit) RCD AB
			Hostile	SCD (if beyond elastic limit) RCD AB
		None	Normal	AD
			Hostile	SCD (if beyond elastic limit) RCD OX (with metals and ceramics) TH (with polymers) TF (with plastics, composites and ceramics)
				AD SCD (if beyond elastic limit) RCD OX (with metals and ceramics) TH TF (with plastics, composites and ceramics)
			Hard particles	Normal
	Hostile	AD SCD (if beyond elastic limit) RCD OX (with metals and ceramics) TH TF (with plastics, composites and ceramics) AB		
	Lubricated	None	Normal	SCD (if beyond elastic limit) RCD
			Hostile	SCD (if beyond elastic limit) RCD
		Hard particles	Normal	SCD (if beyond elastic limit) RCD AB
			Hostile	SCD (if beyond elastic limit) RCD AB

(continued)

Table 1 (Continued)

Motion	Environment ^a			Significant mechanisms ^b		
	Lubrication	Particulates	Ambient			
Trends: RCD mechanisms tend to be the dominant and limiting mechanisms; wear tends to increase with particles and abrasion can dominate; with stationary body, induced vibrations and misalignment can cause slip and fretting, which tends to result in increased wear; acceptable v generally requires stresses be in the elastic range; with moving objects, wear increases with the amount of sliding and sliding effect can dominate wear behavior; fluid lubrication can be very significant in reducing wear.						
Sliding	Unidirectional	None	None	Normal	AD SCD (if beyond elastic limit) RCD OX (with metals and ceramics) TH (with polymers; high speeds) TF (with plastics, composites and ceramics)	
				Hostile	AD SCD (if beyond elastic limit) RCD OX (with metals and ceramics) TH TF (with plastics, composites and ceramics)	
				Hard particles	Normal	AD SCD (if beyond elastic limit) RCD OX (with metals and ceramics) TH (with polymers; high speeds) TF (with plastics, composites and ceramics)
		Lubricated	None	None	Normal	AB SCD (if beyond elastic limit) RCD
					Hostile	AD SCD (if beyond elastic limit) RCD OX (with metals and ceramics) TH TF (with plastics, composites and ceramics)
					Hard particles	Normal

Table 1 (Continued)

Motion	Environment ^a			Significant mechanisms ^b	
	Lubrication	Particulates	Ambient		
Cyclic, large amplitude	None	None	Hostile	SCD (if beyond elastic limit) RCD AB AD	
			Normal	SCD (if beyond elastic limit) RCD OX (with metals and ceramics) TH (with polymers; high speeds) TF (with plastics, composites and ceramics)	
			Hostile	AD SCD (if beyond elastic limit) RCD OX (with metals and ceramics) TH TF (with plastics, composites and ceramics)	
			Normal	AD SCD (if beyond elastic limit) RCD OX (with metals and ceramics) TH (with polymers; high speeds) TF (with plastics, composites and ceramics)	
			Hostile	AD SCD (if beyond elastic limit) RCD OX (with metals and ceramics) TH TF (with plastics, composites and ceramics)	
			Normal	AD SCD (if beyond elastic limit) RCD OX (with metals and ceramics) TH (with polymers; high speeds) TF (with plastics, composites and ceramics)	
	Lubricated	None	None	Normal	AB SCD (if beyond elastic limit) RCD
				Hostile	SCD (if beyond elastic limit) RCD
				Normal	SCD (if beyond elastic limit) RCD AB
				Hostile	SCD (if beyond elastic limit) RCD AB
				Normal	SCD (if beyond elastic limit) RCD AB
				Hostile	SCD (if beyond elastic limit) RCD AB

(continued)

Table 1 (Continued)

Motion	Environment ^a			Significant mechanisms ^b	
	Lubrication	Particulates	Ambient		
Cyclic, small amplitude	None	None	Normal	AD SCD (if beyond elastic limit) RCD OX (with metals and ceramics) TH (with polymers; high speeds) TF (with plastics, composites and ceramics)	
			Hostile	AD SCD (if beyond elastic limit) RCD OX (with metals and ceramics) TH TF (with plastics, composites and ceramics)	
			Hard particles	Normal	AD SCD (if beyond elastic limit) RCD OX (with metals and ceramics) TH (with polymers; high speeds) TF (with plastics, composites and ceramics)
				Hostile	AD SCD (if beyond elastic limit) RCD OX (with metals and ceramics) TH TF (with plastics, composites and ceramics)
				AB	
			Lubricated	None	Normal
	Hostile	SCD (if beyond elastic limit) RCD			
	Hard particles	Normal			SCD (if beyond elastic limit) RCD AB
		Hostile			SCD (if beyond elastic limit) RCD AB

(continued)

Table 1 (Continued)

Motion	Environment ^a			Significant mechanisms ^b
	Lubrication	Particulates	Ambient	
Trends: RCD mechanisms tend to be the dominant and limiting mechanisms; abrasion can dominate; low contact stresses and conditions that minimize adhesive wear and abrasion are preferred; mild to severe wear transitions often associated with a change in stresses from below to above the elastic limit; nature of contact (such as large/small area, conforming, line, and point) can be significant in wear behavior; lubrication very significant.				
Contact Type: One-Body				
Motion	Environment ^a			Significant mechanisms ^b
		Particulates	Ambient	
Impingement with fluid	Low angle	None	Normal	SCD (if beyond elastic limit)
			Hostile	RCD OX (with metals and ceramics) SCD (if beyond elastic limit)
			Normal	RCD OX (with metals and ceramics) SCD (if beyond elastic limit)
		Hard particles	Normal	RCD OX (with metals and ceramics) AB (cutting modes)
			Hostile	SCD (if beyond elastic limit) RCD OX (with metals and ceramics) AB (cutting modes)
			Normal	SCD (if beyond elastic limit) RCD OX (with metals and ceramics)
	High angle	None	Normal	SCD (if beyond elastic limit) RCD OX (with metals and ceramics)
			Hostile	SCD (if beyond elastic limit) RCD OX (with metals and ceramics) AB (deformation modes)
			Normal	SCD (if beyond elastic limit) RCD OX (with metals and ceramics) AB (deformation modes)
		Hard particles	Normal	AB (cutting modes)
			Hostile	OX (with metals and ceramics) AB (cutting modes)
			Normal	AB (deformation modes)
Impingement without fluid	Low angle	Hard particles	Normal	OX (with metals and ceramics)
			Hostile	AB (cutting modes)
	High angle	Hard particles	Normal	AB (deformation modes)
			Hostile	OX (with metals and ceramics)

(continued)

Table 1 (Continued)

Motion	Environment ^a		Significant mechanisms ^b	
	Particulates	Ambient		
Flow	Streamline	None	Normal	AB (deformation modes) None
			Hostile	OX (with metals and ceramics)
		Hard particles	Normal	AB (cutting modes)
			Hostile	OX (with metals and ceramics) AB (cutting modes)
	Turbulent	None	Normal	SCD (if beyond elastic limit) RCD OX (with metals and ceramics)
				Hostile
			Hard particles	Normal
		Hostile		

Trends: in flow situations without particles cavitation is principal cause for wear; impinging fluid droplets act like particles; oxidation and corrosion effects tend to be significant in situations with fluids.

Abrasion

Particles	Environment	Significant mechanisms ^b
Harder than surface	Dry	SCD
	Fluid	SCD OX
Softer than surface	Dry	RCD
	Fluid	RCD OX

Trends: minimum order of magnitude (generally larger) reduction in wear rate when surface becomes harder than particles; can dominate wear behavior in sliding, rolling, and impact situations; there can be synergistic effects between corrosion and wear when fluids are involved.

AD, adhesive wear mechanisms; **SCD,** single-cycle deformation wear mechanisms; **RCD,** repeated-cycle deformation wear mechanisms; **OX,** oxidative wear mechanisms; **TH,** thermal wear mechanisms; **TF,** tribofilm wear mechanisms; **AB,** abrasive wear mechanisms

^a **Hostile** environments are ambient conditions involving high temperatures, corrosive atmospheres, or corrosive liquids.

^b **These** are the most common and more important mechanisms that typically need to be considered in engineering situations. Other mechanisms are also possible in these situations. In some circumstances these may be significant and need to be taken into consideration as well.

mechanisms as well. Depending on the amount, sharpness, and size of these particles, their wearing action can predominate and mask the adhesive and repeated-cycle deformation wear behavior. This is more likely to occur as the number, sharpness, and size of the particles increase.

Of these three general types of motions, rolling, sliding, and impact, rolling generally produces the mildest wear condition. Furthermore, in rolling and impact conditions, wear rates are generally lowest when sliding is not present. As the degree of sliding or the amount of slip increases in these contacts, wear rates increase and sliding effects begin to dominate the wear behavior. In both rolling and impact stress levels are important, with wear tending to increase with increasing stress levels. When stress levels exceed the elastic limits of the materials involved, abrupt and significant changes in wear behavior can occur. To achieve long lives under rolling and impact conditions (e.g., $> 10^6$ cycles), it is desirable to keep the stress levels to a fraction of the yield stress. With both impact and rolling situations, it is important to recognize the significance of alignment and dimensional tolerance in wear behavior. These elements can not only influence stress levels, but can also introduce slip or sliding into the contact situation as well.

Under sliding conditions, it is useful to identify three situations: unidirectional, large amplitude cyclic, and small amplitude cyclic sliding. Small amplitude sliding occurs when the amplitude of the motion is comparable to or less than the contact width in the direction of motion. Large amplitude sliding is when the amplitude is larger than that width. Unidirectional and large amplitude slidings are similar. Without the presence of particles at the interface and for typical roughnesses used in engineering applications, the major mechanisms are repeated-cycle deformation and adhesion. Repeated-cycle deformation generally predominates for mild conditions, but the effect of adhesion cannot be ignored even under those conditions. Under severe conditions (e.g., high stress and unlubricated), adhesion can predominate. When particles are present, abrasion can also occur and predominate, depending on the size, shape, and hardness of the particles.

In sliding wear situations, transitions between mild and severe wear occur and generally are associated with elements such as surface temperature, formation of transfer and third-body films, oxide formation, and stress level. In sliding situations, temperature rise and film formation can be affected by the relative size of surfaces and the nature of the contact (e.g., point, line, or area contact), speed, load, and material properties. Low and acceptable wear rates generally require that the maximum shear stress be a small fraction of the yield shear stress. Lubrication is a significant factor in the reduction of sliding wear.

Small amplitude sliding is frequently referred to as fretting. Fretting typically occurs as a result of induced vibrations and is usually not an intentional motion. Initially, the predominant wear mechanisms are similar to those occurring in the other two categories of sliding. With fretting, however, wear debris, generated by these mechanisms, can be trapped in the contact zone and lead to catastrophic abrasive wear.

As mentioned previously, the severity of the wear tends to increase with increasing contact stress in two-body wear situations. Consequently, it is generally desirable to select sizes and geometries, so that contact stresses are significantly below the yield stresses of the materials involved. Under sliding conditions, repeated-cycle deformation mechanisms tend to become more dominant as stress levels decrease. While this is the case, adhesive aspects are significant in the low stress range and cannot be ignored. Generally, the selection of material pairs which exhibit lower tendency towards adhesion, reduction of stress, and the use of a lubricant are ways to minimize adhesive wear and its significance. Frequently, different wear behavior is observed for conditions in which the elastic limits of the materials are not exceeded as compared to those in which they are. In the latter case,

wear tends to be more severe and service lives tend to be shorter. It is not unusual to observe a mild-severe wear transition when stresses exceed the elastic range.

When lubricants are used, complete separation of the surface can result under sliding (e.g., hydrodynamic lubrication). Adhesion is eliminated under those circumstances and any wear that occurs is likely to be associated with the presence of particles in the lubricant. In some cases, complete separation may not occur and occasional asperity contact results. Under those conditions, adhesive, single-cycle deformation and, more likely, repeated-cycle deformation might take place as well. Smooth surfaces are desirable to minimize asperity contacts and reduce the contributions of these mechanisms. Also, while hydrodynamic lubrication can occur under high stresses and loads conditions, such conditions tend to decrease the likelihood of complete separation, especially when the design is not specifically formulated for this type of lubrication.

In any of the wear situations considered, particles in the interface can trigger abrasive wear mechanisms. If the particles are sharp and hard (relative to the wearing surface), the primary mechanisms are cutting and plowing. If blunt or soft, the primary mechanism is likely to be fatigue or fatigue-like, involving progressive deformation and damage. As particle size becomes smaller, fatigue or progressive deformation becomes the more likely mechanism, with worn surfaces taking on a polished appearance. Wear rates associated with cutting and plowing are generally more severe than with repeated-cycle deformation mechanisms.

1.7. ONE-BODY TRIBOSYSTEMS

In one-body tribosystems, particles can also be associated with both single-cycle and repeated-cycle wear mechanisms. In this case, however, material properties and particle properties and speed are not the only factors that influence the selection of the predominant mode. Angle of attack or impingement is a factor as well. With a low angle of impingement (i.e., grazing), abrasion mechanisms tend to become more predominant, but as the angle increases, repeated-cycle deformation becomes more significant.

Without particles, wear in one-body tribosystems is generally limited to fatigue mechanisms and are strongly dependent on the nature of fluid flow or impingement. Pressure pulses produced by a fluid stream or droplets impinging on a surface can stimulate fatigue wear mechanisms. Under turbulent flow, cavitation is another source for fatigue. All three of these situations can result in significant wear. On the other hand, with streamline flow without the presence of particles, wear is generally negligible. Under any of these conditions involving a fluid, corrosion and corrosion effects can be significant and may be the predominant factors in achieving life or selecting a design. With corrosion of a surface, even streamline flow can produce wear by removing loose oxide from the surface. There can be a synergistic effect between wear and corrosion. Corrosion rate can change (increase or decrease) in the presence of wear. Wear rates can be affected by corrosion (6–8).

1.8. MATERIALS AND WEAR BEHAVIOR

Wear behavior of a material is complex, involving chemical, thermal, mechanical, and physical properties of materials and the interaction of pairs of materials. While models exist for the effect of some of these individual parameters, they generally do not take into account the effect of other material parameters and are limited to specific wear situations.

As a result, it is generally more useful in engineering to simply be aware of the range of parameters that can affect wear behavior and to identify general trends with typical engineering material parameters and types of materials. Useful trends with hardness, toughness, ductility, modulus, and strength properties can be identified and are important in design. However, the use of these trends has to include other considerations, since materials tend to differ in more than one property. Similarly, general trends for seven material categories, metals, plastics, ceramics, elastomers, coatings, composites, and specialty wear materials, can also be identified and are significant to design.

However, before considering these categories, it is worthwhile to make some overall observations regarding wear behavior of materials. One is that superior wear performance of a material may be the result of the material being able to maintain moderate wear performance under adverse conditions, rather than the result of “intrinsic” superior wear resistance. This is often the case with materials used in applications associated with high speeds, temperatures, and hostile environments. In such cases, the better performing materials may have similar or even poorer performance under less demanding conditions than other materials. This concept is illustrated in Fig. 1.1. In these cases, the poorer performers under severe conditions often undergo a transition from mild to severe wear at some point. Such transitions often can be associated with such things as the glass transition temperatures, oxidation rates, or strain rate effects. This type of behavior is significant from two standpoints. The first is that exotic or costly materials used in special applications may offer no advantage in more typical (i.e., less demanding) applications. The second is that the designer has to be sensitive to the basic stability of materials. If a material is used at or near conditions under which some of its properties significantly degrade, it is likely that wear behavior will undergo a transition from mild to severe wear as well. A corollary of this is that a fundamental rule for selecting a material for a wear application is that it maintains its properties or is stable in the operating environment. If it does not, wear is generally severe.

Another observation regarding wear behavior that is useful in design is that materials have a region of mild wear behavior. This means that acceptable wear behavior can be achieved by adjusting and controlling the parameters of the tribosystem. This

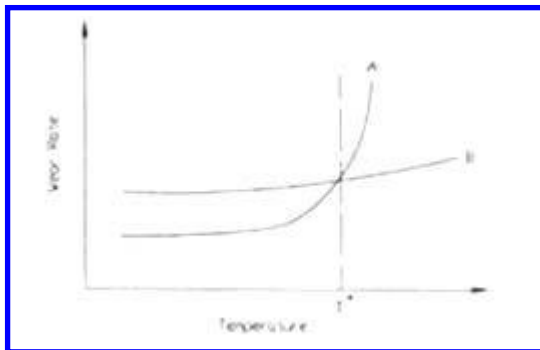


Figure 1.1 Illustration of the significance of transitions in wear behavior on material comparisons. In this case, material A undergoes a mild to severe wear transition at temperature T^* , while material B does not. Ranking of the two materials would be reversed in tests conducted in environments above and below this temperature.

perspective is useful in those design situations, where it is necessary or desirable to use a certain type of or a specific material for reasons other than wear. The problem in this case is to identify the range of parameters needed to insure the required wear behavior and then to implement them in the design. For example, such considerations might result in specifying lubrication, cooling, or a particular geometry. An exaggeration of this concept is that any material can be used, provided there is enough freedom to establish the appropriate values for the various tribosystem parameters. In practice, this means that modifications of the tribosystem, in addition to material selection, can and should be considered in design.

The most general trend associated with mechanical parameters of materials is the one with hardness. Wear tends to decrease with increasing hardness. Most mechanism models show an inverse relationship between wear and hardness. Generally, there are two reasons for this. One is an inverse relationship between the real area of contact and hardness. The other is the relationship between hardness and some strength parameter of the material, such as yield stress. However, this trend can be masked by the effect of other material parameters. This is particularly true when there are significant differences, other than hardness, between materials, such as those that occur between classes or types of materials. Figure 1.2 illustrates the effect that other material parameters can have in this trend. Such effects can often mask the effect of a factor of 2 or more change in indentation hardness.

A similar trend exists between a stress ratio, that is, the ratio of shear stress to shear yield stress, and wear. For impact and rolling situation with no slip or traction involved, this ratio may be replaced by the ratio of contact pressure to compression yield stress. Wear and wear rates tend to decrease with decreasing values of this ratio. Experience indicates that if these ratios exceed 1, wear is typically severe and wear rates generally too large for most applications. Experience also indicates that acceptable behavior in rolling and impact situations generally require that this ratio be between 0.5 and 1. For sliding, this ratio generally has to be smaller than this, often of the order a few tenths or less. Higher values of these ratios are acceptable where more wear can be tolerated or required life is shorter.

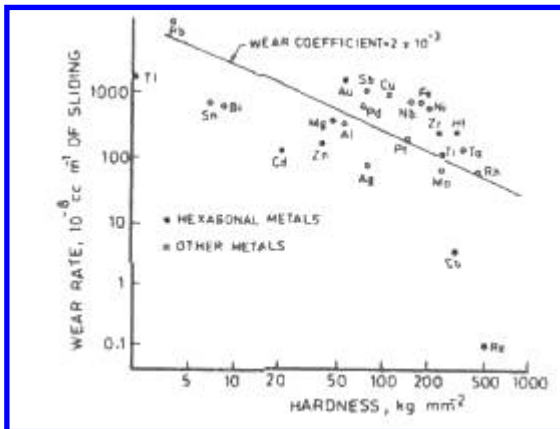


Figure 1.2 Wear rate as a function of hardness for pure metals in a pin-on-disk test at a load of 2 N. (From Ref. 31, reprinted with permission from The McGraw-Hill Companies.)

Ductility (brittleness), toughness, and modulus can also affect wear behavior. Significant trends with these tend to be observed in situations involving impact and single-cycle deformation mechanisms. Ductile and tough materials tend to experience less wear in these situations than brittle materials. For single-cycle deformation mechanisms in abrasive wear situations, wear tends to decrease with increasing modulus. However, for rolling, impact, and sliding situations increased modulus tends to increase wear as a result of its effect on contact stresses. Contact stresses increase with increasing modulus. As with hardness and the stress ratio these trends can often be masked by the effect of changes in other material properties. It is significant to note that in most wear situations, significant plastic deformation and flow are found to occur. This is also found with brittle material and is attributed to the hydrostatic compression that occurs in these contact situations.

The combined effect of material parameters on wear resistance can be found in tables of wear factors and other wear coefficients for generic wear situations. Examples of these are Appendices II, III, and V. Trends observed in these data can be used as a guide in selecting materials. With such data, it is often possible to identify individual materials, materials types, or pairs of materials that tend to perform poorer than most. The use of the poorer performers should be avoided. However, as stated previously, it is sometimes possible to use any material by adjusting various design parameters. Consequently, adequate wear performance with these materials may be obtainable in some applications. The term incompatible is sometimes applied to material pairs that tend to exhibit poorer wear resistance than other materials of similar hardness. Such behavior is often associated with adhesive mechanisms

Wear resistance of metals tends to improve with increasing hardness. However, this is a very crude generality and other factors can significantly modify the performance of metals. For example, the scatter bands in terms of wear resistance that are associated with a hardness trend can be quite large (e.g., from a factor of 2 to an order of magnitude or more). This is illustrated in [Fig. 1.3](#). One of the major contributors to this scatter in unlubricated situations is the nature of the oxide films that form. Changes in the type of oxide formed, its thickness, and uniformity can affect wear behavior, as well as friction. These properties can affect single-cycle deformation wear and repeated-cycle deformation wear. In addition, in sliding situations, these films can affect the degree of adhesion between surfaces, i.e., adhesive wear behavior. The tendency of the metal itself to form and propagate cracks (i.e., its ductility or toughness) can also be another contributor to these scatter bands. This frequently is a significant factor for situations involving impact, high stresses, or high thermal gradients. With metals, transitions in wear behavior frequently can be associated with changes in the oxide films that are formed or with the transition from elastic to plastic contact conditions.

Lubrication is a major factor in the wear behavior of metals. With sliding, the use of any lubricant typically results in at least one to two orders of magnitude improvement in wear behavior over that experienced unlubricated. The use of selected lubricants can result in several orders of magnitude improvement. In addition to this reduction in wear, the use of a lubricant frequently results in more stable and consistent wear behavior. The use of mixed or boundary lubrication is generally associated with a reduction in adhesive wear and adhesion phenomena, possibly with the formation of oxide or other layers on the surface of the metals. While it is not impossible to achieve acceptable metal-to-metal wear behavior without the use of lubricant, the use of a lubricant is generally recommended for sliding conditions. A lubricant is frequently beneficial for nominal impact and rolling situations as well. However, the improvement is generally not as great and depends on the amount of sliding or slip that is associated with these types of contacts.

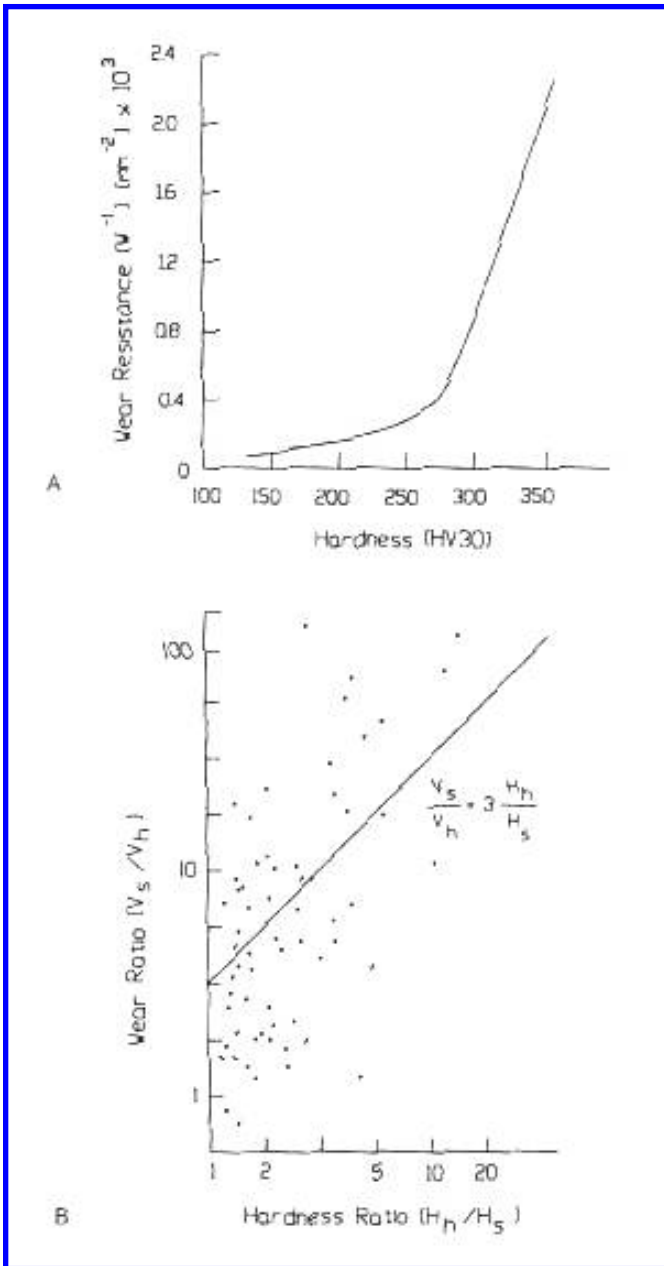


Figure 1.3 Examples of hardness trends in wear behavior. “A” shows the improvement in wear resistance of pearlite and pearlite / ferrite steel pins in an unlubricated pin-on-disk test. “B” shows the general trend and scatter in relative wear of a number of metal couples for unlubricated sliding. (“A” from Ref. 21; “B” from Ref. 22.)

For low bearing or contact pressures (e.g., in the range of 10 kpsi or less) Cu alloys, cast irons, and mild steels frequently provide good wear behavior. In most cases, the practical use of aluminum as a wear surface requires anodization on that surface. However, with lubrication and low contact pressure, aluminum alloys can also provide adequate wear resistance without anodization. For higher pressures, hardened steels are generally required for adequate wear behavior. Particularly for adverse conditions the use of high alloy and specialty steels, which maintain good properties under those conditions, might be required. Precipitation hardening and martensitic stainless steels (400 series) often provide good wear resistance. However, the wear performance of the austenitic stainless steel (300 series) is generally poor. There is a strong tendency towards galling for both the 300 series stainless steels and aluminum alloys.

Work hardening, associated with wear, can occur with some metals and be a significant factor in long-term behavior. When this occurs, the long-term wear rate can generally be correlated to the increased hardness, not the initial hardness of the metal. Finally, it is worthwhile to note that many of the softer metals (e.g., lead, silver, and gold) are used as lubricants for harder metal surfaces; these metals tend to form transfer films on the surface of the rubbing members.

As a class, ceramics and carbides tend to be harder than most steels and tend to retain their hardness at elevated temperatures. Because of the general trend for wear resistance to increase with increasing hardness, ceramics and carbides can provide improved wear resistance over hardened steels in many cases. This is particularly true for those situations where steels tend to degrade because of elevated temperatures. However, because of the complexities of wear, it is possible for steels and other materials to provide better wear resistance in many cases as well. [Figure 1.4](#) shows examples of this relative behavior. There are several reasons usually cited for this. One is that ceramics and carbides tend to be brittle and this brittleness can result in reduced wear resistance in some applications. At the same time, it must be noted that these materials often exhibit ductile behavior in many wear situations because of the stress fields that are produced in the contact (9). Another aspect is that many of the engineering carbides are composite materials in which the carbides are contained in a more ductile matrix. For example, most tungsten carbide (WC) tools contain WC particles in a Co matrix or binder. In this case, the wear behavior is a function of both materials and their relative mixture (e.g., percentage of the carbide to binder and size of the carbide particles) (10). Because of this sensitivity to both sets of properties, as well as to those of the mixture, a wide range of wear behavior is possible with carbide composites.

The environment has been found to be a major factor in the wear behavior of ceramics. For example, wear resistance of alumina has been found to be sensitive to the amount of moisture and oxygen present gases (11). Adhesive wear behavior and the formation of tribofilms are also factors associated with the wear of and by these materials. As with metals, the wear behavior of ceramics and carbides can often be improved with the use of lubricants (12). However, in many of the situations, where these materials are used, lubrication might not be possible because of the properties of conventional lubricants. For example, in applications associated with high temperatures, the use of oils might not be possible because of the degradation of oils.

Since ceramics and carbides are often significantly harder than the surface they contact, surface roughness can be a major factor in the overall wear of the tribosystem. The surfaces of the ceramic or the carbide should be smooth enough so that a severe single-cycle deformation wear situation is not produced on the counterface. At the same time, the designer must be sensitive to the surface preparation technique used, since the

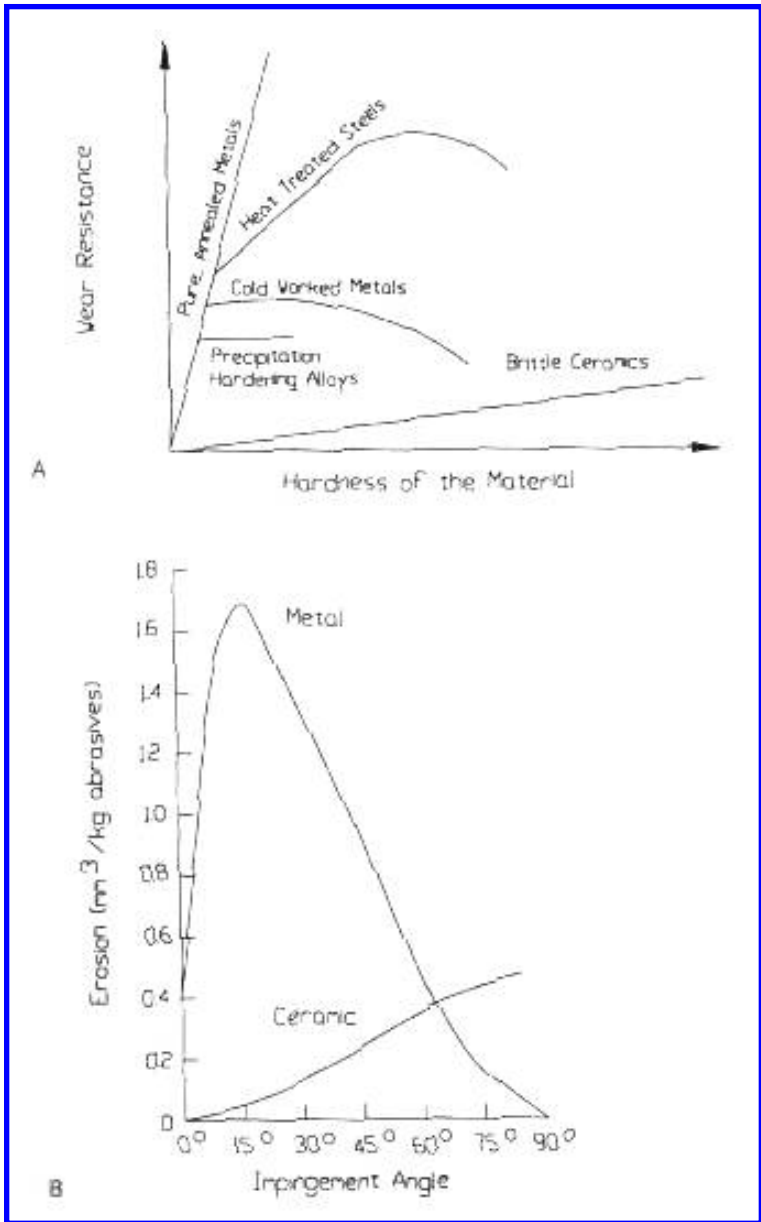


Figure 1.4 Examples of trends in wear resistance under abrasive conditions, “A”, and erosion conditions, “B”. (From Ref. 21.)

surface of these materials should be free of cracks or other types of damage that would intensify brittle behavior (13).

A major factor in the good wear performance of many plastics is the formation of beneficial tribofilms (i.e., transfer and third-body films). This is often the case when the counterface is either a ceramic or a metal. For these materials, the use of a lubricant can result in increased wear as a result of the lubricant's adverse effect on the formation of such films. Consequently, additional lubrication is generally not needed or desirable in these cases. Because of this and the fact that couples involving plastics tend to have lower coefficients of friction than most metal and ceramic couples, many plastics are often referred to as self-lubricating materials. To enhance this self-lubricating behavior, additives, such as PTFE, graphite, or MoS_2 , are often added to a base polymer. These type of additives are often combined with harder additives to form wear resistance grades of polymers. For those wear situations in which a plastic does not form a beneficial tribofilm, wear performance can generally be improved by the use of a lubricant. However, since the surface energy of plastics is generally lower than metals or ceramics, the magnitude of the improvement is frequently not as large as those obtained in tribosystems where a plastic is not used.

Because of the low hardness or strength of plastics, their applications in wear situations are generally confined to those situations in which the bearing or contact pressure is low. To enhance the load carrying capacity of basic polymers, fillers, such as glass and carbon fibers and glass particles, are often added to provide bearing or wear-resistant grades. Without such additives, the useful (i.e., mild) wear range of some thermoplastics are limited to a few kpsi or even lower. With the use of fillers in some of the better wearing thermoplastics, mild wear behavior can be extended up to the range of 10–15 kpsi. The range tends to be slightly higher for thermosets. Plastics, both thermosets and thermoplastics, undergo transitions in wear behavior as a function of temperature. At temperatures near the T_g (i.e., glass transition temperature), many plastics exhibit a sharp transition from mild to severe wear. These transitions can be associated with ambient or bulk temperatures, as well as with surface temperatures resulting from frictional heating. For sliding, this type of transition is often related to a critical sliding velocity above which severe wear occurs. Because of this sensitivity to sliding speed and temperature, heat conduction away from the wearing interface can be a significant factor in the wear performance of systems in which polymers are used. In some cases, a transition from severe to mild wear can be achieved by the use of a lubricant; the lubricant improves the wear by conducting heat away from the contact. Similarly, a plastic might be used at a higher speed when the counterface is a metal than when it is a polymer, because of the better heat conduction provided by the metal. Critical velocities for plastics can be affected by contact pressure.

Skin effects can also be a factor in the tribological behavior of systems involving plastics. With molded plastics, there is frequently a skin layer on the surface of the part. With filled plastics, this layer can have a different composition than the bulk of the plastic. It can be filler or polymer rich, or, if several fillers are involved, the relative concentration of the fillers can be different in the surface layer than the bulk. An example of the effect that these layers can have on wear and friction behavior is shown in Fig. 1.5. In general, there is a transition in wear behavior as this layer is worn off. In applications, which are sensitive to small amounts of wear, the effects associated with these skin layers can often be significant. For small amounts of allowed wear, the life of the skin layer is a greater percentage of the total life, as is demonstrated by the data in Fig. 1.5. In addition to this aspect, skin layers can also influence break-in behavior and have a long-term effect on wear behavior, by affecting tribofilm formation.

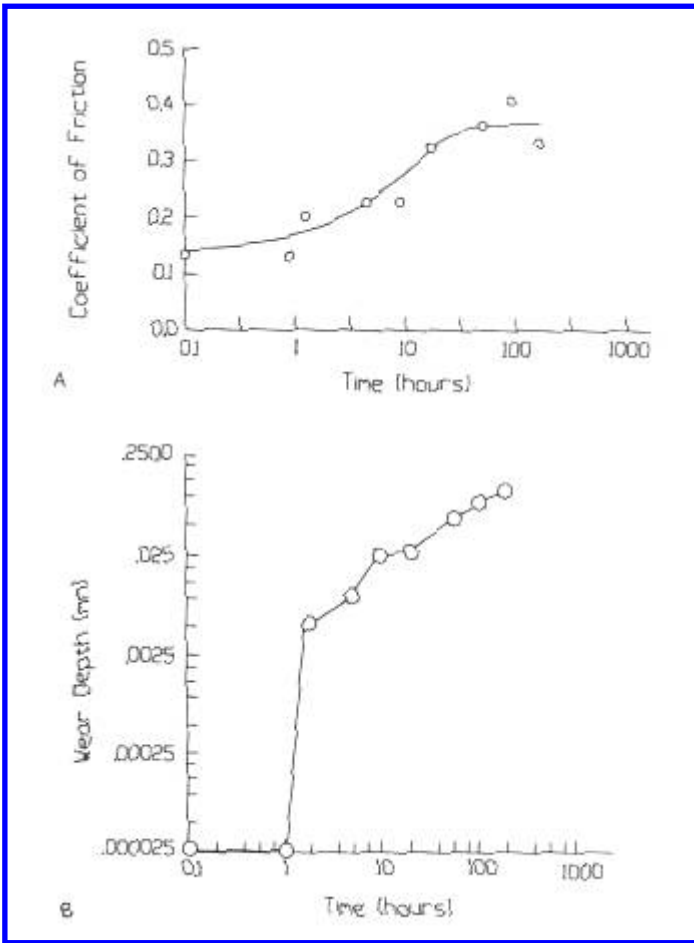


Figure 1.5 The effect of a skin on the friction and wear of molded plastics. (From Ref. 23.)

Since many of the bearing and antiwear grades of plastics utilize glass as a filler material, it is frequently necessary to use a hard metal counterface to avoid abrasion (single-cycle deformation) by exposed glass. Because of the skin effect, the need for this may not be evident during the initial stages of wear. This is because the glass is not exposed and only wear on the plastic is evident during this phase. Once the surface of the plastic is sufficiently worn so that the glass is exposed, wear on the counterface becomes evident. If the counterface is not sufficiently hard, such as with an unhardened steel, the wear of the counterface can predominate. To avoid this effect entirely, it is generally sufficient to make the counterface harder than the glass fibers. In effect this

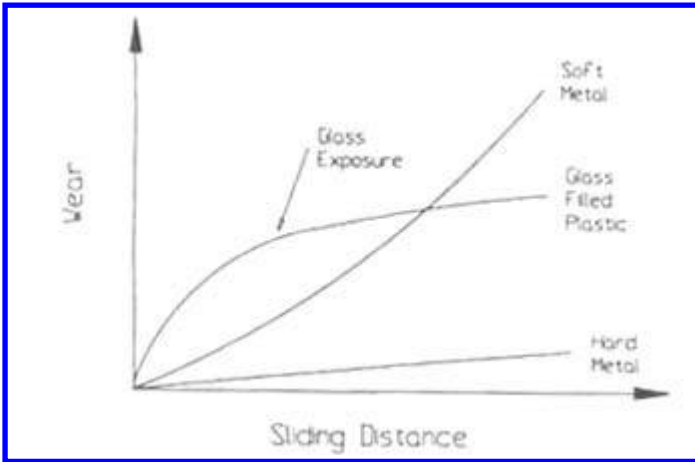


Figure 1.6 Illustration of the effect of glass exposure on the sliding wear of a glass-filled plastic and metal couples.

means that the counterface should have hardness in excess of Rc 60. However, lower hardness surfaces may be adequate in some cases, but generally their hardness should be greater than Rc 50. This scenario is illustrated in Fig. 1.6.

Toughness is the ability of a material to undergo deformation or strain and recover. As a class, elastomers tend to have high toughness, along with a low modulus, as compared to other materials. Typical stress-strain curves of different material classes are shown in Fig. 1.7. It can be illustrated by this figure that elastomers are capable of withstanding strains that are an order of magnitude or more higher than most other materials.

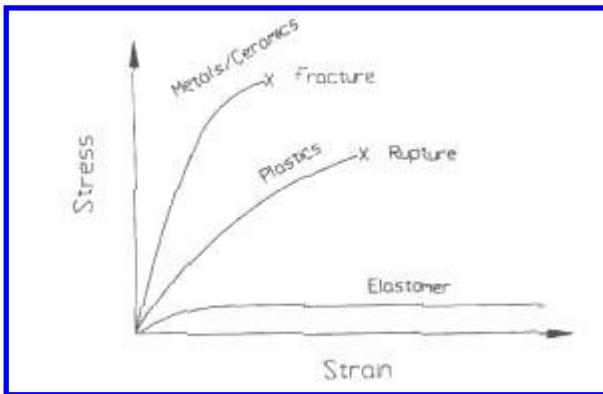


Figure 1.7 Comparative stress—strain behavior of material classes.

This particular characteristic of elastomers is an important aspect in their ability to resist wear. It allows them to out perform harder materials in certain situations, such as erosion by solid particles and three-body abrasion. In these two situations, elastomers tend to trap or hold the particles, rather than have them slide across the surface. In the case of erosion this can result in the particle being held until it rebounds from the surface. In the case of three-body abrasion, this behavior can result in sliding at the counterface, rather than at the elastomer surface. It can also create a situation where the particle rolls or tumbles across the elastomer surface. These situations are illustrated in Fig. 1.8. With all of these mechanisms, a more severe sliding situation is avoided. These mechanisms can occur with other materials and for the same reason (i.e., reduction of sliding at the surface) tend to reduce wear in those cases, as well. This is illustrated by the general tendency for three-body abrasive wear coefficient to be lower than two-body abrasive coefficients. However, the effect is more pronounced with elastomers because of their low modulus and toughness. Toughness is a factor with these mechanisms because there can be a high degree of strain associated with some of these conditions. The high toughness of elastomers enables them to withstand a higher degree of strain without severe damage than is possible with the other classes of materials.

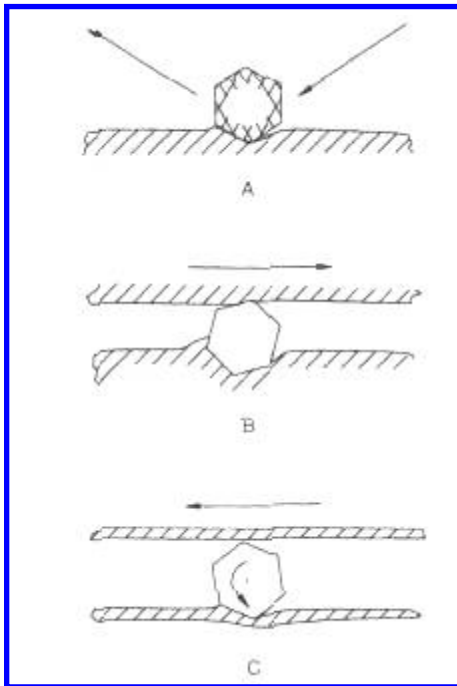


Figure 1.8 Contact situations between abrasive particles and an elastomer (lower) surface. “A”, erosion; “B” and “C”, three-body abrasion.

The toughness of elastomers is also a factor in impact wear. Elastomers are often used in impact situations. In these the elastomer tends to provide a softer impact than stiffer materials. Fig. 1.9 compares the characteristics of an impact with an elastomer and a metal. The peak force is lower and the duration of the pulse is longer with the elastomer. The stress is also lower in the elastomer, but the strain is much higher than with a stiffer material. Because of their high toughness, it is possible for elastomers to exhibit mild wear behavior under the high strain conditions associated with some impact situations. Because of their ability to provide a soft impact, elastomers are frequently used as one member in two-body impact wear situations. The softer impact results in lower stress in the other member of the contact, allowing materials with lower impact wear resistance to be used.

Elastomers tend to have high coefficients of friction. Because of this, another common use of elastomers is in situations involving traction, such as in automobile tires, rollers, and belts. As a result of their high coefficient of friction and low modulus, elastomers in these applications tend to adhere to the counterface and deform rather than slip, which is a more severe wear condition. This action is illustrated in Fig. 1.10. In these situations, high toughness is a desirable property because of the high strains that can result from the shearing and deformation that occurs.

As with plastics, elastomers tend to undergo mild to severe wear transitions as a function of temperature. With elastomers, three contributions to the surface temperature need to be considered. One is the ambient temperature associated with the application. The second is the frictional heating at the surface, which is a function of the sliding that takes place at the surface. The third is hysteretic heating of the elastomer as a result of cyclic strain both on and below the surface. The last can be a factor in sliding, impact, and rolling modes, as well as in the traction mode described above. With increasing temperature, elastomers soften and can degrade chemically (e.g., oxidation). As a result, a transition from mild to severe wear can occur with increasing speeds, higher repetition

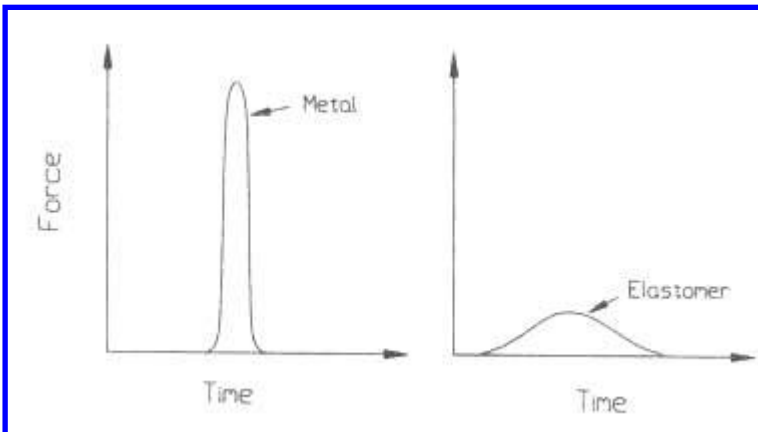


Figure 1.9 Comparative nature of the force pulses resulting from the impact between a metal and a metal, “A”, and an elastomer, “B”.

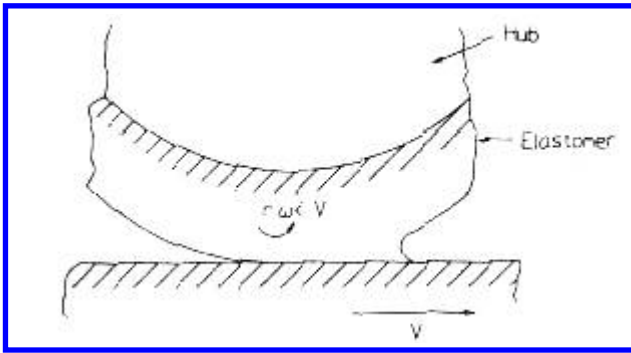


Figure 1.10 Illustration of elastomer deformation as a result of a difference in surface speeds between an elastomer-coated roller and a moving flat surface.

rates, higher ambient temperatures, and any other aspects which tend to increase surface temperatures (4,5). Since the wear behavior of an elastomer is strongly related to their toughness, a mild to severe wear transition can also occur with decreasing temperature. This is because the elastomer toughness decreases and their modulus increases as the temperature is lowered (14). At temperatures near and below their glass transition temperatures, elastomers tend to exhibit less ductile more brittle behavior, which results in more severe wear.

Effects other than temperature can result in a mild-severe wear transition as well. For impact wear, elastomers can exhibit mild to severe wear transitions as a function of severity of the impact, as shown in Fig. 1.11. In this case, the development of an overstressed condition in the elastomer is associated with the transition (4,5). As the severity of the impact increases, the strain and stress levels in the elastomer tend to increase. Because of the nonlinear characteristics of the stress-strain curve of these materials, elastomers will tend to deform over a wide range of impact conditions with relatively little increase in stress. However, because of constraints on the elastomers, an impact condition may be reached where its ability to deform without a significant increase in stress is lost. At this point elastomers tend to exhibit a transition from mild to severe wear. Often the wear takes on a catastrophic characteristic with large cracks and tears. This is illustrated in Fig. 1.12 for a situation where the thickness of the elastomer layer provided a constraint on its ability to deform.

As indicated previously, a significant aspect in the mild wear behavior of elastomers is their ability to reduce or eliminate sliding under conditions that would normally result in sliding with other types of materials. As a result, transitions in wear behavior can be associated with changes in operational parameters, which result in the introduction or elimination of slip on the surface of the elastomer. With increasing slip, wear rate increases and often a transition from mild to severe wear results. For example, the presence of lateral vibrations in impact applications can significantly increase the wear rate of elastomer (4). Also there is a noticeable difference in the wear resistance of elastomers to two- and three-body abrasion. As mentioned earlier, resistance to three-body abrasion is often much higher than what would be expected in terms of their hardness. However, under two-body abrasion their wear resistance is low, reflecting their hardness. An

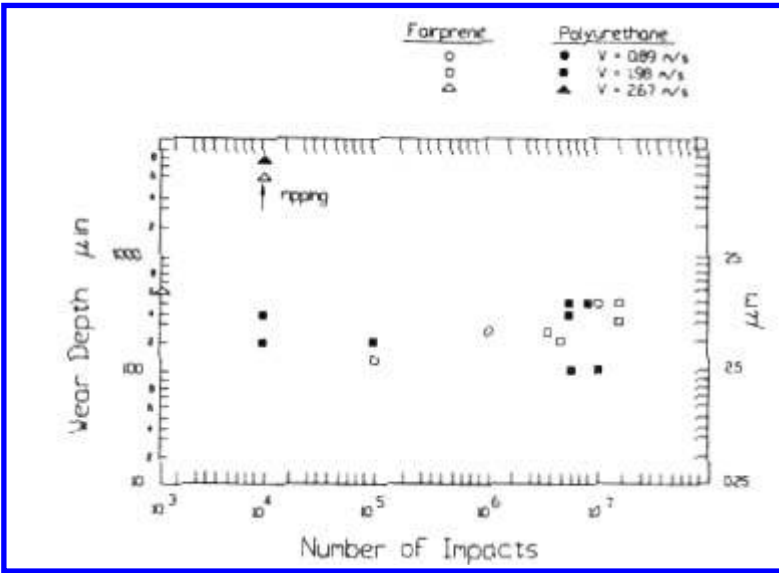


Figure 1.11 Example of a mild-severe wear transition in the case of impact wear of thin elastomer films. (From Ref. 24.)



Figure 1.12 Example of the impact wear of an elastomer, when its ability to deform is constrained. (From Ref. 25, reprinted with permission from ASME.)

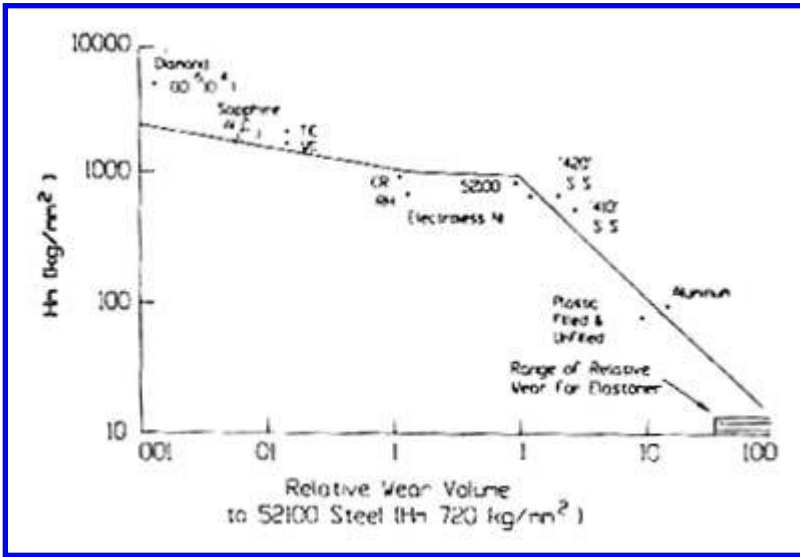


Figure 1.13 Example of the relative wear resistance of elastomers in two-body abrasion. (From Ref. 26.)

example of this is shown in Fig. 1.13, where the resistance of various materials to abrasive wear by paper is compared. The detrimental effect of automobile tire skidding or misalignment is another example of this type of transition.

When materials are used as coatings, their wear performance can be affected by the substrate. In general, the wear behavior of the coating can be considered independent of the substrate only when the coatings are sufficiently thick. As coatings become thinner, the effect of the substrate on wear behavior becomes more significant. Substrate effects generally can be related to differences in the mechanical and thermal properties between the substrate and the coating, and the existence of an interface region between the coating and the substrate. Differences in physical properties can influence wear behavior in a variety of ways. For example, if the substrate is softer than the coating, plastic deformation can occur in the substrate as a result of sub-surface stresses. When this occurs, it tends to result in degraded wear performance of the coating. An example of this type of behavior for a ductile coating is shown in Fig. 1.14. In this case, the plastic deformation of the substrate resulted in increased wear of the Au coating. In the case of brittle coatings, cracks can form in the coating as a result of this deformation, as illustrated in Fig. 1.15. To achieve optimum performance of the coating material, it is generally required that the substrate be sufficiently hard so that plastic deformation does not occur. Another mechanical effect that can occur is associated with the difference in stiffness between the substrate and the coating. A stiffer substrate will tend to increase stresses in the coating during contact, while a more flexible substrate would tend to decrease stresses in the coating (15). Higher stresses generally result in higher wear rates. An extreme example of this type of effect is the over-stressed condition produced in thin elastomer layers on a steel substrate.

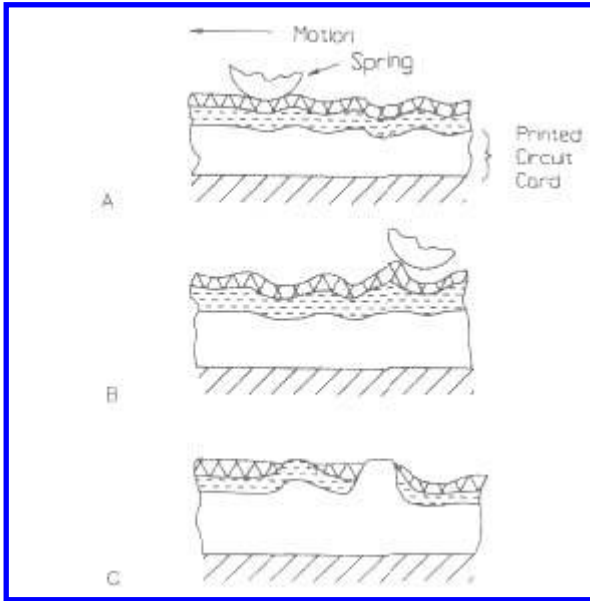


Figure 1.14 Illustration used to describe the wear process observed in electrical contacts, when flow of the substrate occurred. The flow produced local high spots on the surface, "A", which were preferentially worn, "B". The continued flow and preferential wear resulted in the local exposure of the substrate, "C". The nominal metallurgies for which this was found to occur consisted of 3–10 μ in. layer of gold, 3–10 μ in. layer of Ni, 100 μ in. layer of Cu on a glass-epoxy substrate or a 0.5 μ in. of Au, 5 μ in. of Pd-Ni, 0–3 μ in. of Ni, 100 μ in. of Cu on a glass-epoxy substrate. (From Ref. 27.)

The substrate can also effect the wear of the coating because of differences in thermal properties, such as heat conduction and coefficient of thermal expansion. The substrate can influence the temperature of the coating by conducting heat from the contact. This effect can be an important factor with polymer coatings, whose thermal conduction properties are generally poor and whose wear properties degrade with increasing temperature.

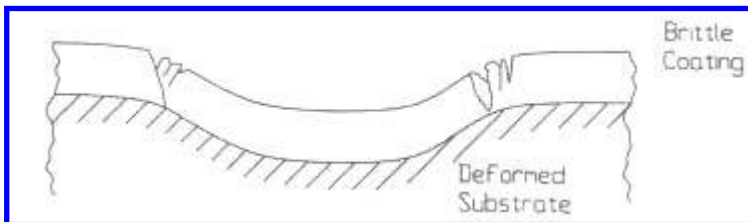


Figure 1.15 The effect of substrate deformation on brittle surface layers.

Since the influence of the substrate on surface temperature would tend to decrease with coating thickness, thin coatings may perform better than thicker coatings in applications where temperature rise is a factor. Thermal stresses developed as a result of differences between the coefficients of thermal expansion of the coating and the substrate can also be a factor in wear performance as well. Depending on the nature of these stresses (e.g., compressive or tensile), and the wear mechanisms involved, these stresses have the potential for improving or degrading wear performance.

In many coating situations, significant stresses can be transmitted to the interface between the coating and the substrate. As a result of the repeated stressing of this region, failure can occur at the interface, resulting in the onset of catastrophic failure of the coating after some amount of usage (e.g., large-scale delamination of the coating). The typical failure mode would involve the formation and propagation of cracks in this interface region. Large difference between the properties of the coating and the substrate will tend to increase the stresses in this region and result in reduced life. On the other hand, increased coating thickness will tend to decrease this effect by reducing the stresses at the interface.

These effects tend to be the typical ones associated with coatings in the thickness range from 0.0002 to 0.020 in. For thicknesses above 0.020 in., these effects tend to be negligible. For thickness below 0.0002 in., other substrate effects may be introduced. In particular, the topography of the substrate can become a factor in the wear performance of the coating. For example, in this region, it is possible for asperity wear to involve both the coating and substrate. This is illustrated in Fig. 1.16 where an abrasive particle is

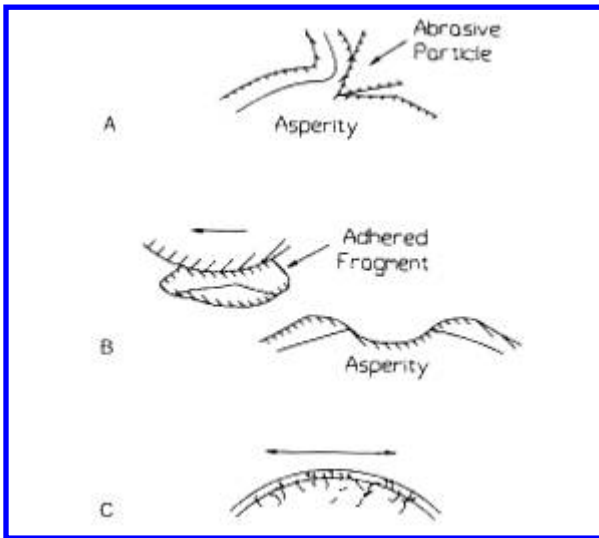


Figure 1.16 Examples of asperity wear situations for thin coatings, where both the material properties of the coating and substrate would be significant: “A”, abrasion; “B”, adhesion; and “C”, surface fatigue.

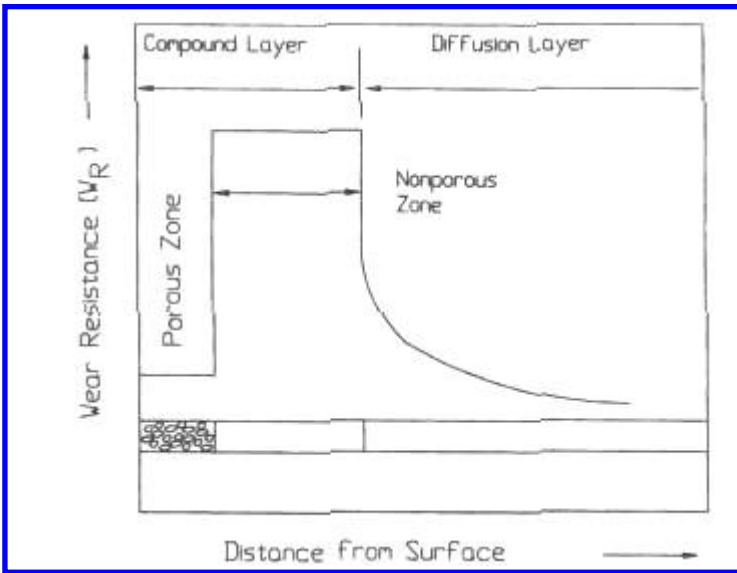


Figure 1.17 Adhesive and abrasive wear resistance for a nitrided layer. (From Ref. 28.)

illustrated cutting through both the coating and the substrate. Fig. 1.16 illustrates this concept for a fatigue and an adhesive wear mechanism as well. In this thickness range, it also becomes more likely that third-body and transfer films involving both the coating and substrate materials are a major factor in the wear performance.

The substrate effects discussed can also be viewed as thickness effects, since their significance is dependent not only on substrate properties but on the thickness of the coating. It should be recognized that these effects are in addition to any processing effects that can be related to thickness and substrate or to intrinsic variations in the properties of the coating as a function of depth. An example of the former is in the case of platings. In this case, properties of the plating can degrade with thicknesses beyond a certain range because of effects of residual stresses or variations in gas evolution during plating. An example of the latter is case hardened layers on steels. The hardness of these layers varies as a function of depth, as shown in Fig. 1.17.

With coatings, it is often necessary to differentiate between the wear rate of a coating and the duration or wear life of a coating. The former is associated with the instantaneous behavior, while the latter is an integrated behavior of the coating and is frequently more important in practical applications. For example, a thicker coating of a higher wearing material may provide a longer service life than a thin coating of a low wear rate material, simply because there is more material to be worn away. This is illustrated in Fig. 1.18. Another factor that can be involved is variation in wear rate of the coating. Because of the effects that thickness can have on wear behavior, wear rate is often a function of wear depth, as illustrated in Fig. 1.19. Since the purpose of the coating is to enhance wear

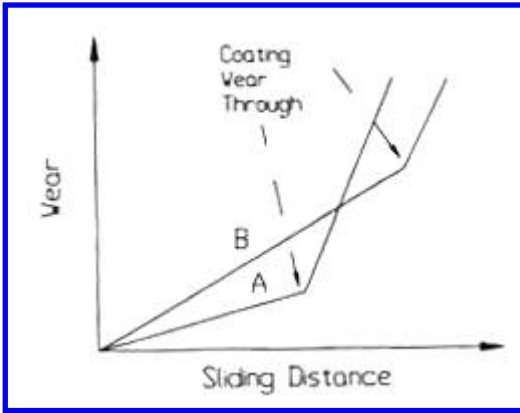


Figure 1.18 Illustration of the difference between wear rate of a coating and wear life of coating.

behavior, initial performance improves with thickness. After some point, however, wear performance tends to become independent of thickness but an optimum condition might exist because of competing effects. For example, as thickness increases, substrate effects tend to decrease and the intrinsic wear performance of the coating material is approached. However, if the wear performance of the coating material is influenced by temperature, its wear performance would degrade as the thickness is increased because of poorer heat conduction. Changes in residual stresses with thickness could also result in an optimum as well. [Figure 1.20](#) illustrates the equivalent behavior in terms of coating wear life. The variations of wear rate and wear life with thickness depend on the materials involved and can depend on the nature of the wear situations. It should not be assumed that the same coating thickness is equally effective or beneficial in all wear situations or that the effect of thickness is the same for all coatings.

Coatings in wear applications are used for two general purposes. One is to provide a surface layer with better wear resistance than the substrate. In this case, a thickness greater

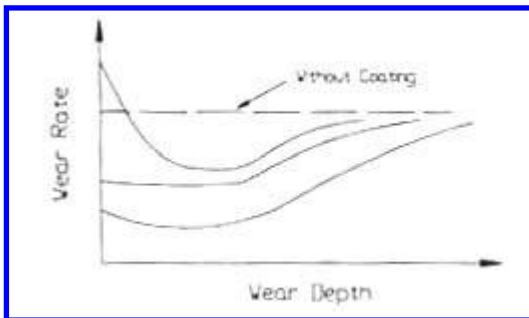


Figure 1.19 Trends in wear rates of coatings as a function of wear depth.

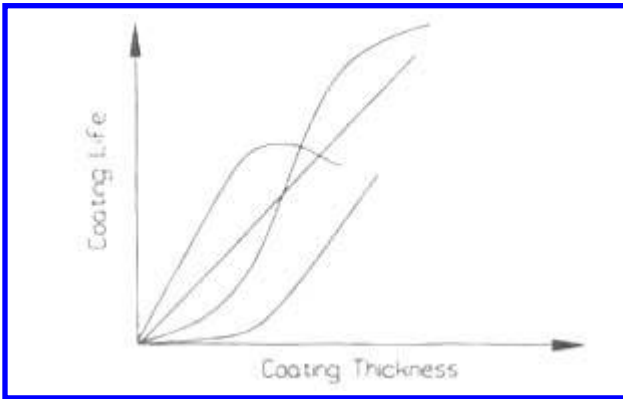


Figure 1.20 Trends in coating life as a function of coating thickness.

than 0.0002 in. is generally required to provide significant improvement. For many of the conventional platings, a minimum of 0.0005–0.001 in. is needed. The second use is to provide lubrication to the substrate surface. In this case, tribofilm formation is often a major factor and thinner coatings are preferred, since these materials frequently have high wear rates. Thicknesses of less than 0.0002 in. are typical in these situations.

With coatings, transitions from mild to severe wear can occur as a result of the properties of the coating, coating thickness, substrate materials, and the parameters of the wear situation. With polymer coatings, a transition as a function of sliding speed is likely. The introduction of impact into a wear situation might result in rapid degradation of a brittle coating. Too thin a layer of an elastomer can result in an over-stressed condition in impact situations. A mild to severe transition can also occur as a function of load, as a result of the occurrence of plastic deformation in the substrate. In addition, these types of transitions in wear behavior tribosystems, which utilize coatings, frequently exhibit mild to severe wear transition as a function of time or exposure. This can occur as the result of coating wear-through, the effect of changing wear modes as the thickness changes with wear, or when substrate failure occurs as a result of a fatigue mechanism.

There are various types of composite materials that are used or can be used in wear applications. Multi-phase materials, such as those shown in Fig. 1.21, are one type of a composite; a second type would be where particles are held together by a binder (Fig. 1.22) and another type is where fillers are added to a material (Fig. 1.23). As was briefly mentioned in the discussion of plastics, there are additional elements associated with the wear of these types of materials. One element is the intrinsic wear properties of the different components or materials that make up the composite. The properties of the interfaces between the materials are another. A third is the size, shape, and relative amounts of the various components. Some preferential wear of the soft component can often be observed on worn surfaces of composite materials, as illustrated by the diagram in Fig. 1.24. The relative significance and the optimum properties for each of the components can vary with the wear situation. Because of the sensitivity to the wear situation, wear resistant composites are usually developed for specific wear situations and good



Figure 1.21 Microstructure of a multiphase material. (From Ref. 29, reprinted with permission from ASM International.)

wear performance of the composite may be limited to that type of wear situation. This can be illustrated in the case of a diamond composite as shown in [Fig. 1.22](#).

The diamond composite in [Fig. 1.22](#) performs well in abrasive wear situations where the wear is controlled by the properties of the diamond and not by the properties of the matrix (16). Loading and the size of the abrasive particles can alter this condition. For light loads, stresses in the binder are low; at higher loads, significant stress can occur in the binder or matrix, and, as a result, fatigue cracks could develop and propagate in the binder. This would result in the diamond particle being lost from the surface prematurely. Such a stress condition might occur when there is a large abrasive particle or only a few large particles at the interface supporting a significant portion of the load. Consequently, in applications where the frequency of encounter with large particles is low, this coating would have good wear resistance. In situations where such encounters are frequent, the wear resistance would be poorer as a result of failure of the binder. Similarly, this coating could exhibit very poor wear resistance in a solid particle erosion situation, where the particles are small enough to erode the binder from around the particle. This difference is illustrated in [Fig. 1.25](#).

Another illustration of this sensitivity to the wear situation is the use of PTFE as a filler in coatings, sintered materials, and plastics. PTFE is a major factor in the formation of transfer films under sliding conditions. The amount of PTFE used as a filler is optimized for such applications and can result in a significant improvement in performance. However, in rolling or in impact situations, the PTFE would not provide any advantage over the base material. Furthermore, it could also result in poorer performance, because of effect of the presence of the filler on the strength of the composite.

This same aspect applies to the use of special wear or tribomaterials, which may not be composites. Babbitt, DU, and oil impregnated sintered materials are examples of these other types of tribomaterials. These types of materials generally have good wear performance in only a limited number of wear situations. Certain conditions for optimum

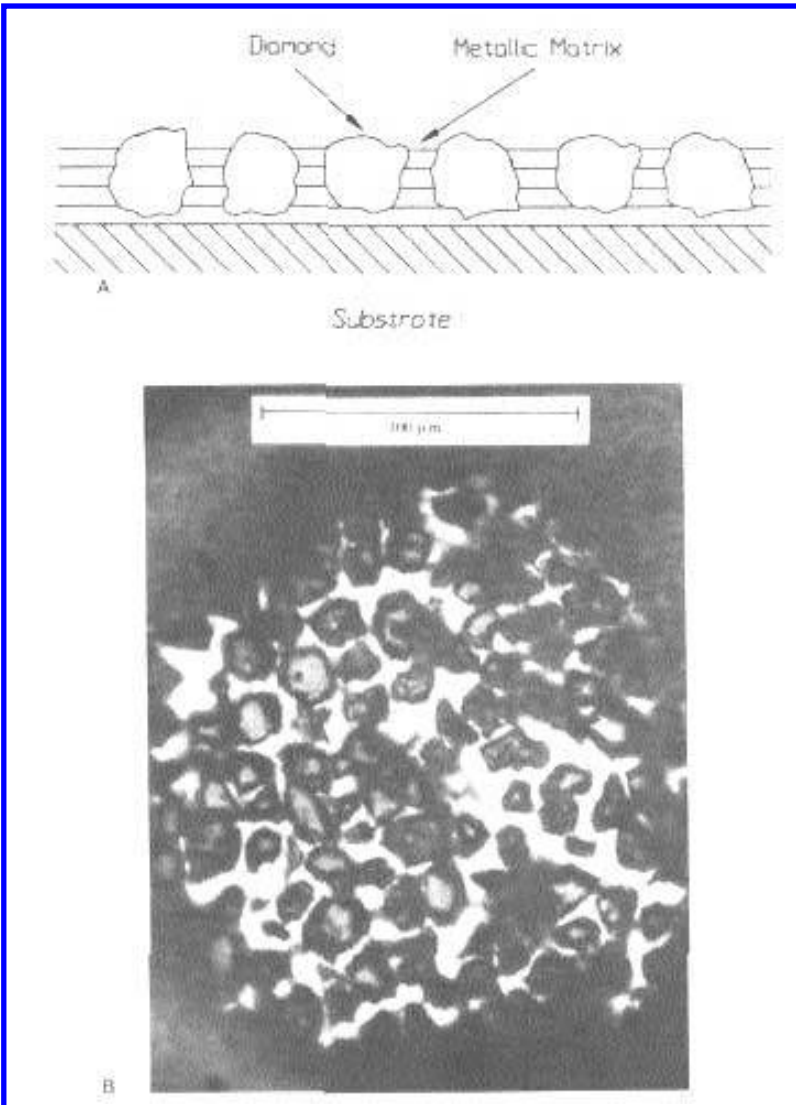


Figure 1.22 Single-layer diamond composite plating. “A” illustrates a cross-section of the plating; “B” is a micrograph of a worn surface. (From Ref. 16.)

performance are required, such as pressures, speeds, and temperatures, and there may be limits to the forms or shapes for which these materials these materials can be used. As a result, it is generally necessary to design around these requirements to insure good performance when these materials are used.

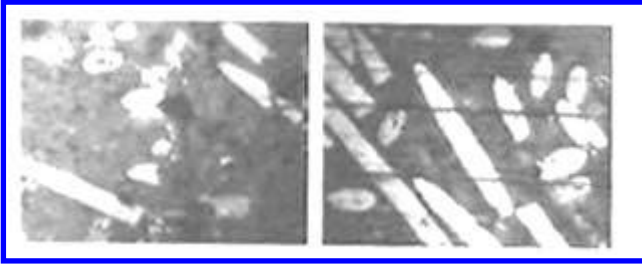


Figure 1.23 Micrographs of wear surfaces of filled plastics, showing the fillers and the polymer matrix. (From Ref. 30.)

In most applications, metal-to-metal contacts, involving sliding and rolling, require lubrication in order to achieve the desired wear performance. In these types of situations, the use of any lubricant typically results in a significant decrease in wear (i.e., an order of magnitude or more). By optimizing the lubricant for the materials and conditions, it is often possible to achieve significantly greater improvements (e.g., up to several orders of magnitude reduction in wear). When lubricants are used to reduce wear, the ability of the lubricant to provide continuous protection to the surface is an important element, as is the supply of the lubricant to the surface. High shear rates and elevated temperatures can result in degradation of the lubricant. Since lubricants can evaporate and spread along surfaces, the lubricant can disappear from the wearing interface as well. When the lubricant degrades or disappears from the surfaces, a transition from mild to severe wear typically occurs. Consequently, an important element associated with wear design is to select a lubricant and lubricant supply system that will maintain lubrication at the wearing

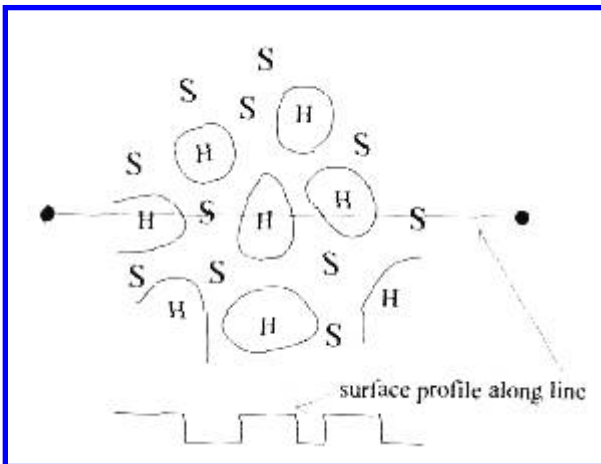


Figure 1.24 Illustration of the relief that can occur on worn surfaces when there are hard and soft regions across the surface, such as those associated with hard and soft phases in a composite material or with a hard filler in a soft matrix.

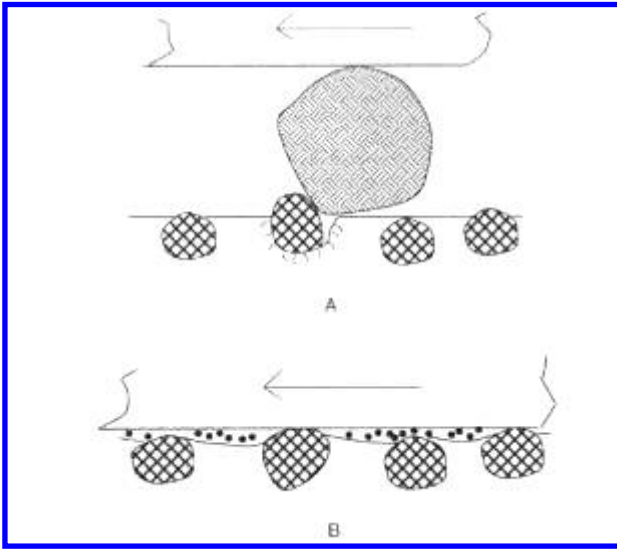


Figure 1.25 Illustration of different modes of wear of a filled material. “A” shows large particles causing matrix failure; “B” shows gradual wear of the filler and matrix resulting from smaller particles.

interface. In sliding and rolling wear, problems with these elements can often be a major factor and should be considered in any failure analysis of lubricated tribosystems.

The three types of lubricants commonly used (i.e., oils, greases, and solid lubricants) have characteristic differences in terms of their ability to provide continuous protection. With oil, evaporation and migration are major factors in depletion from the contact region. When there is sufficient quantity of oil available, displacement from the contact region is usually not a concern because oils tend to rapidly reform a continuous film. Solid lubricants do not have this ability and depletion and displacement from the contact region is a concern. On the other hand, evaporation and migration are not factors with solid lubricants. Greases are composed of a solid and a liquid phase and are able to provide lubrication both as a composite and as a reservoir for the liquid phase. As a composite, their behavior is similar to a solid lubricant and displacement from the contact region is a concern. As a composite they can also act as a very viscous fluid and provide fluid lubrication. Also with this mode the loss of the liquid phase as a result of separation and evaporation is an additional concern. This is because the ability of the grease as a composite to lubricate is generally strongly dependent on the oil phase. As a reservoir, it is the liquid phase or the oil of the grease that provides lubrication. In this mode, self-healing is not a concern, but evaporation and migration of the liquid phase are factors in the ability to provide long term or continuous protection.

Table 1.2 presents an overview of typical applications for various material types. Further information on material wear behavior can be found in Refs. (17–19,32).

Table 1.2 Typical Wear Applications for Materials

Material	Sliding			Rolling			Three-Body Impact	
	Unlubed	Lubed	Abrasion	Unlubed	Lubed	Abrasion	Impact	Abrasion
Structural alloys	X		X			X		X
Surface treatments	X	X	X			X	X	X
Hard surfacing	X	X	X					
Soft coatings	X	X	X	X	X	X	X	X
Alloy steels	X	X	X	X	X	X	X	X
Tool steels	X	X	X	X	X	X	X	X
Stainless steels			X	X	X			X
Precipitation hardened			X	X	X			X
Martensitic			X	X	X			X
Cast irons			X	X	X			X
Graphitic	X	X	X	X	X	X		X
White	X	X	X	X	X	X		X
High temperature alloys	X						X	X
Refractory alloys								
Super-alloys				X				
Copper alloys								
Bronze			X				X	
Beryllium copper			X					
Babbitts			X					
Carbides	X		X					X
Ceramics	X		X					X
Polymers	X							
Thermosets	X							
Thermoplastics	X	X		X	X		X	X
Elastomers	X	X		X	X		X	X
Carbons	X							
Lubricating composites	X							

(Continued)

Table 2 (Continued)

	Fluid Erosion	Cavitation	Drop Erosion	Particle Erosion
Structural alloys				
Surface treatments				
Hard surfacing			X	X
Soft coatings				
Alloy steels				
Tool steels		X		X
Stainless steels				
Precipitation hardened				
Martensitic	X			
Cast irons				
Graphitic				
White				
High temperature alloys				
Refractory alloys				
Super-alloys		X	X	X
Copper alloys				
Bronze			X	
Beryllium copper				
Babbitts				
Carbides			X	X
Ceramics			X	X
Polymers	X			
Thermosets				
Thermoplastics			X	
Elastomers			X	
Carbons		X		X
Lubricating Composites				

Source: adapted from Ref. 20.

REFERENCES

1. J Anderson. Wear of commercially available plastic materials. *Trib Int* 15(5):255–264, 1982.
2. G Nathan, W Jones. The empirical relationship between abrasive wear and the applied conditions. *Wear* 9:300–303, 1966.
3. R Richardson. The wear of metals by relatively soft abrasives. *Wear* 11:245–275, 1968.
4. R Bayer, P Engel, E Sacher. Impact wear phenomena in thin polymer films. *Wear* 32:181–194, 1975.
5. P Engel. *Impact Wear of Materials*. New York: Elsevier, 1978, pp 282–289.
6. Standard Guide for Determining Synergism Between Wear and Corrosion, ASTM International G119.
7. BW Madsen. Measurement of wear and corrosion rates using a novel slurry wear test. *Mater Perform* 26(1):21–28, 1987.
8. BW Madsen. Measurement of erosion-corrosion synergism with a slurry wear test apparatus. *Wear* 123(2): 127–142, 1988.
9. C Yust. Low speed sliding damage in TiB₂-Ni composites. *Proc Intl Conf Wear Mater ASME* 167–173, 1983.
10. J Larsen-Basse. Binder extrusion in sliding wear of WC-Co alloys. *Proc Intl Conf Wear Mater ASME* 39–44, 1985.
11. G Tennenhouse, F Runkle. Pin-on-disk wear tests for evaluating ceramic cutting tool materials. 43–57; West Conshohoken, PA. In: C Yust, R Bayer, eds. *Selection and Use of Wear Tests for Ceramics*. STP 1010: ASTM, 1988.
12. J Hines, R Bradt, J Biggers. Delta alumina formation during the abrasive wear of a polycrystalline alumina. *Proc Intl Conf Wear Mater. ASME*, 1979, pp 540–550.
13. R Gates, J Yellets, D Deckman, S Hsu. The development of a wear test methodology. In: C Yust, R Bayer, eds., *Selection and Use of Wear Tests for Ceramics*. STP 1010, West Conshohocken, PA ASTM, 1988, pp 1–23.
14. B Bhushan, B Gupta. *Handbook of Tribology*. New York: McGraw-Hill, 1991.
15. W Chen, P Engel. Impact & contact stress analysis in multilayer media. *Int J Solid Struct* 8:1257–1281, 1972.
16. D Roshon. Electroplated diamond composite coating for abrasive wear resistance. *IBM J R&D* 22(6):681–686, 1978.
17. P Blau. *Friction and Wear Transitions of Materials*. Park Ridge, NJ: Noyes Publications, 1989.
18. M Peterson, W Winer, eds. *Wear control handbook*. New York, NY: ASME, 1980.
19. P Blau. ed. *Lubrication, and wear technology*, ASM Handbook. Vol. 18. Metal Parks, OH: ASM Intl, 1992.
20. W Glaeser. Wear resistant materials. In: M Peterson, W Winer, eds. *Wear Control Handbook*. New York, NY: ASME, 1980, pp 313–326.
21. W Glaeser. Light Microscopy. In: P Blau, ed. *Lubrication, and Wear Technology*, ASM Handbook. 18. Metals Park, OH: ASM Intl., 1972, pp 370–375.
22. E Rabinowicz. Wear Coefficients–Metals. In: M Peterson, W Winer, eds. *Wear Control Handbook*. NY: ASME, 1982, pp 475–506.
23. R Bayer, N Payne. Wear Evaluation of Molded Plastics; *Lub Eng*, 41(5):290–293 May: 1985.
24. P Engel. *Impact wear of materials*, Tribology Series 2. New York: Elsevier Science Publishing Co., 1978.
25. P Engel. Experimental and analytical approaches in impact wear. *Proc Int Conf Wear Mater. ASME*, 1977, pp 401–412.
26. R Bayer. The influence of hardness on the resistance to wear by paper. *Wear* 84:345–351, 1983.
27. R Bayer, E Usue, J Turner. A motion-induced sub-surface deformation wear mechanism. *Wear* 154:193–204, 1992.
28. F Hoffmann, P Mays. Nitriding and nitrocarburizing. In: P Blau, ed. *Lubrication, and Wear Technology*, ASM Handbook. 18. Metals Park, OH: ASM Intl., 1992, pp 878–883.

29. K Cooper. Laser surface processing. In: P Blau, ed. *Lubrication, and Wear Technology*, ASM Handbook. 18. ASM Intl Metals Park, OH, 1992, pp 861–872.
30. R Bayer, J Sirico. Influence of ink jet printing inks on wear. *IBM JR Dev* 22(1) 90–93, 1978.
31. B Bhushan, B Gupta. *Handbook of Tribology*. New York: McGraw-Hill, 1991, pp 4.2–4.41.
32. B Bhushan, B Gupta. *Handbook of Tribology*. New York: McGraw-Hill, 1991.

2

Engineering Models for Wear

2.1. INTRODUCTION

A single, universal model for wear does not exist and is probably not possible because of the many parameters, both fundamental and operational, that are involved (1). One aspect of this complex nature of wear is the occurrence of transitions in wear behavior that can be associated with operational parameters of a tribosystem. Changes in loads, speeds, and geometry can result in changes in wear mechanisms, as has been described in Part A of MWFT2E and elsewhere (2). While this is the case, it is also true that most systems exhibit regions of stable wear behavior on either side of such transitions. For many of these stable regions, there are empirical expressions relating wear to the primary design parameters, such as load and geometry, and to usage (or exposure). These expressions provide the basis for what may be termed engineering models for wear and can be used in the development of design approaches to wear.

There are two general types of empirical relationships, which can be used for design. One type relates the amount of usage, required to produce a certain level of wear, to operating parameters. Assuming the amount of wear associated with these relationships define life, this type of relationship provides a direct relationship between life and operating parameters. However, these equations do not provide a relationship between wear and operating parameters. Wear is not explicitly included in these relationships. Such relationships exist for sliding, rolling, and impact and other situations as well. The second type of empirical relationship basically relates wear, directly or indirectly through wear rate, to operating parameters and usage. Relationships between wear and operating parameters can be obtained from wear rate equations by integration. This type does not directly provide a relationship between operating parameters and life. Such wear life relationships can be developed from this second type of empirical relationships by defining a certain amount of wear as an end-of-life condition. A summary of both types of these empirical relationships for various wear situations is presented in [Table 2.1](#). It can be seen that the forms of the relationships relating usage with operating parameters are quite similar. However, there is considerable difference in the forms relating wear, operating parameters, and usage. The basis of these relationships and the associated models, as well as some more specific models for particular situations, will be discussed in detail further in this section. However, before this is done, it is necessary to consider general aspects of these models and relationships.

While the form of these equations have rather broad applicability, the coefficients and, in some cases, the exponents may vary with the tribosystem. In general, the coefficients are at least material-dependent but they can also depend on other aspects of the tribosystem, such as speed, environment, and lubrication, which are not specifically

Table 2.1 Forms of Engineering Wear Equations

Sliding	$W = K L S, W = K L(S - S_0) + S_0, W = k L^{m \geq 1} S^{n \leq 1}$ $W = K L^{m > 1}, h = K P V$ $dW'(E, S') = W'_E dE + W'_{S'} dS'$ $\sigma_1^q S_1^r = \sigma_2^q S_2^r$ <p> W, wear; W', normalized wear; W, wear rate $W'_{E, S'}$, partial derivatives h, depth wear rate S, sliding distance S' normalized sliding distance L, load; σ, stress; E, energy; V, velocity K, wear coefficients </p>
Rolling	$W = K L^{m > 1} N$ $\sigma_1^{m > 1} N_1 = \sigma_2^{m > 1} N_2, L_1^{m > 1} N_1 = L_2^{m > 1} N_2$ $\log K = \frac{B - \log N}{A}$ <p> W, wear N, number of revolutions L, load; σ, stress K, A, B wear coefficients </p>
Impact	$W = K V^m N$ $\sigma_1^{m > 1} N_1 = \sigma_2^{m > 1} N_2$ $dW(E, N) = W'_E dE + W'_N dN$ <p> W, wear; $W'_{E, N}$, partial derivatives V, impact velocity, σ, stress N, number of impacts K, wear coefficient </p>
Erosion	$e(t) = K(t) A$ (angle) I (intensity) general $e(t) = K(t) \sin^n \alpha M v^n$ liquid drops $e(t) = [K(t)_d v^n \cos^n \alpha \sin(\pi \alpha / \beta) + K(t)_b v^m \sin^m \alpha] M$ particles $e(t) = K(t) \delta^n$ vibration-induced cavitation $e(t) = K(t) v_j^n$ jet-induced cavitation <p> e, erosion rate M, erodent rate; v, velocity; α, angle of impact δ, amplitude of vibration; v_j, velocity of jet $K(t), \beta$, wear coefficients </p>
Ball and roller bearings	$N_L = C \pi_1 F_1 L^{-n}$ <p> N_L, bearing life F_1, empirical factors related to application and bearing design aspects L, load C, reference coefficient </p>
Journal bearings	$W = K L$ $h = K (L S)^{2/3}$ $h = K L^{1 < n < 6} S^{m \leq 67}$ <p> W, wear rate; h, depth of bearing wear L, load; S, sliding distance K, wear coefficient </p>

(continued)

Table 2.1 (Continued)

Tool wear

$$\begin{aligned}
 V_1 T_1^\alpha &= V_2 T_2^\alpha \\
 V_1^\beta F_1^\gamma D_1^\delta &= V_2^\beta F_2^\gamma D_2^\delta \\
 \ln T &= c_{10} + c_{11} \ln V + c_{12} \ln F + c_{13} \ln D \\
 &\quad + c_{14} (\ln V)^2 + c_{22} (\ln F)^2 + c_{33} (\ln D)^2 \\
 &\quad + c_{12} \ln V \ln F + c_{13} \ln V \ln D + c_{23} \ln F \ln D
 \end{aligned}$$

 T , tool life V , cutting speed; F , feed rate; D , geometry parameter c_n , experimental coefficient

addressed by the equations. The exponents can also exhibit similar dependencies. In sliding systems, for example, different exponents have been found with different material systems (3–6). In effect, the coefficients and exponents of these relationships are experimental parameters, which can vary with the tribosystem. Consequently, design approaches utilizing these models cannot be completely analytical or theoretical. They must also involve a complimentary experimental element, either explicitly (from testing) or implicitly (from existing data).

These engineering models are primarily based on experimental observations and correlations. However, the general form of the relationships and, in some cases, the range of the exponents involved can be developed on the basis of physical and theoretical models. While this is the case, the relationships between these engineering models and specific wear mechanisms are weak. There are several reasons for this. One is the complex nature of most wear scars themselves; others are associated with various aspects of the modeling approaches. Typically, evidence for the occurrence of several wear mechanisms and associated phenomena can be found in most worn surfaces. Consequently, it is difficult to relate these engineering models to any one specific mechanism, solely on the basis of experimental observations.

The theoretical models, which support the general nature of these relationships, tend to be either very conceptual or very specific. Both characteristics tend to reduce their effectiveness in practical applications. With the conceptual models, the common features of different wear mechanisms or different combinations of wear mechanisms tend to be emphasized, rather than the features, which are often important for providing specific values or relationships for coefficients and exponents. Because of this such models tend to be equivalent to empirical models. On the other hand, specific theoretical models for unique mechanisms tend to use simplifying assumptions regarding the tribosystem. This tends to compromise their extension to practical systems and to limit their range of applicability. Another reason for the weak correlation between engineering models and specific mechanisms is the fact that it is possible to develop the same basic relationship between wear and primary design parameters by considering significantly different physical mechanisms. In the case of sliding wear, for example, it is possible to predict a linear dependency between wear volume and load for most mechanisms depending on assumptions used (7–16).

Because of the general weakness of the correlation between specific wear mechanisms and the engineering models, there is an additional benefit obtained from including an experimental element in a design approach. The combining of experimental and analytical elements in an overall design approach helps to remove the ambiguities associated with the more general relationships and concepts. This often enables the development

of specific correlation between wear mechanism(s) and engineering models for the specific application, such as determining which of several models is the more applicable or valid or what is the dominant mechanism.

As was initially indicated, these empirical wear relationships and associated engineering models apply to stable wear regimes. In addition to this, there are two other conditions associated with these. The relationships generally assume that there is wear on only one member. In two-body wear situations, this means that these relationships presume that there is no wear on the counterface or changes to the counterface as a result of wear. The relationships also are for constant values of the parameters identified in the relationship. These conditions are often not representative of engineering situations. In many engineering situations, both surfaces in two-body tribosystems simultaneously wear or model parameters may not be constant or singled-valued. For example, the load might vary as a function of time in a sliding situation or there can be a distribution of particle sizes and velocities in an erosion situation. While this is the case, it is still possible to utilize these empirical relationships in design approaches. There are several ways of accounting for the simultaneous wear of two surfaces, which are dependent on the engineering model used and the overall design approach that is developed. These approaches to two-body wear will be discussed in the treatment of the individual models, design approaches, and examples. A common approach to treating situations in which there is a distribution associated with a model parameter is to determine an effective or equivalent value for that parameter. An equivalent value is typically determined by assuming that the effective wear, wear rate, or life is a sum of weighted individual amounts of wear, wear rates, or lives, associated with the different values of the parameters. For example, if the wear rate is proportional to P^n , where P is the load, then the effective value of P to be used in the equation for wear rate, P_e , would be

$$P_e = \left[\sum_i x_i P_i^n \right]^{1/n} \quad (2.1)$$

for discrete loads or

$$P_e = \left[\int_0^1 \mathbf{P}(\alpha)^n d\alpha \right]^{1/n} \quad (2.2)$$

for a continuous load distribution, α_i is the fraction of time under load P_i for discrete loads and $\mathbf{P}(\alpha)$ is a distribution function for P for a continuous load distribution. This approach, which essentially is an extension of Miner's rule to wear applications, is illustrated in several of the case studies (Secs. 5.2 and 5.7–5.8). It is also used in the method for determining rolling bearing life, when the load is not constant (17).

The engineering models for sliding, rolling, and impact conditions apply to both unlubricated and lubricated conditions. Since these models are for stable wear behavior, it is implied for lubricated situations that the state of the lubricant and the lubrication (e.g., film thickness and condition of the lubricant are constant). The effect of the lubricant is generally reflected in the values of the wear coefficients of the model, as are the other material and environmental elements.

The purpose of these engineering models is to provide relationships between wear, major design parameters, and usage, so that design relationships and approaches can be developed to control wear and analyze wear situations. As will be illustrated later in this book, sometimes the relationships of these models can be directly applied to design

situations. In others, they may need to be modified, extended, or combined to develop a design model or approach. In addition, it may also be necessary to develop or identify additional relationships for less common wear mechanisms.

2.2. WEAR AND WEAR RATE RELATIONSHIPS FOR SLIDING WEAR

One of the earliest and most frequently cited relationship for sliding wear is one that is associated with Archard. Based on experimental data in the early 1950s, it was concluded that for sliding between two surfaces, stable wear behavior can be described by the following:

$$V = K \times P \times S \quad (2.3)$$

or

$$\mathbf{V} = K \times P \quad (2.4)$$

where V is the volume of wear; P , the normal load; S , the sliding distance; \mathbf{V} , wear rate; and K is an empirical wear factor or coefficient (13,18,19). Using adhesive wear concepts, an explanation for these simple relationships was proposed at that time. Since then, however, additional data have showed that while these relationships describe the wear of some tribosystems, they do not necessarily describe the wear behavior of all systems (3,20–24). In addition, a variety of explanations for Eqs. (2.3) and (2.4) have been proposed, including some which do not involve adhesive wear (7–11,25).

One modification or extension of this simple model is associated with need to account for break-in behavior that is exhibited by some systems (19,26,27). One interpretation is that for those systems exhibiting such behavior, the rate equation is valid after break-in. In this case, the relationship for total wear and sliding can be modified in the following manner to account for break-in:

$$V = K \times P \times (S - S_b) + V_b \quad (2.5)$$

where V_b is the volume of wear associated with break-in and S_b is the amount of sliding associated with the break-in period. Obviously, when $S > S_b$ and $V_b \ll V$, Eq. (2.5) reduces to the original relationship for wear, Eq. (2.3). In this approach initial nonlinear behavior is viewed as a non-stable wear regime rather than as part of a continuous process.

In addition to break-in behavior, several investigators have reported that the relationship between V or \mathbf{V} and load is not necessarily linear (3,20–22,24,28–30). In most cases, the expression for \mathbf{V} is then modified to the following:

$$\mathbf{V} = K \times P^m \quad (2.6)$$

where m can be significantly larger than 1. Most explanations that have been proposed to explain such a nonlinear dependency on load, involve repeated-cycle deformation mechanisms, typically a fatigue, fatigue-like, or stress dependent wear mechanisms, rather than an adhesive-type mechanism. As was discussed in Part A of MWFT2E, theoretical models for these mechanisms indicate that m can range from 1 to much larger values. While typical values may be in the range of 2–3, values over 5 have also been reported. Since similar models for other types of mechanisms (e.g., adhesive, oxidation, single-cycle deformation, or abrasion) result in values close to 1, large empirical values for m indicate that fatigue or some other stress-dependent wear mechanism is likely to be the predominant one for that tribosystem. On the other hand, since small values of m can also

be associated with fatigue or stress-dependent mechanisms, the observation of small empirical values cannot be used to eliminate the possibility of these types of mechanisms.

In tribosystems where the apparent contact area changes with wear, such as a sphere on a flat, it has been observed that V is not necessarily constant, even under conditions of stable wear behavior (3). Examples of this type of wear behavior are shown in Fig. 2.1. The shape of these curves is similar and suggests a relationship of the following form for V :

$$V = K \times P^m \times S^n \quad (2.7)$$

where $n \leq 1$, which includes the situation where a linear relationship is observed. In this case,

$$V = \frac{K \times P^{1/n} \times S^{n-1}}{n} \quad (2.8)$$

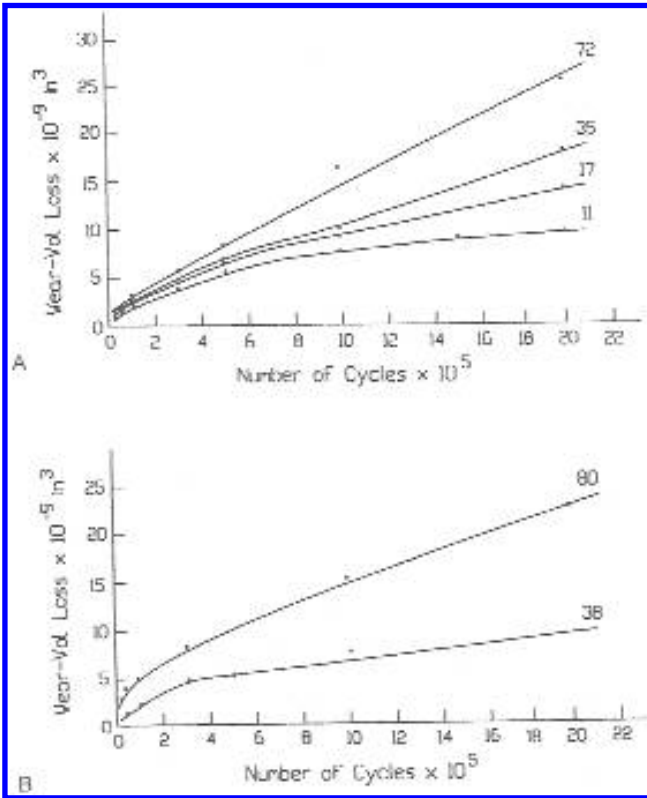


Figure 2.1 Wear curves for slider wear in reciprocating ball-plane tests. “A” is for unlubricated sliding of a soft steel against a hard steel flat; “B” is for a hard steel slider. The CLA roughness values ($\mu\text{in.}$) of the flat specimen are shown on the graphs. (From Ref. 76, 148.)

or

$$V = K' \times \frac{P^m}{S^{1-n}} \quad (2.9)$$

where $1-n \geq 0$. The occurrence of values of $n < 1$ is generally explained in terms of fatigue wear mechanisms or similar repeated-cycle deformation mechanisms, which can be related to the contact stress. However, a value of $n = 1$ does not eliminate the possibility of fatigue as a major wear mechanism in that situation.

One way of interpreting the value of n in these relationships is in terms of the energy expended in wear. If this energy remains constant as sliding progresses, it is reasonable to infer that $(1 - n)$ should be 0. This would be true for contacts in which the area changes with wear and in which the area stays constant. If the energy associated with wear decreases with sliding, values of $n < 1$ can be inferred. The energy going into wear can be influenced by a large number of factors, such as material properties, surface conditions, wear mechanisms, load, and stress level. With a constant load, stable wear behavior implies constant material properties, surface parameters, and mechanisms. Therefore, the only possibility for the energy to decrease in these stable regimes of wear is for the energy and wear mode to be stress dependent. If the stress also remains constant, such as with a constant contact area, then n equals 1 (i.e., $(n - 1)$ equals 0). If the contact area changes, stress also changes and values of $n < 1$ are possible. Consequently, different values of n should only be expected in situations where the contact area changes with wear. In these situations, it has been found that different values of n can be obtained for the same contact geometry but with different material couples (Fig. 2.2). This suggests that material properties are primary factors in determining n .

These further observations and considerations indicate that Eqs. (2.3) and (2.4) are best viewed as particular examples of the more general relationships, Eqs. (2.7) and (2.9). In addition, these more general relationships provide a means of accounting for the initial higher wear rates of some systems, other than with a break-in concept. With this approach the "initial period" is considered to be an integral part of a stable wear regime, which can be described by a single nonlinear expression. The practical difference between these two approaches in analyzing wear data can be illustrated by considering Fig. 2.3, which compares the shape of two theoretical wear curves to typical data. One has a break-in period, followed by a period in which wear rate is constant. In the other, a single, nonlinear expression is used for the entire period. It can be seen that over a limited range both have similar shapes, but over longer periods there is obviously a difference. Because of the scatter that is involved with wear data, it is generally required to take data over a long period so that this difference can be identified. If this is not done, it is often a moot question as to which type of model better describes the observed wear behavior.

While Eqs. (2.3) and (2.4) have limited applicability, they have been used to provide design information. One application is to use of V/P values to quantify the wear behavior of material pairs, that is, the "K Factor" approach (31–33). The other application is the PV factor (pressure times velocity) approach or concept, which is generally limited to situation in which the nominal area of contact does not change with wear, such as in many sliding bearing situations (34–40).

With the K factor approach, wear tests are usually performed long enough so that stable wear behavior is achieved. The wear rate in this region is determined from two successive wear measurements in this region. K values determined in this manner cannot be directly related to the wear coefficients of the more general relationships. Because of

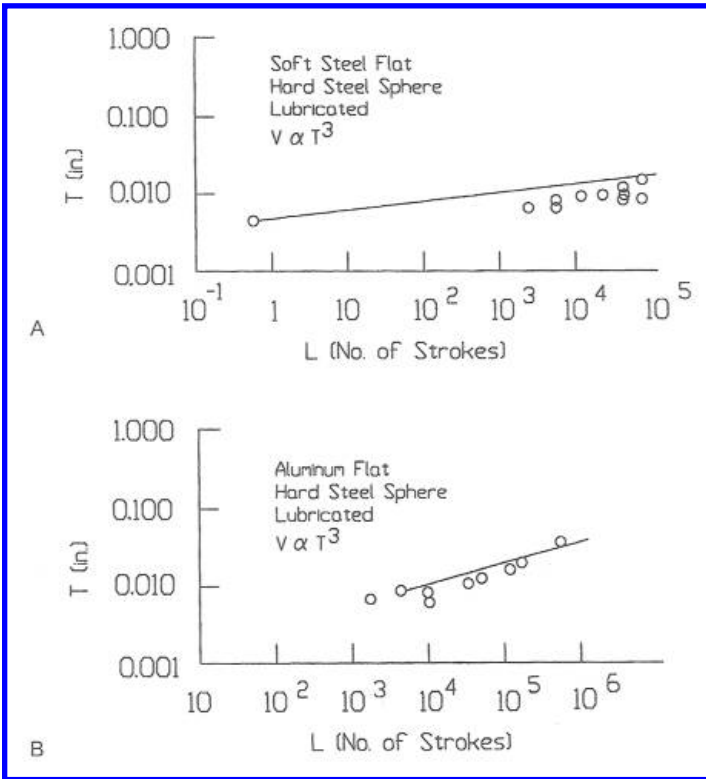


Figure 2.2 Wear curves from reciprocating ball-plane tests. In “A” and “B”, T is the width of the wear scar on the flat; V is the wear volume; in “C” and “D”, T is on the spherical slider. In “B” and “C”, the slopes are equivalent to $n = 1$ in Eq. (2.6). In “A” and “D”, $n < 1$.

this and the fact that this approach does not address the possibility of values of n and m other than 1, its use in design tends to be more qualitative than quantitative. K values determined in this way can often be used for the qualitative investigation of major sensitivities or effects and in this way provide useful design information. For example, the same general trend of K values with hardness is similar to trends of the wear coefficient of the more general model. However, specific rankings or relative performance may be different. In addition, there is some evidence that the variation of K values determined in this manner for a tribosystem follows a log normal distribution rather than a normal distribution (41).

With the PV factor, the experimental approach is similar to that used in the K factor approach, but tests are performed using conformal contacts of constant area. For such geometries, Eq. (2.3) can be written as

$$A \times h = K \times P \times S \quad (2.10)$$

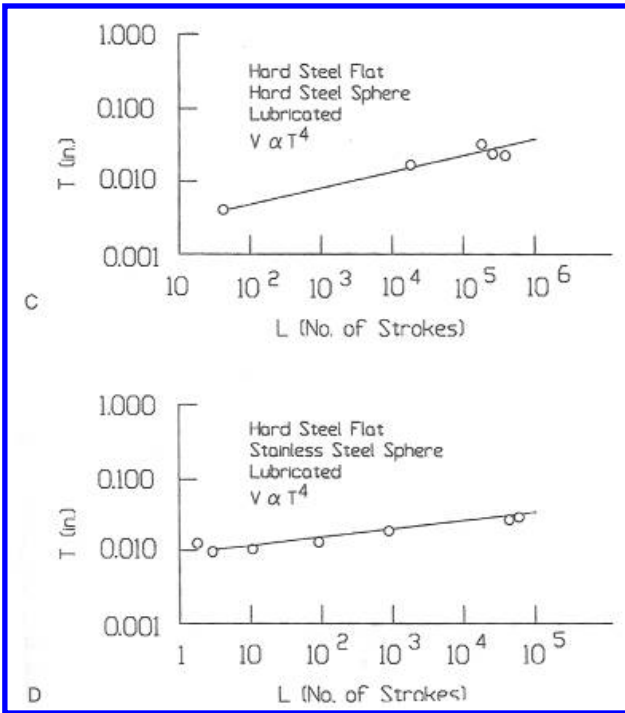


Figure 2.2 (continued)

where A is the area of contact and h is the depth of wear. Therefore,

$$h = K \times \left(\frac{P}{A}\right) \times S \tag{2.11}$$

$$\frac{dh}{dt} = \mathbf{h} = K \times \frac{P}{A} \times \left(\frac{dS}{dt}\right) \tag{2.12}$$

where t is time, \mathbf{h} is the depth rate of wear, (P/A) is the pressure, and (dS/dt) is the sliding velocity and the product of the two is the PV factor. Equation (2.12) is then written as

$$\mathbf{h} = K \times PV \tag{2.13}$$

In this approach, this formulation is used as a basis to relate wear to the operating parameters of pressure and velocity. This is done by experimentally determining K as a function of PV (Fig. 2.4). Usually the experimental matrix is extensive enough to characterize a transition from mild to severe wear in terms of PV , as is shown in this figure. This transition point is called the PV limit of the material. While the formal derivation implies that K is constant for values under this limit, frequently K is found to be a function of PV in the region of mild wear.

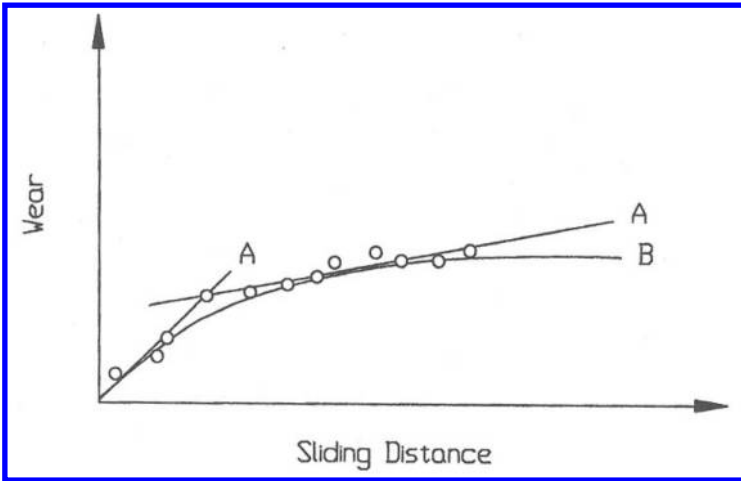


Figure 2.3 Alternatives for analyzing wear data. “A” illustrates a piece-wise fit using two linear relationships; “B” illustrates a continuous fit using a single nonlinear relationship.

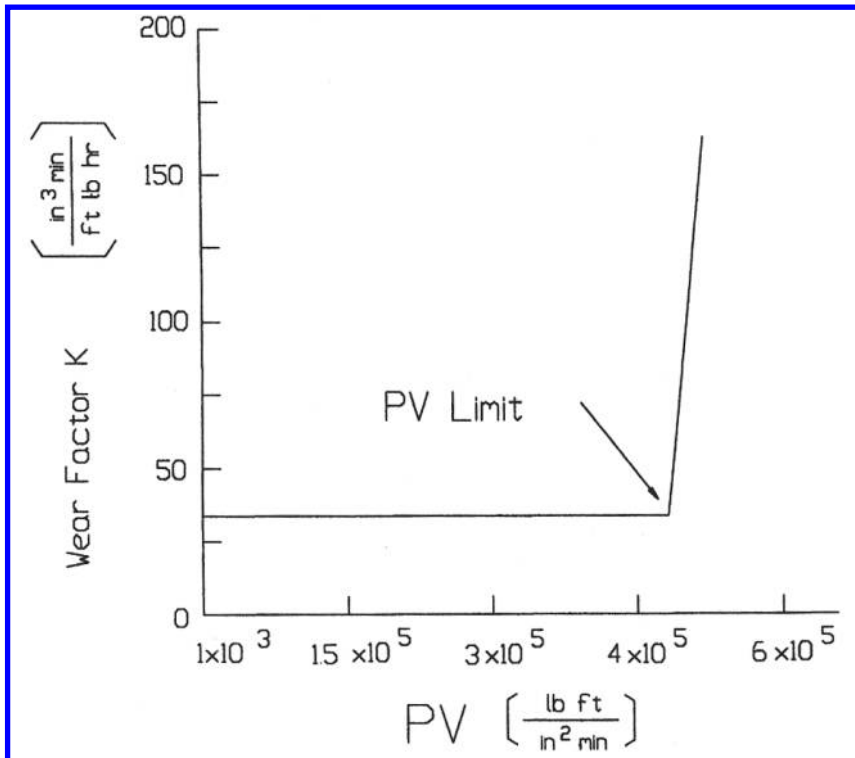


Figure 2.4 The wear coefficient, K , of a filled polyimide as a function of PV . Data were obtained in a thrust washer test. (From Ref. 146.)

Since this model is also based on Eq. (2.3), its application to design is subject to the same limitations as the K factor approach but there are differences. One is that it is limited to those situations for which the contact area remains constant with wear. While this is an additional limitation, it also removes concerns associated with the value of n since $n = 1$ for all geometries of this type. Also, the ability of the formulation to accommodate different relationships between K and PV tends to account for values of m other than 1, as well. An additional concern with this model is associated with the implied assumption that it is the product of pressure and velocity that controls the wear. It is this aspect which is most appealing in design, since it means that wear behavior can be simply related to this PV factor. However, as was pointed out in Part A of MWFT2E, this is not necessarily the case. Both pressure and velocity can independently influence wear behavior and there are also different ways by which the product of pressure and velocity can be related to wear behavior.

This type of model is often found to be useful in journal and thrust bearing applications, since in both of these situations the contact area tends to stabilize after some initial period of small wear. In these types of applications, there are two distinct situations, which can occur and involve different concepts regarding PV factors. One is unlubricated sliding, the other is lubricated sliding. For unlubricated situations, particularly those involving a plastic, the PV limit and the behavior of K is usually associated with sliding temperature. In lubricated situations, the PV factor is generally related to lubricant behavior, that is, fluid lubrication. In the former case, PV is related to the power expended in sliding and through this, temperature. Heat conduction paths, as well as basic material wear behavior, are important factors in this situation. In the latter situation, PV is often related to the nature of the lubricant film that is maintained in the bearing and the likelihood of penetration of this film. In such situations the boundary lubrication qualities of the lubricant, the basic wear properties of the surfaces, and the possibility of fluid lubrication effects are factors that can be involved in the wear behavior. These two situations indicate some of the difficulties and concerns associated with the use of PV factors to characterize general wear behavior. However, these factors can be of use in design if their limitations and range of applicability are understood and recognized.

The formalism of this PV model and its application to journal bearings, both lubricated and dry, are treated further in the consideration of journal bearing models.

2.3. WEAR AND WEAR RATE RELATIONSHIPS FOR ABRASIVE WEAR

With abrasive wear, the situation is much simpler than with general sliding wear. While there are some exceptions, most experimental studies indicate that abrasive wear behavior can be fitted to the following relationship, when the hardness of the abrasive, H' , is larger than the hardness of the abraded material, H

$$V = K \times P \times S \quad (2.14)$$

where V is the volume of wear; P , the normal force; S , the distance of sliding; K , a wear coefficient affected by the other parameters of the tribosystem (42–48). There is some evidence that when $H > H'$, the same linear relationship also applies, but that the values of K for each region are significantly different (42,49). Generally, the K values in these two regions differ by a factor of 10–100, with the value being lower when $H > H'$.

The primary mechanical parameter of the abraded material that affects K is generally its hardness, H . When $H < H'$, K generally is proportional to H^{-1} (43–50). When H approaches H' , this relationship is modified but K still tends to decrease with H . This is

also true in the situation when $H > H'$. For all three regions, there is some evidence that exponential relationships can be used to describe the relationship between K and hardness. In the case of abrasive wear by paper (49), it has been found that the experimental data fit the following:

$$K \propto H^m \quad (2.15)$$

where $m = -1$ for $H < H'$; $m = -10$, $H \approx H'$; and $m = -5$, $H > H'$.

Of these three relative hardness conditions, the first, $H < H'$, has received most attention in terms of modeling. Theoretical models for abrasive wear processes based on single-cycle deformation mechanisms for this condition tend to support the empirical relationships given by Eqs. (2.14) and (2.15) for this condition. Most of these, but not all, result in dependencies on load, sliding distance, and hardness similar to the empirical ones given in these equations (50–53). Some of these models for abrasive wear introduce dependencies on other parameters of the tribosystem. Such dependencies and relationships are generally considered as part of the wear coefficient, K , as is the dependency on hardness. This general agreement between theory and form of Eq. (2.14) and the inverse relationship to hardness provide a high degree of confidence in the use of this relationship in design for conditions, when the abrasive is harder than the abraded material.

Unfortunately, this cannot be claimed for the other two conditions of relative hardness. These two regions have not received as much attention, either theoretically or experimentally. For these conditions, it is reasonable to consider a more generic form of these equations, similar to the ones used for sliding, for use in these regions,

$$V = K \times H^m \times P^n \times S^k \quad (2.16)$$

In this form, the values of m , n , and k are functions of the tribosystem and need to be determined experimentally for each range of relative hardness. However, energy arguments, like those used in the discussion of the relationships for sliding wear, and the limited data cited previously suggest that values of n and k are likely to be 1. When values of k less than 1 are observed, this behavior can generally be attributed to degradation or changes with the abrasives, the protection of the surface by debris, or some other change to the tribosystem, as discussed in 3.8 of MWFT2E.

2.4. ZERO WEAR AND MEASURABLE WEAR MODELS FOR SLIDING

There are two other models for sliding wear that were developed for design (3,54–64). One of these models, the Zero Wear Model, is concerned with the conditions needed to insure that a certain low level of wear is not exceeded. The companion model is concerned with the progression of wear and is called the Measurable Wear Model.

In the Zero Wear Model, “zero wear” is defined as wear of such a magnitude that the average depth of the wear scar is equal to or less than half the initial roughness of the rougher of the two surfaces. The wear condition, when the average depth is just equal to half the roughness, is referred to as the zero wear criteria. The basic concept of zero wear is that wear of such a magnitude is generally negligible in terms of engineering performance and that contact conditions remain nominally the same for this amount of wear. The zero wear criteria is a large enough amount of wear, so that a wear groove can just barely be identified by a profilometer measurement across the wear scar. Fig. 2.5 illustrates some zero wear conditions and the zero wear criteria and compares them to what is termed measurable wear, where a wear groove can be clearly identified

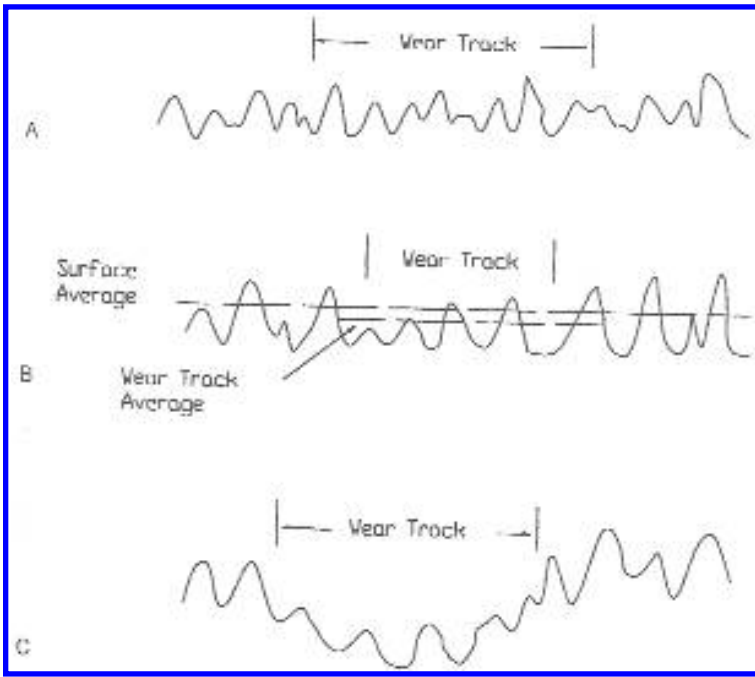


Figure 2.5 Illustration of zero and measurable wear conditions. “A” illustrates the zero wear condition; “B”, the condition near the zero wear criteria; and “C”, the measurable wear condition.

by a profilometer trace. Measurable wear is a term used to identify wear above the zero wear criteria. Additional examples of zero and measurable wear are shown in Figs. 2.6 and 2.7. The basic concept of zero wear allows for differences in wear scar topography for conditions where the worn member is smoother or rougher than the counterface. Since on a practical basis this difference would be negligible for most engineering applications, a single criterion can be used. Mathematically, the zero wear criterion is defined as

$$h = \delta \tag{2.17}$$

where h_{avg} is the average depth of the wear scar and δ is the center line average roughness of the rougher of the two surfaces in contact. This condition is illustrated in Fig. 2.8.

The Zero Wear Model identifies conditions of loading and sliding which result in zero wear. The conditions of loading and sliding for the zero wear criteria to be reached are given by the following relationship:

$$2000 \times (\Gamma_r \tau_y)^9 = N \times \tau_{max}^9 \tag{2.18}$$

provided

$$\tau_{max} \leq 0.54 \tau_y \tag{2.19}$$

where τ_{max} is the maximum shear stress produced in the contact; τ_y , the yield point in shear of the material; Γ_r , an empirically determined wear coefficient, which depends on the

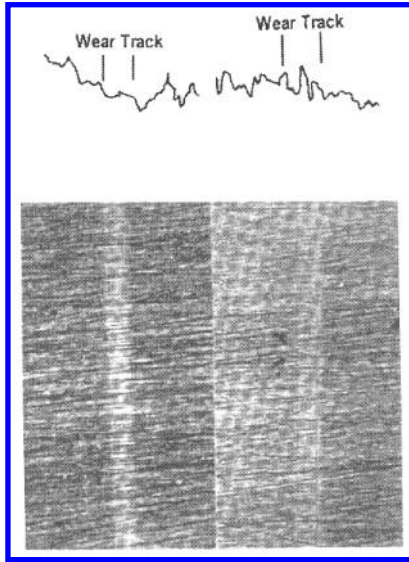


Figure 2.6 Zero wear examples. The profilometer traces above the micrograph were taken across the wear scars shown in the figure. While the wear scars were visible, they were undetectable in the traces. (From Ref. 60.)

materials and environment; N , the number of passes required for zero wear. Γ_T is referred to as the Zero Wear Factor.

A pass is defined in the model to be a distance of rubbing equal to the width, W , of the apparent area of contact measured in the direction of sliding. If a surface experiences a total amount of rubbing, S ,

$$N = \frac{S}{W} \quad (2.20)$$

In many contact situations, the two members experience different amounts of sliding so that in a unit operation (e.g., a revolution or an engagement) or a unit of time the number of passes that each member of sliding couple experience is not necessarily the same. This can be illustrated by considering a typical test configuration of a sphere sliding back and forth across a flat surface (Fig. 2.9). Letting A be the amplitude of the motion, two conditions can be considered. One is when $A > W$. In this case, the contact area on the flat is completely unloaded during the course of the sliding and each region of the surface experience rubbing only while the sphere passes over it. In each $1/2$ cycle, the amount of rubbing that the flat experiences is W , while the sphere experiences A . The number of passes in that $1/2$ cycle for the flat is W/W or 1; for the sphere, A/W . The other condition is when $A < W$. In this case, the surfaces of the sphere and the flat experience the same amount of rubbing, A , and the number of passes in a $1/2$ cycle is A/W for both. It is also important to recognize that for these two situations, the number of passes of rubbing in a half-cycle is different. For each member, it is less for the case when $A < W$, than when $A > W$. For the flat, $N < 1$ and $N = 1$, respectively. For the sphere, $N < 1$ and $N > 1$, respectively. It can be seen that this concept of pass allows the model to differentiate between the two members of a couple and also to account for the difference between large amplitude motion and small amplitude motion (i.e., large amplitude oscillatory motion

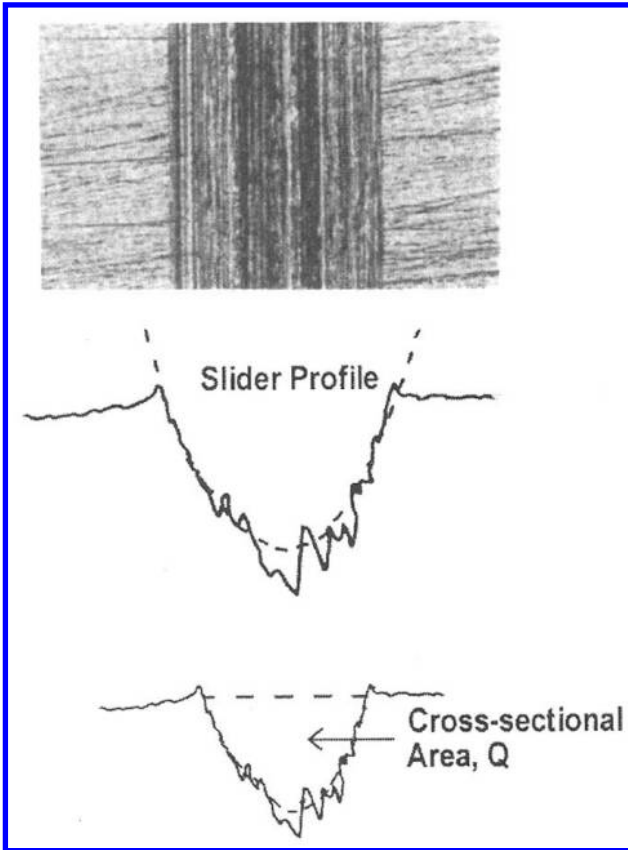


Figure 2.7 Measurable wear examples, illustrating Q , the cross-sectional area of the wear scar used in the Measurable Wear Model. The micrographs are of a wear scar produced on a flat surface by a spherical slider. The profilometer trace is across the wear scar. A profilometer trace of the slider is super-imposed on the trace through the wear scar.

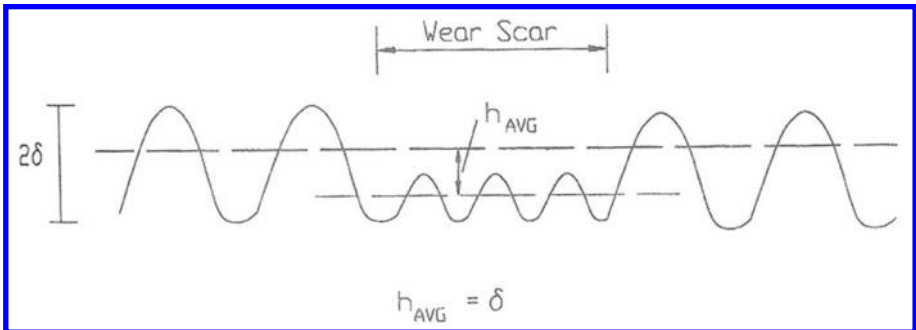


Figure 2.8 Definition of the zero wear criteria.

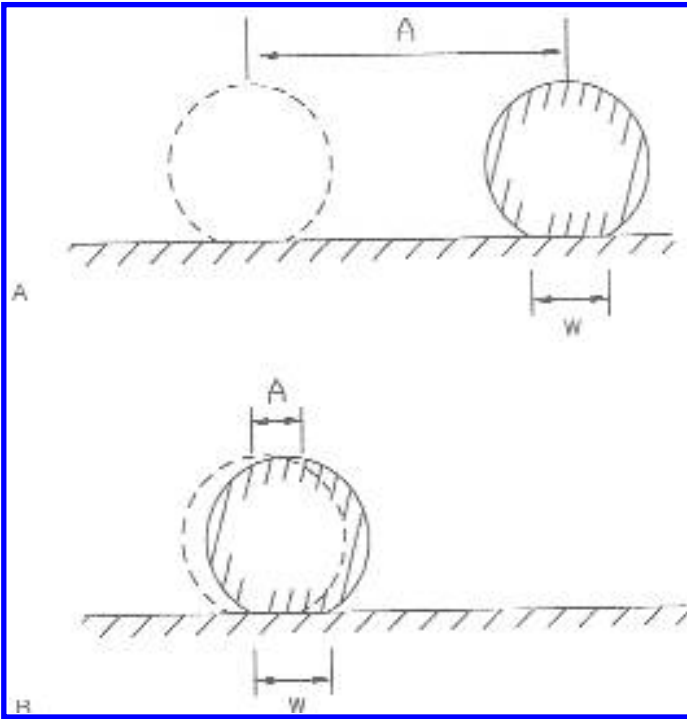


Figure 2.9 Illustration of the concept of a pass in an oscillating ball-plane test. “A” is for large amplitude motion (i.e., when the contact area is fully unloaded); “B”, for small amplitude motion or fretting (i.e., when the contact area is not fully unloaded).

and fretting conditions). This concept is an important aspect in the application of this model to the fretting situations (65,66).

The maximum shear stress in Eqn. (2.18), τ_{\max} , includes the combined effects of load, geometry, and friction. For this model, the stress concentration effects associated with any edges involved in the contact situation must be considered in determining τ_{\max} . In most situations, this can be described in terms of a stress concentration factor, K , which is a multiplier of the stress determined on the basis of the gross geometry. This is illustrated in Fig. 2.10. The value of K is associated primarily with the shape of the edge (e.g., the radius) but can also depend on the gross dimensions of the contact, as well as the moduli of the materials in contact (67). Equations for τ_{\max} and K for several contact situations are given in Table 2.2 (54,58–59,67–69).

Since the model indicates that the amount of rubbing required for zero wear criteria to be reached is proportional to τ_{\max}^2 , the effects of friction and stress concentration can be significant. Both can easily account for an order (or orders) of magnitude change in wear behavior. From examination of the equations in Table 2.2, it can be seen that the normal load and shape are the predominate factors when the coefficient of friction is small (e.g., < 0.2) which is characteristic of lubricated conditions. For much higher values of μ , such as those associated with many unlubricated metal couples, friction significantly increases τ_{\max} (e.g., doubling the stress if μ is in the range of 0.5–0.6).

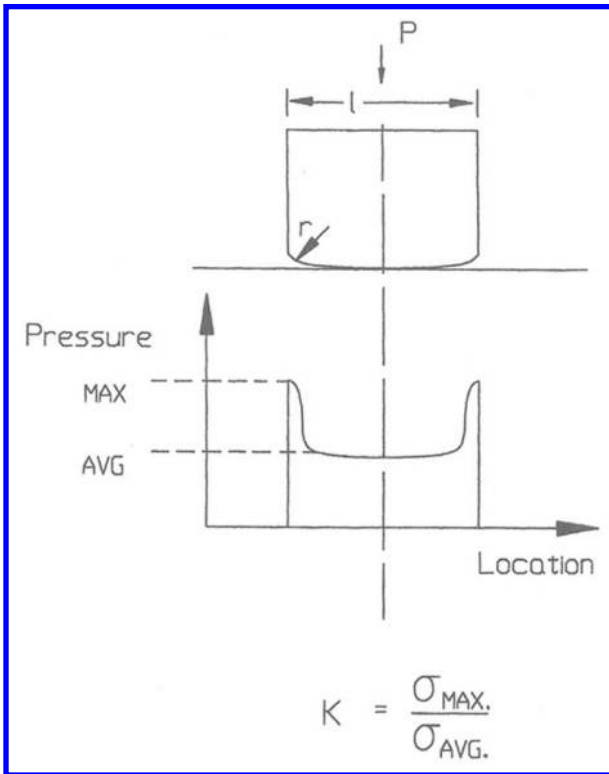


Figure 2.10 Stress concentration factor.

Edge conditions can also result in significant increases. Evaluations of the expressions for K indicate that large edge radii (e.g., > 0.10 in.) are often required to obtain stress concentration factors less than 2 and that values as high as 10 can occur with smaller radii. While the effects of an edge on wear can persist, they tend to be more pronounced during the initial stages of wear and are localized to the regions of edge contact. In most cases, wear tends to eliminate stress concentration. In particular, there is generally no stress concentration (i.e., $K = 1$) associated with edges formed by wear.

In addition to affecting the magnitude of the maximum shear stress, friction and edge conditions can also influence the location of the maximum shear stress. However, the location is also a function of the general contact geometry. As can be seen in [Table 2.2](#), the maximum shear stress is on the surface for most cases. However, in the case of Hertzian point contact, it is below the surface if $\mu < 0.31$. Where there is a stress concentration effect, the maximum stress occurs at the location of the stress concentration. While the model is concerned with the average wear, it suggests that the regions associated with the stress concentration should exhibit the earliest and most severe wear.

These trends of degraded wear performance that are predicted by the model (i.e., with unlubricated couples and sharp edges) are consistent with observations. For example, higher wear is generally observed in unlubricated conditions and wear scars frequently show the effects of sharp edges. [Fig. 2.11](#) shows example of the influence that edges have on wear behavior. The effects of edge conditions on wear behavior and how to account for these situations in design are illustrated in several of the case studies (5.2–5.4).

Table 2.2 Stress Equations

<i>Symbols</i>	
σ contact pressure	τ shear stress
E Young's Modulus	ν Poisson's ratio
μ coefficient of friction	K stress concentration factor
P load	$k = (1 - \nu^2)/(\pi E)$
(subscripts identify the two surfaces in contact)	
<i>Non-conforming contacts</i>	
General	
$2a$ major axis of contact area	$2b$ minor axis of contact area
R and r radii of surface (negative if concave)	
$\sigma_{\max} = 0.477P/ab$, $\tau_{\max} = 0.31\sigma_{\max}$, $\mu \leq 0.31$	$0.5a$ below center of contact on contact surface
$\tau_{\max} = \mu\sigma_{\max}$, $\mu \geq 0.31$	
$a = 1.33 m [P(k_1 + k_2)/(B + A)]^{1/3}$	$b = 1.33 n [P(k_1 + k_2)/(B + A)]^{1/3}$
$B + A = 0.5(R_1^{-1} - r_1^{-1} + R_2^{-1} + r_2^{-1})$	$B - A = 0.5[(R_1^{-1} - r_1^{-1} + R_2^{-1} - r_2^{-1})]$
m and n given in Appendix I in terms of $\cos \theta$ where $\cos \theta = (B - A)/(B + A)$	
<i>Parallel cylinders</i>	
L length of shorter cylinder, x edge radius of shorter cylinder	
$\sigma_{\max} = 0.637 P/(L b)$, $\tau_{\max} = K \sigma_{\max} (0.25 + \mu^2)^{1/2}$, sliding parallel to the axis; on contact surface	
$\tau_{\max} = K \sigma_{\max} ([1 + \mu]/2)$, sliding perpendicular to the axis; on contact surface	
$b = 2(R_1 R_2 P/L)[k_1 + k_2]/[R_1 + R_2]^{1/2}$, $K = (1 + [x^{-1}/(R_1^{-1} + R_2^{-1})]/(2/m^2 n))$	
m and n given in Appendix I in terms of $\cos \theta$; $\cos \theta = (x^{-1} - R_1^{-1} + R_2^{-1})/(x^{-1} + R_1^{-1} + R_2^{-1})$	
<i>Conforming contacts</i>	
A area of conformity	L contact length } same plane
$\sigma_{\text{avg}} = P/A$	x radius of edge }
$K = 0.34 ([k_1 + k_2][x/L]\sigma_{\text{avg}})^{-1/3}$	$\tau_{\max} = K \sigma_{\text{avg}} (0.25 + \mu^2)^{1/2}$ on contact surface

The Zero Wear Model reflects the influences of speed, environmental conditions, temperature, counterface material, lubrication, etc., in the values of the empirical Zero Wear Factor, Γ_r . Γ_r can be determined as a function of these parameters in several ways, but all involve the simulation or replication of these conditions in a sliding wear test. The most direct is to perform a series of wear tests, which simulate the significant parameters at different loads but for a fixed amount of sliding. The purpose of this series of tests is to determine the maximum load for which the zero wear criteria is reached for that fixed amount of sliding. The number of passes in these tests should be equal to or greater than 2000. Once the maximum load for zero wear is determined, τ_{\max} is calculated and the following form of Eq. (2.16) is used to determine Γ_r :

$$\Gamma_r = 0.43 \left(\frac{S}{W} \right)^{1.9} \times \left(\frac{\tau_{\max}}{\tau_y} \right) \quad (2.21)$$

For some geometries, such as point and line contacts, W may also be a function of load and would also have to be calculated (see Table 2.2).

An alternate way to determine Γ_r is to perform a series of tests at a fixed load and stress to determine the amount of sliding required to reach the zero wear criteria. Equation (2.21) is again used to determine Γ_r . A third way is to develop a wear curve (i.e., a plot of wear against distance of sliding for a fixed load) and to use the Measurable

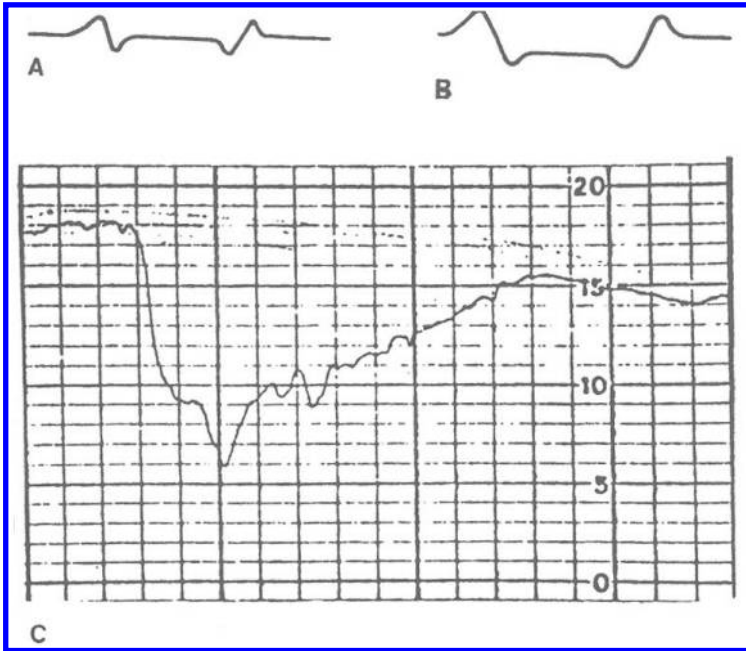


Figure 2.11 Profilometer traces through wear scars, showing the effect of stress concentration in the exaggerated wear at the edges of the scars. “A” and “B” are for well-aligned fretting situations; “C”, for a misaligned sliding situation. (“A” and “B” from Ref. 82, reprinted with permission from Elsevier Science Publishers.)

Wear Model to determine Γ_r . This approach will be described in the discussion of the Measurable Wear Model. The first two methods are illustrated in Fig. 2.12.

Since there is little or no change to the initial contact configuration in the zero wear range, any contact configuration can be used to determine Γ_r , including those geometries for which the stress level change with wear (e.g., a sphere on a flat). In fact, such geometries are preferred for this type of evaluation, since alignment and stress concentration problems tend to be eliminated with this type of contact. Since the Zero Wear Model only applies to situations in which $\tau_{\max} \leq 0.54 \tau_y$, only test conditions which satisfy that criteria can be used to determine Γ_r .

Tests of these types have been performed with a large number of material pairs, with and without lubrication (54,60,65,70). The results of these tests indicate that values of Γ_r are not uniformly distributed but tend to cluster around two characteristic values, 0.54 or 0.2. An analysis of the tabulation of approximately 700 values of Γ_r for different material pairs and lubricants, given in Appendix II, indicated that approximately two-thirds of the combinations were associated with the characteristic value of 0.2. This indicates that it is more likely for a tribosystem to have a value of 0.2 than a value of 0.54. Examination of these same data also indicates that some trends exist regarding individual materials. While Γ_r is a function of the material pair and lubricant, the analysis indicates that some materials tend to be associated with one of the characteristic values, more than the other. This trend is consistent with practical engineering experience that some materials tend to exhibit better wear performance and others, poorer wear performance. At the same time, the analysis of this tabulation indicates that even though some materials exhibit such a tendency, a non-typical value can be associated with this material when it is used with a

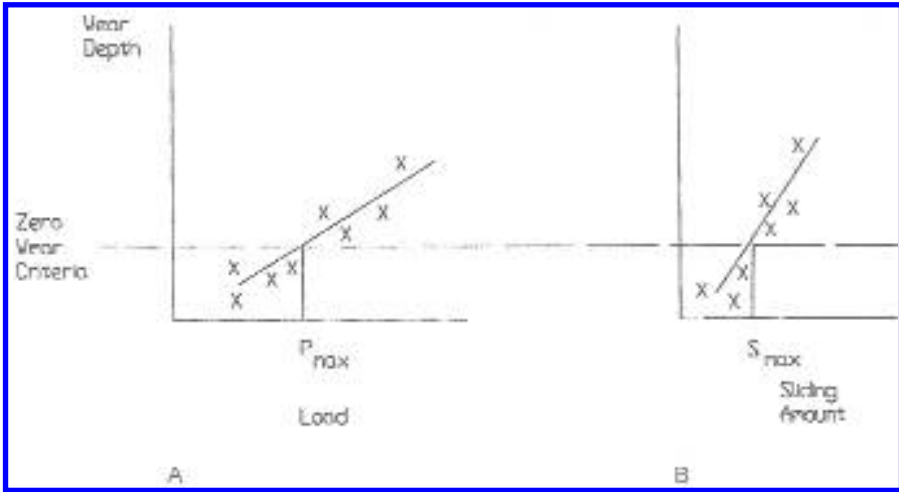


Figure 2.12 Experimental methods for determining Γ_T . “A” involves a series of tests at different loads and a standard amount of sliding; “B” involves a series of tests of different durations and a standard load.

specific counterface material or lubricant. Another trend that is observed in this tabulation is that, except for polymer / metal couples, most unlubricated systems tend to have the characteristic value of 0.2; polymer / metal couples tend to have the characteristic value of 0.54 under both dry and lubricated conditions.

The fundamental understanding of the relationships between Γ_T and various physical, material, and environmental parameters is not known. However, these general trends exhibited by Γ_T suggest that Γ_T is likely to be inversely related to the material couple’s tendency for adhesion. On a practical basis, this indicates the desirability of selecting material pairs which exhibit low adhesive wear characteristics and the use of a lubricant to reduce the tendency for adhesion in sliding wear applications.

The concept underlying the development of the Zero Wear Model is that under low stress conditions the governing wear mechanism in sliding is fatigue or at least fatigue-like. The condition of the model that $\tau_{max} \leq 0.54\tau_y$ is needed to insure that wear due to adhesive and single-cycle deformation mechanisms do not exceed the zero wear criteria after a single pass. This condition was determined empirically by examining wear scars produced with a single pass at different stress levels (60). This condition is not sufficient to insure that adhesive and single-cycle deformation elements are completely eliminated or insignificant with repeated or continuing sliding. The fact that Γ_T can have values significantly lower than 0.54 implies this. Lower stress values (e.g., $0.2\tau_y$) are required to insure this with some material systems. There is direct evidence correlating micro-crack formation and growth with Eq. (2.18) (71). This is shown in Fig. 2.13. In addition, numerous investigations have indicated the significance of fatigue or fatigue-like mechanisms in sliding wear, as well as a high stress dependency for such mechanisms (7–9,20,21,30,72).

Two aspects of the model must be recognized in order to utilize this model in design. One is that it is a conservative model in that it is concerned with dimensional changes resulting from wear that are the order of surface roughnesses. In practice, most devices can experience significantly greater dimensional changes and still function properly.

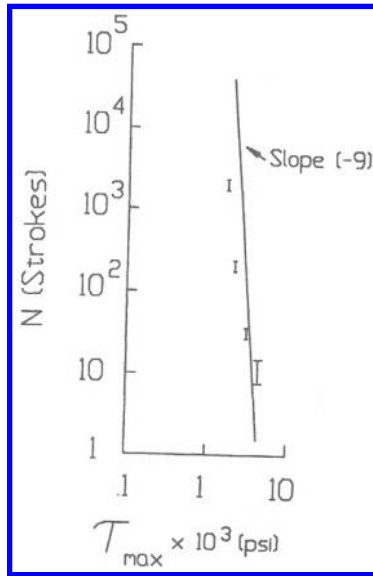


Figure 2.13 Data showing the correlation between stress level and the number of sliding cycles required to initiate surface cracks in Cu. (From Ref. 71.)

The second is the high stress dependency and its implication on predicted wear life. For example, a 10% variation in stress results in a factor of 2 difference in the amount of sliding required for the zero wear criteria. In practice, it is often difficult to determine value of the stress to within 10%, particularly if a stress concentration effect has to be included (73); on the other hand, this sensitivity indicates the importance of controlling design elements, which affect stress.

One way of utilizing this model that has been found to be useful in a design environment and allows for this aspect is the “Allowable Load” concept. In this concept, the model is used to determine the maximum load that can be applied to a design and still achieve a specified lifetime. This allowable load for the design is then compared to the anticipated or actual load. A design is finally selected so that there is a sufficient safety factor in terms of the allowed and anticipated load (58). This approach is also useful for evaluating designs for potential wear problems. Potential wear problems can be viewed as designs for which the actual load is similar to or exceed the allowable load. The wear performance of such designs would be monitored closely in development tests to insure adequate performance. The utilization of the allowable load concept in design is further described in Sec. 3.6. Expressions for allowable loads can be found in Appendix VI.

The conservatism associated with the Zero Wear Model can be reduced when it is combined with its companion model, the Measurable Wear Model, which is concerned with the progression of wear. The basic hypothesis of the Measurable Wear Model is that the wear per unit distance of sliding, Q , is a function of the energy going into wear per unit surface area per unit distance of sliding, E , and the amount of sliding per unit distance of sliding, N (3,54,61). The model proposes the following relationship between these three terms:

$$dQ = Q_E dE + Q_N dN \tag{2.22}$$

where Q_E and Q_N are the partial derivatives of Q with respect to E and N . In this formulation Q is basically the cross-sectional area of the wear scar in a plane perpendicular to the sliding direction (Fig. 2.14). The unit distance of sliding is defined as the width of the contact area in the direction of sliding, W , which also is used to define a pass in the Zero Wear Model. Therefore, N is the number of passes. A further hypothesis of the model is that there are two types of wear systems. In one, E changes as wear progresses; in the other, E stays constant as wear progresses.

When E is constant, $dE \equiv 0$ and Eq. (2.22) reduces to

$$dQ = Q_N dN \quad (2.23)$$

which is equivalent to the following:

$$V \propto S \quad (2.24)$$

where V is the volume of wear and S is the sliding distance. This can be shown in the following manner. Eq. (2.23) can be expressed as

$$\frac{dQ}{dN} = Q_N \quad (2.25)$$

Since

$$dV = W dQ \quad (2.26)$$

and

$$dS = W dN \quad (2.27)$$

$$\frac{dQ}{dN} = \frac{dV}{dS} \quad (2.28)$$

Therefore, since dV / dS is constant for a constant energy system (as discussed in Section 2.2), Q_N is also constant (i.e., not a function of N). Integration leads to

$$V = Q_N S \quad (2.29)$$

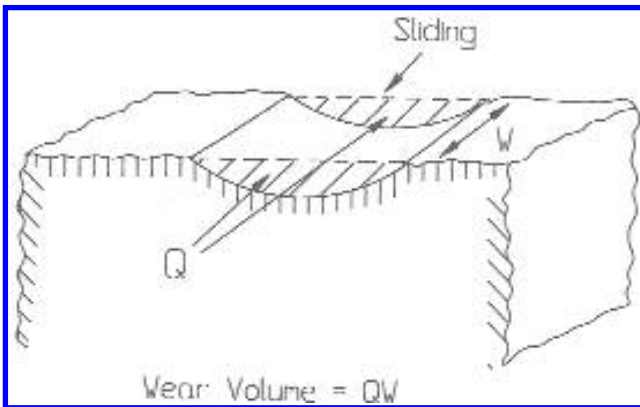


Figure 2.14 Diagram of a wear scar of uniform cross-section in a flat surface.

where Q_N is not a function of S or N but a function of other tribosystem parameters, such as load, material properties, etc. In this form Q_N can be treated as an empirical wear coefficient.

For the general wear situation, it is assumed that Eq. (2.18) of the Zero Wear Model can be used to deduce general relationships for the partial derivatives of Q . Within the framework of these models this is reasonable, since Eq. (2.18) is not limited to a particular type of system. In doing this, a further hypothesis is introduced. It is argued that it is plausible to assume that the energy going into wear would be proportional to the product of the stress produced during sliding and the amount of sliding that takes place in a unit distance of sliding. Specifically, it is proposed that

$$Q = C \tau_{\max} W \tag{2.30}$$

where C is a constant of proportionality.

Since Eq. (2.18) relates conditions for equivalent wear, it can be expressed in the same form as

$$Q = C' \tau_{\max}^9 N \tag{2.31}$$

where C' is a constant for a given system. Recognizing that τ_{\max} can be proportional to W , as can be seen in Table 2.2, this can be expressed as

$$Q = C'' (\tau_{\max} W)^{9/2} N \tag{2.32}$$

or

$$Q = C''' E^{9/2} N \tag{2.33}$$

where C'' and C''' are system constants. Since Eqs. (2.32) and (2.33) can be viewed as the integrated form of Eq. (2.22), they can be used to determine the partial derivatives of that equation. Doing this, it can be shown that

$$Q_N = C (\tau_{\max} W)^{9/2} \tag{2.34}$$

$$Q_E = \frac{4.5}{\varepsilon} (\tau_{\max} W)^{-1} Q \tag{2.35}$$

where ε is the constant of proportionality implied in Eq. (2.30). Using Eqs. (2.34) and (2.35), it can be shown that Eq. (2.22) reduces to the following:

$$d \left[\frac{Q}{(\tau_{\max} W)^{9/2}} \right] = C dN \tag{2.36}$$

Since $\tau_{\max} W$ represents the energy going into wear, Eq. (2.36) can be written as

$$dQ = C dN \tag{2.37}$$

for constant energy systems.

It should be noted that Eqs. (2.36) and (2.37) are general relationships for the two types of tribosystems considered by the model and are not limited to low stress conditions. For convenient reference, the expressions for the Measurable Wear Model are summarized in Table 2.3.

The relationships of this model describe the progression of wear in a sliding system. They do not determine either the absolute amount of wear or the absolute magnitude of the rate of wear. These absolute values are determined by the various parameters that can effect the wear of a tribosystem, such as the shape and size of the bodies in contact, the

Table 2.3 Measurable Wear Equations for Sliding

Variable energy mode, $dQ/(\tau_{\max} W)^{0.75} = C dN$
 Constant energy mode, $dQ = C dN$

Symbols

Q , cross-sectional area of the wear scar in a plane perpendicular to the sliding direction

W , width of contact area in the direction of sliding

τ_{\max} , maximum shear stress

N , number of passes (a pass is a distance of sliding equal to W).

C , wear coefficients determined empirically or by use of the Zero Wear Model for Sliding

load, materials, lubrication, and the environment. The dependencies of these parameters are implicitly contained in the values of the various wear coefficients (e.g., the C 's) which can be empirically determined and related to these parameters. In this respect, these equations are similar to the general wear and wear rate expression discussed previously (e.g., Eqs. (2.3) and (2.4)). In the context of the Measurable Wear Model, these same factors also determine which mode of wear occurs. This is particularly true with respect to the counterface material, the lubrication, and environment. The determination of which mode applies to a given system (i.e., the constant energy or variable energy modes) needs to be done empirically as well.

As was previously discussed in the section on Wear and Wear Rate Relationships for Sliding Wear (Sec. 2.2), wear is not always found to be proportional to sliding distance. In situations where this is observed, it has been found that the variable energy formulation can describe the nonlinear behavior (3,61,74). This is illustrated for cases involving a sphere sliding on a flat in Fig. 2.15. Since the constant energy formulation is equivalent to a linear relationship between wear and sliding, the combined expressions of the Measurable Wear Model provide an explanation for the range of the observed relationships between wear and sliding distance. While this is the case, the nature of the model does not provide any guidance as to which mode will be followed. However, as with Γ_r of the Zero Wear Model, some trends have been observed regarding these two modes of wear. One trend is that the constant energy mode tends to be more common than the variable energy mode. Another trend that has been observed is that the constant energy mode tends to be the characteristic mode of unlubricated systems and other system, which exhibit a high degree of or tendency for adhesive wear. However, the constant energy mode is not limited to such systems, since it has also been observed in systems in which adhesive wear is not the predominate feature (e.g., lubricated systems in which $\tau_{\max} \leq 0.54$). On the other hand, data suggest that a low tendency for adhesion is required if the variable energy mode is to apply.

The determination of the wear coefficients of this model and the identification as to which mode of wear the systems follows is a two-step process. The first step is the determination of which mode of wear the system follows and the second is the determination of wear coefficient. To do this, it is necessary to develop a wear curve in a simulative wear test so that the empirical relationship between wear and sliding can be determined and compared to those predicted by both equations. This means it is also necessary to develop the theoretical relationships for both modes for the geometries involved in the simulative test. Once the mode of wear is determined by this comparison for the system, the wear data can be used to determine the value of the wear coefficient by fitting the appropriate theoretical expression to the data. To determine the wear

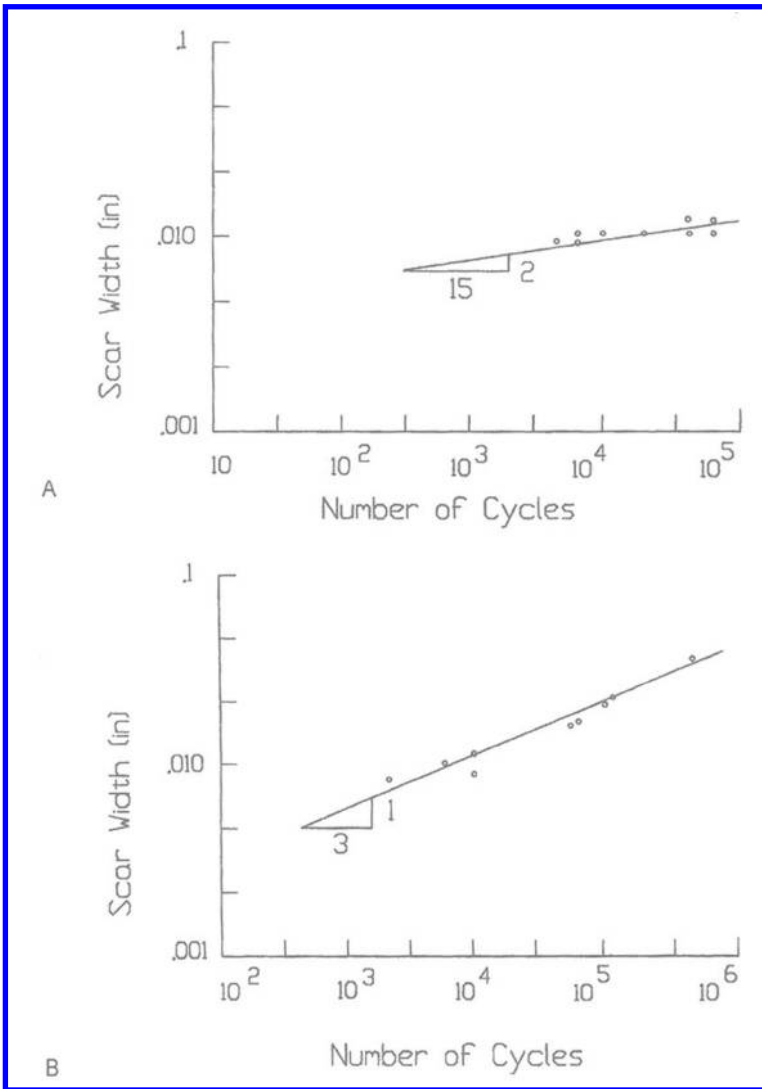


Figure 2.15 Wear data from reciprocating ball-plane tests, involving a harder unwearing sphere and a softer flat counterface. “A” shows the behavior for the lubricated wear of a soft steel flat which is consistent with the variable energy model; “B” shows the behavior for lubricated wear of an aluminum flat which is consistent with the constant energy model, (see pages 70–71).

coefficients, per se, any contact geometry may be used for such test. However, not all contact geometries can be used for the determination of the mode of wear. It is necessary that special, contact configurations be used for this determination. It can be shown that for contact geometries in which the contact area remains constant, the two equations predict the same relationship between wear and sliding distance. Therefore, to determine which mode applies to a tribosystem, it is necessary to use contact geometries in which the size of the contact increases perpendicular to the motion with wear (e.g., a sphere on a flat or

crossed cylinders). The basic elements of this approach can be illustrated by considering such a system.

Fig. 2.16 shows a wear test where a flat is worn on the surface of a sphere, which is sliding back and forth across a non-wearing flat surface. By consideration of the geometry, it can be shown that for $h < r$,

$$Q \approx 0.5 Wh \quad (2.38)$$

$$W^2 \approx 8 rh \quad (2.39)$$

Combining Eqs. (2.38) and (2.39) results in

$$Q \approx \frac{W^3}{16r} \quad (2.40)$$

From Table 2.2, τ_{\max} is given by

$$\tau_{\max} = \frac{KP(0.25 + \mu^2)^{1/2}}{\pi W^2} \quad (2.41)$$

As was discussed previously in this section, the stress concentration factor is assumed to be 1 for edges that are formed by wear. Therefore,

$$\tau_{\max} W = \frac{P(0.25 + \mu^2)^{1/2}}{\pi W} \quad (2.42)$$

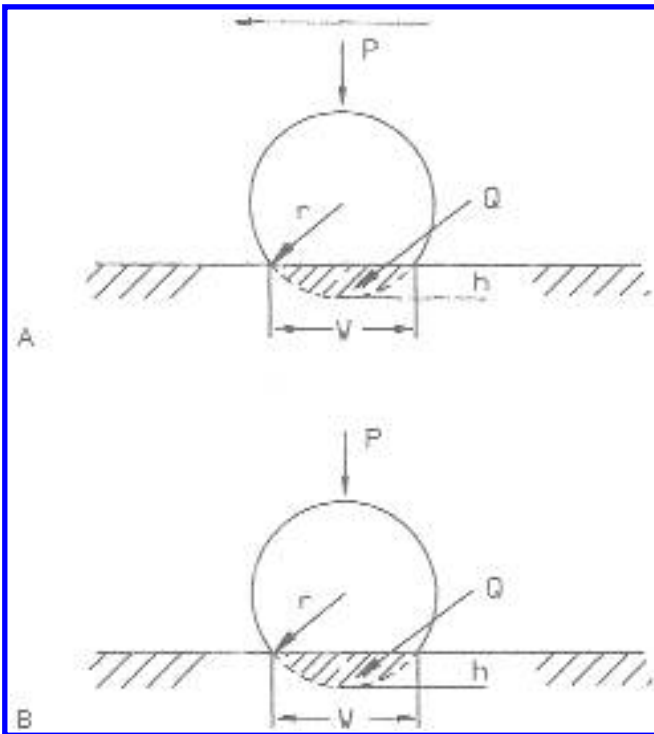


Figure 2.16 Wear scar geometry of a sphere wearing against a flat surface. “A”, view parallel to the sliding direction; “B”, perpendicular to the sliding direction.

Also

$$dN = \frac{dS}{W} \tag{2.43}$$

where S is the total amount of sliding.

Substituting these into Eq. (2.37) and integrating the following expressions results for the variable energy mode,

$$W = 53.8C[rP^{9/2}(0.25 + \mu^2)]^{2/17} S^{2/17} \tag{2.44}$$

The integration constant is 0 since the wear is 0 when the sliding is 0. Since C can also be a function of r , P , and μ , as well as other factors, this expression can be simplified to the following:

$$W = KS^{2/17} \tag{2.45}$$

where K is an empirical wear coefficient, which is constant of the tribosystem. It can be shown in a similar manner that the expression for the constant energy wear mode is

$$W = KS^{1/4} \tag{2.46}$$

If W , the width of the flat on the sphere, is measured in such a wear test as a function of the amount of sliding, the appropriate mode can easily be identified by plotting $\log W$ against $\log S$ and determining which exponent fits the data better. This type of comparison is illustrated in Fig. 2.17. Once the mode is determined, the appropriate equation (e.g., Eq. (2.45) or Eq. (2.46)) can be used with the individual data points to determine the value of K . By performing a series of tests, the dependency of K on load, lubrication, and other tribological parameter can be determined. Example of this approach can be found in the literature, as well as in Secs. 5.7–5.9 and 7.2 (61,74).

For low stress conditions, the Measurable Wear Model can be combined with the Zero Wear Model to determine K (3,54). In general, this is done by using the zero wear point to determine the coefficients of the Measurable Wear Model. The zero wear point is defined as the amount of sliding, S_0 , that results in wear equal to the zero wear criteria, namely a scar whose average depth is equal to the center line average, δ , of the rougher surface. (See Eq. (2.17).) Using this condition, the load and geometry dependencies of

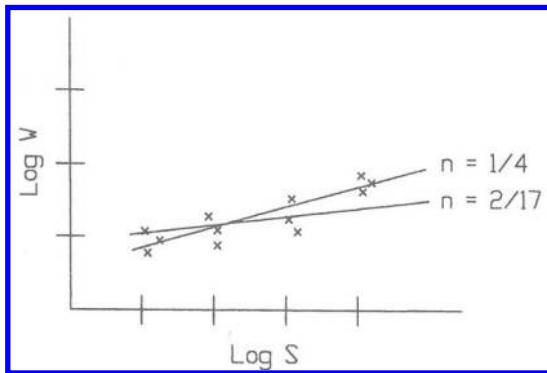


Figure 2.17 Method for determining Measurable Wear Model wear modes. The example indicates agreement with the constant energy wear mode.

these coefficients are explicitly determined and only the zero wear factor, Γ_r , needs to be determined empirically. This method can be illustrated by further consideration of the example of the sphere wearing to a flat.

If Q_0 is the cross-sectional area of the scar at the zero wear point, then

$$Q_0 \approx 1/2 \delta W_0 \quad (2.47)$$

where W_0 is the diameter of the flat at the zero wear point and equal to

$$W_0 \approx (8r)^{1/2} \delta^{1/2} \quad (2.48)$$

Assuming that the system is described by the variable energy mode,

$$K = \frac{W_0}{S_0^{2/17}} \quad (2.49)$$

S_0 is obtained from Eqs. (2.18) and (2.20) of the Zero Wear Model

$$S_0 = 2 \times 10^3 W_0 \left(\frac{\Gamma_r \tau_y}{\tau_{\max i}} \right)^9 \quad (2.50)$$

where $\tau_{\max i}$ is the maximum shear stress for the unworn contact. Since in the zero wear region, there is little change to the contact, it is assumed that the width of the contact is constant during the zero wear period ($S \leq S_0$). Therefore, W_0 is assumed to be equal to the diameter of the initial contact area. Combining Eqs. (2.48)–(2.50), the following results:

$$K = \frac{r^{15/34} \delta^{15/34} \tau_{\max i}^{18/17}}{\Gamma_r^{18/17} \tau_y^{18/17}} \quad (2.51)$$

Therefore,

$$W = \frac{r^{15/34} \delta^{15/34} \tau_{\max i}^{18/17}}{\Gamma_r^{18/17} \tau_y^{18/17}} S^{2/17} \quad (2.52)$$

By using Eq. 2.39, this can be transformed into similar relationships for wear depth, h ,

$$h = \frac{\delta^{15/17} \tau_{\max i}^{36/17}}{8r^{2/17} \Gamma_r^{36/17} \tau_y^{36/17}} S^{4/17} \quad (2.53)$$

As can be seen, Γ_r is the remaining empirical wear coefficient and this can be determined from the data used to establish the wear curve. Alternatively an equation, like Eq. (2.53), which is developed on the basis of these two models, can be used to project the wear once Γ_r is known.

Using the expression for $\tau_{\max i}$ from Table 2.2, these equations can be further developed to identify the dependency on load, radius, material properties (modulus and hardness), and μ . For example, Eq. (2.53) can be written as

$$h = \frac{0.0078 \delta^{15/17} \mu^{36/17} P^{12/17}}{r^{26/17} \Gamma_r^{36/17} \beta^{24/17} \tau_y^{36/17}} S^{4/17} \quad (2.54)$$

where

$$\beta = \frac{1 - \nu_1^2}{\pi E_1} + \frac{1 - \nu_2^2}{\pi E_2} \quad (2.55)$$

and E and ν are Young's modulus and Poisson's ratio of the two bodies.

In the general situation, where τ_{\max} depends on the coefficient of friction, μ , the coefficient of friction must be known, if Γ_r is to be determined. If μ is not known, it has to be determined as well. This is usually not a problem in practice, since wear testers frequently provide means of determining μ , that is, by measuring the friction force. However, it is not always necessary to determine the coefficient of friction. If the dependency on μ is the same in the test geometry and the intended application, then a single coefficient, combining both Γ_r and μ , can be determined instead of Γ_r . Since μ or some function solely of μ appears as a multiplier in the expression for τ_{\max} , it is possible to combine the two to form a geometry-specific wear coefficient, which can be used in design. This combined coefficient can be determined by the same methods that are used to determine Γ_r (75).

When the Zero Wear and Measurable Wear Models are combined, the zero wear criteria results in an explicit relationship between roughness and wear. When wear depth, h , is used as the measure of wear, this relationship is linear or close to linear,

$$h \propto \delta \quad (2.56)$$

where δ is the center line average of the rougher of the two surfaces. For example, such a dependency is shown in Eq. 2.54. Actual behavior tends to be somewhat different than this but experience indicates that it is a reasonable approximation for the range of surface roughness typically used in engineering. The experimentally determined dependency on the wear coefficient of a brass sphere sliding on a steel flat of various roughnesses is shown in Fig. 2.18 (76). It can be seen that for relatively smooth surfaces (i.e., $\delta < 20 \mu\text{in.}$), a linear relationship provides a reasonable approximation. However, for rougher surfaces, such a relationship tends to over-estimate the effect of surface roughness. This can be corrected by a modification to the theoretical relationship.* This involves the replacement of the approximately linear factor for δ in a relationship for wear depth by $(5.4 \delta^{0.3})$ (for $\mu\text{in.}$) for roughnesses greater than $10 \mu\text{in.}$

The Measurable Wear Model can be applied to situations involving the simultaneous wearing of two mated surfaces. Applying the measurable wear equations (Eqs. (2.36) and (2.37)) to both surfaces and solving the resultant set of differential equations does this. Because of the influence that the geometry of one body has on the wear of the other body, these equations are usually coupled and must be solved simultaneously. While this can be complex, this approach has been successfully used (54,66). The wear coefficients in these applications and their dependencies were determined experimentally.

Lubrication is generally a very significant factor in wear behavior and it is also a very significant factor in both the Zero Wear and the Measurable Wear Models. A lubricant can influence the values of Γ_r and τ_{\max} , as a result of its dependency on μ . Lubrication can also determine which wear mode associated with the tribosystem, that is, the constant energy or variable energy wear mode. Changes in these parameters associated with lubrication typically result in orders of magnitude changes in wear behavior. This is shown

*Another method has been proposed for correcting this relationship (76). A description of this alternate method and its application can be found in the case studies, Sec. 5.7.

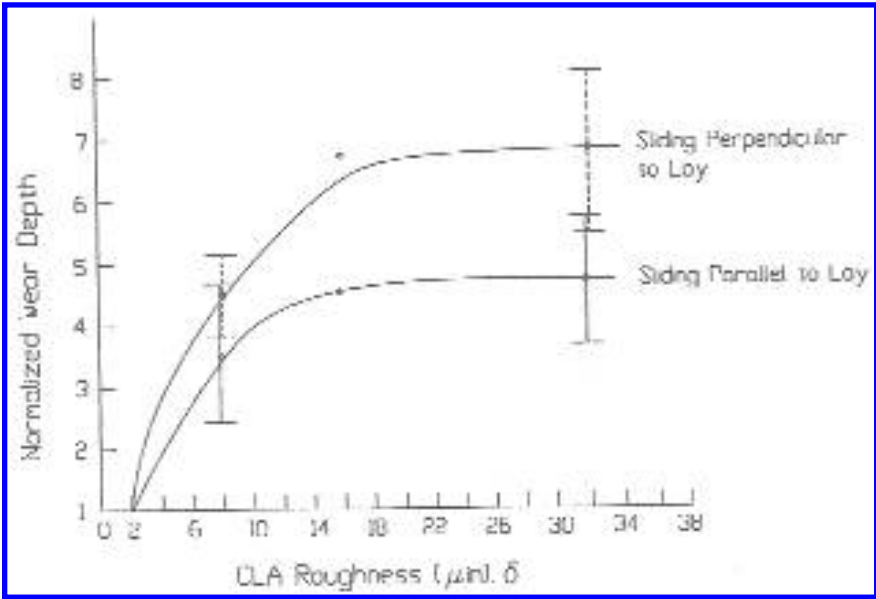


Figure 2.18 Wear depth as a function of surface roughness. (From Ref. 76.)

in Fig. 2.19, where the theoretical effects of such changes on two systems are illustrated. This behavior was experimentally confirmed by wear tests (61,77).

The value of the zero wear coefficient can be affected by the development of fluid films, that is, fluid or hydrodynamic lubrication as a result of reduced contact between the surfaces (78). This is shown in Fig. 2.20. In this figure, zero wear factors corresponding to different film thickness are plotted as a function of the lubrication thickness parameter, Λ . This is defined as

$$\Lambda = \frac{h}{(\delta_1^2 + \delta_2^2)^{1/2}} \quad (2.57)$$

where h is the thickness of the EHD (elastohydrodynamic) film. The δ 's are either the AA (arithmetic average) or the RMS (root mean square average) values for the surface roughness of the two surfaces. The model proposed for this relationship is described in Appendix VII. Its application in journal bearing situations is discussed in Sec. 2.8.

For most situations, integration of the measurable wear equations result in or can be approximated by a simple power relationship, which has the following form:

$$h = K S^n \quad (2.58)$$

With the use of the Zero Wear Model, the following forms can be obtained:

$$h = K \frac{S^n}{S_0^n} \quad (2.59)$$

$$h = K \tau_{\max}^n S^n \quad (2.60)$$

Values of n for a range of contact situations can be found in Appendix VI.

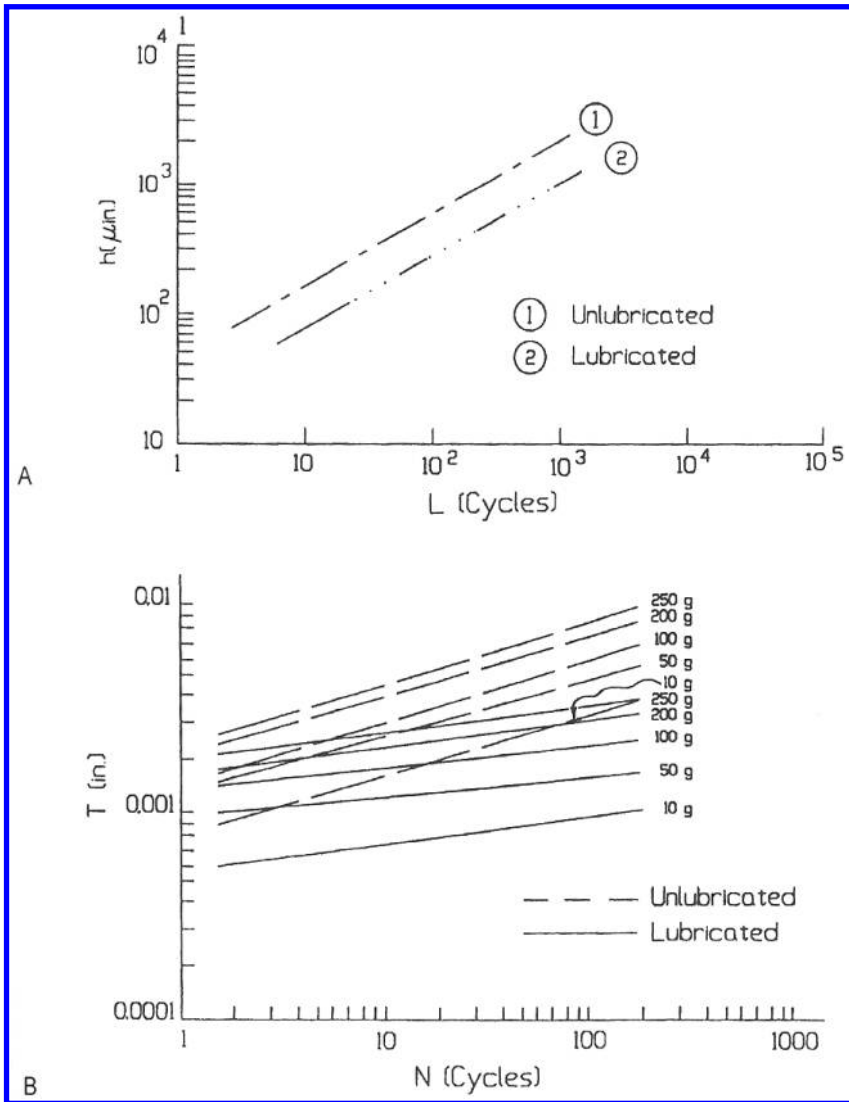


Figure 2.19 The effect of lubrication on wear behavior. “A” shows the effect in steel / ceramic system; “B”, in an Au / Au system. In the steel/ceramic system, the use of the lubricant only affected the ratio of Γ_r to t_{max} ; in the Au / Au system, it also changed the wear mode. (“A” from Ref. 77; “B” from Ref. 61.)

2.5. PERCUSSIVE IMPACT WEAR MODELS

Percussive impact wear refers to the wear generated by the repeated impacts between two surfaces or bodies. Studies of this type of wear have shown that the following expression can be used to describe wear behavior:

$$W = KV^n N \tag{2.61}$$

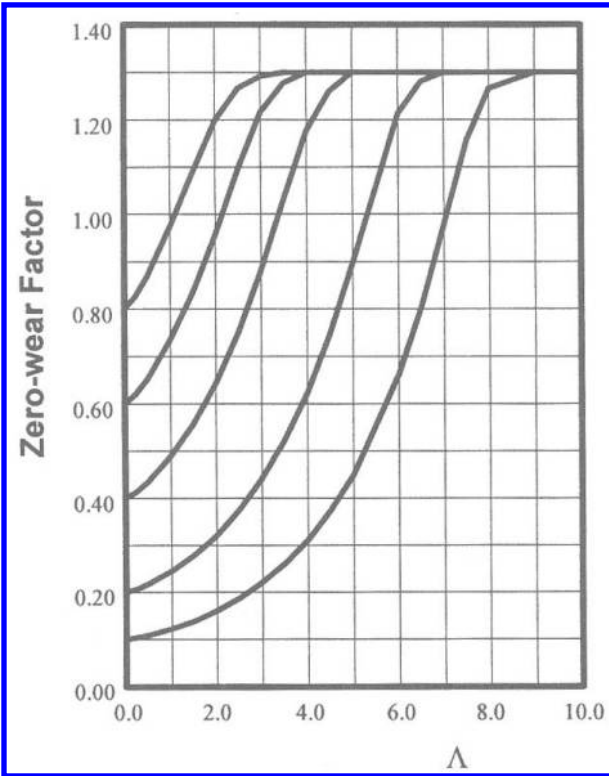


Figure 2.20 The effect of fluid lubrication film thickness on zero wear factors. Λ is the ratio of the film thickness to the composite roughness $(\sigma_1^2 + \sigma_2^2)^{1/2}$. The value of the zero wear factor at $\Lambda = 0$ is the value for boundary lubrication.

where W is the volume of wear; V , the impact velocity; N , the number of impacts (79). In this equation, K and n are empirical coefficients which can depend on geometry, mass, and material properties. While this is the case, the value of n is often found to be in the range of 2 or 3. In addition to this type of empirical model for percussive impact wear, there are two engineering models, similar to the Zero Wear Model and Measurable Wear Model for Sliding, which have been used to describe wear behavior under these conditions. One model is called the Zero Wear Model for Impact Wear and the other, the Measurable Wear Model for Impact Wear (80,81). The Zero Wear Model for Impact Wear is concerned with those conditions which result in the zero wear criteria being reached, while the Measurable Wear Model is concerned with the progression of wear. With both of these models, an underlying hypothesis is that the predominant mechanism for percussive impact wear is fatigue.

Both of these engineering models are formulated for compound impact situations, namely situations involving both impact and sliding. Pure impact situations are covered by these models as well, since they can be viewed as compound impact situations in which there is zero or negligible sliding. The zero wear equation for compound impact is

$$N_0 = \frac{2000}{1 + \beta} \left(\Gamma \frac{\sigma_1}{\sigma_0} \right)^9 \quad (2.62)$$

where N , is the number of impacts required for the zero wear criteria; σ_y , the tensile yield stress of the wearing material; σ_0 , the peak contact pressure during the impact; Γ_r' and β ; are system wear coefficients. This equation is valid only for elastic impact conditions, namely,

$$\sigma \leq \sigma_y \quad (2.63)$$

Γ_r' is referred to as the zero wear coefficient for impact and is dependent on the properties of the wearing material, β is dependent on the friction of the tribosystem and the amount of sliding that takes place during impact. It is defined as the ratio of the damage, D_2 , produced by the surface shear stress as a result of the sliding which may be present during the impact, to the damage, D_1 , produced by the subsurface shear stress, which is produced by the impact,

$$\beta = \frac{D_2}{D_1} \quad (2.64)$$

For impact situations in which there is no sliding, β is zero. β is called the surface damage factor for impact wear.

Like the zero wear coefficient for sliding, Γ_r' , is an empirical wear coefficient. It can be determined in the same manner as those used for determining Γ_r , with the exception that an impact wear test is used instead of a sliding wear test and that β must also be known. While impact wear test involving sliding can be used, pure or simple impact tests (i.e., those in which the sliding component is 0) are generally used. This is because such tests are easier to implement and β is equal to 0 under this condition. While Γ_r' can vary with materials, there is evidence that for design applications a value close to 1 can be assumed for most materials (82). There is both theoretical and experimental evidence, which suggests that such a single value may be used for most ductile materials. The theoretical considerations are based on an implied relationship between the zero wear models for impact and sliding.

The sliding model can be viewed as an extension of the impact model. This can be seen by noting that an impact situation, which involves a large amount of sliding, can also be viewed as a sliding situation in which the load varies with time. Furthermore, the assumptions of both models are similar, including the correlation between wear and stress and the predominance of fatigue and fatigue-like mechanisms in the wear process. Based on these observations, the Zero Wear Model for Sliding can be viewed as the limit of the Zero Wear Model for Impact as the amount of sliding during impact increases. As a consequence, a relationship between the two zero wear factors can be obtained. For a sphere wearing against a flat, it can be shown for this limiting condition that

$$\Gamma_r' = \frac{\Gamma_r \Phi}{0.31} \quad (2.65)$$

where Φ is the ratio between the yield point in shear, τ_y , and the yield point in tension, σ_y (80). For most ductile materials, $\Phi \approx 0.57$. Therefore,

$$\Gamma_r' = 1.84 \Gamma_r \quad (2.66)$$

This implies that there should be two predominate values for Γ_r' , 0.4 and 1, corresponding to the two predominate values of Γ_r . The lower would apply to systems which have a high tendency for transfer and the higher to systems which have a low tendency for transfer. Since transfer or adhesive wear phenomena generally have not been

found to be a major factor in percussive impact wear, Γ_R , should 0.54 for most materials under this limiting situation of compound impact wear (80,82). Consequently, it is implied that $\Gamma_R' \approx 1$ for most materials. Experimental data support this. (See Fig. 2.21.) In this figure the values of Γ_R' , determined from several different compound impact tests, are given for two different materials. These tests were unlubricated and the materials systems were known to have a Γ_R of 0.2. It can be seen that the average value for both materials is approximately the same, 1.2, which is slightly higher than the theoretical value of 1. Based on a larger database, it has been recommended that for design, a value of 1.1 be used for Γ_R' in lieu of actual experimental determination (82).

While Γ_R' appears to be a single value for most materials and independent to impact conditions, β is extremely dependent on the impact conditions that cause sliding or affect the amount of sliding, which occurs, β can take on values ranging from 0 to 10^5 , as shown in Table 2.4. The reason for this range can be related to the nature of compound impacts and the effects that various aspects can have on the relative amount of damage associated with surface stresses to the amount of damage associated with subsurface stresses.

In compound impact situations, there can be significant surface shear stresses as a result of the relative sliding that takes place at the interface. The model assumes that the damage that is associated with the surface shear stress is not only a function of its magnitude but the amount of sliding that takes place. The amount of sliding that takes place in compound impact situations can be related to a parameter of the system called the slip factor, f . For the general situation of a mass striking a surface (Fig. 2.22) f is defined as

$$f \equiv \frac{(\pi m \nu) / (\mu P_0 t')}{1 + (m L^2 / I_{cx})} \quad (2.67)$$

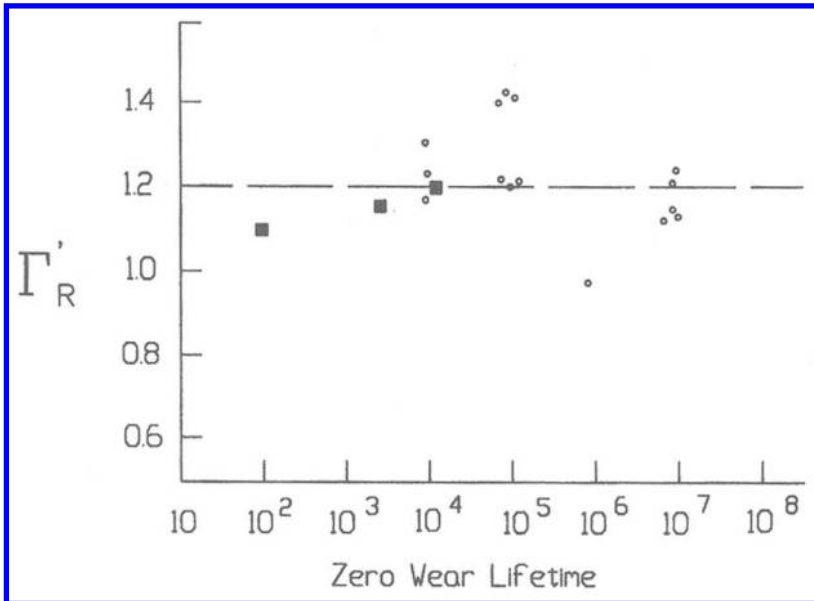


Figure 2.21 Experimentally determined values of Γ_R' for two unlubricated metal pairs. (From Ref. 80.)

Table 2.4 Damage Contribution Factor, β , for Various Conditions of Elastic Impact

	Normal impact		Compound impact
	Without fretting motions	With fretting motions	
Dry	$\beta \approx 0$	$0 < \beta \leq 10$	$0 < \beta \leq 10^8$
Lubricated (boundary)	$\beta \approx 0$	$\beta \approx 0$	$0 < \beta \leq 10^8$ ($\beta \approx 0$ possible with high viscosity lubricants)

Source: Ref. 144.

where m is the impacting mass; v , the relative tangential velocity between the two surfaces prior to the impact; μ , the coefficient of friction for the two surfaces; P_0 , the peak impact force; t^* , the duration of the impact or contact time; L , the distance of the impactor's center of gravity from the impact point; and I_{CG} , the moment of inertia of the impactor about its center of gravity. If the impactor is not free to rotate, I_{CG} is infinite and the expression for f reduces to

$$f \equiv \frac{\pi m v}{\mu P_0 t^*} \tag{2.68}$$

As f increases, the amount of sliding that takes place during the impact increases. However, because of the friction between the two surfaces, the relative tangential velocity will decrease during the impact. For values of f below a critical value, f_c , sliding will stop during the impact and the two surfaces will adhere (i.e., the relative tangential velocity goes to 0). f_c is dependent on the shape of the impact pulse and on the stiffness of the system and is typically less than π . For values of $f < f_c$, the portion of the contact time for which sliding takes place increases with increasing values of f . The exact relationship between the duration of the slip period, t' , and the slip factor has been developed for the

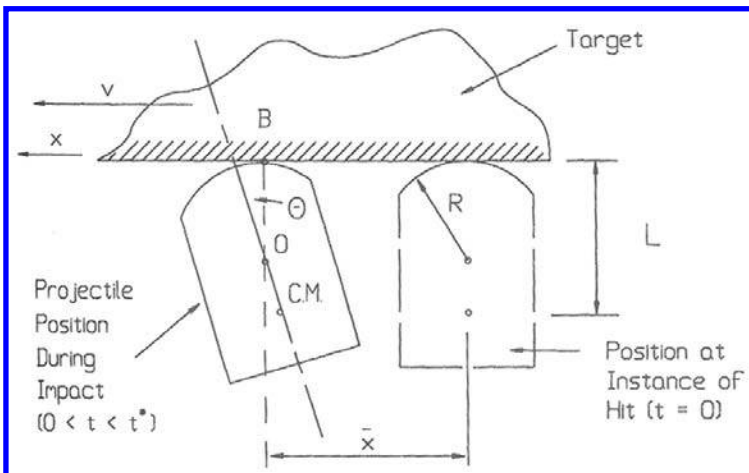


Figure 2.22 Compound impact situation between a projectile and a surface. (From Ref. 82.)

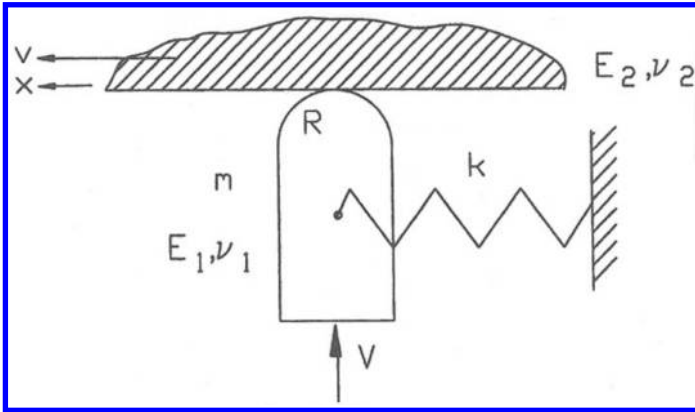


Figure 2.23 Spring-restrained projectile impacting a moving infinite mass. (From Ref. 82.)

case of a sinusoidal-shaped impact pulse and an impactor constrained by spring as illustrated in Fig. 2.23. In this case

$$P(t) = P_0 \sin \frac{\pi t}{t^*} \quad (2.69)$$

and the relationship between f and t'' is given by the solutions of the following equation:

$$\cos w t'' - \cos \phi t'' - f [1 - (w/\phi)^2] = 0 \quad (2.70)$$

where

$$w \equiv \left(\frac{k}{m} \right)^{1/2} \quad (2.71)$$

$$w/\phi \equiv \frac{\pi}{t^*} \quad (2.72)$$

k is the stiffness of the spring constraint. The solutions of this equation are graphically shown in Fig. 2.24 for several values of w/ϕ . In these graphs f' is the value of f at which $t''/t^* = 1$. For values of impact situations with values of f above f' , sliding takes place during the entire contact. By comparison of Eqs. (2.67) and (2.68), it can be seen that rotation reduces f and therefore tends to reduce the amount of sliding that takes place during an impact.

The model assumes that the rate of damage, \mathbf{D} , associated the shear stress system is proportional to the ninth power of the stress,

$$\mathbf{D} \propto \tau^9 \quad (2.73)$$

If D_1 is the damage associated with the subsurface shear and D_2 , the damage associated with the surface shear, β in Eq. (2.62) is defined as

$$\beta = \frac{D_2}{D_1} \quad (2.74)$$

Letting q_0 be the maximum contact pressure at any time during the impact, the subsurface shear stress is defined as $0.31q_0$ and the surface shear stress as μq_0 . For $f \leq f'$,

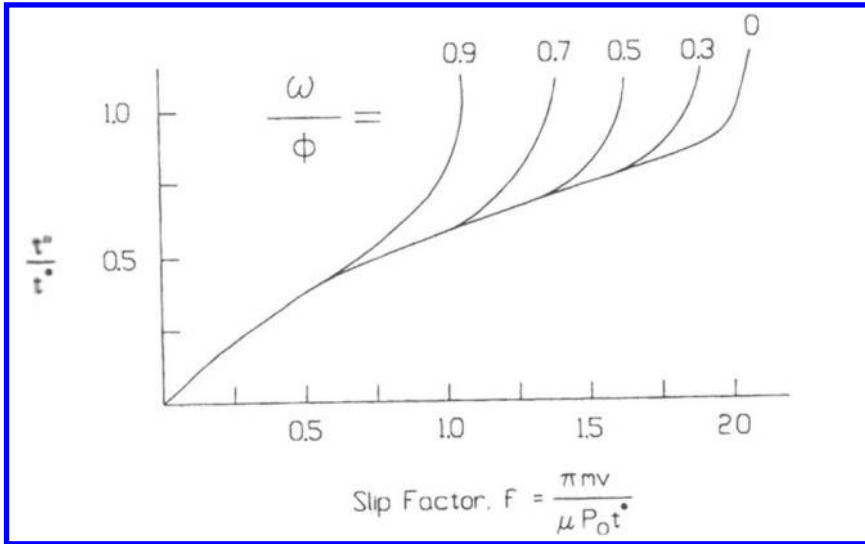


Figure 2.24 Relationship between slip factor and slip time for system shown in Fig. 2.23. (From Ref. 82.)

sliding only occurs until t equals t'' . Therefore, for $f \leq f'$ the following expression for β is obtained:

$$\beta = \frac{\int_0^{t''} (\mu q_0)^y dt}{\int_0^{t''} (0.31 q_0)^y dt} \tag{2.75}$$

For $f > f'$, β is modified to the following:

$$\beta = \frac{v \int_0^{t''} \tau_2^y dt}{v' \int_0^{t''} \tau_1^y dt} \tag{2.76}$$

where v' is the velocity which corresponds to f' . Physically, this is the maximum sliding velocity which would result in adherence by the end of the contact time. The ratio of v / v' which is equivalent to f / f' , is introduced to account for the increased amount of sliding that takes place during the impact when the velocity is above v' .

If a sinusoidal approximation is used for the impulse (Eq. (2.69)), the expressions for β are as follows:

$$\beta = 4.65 \times 10^4 \mu^y \int_0^{\arccos 1/f'} \sin^y \Phi d\Phi, \quad f \leq f' \tag{2.77}$$

$$\beta = 3.78 \times 10^4 \mu^y \frac{f}{f'}, \quad f \geq f' \tag{2.78}$$

The high order dependency on μ , the coefficient of friction, is the primary reason for the large range of values possible for β . For a coefficient of friction change from 0.1 to 1, β changes by a factor of 10^9 . Increased sliding speeds can also increase β , but the effect is much less pronounced than that associated with a change in friction. Because of the strong influence of friction, higher sliding speeds can lead to the reduction of β under lubricated

conditions. For lubricated conditions, higher sliding speeds can result in hydrodynamic lubrication, which significantly reduces friction (e.g., < 0.1). When this happens, β is approximately 0 and the wear performance is greatly enhanced.

The development and formulation of the Measurable Wear Model for Impact is very similar to that for sliding (81). The major difference is that the concept of a pass is not needed and it is replaced by the concept of a single impact. The model assumes that for elastic conditions the progression of wear in a compound impact wear situation is a function of the amount of energy going into wear and the number of impacts. This can be expressed in the following manner:

$$dW = W_e dE + W_n dN \quad (2.79)$$

where W is the amount of wear; W_e and W_n are the partial derivatives with respect to the energy going into wear per impact, E , and number of impacts, N , respectively. The model also proposes two types of wear modes, a constant energy mode and a variable energy mode. For the constant energy wear mode, $W_e = 0$. As with sliding, the zero wear relationship is interpreted as resulting from the integration of this differential equation and is used to infer the form of the partial derivatives. The following equation for measurable impact wear was developed in this manner:

$$dW = \frac{W}{N} dN + g \frac{9W}{\sigma} d\sigma \quad (2.80)$$

σ is the contact pressure, g is 1 for the variable energy mode and 0 for the constant energy mode.

To integrate this equation when $g = 1$, a relationship between some parameter associated with the shape and size of the wear scar and stress is needed. The development of such a relationship requires some information regarding the nature of the contact configuration in the worn state. The fact that sliding wear produces a conforming contact between the two surfaces is used to develop such a relationship in the case of sliding. However, this situation is different and the assumption of conformity cannot be used. In the case of impact wear, experimental data show that while conformity is approached with wear, conformity is never actually achieved. Profilometer traces through progressive impact wear scars show this changing nature of the contact (Fig. 2.25). Formally, this behavior is called *The Principle of Variable Curvature for Impact Wear* and is stated as: Impact wear proceeds with continuously changing curvature on the softer (wearing) body, toward conformity with the shape of the harder (unwearing) body, with the current worn area coinciding with current peak contact area. This principle is also a factor in the integration of Eq. (2.80) when $g = 0$. In this case, the integration is simple and results in the following linear relationship:

$$W = KN \quad (2.81)$$

However, since the assumption of conformity cannot be used, the shape of the wear scar is unknown and this cannot be reduced to a relationship for wear depth or scar width. As a result, it is even necessary in this case to use the more general approach, which involves applying the variable curvature principal principle, to determine the shape of the wear scar and develop relationships for depth or width.

To utilize the variable curvature principle in the integration of Eq. (2.80), a non-dimensional curvature parameter, Γ , is introduced and used to describe both the wear

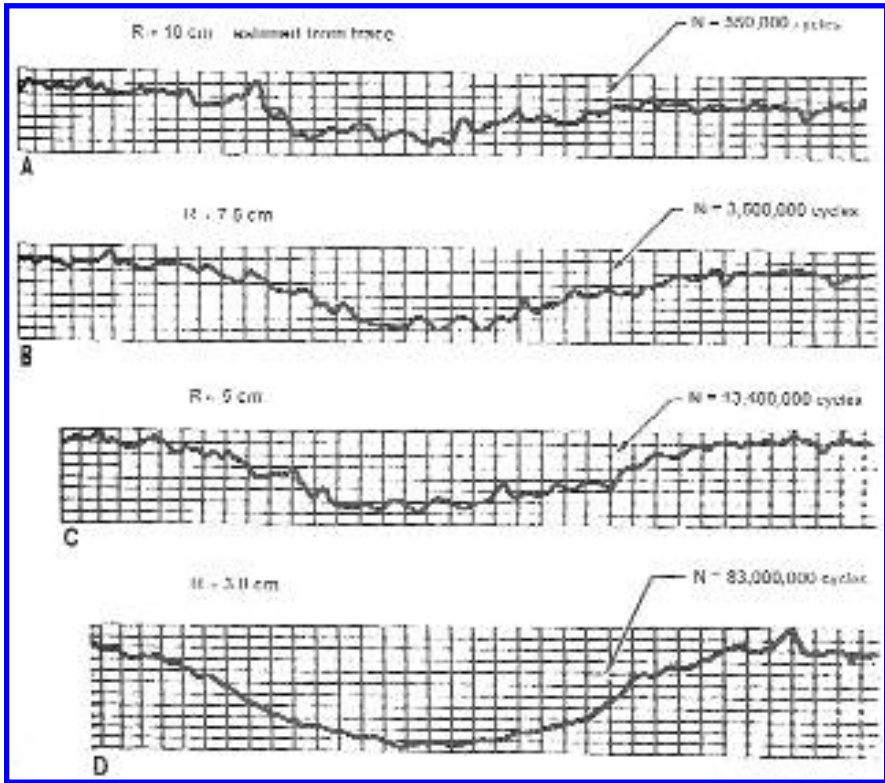


Figure 2.25 Profilometer traces of impact wear scars and the radius of the crater produced on a flat by a cylindrical hammer (3.5 cm radius). As the number of impacts increases, the radius of the crater approaches that of the hammer. (From Ref. 82, reprinted with permission from Elsevier Science Publishers.)

and the stress (81,83). For example, in the case of a hard sphere wearing a softer plane (Fig. 2.26), Γ is defined as the ratio of the radius of the sphere, R_1 , to the radius of the wear scar, R . Since the surface is initially flat (R infinite) and the wear scar is concave (R is negative), Γ goes from 0 to -1 as wear progresses. In the case of a soft sphere being worn against a hard flat (Fig. 2.27), the relationship for Γ is different. In this case, Γ is defined as the ratio of the initial radius of the sphere, R_1 , to the worn radius of the sphere, R , and goes from 1 to 0, as wear increases.

In order to illustrate this approach further, its application to the case of a hard sphere wearing a soft flat in the variable energy mode (i.e., $g = 1$) will be considered in greater detail. In this case, it can be shown that the peak contact stress predicted by the Hertz impact theory is related to Γ by the following equation:

$$\sigma = K_f(1 + \Gamma)^{3/5} \tag{2.82}$$

where

$$K_f = 0.126(E_f^4 V^2 m R_1^3)^{1/5} \tag{2.83}$$

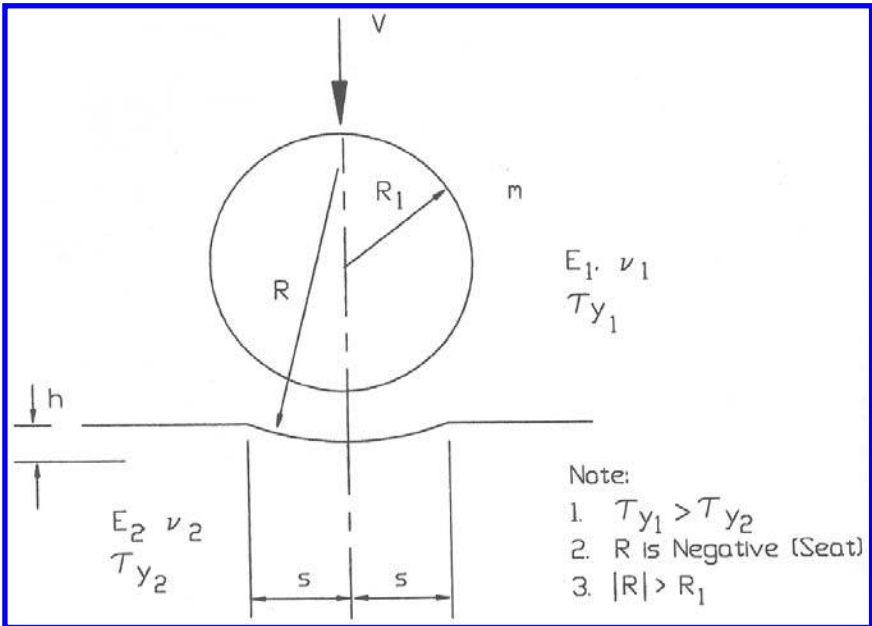


Figure 2.26 Impact wear of a soft plane by a hard sphere.

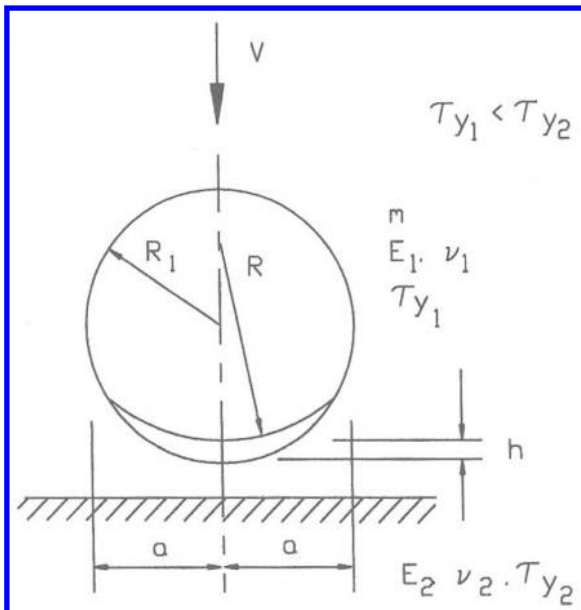


Figure 2.27 Impact wear of a soft sphere by a hard plane.

In this equation, E_r is the reduced modulus for the material pair; V , the impact velocity; and m is the mass of the sphere. By means of the same theory, the radius of the contact area corresponding to the peak stress can also be related to Γ . The equation for this is

$$a_0 = K_2(1 + \Gamma)^{-2/5} \quad (2.84)$$

where

$$K_2 = 1.24(E_r^{-1} V^2 m R_1^2)^{1/5} \quad (2.85)$$

By examination of equations (2.82) and (2.84), it can be seen that as wear progresses, σ decreases and a_0 increases. By consideration of the geometry of the wear scar, the wear, W , can also be expressed in terms of Γ . Since the shape of the wear scar is a paraboloid of base a_0 and meridional radius of curvature, R , and noting that the wear scar is concave

$$W = -\frac{\pi a_0^4}{4R} \quad (2.86)$$

The corresponding depth of the wear scar is

$$h = -\frac{a_0^2}{2R} \quad (2.87)$$

Substituting for a_0 ,

$$W = -\frac{\pi K_2^4 \Gamma (1 + \Gamma)^{-8/5}}{4R_1} \quad (2.88)$$

$$h = -C_s \Gamma (1 + \Gamma)^{-4/5} \quad (2.89)$$

where

$$C_s = 0.77(V^4 m^2 E_r^{-2} R_1^{-1})^{1/5} \quad (2.90)$$

C_s is referred to as a stress severity factor.

When these are substituted into Eq. (2.80), the following differential equation, describing the progression of wear, is obtained:

$$\frac{dN}{N} = \frac{1 - 6\Gamma}{\Gamma(1 + \Gamma)} d\Gamma \quad (2.91)$$

The solution of this equation can be shown to be

$$N = N_0 \frac{\Gamma/\Gamma_0}{[(1 + \Gamma)/(1 + \Gamma_0)]^7} \quad (2.92)$$

where N_0 and Γ_0 are reference values. Γ_0 is the values of Γ after N_0 . The relationship between the number of impacts and the depth of wear can be numerically determined by means of this equation and Eq. (2.89).

The values of N_0 and Γ_0 can be determined empirically by measuring the depth of wear after a certain number of impacts and using Eq. (2.89) to convert this depth to Γ_0 (83). The zero wear relationship can also be used to determine their values. When this approach is used, they can be thought of as initial conditions. In this case, N_0 is the

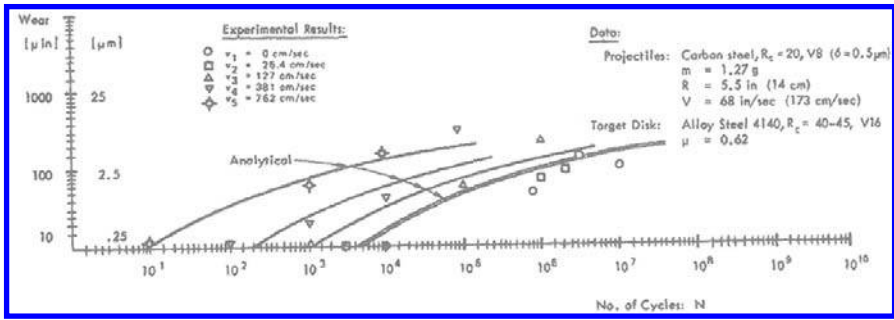


Figure 2.28 Example of the general shape of wear curves obtained by solving the measurable wear relations for impact, showing the agreement with observed behavior. (From Ref. 82.)

zero wear lifetime as given by Eq. (2.62). Γ_0 is then determined from Eq. (2.89), using the definition of the zero wear criteria (Eq. 2.17), namely, $h = 2\delta$, where δ is the CLA or RA roughness of the surface (81).

The determination of the wear mode for a given system (i.e., $g = 1$ or 0) must be done empirically, as is the case with sliding. However, in the case of impact wear, the variable energy mode ($g = 1$) appears to predominate. In general, it has been found that this model gives good agreement with observed behavior (84). However, there are exceptions. This model does not agree with behavior observed with unlubricated impact situations in which severe fretting occurs (85). The model also does not agree with the wear behavior found with elastomers (86). An example of the general shape of impact wear curves and agreement with this model is shown in Fig. 2.28.

To account for the wear behavior observed in these unlubricated fretting situations, a more general form of the Measurable Wear Model was proposed. For this model, a general power relationship between wear and stress was assumed, that is, wear proportional to σ^n , not simply σ^9 . In effect this results in one more empirical factor, n , that needs to be determined. This more general model has been applied to various impact conditions involving spheres and cylinders (84). The differential equations and their solutions for these conditions are summarized in Table 2.5. While the wear behavior of most systems corresponds to a value of 9 for n and generally a value of 1 for g , wear behavior in unlubricated impact involving severe fretting wear behavior was found to correspond to $n = 3$ and $g = 0$ (85). This is shown in Fig. 2.29. The contact geometry in this test was a hard sphere against a softer flat. Because stress is proportional to the cube root of the load in Hertzian contacts, this result suggests that wear is proportional to load in this situation, rather than stress. As a result, the mode of impact wear characterized by these values of n and g is sometimes referred to the load-dependent mode and the more typical mode as the stress-dependent mode (87). It is hypothesized that the load-dependent mode is the result of abrasive wear behavior associated with fretting.

For reference, some general relationships for impact load, contact pressure, and impact areas are given in Table 2.6 for elastic ballistic impact.

The following model, which takes into account the unique nature of elastomer, has been found to agree with the observed impact wear behavior of elastomers (86).

With elastomers, two modes of impact wear have been identified (86). In one mode, the material deforms without material loss and the deformation is progressive but

Table 2.5 Solutions of the Impact Measurable Wear Equation

Non-conforming Geometries	
Hard shape/soft plane	Soft shape/hard plane
Variable curvature ration, Γ (R_1 , radius of hard shape; R , radius of wear shaper)	
$\Gamma = R_1/R, 0 > \Gamma > -1$	$\Gamma = R/R, 1 > \Gamma > 0$
Form of the differential equation (B, D, and E constants)	
$\frac{1 - B\Gamma}{\Gamma(1 + \Gamma)} d\Gamma = dN/N$	$\frac{D\Gamma - E}{\Gamma(1 - \Gamma)} d\Gamma = dN/N$
Initial conditions	
$\Gamma = \Gamma_0$ at $N = N_0$	$\Gamma = \Gamma_0$ at $N = N_0$
Form of solution	
$N = \frac{N_0(\Gamma - \Gamma_0)}{[(1 + \Gamma)/(1 - \Gamma_0)]^{1/B}}$	$N = N_0 \frac{(1 - \Gamma)/(1 - \Gamma_0)^{D/E}}{(\Gamma - \Gamma_0)^{D/E}}$
Hard sphere/soft plane	
$B = (3/5)(1 + gn)$	$D = (3/5)(1 + gn), E = (1/5)(8 + 3gn)$
$h = -C_s \Gamma(1 + \Gamma)^{-4.5}$	$h = C_s(1 - \Gamma)\Gamma^{-4.5}$
Hard cylinder/soft plane	
$B = (1/2)(1 + gn)$	$D = (3/5)(1 + gn), E = (1/2)(3 + gn)$
$h = -C_c \Gamma(1 + \Gamma)^{-1}$	$h = C_c(1 - \Gamma)\Gamma$
$C_s = 0.77 [v^4 m^2 E_t^{-2} R_1^{-1.5}]$	$C_c = 2\pi \left[\frac{vm}{E_t t W} \right]$
Conforming surfaces	
$h = h_0 \frac{N}{N_0}$	

h, wear depth; *N*, number of impacts; *g* = 1, variable energy mode; *g* = 0, constant energy mode; wear \propto stress^{*n*} (See Table 2.6 for definition of symbols)

asymptotically approaches a limit. The second mode involves material loss and is the result of fatigue. The deformation mode predominates in the initial stages of impact wear, while the fatigue mode predominates in the latter stages. The behavior and superposition of these two modes are graphically illustrated in Fig. 2.30. Another unique feature of elastomers in impact situations is that, when unconstrained, they tend to flow until a characteristic pressure is achieved, independent of the severity of the impact or the geometries involved (88). When this flow is constrained, the stress level increases. This concept is shown in Fig. 2.31 for an elastomer layer or slab on a rigid substrate. For a fixed impact condition, the stress level will remain constant as a function of thickness until a critical thickness. At this point, the deformation is large enough in comparison to the thickness, so that substrate begins to influence the flow and stress level in the elastomer. Conditions, which result in this increased stress level in the elastomer, are referred to as over-stressed conditions and result in degraded and often catastrophic wear behavior (88,89). There are large cracks formed in this region of the material and there is often evidence of thermal degradation. The wear rates under these conditions are generally too high for most engineering applications. Examples of the surface topography for the three wear modes are shown in Fig. 2.32.

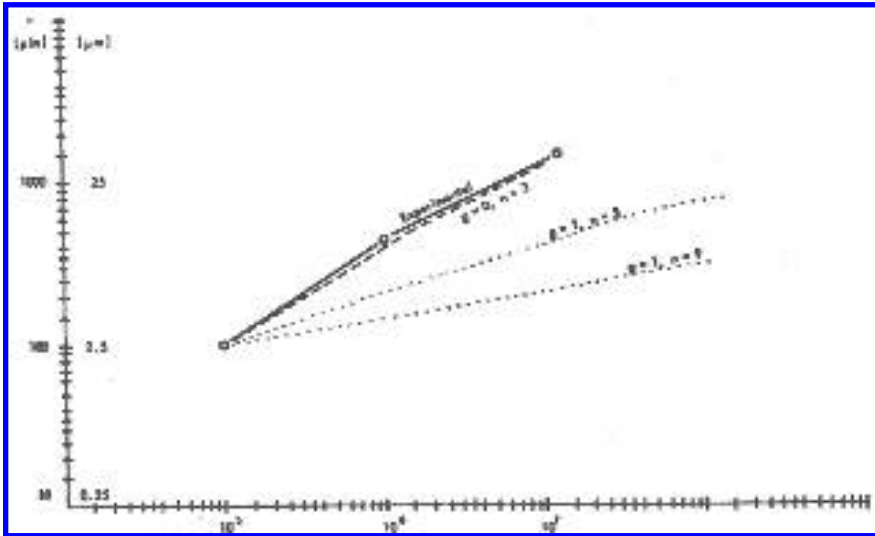


Figure 2.29 Wear curve for an impact wear situation between a hard steel hammer and a softer steel plate in which there was fretting. Integration of the measurable wear equations for impact, assuming different values of g and n , resulted in the dashed Scurves. (From Ref. 82.)

The expressions for the impact wear of elastomers, based on these considerations, are

$$h = \alpha_0 T \left(\frac{P}{A_a} \right) e^{-\beta/N} + \frac{\mathbf{h}(P/A_a)PN}{\sigma_f}, \quad P \leq P_c \quad (2.93)$$

$$h = \alpha_0 T \sigma e^{-\beta/N} + \mathbf{h} \left(\frac{\pi \sigma}{\sigma_f} \right)^{10} N, \quad P \geq P_c \quad (2.94)$$

In these expressions, h is the depth of wear of the elastomer, α_0 and β are material parameters describing the deformation mode, P is the peak impact force, σ_f is the flow pressure of the elastomer, T is the thickness of the elastomer, A_a is the apparent area of contact, N is the number of impacts, \mathbf{h} is a characteristic wear rate of the elastomer, σ is the contact stress in the over-stress region, and P_c is the peak impact force corresponding to the onset of the over-stressed condition (86). Since Eq. (2.94) applies to a region of wear behavior that is generally unacceptable, Eq. (2.93) is of more engineering significance. The high exponential dependency on stress in Eq. (2.94) indicates the rapid rise in wear that occurs in the over-stressed region.

The set of coefficients, α_0 , β , \mathbf{h} , and σ_f are wear parameters, which need to be determined experimentally. They are characteristic values of a material and need only be determined once. However, wear curves (i.e., h vs. N) for several different conditions are needed to provide a sufficient number of equations to solve for their values. Test conditions, which are below the over-stressed condition, should be used for these tests. In this range, the deformation mode tends to predominate for $< 10^6$ impacts. Consequently, impact wear tests into the range of 10^7 or more impacts are generally required for these determinations.

This impact wear model for elastomers is primarily for impact situations which do not involve sliding but it can be extended to some compound impact situations. With

Table 2.6 Contact Relationships for Elastic Impact

Between spheres

$$P_0 = 0.407[v^6 m^3 R_1 E_r^2 (1 - \rho)^{-1}]^{1/5}$$

$$t_c = 4.525[v^{-1} m^2 R_1^{-1} E_r^{-2} (1 + \rho)]^{1/5}$$

$$\sigma_0 = 0.1258[v^2 m R_1^{-3} E_r^4]^{1/5} (1 + \rho)^{3/5}$$

$$a_0 = 1.2411[v^2 m R_1^2 E_r^{-1}]^{1/5} (1 + \rho)^{-2/5}$$

Between parallel cylinders

$$P_0 = \frac{\pi m v}{t_c}$$

$$\sigma_0 = \frac{1}{\pi} \left[\frac{P_0 E_r}{W R_1} \right]^{1/2} (1 + \rho)^{1/2}$$

$$b_0 = 4 \left[\frac{P R_1}{W E_r} \right]^{1/2} (1 + \rho)^{-1/2}$$

General impact

$$P_0 \approx \frac{\pi m v}{t_c}$$

$$\sigma_0 = \frac{P_0}{A_0}$$

$$\rho = R_1/R_2 \quad E_r = \left(\frac{1 - \nu_1^2}{\pi E_1} + \frac{1 - \nu_2^2}{\pi E_2} \right)^{-1} \quad m = \left(\frac{1}{m_1} + \frac{1}{m_2} \right)^{-1}$$

t_c are determined empirically or by finite element modeling in the relationships for parallel cylinders and general impact.

P_0 , peak impact force; t_c , contact time; v , impact velocity (normal to surface); m , reduced mass; R 's, radii; E_r , reduced modulus; E 's, Young's moduli; ν 's, Poisson's ratios; σ_0 , peak maximum contact pressure; a_0 , radius of contact area at peak; b_0 , width of contact at peak; W , length of shorter cylinder; A_0 , apparent contact area at peak.

elastomers, sliding during impact generally results in significant increases in the amount of wear and tends to modify the nature of the wear. Temperature rises at the interface because of sliding can often lead to catastrophic wear behavior. While this is the case, a certain amount of tangential relative velocity can often be tolerated in impacts before significant changes in wear behavior occur. This is because of the ability of the elastomer to experience a large degree of deformation prior to slip or the onset of sliding in these impact situations. As a consequence of this, the model can be applied to compound impact situations which result in only deformation or moderate sliding. To do this, \mathbf{h} needs to be considered as a function of the compound impact conditions, as well as of the material. Consequently, \mathbf{h} needs to be determined from impact tests which simulate the application.

2.6. MODEL FOR ROLLING WEAR

A model for rolling contact wear situations has been developed that is very similar to the zero wear models for sliding and impact wear (90–94). The similarity between these models will become apparent as the various aspects of the model for rolling are discussed and these similarities identified.

The model for rolling wear between cylinders is based on the observed correlation between stress and the onset of macro-surface deterioration, which is characterized by

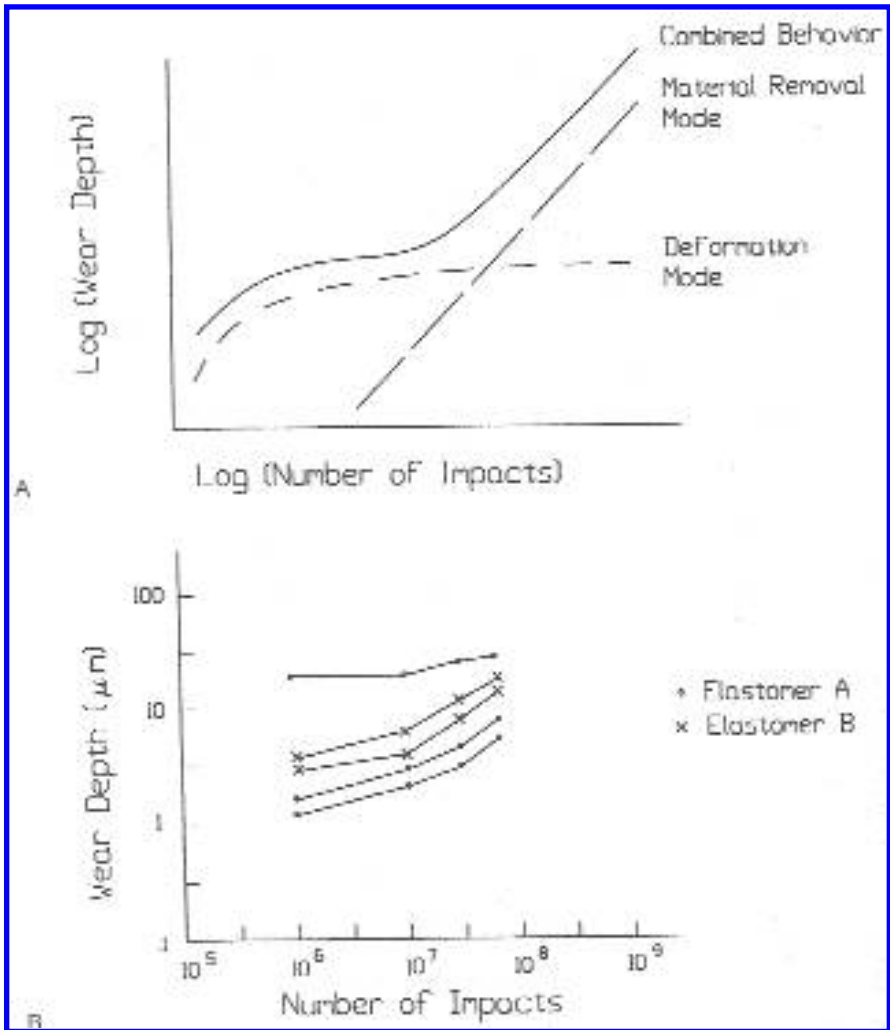


Figure 2.30 Impact wear curves for elastomers. “A” shows the behavior of the two modes involved and the general shape of the curves. In “B”, wear curves for two different elastomers, obtained for different impact conditions, are shown. (From Ref. 86.)

the sudden appearance of cracks, spalls, or pits on the surface. In the case of materials, which exhibit a tendency to creep, the onset of surface deterioration can be associated with the sudden occurrence of macro-flow of the material. This is often the case with polymers. For both pure rolling and rolling with sliding (e.g., slip), the general form of the relationship between maximum contact stress, σ , and the number of revolutions, N , required for the onset of this level of surface deterioration, is

$$N_1 \times \sigma_1^m = N_2 \times \sigma_2^m \quad (2.95)$$

where m is typically significantly greater than 1. This form and the general character of the surface deterioration that is characteristic of rolling wear indicate the predominance of a

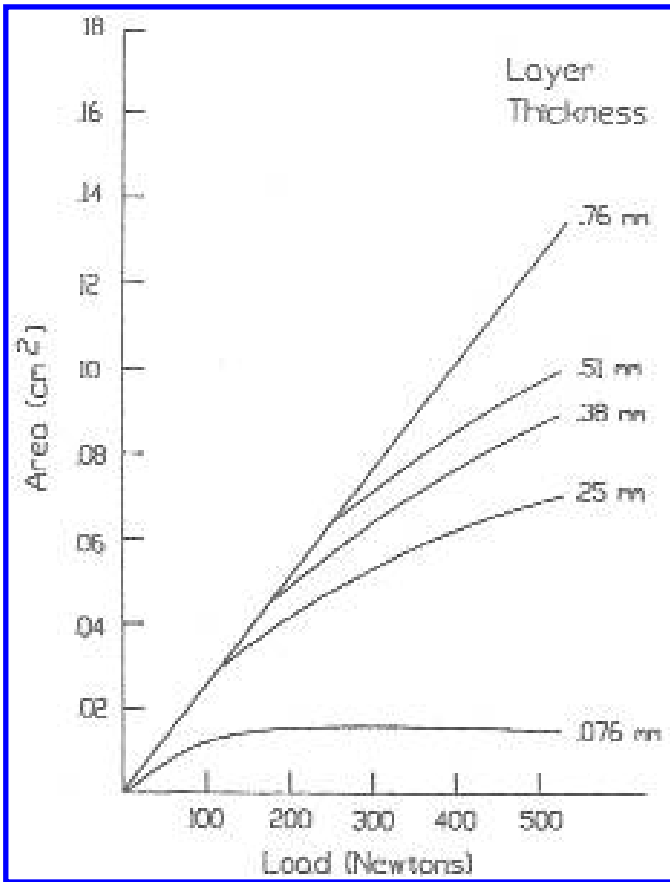


Figure 2.31 Relationship between contact area and peak impact load as a function of elastomer thickness. (From Ref. 86.)

fatigue wear mechanism under these conditions. The similarity between this and the ninth power relationships of the zero wear models for sliding and impact (i.e., Eqs. (2.18) and (2.62)) and their common association with fatigue and repeated-cycle deformation wear is evident.

While the zero wear models use this type of expression explicitly, the rolling wear model is formulated in terms of a load-stress factor, K_f , which is related to the stress but also includes material parameters. The formulation of this model can be developed from Eq. (2.95) as follows.

For parallel cylinders, the contact stress is given by the following equation:

$$\sigma = \frac{P^{1/2}(1/R_1 + R_2)^{1/2}}{\pi L^{1/2}(k_1 + k_2)^{1/2}} \tag{2.96}$$

$$k_{1,2} = \frac{1 - \nu_{1,2}^2}{E_{1,2}} \tag{2.97}$$

where P is the load, L is the width of the smaller cylinder, R_1 and R_2 are the radii of the two cylinders, and ν and E are Poisson’s ratio and Young’s modulus, respectively, of the

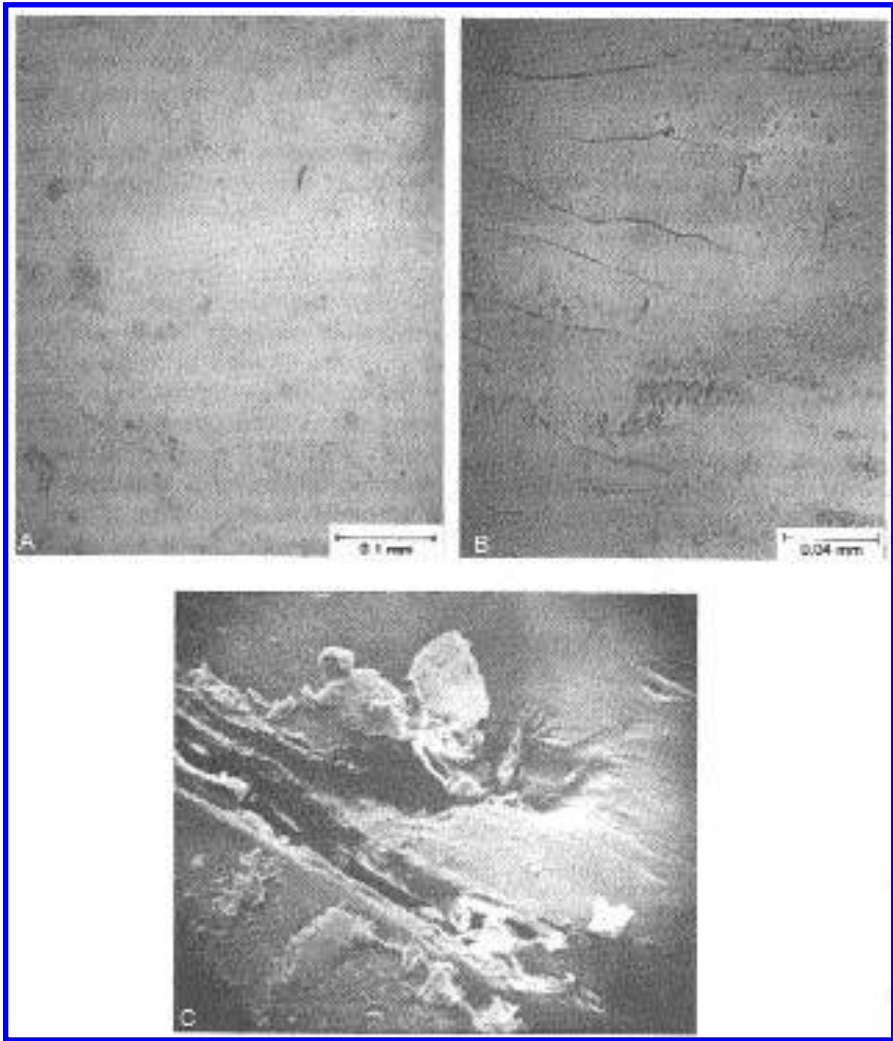


Figure 2.32 Morphology associated with the different modes of elastomer wear behavior. “A”, deformation; “B”, surface fatigue; and “C”, overstressed. (“A” and “B” from Ref. 86, reprinted with permission from Elsevier Sequoia S.A.; “C” from Ref. 147, reprinted with permission from ASME.)

two cylinders. Solving for P , the following results:

$$P = \sigma^2 \pi (k_1 + k_2) \frac{L}{1/R_1 + 1/R_2} \quad (2.98)$$

Since the stress level for the onset of surface deterioration is a function of the materials involved, σ and the k term can be combined into a single material coefficient, K_I , which is called the load-stress factor, namely,

$$K_I = \sigma_s^2 \pi (k_1 + k_2) \quad (2.99)$$

where σ_s is the stress at which the onset of surface deterioration occurs in N revolutions. The corresponding load for that number of revolution, which is called the endurance load, P_e , is

$$P_e = K_I \frac{L}{1/R_1 + 1/R_2} \tag{2.100}$$

Consequently, it can be seen that if K_I is known for a given pair of materials, the allowed load for any size rollers of those materials can be determined.

To obtain values of K_I for different numbers of revolutions, Eq. (2.95) is used but in an altered form. An equivalent form of this relationship in which σ is replaced by K_I is

$$\log K_I = \frac{B - \log N}{A} \tag{2.101}$$

where A and B are empirical coefficients. In this model, A and B are dependent on the material pairs, surface conditions, and the amount of slip but are independent of the load and size of the rollers. A and B are determined by performing rolling wear tests, using an apparatus similar to that discussed in Sec. 9.2 of MWFT2E and determining the number of revolutions at which surface deterioration occurs. A minimum of two tests at different loads for each combination of materials, surface conditions, and slip are required. B and A are determined by fitting Eq. (2.101) to the data. Once these values are obtained, Eqs. (2.100) and (2.101) can be used to determine a safe load for a given number of operations or appropriate roller size for a given load and life requirement.

Several graphical examples of the relationship between K_I and N are shown in Fig. 2.33 for different materials and rolling conditions. It should be recognized that since

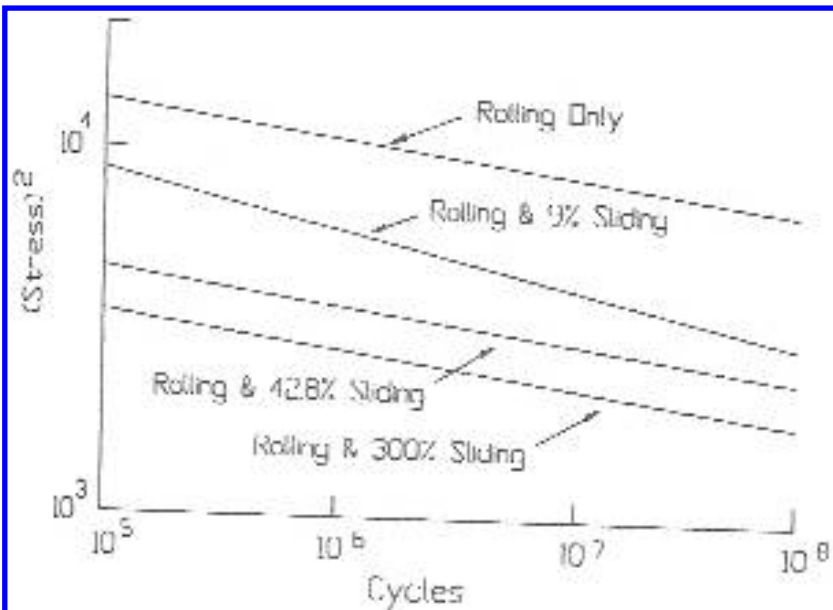


Figure 2.33 Examples of rolling load / life curves for two self-mated materials. (From Ref. 90.)

these curves are not parallel, both A and B can vary as a function of rolling conditions. It also implies that the exponent in Eq. (2.95) is a function of materials and rolling conditions. While this is the case, these curves indicate a general trend. Slip or sliding tends to reduce K_I . The degree of sliding or slip in a rolling contact is often expressed as % sliding, where

$$\% \text{ sliding} = 100\% \times \frac{2|V_1 - V_2|}{V_1 + V_2} \quad (2.102)$$

The V 's are the surface velocities of the two rollers. Higher percentages indicate higher amounts of slip or sliding in the contact zone. Except in situations where higher speeds or velocity result in significant temperature increases, A and B are typically independent of speed or velocity, per se, even though they are dependent on % sliding.

Values of A and B for a number of material pairs for two different rolling conditions, pure rolling and rolling with 9% sliding, are given in Table 2.7. Values of K_I for 10^8 revolutions are also given for reference. The data in this table indicate that there is considerable variability in the values of A and B and does not suggest any significant trends for these two parameters. Values of K_I on the other hand indicate two trends; one is the trend regarding % sliding, discussed previously and the other is that K_I tends to increase with hardness. However, as can be seen in the data, there are exceptions to this rule.

The formulation of the model assumes uniform loading across the contact (i.e., no stress concentration point as a result of alignment or edge conditions). Since the basis of the model is the strong sensitivity of wear to stress, the occurrence of such stress risers in a rolling contact can significantly reduce values for K_I . Consequently, it is desirable in both the tests to determine A and B and in applications to insure good alignment and edge conditions.

This model has been effectively applied to gears, cam follower applications, and wheel-on-a-rail applications. In the case of gears, it is recommended that values of A and B for 9% sliding be used to account for slip at the interface. In the other two types of applications, the values for pure rolling can be used, provided there is no slip. To allow for experimental scatter and error in the determination of the coefficients, it is generally recommended that only 3 / 4 of an experimentally determined value of K_I be used in design.

Equation (2.95) can be put into a form similar to the zero wear equations used for sliding and impact. In this case, the zero wear criteria would correspond to the onset of surface damage. Using 10^8 revolutions as the reference point, Eq. (2.95) can be changed to

$$N = 10^8 \left(\frac{\gamma_r \sigma_y}{\sigma_{\max}} \right)^{2A} \quad (2.103)$$

$\gamma_r \sigma_y$ is the stress corresponding to a zero wear lifetime of 10^8 revolutions. While the data shown in Table 2.7 indicate a range of values for A , ranging from about 3 to 14, the average value is close to 7. Rolling bearing studies suggest that the nominal value for A is somewhat smaller than this average, approximately 4.5 ($2A = 9$) (17). Converting to shear stress and using a value of 4.5 for A , the following relationship is proposed, which is similar to that for sliding:

$$N = 10^8 \left(\frac{\Gamma_r'' \tau_y}{\tau_{\max}} \right)^9 \quad (2.104)$$

Table 2.7 Experimental Load/Stress Factors: K_L , A , and B

Materials	Rolling			Rolling with 9% Slip		
	K_L (psi)	A	B	K_L (psi)	A	B
<i>Rc 60 tool steel against</i>						
Carburized 1020	12,700	7.39	38.33	10,400	13.20	61.06
1020 130–150 Bhn				1,720	4.78	23.45
1117 130–150 Bhn	1,500	4.21	21.41	1,150	3.63	19.12
Spring steel 40–50 Rc	2,470	4.00	21.57			
4150 350–370 Bhn				11,300	17.76	80.00
4150 270–300 Bhn, phosphate-coated	10,500	10.10	48.67	7,460	13.52	60.42
4150 270–300 Bhn, flash Cr-plated	6,060	11.18	50.29			
4150 270–300 Bhn				2,850	17.86	69.72
4340 Induction hardened, 50–58 Rc	13,000	14.15	66.22	9,000	14.02	63.44
4340 270–300 Bhn				5,500	18.05	75.55
6150 270–320 Bhn	1,170	3.10	17.51	1,820	8.30	35.06
18% Ni maraging tool st., 48–50 Rc				4,300	3.90	22.18
Gray-iron, Class 20, 160–190 Bhn, phosphate-coated	940	3.90	19.60			
Gray-iron, Class 20, 140–160 Bhn	790	3.83	19.09	740	4.09	19.72
Gray-iron, Class 30, 200–220 Bhn	1,120	4.24	20.92			
Gray-iron, Class 30, 255–300 Bhn, phosphate-coated	2,920	5.52	25.79	2,510	6.01	28.44
Gray-iron, Class 30, 270–415 Bhn	1,850	5.45	25.79			
Gray-iron, Class 35, 225–255 Bhn	2,000	11.62	46.35	1,900	8.39	35.51
Nodular-iron, Grade 80-60-03 240–270 Bhn	2,100	10.09	41.53	1,960	5.56	26.31
Nodular-iron, Grade 100-70-03 240–260 Bhn				3,570	13.04	54.33
Yellow brass, 157–162 Bhn	1,280	3.69	19.45			
Nickel bronze, 80–90 Bhn	1,390	6.01	26.89			
Phosphor bronze, SAE 65, 65–75 Bhn	730	2.84	16.13	350	2.39	14.08
Bronze, SAE 660, 75–80 Bhn				320	1.94	12.87
Aluminum bronze	2,500	5.87	27.97			
Zinc die casting, 70 Bhn	250	3.07	15.35	220	3.11	15.29
Phenolic, cotton-base, fiber filled	1,000	6.03	26.11	900	5.95	25.60
Phenolic, graphitized, laminated	900	6.58	27.43			
Phenolic, linen-base, laminated	830	8.54	32.90	670	6.46	26.25
Acetal	620			580		
Polyurethane	240					
Polycarbonate	60					
HMWPE				370	8.03	28.61
<i>Self-mated</i>						
1020, 130–170 Bhn, phosphate-coated	2,900	7.84	35.17	1,450	6.38	28.23
1144, 260–290 Bhn				2,290	4.10	21.79
4150, 270–300 Bhn, phosphate-coated	6,770	10.46	48.09	2,320	9.58	40.24
4150 leaded, 270–300 Bhn, phosphate-coated				3,050	6.63	31.10
4340, 320–340 Bhn, phosphate-coated	10,300	18.13	80.74	5,200	26.19	105.31
Gray-iron, Class 20, 130–180 Bhn	960	3.05	17.10	920	3.55	18.52
Gray-iron, Class 30, 270–290 Bhn	3,800	7.25	33.97	3,500	7.87	35.90
Nodular-iron, Grade 80-60-03, 207–241 Bhn	3,500	4.69	24.65	1,750	4.18	21.56
Mechanite, 190–240 Bhn	1,600	4.77	23.27	1,450	4.94	23.64
Aluminum 6061-T6, hard anodized	350	10.27	34.15	260	5.02	20.12
Magnesium HK31XA-T6, HAE coal	175	6.46	22.53	275	11.07	35.02

Source: Ref. 90.

In this equation Γ''_r is the zero wear factor for rolling, similar to the other zero wear factors. In addition to being material dependent, it is also dependent on the amount of slip that occurs. Analysis of the data in Table 2.7 indicates an average value of 0.86 for Γ''_r for pure rolling. For 9% slip, this value decreases to 0.70. For pure rolling without lubrication or with boundary lubrication, a value of 0.80 is used for Γ''_r . With slip, the following relationships are used to determine Γ''_r for these conditions. The development of these relationships can be found in Appendix VII

$$\Gamma''_r = \left(\frac{p_s}{\beta} + (1 - p_s) \Gamma''_{r0} \right)^{-1/9} \quad (2.105)$$

$$\beta = \frac{0.26}{\left(\frac{0.54}{\Gamma_r} - 1 \right) p_s + 1} \quad (2.106)$$

In these equations, p_s is the slip ratio, which is the ratio of the amount of slip to the width of the contact area in the direction of motion. Γ''_r is the zero wear factor for rolling without slip, normally 0.80. Γ_r is the zero wear factor for sliding, 0.54 or 0.20. As can be seen from Eq. (2.106) Γ''_r becomes lubricant dependent when there is slip. Expressions for the effect of fluid lubrication on Γ''_r can be found in Appendix VII.

2.7. MODEL FOR BALL AND ROLLER BEARING WEAR

This model is based on an empirical correlation between bearing life and load. Bearing life (i.e., number of revolutions) has been generally found to be inversely proportional to P^3 for ball bearings and $P^{3.3}$ for roller bearings, where P is load (95–97). Since stress is proportional to $P^{1/3}$ for spherical contacts and $P^{1/2}$ for cylindrical contacts, this implies that life in these bearings is inversely proportional to stress level to the seventh or ninth power. This type of relationship is suggestive of fatigue wear. Typical features of the wear scars observed on the rollers, balls, and races of failed bearings (e.g., cracks, spalls, and pits), are also suggestive of fatigue wear. Examples of these features are shown in Fig. 2.34. These aspects of roller and ball bearing wear are very similar to those for general rolling wear, as discussed in Sec. 2.6. However, there is a significant difference associated with the models used for general rolling and rolling bearings. With the former, the model is associated with a single wearing interface where the motion is rolling and a specific percentage of sliding. With the latter, the model is associated with the overall performance of a device, which involves several wearing interfaces. At the primary interfaces (i.e., between the ball or rollers and the race) the motion is nominally rolling, but the percentage of sliding at these interfaces can be influenced by a large number of parameters. To account for these and other effects, the model generally used for bearings assumes that the basic relationship between life, L , load and these other parameters can be expressed as

$$L \propto \pi_i^m F_i P^{-n} \quad (2.107)$$

where n is 3 for ball bearings and 3.3 for roller bearings. F_i are factors associated with various aspects of the bearing design and environment. These concepts and relationships are the basis of the AFBMA's (Antifriction Bearing Manufacturers Association) model for ball and roller bearing life, (17,98–101).

A basic load rating, C , is established in the AFBMA model for a general bearing design or type. At a standard set of conditions, C is an equivalent radial load, which will

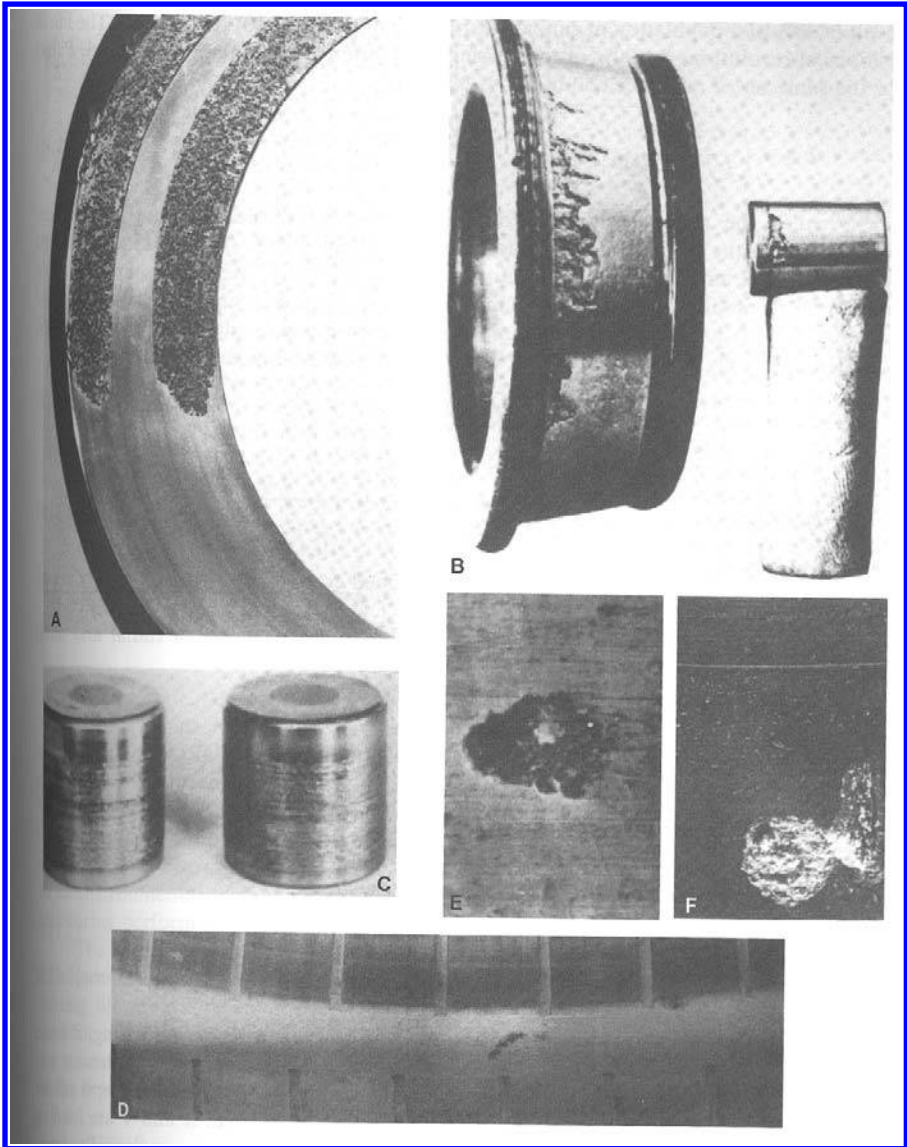


Figure 2.34 Examples of wear in roller and ball bearings. “A”, advanced stages of fatigue wear under normal conditions; “B”, fatigue wear on race and roller, resulting from misalignment and overloading; “C” damage associated with ineffective lubrication; “D”, false brinelling or fretting under stationary conditions; “E” and “F”, examples of spalling. (“A”–“D” from Ref. 99, “A” and “D” original source The Torrington Co., “B” and “C” original source SKF Industries, reprinted with permission from Texaco’s magazine *Lubrication*; “E” and “F” from Ref. 101, reprinted with permission from the Council of the Institution of Mechanical Engineers.)

result in 90% of a population of similar bearings having a life $\geq 10^6$ revolutions. The life in millions of revolutions for 90% of the bearings at a different equivalent radial load, P , but for the same set of reference conditions is given by

$$L_{10} = \left(\frac{C}{P}\right)^n \quad (2.108)$$

L_{10} is called the rating life. To account for the effect of non-standard conditions, adjustments to the rating life are made to obtain actual life, L . This is done by means of factors, such as F_j in Eq. (2.107). In the AFBMA model, five factors are generally considered to modify bearing performance. They are materials, material processing and finishing, lubrication, speed, and alignment, which are typically identified as D , E , F , G , and H , respectively. Consequently, the equation for bearing life is written as

$$L = D \times E \times F \times G \times H \times L_{10} \quad (2.109)$$

or

$$L = D \times E \times F \times G \times H \times \left(\frac{C}{P}\right)^n \quad (2.110)$$

The factors D , E , F , G , H , and C are determined empirically, n is 3 for ball bearings and 3.33 for roller bearings, as stated previously.

To account for different bearing sizes and different mixtures of radial and axial loads, C and P are further defined as follows.

For ball bearings,

$$C = f_c(i \cos \alpha)^{0.7} Z^{0.67} D^{1.8}, \quad D < 1 \quad (2.111)$$

$$C = f_c(i \cos \alpha)^{0.7} Z^{0.67} D^{1.4}, \quad D > 1 \quad (2.112)$$

$$P = XF_r + YF_a \quad (2.113)$$

for roller bearings,

$$C = f_c(i l_{\text{eff}} \cos \alpha)^{0.78} Z^{0.75} D^{1.1} \quad (2.114)$$

$$P = XF_r + YF_a \quad (2.115)$$

In these equations, i is the number of rows of rolling elements in the bearing, Z is the number of rolling elements per row, α is the contact angle between the rolling element and the race (Fig. 2.35), D is the rolling element diameter, l_{eff} is the effective length of the roller, F_r is the applied radial load, and F_a is the applied axial load. X and Y are loading factors for the bearing type and provided by the manufacturer. f_c is an empirically determined wear coefficient, referenced to a life of 10^6 revolutions under the standard test conditions for a given bearing type and design. Standard values for these have been developed and published. One source is Ref. 17

The materials factor in the AFBMA model, D , is used to account for relative performance of different bearing materials in a specific state, condition, or combination. The reference material condition used for this factor is self-mated air-melted 52100 steel with a minimum hardness of Rc 58, lubricated with a super-refined naphthenic mineral oil with a kinematic viscosity of 79 cs at 100°F. The processing factor in the model, E ,

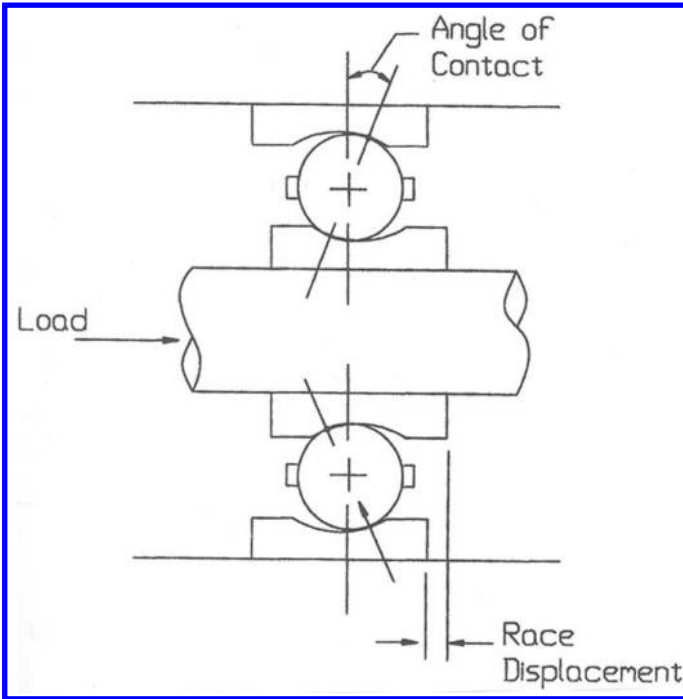


Figure 2.35 Contact angle between the roller and race.

is used to account for changes in material properties from those associated with a determined value of D . For example, this factor is used to adjust for generic differences associated with different melting techniques for steels and generic effects associated with hardness changes. Examples of D and E values illustrating this are shown in Table 2.8. These two factors are generally referred to as bearing design factors, since they relate to the selection of bearing materials. The remaining three factors, F , G , and H , are referred to as environmental factors, since they are concerned with the effects of use conditions on bearing performance.

The lubrication factor, F , is used to adjust for differences in bearing life as a result of differences in elastohydrodynamic lubrication. Other effects that a lubricant might have on bearing life are addressed through the material's factor, D . The effect of elastohydrodynamic lubrication on bearing life is related to a film parameter, Λ , which is defined as the ratio of the elastohydrodynamic film thickness, h , to the composite surface roughness of the bearing, σ , namely

$$V = K \times H^m \times P^n \times S^k \tag{2.16}$$

where

$$h = \delta \tag{2.17}$$

σ_r and σ_{re} are the RMS values of the surface roughness for the race and rolling element (i.e., the ball or roller), respectively. Expressions for h are given in Table 2.9. A graph of an experimentally determined trend in F values as a function of Λ ; is given in Fig. 2.36.

Table 2.8 Bearing Design Factors

Materials	D factor
<i>Materials factor D: values for air-melted through hardened bearing materials</i>	
52100	2.0
M-1	0.6
M-2	0.6
M-10	2.0
M-50	2.0
T-1	0.6
HALMO	2.0
M-42	0.2
WB-49	0.6
<i>Processing factor E</i>	
Processes	E factor
Air melting	1
Consumable electrode vacuum melting	3
Thermomechanical vacuum (M-50 only)	3
<i>Hardness scaling factor for use with D and E^a</i>	
$(L'L'') = \exp 0.1 (Rc' - Rc'')$	

^aTo adjust for changes in hardness as a result of different heat treatments and bearing operating temperatures.
Source: Ref. 100.

Table 2.9 Expressions for Lubricant Film Thicknesses for Use with Ball and Roller Bearings

Line (roller) contact

$$h = 1.18 [(a \mu_0 \{u_1 + u_2\})]^{0.73} [E I (\{1 - \nu^2\} P')]^{0.091} [r]^{0.36}$$

Point (ball) contact

$$h = 1.22 [(a \mu_0 \{u_1 + u_2\})]^{0.74} [E I (\{1 - \nu^2\} P)]^{0.074} [1 + [0.667 (r/R)]]^{-0.74} [r]^{0.407}$$

h Film thickness, in.

u_1, u_2 Surface velocities of rolling elements, in./sec

P' Contact load per unit length between rolling elements, lb/in.

P Contact load between rolling elements, lb.

r $(r_1^{-1} + r_2^{-1})^{-1}$, in.

r_1, r_2 Radii of rolling elements in direction of rolling, in.

R $(R_1^{-1} + R_2^{-1})^{-1}$, in.

R_1, R_2 Radii of rolling elements perpendicular to rolling direction, in.

E Young's modulus, psi

ν Poisson's ratio

μ_0 Lubricant absolute viscosity at atmospheric pressure, reyns, lb sec/in.²

a Pressure coefficient at atmospheric pressure from the viscosity formula $\mu = \mu_0 e^{ap}$,
where p (lb/in.²) is pressure, in.²/lb

Note: for many types of oils, $(\mu_0 a)^{0.7} = 10^{-9} \text{SUS}^{-1} \nu_0$, the kinematic viscosity at atmospheric pressure in SUS

Source: Ref. 100.

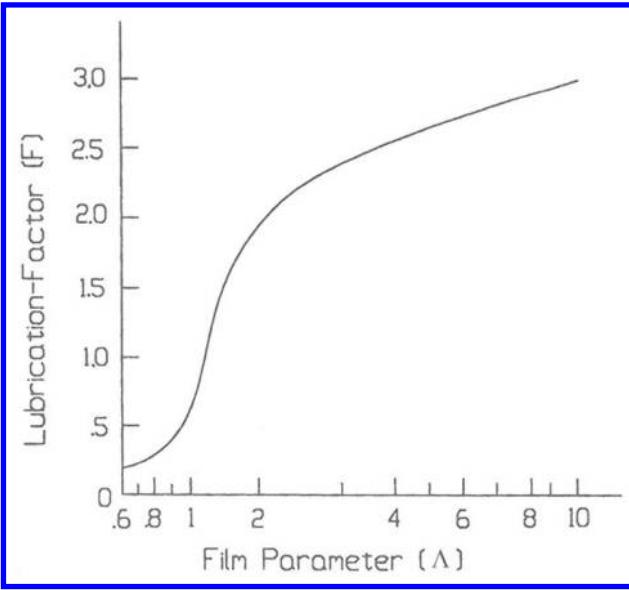


Figure 2.36 Lubrication factor, F , as a function of film parameter, Λ . (From Ref. 100.)

As described in Appendix VII, this trend can be related to the zero wear factors of the models for sliding and rolling wear.

Centrifugal effects become increasingly important in bearing performance as the speed is increased. These effects can influence the nature and location of contact points within the bearing, as well as the loading. The graph in Fig. 2.37 illustrates the degradation that can be expected in bearing life as a result of these effects. The speed factor, G , is used to adjust for these effects. Table 2.10 contains experimentally determined values of G for ball and roller bearings in terms of a speed parameter, DN. DN is the product of the bearing bore diameter (mm) with the inner race speed in revolutions per minute (rpm).

Load distribution is a critical factor in bearing performance. External alignment or misalignment can influence load distribution and, as a result, influence bearing life (17,102–104). The remaining factor the AFBMA model, H , is used to account for the effects of misalignment. Experimentally determined values of this factor are given in Table 2.11 for various alignment conditions.

Temperature, distortion due to heavy loads, contamination, amount of lubrication, load fluctuations, and traction are some of the other aspects that can affect bearing life. As with the elements identified with the adjustment factors, these and other conditions, which can affect bearing life, are also taken into account by modification of these adjustment factors, combined with their effect on P (17,105). Fig. 2.38 shows an example of the effect of traction on bearing life. Traction can reduce rolling bearing life by reducing the thickness of lubricating films, cause or increase slip in bearings, and increase shear stresses. It is taken into account by modification of the lubrication factor, as is the amount and type of lubrication.

It has been found that the life for oscillating bearing follows the same basic relationship of the AFBMA model for rotating bearings, Eq. (2,108), with N being the number of oscillations (106). The amplitude of the oscillation can affect bearing life as a result of changes in the number of loading cycles that are experienced by individual regions.

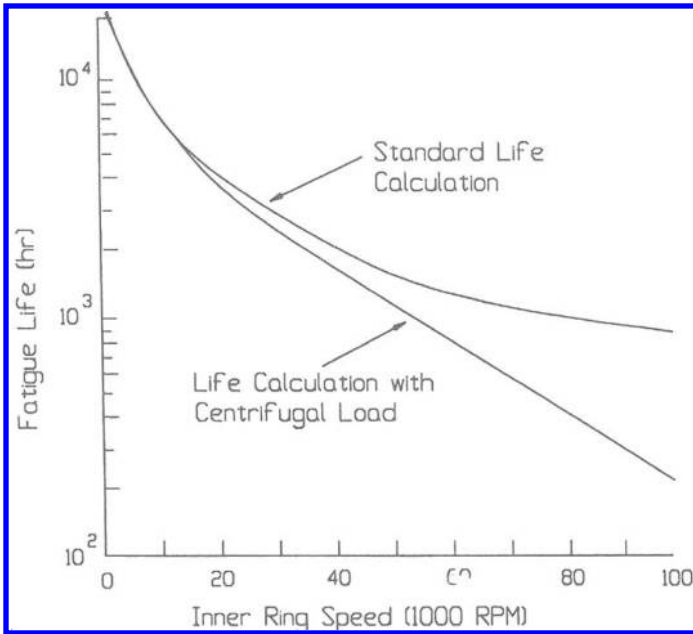


Figure 2.37 Example of the influence of centrifugal effects on bearing life. (From Ref. 100.)

In general, this results in an increase in life (number of oscillations) with decreasing amplitude. Three different regions of amplitude are associated with this effect. One is when the amplitude is greater than the angular separation of the rolling elements. This angle in general is referred to as the critical angle. The second is when the amplitude is less than the critical angle but larger than the angle subtended by the contact area between the rolling element and the race. The third is when the amplitude is less than the subtended angle. Fig. 2.39 illustrates this effect for amplitudes greater than the critical angle, where the effect is the most pronounced. Amplitude is less of a factor in the second region and becomes negligible in the third region. For amplitudes above the critical angle, the following relationship exists between the dynamic capacity of rolling bearings, C , and the dynamic capacity of oscillating bearings, C_{osc} (107)

$$C_{osc} = C \left(\frac{180}{\Phi_{crit}} \right)^{1/n} \quad (2.118)$$

Φ_{crit} is the critical angle and n is 3 for ball bearings and 4 for roller bearings. This effect is not the only way that oscillations can affect bearing life and performance. The speed and amplitude of the oscillations can also affect bearing life through their effect on fluid lubrication. With oscillations fluid films degrade (become thinner) and collapse with oscillatory motion (at reversals). In fact the amplitude and speed can be such that fluid lubrication does not occur at all. As described with rolling bearings, reduced lubricant film thickness results in lower values of the lubrication adjustment factor and in reduced life. With oscillating bearings, this effect, that is reduction in the value of a lubrication adjustment factor, will become more significant with decreasing amplitude and may

Table 2.10 Speed Effect Factor

Speed $DN^a \times 10^6$	Thrust load															
	5% C						10% C						20% C			
	Bearing bore (mm)															
	<20	20-39	40-69	70-100	101-120	<20	20-39	40-69	70-100	101-120	<20	20-39	40-69	70-100	101-120	
0.1	0.8	0.7	0.7	0.7	0.8	0.9	0.8	0.8	0.8	0.9	1.1	1.0	1.0	0.9	1.0	
0.3	1.0	0.8	0.8	0.9	1.0	0.9	0.8	0.8	0.9	1.0	1.0	1.0	0.9	1.1	1.1	
0.5	1.3	1.1	0.9	0.9	1.0	1.2	1.0	0.9	0.9	1.0	1.1	1.0	1.0	1.0	1.1	
0.7	1.4	1.2	1.1	1.0	1.1	1.6	1.2	1.1	1.0	1.2	1.2	1.1	1.1	1.1	1.2	
0.9	1.0	1.1	1.0	1.0	1.0	1.7	1.4	1.2	1.1	1.3	1.3	1.2	1.2	1.2	1.3	
1.1		0.8	0.8	0.7	0.7		1.4	1.2	1.1	1.2	1.2	1.1	1.2	1.2	1.4	
1.3		0.4	0.5	0.4	0.4		1.2	1.1	1.0	1.1	1.2	1.1	1.0	1.1	1.2	
1.5		0.3	0.3	0.3	0.2		1.0	1.0	0.8	0.8	1.0	1.0	0.8	0.8	1.2	
<i>Radial cylindrical roller bearings</i>																
Speed $DN^a \times 10^6$	Radial load															
	5% C						10% C						20% C			
	Bearing bore (mm)															
	5-50	50-100	100-150	150-200	5-50	50-100	100-150	150-200	5-50	50-100	100-150	150-200				
0.1	1.0	1.0	1.0	1.0	1.0	1.0	1.0	1.0	1.0	1.0	1.0	1.0				
0.3	1.0	1.0	1.0	1.0	1.0	1.0	1.0	1.0	1.0	1.0	1.0	1.0				
0.5	1.0	1.0	1.0	1.0	1.0	1.0	1.0	1.0	1.0	1.0	1.0	1.0				
0.7	1.0	0.8	0.8	0.8	1.0	0.9	0.9	0.9	1.0	0.9	1.0	1.0				
0.9	0.9	0.2	0.2	0.2	1.0	0.7	0.9	0.7	1.0	1.0	1.0	1.0				
1.1	0.9	0.1	0.1	0.1	0.9	0.2	0.7	0.2	0.7	0.2	1.0	0.9				
1.3	0.8	0.9	0.2	1.0	0.8	0.8	0.9									
1.5	0.7	0.9	0.9	0.2	0.2											

Note: Use above factors with lubricant life factor greater than 1, otherwise, use a minimum speed effect life factor of 1.
^a D is the bearing bore diameter in mm. N is the inner race speed in revolution per minute.
 Source: Ref. 100.

Table 2.11 Misalignment Factor

Bearing type	Misalignment (rad)	H
Cylindrical and tapered roller bearings	≤ 0.001	1
Spherical bearings	≤ 0.0087	1
Deep groove bearings	≤ 0.0047	1
Cylindrical and tapered roller bearings with crowning	0.001	1
	0.002	0.8
	0.003	0.6
	0.004	0.5
	0.005	0.4
Cylindrical and tapered roller bearing without crowning	0.001	0.8
	0.002	0.55
	0.003	0.35
	0.004	0.2
	0.005	0.1
Spherical bearings	> 0.0087	< 1
Deep groove bearings	> 0.0047	< 1

Source: Ref 100.

over-ride the increase in life based on number of loading cycles. Both of these elements generally should be considered when selecting bearings for oscillatory applications.

While there is considerable formalism and the use of analytical relationships associated with the AFBMA model for rolling bearings, the model is fundamentally an empirical model, based on the empirical determination of the basic load rating, C , or the factor f_C . Values for these are determined by testing bearings to failure. The failure criteria in these tests are somewhat variable but generally are related to a noticeable change in performance, such as the onset of vibrations or increase in torque, for a specified percentage of the population. Typically, the standard tests involve continuous rotation and constant load and use a small percentage (e.g., 10% failure rate). Obviously, these conditions do not apply to all applications. Applications can be sensitive to different levels of vibration, noise, and torque or a different failure percentage might be required or tolerated. Adjustment factors can also be used to account for such difference in what is considered failure (108). Since bearing failure rates generally conform to the Weibull statistics, these relationships are typically used to adjust for different failure rate requirements.

2.8. MODELS FOR JOURNAL BEARING WEAR

Models for journal bearing wear can be grouped into three categories, based on the lubrication regime for which they are appropriate (109,110). One category covers models for bearings operating under dry and boundary lubricated conditions. A second is for bearings, which operate in the mixed lubrication regime, and the third category is for those bearings, which operate in the full fluid or hydrodynamic lubrication regime. The models in the first category are basically sliding wear models that are applied to a journal bearing configuration. The models for mixed and fluid lubrication operation are complicated by the consideration of the effect of fluid film formation on wear behavior. As these films form and become thicker, there is less asperity interaction and wear decreases. In the full fluid lubrication regime ultimately there is complete separation and wear is eliminated.

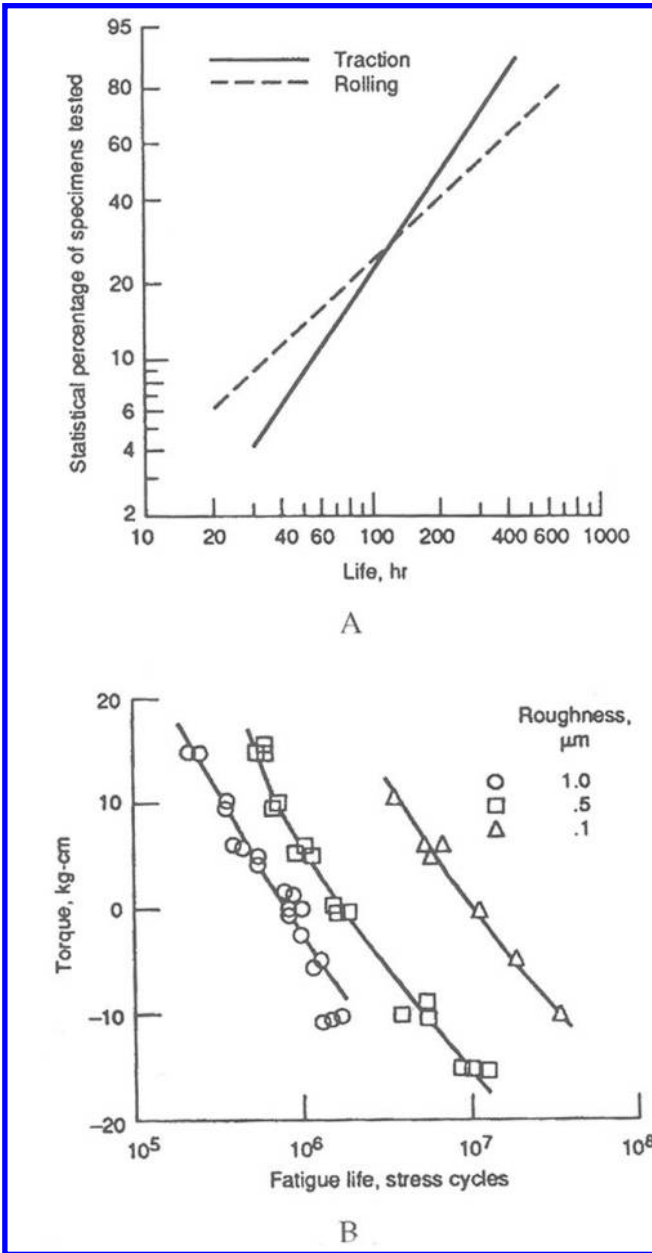


Figure 2.38 Examples of the effect of traction in rolling contacts. “A” shows the life of a rolling bearing with and without traction. “B” shows the influence of torque transmitted as a result of traction on the life of another rolling bearing. (From Ref. 17. Reprinted with permission from STLE.)

However bearings, which operate in this regime, do experience wear as the result of stop / start cycles. During these cycles, boundary and mixed lubrication conditions are encountered and wear results from rubbing contact between the journal and the bearing. Generally, wear life is least for bearings operating in the dry and boundary lubricated regime and longest for those operating in the fluid regime. In the mixed lubrication regime,

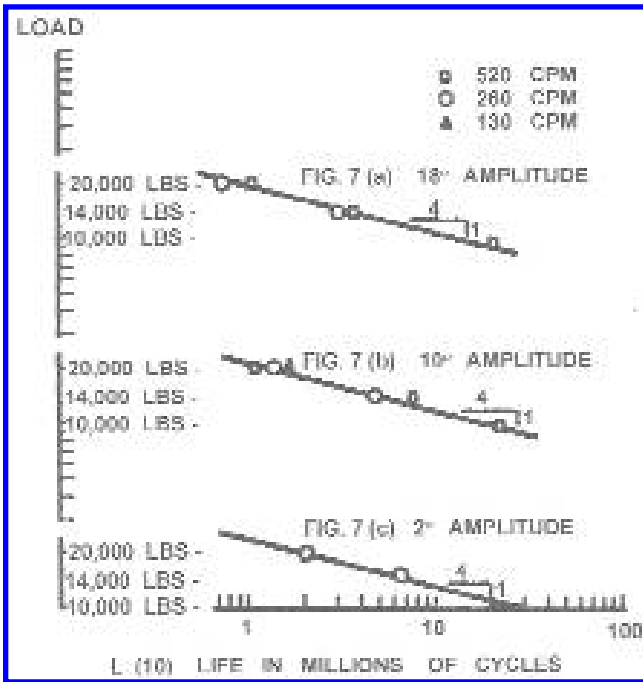


Figure 2.39 Examples of the effect of oscillatory motion on the life of rolling bearings. L_{10} is bearing life based on 10% failure—that is, 90% of the bearings will have a lifetime equal to or greater than L_{10} . (From Ref. 106. Reprinted by permission from ASME.)

intermediate lives are achieved, depending on the thickness of the fluid film. For thin films, wear lives approaching those of boundary lubricated operation are achieved, while for thick films, wear lives are closer to those of fluid lubrication.

Good design practice for journal bearings is to have the journal harder than the bearing to insure that there is negligible wear of the journal. In this way greater conformity is achieved as wear occurs on the bearing, tending to enhance bearing life. If the journal wears significantly, conformity is reduced and bearing life degrades. Consequently, a common assumption of all the models that will be discussed is that negligible wear occurs on the journal.

Knowing the transitions from boundary to mixed lubrication and from mixed to complete fluid lubrication in terms of design parameters is significant in design for two reasons. First, it enables the selection of the wear model to be used and, second, this information can be used to select parameters so that the bearing operates in a preferred regime to minimize or eliminate wear. These transition points are defined in terms of changes in the coefficient of friction as a function of the Sommerfeld number, S , as is indicated in the Stribeck diagram (Fig. 2.40). The Sommerfeld number, S , for the bearing, is defined as

$$S = \frac{\Omega N}{p} \left(\frac{R}{C} \right)^2 \quad (2.119)$$

where Ω is the absolute viscosity of the lubricant, N is the shaft rotational speed in revolutions per second, p is the bearing pressure, R is the radius of the journal, and C

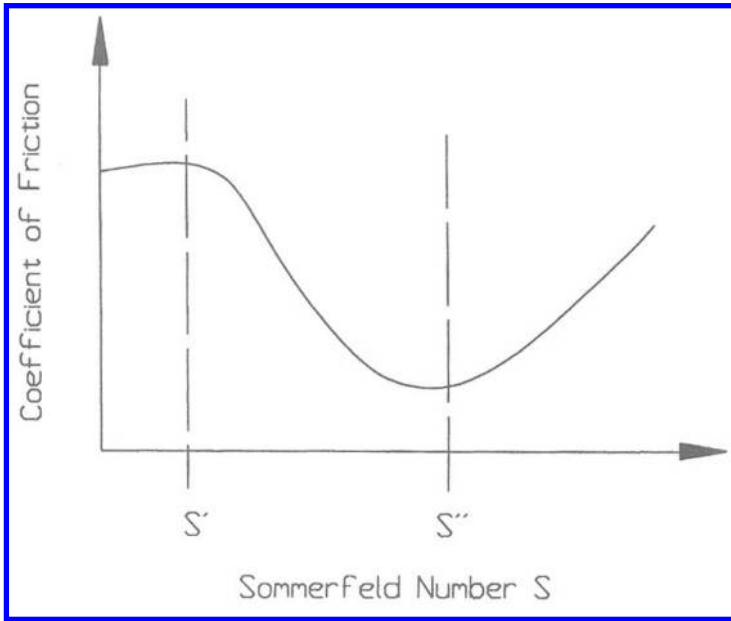


Figure 2.40 Stribeck diagram.

is the radial clearance. The transition from boundary to mixed lubrication occurs at S' , which is the Sommerfeld number at which the coefficient of friction starts to decrease. The transition from mixed to fluid lubrication occurs at S'' , which is the Sommerfeld number at which the coefficient of friction starts to increase.

S' and S'' can be determined empirically by measuring bearing friction as a function of the Sommerfeld number. Also there are analytical relationships, which can be used to estimate the values for many cases. These relationships are based on correlations between film thickness and journal and bearing roughnesses. The thickness of the film, H , that is formed, is related to the Sommerfeld number, increases with increasing values of S . For large length, L , to diameter, D , ratios, where leakage from the ends of the bearing can be ignored, the relationship is shown in Fig. 2.41 in terms of the eccentricity, e , of the bearing, e is related to H by the following:

$$H = C(1 - e) \quad (2.120)$$

For bearings in which flow from the ends cannot be ignored and the L/D ratio is less than 1, there is the following relationship:

$$S \left(\frac{L}{D} \right)^2 = \frac{(1 - e^2)^2}{\pi e} [\pi(1 - e^2) + 16e^2]^{-1/2} \quad (2.121)$$

It has been found that values of S' and S'' depend on the ratio of an effective roughness to the film thickness (111–113). In particular, studies have indicated that the transition from boundary to mixed is related to the initial roughness of the journal, namely

$$H' = 0.2\delta_{0j} \quad (2.122)$$

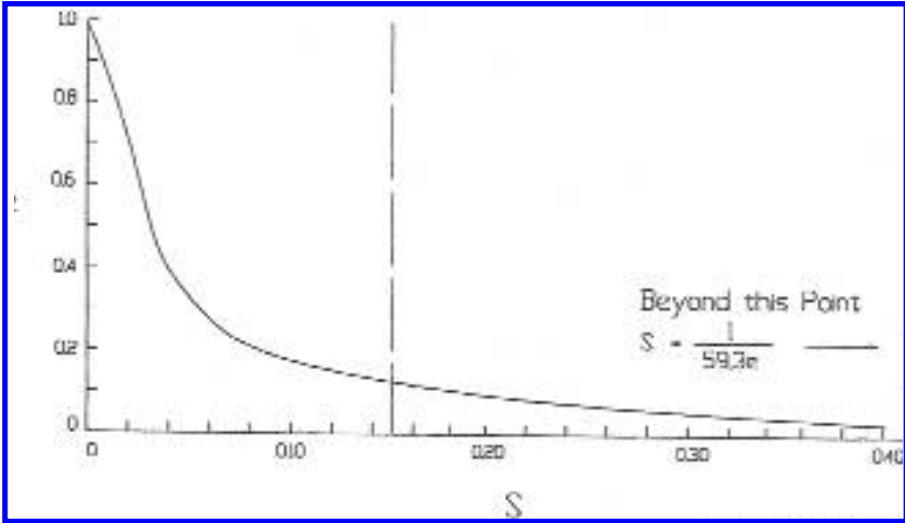


Figure 2.41 Relationship between bearing eccentricity, e , and the Sommerfeld number, S , for large L/D ratios. (From Ref. 114.)

H' is the film thickness at the transition and δ_{0J} is the initial RMS roughness of the journal. The corresponding value for e , e' , is

$$e' = 1 - \frac{0.2\delta_{0J}}{C} \quad (2.123)$$

Studies have shown that the transition from mixed to full fluid lubrication can be related to sum of the predominant peak roughnesses of the journal and the bearing (111,112). The predominate peak roughness is related to the RMS roughness by a factor called the Tarasov factor, K_S . There are characteristic values of K_S for different surface finishing processes. A list of values for different processes is given in Table 2.12. Basically, the criteria for the transition from the mixed to the full fluid regime are that the film thickness, H'' , is equal to the sum of the predominate peak roughnesses, namely

$$H'' \simeq (\delta_{0B} + \delta_{0J}) \times K_S \quad (2.124)$$

Table 2.12 Tarasov Factor

Type of finish	K_S		
	Average	Maximum	Minimum
Ground	4.5	5.0	3.5
Hydrolapped	6.5	7.5	5.5
Loose-abrasive lapped	10.0	13.0	7.5
Abrasive paper	7.0	9.0	5.5
Super-finished	7.0	9.5	7.0

Source: Ref. 112.

H'' is the film thickness at the transition and the δ_0 's are the RMS value of the surface roughnesses. The corresponding value of the eccentricity, e'' , is

$$e'' \approx 1 - \left[(\delta_{0B} + \delta_{0J}) \times \frac{K_s}{C} \right] \tag{2.125}$$

The corresponding value of S can then be obtained by using the appropriate relationship between e and S obtained from fluid lubrication theory, such as the ones shown by Fig. 2.41 and Eq. (2.119) (114). Effects associated with non-Newtonian fluid characteristics, micro-elastic and micro-plastic deformations, pressure and temperature effects on fluid properties, and oil supply can influence film thickness and its relationship to the Sommerfeld number (115). An example of this is the situation with oil-impregnated porous bearings.

Both the wear models and this method of identifying the transitions between lubrication regimes apply to both solid and porous bearings. However, the relationships between film thickness and the Sommerfeld number is different for porous bearings as a result of flow through the pores (115–119). With porous bearings, there is a critical value of the Sommerfeld number, S_c , that must be achieved before a porous bearing can support a film. The value of S_c depends on the porosity of the bearing. Studies have shown that for values of $S \geq 2S_c$, the porosity has a negligible effect and the relationship between film thickness or eccentricity and S is essentially the same as for a solid bearing. This behavior is shown in Fig. 2.42. The approximate relationship between S_c and the permeability coefficient of the bearing, Φ , is shown in Fig. 2.43. The permeability coefficient is related

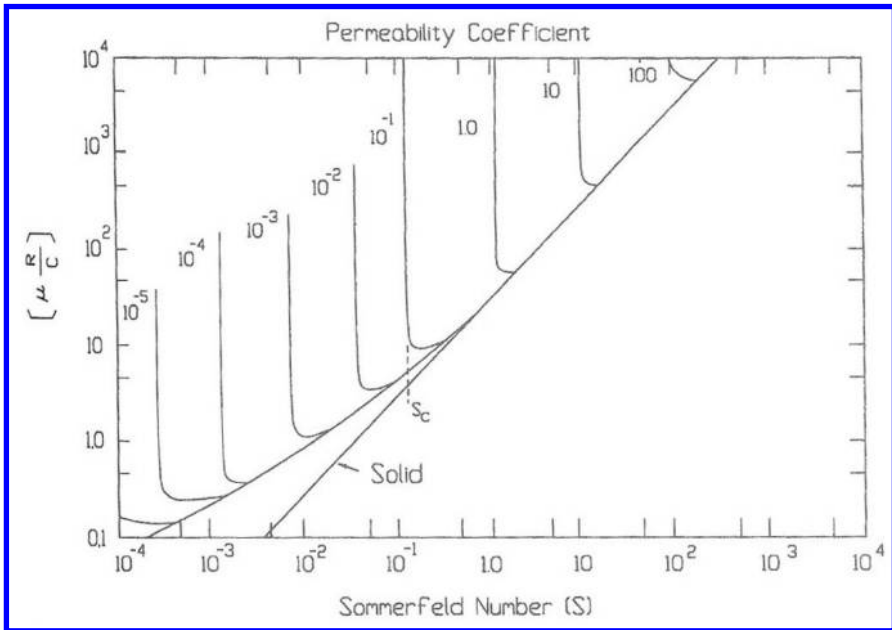


Figure 2.42 The effect of porosity on friction behavior of porous bearings. (From Ref. 109.)

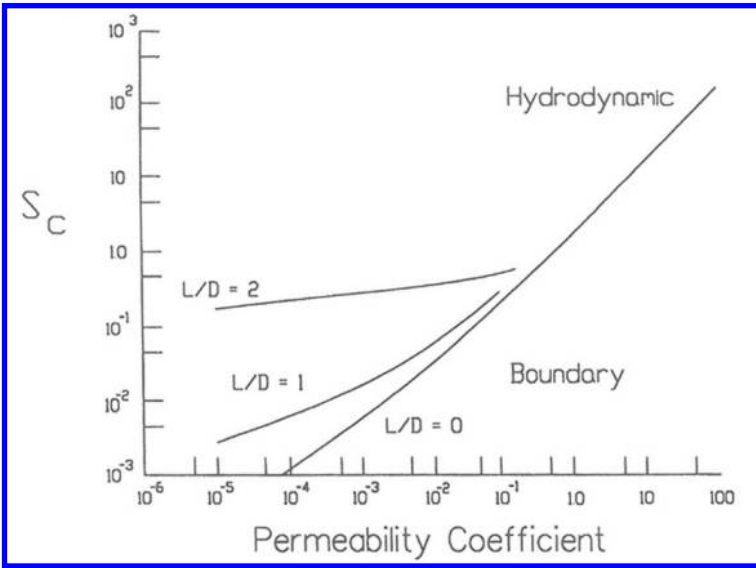


Figure 2.43 Relationship of S_C and the permeability coefficient of porous bearings, Φ . (From Ref. 109.)

to the permeability of the bearing, Θ , by the following:

$$\Phi = \frac{\Theta T}{C^3} \quad (2.126)$$

where T is the wall thickness of the bearing. Θ of the bearing is defined in terms of Darcy's equation for flow through a porous media,

$$\frac{\delta p}{L} = \frac{\Omega Q}{\Theta A} \quad (2.127)$$

where Q is the flow through a cross-section, A , δp is the pressure drop over a length L , and Ω is the absolute viscosity of the fluid.

Estimates of S' and S'' for porous bearings can be obtained by first determining the value of S_C . The graph in Fig. 2.43 may be used for that purpose. A value for e is obtained from the value of S_C using the relationships for solid bearings. If $e > [1 - 0.28\delta_{OJ}/C]$, S' equals S_C and S'' is determined as for a solid bearing. If $e < [1 - 0.28\delta_{OJ}/C]$, S' and S'' are determined as for a solid bearing.

The amount of oil in the porous bearing is also a factor that can influence the type of lubrication or the lubrication regime. Studies have indicated that porous bearings can sustain a significant film of oil, even when they are not completely impregnated but film thickness does decrease with oil loss (118,120). The data indicate that above 70–80% of capacity there is little affect on film thickness. Below this level, however, film thickness decreases and by 50% of capacity the operation is in the boundary lubrication range for any value of S . This means that as lubricant is lost from the bearing, the lubrication regime can change from full fluid to boundary, resulting in increased wear. The same studies also indicate that oil loss is proportional to some power of running time,

$$\% \text{ loss} = K_t^n, \quad n > 0 \quad (2.128)$$

where t is running time.

There are three models used for the dry and boundary lubricant regimes. In one it is assumed that after an initial run-in period a constant volume wear rate, V , is achieved and that wear behavior in this region can be characterized by a wear coefficient, K , determined from a reference or standard test (39,109,110,121). This concept is illustrated in Fig. 244. In this model, V is related to K by means of the following:

$$V = \frac{dV}{dS} = KP \tag{2.129}$$

where V the volume of wear; S , the distance of sliding; and P , the load. K is determined from the wear rate, v , after the break-in period of the reference test by the following:

$$K = \frac{v}{P'} \tag{2.130}$$

where P' is the load used in this test. While non-bearing tests (i.e., pin-on-disk and block-on-ring tests) are often used to determine K , a bearing test provides better simulation. With this model, K is often determined as a function of such parameters as surface finish, pressure, velocity, temperature, and lubricant. This type of characterization is shown in Table 2.13 for several materials. Values of K for a number of material pairs are given in Appendix III.

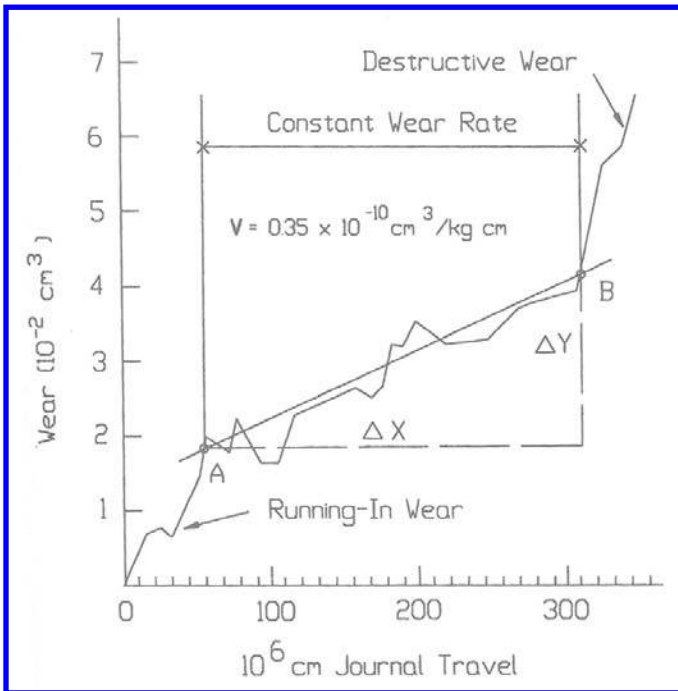


Figure 2.44 Model for journal bearing wear. (From Ref. 26.)

Table 2.13 Matrix Used in Determining K Values for Various Test Parameters from Bearing Tests

Load (psi)	Velocity (ft/min)	Shaft conditions		
		Material	Hardness (R_c)	Roughness μ
25	11	4037	61	16
150	105			32
300	300	1137	12	16
				32
		1137	42	16
				32
		4142	49	16
				32

Source: Ref. 109.

In practice, journal bearing wear and performance are usually related to the increase in clearance between the journal and the bearing. This increase in clearance is the depth of the wear scar, h , on the bearing (Fig. 2.45). Approximate relationships between h and V are as follows:

journal aligned

$$h \approx 0.66 R_j^{-1/3} V^{2/3} \quad (2.131)$$

journal misaligned

$$h \approx 0.54 R_j^{-1/5} \alpha^{2/5} V^{2/5}, \quad h/\alpha \leq L \quad (2.132)$$

where R_j is the radius of the journal; L , the length of the bearing; and α , the axial misalignment of the journal in radians, α is the depth of the wear scar divided by the length of the wear scar (Fig. 2.46).

Total wear with this model is the sum of the wear produced during the run-in period and the wear produced during the stable wear rate period. As a consequence, additional information or assumptions about wear during the run-in period are needed to provide

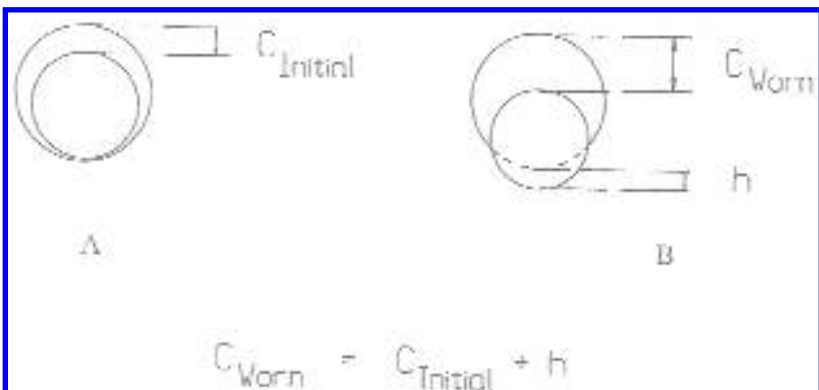


Figure 2.45 Relationship between bearing clearance and wear.

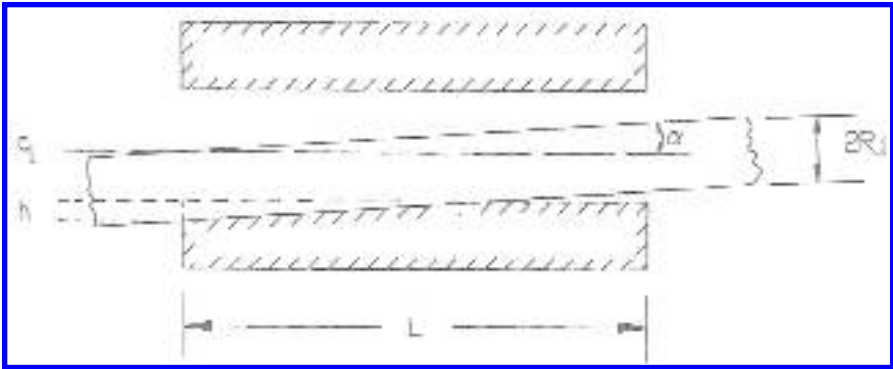


Figure 2.46 Wear in misaligned bearings.

a complete model for bearing wear. One way of treating the run-in wear is to assume that this is a period of a higher but constant wear rate with a wear coefficient, K_i . (See Fig. 2.47.) With this assumption the following relationship for h results for an aligned bearing:

$$h \approx \frac{0.65(KPS)^{2/3} [1 + [(K_i/K) - 1][S_i/S]^{2/3}]}{R^{2/3} J^{2/3}} \tag{2.133}$$

where S_i is amount of sliding during the run-in period. The factor outside the brackets is the increased clearance that would be predicted if the run-in period was neglected. This equation shows that when the effect of run-in is neglected in this model, the model tends to underestimate the wear. The error is a function of both the relative duration of the run-in period to total duration and the relative severity of run-in and stable wear behavior. If K_i is much larger than K , a significant error could result, even for long periods of

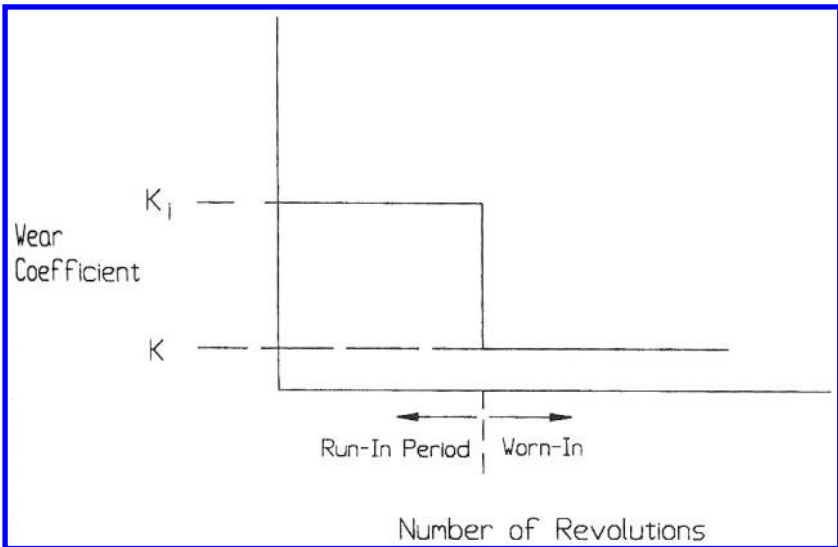


Figure 2.47 Approximate method for including the effect of run-in on bearing life.

operation. For example, in the case where K_i / K is of the order of 100 and (S / S') is of the order of 10^4 , the model would predict 50% less wear if run-in was ignored. If K_i is similar to K , the error tends to be small in most practical situations and can often be neglected, particular for long-term behavior.

Run-in behavior can be characterized by short-term tests with bearings. This is the preferred method. If necessary, estimates can also be made from characterizing the wear in the initial stages of pin-on-disk and block-on-ring tests. The magnitude of the run-in wear and the duration of the run-in period in these tests can be used to estimate K_i and S_i . There is a second model, which is simpler and more limited, that is often used for plastic bearings (39,121–123). Like the first model, it also assumes that the wear follows linear relationship:

$$V = KPS \quad (2.134)$$

However, it does not consider or identify a run-in period as does the first. In addition, it assumes a simpler and less realistic wear geometry. A constant contact area of uniform wear depth is assumed. These assumptions allow the use of the PV approach discussed in Sec. 2.2 for general sliding. This approach leads to a constant rate of radial wear, h , which is proportional to the product of pressure and velocity, namely

$$h = \frac{dh}{dt} = Kpv \quad (2.135)$$

where p is the pressure and v is the sliding velocity. With this model, K is assumed to be independent of pressure and velocity for velocities and pressure under certain limits defined by a limiting PV curve. K may be and usually is a function of other parameters such as counterface material, roughness, and lubrication. The limiting PV curve is the locus of pressure and velocity values above which there is a significant and abrupt increase in wear rate. Typically, this model is used to provide general guidance for the selection of plastic bearings in terms of average wear, rather than to provide a quantitative relationship for maximum radial wear or increased clearance.

Both K and the limiting PV curve used in this approach are determined empirically. Different tests are usually used for this purpose. K is generally determined from thrust washer tests because of its similarity to bearing situations. The limiting PV curve is usually determined by a test using the half-bearing configuration shown in Fig. 2.48. The mounting block for the half bearing is instrumented so that load, torque, and temperature can be monitored. The limiting values are determined by running at constant speed and incrementally increasing the load until there is either a dramatic increase in torque or temperature, or the temperature does not stabilize after 30 min. An example of this testing profile is shown in Fig. 2.49. This test is done for several speeds, so that the limiting PV curve can be drawn (Fig. 2.50). Other methods can be used to develop this curve. For example, a series of wear tests in which wear rates are determined as a function of speed and load can be used, as well (121). However, this is usually a more involved and lengthy process.

This second model allows the development of a very simple graph, which can be used in design. The relationship between radial wear rates and PV values for bearings is graphically shown as a function of K in Fig. 2.51. If an allowable wear rate is known, this figure can be used to determine either the maximum allowable value of K for a bearing or the maximum PV allowed for a given K . Alternatively, it can be used to estimate the wear rate if K and PV are known. From Eq. (2.135), it can also be seen that with this model wear depth or radial clearance is given by the product of h with the duration of operation.

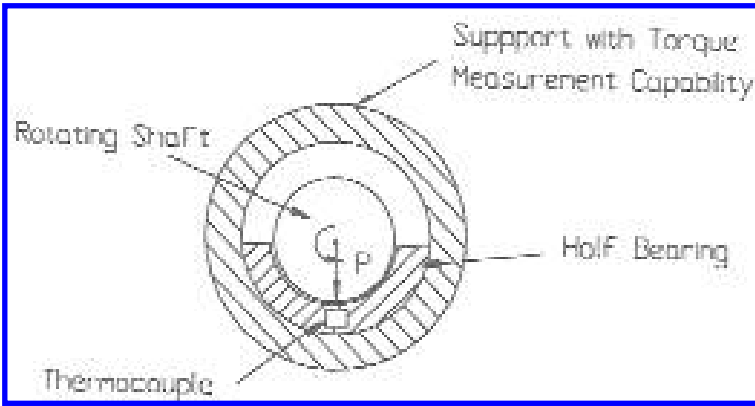


Figure 2.48 Test configuration used to determine the limiting PV curve for plastic bearings.

Therefore, the maximum allowable wear rate is the maximum increase in radial clearance allowed in the application divided by the desired lifetime. For all of these uses, it is also necessary to verify that the values of the pressure and velocity in the application are below those of the limiting *PV* curve of the bearing material. It is generally recommended that bearings be operated well below these limits. *PV* data for several materials are given in Table 2.14.

The Zero and Measurable Wear Models for Sliding can also be applied to a journal bearing configuration, providing a third model for the boundary regime. For the same worn geometries considered with the first model, the Measurable Wear Model results in the following relationships for wear depth or increased clearance and usage:

$$h = CS^n \tag{2.136}$$

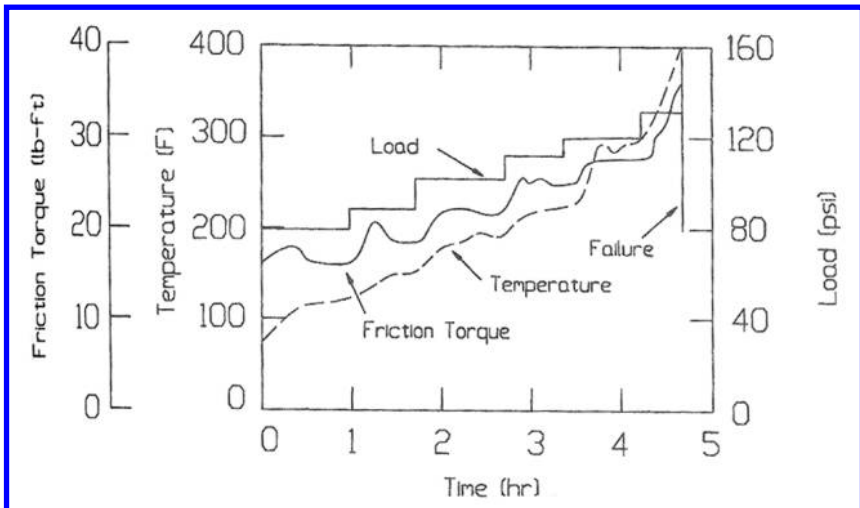


Figure 2.49 Load-stepping diagram used to determine limiting PV values. (From Ref. 122.)

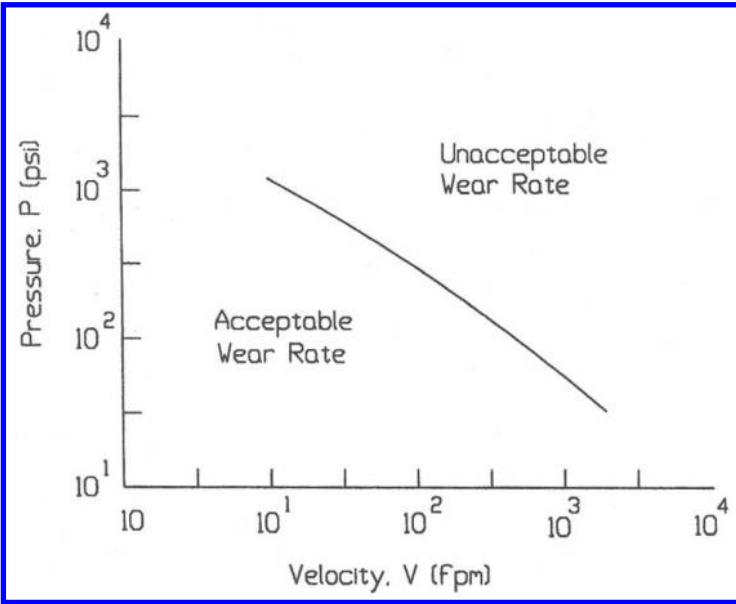


Figure 2.50 Limiting PV curve. (From Ref. 122.)

For an aligned bearing, n is $2/3$ for both the constant and variable energy modes. For a misaligned bearing, n is $2/5$ for the constant energy mode and $1/7$ for the variable energy mode. Stress levels in most bearing situations are generally low in comparison to the yield points of the bearing material. Assuming that this is the case, C in this equation

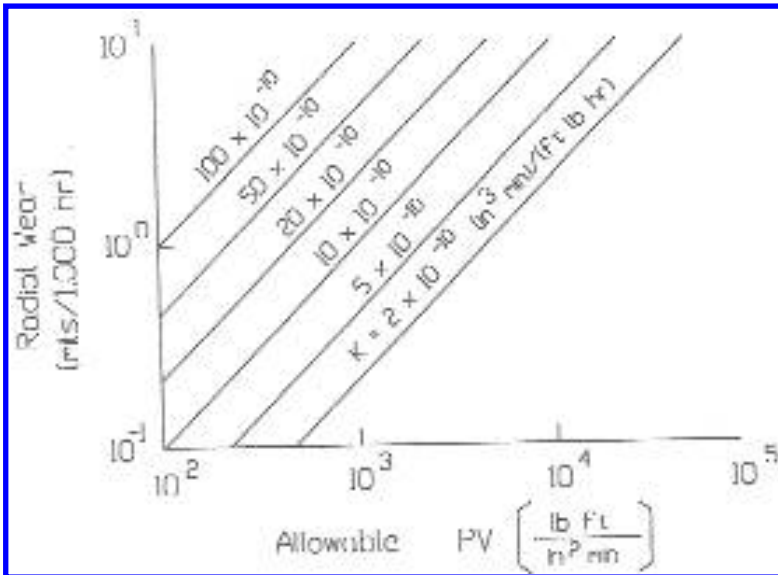


Figure 2.51 Relationship between radial wear rate and PV factors for different wear factors. (From Ref. 122.)

Table 2.14 Wear Factor and *PV* Limits for Plastics Against Steel

Plastic	<i>PV</i> limit (lb ft/in ² min)			
	<i>K</i> (in. ³ min/ ft lb h) × 10 ⁻¹⁰	10 ft/min	100 ft/min	1000 ft/min
ABS, 15% TFE	300	18,000	4000	2000
Acetal	65	4000	3500	< 2500
Acetal, 20% TFE	17	> 40,000	12,500	5500
Acetal, 30% glass, 15% TFE	200	12,500	12,000	8000
Fluorocarbon	2500		1800	
Fluorocarbon filled	1 20		30,000	
Nylon type 6, 30% glass, 15% TFE	17	17,500	20,000	13,000
Nylon type 6/10, 30% glass, 15% TFE	15	20,000	15,000	12,000
Nylon type 6/6	200	3000	2500	2500
Nylon type 6/6, 20% TFE	12	> 40,000	27,500	8000
Nylon type 6/6, 30% glass, 15% TFE	16	17,500	20,000	13,000
Nylon graphite filled	50		4000	
PEEK, 30% carbon	60			
PEEK, 5% carbon, 15% TFE	60		40,000	
Phenolic	250 2000		5000	
Phenolic, TFE filled	10		40,000	
Polycarbonate	2500	750	500	
Polycarbonate, 30% glass, 15% TFE	30	27,500	30,000	13,000
Polyester	210			
Polyester, 30% glass, 15% TFE	20	> 40,000	30,000	5500
Polyimide	150		100,000	
Polyimide, graphite filled	15		100,000	
Polyimide, SP211 filled	33		500,000	200,000
Polypropylene, 30% glass, 15% TFE	36	14,000	12,000	7500
Polysulfone	1500	5000	5000	3000
Polysulfone, 30% glass, 15% TFE	70	20,000	35,000	15,000
Polyurethane	340	2000	1500	< 1500
Polyurethane, 30% glass, 15% TFE	35	7500	10,000	5000
PPS, 30% glass, 15% TFE	110	27,000	30,000	> 30,000
Styrene acrylonitrile, 30% glass, 15% TFE	65	17,500	10,000	10,000

can be determined by the zero wear condition. This result in

$$h = \beta \frac{\delta \tau_{\max}^{2n}}{W^m (\Gamma_r \tau_y)^{2n}} S^n \quad (2.137)$$

where δ is the peak-to-valley roughness of the journal; τ_y , the yield point in shear of the bearing material; Γ_r , the zero wear factor of the model; and τ'_{\max} and W are the maximum shear stress and contact width in the unworn state, respectively, β is 0.0031 for $n = 2/3$, 0.048 for $n = 2/5$, and 0.34 for $n = 1/7$.

With most bearings, the initial clearance or difference in radii is so small that the standard Hertz formulas cannot be used to determine the stress or the contact width. At the same time, there is sufficient difference so that complete conformity between the

Table 2.15 Characteristics Coefficients of Friction for the Mixed and Boundary Lubrication Regimes for Several Bearing Materials*

Bearing material	μ_b	$\mu_m (\times 10^6)$
CuSn(90/10) (with Pb and Zn)	0.145	0.041
CuSn(90/10)	0.13	0.059
CuZn(60/30)	0.10	0.032
CuPb(70/30)	0.074	0.019
AlSn(90/10)	0.074	0.020
SnSb(75/10)	0.15	0.0058
PbSbSn(75/15/10)	0.185	0.0074
*Journal	JIS S45C carbon steel Hardness $226 \times 10^3 \text{ N/mm}^2$ Roughness 0.14 0.60 $\mu\text{m rms}$	
Lubricant	Turbine oil Kinematic viscosity, cS at 37.8 C 32 at 98.9 C 5.4	

Source: Ref. 113.

journal and the bearing does not occur. An approximation that may be used in these cases is to determine the arc under which the separation between the two surfaces is less than the sum of the roughnesses and assume conformity over that region defined by that arc. This region is illustrated in Fig. 2.52. Letting ϕ be that angle in radians, the projected area of contact for an aligned bearing is then $\phi / \pi DT$, where D is the diameter of the journal and T is the length of the bearing. For this case, W is $(\phi / \pi)D$. For many bearing conditions, ϕ is of the order of 1 and typically ranges from 0.5 to 1.5. A similar approach can also be applied in the axial direction to account for initial misalignment, which is also illustrated in Fig. 2.52. The criterion in this case is used to determine the axial length, L , over which the separation is less than the sum of the roughnesses. The projected contact area in this case is $(\phi / 2\pi)DL$. With misalignment, the average width of the contact region should be used for W (i.e., $(\phi / 2\pi)D$). For all these cases

$$\tau'_{\max} = \frac{P}{A} (0.25 + \mu^2)^{1/2} \quad (2.138)$$

where P is the load, A is the projected area, and μ is the coefficient of friction.

For situations where the clearance is large enough, the Hertz parallel cylinder formulation should be used for τ'_{\max} . These equations can also be used for situations where the axial misalignment is so large that contact is primarily with the edge of the bearing. Determining the radius of the edge and approximating the contact situation by a cylinder, whose length corresponds to ϕ and radius is the radius of the edge, can do this. If the clearance is also too large to use the conforming assumption, the contact can be treated as a Hertzian point contact.

This model provides two explanations for an initial period of higher volume wear rate observed with some bearings and methods to account for this behavior. If the initial period of high wear is associated with wear depth equivalent to or less than the surface roughnesses, this behavior is consistent with behavior in the zero wear regime, during which some wear can and does occur. Higher volume wear rates in this region are the result of higher

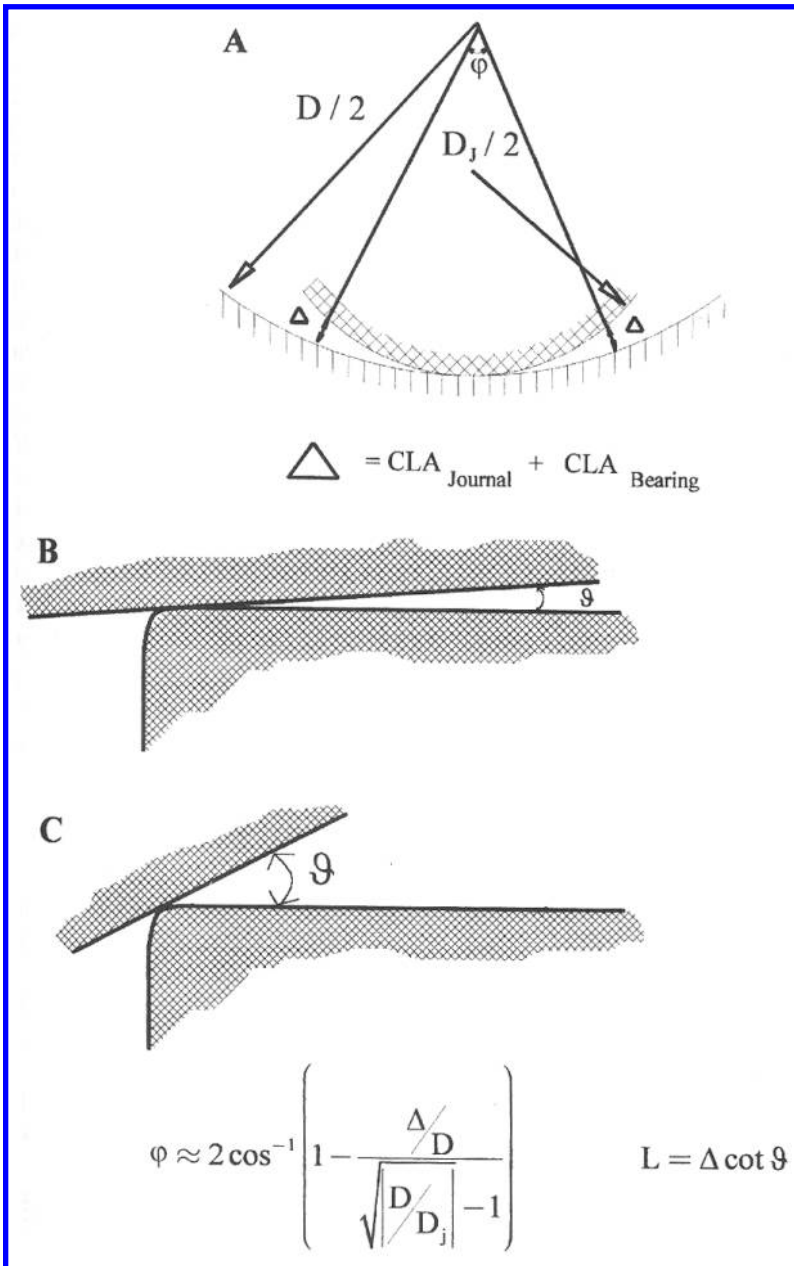


Figure 2.52 Possible journal bearing contact conditions. “A” illustrates the situation resulting from radial clearance. “B” and “C” indicate axial misalignment conditions. L is the contact length for condition “B”, based on the assumption that separation occurs at the sum of the contact roughnesses. “C” is an extreme situation where contact occurs on the edge and is approximated by a Hertzian line or point contact, depending on whether or not there is conformity in the radial direction.

initial stresses because of initial non-conformity and the initial contribution of other wear mechanisms, such as single-cycle deformation and adhesion. This level of run-in wear is included in the wear described by the zero wear relationship, which predicts the depth of wear after a certain amount of rubbing. For this situation, there is no need for special consideration of run-in. If the higher volume wear rates in the run-in are associated with wear depths greater than the surface roughnesses, initial axial misalignment is considered the cause because of the higher stress levels associated with the misaligned condition. In this case, the wear relationships for misaligned conditions are used for the initial period of wear and until axial conformity is achieved. Once conformity is achieved, the progression of wear is described by Eq. (2.136) with the exponent for conforming contact (i.e., $n = 2/3$). C in this equation is determined by matching the two relationships at the point of conformity, that is, the amount of sliding at which axial conformity is achieved. This is illustrated graphically in Fig. 2.53. To determine which approach is to be used, the design should be examined to determine the degree of initial misalignment. If the initial misalignment is such that conformity can be achieved with a depth of wear equal to or less than the roughness (i.e., the zero wear condition), conformity can be assumed throughout; if not, the more complex method, assuming initial misalignment, should be used.

Using the relationship between Γ_r and film thickness, this model can also be used for the mixed region of lubrication. Equation (4) of Appendix VII, which is applicable for any zero wear factor, can be used for this. Using a value of 1.30 for Γ_m (see Appendix VII), this relationship for sliding is

$$\Gamma_r^* = \left[\frac{p_a}{\Gamma_r^9} + \frac{(1-p_a)}{10.6} \right]^{-1/9} \quad (2.139)$$

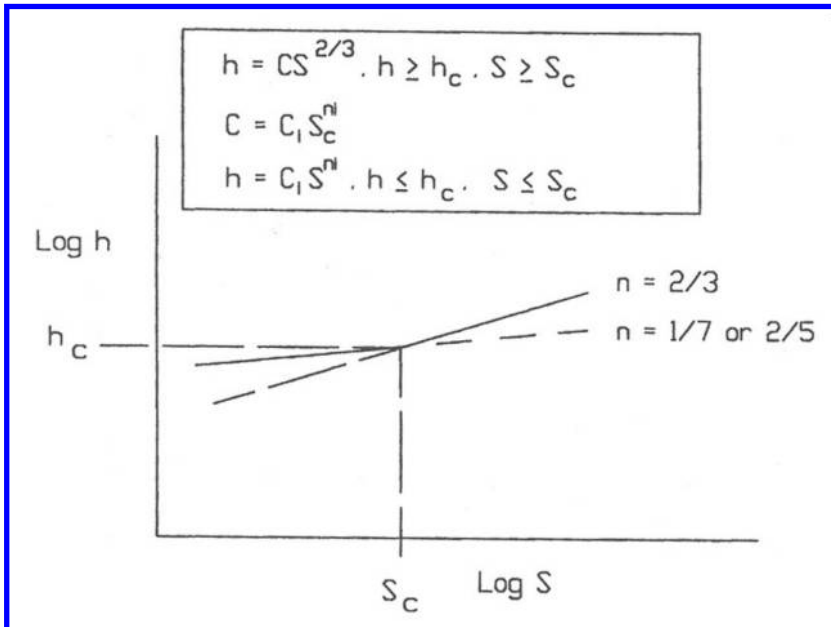


Figure 2.53 Wear model for journal bearings based on the Zero and Measurable Wear Models for sliding.

where

$$p_s = \exp(-1.81\Lambda^{1.25}) \tag{2.140}$$

Γ_r^* is the zero wear factor for a film thickness, h . Λ is the lubrication thickness parameter defined by Eq. (2.57). p_a is the fraction of the contact area over which there is asperity interaction. The effect is graphically illustrated in Fig. 2.20. The model, using the K factor, can also be applied to the mixed region. The common assumption for the effect of film thickness on the value of the wear factor, K , is that it is proportional to P_a , namely,

$$K^* = p_a K \tag{2.141}$$

where K^* is the reduce value of K .

Another model for wear in this region is one based on a correlation between the coefficient of friction and wear rate. This has been proposed for design use (113). Empirically, it has been found that

$$V = C\mu^5 \tag{2.142}$$

where V is the specific wear rate (i.e., wear volume divided by load and sliding distance); μ , the coefficient of friction; and C , a coefficient which is a function of materials. This is shown in Fig. 2.54 for two bearing systems. C is determined by fitting this expression to the wear rate of the boundary region, namely

$$C = \frac{V_b}{\mu_b^5} \tag{2.143}$$

where V_b and μ_b are the boundary wear rate and coefficient of friction, respectively.

This is based on the concept that both wear rate and friction should decrease with decreasing asperity interaction. In the boundary region, interface conditions regarding asperity interaction are considered to be constant. Wear rate is therefore constant over that region, as is the coefficient of friction, μ_b . As fluid lubrication begins to develop in the mixed region, the surfaces separate and the smaller asperities no longer interact and do not contribute to wear and friction. When full film lubrications occur, none of the asperities interact and wear rate goes to 0. Therefore, friction in this region is purely viscous. μ_m is the coefficient of friction at the transition from mixed to full film lubrication.

The model also includes the following empirical relationship for the coefficient of friction in the mixed lubrication regime:

$$\mu = \mu_b \left[1 + \left(\frac{\mu_b P'^{1/2} H}{\mu_m} \right)^2 \right]^{-1/2} \tag{2.144}$$

μ_b and μ_m , the characteristic coefficients of friction for the mixed and boundary regimes, respectively, are determined empirically. P' is a non-dimensional load parameter, defined as

$$P' = \frac{P}{TE'R} \tag{2.145}$$

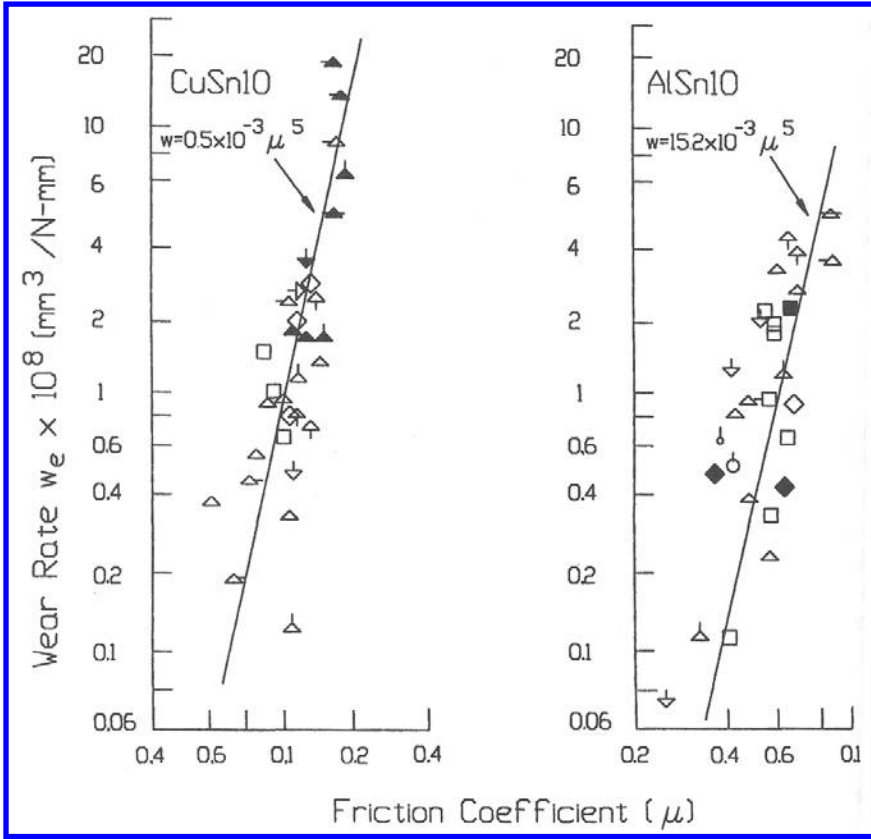


Figure 2.54 Relationship between wear rate and coefficient of friction in the mixed lubrication region of bearing operation. (From Ref. 113.)

where P is the load; T , the bearing length; E' , the reduced modulus,

$$E' = \frac{1 - \nu_j^2}{E_j} + \frac{1 - \nu_B^2}{E_B} \quad (2.146)$$

and R' , the equivalent radius of curvature,

$$R' = \frac{R_j R_B}{R_j + R_B} \quad (2.147)$$

\mathbf{H} is called the non-contact parameter and is the inverse of Dowson's D -ratio (124). \mathbf{H} is the ratio of the EHD film thickness, H , to a combined surface roughness, δ^* . For journal bearings,

$$\delta^* \approx 1.4 \delta_{j0} \quad (2.148)$$

where δ_{JO} is the initial RMS surface roughness of the journal (113), H is given by

$$H = 1.6R'W^{-0.13}U^{0.7}\alpha^{0.6}E^{0.6} \quad (2.149)$$

where α is the pressure coefficient of viscosity of the lubricant and U is a non-dimensional speed parameter defined as

$$U = \frac{\Omega\nu}{E'R'} \quad (2.150)$$

Ω is the viscosity of the lubricant and ν , the speed (125).

In the full film region, wear only occurs when the film is collapsed during stop-start cycles. The amount of sliding that occurs during a stop-start cycle can be estimated by the following expression:

$$S = \frac{Jw_c^2}{\mu_b P} \quad (2.151)$$

where J is the moment of inertia of the journal, and w_c is the angular velocity at the critical Sommerfeld number (110). To determine the increased clearance or wear depth in this mode of operation, the amount of sliding given by Eq. (2.151) is multiplied by the number of start-stop cycles and the product is used as the amount of sliding in the models for boundary lubrication. It is assumed in this approach that the kinetic energy of the journal can be equated to the energy dissipated by friction in the boundary lubrication region. The effect of the mixed region is considered to be negligible.

As these discussions indicate, the constant wear rate models and the Zero / Measurable Wear Models can be used to determine wear in all three lubrication regions. The implicit assumption of this approach is that the fundamental wear behavior is the same for all three regions; only the extent of exposure to this wear is different. For mixed lubrication, the exposure is related to the number of asperities in contact to those occurring in the boundary region. For bearing using full film lubrication, it is the amount of sliding that occurs under boundary lubrication conditions during stop-start cycles.

2.9. MODELS FOR EROSIWE WEAR

There is an absence of formally developed engineering models of erosion that have wide applicability. However, a review of studies of these wear situations indicates the existence of some common elements and trends which may be consolidated to form the basis of an engineering model. These studies indicate that the erosion wear rate, e , can often be expressed as the product of several factors (126–135). For limited ranges of erosive conditions, it is often possible to approximate e as the product of three terms, namely,

$$e(t) = K(t)A I \quad (2.152)$$

In this expression, K is a wear coefficient that is dependent on the materials (e.g., the erodent's composition, size, and shape and hardness and ductility of the wearing material) and environmental conditions (e.g., temperature and atmosphere). This is determined by a simulative erosion test and may be a function of time, t (128,136,137). A is a function of the impingement angle of the erodent and I is a factor expressing the intensity of wear situation. Both the tests used to determine K and the forms of the expressions for I and A depend on the nature of the erosive wear situation. These are different for particle erosion,

liquid erosion, and cavitation erosion and may vary within these categories. In the case of liquid and particle erosion, I is generally expressed as the product of two other factors, M and i . M is the rate of supply of the erodent. i is the intensity factor associated with an individual particle or droplet. Therefore, for these two situations Eq. (2.152) can be modified to the following:

$$e(t) = K(t)AMi \quad (2.153)$$

With many materials, the wear coefficient is found to vary with time. Characteristic patterns for erosion rates as a function of time are shown for cavitation and liquid and particle erosion in Figs. 2.55 and 2.56, respectively. Data indicate that for cavitation long-term values of K can be as low as a third of the peak value. For liquid and particle erosion, however, the effect appears to be less severe (e.g., typically less than a 20% reduction).

One reason for this type of behavior is the existence of fatigue wear processes in erosion (137). With fatigue wear processes, there is generally an incubation period before material loss occurs. Since erosion situations generally involve a distribution of impact conditions, this characteristic would be exhibited as a gradual increase to a stable erosion rate rather than as a sharp transition. Another reason for a time dependency is the modifications of the surface, which are caused by the erosion process. These modifications are used to explain differences between short- and long-term behavior (128,136,137). This type of behavior is generally associated with two changes that can occur as a result of initial wear or erosion. One is a change in surface topography or roughness and the other is a change in the physical properties of the material, such as work hardening in the case of some metals. In general, once these changes occur and a stable condition is established, K becomes independent of time. Prior to the development of this stable condition, erosion rates may be higher or lower, depending on the effects that these changes have on erosion behavior.

For liquid drops, there is evidence that the following forms for A and i can be used:

$$A = \sin^n \alpha \quad (2.154)$$

$$i = v^m \quad (2.155)$$

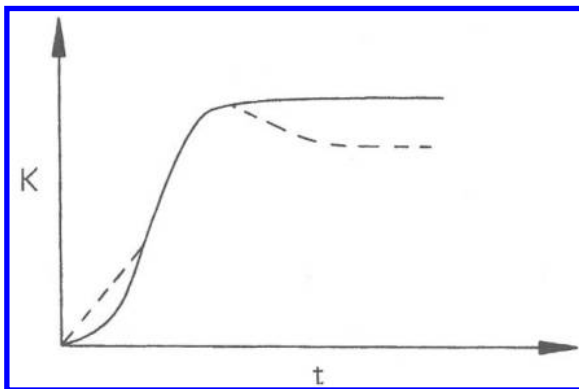


Figure 2.55 Typical behavior of erosion wear coefficients as a function of time in the case of cavitation.

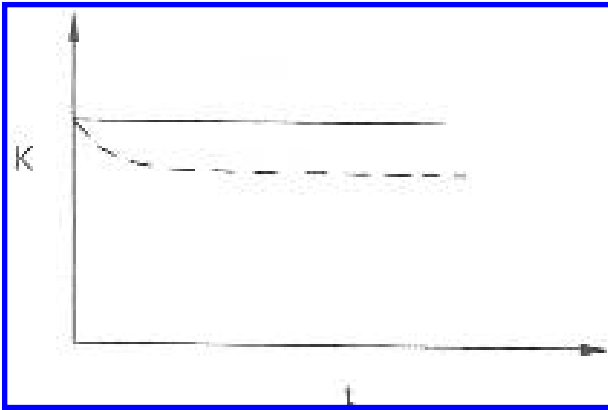


Figure 2.56 Typical behavior of erosion wear coefficients as a function of time in the case of solid and liquid particle erosion.

where α is the impingement angle and v the velocity of the drop, m and n are determined experimentally as a function of material and drop size. Typical values for m range from 2 to 10; for n , 2 to 3 (134).

With particle erosion, two modes are generally identified, a ductile mode and a brittle mode (133,138). Actual erosion behavior is considered to be the sum of these two components. This is illustrated in Fig. 2.57. In this case, Eq. (2.153) is applied to the two individual modes. For ductile behavior, the following is often used:

$$A = \cos^n \alpha \sin\left(\frac{\pi\alpha}{2\beta_0}\right), \quad \alpha < \beta_0 \tag{2.156}$$

$$A = \cos^n \alpha, \quad \alpha \geq \beta_0 \tag{2.157}$$

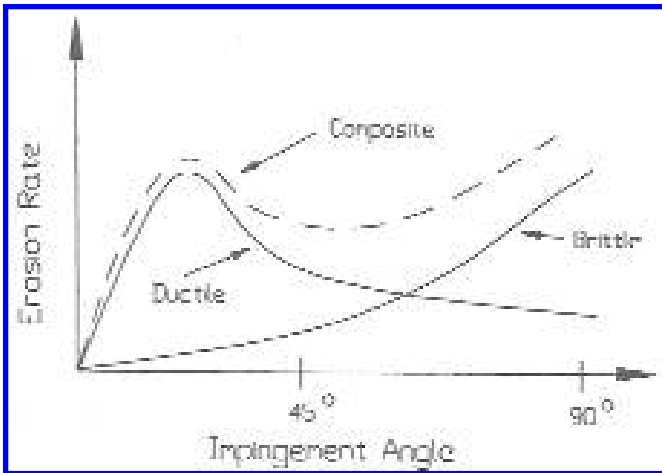


Figure 2.57 Erosion wear models.

$$i = \nu^n \quad (2.158)$$

$$K = K_d \quad (2.159)$$

For the brittle mode, the corresponding relationships are

$$A = \sin^m \alpha \quad (2.160)$$

$$i = \nu^m \quad (2.161)$$

$$K = K_b \quad (2.162)$$

The total erosion rate is given by

$$e = \left[K_d \nu^n \cos^n \alpha \sin \left(\frac{\pi \alpha}{2\beta_0} \right) + K_b \nu^m \sin^m \alpha \right] \mathbf{M}, \quad \alpha \leq \beta_0 \quad (2.163)$$

$$e = (K_d \nu^n \cos^n \alpha + K_b \nu^m \sin^m \alpha) \mathbf{M}, \quad \alpha \geq \beta_0 \quad (2.164)$$

In this case K_d , K_b , β_0 , m , and n are determined empirically by fitting Eq. (2.163) or Eq. (2.164) to the data, n and m typically are in the range of 2 or 3. In addition, there is some evidence to indicate that when particle velocities are sufficient to cause inelastic deformation, m and n may be considered to be the same (133).

There is usually no angular dependency in cavitation erosion as there is for particle and droplet erosion. As a result, Eq. (2.153) can be simplified to

$$e(t) = K(t) I \quad (2.165)$$

In this case I is a measure of the intensity of the cavitation field. For example in the case of a vibrating source, the intensity is related to the amplitude of the vibration, δ (136). Namely,

$$I \propto \delta^n \quad (2.166)$$

In the case of a cavitating jet, it is related to the velocity of the jet (137)

$$I \propto v_j^n \quad (2.167)$$

v_j is the jet velocity. An example of the effect on source intensity on erosion rate is shown in Fig. 2.58. The exponents in each case need to be determined experimentally. The constant of proportionality can be combined with K . In the case of the vibrating horn, n has been found to be near unity; for the jet, it is considerably higher. For example, values in the range of 7–8 have been found with jet induced cavitation.

It is sometimes possible to expand this general approach to other parameters affecting erosion. In the case of particle erosion, for example, there is some evidence that

$$K \propto D^m \quad (2.168)$$

where D is particle diameter and m is an empirical constant dependent on material (128,139). In this case, Eq. (2.153) can be expanded to

$$e(t) = K(t) A I D^m \quad (2.169)$$

where K is now independent of particle size.

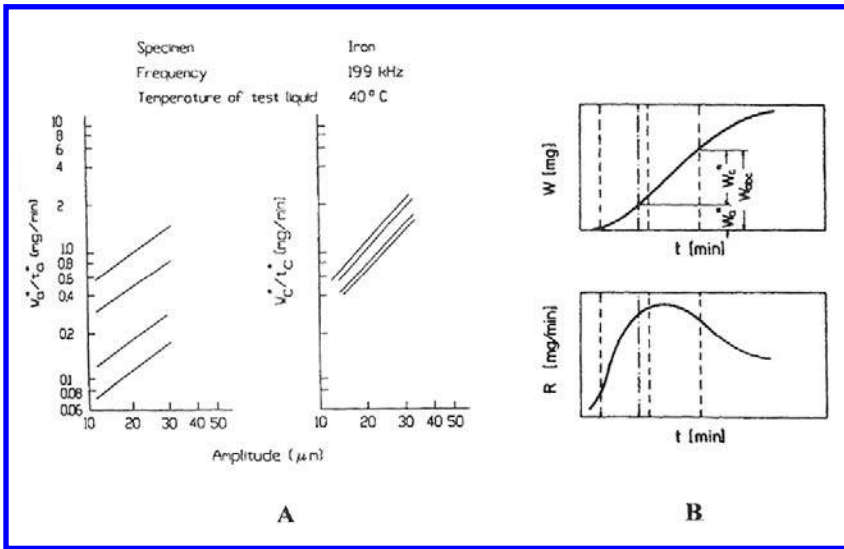


Figure 2.58 “A” shows the effect of the intensity of a cavitation field, induced by a vibrating source, on erosion rate for two different regions of the erosion curve. “B” illustrates the different regions of a typical cavitation erosion curve and the erosion rate behavior in those regions. The data are for initial and maximum erosion rate periods. (From Ref. 136. Reprinted with permission from ASTM).

2.10. MODELS FOR TOOL WEAR

The majority of tool wear models relate tool life to operational parameters, such as speed, feed, and tool geometry. The oldest and simplest relationship of this type is Taylor’s equation, which relates tool life, T , to cutting speed, V ,

$$VT^n = C \tag{2.170}$$

n and C are empirical coefficients that are determined in controlled machining tests (140,141). Both of these coefficients are dependent on materials, tool shape, and other machining parameters. More complex empirical models have also been proposed which relate tool life to various machining parameters (142). Up to three operational parameters are usually considered in these type of relationships, namely, speed, V , feed, F , and a geometry or design factor, such as size or angle, D . A general form that summarizes these is

$$\begin{aligned} \ln T = & c_0 + c_1 \ln V + c_2 \ln F + c_3 \ln D \\ & + c_{11}(\ln V)^2 + c_{22}(\ln F)^2 + c_{33}(\ln D)^2 \\ & + c_{12} \ln V \ln F + c_{13} \ln V \ln D + c_{23} \ln F \ln D \end{aligned} \tag{2.171}$$

The c ’s are determined by fitting this type of expression to experimental data.

This form is equivalent to the original Taylor equation if all the c ’s, except c_0 and c_1 , are assumed to be 0. When only the first-order terms are considered, the form is referred to as the *Extended Taylor Relationship* for tool life.

There is evidence that a more physical model can be used, as well. It has been found that the following expression can be applied to tool wear (143).

$$h = C' V \sigma_t e^{-C''/\theta} \quad (2.172)$$

In this expression h is the depth rate of wear, V is the tool speed, σ_t is the pressure between the tip of the tool and the work piece, and θ is the absolute temperature of the tool tip. C' and C'' are empirical coefficients. The ability of this type of expression to describe tool wear is shown in Figs. 2.59 and 2.60 for flank and crater wear, respectively. In examining this expression, it can be seen that the first-order terms are basically equivalent to a PV factor that is associated with a linear wear model, such as those used for sliding. The exponential factor, on the other hand, has the form of the Arrhenius relationship, which is often used to describe chemical reactions.

The significance of temperature in tool wear is to be anticipated because of the high temperatures that can occur in machining and the presence of highly reactive surfaces

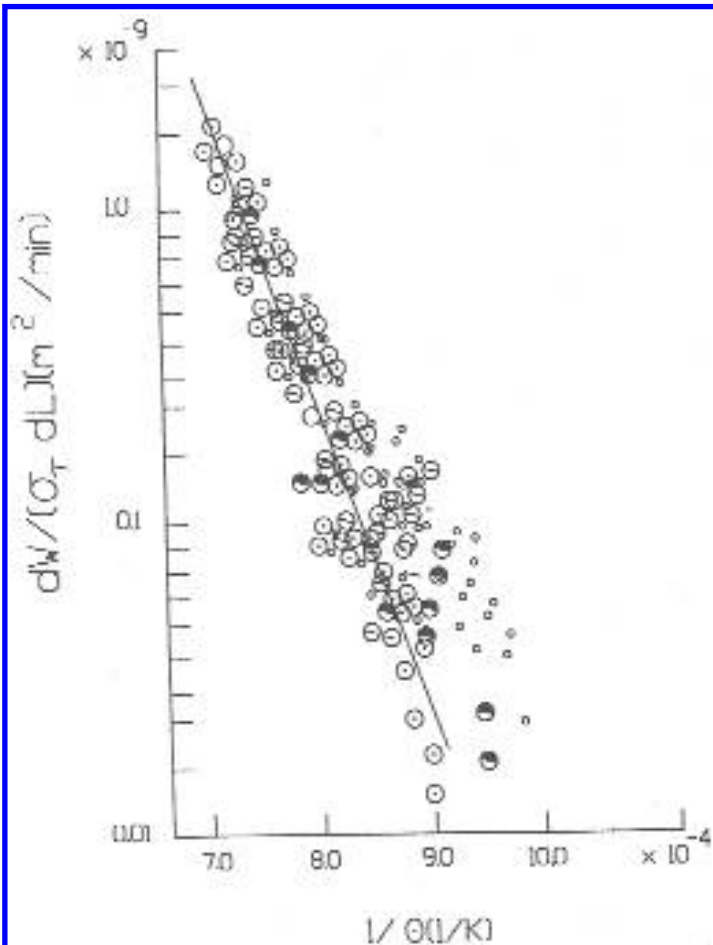


Figure 2.59 The effect of temperature on crater wear. (From Ref. 6.)

(newly formed) in the tip region. Often more than one type of reaction is possible and transitions in wear behavior or tool life can occur because of changes in the relative significance of these individual reactions. Two distinct regions of the wear of a carbide tool can be seen in Fig. 2.60. Different complex Fe–W–Co carbides are found in the two regions.

By specifying a maximum allowed wear depth, H , Eq. (2.172) can be used to obtain the life of a tool, T . Namely,

$$T = B' V^{-1} \sigma_T^{-1} e^{C'/\theta} \tag{2.173}$$

where

$$B' = \frac{H}{C'} \tag{2.174}$$

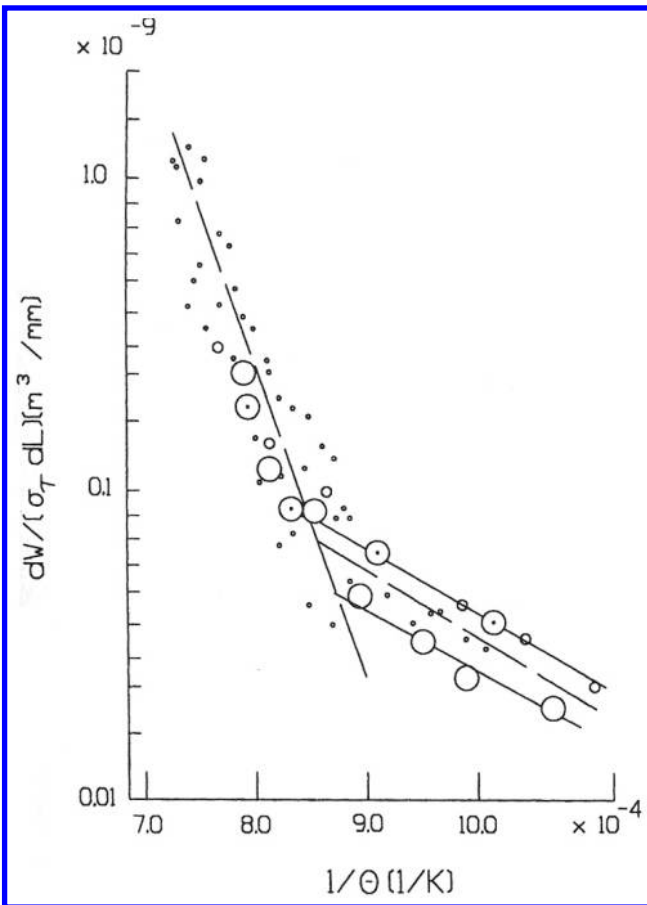


Figure 2.60 The effect of temperature on flank wear. (From Ref. 6.)

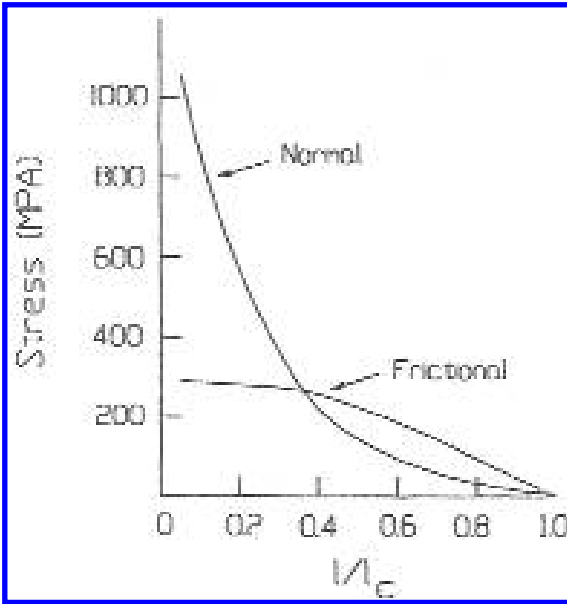


Figure 2.61 Stress distributions on a rake face as a function of distance from the tip. L_c is the position where the chip leaves the tool face. (From Ref. 6.)

Additional information is required to use this model, namely, σ_t and Θ . These may be determined by suitable analytical techniques (e.g., finite element modeling and heat transfer analysis). Experimental methods may be used as well. For example, Θ may be determined by the use of thermocouples or IR (infrared) instrumentation. σ_t can also be estimated by measuring the normal force between the tip and the work piece, N , and solving the following equation for the constant, D :

$$N = \int_{A_t} \alpha e^{D(1-L/L_c)} dA_t \quad (2.175)$$

since

$$\sigma_t \approx \alpha e^{D(1-L/L_c)} \quad (2.176)$$

L is the position along the tool face, as indicated in Fig. 2.61. L_c is the tool–chip contact length, A_t is the tool–chip contact area, α is the stress at which the chip leaves the tool ($L = L_c$). To use this approach A_t , L_c , and α need to be determined. A value of 10 MPa has been used for α (for steel) (143).

REFERENCES

1. K Ludema, R Bayer, eds. *Tribological Modeling for Mechanical Designers*. West Conshohocken, PA, STP 1105, ASTM, 1991.
2. P Blau. *Friction and Wear Transitions of Materials*. Park Ridge, NJ: Noyes Publication, 1989.
3. R Bayer. Prediction of wear in a sliding system. *Wear* 11:319–332, 1968.
4. V Jain, S Bahadur. Experimental verification of fatigue wear equation. *Proc Intl Conf Wear Mater. ASME* 700–706, 1981.

5. P Clayton, D Danks. Rolling / sliding conditions. *Proc Intl Conf Wear Mater. ASME* 191–204, 1989.
6. E Usui, T Shirakashi, T Kitagawa. Analytical prediction of cutting tool wear. *Wear* 100: 129–152, 1984.
7. O Vingsbo. Wear and wear mechanisms. *Proc Intl Conf Wear Mater. ASME* 620–635, 1979.
8. N Suh. The delamination theory of wear. *Wear* 25:111–124, 1973.
9. A Rosenfield. Modelling of dry sliding wear. *Proc Intl Conf Wear Mater. ASME* 390–393, 1983.
10. D Kuhlmann-Wildorf. Parametric theory of “Adhesive” wear in uni-directional sliding. *Proc Intl Conf Wear Mater. ASME* 402–413, 1983.
11. T Quinn, J Sullivan, D Rowson. New developments in the oxidational theory of the mild wear of metals. *Proc Intl Conf Wear Mater. ASME* 1–11, 1979.
12. H Chang. Fundamentals of elasto-hydrodynamic contact phenomena. In: N Suh, N Saka, eds. *Fundamentals of Tribology*. Cambridge, MA: MIT Press, 1980, pp 1009–1048.
13. J Archard. Contact and rubbing of flat surfaces. *J Appl Phys* 24:981–988, 1953.
14. S Lim, M Ashby. Wear-mechanism maps. *Acta Metal* 35(1):1–24, 1987.
15. A Bower, K Johnson. The influence of strain hardening on cumulative plastic deformation in rolling and sliding line contact. *J Mech Phys Solids* 37(4):471–493, 1989.
16. K Johnson. *Proceedings of the 20th Leeds-Lyon Symposium on Tribology*. Vol. 21. Elsevier, 1994.
17. E Zaretsky, ed. *Life Factors for Rolling Bearings*. STLE SP-34. Park Ridge, IL: STLE, 1999.
18. J Archard, W Hirst. The wear of metals under unlubricated conditions. *Proc Roy Soc A* 236:397–410, 1956.
19. J Archard. *J Appl Phys* 23:18, 1952.
20. Atkins, M Omar. The load-dependence of fatigue wear in polymers. *Proc Intl Conf Wear Mater. ASME* 405–409, 1985.
21. J Hailing. A contribution to the theory of mechanical wear. *Wear* 34(3):239–250, 1975.
22. I Kraghelskii, R Loginov. Prediction of wear rate by theoretical experimental method. *Proc Intl Conf Wear Mater. ASME* 394–401, 1983.
23. R Fusaro. Effect of load, area of contact, and contact stress on the tribological properties of polyimide bonded graphite fluoride films. *Proc Intl Conf Wear Mater. ASME* 625–636, 1981.
24. H Da-Yue, G Ting-Hong, L Hang-Chou, Q Rui-Zhong. *Proc Intl Conf Wear Mater. ASME* 644–647, 1981.
25. T Quinn, J Sullivan. A review of oxidational wear. *Proc Intl Conf Wear Mater. ASME* 110–115, 1977.
26. J McGrew. *Standard news* 2(9):22–28, 56–57, 1974.
27. G Massouros. Model of wear in a plain bearing under boundary lubrication. *Trib Intl* 15(4):193–198, 1982.
28. K Kato. Tribology of ceramics. *Wear* 136:117–134, 1990.
29. Z Rymuza. Wear in polymer micropairs. *Proc Intl Conf Wear Mater. ASME* 125–132, 1981.
30. V Sastry, D Singh, A Sethuramiah. Modeling of wear under partial elasto-hydrodynamic lubrication contacts. *Proc Intl Conf Wear Mater. ASME* 765–770, 1989.
31. H Veerbeek. Tribological systems and wear factors. *Wear* 56:81–92, 1979.
32. E Rabinowicz. *Friction and wear of materials*. New York: John Wiley and Sons, 1965.
33. M Peterson, W Winer, eds. *Wear control handbook*. New York: ASME, 1980.
34. G Pratt, W Wilson. The performance of steel-backed acetal copolymer bearings. *Wear* 12(2):73–90, 1968.
35. G Chen, G Jiao, Y Wang. Wear prediction for unlubricated piston rings. *Proc Intl Conf Wear Mater. ASME* 645–652, 1989.
36. J Anderson. Wear of commercially plastic materials. *Trib Intl* 15(5):255–264, 1982.
37. M Wolverson, J Theberge. How plastic composites wear against metals: machine design, 2 / 6 / 86, 67–71. Cleveland, OH: Penton Publishing Co., 1986.

38. R Steijn. Friction and wear of plastics. In: D Rigney, W Glaeser, eds. Source Book on Wear Control Technology. Metal Park: ASM, 1978, pp 371–383.
39. M Neale, ed. Tribology Handbook. New York: John Wiley and Sons, 1973.
40. A Beerbower. Boundary Lubrication. Scientific and Technical Applications Forecast, DAHC19-69-C-0033, Department of the Army, 1972.
41. M Wallbridge, D Dowson. Distribution of wear rate data and a statistical approach to sliding wear theory. Proc Intl Conf Wear Mater. ASME 101–110, 1987.
42. R Bayer. A model for wear in an abrasive environment as applied to a magnetic sensor. Wear 70:93–117, 1981.
43. K Zum Gahr. Relation between abrasive wear rate and the microstructure of metals. Proc Intl Conf Wear Mater. ASME 266–274, 1979.
44. B Briscoe, P Evans, J Lancaster. The influence of the mean debris particle size on the abrasive wear rate of PTFE. Proc Intl Conf Wear Mater. ASME 607–618, 1987.
45. Y Wang, Z Wang. An analysis of the influence of plastic indentation on three body abrasive wear of metals. Proc Intl Conf Wear Mater. ASME 607–618, 1987.
46. K Zum Gahr. Relation between abrasive wear rate and the microstructure of metals. Proc Intl Conf Wear Mater. ASME 266–274, 1979.
47. K Hokkirigawa, K Kato. Theoretical estimation of abrasive wear resistance based on microscopic wear mechanism. Proc Intl Conf Wear Mater. ASME 1–8, 1989.
48. R Mayville. Abrasive concentration effects on wear under reciprocating conditions. Proc Intl Conf Wear Mater. ASME, pp 83–88, 1989.
49. R Bayer. The influence of hardness of the resistance to wear by paper. Wear 84:345–351, 1983.
50. E Rabinowicz. Abrasive wear resistance as a materials test. Lub Eng 33:378–381, 1977.
51. R Bayer. The influence of hardness of the resistance to wear by paper. Wear 84:345–351, 1983.
52. G Yampolski, I Kragelskii, I Yushakov. Abrasive wear of rolling bearings. Trib Intl 14(3): 137–138, 1981.
53. M Moore, F King. Abrasive wear of brittle solids. Proc Intl Conf Wear Mater. ASME 275–285, 1989.
54. R Bayer, T Ku. Handbook of Analytical Design for Wear. New York: Plenum Press, 1964.
55. R Bayer, W Clinton, T Ku, C Nelson, R Schumacher, J Sirico, A Wayson. An engineering model for wear. Paper No. 66-MD-11. Design Eng Conf Show. ASME Feb, 1966.
56. R Bayer, W Clinton, T Ku, C Nelson, R Schumacher, J Sirico, A Wayson. Applying the wear model to design problems. Paper No. 66-MD-12. Design Eng Conf Show. ASME Feb, 1966.
57. R Bayer, W Clinton, T Ku, C Nelson, R Schumacher, J Sirico, A Wayson. Special considerations relating to the engineering model for wear. Paper No. 66-MD-13. Design Eng Conf Show. ASME Feb, 1966.
58. R Bayer, A Shalkey, A Wayson. Designing for zero wear: machine Design, 1 / 9 / 69, 142–151 Cleveland, OH: Penton Publishing Co., 1969.
59. R Bayer, A Wayson. Designing for measurable wear: machine design, 8 / 7 / 69, 118–127. Cleveland, OH: Penton Publishing Co., 1969.
60. R Bayer, W Clinton, C Nelson, R Schumacher. Engineering model for wear. Wear 5: 378–391, 1962.
61. R Bayer, W Clinton, J Sirico. A note on the application on the stress dependency of wear in the wear analysis of an electrical contact. Wear 7:282–289, 1964.
62. A Beerbower. Boundary Lubrication, Scientific and Technical Applications Forecast, DAHC19-69-0033. Department of the Army, 1972.
63. J Dumbleton, S Rhee. The application of a zero wear model to metal / polyethylene sliding pairs. Wear 35:233–250, 1975.
64. E Finkin. What happens when parts wear: machine design 3 / 19 / 70, 149–154. Cleveland, OH: Penton Publishing Co., 1970.
65. A Wayson. A study of fretting on steel. Wear 7:435–150, 1964.
66. R Bayer, J Sirico. Wear of electrical contacts due to small-amplitude motion. IBM J R&D 15(2):103–107, 1971.

67. C Moyer, H Neifert. A First-order solution for the stress concentration present at the end of roller contact. *ASLE Trans* 6:324–326, 1963.
68. S Timoshenko, J Goodier. *Theory of elasticity*. 2nd Ed. New York: McGraw-Hill, 1951.
69. J Goodier, C Loutzenheiser. Pressure peaks at the ends of plane strain rigid die contacts (Elastic). *Trans ASME* June:462–463, 1965.
70. W Clinton, T Ku, R Schumacher. Extension of the engineering model for wear to plastics, sintered metals and platings. *Wear* 7:354–367, 1964.
71. R Bayer, R Schumacher. On the significance of surface fatigue in sliding wear. *Wear* 12: 173–183, 1968.
72. J Hailing, R Arnell. Ceramic coatings in the war on wear. *Wear* 100:367–380, 1984.
73. J Dumbelton. *Wear* 24:229, 1973.
74. R Bayer, E Hsue, J Turner. A Motion-induced sub-surface deformation wear mechanism. *Wear* 154:193–204, 1992.
75. R Bayer. Influence of oxygen on the wear of silicon. *Wear* 69:235–239, 1981.
76. R Bayer, J Sirico. The influence of surface roughness on wear. *Wear* 35:251–260, 1975.
77. R Bayer, J Sirico. Some observations concerning the friction and wear characteristics of sliding systems involving cast ceramics. *Wear* 16:421–430, 1970.
78. RG Bayer. *Wear Analysis for Engineers*. Chapters 6.1.2 and 7.2. NY: HNB Publishing, 2002.
79. K Wellinger, H Breckel. *Wear* 13:257–281, 1969.
80. P Engel, T Lyons, J Sirico. Impact wear model for steel specimens. *Wear* 23:185–201, 1973.
81. P Engel, R Bayer. The wear process between normally impacting elastic bodies. *J Lub Tech* Oct:595–604, 1974.
82. P Engel. *Impact wear of materials*. Tribology Series 2. New York: Elsevier Science Publishing Co., 1978.
83. P Engel. Measurable impact wear theory; Impact wear of materials. Vol. 214–221. Chapter 8. Tribology Series 2. New York: Elsevier Science Publishing Co., 1978.
84. P Engel. Measurable impact wear theory. Impact wear of materials, Chapter 8. Tribology Series 2. New York: Elsevier Science Publishing Co., 1978.
85. P Engel. Measurable impact wear theory. Impact wear of materials, Chapter 8. Tribology Series 2. New York: Elsevier Science Publishing Co., 1978, pp 228–235.
86. R Bayer. Impact wear of elastomers. *Wear* 112:105–120, 1986.
87. RG Bayer. *Wear Analysis for Engineers*, Chapters 6.1.3. NY: HNB Publishing, 2002.
88. P Engel. Impact wear through flexible media. Impact Wear of Materials, Chapter 10. Tribology Series 2. New York: Elsevier Science Publishing Co., 1978, p. 277.
89. R Bayer, P Engel, E Sacher. Impact wear phenomena in thin polymer films. *Wear* 32:181–194, 1975
90. R Morrison. Test data let you develop your own load / life curves for gear and cam materials: machine design, 8 /1/ 67, 102–108. Cleveland, OH: Penton Publishing Co., 1967.
91. E Buckingham, G Talbourdet. Roll test on endurance limits of materials. *ASME* Jan, 1950.
92. G Talbourdet. A progress report on the surface endurance limits of materials. *ASME Paper* No. 54-LUB-14, 1954.
93. W Cram. *Cam Design*. Proceeding of the Third Mechanisms Conference. Purdue University, 5/56, 1956
94. E Buckingham. *Analytical mechanics of gears*. New York: McGraw-Hill, 1949.
95. T Harris. *Rolling Bearing Analysis*. 2nd ed. New York: John Wiley and Sons, 1984.
96. G Lundberg, A Palmgren. Dynamic capacity of rolling bearings. *Acta Polytechnica*. Roy Swedish Acad Eng Sci, ME Series 1(3):7, 1947.
97. G Lundberg, A Palmgren. Dynamic capacity of roller bearings. *Acta Polytechnica*. Roy Swedish Acad of Eng Sci, ME Series 2(4):96, 1952.
98. ANSI/AFBMA Standards 9 and 11, Standard 9, Load Ratings and Fatigue Life for Ball Bearings; Standard 11, Load Ratings and Fatigue Life for Roller Bearings. American National Standards Institute and Anti-Friction Bearing Manufactures Association, 1990.
99. *Lubrication*, 60(Jul-Sept, Oct-Dec), 1974, and 61(Jan-Mar), 1975, Beacon, NY: Texaco.

100. An Engineering Design Guide. Life Adjustment Factors for Ball and Roller Bearing an Eng Design Guide, New York. ASME, 1971.
101. L Valentin, A Bianchi. Life adjustment factors for tapered roller bearings. Proceedings of the First European Trib. Congress. Inst Mech Eng 1973, pp 377–381.
102. D Dareing, E Radzimovsky. Misaligned roller bearings - how fast will they fail: machine design 36(4), 2 / 13 / 64, 175–179. Cleveland, OH: Penton Publishing Co., 1964.
103. J Liu. J Lub Tech 93(1):60, 1971.
104. E Ellis. Tribology 3(1):29, 1970.
105. TA Harris. Rolling bearing fatigue rolling bearing analysis. 3rd ed. Chapter 18. 665–776 NY: John Wiley & Sons, 1991.
106. JH Rumbarger, AB Jones. Dynamic capacity of oscillating rolling element bearings JOLT. ASME Trans 90 Series F(1):130–138, 1997.
107. TA Harris. Rolling Bearing Fatigue. Rolling Bearing Analysis. 3rd. ed. NY: John Wiley & Sons, 1991, pp 772–774.
108. E Zaretsky ed. Current Practice Life Factors for Rolling Bearings, STLE SP-34, Chapter 1. 1–46. Park Ridge, II: STLE, 1999.
109. J McGrew, G Han, R Lee, W MacFarland, R Thompson. Synthesis of Strength Distributions as Functions of Wear. Tech. Report No. RADC-TR-67-557, Rome Air Dev. Center, Nov 1967.
110. J McGrew. Design for wear of sliding bearings. Standard News 2(9):22–28, 56–57, 1974.
111. J Burwell et al. Effects of surface finish. J Appl Mech June: 1941.
112. L Tarasov. Relation of surface roughness to actual surface profile. Trans ASME 67: 186–189, 1945.
113. Y Doi, T Haba. Friction and wear characteristics of bearing materials under boundary lubricated conditions. Proc Intl Conf Wear Mater. ASME 310–316, 1977.
114. M Shaw, F Macks. Analysis and Lubrication of Bearings. New York: McGraw-Hill, 1949.
115. M Neale ed. Tribology Handbook. New York: John Wiley and Sons, 1973.
116. Mechanism of Lubrication in Porous Metal Bearings. Paper No. 89, 151–157, Inst Mech Eng Conf Lub Wear Oct. 1957.
117. A Cameron, V Morgan, A Stainsby. Critical conditions for hydrodynamic lubrication of porous metal bearings. Proc Inst Mech Eng 176(28):761–770, 1962.
118. V Morgan. Hydrodynamic porous metal bearings lub. Eng. Dec. 448–455, 1964.
119. W Roulea. Hydrodynamic lubrication of narrow press-fitted porous metal bearings; Journal of Basic Engineering, March 1963, Transactions of ASME. ASME Paper No. 62-LUB-54, 1962.
120. V Morgan. Study of the design criteria fir porous metal bearings Paper No. 88, Proc Inst Mech Eng Conf Lub Wear Oct: 1957.
121. J Lancaster. Dry bearings: A survey of materials and factors affecting their performance. Trib Intl 6:219–251, 1973.
122. J Theberge. A guide to the design of plastic gears and bearings. Machine Design 2/5/70, 114–120. Cleveland, OH: Penton Publishing Co., 1970.
123. M Neale ed. Tribology Handbook. New York: John Wiley and Sons, 1973.
124. D Dowson. J Mech Eng Sci 4(1): 1962.
125. D Dowson, G Higginson. Elastohydrodynamic Lubrication. Elmsford, NY: Pergamon Press, 1966.
126. C Dimond, J Kirk, J Briggs. The evaluation of existing models for impact erosion and abrasive wear of ceramic materials. Proc Intl Conf Wear Mater. ASME 333–339, 1983.
127. I Finnie, A Levy, D. McFadden. In: W Adler, ed. Erosion: Prevention and Useful Applications. STP 664. ASTM, Fundamental Mechanisms of the Erosive Wear of Ductile Metals by Solid Particles; West Conshohocken, PA 36–58, 1979.
128. C Sargent, P Mehrotra, H. Conrad. Multiparticle erosion of pyrex glass. In: W Adler, ed. Erosion: Prevention and Useful Applications. STP 664. ASTM, West Conshohocken, PA 77–100, 1979.

129. M Gulden. Solid-Particle Erosion of high-Technology Ceramics (Si_3N_4 , Galss-Bonded Al_2O_3 , and MgF_2). In: W Alder, ed. Erosion: Prevention and Useful Applications. STP 664. ASTM, West Conshohocken, PA 100–122, 1979.
130. H Shimura, Y Tsuya. Effect of atmosphere on the wear rate of some ceramics and cermets. Proc Intl Conf Wear Mater. ASME 452–461, 1977.
131. B Madsen. A comparison of the wear of polymers and metal alloys in laboratory and field slurries. Proc Intl Conf Wear Mater. ASME 741–752, 1989.
132. A Ruff, S Wiederhom. Erosion, Treatise on Materials Science and Technology. Vol. 16. San Diego: Academic Press, 1979.
133. M Menguturk, E Sverdrup. Calculated tolerance of a large electric utility gas turbine to erosion damage by coal gas ash particles. In: W Adler, ed. Erosion: Prevention and Useful Applications. STP 664. ASTM, West Conshohocken, PA 193–226, 1979.
134. G Schmitt. Influence of materials construction variables on the rain erosion performance of carbon-carbon composites. In: W Adler, ed. Erosion: Prevention and Useful Applications. STP 664. ASTM, West Conshohocken, PA 376–405, 1979.
135. G Sheldon, I Finnie. Trans ASME 1966; 888:393–400.
136. M Matsumura. Influence of test parameters in vibratory cavitation erosion tests. In: W Adler, ed. Erosion: Prevention and Useful Applications. STP 664. ASTM, West Conshohocken, PA 434–458, 1979.
137. A Lichtarowicz. Cavitating jet apparatus for cavitation erosion testing. In: W Adler, ed. Erosion: Prevention and Useful Applications. STP 664. ASTM, West Conshohocken, PA 530–579, 1979.
138. L Ives, A Ruff. Electron microscopy study of erosion damage in copper. In: W Adler, ed. Erosion: Prevention and Useful Applications. STP 664. ASTM, West Conshohocken, PA 5–35, 1979.
139. G Sheldon, I Finnie. J Eng Industry Nov:393–400, 1966.
140. M Peterson, W Winer, eds. Wear Control Handbook. New York: ASME 1980.
141. E Usui, T Shirakashi, T Kitagawa. Analytical prediction of cutting tool wear. Wear 100:129–152, 1984.
142. M Peterson, W Winer, eds. Wear Control Handbook. New York: ASME 924, 1980.
143. E Usui, T Shirakashi, T Kitagawa. Analytical prediction of cutting tool wear. Wear 100: 129–152, 1984.
144. P Engel. Percussive impact wear. Trib Intl Jun:169–176; 1978.
145. K Cooper. Laser Surface processing. In: P Blau, ed. Lubrication and Wear Technology, ASM Handbook. Vol. 18. ASM Intl, 1992, pp 861–872.
146. R Lewis. Paper No. 69AM5C-2. Proceedings of the 24th ASLE Annual Meeting, Philadelphia, 401–412, 1969.
147. P Engel. Experimental and analytical approaches in impact wear. Proc Intl Conf Wear Mater ASME 401, 1977.
148. R McClocklin, IBM Technical Report No. 07.436, General Systems Division, Rochester, MN, 1971.

3

Wear Design

3.1. GENERAL

Wear design is a process in which values of design parameters are selected in order to achieve a specific wear performance. This process is different than a simple materials approach to wear. In a basic materials approach, the concern is limited to selecting the best material for the application. This is usually based on the rankings of materials obtained in a simulative wear test. In wear design, however, the concern or focus is not limited to the selection of materials but includes the potential modification and determination of any design parameter that can affect wear performance in the application. Wear design is also different than a problem solving. Wear design is an anticipatory approach, which is an integral part of a design methodology. Problem solving is a reactionary approach in response to wear failure. It often focuses on determining the parameter or element whose change has caused the failure and making the necessary modifications to eliminate the failure. A methodology for problem solving is described in Part B, along with examples of this approach. The analysis of wear situations is a central element of problem solving and wear design (1). A useful methodology for performing this type of analysis for both problem solving and wear design is described in *Wear Analysis for Engineers* (1). A flow-chart of the wear analysis process is shown in Fig. 3.1 and the information generally required for a wear analysis is shown in Table 3.1. Many of the elements involved in a wear analysis and the information required are also involved in wear design and problem solving. The common elements of these processes, as they apply to wear design, are discussed in this section on wear design. The common elements of these processes as they apply to problem solving are covered in Part B. Most elements are common to all three processes.

Wear design is an element in the overall development of a design. The first step in a wear design process involves the characterization of a tribosystem in terms of key design parameters. The second step in the process is the selection of and use of a model to either project wear performance or to determine values of a parameter or parameters to achieve a particular wear life. Using these models, different design options are evaluated until an acceptable design(s) is achieved. If an initial set of parameters (selected for reasons other than wear) results in a satisfactory design, the process is complete. If not, the tribosystem is examined for options, which are evaluated, until an acceptable design is obtained. In practice, material changes are often considered first in this iterative cycle. However, changes to other elements, such as size, shape, and lubrication, are also included. Ultimately in this process, changes in the basic nature of the tribosystem may need to be considered. An example of this type of consideration would be the consideration of the use of a roller bearing in place of a sliding bearing.

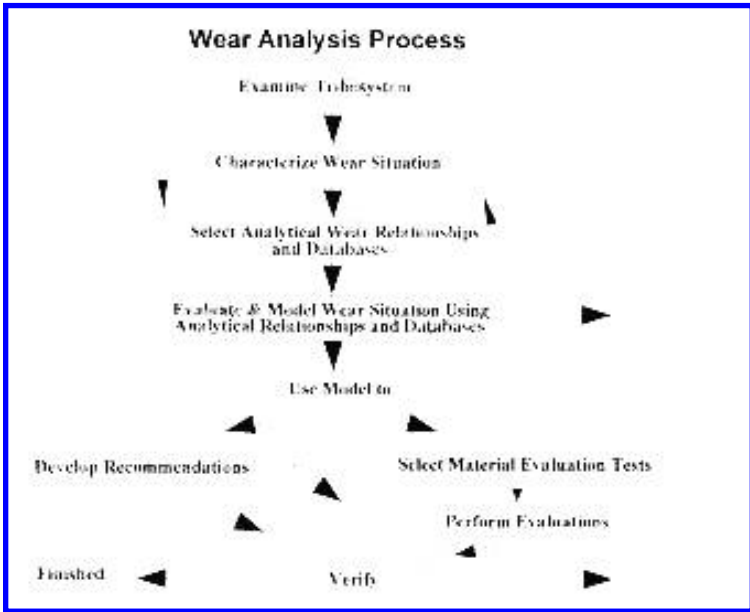


Figure 3.1 Flow diagram showing the elements involved in wear analysis. (From Ref. 1.)

Because of the complex nature of wear and the scatter characteristic of wear data, there can be considerable variation in the accuracy and precision associated with a wear design approach. To some extent, these are influenced by the nature of the tribosystem. To a much larger extent, the accuracy and precision that can be obtained are influenced by the amount of effort expended and the degree to which experimental and theoretical aspects are blended. Figures 3.2 and 3.3 indicate the general trend found in practice. Normally with a minimal amount of effort and a mainly theoretical approach an order of magnitude to a factor of 2 accuracy can be anticipated in estimating life. This can be reduced to 10–20% with the inclusion of more experimental elements and the expenditure of more effort in characterizing and understanding the tribosystem. This aspect of a wear design approach can be considered in the context of a safety margin for the design or a safety factor associated with the values of the parameters involved or the life required. For example, the analysis could be performed using as a goal twice the required life or twice the actual load. By using this conservative approach, the accuracy and precision required for practical design can be reduced, allowing the use of more theoretical or analytical approaches and reducing the amount of effort required by the approach. Similarly, if the situation requires a low margin of safety or a less conservative approach is desirable, more empirical aspects need to be included and a greater amount of effort will be required to satisfactorily complete the process.

Typically, a wear design approach involves four major elements. One is system analysis that includes all those activities, which are necessary to sufficiently characterize

1	Component information (a) Geometry (b) Dimensions (c) Materials
2	Contact condition information (a) Orientation (b) Location (c) Loading (d) Motion
3	Lubrication information (a) Type of lubrication (b) Lubricant (c) Conditions
4	Environmental information (a) Temperature (b) Humidity (c) Atmosphere (d) Contamination
5	Wear information (a) Amount of wear (b) Usage (c) Appearance (d) Location of wear

the tribosystem to allow the selection and use of a model. Another element is the selection and, if necessary, the development of an analytical model, which relates wear to the parameters of interest. In general, all wear models involve one or more empirical wear coefficients, which are dependent on materials. The third element is the identification and development of a database for those material-dependent coefficients. The fourth is verification, a common element in many engineering approaches. The need for and desirability of such an element with a wear design approach is apparent because of

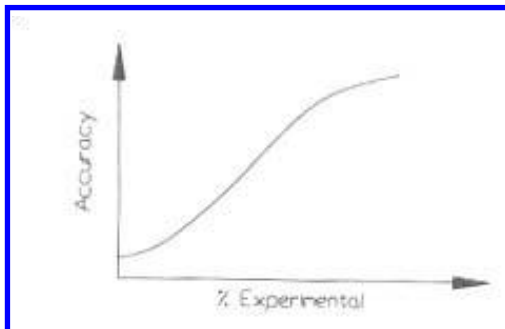


Figure 3.2 The relationship between the inclusion of experimental methods in wear design and accuracy of wear projections.

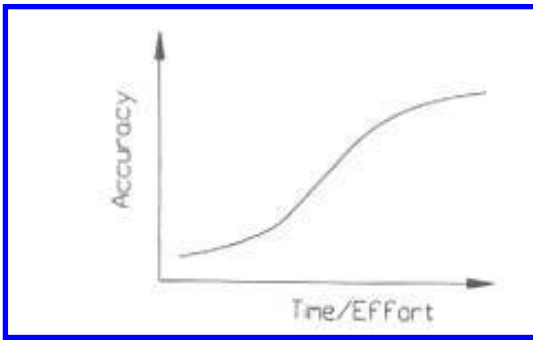


Figure 3.3 The general trend relating the accuracy of wear projections and the amount of effort put into a wear design approach.

the complexity of wear behavior. This element includes such aspects as verification of projections, the applicability of the model, and any of the assumptions made as part of the wear design. Each of the four elements of wear design will be considered in further detail in the Secs. 3.2–3.5 and illustrated by the case studies described in Sec. 5. A design practice that has been found to be useful in the development of sliding mechanisms is described in Sec. 3.6.

3.2. SYSTEM ANALYSIS

Wear design begins with system analysis, which, in turn, begins with the identification of the wear points of a mechanism and classifying them in terms of their general operational characteristics. This generally enables the identification of models, which might be used, and the likely significance of various parameters and factors associated with the application. The relationship between wear and performance needs to be considered at this stage as well. Two aspects need to be identified with respect to performance and wear. One is what feature or dimension of the wear scar is significant to the performance and the other is the acceptable level of wear in that application. These points comprise the minimal level of system analysis that can be done. By itself it is usually only sufficient in situations where the approach is to project long-term wear from short-term machine or field data. More sophisticated wear design approaches require additional system analysis elements, needed for a variety of purposes.

A further element of system analysis is the determination of values for the parameters of the tribosystem. This includes any parameter or element, which can influence wear behavior. In general, the degree to which each has to be known is not the same. This depends on how significant the parameter is and how its value will be used. This type of information is needed for several reasons. Values of tribosystem parameters are needed for the selection (and development) of models, use with analytical wear relationships, to insure adequate simulation in tests used to determine empirical wear coefficients, and to aid in the evaluation of existing data for relevance to the current application. Typically, more nominal values are adequate for parameters that tend to be constant or whose variations tend to be insignificant and whose effects are taken into account by empirical coefficients

of models. However, it is generally necessary to have some knowledge about the values of all parameters. This activity can include characterizing the abrasives in various environment, determining the composition of hostile environments, determining the severity of a cavitation field, as well as determining loads, dimensions, and motions.

As part of system analysis, the design parameters of the tribosystem should be examined to determine parameters or elements that could be used to optimize wear behavior (e.g., insure mild wear behavior). Appropriate elements can then be incorporated into the design to insure that those optimum conditions are satisfied. Examples of this type of activity would be as follows: the recognition of the importance of lubrication in a sliding mechanism and the inclusion of a lubrication system in the design; recognition of the critical nature of alignment in a bearing application and the design of a mounting system to insure good alignment; recognition of the potential severity of abrasive wear and the incorporation of a filter system to avoid the introduction of abrasive particles to the wear interface; recognition of the significance of abrupt changes in a pipeline containing a slurry on erosion and the use of more gradual changes in the contour to encourage a more streamlined flow. With some, it might be necessary or appropriate to include these elements in the modeling to determine specific values or limits for them. With others the simple introduction might be sufficient to optimize wear behavior. Examples of the former might be the determination of the amount of lubrication required or the degree of misalignment that can be allowed. Examples of the latter would be the use of shields and seals to prevent abrasives from reaching the interface or reducing the ambient temperature by cooling.

The identification of the parameters and elements involved in the tribosystem and knowledge of their values can also be useful in selecting or eliminating materials. Certain parameters, such as temperature, the hardness range of the abrasives, and the corrosive nature of the fluid involved, can lead to the immediate elimination and selection of materials types thereby simplifying the overall effort. For example, high ambient temperatures would generally result in the exclusion of most polymers. In the abrasive case, the design activity should focus on materials harder than the abrasives. Highly reactive materials would be eliminated from consideration for use in a corrosive environment.

To obtain the necessary information required from a system analysis a variety of techniques may be required (1). As a minimum, a review of the mechanism and its operation is required. Beyond this, finite element analysis, CAD-CAM simulation, dynamic analysis, or fluid flow analysis might be required, as well as various measuring and examination techniques (e.g., strain gage measurements, environmental sampling, and determination of vibration levels). Examination of worn components can also be useful in system analysis in determining the nature of the contact, characterizing the mode of wear that is occurring, and the motions that are involved. While often not possible in the initial stages of a wear design approach, it should be done when used parts become available. Examination of components from a similar or previous application is also beneficial. In performing these examinations, it is well to do so with a variety of techniques, since different aspects of the wear situation frequently are more easily identified with one technique than another. A significant amount of information about the wear situation can often be obtained from visual and low-power optical examination.

Wear analysis can be performed with various degrees of rigor and completeness associated with the identification and determination of the parameters. However, the cruder and less complete this portion is, the lower the accuracy associated with the analysis and the larger the safety margin that should be employed. In general, all the parameters associated with a tribosystem do not have to be determined to the same amount of

precision. Either because of the nature of the overall analysis or the sensitivity of wear behavior to the parameter, a crude estimate of the value of some parameters may only be necessary (e.g., the general range of its value may be adequate). On the other hand, it may be necessary to determine other parameters very precisely.

While wear design starts with system analysis, system analysis is frequently not limited to this initial stage of wear design. Some elements of system analysis are often involved throughout wear design. This is often in the form of activities leading to refinements in knowledge about the tribosystem, which is required for the modeling activity.

3.3. MODEL SELECTION AND DEVELOPMENT

There are three general approaches in wear design and each involves the use of wear models. One of these may be termed a theoretical approach; the other two, empirical approaches. In the theoretical approach, the model provides an analytical relationship for wear which usually contains explicit dependencies on a number of design parameters and one or more wear coefficients that are determined from laboratory tests or existing databases. In both the empirical approaches, the model again provides analytical relationships but these are generally simpler and contain a fewer number of explicit dependencies. In one case, the coefficients of the relationship are determined by fitting the relationship to data obtained from measurements on actual or prototype hardware. This approach is often used for the determination of a usage factor so that long-term projections can be made from short-term data. In the other case, the analytical relationship is used for the correlation of field or application performance to the performance in a laboratory test; here the model provides a basis for estimating field performance on the basis of laboratory tests.

The selection and development of the analytical relations are basically the same for all these approaches. Based on information gathered in the system analysis, an appropriate engineering model for wear or form of a wear relationship is selected. This is done by comparing the operational aspects of the application to those associated with the various engineering or other models available and selecting the most appropriate one. If an existing model is not completely adequate for the analysis, it may be necessary to expand or modify the model by using some of the more fundamental physical relations and theories regarding wear behavior. Information obtained from the system analysis is needed to guide the development of such a model or the modification. Typically, these more fundamental considerations lead to the identification of an analytical form, which can be fitted to either laboratory or application wear data. It is worthwhile to note that while the initial consideration of a unique wear situation may require an empirical approach, information obtained from the initial application may enable the use of a theoretical approach in similar or future applications. More elaborate and refined engineering models may be developed for specific applications in this manner.

Two types of required modifications often occur. One type is the expansion or refinements of factors contained in the original model or formulation. An example of this might be the refinement of a material factor to explicitly address a hardness or modulus dependency. A second type of modification is the combining of or the allowing for more than one wear mechanism or a change in wear mechanism. An example would be the need to specifically include an abrasion mode in a nominally non-abrasive sliding situation. Another example is the impact wear behavior of elastomers, where the dominant mode changes from "creep-like" to fatigue as the number of impacts increases.

One aspect that should be kept in mind when attempting to select a model is the conditions required in order to allow the use of a particular model. For example, with the Zero Wear Model for sliding, it is required that contact stresses be less than approximately one half the yield point. If this condition is not satisfied, the model is not applicable. When the initial selection of design parameters is limited to those combinations which satisfy this requirement (e.g., in this case appropriate values of size and material hardness), these models are now candidates for use in the wear analysis.

It is often useful to analyze wear data in empirical approaches in terms of log—log plots, particularly for relationships with normal engineering parameters. This method is convenient for determining approximate relationships or trends, even with the scatter that is often associated with wear data, particularly field or machine data. Experience has shown that most wear relationships can be approximated by a power relationship, which is a straight line on a log—log plot. This is illustrated in Fig. 3.4. Experience with this type of analysis has indicated that when wear data deviate from a straight line on a log—log scale, it is likely the result of a transition in wear behavior. When this type of deviation is observed, the wear situation should be investigated to verify the existence of a transition, if there is one, and determine the reason for it. This type of behavior for two situations in which a transition has been verified is shown in Figs. 3.5 and 3.6. While transitions are the likely explanation for such behavior, another explanation is also possible and needs to be recognized, namely, that the range covered is so large that a simple power relationship is not a good approximation of a more complex form.

The theoretical approach to wear design can be completely analytical if existing data are used to provide values for the coefficients required by the models. While this type of approach is highly desirable for design, there are often limitations associated with it. For example, without specific experimental data for the tribosystem being considered, it may be impossible to eliminate different alternatives from consideration when more than one model can be assumed for the application. In the case of sliding wear for instance, both a PV-type model and the Zero and Measurable Wear Models might potentially apply. In addition, existing data often indicate a range of values or nominal values for particular coefficients rather than specific values for the application. In these types of situations (i.e., where it is necessary to consider different theoretical options as possibilities or a range of values for different wear coefficients), a technique called bracketing has been found to be useful. In this approach, wear projections are made for the design with each of the models, using the extremes for the various coefficients indicated by existing data

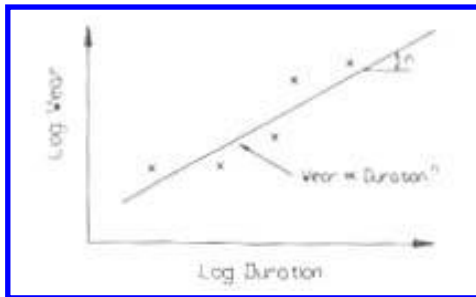


Figure 3.4 Use of log—log plots in wear analysis.

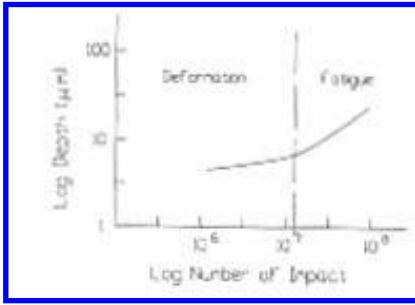


Figure 3.5 A log—log plot for the impact wear of an elastomer, showing the effect of a change in wear modes on the slope of the curve.

for different materials. The range of likely wear behavior can be estimated in this manner. This range in performance is then compared to the requirements. Three possible conditions can result and these are shown in Fig. 3.7. One is when the worst case wear projection satisfies the requirements and therefore a design can be selected without further analysis. The second condition is when the best case wear projection does not satisfy the requirements. In this case, practical experience has indicated that the design concept should be changed. It is unlikely that an existing material or pair of materials can be found which will provide adequate performance. If this condition exists for all the design options, experience indicates that it should be recognized that it is very unlikely that the wear performance goal can be achieved and reduced performance should be accepted. The third condition is when the desired wear performance is bracketed by the worst-case and best-case conditions. Several options are possible in this situation. If the wear design is

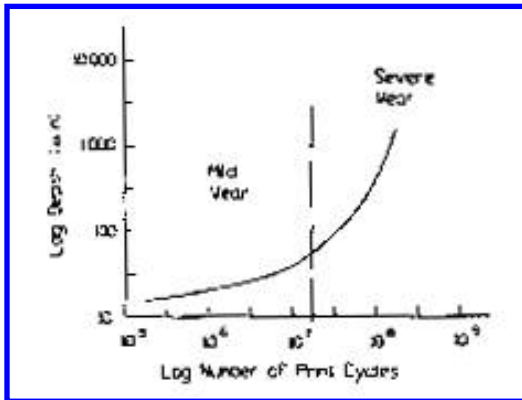


Figure 3.6 A log—log plot of the wear in a band printer at the band-platen interface, showing the effect of a mild to severe transition that occurs after a certain amount of usage.

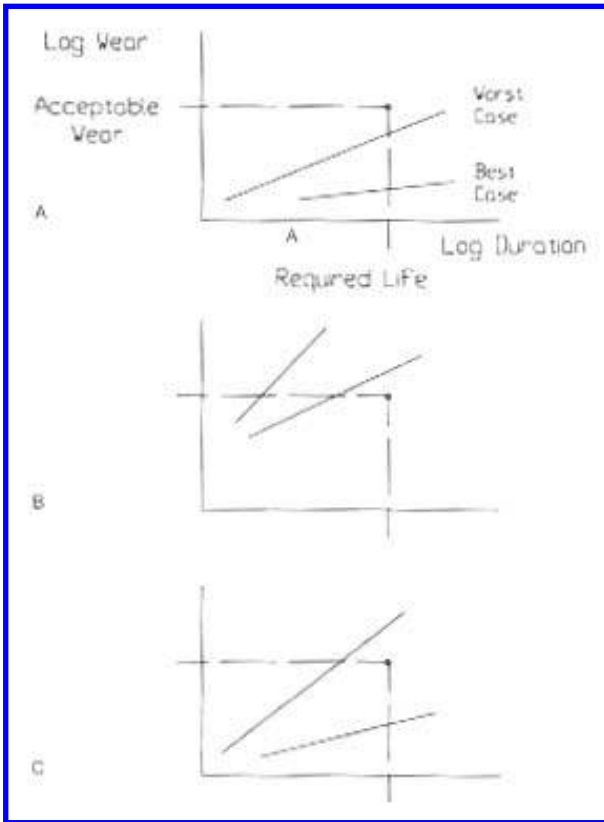


Figure 3.7 Illustration of the bracketing method in wear design. For the condition indicated in “A”, the design is satisfactory and no further work needed. In “B”, a design change is needed. In “C”, further work is needed to identify correct model and required materials.

limited to an analytical approach, additional design options (e.g., maintenance strategies, lowering replacement costs, the use of wear compensation techniques, etc.) can be considered to make the worst-case condition acceptable. An example would be inserting a replaceable interposer between the two surfaces. It might also be possible to eliminate the worst-case from consideration by changing elements of the design to insure that those conditions do not occur or that best-case conditions are achieved. An example of this might be to improve tolerances so that good alignment is assured. If the wear design is not limited to analytical methods, an empirical approach can be incorporated into the

wear analysis to determine the correct model and proper values of the coefficients before a design is selected.

In many applications it is possible that both contacting surfaces can wear. In these cases, it is necessary to consider the wear of each member in the wear design approach. In addition, since the wear of one surface can be influenced by the conditions of the counterface, it is necessary to account for the effect of counterface wear in these approaches. The treatment of these two-body wear situations in a wear design approach can be complex. One reason for this is the increased number of wear coefficients or exponents that may be involved. Another is that general engineering wear models tend to be developed in the context of one-body wear (i.e., they assume a constant counterface) and, as a result, modifications to or extensions of existing models are often required. The relationships between wear volumes and engineering wear measures, such as depth, also can change as a result of a geometry change of the counterface with wear, leading to increased complexity. One approach that can be used in these wear design situations is to model the wear of each member, assuming that the counterface does not wear. The sum of the wear projected for each member is then used to determine whether or not acceptable wear performance is achieved. In practice, this is a conservative approach because in mild wear situations experience indicates that, if there is a change, individual wear rates tend to decrease with counterface wear. An exception to this would be a situation in which the properties or characteristic of a counterface might change dramatically with only a small amount of wear or usage, as is the case of a molded glass-filled plastic. With wear through of the skin and exposure of the glass, the properties of the plastic surface change dramatically (i.e., from a non-abrasive to an abrasive surface). This type of behavior can be taken into account by using the properties of the modified surface in the analysis.

A second, more rigorous, analytical approach would be to account for the changing conditions of the counterface in the model used to describe the wear of one member. Since wear on both members is of concern in these situations, a pair of coupled relationships would be obtained in this manner. Generally, this pair of equations would have to be simultaneously solved to obtain expression for total wear of the system and individual wear of each member. The complexity of such an approach depends on the nature of the models used, the geometries of the two members, and the engineering wear measure required in the application. In its easiest form, the coupling can be in the form of a sliding wear coefficient that has to be determined under conditions of simultaneous wear. In a more complex form, it might be in the form of simultaneous differential equations.

With an empirical approach (curve fitting or regression analysis) to two-body wear a single form for total wear can be used as a basis or two forms can be used, one for each member.

In two-body wear situations, it is possible that the wear rate of one member is so much smaller than the wear rate of the other that it can be ignored. This can be assessed in an empirical manner by suitable system analysis to see if it is reasonable to expect negligible wear on one member or not, review of wear data from tests, and the examination of used parts. It can also be assessed analytically, using models to estimate or project wear or wear lives. For example, based on the assumption that only one member wears at a time, if there is a difference of several orders of magnitude in their projected wear lives, the wear on the member with the larger projected life can generally be ignored. It should be kept in mind that if changes in the design are introduced, this aspect needs to be reexamined since the changes could result in increased wear on the originally low-wearing member. For example, initially an unhardened steel surface might engage a hardened surface. As a result the hard surface might experience negligible wear. If the softer member is hardened to

reduce its wear, significant wear might now occur on the original hardened member. As a result, a more general two-body wear approach now needs to be used in the wear design.

3.4. DATABASE IDENTIFICATION AND DEVELOPMENT

This element of wear design is concerned with obtaining all the empirical data needed for the implementation of a wear design approach. In addition to material wear coefficients, the databases required for these approaches can include a variety of experimental data. For example, the database may include such information as values of variable exponents, wear coefficients associated with other parameters of the tribosystem, and the association of wear modes and transitions in wear behavior with various parameters of tribosystems. It can also include data regarding the characterization of the tribosystem, including the environment in which the device operates. Such aspects as the determination of the size and type of abrasives encountered, determination of loads, and the characterization of a cavitation field would be examples of these types of data.

If not known beforehand, the data associated with the characterization of the tribosystem can usually be obtained from direct or indirect measurements of various aspects of the system. Generally, using conventional measurement techniques for the property or aspect of interest can do this. The other types of data required, such as material wear coefficients, values of exponents, and information regarding wear modes, can be obtained from a variety of sources. Technical and vendor publications provide one source of such data. However, the tests upon which these data are based usually do not provide sufficient simulation of the application to provide specific values. Typically, data from such sources can be used to identify ranges or estimates that are useful in a bracketing approach. In general, simulative wear tests are needed to provide specific values for these quantities. The first time a situation is encountered it might be necessary to develop a unique test to determine the appropriate values; in subsequent applications, however, the previously obtained data may be adequate. An in-house database that is built on these unique tests that provide good simulation can be a valuable tool in facilitating analytical wear design approaches. Another source of values for these data can be application data. Machine or field wear data for the application or from a similar application can be analyzed to determine the model and values, which best satisfy the data. Data from robot tests can be used in the same manner.

3.5. VERIFICATION

There are usually two general concerns associated with verification activities in wear design. One is a design engineering concern, namely to verify that the selected design is performing properly. Basically, this is verifying the wear projections made with the model. The second type of concern is more fundamental. It is concerned with verification of tribological behavior. This includes verification of the assumptions and hypotheses used in the development of the wear design approach, verification of the wear mode and models, and the determination of the range of validity of the model. It includes verification of aspects associated with the wear, such as the nature or size of the contact area and location of the wear.

For the design engineering concern, verification generally requires machine or field data. One way of providing this verification is by determining field life. A long time might

be need for gathering of these types of data and is often impractical. An alternative that does not require as much time is to determine the amount of wear as a function of usage (empirical wear curve) and comparing this to what was predicted with usage (theoretical wear curve). For tribological concerns, verification is not limited to field or machine data. Laboratory and robot tests can often be used and are often preferred to verify assumptions and to define limits of applicability. It should be recognized in these activities that confirmation is not limited to quantitative aspects. Qualitative aspects, such as the morphology, shape, and location of the wear scars and wear debris characteristics can also be used in verifying assumptions and determining limits. Often one way of verifying hypotheses and assumptions is to perform special tests and vary significant parameters, in order to confirm trends predicted by the model used in the wear analysis.

While there is always some need for verification, the need and extent for this can vary. With new types of applications there is generally a greater need for more extensive verification elements, particularly those covering the tribological aspects. However, when the application and situation are similar to previous ones, the need and extent can decrease because of the information and experience gained from prior applications. In these cases, only a cursory engineering verification might be needed. The tribological verification is the more fundamental of the two types and has the most impact on a wear design methodology. If done well, the extent of engineering verification activity can be greatly reduced, both in the current application and future similar applications. It also provides the basis for developing improvements and refinements in modeling.

3.6. DESIGN TRIAGE

This is a wear design method that was used at the IBM development laboratory in Endicott, NY. It was based on the Zero and Measurable Wear Models for sliding and used in conjunction with a three-stage product test program. The first stage of this program was essentially a feasibility evaluation of the machine concept. In the second stage the machine, built with engineering-level parts, was evaluated against set performance and life requirements, including wear life. The final stage of testing was done with production-level parts and focused on the evaluation of these level parts. The most intensive and extensive stage of testing regarding wear concerns was typically the second.

In the Design Triage method, all mechanisms were evaluated using the allowable load concept described in Sec. 2.4. Using the Zero Wear Model, allowable loads were determined for proposed designs. These loads were then compared with estimates for the actual load. If a design, which met all other design criterion, could be identified for which the allowable load was below the applied load, it was accepted. Designs in this category were only examined when the opportunity became available, which was typically at the end of a testing stage, to insure that the wear was acceptable.

If a design, which satisfied all other requirements, could not be found for which the allowable load exceeded the actual load or if a preferred design did not satisfy this condition, the Measurable Wear Model was used to estimate the depth of wear at the end of the required life. The effect of this amount of wear on function was then assessed. If the projected wear depth was an order of magnitude or smaller than that which was estimated to effect function, it was considered negligible. Designs, which fell into this category, were treated in the same manner as those in the first category.

Designs for which the projected wear was greater than this but still acceptable were treated in a different manner. These designs were subjected to scheduled inspections and

measurements in the test program to insure that the wear was acceptable. In addition, if the parts were considered critical, more elaborate wear design or wear analysis methods were used to establish confidence and optimize parameters. In these cases, special test programs were also frequently established to verify wear behavior. Designs for which the projected wear exceeded the allowable amount were subjected to these same types of extended studies and evaluations. In these situations different design concepts to achieve functionality were also explored in the case where acceptable wear could not be obtained with the design.

To facilitate this methodology, relationships for determining allowable loads and projecting end-of-life wear were developed for common contact situations (2,3). With these relationships, the following expression is used to estimate end-of-life wear, h , when the actual load, P , exceeds the allowable load, P_a .

$$h = 2\delta_0 \left\{ \frac{P}{P_a} \right\}^{sn^9} \quad (3.1)$$

δ_0 is the CLA or RMS roughness and s is the exponent of the load in the relationship between load and stress.

$$\tau_{\max} \propto P^s \quad (3.2)$$

n is the exponent in the relationship between wear depth and usage.

$$h \propto (\text{usage})^n \quad (3.3)$$

A summary of expression for the allowable load and values of n can be found in Appendix VI. Values of m can be found in Appendix I.

REFERENCES

1. RG Bayer. *Wear Analysis for Engineers*. NY: HNB Publishing, 2002.
2. R Bayer, A Shalkey, A Wayson. Designing for zero wear, *Machine Design*, 1 / 9 / 69, 142–151. Cleveland, OH: Penton Publishing Co. 1969.
3. R Bayer, A Wayson. Designing for measurable wear, *Machine Design*, 8 / 7 / 69, 118–127. Cleveland, OH: Penton Publishing Co., 1969.

4

Design Guidelines

4.1. INTRODUCTION

A collection of guidelines which have been found to be useful in wear design are presented in this chapter. Basically, these guidelines comprise general and mainly qualitative trends and recommendations regarding wear behavior that are useful in design. Exceptions to these trends are possible and it is also not necessary for these guidelines to be followed in order to achieve an adequate design. However, if followed, these guidelines generally help to facilitate the implementation of a wear design approach. As may be observed, several of the guidelines presented in this section have also been discussed in prior sections. They are included in this section for completeness with respect to design approaches.

4.2. GUIDELINES

4.2.1. Reliance on Analytical Design Methods Increases the Degree of Conservatism Required

Conservatism can be introduced into a design approach in several ways. One is to use exaggerated worst case assumptions. For example, load levels used in the analysis can be higher than that occurring in the application or wear coefficients can be poorer than data suggest. Another method is to design for less wear than can be allowed or for a greater life than required. The ratio between the values used in the analysis and those actual occurring or required can be thought of as safety factors. Some degree of conservatism or safety should be incorporated into most wear design approaches because of the complex nature of wear behavior. Appropriate values for these safety factors depend on a variety of aspects, including both the nature of the wear situation, the materials involved, and engineering or design needs. Maximum values for safety factors are recommended with a completely analytical approach. However, by including empirical elements into the approach, lower values for safety factors can be used.

4.2.2. Wear is a System Property; Utilize All Design Parameters That Can Influence Wear

It is important not to think of wear simply in terms of materials but also to recognize all the factors and parameters, which affect wear. Limiting the consideration to materials or material selection may result in not finding a satisfactory or optimum design. Modification of other parameters (e.g., shape, size, alignment, and counterface roughness) can also be used to achieve or influence wear behavior. Modification of other parameters may be required to achieve a satisfactory or optimum design. For example, in some cases, adequate performance might be achieved

simply by improving tolerance, modifying the shape, or reducing the amount of slip that occurs in a rolling contact, rather than utilizing a more expensive material. Experience has shown that in problem solving situations changes, other than material changes can often resolve the wear problem alone or in conjunction with material changes.

4.2.3. Approach Extrapolation of Data and Extension of Designs Cautiously

Because transitions in wear behavior are common, extrapolation of data beyond the ranges or regimes in which it was generated is risky. Interpolation of data is much preferred but does not eliminate the possibility of transitions. The possibility of such transitions and other types of nonlinear behavior also makes the extension or application of designs to conditions beyond those previously evaluated risky. It is possible that a dramatic reduction in wear performance may occur for relatively minor changes with respect to some parameters. Understanding the wear behavior in the regions for which data and experience exist and the nature of the materials involved can reduce this risk. Using this knowledge and the knowledge of the new conditions, estimates of likely behavior can often be made. In addition tests may be used to verify the projections or to bracket the range so that interpolations may be made.

4.2.4. Design with Limits and Characteristics of Materials in Mind

Classes of materials and, in some cases, individual materials within a class have different properties and limits, which are significant in terms of their relative wear behavior. Because of this, it is sometimes necessary to select design parameters to accommodate or optimize the use of specific materials. This implies that a design that is appropriate for one type of material may not be suitable for another. For example, plastics tend to require lower contact stresses than metals and specific counterface conditions for low wear. They also tend to be more sensitive to temperature and have poorer thermal conductivity. Consequently, a design which is appropriate for case hardened steel may not be appropriate for a plastic since the plastic might require a larger contact area, a specific roughness for the counterface to establish a beneficial transfer film, and a means of dissipating frictional heat to lower the operating temperature. Differences in dimensional stability, tolerances that are obtainable, sensitivity to impact, chemical properties, and sliding motions are among other aspects that might be significant in considering designs utilizing different types of materials. An extension of this concept is that whenever possible the design should be developed around and be consistent with the properties of typical engineering materials used in that type of application. A design or application, which requires a new material or the use of an existing material in a new type of application, generally requires a lengthy development and research effort without a guarantee of success.

4.2.5. Metals and Polymers Tend to Require Different Designs

This is a corollary of the previous design rule. A more general version of this corollary is that "Different classes of materials tend to require different designs" However, the specific form is of particular importance because of the tendency to convert a design fabricated with metals to one fabricated with plastics, without compensating for the difference in wear characteristics of these two types of materials. When converting from a metal to a plastic, it is frequently necessary to enlarge the apparent area of contact and modify the roughness of the counterface. Changes in lubrication might also be required. The lubrication may have to be eliminated to enhance transfer film development, changed for compatibility

reasons, or increased to enhance cooling. Since a goal of this type of change is often the elimination of the need for lubrication, the first aspect is often an intrinsic element with the change to a plastic; however, the latter two aspects are generally not.

4.2.6. Design So That a Mild Wear Condition Exists

In terms of most wear parameters there tends to be two broad regimes of wear behavior, mild and severe, separated by relatively sharp boundaries. Associated with these two regimes are differences in wear morphology and in wear rates. Wear features are coarser and wear rates higher in the severe region. In general, the high wear rates associated with the severe regime are unsuitable for applications where long life is desired and at least undesirable for most other applications. Therefore, a first step in a wear design approach should be to establish general conditions that will enhance the probability of being in the mild wear regime. For example, in many cases, the transition for mild to severe wear is associated with exaggerated abrasion, single-cycle deformation, or adhesion phenomena. This suggests that the design trend should be to select parameters and provide conditions, which tend to minimize these types of wear mechanisms. The magnitudes of these types of mechanisms tend to be reduced by the use of dissimilar materials, low contact stresses, the use of lubrication, and elimination of sources of abrasion. Consequently, the overall design approach should allow for such aspects as the use of dissimilar materials, the use of shapes and sizes that will result in low stresses, the use of a lubricant, and the prevention of abrasives from the contact region. This type of approach is not limited to these types of transitions and wear situations. It should be applied to all wear situations, focusing on the appropriate parameters for that wear situation. For example, in an application in which slurry erosion is a factor, the overall design should tend to minimize impingement by the abrasives in the slurry. Another example would be in the case of an application in which plastics are to be used. In this case, the overall design approach should anticipate a possible need for enhanced cooling so that the temperature of the plastic can be kept under its glass transition temperature or the need to reduce surface speeds under a critical value.

4.2.7. A Minimum Requirement for Material Selection is That the Material Should be Stable in the Operating Environment

Severe wear behavior results when material properties degrade. Consequently, to obtain acceptable wear performance, it is generally necessary to utilize materials that do not degrade in the operating environment as a result of chemical reactions and temperature.

4.2.8. While Fluid or EHD Lubrication is very Effective for Reducing Wear, Specific Designs are Required to Insure this Form of Lubrication

Since EHD lubrication reduces asperity contact, it not only reduces wear, but also can effectively eliminate wear during continuous motion. The ability of this type of lubrication to control or eliminate wear depends on the formation, thickness, and stability of the fluid wedge or film formed in the contact region. These films depend on a number of factors, including shape of the counterfaces, speeds, loads, lubricant properties, and supply of lubricant. In addition, the effectiveness of a given film is a function of the roughnesses of the counterfaces. With this degree of complexity, there is a limited range of parameters associated with these factors that will provide a suitable film or desired wear performance. At the same time, these factors are also important in controlling wear in the boundary

lubrication regime. While this is the case the relationships between wear and these factors are not necessarily the same in both regimes. In fact, they tend to be quite different. A wear design approach, assuming boundary lubrication, is unlikely to lead to the same design as that obtained with a wear design approach that assumes fluid lubrication. Consequently, if it is decided to use EHD lubrication to obtain the desired wear performance, a design has to be selected specifically in terms of the requirements for developing and maintaining the appropriate film thickness. An important corollary to this is that a design based on EHD lubrication principals may not perform as well in a new application which appears milder than the original application for which it was developed. A scenario of this is a device that performs well in a high-speed application but fails in a low-speed application. The reason for this is that, in the low-speed application, the EHD film may not form as a result of the lower speed and the material couple, not being selected for good boundary lubrication wear properties, wear at a high rate.

4.2.9. Minimize Exposure to Abrasive Particles

The presence of abrasive particles in most contact situations is undesirable because of the high wear rate that is associated with abrasion, which can result in a significant decrease in wear life. When there is an exposure to abrasive particles, it is often necessary to include features in the design, which tend to eliminate or prevent abrasive particles from the interface. Filters on oil supplies, the use of seal and shields, and allowing for flushing of the interface are some ways of doing this. Another way is to select materials harder than the abrasives, which will be present. This will significantly reduce the wear rate associated with the abrasive particles, as discussed in the next rule.

4.2.10. In Abrasive Situations Make the Wear Surfaces Harder than the Abrasives

As discussed in the treatment of abrasive wear, wear rates typically decrease by at least one to two orders of magnitude when the wear surface becomes harder than the abrasive. This is the result of a transition in wear behavior. While increases in hardness in the range above and below the hardness of the abrasive also tend to reduce wear, these improvements are generally not as great as that associated with this transition. Therefore, the initial step in designing for an abrasive wear situation should be characterizing the abrasives involved and then trying to incorporate materials harder than the abrasive into the design.

4.2.11. Optimize Contact Geometry to Minimize Stresses

Wear life tends to decrease with increasing contact stresses for two reasons. One is that some wear mechanisms are stress dependent. The other is that wear life tends to be determined by the depth of wear (rather than wear volume) and the depth rate of wear is generally related to stress. Because of this trend, it is generally desirable to design so that stress levels are reduced as much as possible. To do this, three aspects need to be considered. One, the most evident, is the size and shape of the contacting members. The second and third tend to be overlooked. The second factor in minimizing stress is to insure proper alignment so that the load is uniformly distributed over the interface. The third is to avoid sharp edges and corners. Sharp edges and corners to act as stress risers and should be rounded to reduce stress concentration effects as much as possible. The effects of misalignment and edges on wear can often be observed on worn parts. Misalignment results in tapered wear scars. Sharp edges and comers result in localized regions of increased depth

of wear, usually in the form of local grooves. The following two corollaries of this more general rule emphasize these two aspects: insure good alignment and round the corners.

4.2.12. Use a Lubricant Whenever Possible

Lubrication is a very effective method of reducing the effect of adhesive wear mechanisms. Typically, some form of lubrication needs to be used if long life and low wear rates are to be achieved with metals and ceramics when there is sliding or slip involved. Additional advantages of using a lubricant are generally lower friction and cooling.

4.2.13. Use Dissimilar Materials

The tendency for adhesion tends to be higher between similar or self-mated pairs. Therefore, the use of dissimilar materials in a contact tends to reduce adhesive wear modes. This is the same reason given for the use of a lubricant. As a consequence, lubrication tends to reduce the significance of this rule in design situations where lubrication is used. Experience indicates that it is much more likely to achieve a satisfactory design with similar or self-mated pairs and the use of a lubricant, than it is to achieve a satisfactory design without the use of a lubricant.

4.2.14. Increasing Hardness Tends to Reduce Wear

The magnitude of most wear mechanisms tends to be reduced by increased hardness and, as a result, the wear life of a component should be improved by increasing its hardness. In practice, this tends to be valid only when large changes in hardness (e.g., greater than 30%) are considered. This is because it is not generally possible to only change the hardness of the component and not some other material properties. This is particularly true when the hardness change is accomplished by a change to a different material. Changes in wear behavior associated with these other properties can mask the effect of hardness. It is even possible for a harder material to wear more than a softer material because of difference in these other material parameters.

4.2.15. To Increase System Life (Reduce System Wear), It is Sometimes Necessary to Increase the Hardness of Both Members

When the hardness of one member of contact is increased, wear on the counterface tends to increase. Therefore, the unilateral hardening of one surface to reduce the wear on that member can result in initiating or increasing of the wear on the counterface. Since wear life of a mechanism is a function of the wear on both members of the system, it is possible that the reduction of wear on one member at the expense of increasing the wear on the other may not result in the desired system life. It may have just changed the determining factor for system life. In such a situation, it is necessary to increase the hardness of both members to achieve the desired system life.

4.2.16. Rolling is Preferred Over Sliding

Rolling motion is a milder wear situation than sliding. As a result, it is sometimes possible to improve or extend wear life by replacing sliding elements with rolling elements. An example of this type of approach is the replacing of journal bearings with roller or ball bearings. When rolling contact is used, it is very important to minimize the amount of slip that occurs in the contact. The sliding motion that is associated with this slip can significantly increase the wear in such contact situations and dramatically decrease life.

Alignment and tolerances can be major factors in achieving good wear performance with rolling elements.

4.2.17. Sliding or Fretting Motions Should be Eliminated in Impact Wear Situations

Since sliding motion results in more wear than rolling or impact motions, the occurrence of even a small amount of sliding in an impact or rolling contact can result in significantly increased wear. Alignment between the impacting surfaces can be a factor in controlling fretting under impact conditions, as well as tolerances affecting the structural rigidity of the impacting elements. For example, a loose tolerance in a bearing of a pivoting element could increase the amount of sliding or fretting associated with the impact.

4.2.18. Compound Impact Situations Can Often be Treated as a Sliding Wear Situation in Which the Loads (Stresses) are Determined by the Impact

When slip occurs throughout the contact in compound impact situations, sliding wear behavior tends to dominate the wear situation. In such cases, the wear situation can often be viewed and modeled as sliding wear, using an equivalent load or stress for the impact (see Secs. 2.1, 5.2, 5.8, and 5.9).

4.2.19. Impacts Should be Avoided in Sliding and Rolling Contacts

While impact motion is milder than sliding, loads and stresses that are generated by impact can be quite high. When impact takes place in nominally sliding and rolling mechanisms, the loads and stresses occurring during the impact tend to be much larger than the ones associated with the nominal operation. In these situations, increased wear can often be observed in regions corresponding to these impacts. The increased wear caused by these impacts can reduce wear life in some applications.

4.2.20. Elastomers Frequently Outperform Harder Materials and Reduce Counterface Wear in Impact Situations

Elastomers tend to perform well under impact conditions. Because of their ability to cushion impacts, they tend to outperform most materials with hardness less than 700 kg/mm². However, their relative performance degrades in impact situations that involve slip, tending to be unsuitable for compound impact situations in which there is a large amount of sliding. In those situations, their performance may be comparable to or poorer than many other materials. For those impact situations, which have a tendency to fret, elastomers sometimes have an additional advantage by eliminating the slip or fretting motion. This is because elastomers tend to be able to accommodate more lateral displacement of the counterfaces before slip occurs. This tendency adds to their superior performance in these impact situations. However, if slip or fretting still occurs, their performance degrades rapidly. An additional advantage of using elastomers in impact situation is that wear of the counterface is generally reduced by virtue of the ability of elastomers to reduce impact loads.

4.2.21. Thicknesses of Conventional Coatings Generally Should be Greater than 100 μm

Included in this category of conventional coatings are electrolytic and electroless platings, various polymer coatings, carbide coatings, and anodized coatings. There are several

reasons for the minimum thickness recommendation. One is that below this value their performance tends to be strongly influenced by substrate properties. Also, sensitivity to properties of the coating / substrate interface increases, as the coating becomes thinner because of greater stresses at that boundary. Another reason, often the governing one, is that even for highly wear resistant coatings, like Cr, lower thicknesses do not provide long enough life for most applications. This point is also often a factor with coatings that have high wear resistance, since they are often thin.

4.2.22. Use Moderate Surface Roughnesses

Surface roughnesses for most applications should be in the range from approximately from a CLA or RMS from 5 to 32 μin . ($\sqrt{5}$ to $\sqrt{32}$). While wear tends to increase with increasing roughness in this range, the increase is typically moderate and the difference is often negligible over this range. Single-cycle deformation (cutting and plowing) often becomes significant above $\sqrt{32}$ and wear rates tend to increase significantly. On practical basis, roughnesses below $\sqrt{5}$ tend to increase cost and are usually not required to obtain satisfactory wear behavior. Also, undesirable adhesive and stiction phenomena tend to increase and become significant for the very smooth surfaces, $< \sqrt{5}$.

4.2.23. Avoid the Use of Stainless Steel Shafting with Impregnated Sintered Bronze Bearings

While several theories have been proposed for the poor wear performance that is observed with the use of some stainless steels in impregnated sintered bronze bearings, none are satisfactory. There is some evidence that satisfactory performance can be obtained with some grades of stainless steels with some bearings and lubricants. However, without a complete understanding of the phenomena involved, it is best to avoid the use of stainless steels in this type of application.

4.2.24. When Molded Filled Plastics Tend to Exhibit Significantly Different Initial and Long-Term Wear Behavior

Filled plastic parts tend to have skins when molded, which have different wear properties than the bulk. A reason for this is that there is a tendency for the composition to be different close to the surface. Generally, it is resin rich. Once this layer is penetrated there is a change in wear behavior because of this change in composition. Changes in physical properties could also be a factor. The composition and thickness of skin layer tend to have considerable variations from lot to lot and from part to part. As a result, when small amounts of wear determine life, this skin effect can produce significant variations in wear life. The skin effect also applies to friction. The coefficient of friction for a molded surface is often different than for the bulk.

4.2.25. When Glass or Other Hard Fillers are Used, the Hardness of the Counterface Should be Equal to or Greater than that of the Filler

Once any skin is removed from filled plastics, hard fillers (e.g., glass) create a potential abrasive wear situation. Abrasive wear is significantly reduced when the counterface is harder than the abrasive. When there is a skin on glass-filled plastics, a common experience is that wear tends to initiate on the plastic in a metal / plastic couple. However, with a soft metal, wear tends to stop on the plastic once the skin is penetrated and rapid wearing of the metal occurs. With a hard counterface (i.e., greater than Rc 60–62) this does not

occur. The abrasivity of hard filler depends on their shape and size, as well as their hardness. For example, glass fillers tend to be less abrasive when the glass is in the form of spheres than when they are in the form of fibers.

4.2.26. The Tendency for Galling to Occur can be Reduced by Using Dissimilar and Hard Materials of Low Ductility, Lubrication, and Rougher Surfaces

Galling is an adhesion phenomenon which tends to be exaggerated with materials that exhibit a high degree of plastic behavior. It tends to occur in situations involving high loads, large apparent areas of contact, and sliding. The use of hard and dissimilar materials and a lubricant tends to reduce adhesion under these conditions. The use of materials with low ductility and rougher surfaces generally reduce the effect of plasticity on galling behavior. Both low ductility and higher roughness tend to inhibit the size of the galls that occur, which typically reduce the sensitivity of applications to the occurrence of galling.

4.2.27. Avoid the Use of Designs in Which Fretting Motions Can Occur

Fretting motions are generally not intended (needed) and can be superimposed on the intended motions of contacts. Such motions tend to increase wear in those situations and, as a result, should be reduced or eliminated by design. In nominally stationary contact situations, fretting motion can often occur as a result of machine induced or transmitted vibrations. Ideally, the design should prevent such motions by either reducing the vibrations, using a compliant interposer (elastomer) to prevent slip, increasing the holding forces at those interfaces, or some combination of these. However, since fretting wear has been shown to result from sliding amplitudes as low as 0.5 μm , this may not be always be possible. In such cases, it is then necessary to design the interface on the basis of sliding and abrasive wear behavior.

4.2.28. When Fretting Motions are Present, Design to Optimize Sliding Wear Life and to Minimize Abrasive Wear

When fretting motions cannot be eliminated from nominally stationary contacts, the design of the contact, including material selection, should be to maximize the resistance to sliding wear. To avoid the potential for significant abrasion, the materials used should be ones, which do not produce wear debris that is significantly harder than the original materials. Lubrication of these interfaces is often beneficial if it reduces sliding wear rates and prevents the formation of hard abrasives. Sometimes lubrication can also help flush the wear debris from the contact. However, the use of a lubricant can sometimes increase fretting wear when it allows the formation of a slurry of hard wear debris or foreign abrasives, which is trapped at the interface.

4.2.29. Sacrificial Wear Design Should be Considered an Option When Satisfactory Life Cannot be Achieved with Available Materials

Sacrificial wear design is an approach in which the design is selected to insure that only one member wears and involves the scheduled replacement of that part. This can provide a practical solution to situation where it is not possible to find or utilize materials, which will provide adequate life for both members. One method of this type is to select the material for one member to be sufficiently soft so that wear will occur only on it. An alternate approach to this would be the use of a replaceable interposer between the two surfaces and

have this soft enough that it wears preferentially. Often the key to making this approach practical is the replacement scheme. The overall design should make replacement of the wearing member convenient and the wearing material needs to be selected so that it absorbs all the wear but still last long enough for an appropriate replacement schedule. A typical selection of this type would involve the selection of a soft but relatively good wearing polymer as the sacrificial material against a hard metal surface. An example of this approach is described in Sec. 5.9.

4.2.30. Conform to Vendor Recommendations Regarding Optimum Wear Performance

It is generally advisable to design so that vendor recommendations regarding the use of their materials or components, such as bearings, are followed. These recommendation might include recommended ranges of clearances, pre-loads, break-in, use of lubrication, limiting sliding velocities, counterface conditions, and preferred applications, among others. While deviating from these recommendations generally results in increased wear rates, it does not necessarily mean that the wear rate will be unacceptable. However, it usually does mean that the risk associated with an analytical design or the amount of empirical effort involved in a wear design increases. On the other hand, conformance with the recommendations does not necessarily mean that the specific wear rates cited by the vendor apply, since these can vary with the tribosystem.

4.2.31. Changes Associated with Design Modifications or New Applications Should be Reviewed Carefully with Respect to their Potential Effect on Wear Behavior

The review helps to avoid or anticipate field problems that might result from these changes. Because of the complex nature of wear behavior and, particularly, the sharp transitions that are possible, make this a cardinal rule. A wear design or a wear analysis approach should be used for the review. If the review indicates a potential problem, the information obtained can be used to initiate a wear design approach to find an acceptable modification or new design to avoid a problem in the new application.

4.2.32. Provide Adequate Clearance in Journal Bearings

A minimum clearance is generally required in journal bearings to account for the effects of mechanical tolerances and differential thermal expansion. If there is insufficient clearance, these effects can result in increased loading and binding. In lubricated journal bearings, the use of too small a clearance can also inhibit the formation of beneficial fluid lubrication films, restricting the lubrication to the boundary or, at best, the mixed regime.

4.2.33. The Severity of the Wear (Wear Rate) in Rolling, Sliding, and Impact Wear Situations can Generally be Correlated to the Ratio of Operating Stress Over Yield Stress (Stress Ratio)

In most engineering situations, wear depth is the primary concern and depth rate of wear is a measure of the severity of the wear in that situation. Models for wear mechanisms and engineering models for wear behavior typically show that the depth wear rate is directly related to contact stress and inversely related to some strength property, usually hardness. With most of these models, the two dependencies can be combined as a ratio. Analysis of wear situations generally shows this to be the case as well, that is, a general tendency for

the wear to become more severe as values of the type of ratio increase. Experience gathered from the analysis of wear situations and the resolution of wear problems provided some guidelines for appropriate values of stress ratios in engineering situations. One is that the ratio of shear stress to yield shear stress is more generally applicable than ratios related to tensile properties, since it includes the effect of friction and traction on wear behavior. Another is that the value of this ratio typically should be less than 1. For rolling and impact values in the range of 0.5 or slightly higher are often required for adequate wear performance without fluid lubrication. For sliding values in the range of 0.1–0.2 and lower are often required for satisfactory wear behavior. For some material pairs and lubricants, acceptable ratios might approach 0.5 in some sliding situations.

4.2.34. Design so that Severe Wear Mechanisms Associated with Adhesion and Single-Cycle Deformation do not Occur

While long-term wear behavior tends to be dominated by repeated-cycle deformation mechanisms, the most severe forms of wear and high wear rates are often associated with adhesion and single-cycle deformation mechanisms. Consequently, a starting point and minimal criterion for a wear design approach is to select parameters so that the more severe forms of these mechanisms are prevented from occurring.

5

Design Examples

5.1. INTRODUCTION

A number of case studies are presented in this section to illustrate wear design methodology; they were selected to illustrate different approaches and different elements involved in wear design. As a result, the focus of the individual case studies is typically on selected general aspects involved in that example, rather than on either specific details or all the elements of a complete wear design approach. Furthermore, it is not intended that these case studies provide relationships or data with applicability beyond the situation discussed. However, in some cases, relationships and data might be applicable to other situations, provided the situations are similar enough to allow such uses.

A variety of wear situations are covered in these examples, involving different types of materials, geometries, and motions. Many of these case studies involve examples from computer peripheral equipment, which are from the author's personal experience. In addition to these there are a number, which are taken from the literature and involve a wider range of applications. Additional examples of this methodology can be found in *Wear Analysis for Engineers* (1).

5.2. PRINTER CARTRIDGE

This case study involves a wear design approach used in the development of the print cartridge for an intermediate speed impact printer. It provides an example of the use of the Zero and Measurable Sliding Wear Models and the combining of these models with mechanical analysis and verification to achieve a design with adequate wear life. It also illustrates a method for treating two-body wear situations.

The design of the print cartridge involved type slugs loosely attached to a reinforced elastomer belt that is driven by rotating pulleys. The general configuration is illustrated in Fig. 5.1. The type slugs had a U-shaped cross-section, which allowed them to be placed over the face of the belt. Attachment to the belt was by means of pins through the legs of the slug and between ridges on the back of the belt (Fig. 5.1). This method of attachment prevented translations between the type slug and the belt but allowed rotation of the slug about the axis of the pin. Printing was accomplished by having a hammer impact in a region of paper, driving it and a region of inked ribbon against the moving type slug. This, in turn, drove the type slug against a platen. In the print region, the slugs are confined between the platen surface and the surfaces of upper and lower guides, which are above and below the font line. A ramp at the entrance to this region is used to guide the slug into the print area.

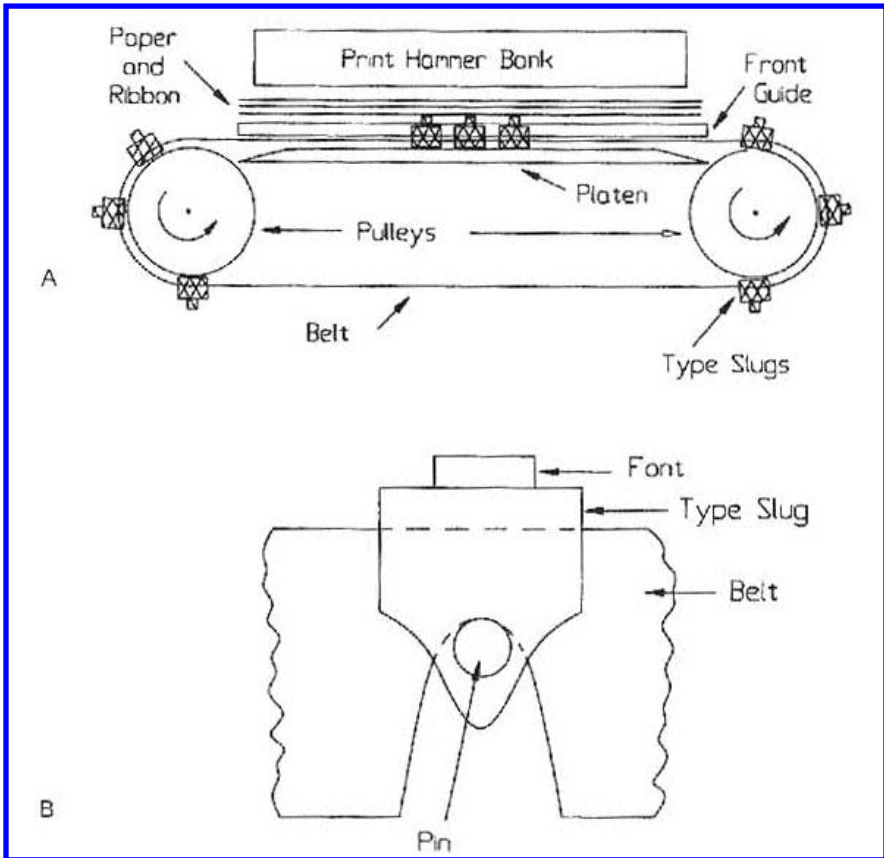


Figure 5.1 Schematic of the printing region of a line printer, “A”. “B” shows the attachment of the individual type slugs to the elastomer timing belt used.

The wear design approach used the analytical relationships of the Zero and Measurable Wear Models, in conjunction with mechanical analysis, to determine a design with adequate wear life and to verify the performance by short-term testing of the cartridge. The first step in this approach was to review the design concept for potential wear points. The next was to estimate the wear life at these sites. If any of these were not acceptable, the third step was to use the relationships to identify design parameters that result in satisfactory lives and to modify the design to incorporate these conditions. This was followed by short duration testing (e.g., 1 / 10–1 / 100 of the desired life) in which the cartridge was periodically inspected and measured for wear. If the wear was equal to or less than predicted by the models, the design was accepted. If not, the last two steps were repeated, taking advantage of the additional information obtained from the tests, until all wear concerns were resolved.

Since this new application involved higher speeds and more usage than previous impact printers, the tendency for and concern with wear were increased over that associated with prior designs. Prior experience with these types of print cartridges had indicated that the most likely wear sites are those involving sliding contact between the

slugs and the platen or guides. This proved to be the case with this cartridge, as well. As a result, while the wear design approach was applied to all the potential or actual wear sites in the cartridge, most of the effort was involved with those sites. Three contacts of this nature were initially identified. One was the engagement of the slug with the ramp at the entrance of the print region. The second was between the platen and the type slug during printing. The third was between the type slug and the front guides as a result of rebound from the platen during printing. Since all wear points were addressed in a similar manner, the general details can be illustrated by considering only one. The wear between the type slugs and the front guides provides a good illustration.

In order to perform this type of wear design, the amount of wear that can be tolerated needs to be known. In this case, prior experience provided an estimate. Generally, dimensional changes of only a few thousandths of an inch in the print region can be tolerated before there is functional degradation (i.e., reduction in print quality). Therefore any design, which provided end-of-life wear depths below this range, was assumed to be acceptable.

In this example, systems analysis consisted mainly of identifying the wear points, characterizing them in terms of geometry, loads, and motions, and determining acceptable limits for the amount of wear. Since the loading at most of the wear points resulted from the dynamics, load determination was generally the most complex and involved portion of the system analysis. In the case of the contact between the type slug and the front guides, the load was determined by mechanical analysis, assuming that the guide to be infinitely stiff and a linear spring rate for the type slug. A description of the impact situation that was modeled is shown in Fig. 5.2. The analysis accounted for both rotation about the pivot and translation of the type slug. This analysis resulted in the following

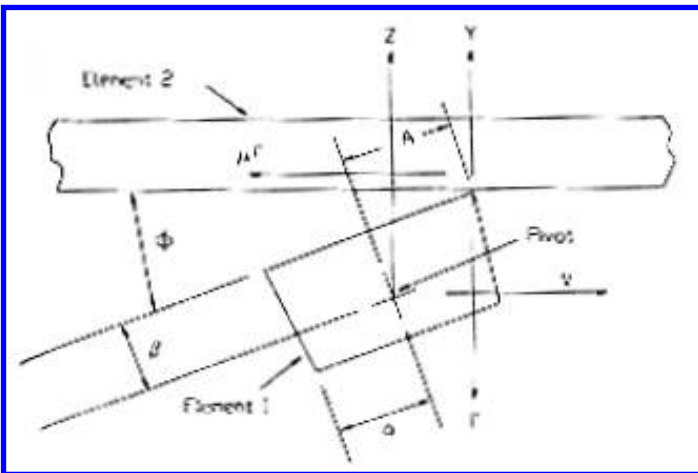


Figure 5.2 Impact condition between the type slug and the front guides. (From Ref. 32.)

expressions for the normal force, P , and contact time, T_c :

$$P = P_{\max} \sin\left(\frac{\pi T}{T_c}\right) \quad (5.1)$$

$$P_{\max} \approx \nu_0 K^{1/2} G^{-1/2} \quad (5.2)$$

$$T_c \approx \pi K^{-1/2} G^{-1/2} \quad (5.3)$$

where

$$G = m^{-1} + \frac{A^2}{J} \quad (5.4)$$

where m is the mass of the type slug; J , its rotational inertia about the pivot; K , its stiffness; ν_0 , its impact velocity normal to the surface of the guide; and A is the dimension shown in Fig. 5.2. Values for J and K were determined by conventional methods; ν_0 was determined through its relationship to the total momentum, M , of the type slug before impact, which could be measured. The following relationship was found to exist between m and ν_0 .

$$M = \frac{\nu_0[(m\alpha^2) + J]}{A\alpha} \quad (5.5)$$

α is a dimension of the slug (Fig. 5.2).

ν_0 , P_{\max} , and T_c were considered as fixed in the wear analysis since their values were primarily determined by printing requirements (e.g., sufficient energy for good print quality). For the values of the parameters specified by the overall design, the following values resulted from this kinematic analysis for ν_0 , P_{\max} , and T_c , 0.5 in./sec, 0.9 lb, and 10 μ sec, respectively.

Since the intention was to apply the Zero and Measurable Wear Models, the mechanical analysis needed to be carried one step further. Contact stresses needed to be determined. Examination of the design indicated that a cylinder of radius, r , contacting a flat surface, could approximate the contact between the type slug and the guide. Assuming good alignment, this is a special case of a Hertzian line contact, r would be the effective radius of the front, leading edge of the slug. The load per unit length would be P/w , where w is the total overlap of the upper and lower guide surfaces and the edge of the type slug. Assuming that the guide and the type slug are made of steel, which is typical for these applications, the equations for maximum stresses and contact width can be reduced to the following:

$$\sigma_c = 2290(\text{lb/in.}^2)^{1/2} K \left(\frac{P}{wr}\right)^{1/2} \quad (5.6)$$

$$W = 0.000556(\text{in.}^2/\text{lb}^{1/2}) \left(\frac{P}{wr}\right)^{1/2} \quad (5.7)$$

where σ_c is the maximum contact stress, W is the contact width, and K is a stress concentration factor. Since sliding is perpendicular to the axis of the cylinder, the maximum shear stress, τ_c , is given by

$$\tau_c = \frac{\sigma_c}{2} (1 + \mu) \quad (5.8)$$

where μ is the coefficient of friction.

The stress concentration factor included in Eq. (5.6) is used to account for a possible increase in stress at the ends of the cylinder. The edges of the type slugs tended to be well rounded. Since some increased amount of local wear could be accepted, a value of 1 was used for K . The validity of this assumption was investigated during the short-term testing of the cartridge by examining the cartridge for signs of significant wear that could be associated with these edges. None was observed. If some were found, the manufacture and the design of the type would have been modified to provide sufficiently rounded edges to insure proper wear performance.

The implicit assumption regarding alignment involved with the use of the Hertz equations was treated in a similar fashion. The overall design, along with the tolerances and clearances, supported this assumption and was later verified during the short-term testing. Again, if an alignment problem was observed, modification would have been introduced into the design to eliminate it. The underlying presumption in the wear design approach was that poor edge conditions and misalignment could not be tolerated and that they could be eliminated by design, since they were not intrinsic elements in the operation of this type of cartridge.

The initial values for w and r were 0.126 and 0.010 in., respectively. With these values, P_{\max} results in a value of 61 kpsi for σ_c and a value of 140 min for W . As a starting point for selecting or determining a wear model, it is necessary to characterize the contact situation. Since both impact and sliding were involved, this was not obvious. To aid in this characterization, an estimate of the amount of sliding that occurs during impact was made. The speed of the belt to which the type slug is attached, V , was 129 in. / sec. Comparing this value to the impact velocity, it was concluded that the impact tends to be a glancing one. Since the belt/type slug system was designed to be stiff in the direction of belt motion, a glancing impact implies that significant sliding is involved. Using T_c and assuming continuous sliding during the impact, the amount of sliding was estimated to be 0.0013 in., which is almost an order of magnitude larger than the maximum contact width. As a result, it was concluded that the model selected needed to account for the sliding motion by characterizing the contact as either a compound impact situation or a sliding situation with a varying load. To decide which was the more appropriate characterization, two general observations were noted regarding wear behavior. One is that studies have indicated that wear behavior in impact situations tends to approach sliding wear behavior as the amount of sliding during impact increases. The second is that tangential motions tend to produce more wear than motions normal to the surface. Therefore, a sliding characterization will tend to be conservative, since it assumes a more severe wear situation. It was decided that this conservative approach was the preferred one, since the amount of sliding occurring during the impact was large enough to suggest that sliding wear may be the predominant mode.

Several of the other wear points in the cartridge involved both sliding and impact and were addressed in a similar fashion. As part of the verification process, the morphology of the wear scars that were produced in the tests was examined to confirm the significance of sliding at those sites. The wear scars produced on the guides and the type slugs indicated that sliding was the predominant mode in this particular situation, supporting the selection.

The desired life of the cartridge was 5.25×10^7 lines of printing and, as indicated previously, maximum dimensional changes that could be allowed were in the range of 0.001–0.005 in. Mild wear behavior is required to satisfy these requirements. Since the Zero and Measurable Wear Models for sliding provide relationships between design

parameters in the mild wear regime and conditions to insure mild wear behavior, they were selected to provide the basis for the wear design. (See Sec. 2.4.)

When these models are applied to a varying load situation, an equivalent stress is used rather than a value based on the peak load. The relationship for the average stress in such a situation is

$$\sigma = \left(t^{-1} \int_0^t \sigma(t)^9 dt \right)^{1/9} \quad (5.9)$$

where t is time. Using the relationship between load and maximum contact stress (Eq. (5.6)) and integrating over the contact time, the following is obtained:

$$\sigma_c = 2222(\text{lb}^{1/9}/\text{in.}) \left(\frac{L_{\text{max}}}{Wt} \right)^{1/9} \quad (5.10)$$

For the specific conditions, σ_c is 59.8 kpsi, which is approximately 3% lower than the maximum value for σ_c .

The models also use a normalized unit of sliding called a pass. A pass is a distance of sliding equal to the dimension of the contact area in the direction of sliding. In this case, the distance is W . A general relationship between the number of passes in an operational unit can be written as

$$n = \frac{sf}{W} \quad (5.11)$$

where s is the amount of sliding experienced in an operational unit and f is the number of operational units. The operational unit for the contact considered was taken to be a line of printing, since the wear only occurred during printing. For some of the other wear points in the cartridge, time was used as the operational unit, because the wear at those sites was associated with belt motion and not printing. The application allowed the cartridge to idle (i.e., the belt moving without printing occurring). As a result this was a significant consideration in the overall wear design of the cartridge. The total number of passes, N , in L lines of printing is Ln .

Since all the type slugs contained in a cartridge do not experience printing during each line of print and not every print site is used in every line of print, values of f were different for the guide and the type slug and could vary with the printing done. Values for f were assigned by considering typical printing situations. This analysis indicated that appropriate values for f were 0.55 for the type slug and 1 for the guide. s is also different for the two members, but independent of print pattern. Since the guide surface experiences sliding only while the edge of the type slug passes over it, is equal to W for the guide. However, the edge of the type slug experiences sliding over the entire contact duration, T_c , so s for the type slug is the product of belt velocity, V , and contact time, T_c . Substituting these into Eq. (5.11), the following relations for n were obtained:

$$n_g = 1 \quad (5.12)$$

$$n_s = 0.00072 (\text{in.}) \frac{f}{W} \quad (5.13)$$

The subscripts, g and s , refer to the guide and slug, respectively.

The first step in a wear design using the Zero and Measurable Wear Models is to determine the zero wear life of both members. The ninth power relationship (Eq. (2.18))

is used to do this. Substitutions into this equation for τ and N result in the following:

$$L_{0g} = 1.07 \times 10^6 \left(\frac{\Gamma_r \tau_{yg}}{(1 + \mu) \bar{\sigma}_c} \right)^9 \quad (5.14)$$

$$L_{0s} = 1.43 \times 10^9 W \left(\frac{\Gamma_r \tau_{ys}}{(1 + \mu) \bar{\sigma}_c} \right)^9 \quad (5.15)$$

where L_{0g} and L_{0s} are the zero wear lifetimes of the guides and the type slugs, respectively. Γ_r is the zero wear factor for the material system and τ_{yg} and τ_{ys} are the yield points in shear for the two materials. These expressions were evaluated using properties of appropriate to the material system being considered.

The particular material system that was being considered consisted of a hardened, high-density sintered steel for the type slug, a hardened tool steel for the guide, and a multi-viscosity motor oil as a lubricant. The lubrication was in the form of a thin film and maintained by sliding contact with a wick. Since the hardness of the steels was the same (i.e., RC 60–62), their values for τ_y were the same, 150×10^3 psi (See Appendix I). It was inferred that the likely value of Γ_r was 0.54, rather than 0.20, from wear tests with similar combinations of hardened steels and previous experience with this particular combination of materials in other applications. This value could have been verified by a specific laboratory evaluation. However, in this case, it was not felt to be necessary. The appropriate value could be inferred from the results of the cartridge wear tests that were to be performed. A value of 0.2 was assumed for μ , the coefficient of friction, which is typical for boundary lubricated steels.

Substitution of the appropriate values into Eqs. (5.14) and (5.15) resulted in the following values for the zero wear lifetimes: 3.0×10^6 lines of printing for the guide (L_{0g}) and 0.6×10^6 lines of printing for the slug (L_{0s}). Both these are less than the lifetime desired for the cartridge, which as stated earlier was 5.25×10^7 lines. Since the values of the material parameters used in the analysis were those normally associated for the best wearing couples, it was decided to use the Measurable Wear Model to determine the amount of wear at end of life. If this amount of wear was not acceptable, changes other than materials would be made to the design, until satisfactory performance was obtained.

The geometry of the wear scars is shown in Fig. 5.3. To use the Measurable Wear Model, it is necessary to develop relationships for the number of passes in an operational unit and stress in terms of the dimensions of the wear scar. The contact geometry in the measurable wear region changes to a flat-on-flat and that the contact width increases with increasing wear (Fig. 5.3). For a flat-on-flat contact,

$$\tau_{\max} \propto (W w)^{-1} \propto W^{-1} \quad (5.16)$$

By considering the worn geometry of the type slug, it can be shown that

$$W = (2r h_s)^{1/2} + h_s \cot \Phi \quad (5.17)$$

where h_s is the depth of wear on the type slug and Φ is the angle between the surface of the slug and the guide. Both are identified in the illustration (Fig. 5.3). As can be inferred from the illustration, it was deduced that the wear scars have rectangular cross-sections, whose areas, Q , are given by

$$Q_g = w h_g \quad (5.18)$$

$$Q_s = w h_s \quad (5.19)$$

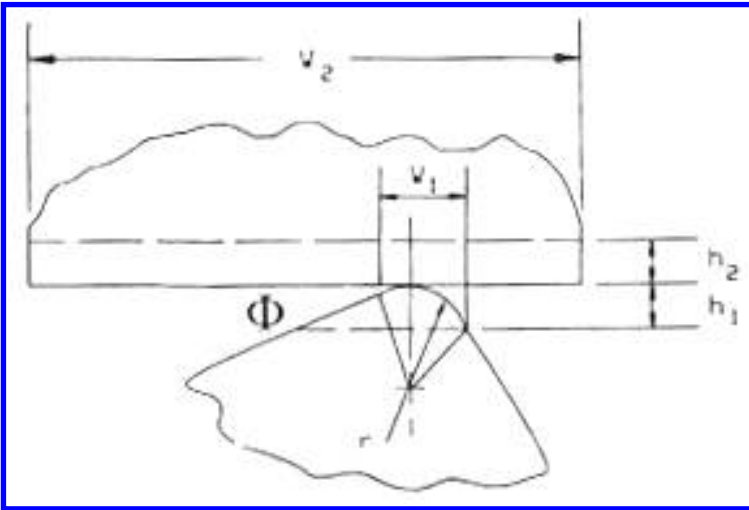


Figure 5.3 Wear scar geometry of the type slug and front guide. (From Ref. 32.)

Since n_g is independent of W , it is constant in both the zero and measurable wear regions. n_s is dependent on W and therefore changes as wear progresses. The expressions for each in the measurable wear analysis are

$$n_g = I \quad (5.20)$$

$$n_s = 0.00072 \text{ (in.)} \frac{f}{(2rh_s)^{1/2} + h_s \cot \Phi} \quad (5.21)$$

Since the product $\tau_{\max} W$ is constant in this situation, there is no distinction between the variable and constant energy wear modes and it is sufficient to only use the following expression for the progression of wear:

$$dQ = C dN \quad (5.22)$$

(See Eqs. (2.36) and (2.37).) For the guide, this reduces to

$$dh_g = C_g dL \quad (5.23)$$

For the type slug,

$$[(2rh_s)^{1/2} + h_s \cot \Phi] dh_s = C_s dL \quad (5.24)$$

Integrating, the following relationships are obtained for the wear of the guide and the type slug:

$$h_g = C_g L \quad (5.25)$$

$$0.667(2r)^{1/2} h_s^{3/2} + \cot \frac{\Phi}{2} h_s^2 = C_s L \quad (5.26)$$

C_g and C_s are determined by means of the zero wear criteria, namely that at the zero wear lifetime, the average depth of the wear scar is equal to half the peak to valley roughness, δ . By considering the geometries of the two scars, it can be shown that

$$H_g = h_g \quad (5.27)$$

$$H_s = 0.5 h_s \quad (5.28)$$

where H 's are the average depths of the wear scars.

Upon substitution, the following were obtained:

$$h_g = 0.5 \delta_g \frac{L}{T_{0g}} \quad (5.29)$$

$$h_s^2 \left[1 + \left(\frac{4}{3 \cot \Phi} \right) \left(\frac{2r}{h_s} \right)^{1/2} \right] = \delta_s^2 \left[1 + \left(\frac{4}{3 \cot \Phi} \right) \left(\frac{2r}{\delta_s} \right)^{1/2} \right] \frac{L}{T_{0s}} \quad (5.30)$$

Once values for Φ , δ_s , and δ_g were determined, these two equations were used to determine the wear at end of life. By analysis of the design, it was concluded that Φ was approximately 20° . The surface roughness of both the type slug and the guide was specified to be $20 \mu\text{in.}$, CLA, implying that δ 's were $40 \mu\text{in.}$ Using these values and the previously determined values for L_0 , the zero wear lifetimes, the projected wear depths on the two members were $340 \mu\text{in.}$ for the guide and $410 \mu\text{in.}$ for the slug. Since 0.002 – 0.005 in. of wear was acceptable, it was concluded that the design was satisfactory.

The amount of wear projected for the guide is an upper-bound estimate, since it does not include the possible effect of slug wear on the zero wear lifetime of the guide. This is likely because of the reduction in stress associated with the change from a cylinder-on-flat configuration to a flat-on-flat configuration.

A cartridge was built to the design parameters selected and tested for approximately $1/50$ of its intended life; the cartridge was examined for wear at the end of the test. For this amount of usage, the analysis indicated that wear on both the guide and front surface of the type slug should only be comparable to the surface roughness (i.e., no pronounced change in contour, but some evidence of rubbing). The examination of the tested cartridge showed that this was the case for the guide. However, a pronounced wear scar was observed on the type slug and the wear depths approached several hundred micro-inches. One possibility that was considered for this disagreement was the assumption used for Γ_r . If the value for Γ_r was 0.2 , the projected wear would be in that range since the depth of wear is approximately proportional to $\Gamma_r^{-4.5}$. However, if this were the case, the wear should also be much larger on the guide. Since this was not the case, other explanations were sought. One approach taken was to look for additional wear points not considered in the analysis. After some study, it was determined that the type slug was rebounding from the entrance ramp and contacting the end of the guide. Analysis of this situation indicated that rebound was sufficient to explain the wear. To eliminate this wear, the entrance ramp was modified to eliminate the rebound. Subsequent testing confirmed this as a solution.

5.3. VACUUM PROBE

This example of wear design is concerned with a vacuum probe used to pick up and place chips in a semiconductor manufacturing line. It illustrates the elements involved with the

use of the Zero Wear Model, the determination of non-material design parameters needed to insure adequate wear performance, and the use of a laboratory tests to provide confirmation. There were two reasons to be concerned with wear. In addition to the typical one, which was related to function, there was also a concern associated with the formation of wear debris. Studies had shown that a major source of contamination in semiconductor manufacturing was often wear debris from the manufacturing equipment. As a result there was a desire to eliminate all wear for the intended life and, if that was not possible, to reduce the amount of wear as much as possible during that period. The intended life of these probes was 10^7 placements.

This example is concerned with the wear design of the needle/bushing interface of the vacuum probe. Figure 5.4 shows the design of the probe. The operation of the probe consisted of pressing the needle against the surface of a chip and providing a suction force to hold the chip. During this operation, the axial displacement of the needle relative to the bushing was approximately 0.010 in. The overall design of the apparatus insured that the axis of the probe was within 5° angle from normal to the surface of the chip. The spring in the assembly provided an axial pre-load of 32–42 g, which needed to be overcome during operation. Instrumentation of a prototype showed that while there was a slight impact when the needle contacted the chip, the loading associated with it was negligible in comparison to the pre-load. In addition to the pre-load provided by the spring, assembly and part tolerances resulted in some loading between the needle and the bushing. The design specified that the maximum force required to move the needle in the bushing in the absence of a pre-load was not to exceed 3 g. The bushing material was a leaded bearing bronze with a Vickers hardness of 225 kg/mm^2 . The needle was to be made from 24-gauge hypodermic needle stock with a Vickers hardness of 420 kg/mm^2 . Because of the concern with contamination in this application, there was to be no lubrication.

The sliding nature of the needle/bushing interface and the goal of having no wear debris generated during life led to the selection of the Zero Wear Model as the basis for the analysis. One reason for the selection was the general applicability of the Zero Wear Model in determining conditions to insure low wear. Another was the judgement that

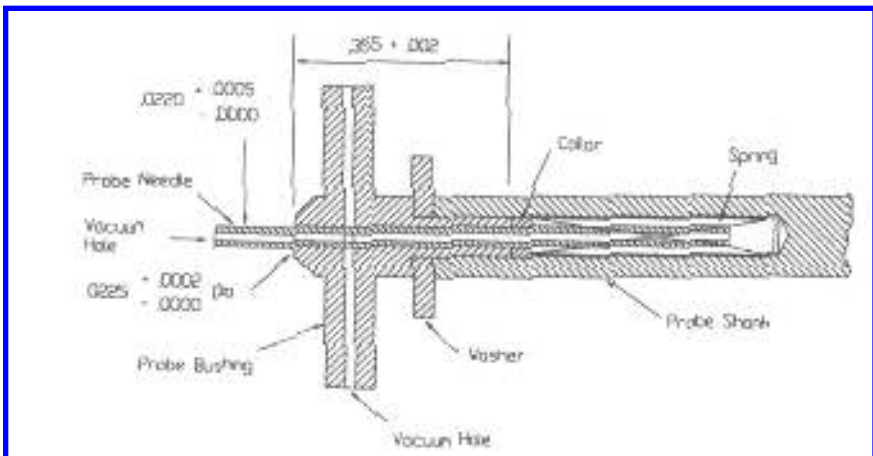


Figure 5.4 Vacuum probe used for chip placement.

the amount of wear debris that would be associated with a zero wear condition would be negligible. The approach was to use the relationships of the Zero Wear Model to determine required values of design parameters, so that a zero wear lifetime of 10^7 operations was achieved. Some laboratory testing was also done to support the analytical predictions and to determine the zero wear factor, Γ_r , for the material pair.

Typical mechanical design considerations had led to the initial material selections as well as initial dimensions and tolerances. A review of those selections and the overall nature of the wear situation, which could be characterized as a linear journal bearing, was performed as the first step in the wear design. This review identified two sources for a radial bearing load. One was assembly interference and the other was pre-load. Available friction data (2) indicated that the likely range for the coefficient of friction was between 0.2 and 0.6. This being the case, the 3 g design specification related to interference implied a radial load of between 5 and 15 g. By considering the geometries involved, it was estimated that the contribution of the pre-load would be less than 0.1 g and as a result, it was concluded that the pre-load could be neglected in the analysis of the bearing. It was also concluded that the material selection was reasonable in that a harder shaft was being used against a typical softer-bearing material. Alignment in the proposed designs was also reviewed. It was found that the indicated dimensions and tolerances would result in less than 7' of axial misalignment and on that basis were acceptable as initial values for the wear design. One area of concern was identified during this review. This was with respect to the edge of the bushing.

In general, edges tend to act as stress risers and increase wear in the region affected by edge. In many cases, the mechanism can tolerate some increased local wear and it is sufficient to simply require that the edges be beveled or rounded, as was the case in the printer cartridge example. However, in this application, there was the need to eliminate all wear debris, so even localized wear could not be tolerated. Consequently, it was decided that the wear design would have to include the effect of the edge. Since the proposed design did not specify any particular edge condition for the bushing, it was decided that the Zero Wear Model would be used to determine the required edge condition, assuming all other parameters were as initially selected.

To apply the Zero Wear Model, two quantities need to be determined. One is the maximum shear stress and the other is the number of passes in a unit operation. Since the clearance in the bearing was sufficient for the Hertz model to be applied, the relationship for the maximum shear stress, τ_{\max} , without accounting for stress concentration, was

$$\tau_{\max} = \sigma_c(0.25 + \mu^2)^{1/2} \quad (5.31)$$

where σ_c is the Hertz contact pressure and μ is the coefficient of friction. Accounting for stress concentration, the equation is

$$\tau_{\max} = K\sigma_c(0.25 + \mu^2)^{1/2} \quad (5.32)$$

where K is the stress concentration factor for the edge. Since the amplitude of the motion is not greater than the length of the bearing, the relationship for the number of passes was the same for both members. The number of passes in a single operation, n , was given by

$$n = \frac{2a}{\beta} \quad (5.33)$$

where a is the amplitude of the stroke and β is the length of the bushing. Because the needle is harder, the zero wear lifetime of the mechanism is the zero wear lifetime of the

bushing. As a result, the zero wear relationship, as applied to the bushing, is used to determine the required edge conditions. When the expressions for t_{\max} and n are substituted into the equation for zero wear lifetime of the bushing, the following expression is obtained for the allowed value of K :

$$K = \left(\frac{\Gamma_r \tau_{yb}}{\sigma_c (0.25 + \mu^2)} \right) \left(\frac{10^3 \beta L_0}{a} \right)^{0.111} \quad (5.34)$$

where Γ_r is the zero wear factor for the material couple; τ_{yb} the yield point in shear of the bushing material; L_0 , the required lifetime in number of placement cycles.

This equation was used to determine the allowed value for K for the proposed design and a lifetime of 10^7 placements. Based on the hardness of the bronze, τ_{yb} was estimated to be 44 kpsi. (See Appendix IV for an approximate relationship between yield point and hardness.) Values for both Γ_r and m had to be assumed. Over the likely range for coefficient of friction (i.e., 0.2–0.6), there was only a 10% difference in K . The possible range for Γ_r was much more significant and results in a factor of 2.7 in possible values for K . Assuming good wearing properties for the couple (i.e., Γ_r equal to 0.54), the allowed value for K was approximately 32; for 0.2, approximately 12.

To relate a stress concentration factor, K , to edge geometry, the following relationship for parallel cylinders was used (Table 2.2, 3):

$$K = \left[1 + \frac{r^2}{R_1^2} + \frac{r^2}{R_2^2} \right]^{1/2} \quad (5.35)$$

where r is the radius of the edge; R 's, the radii of the two cylinders; m and n are the coefficients of the general Hertz formulation, m and n are defined in terms of $\cos \theta$ where

$$\cos \theta = \frac{r^{-1} - R_1^{-1} - R_2^{-1}}{r^{-1} + R_1^{-1} + R_2^{-1}} \quad (5.36)$$

(See Appendix I.) These relationships were used to determine values of K as a function of r . For the nominal values of -0.01125 and 0.0110 in. for the radius of the bushing and the needle, respectively, this relationship is shown in Fig. 5.5. Using this curve, it was concluded that if the couple had good wearing properties, a minimum radius of 0.001 in

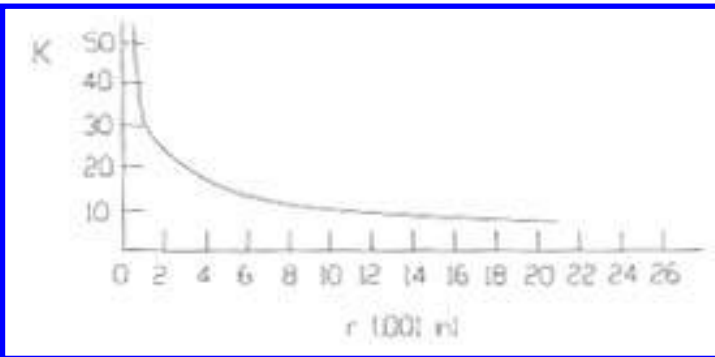


Figure 5.5 Stress concentration factor as a function of edge radius.

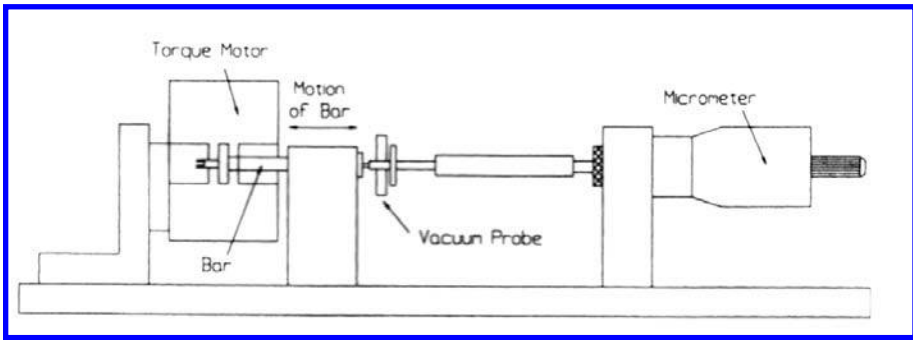


Figure 5.6 Test configuration used in the wear design of a vacuum probe.

would be acceptable; otherwise, a minimum radius of 0.010 in. was required. Without knowing what the appropriate value was for Γ_r , a minimum radius of 0.010 in. was specified for the design.

Verification consisted of demonstrating the significance of edge conditions on the wear of this probe. To do this, it was decided to perform accelerated wear tests on actual probes, which had significantly different edge conditions. A test fixture was developed in which a torque motor was used to move the needle at a frequency of 360 Hz and amplitude of 0.01 in. This test situation is shown in Fig. 5.6. Two probes were selected; one had a noticeably sharp edge, and the other a noticeably rounded edge. After 10^7 cycles, the probe with the sharp edge was examined for wear. The only wear that was observed was on the edge and it approached 0.001 in. In the second case, there was no detectable wear after 2×10^7 cycles. Measurements of the edge radii after the test indicated that the radius for the sharp bushing was approximately 0.0003 in.; for the other, 0.003 in. Because of the actual value of the radius for the second probe, a serendipitous result regarding Γ_r was obtained. For that radius and a value of 0.2, Eq. (5.24) indicated a zero wear lifetime of 1.5×10^3 cycles, implying that the value of Γ_r for this combination was 0.54. As a result, the radius specification could be changed to 0.001 in. However, to provide additional safety, the minimum radius was specified to be 0.003 in.

5.4. FORMS THICKNESS CONTROL

This case history illustrates a non-analytical approach to wear design. In this example, the results from an examination of worn parts provided the basis for a phenomenological model which was used to develop a satisfactory design. Simulative testing was also used to both verify the model and to aid in the selection of specific design parameters.

In most line printers, there is a means of adjusting for different thicknesses of the forms or paper stock that is to be used. In this particular case, this adjustment was accomplished by means of a manually actuated cam-follower device. This device was required to last for 12×10^3 operations. When operated, the follower, which was a compound surface formed by two cylindrical profiles, slid along a flat surface of a ramp. Both parts were molded and made from the same glass and PTFE-filled phenolic. During the qualification of the printer, significant wear was observed on both parts after as little as 50 operations. In printers, which had experienced extensive testing, wear depth was found in the 0.001–0.01 in. range. Because of the significance of the forms adjustment control in

insuring print quality, wear of this magnitude was unacceptable. The wear design approach started with the examination of the worn parts, two of which are shown in Fig. 5.7.

The examination revealed the following characteristics of the wear:

1. Wear was primarily on the surface of the follower; however, the ramp surface did experience sufficient wear to expose glass fibers.
2. The wear zone on the follower showed that contact occurs in the regions where the two cylindrical profiles were blended.
3. Both the wear scar on the ramp and on the follower indicated that, at least during some portion of the operation, the contact extended over the edges of the ramp and that the contact motion was diagonally across the surface of the ramp.
4. The wear scar on the ramp did not exhibit singular wear zones corresponding to individual settings; rather, it appeared continuous. This indicated that the wear was primarily due to the operation of the mechanism rather than any fretting type of motions caused by machine vibrations that could occur in a fixed position.

Based on these observations, a phenomenological model for the wear was formed. It was hypothesized that the wear resulted from the sliding motion associated with the

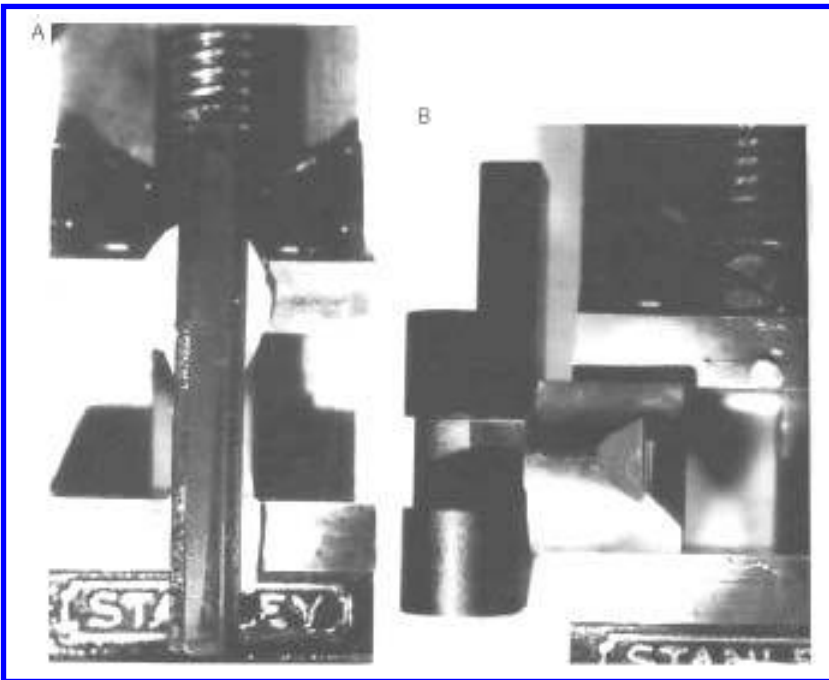


Figure 5.7 Worn components of the forms thickness control unit. “A” shows the ramp; “B” shows the follower.

actuation of the device and the high stress conditions associated with the edge contacts. Initially, the high stresses, resulting in the poor contact geometry (i.e., contact in the region where the two cylindrical profiles merged and contact with the edge of the ramp), caused rapid wear of both surfaces. This exposed the glass fibers used as fillers in the phenolic. Since the matrix material was soft, this resulted in the introduction of a significant abrasive wear contribution to the overall wear behavior. Greater wear would occur on the follower since its surface experienced more rubbing than the surface of the ramp.

To develop this model, it was necessary to estimate the wear in the application in terms of the several models for sliding wear. Estimates of wear rates based on the linear relationship for sliding wear (Eq. (2.3)) and nominal values for the wear coefficient for this type of material (e.g., values in the range of $100\text{--}1000 \times 10\text{--}10$ in.³ min / ft lb hr) tended to be significantly lower than those estimated from the wear measurements. Typically, these estimates were one to two orders of magnitude lower, unless the possibility of thermal degradation was considered. However, both the appearance of the scars and the nature of the operation, as well as the properties of the phenolic, did not indicate thermal degradation to be a factor. On the other hand, it was found that the Zero and Measurable Wear Models could easily account for the observed wear if the effect of stress concentration was taken into account. It was concluded that the influence of stress and geometry predicted by the Zero and Measurable Wear Models provided the most likely explanation. This provided the basis for the phenomenological model. These two models were also used to provide guidance in determining a solution.

This model provided an explanation for the observations and led to the identification of geometry as the primary element to be addressed in redesign. A change in materials was considered to be a secondary element, since the original geometry would be poor for any material system. It was also possible that with the proper geometry, adequate wear might be obtained with the original materials.

After reviewing the design and the existing molds to see what changes were possible, it was decided to modify the follower by replacing the compound surface formed by the two cylindrical profiles with a spherical surface with as large a radius as possible. This would reduce the contact stress and avoid alignment concerns that would be associated with a large radius cylindrical surface. Layouts indicated that this was possible for radii up to 1 in. Estimates of wear behavior using the Zero Wear Model indicated that a radius in the range of 0.75–1 in. would be adequate. Two ways of implementing this design change were considered. One was the use of hard steel insert for the face of the follower. This version made the follower significantly harder than the ramp, which was beneficial since the follower tended to experience more wear than the ramp. In addition, the use of a hard steel surface would greatly improve the abrasive wear resistance of the follower. The second was to modify the mold to provide a spherical phenolic surface. By controlling the location of the spherical section, contact with the edge of the ramp during actuation could be eliminated for nominal dimensions. However, edge contact could not be eliminated over the entire tolerance range and a modification of the mold for the ramp to provide a wider surface was also considered. While this was possible, it was not desirable since additional changes were required to accommodate a wider ramp. A simulative wear test was selected to evaluate these options and verify the proposed model.

It was decided that with modifications a reciprocating ball–plane wear tester could be used to simulate the actual wear situation as it provided the same type of motion and loading. The only modifications that were required were fixtures to allow the use of actual ramps as the plane and of prototypes of the cam surface as the ball. The loads measured in the application were in the 3–4 lb range and could be applied with the wear

tester that was to be used. The maximum stroke length (1 in.) that could be obtained with the tester, while shorter than the full range of the application (1.8 in.), was considered to be representative, but the normal mode of testing with this tester (i.e., continuous, reciprocating sliding) was not. In the application, the control would be manually adjusted, moving the follower from one location on the cam to another, and then it would remain at that new position for some period of time. The conditions in the tester would tend to produce higher interface temperatures than in the application. Since surface temperature is often a significant factor with the wear of plastics, there was concern that this would be a significant factor affecting the simulation. It was decided to resolve this concern by comparing the morphology of the wear produced in the tester to that produced in the application. A 50 cycles / min rate was selected for the test, since it provided an average speed representative of the application and a convenient test duration for the accumulation of the required lifetime cycles (approximately 4 hr). The morphology of the test wear scars was found to be the same as machine-worn parts, and it was concluded that a 1 in. stroke and a 50 cycles / min rate provided good simulation.

The results of the simulative tests that were performed are shown in Table 5.1. As can be seen from the table, several of the tests were done to verify the model. The increase in wear, resulting from exposure of the glass and edge contact, was demonstrated directly. The influence of stress on wear was indirectly demonstrated by using a higher load. A 4.5-fold increase in load was found to result in a 25-fold increase in wear volume, since wear volume is proportional to the depth squared. This result is more consistent with the Zero Wear Model than for the linear wear model. These test results also demonstrated the tendency for the follower to experience more wear. Since surface roughness can be a factor in wear behavior, it was decided to evaluate several different surface roughness conditions for the metal insert. Overall, the test results showed that acceptable wear behavior could be obtained with either of the proposed modifications of the follower. It was also concluded that occasional edge contact could be tolerated with the new

Table 5.1 Wear Test Results

Steel roughness	Wear at 12,000 strokes (2000 g load)	
	Slider	Flat
Hard steel insert, 0.75 in. radius		
V6	Not measurable	Not measurable
V15-20	≈75 μin.	≈75 μin.
V32	Not measurable	≈150 μin.
Test conditions	Wear at 12,000 strokes	
	Slider	Flat
Phenolic follower, 1 in. radius		
2000 g load	Not measurable	Not measurable
2000 g load, sliding on edge of flat	≈ 0.001 in.	≤0.00005 in.
2000 g load, abraded slider surface	≈ 0.0001 in.	≤0.00005 in.
9000 g load	≈ 0.0015 in. avg. 0.0005 in. groove	≤0.00005 in.
9000 g load, abraded slider surface	≈ .0005 in.	≤0.0001 in.

follower, since continuous contact resulted in only 0.001 in. of wear at end of life. Since stress level would be higher in the tests conducted with the steel insert, it was also concluded that a minimum radius of 0.75 in. would also be acceptable for a phenolic follower. Based on this information, the mold for the follower was changed to provide a 0.75 in. radius and the width of the ramp was increased as much as possible. As these changes provided satisfactory performance, it was not necessary to change the materials.

5.5. PLASTIC GEARS

This example of wear design provides an illustration of the development of a theoretical model for design use. The approach is primarily analytical and is guided by general experimental trends and observations. As a result, the relationships developed have more general applicability than the specific situation for which they were developed.

As part of a cost reduction effort for a mid-range impact printer, the replacement of a satisfactorily performing phenolic / metal bevel gear pair, having a gear ratio of 1, with a plastic pair of the same size and geometry was being considered. As part of the design process associated with this change, the potential wear performance of different pairs needs to be evaluated and compared to the performance of the original steel / phenolic pair. One wear design approach that was considered was based on the use of simulative tests. In this case, prototype gear tests or rolling tests with slip would have been required to simulate slip and temperature build-up that is possible with plastic gearing. However, this approach was not considered feasible because of the lack of the specialized equipment needed, the cost and time associated with obtaining the specimens required, and the length of time associated with those tests. Another approach that was considered to be feasible was to build on existing models and theoretical concepts to develop an analytical wear relationship, which involved the principal parameters that would affect relative performance of different material pairs. This relationship could then be used to select an appropriate pair whose performance would be verified by a printer test. This is the approach that was taken and, in effect, resulted in the development of a Figure of Merit for the material pairs considered.

The starting point of this approach was some general observations about relative motion and wear life of gears. While the motion between gear teeth can nominally be described as rolling, it is not pure rolling since relative slip occurs. The amount of slip varies along the tooth profile and is primarily determined by the geometries involved. Gear failures can result from both rolling and sliding wear mechanisms. However, in the case of gears operating under dry or boundary lubrication conditions, lifetimes associated with sliding wear mechanisms tend to be shorter than those associated with rolling wear mechanisms. Under those conditions, the wear life of a gear can be related to the amount of wear that occurs in the regions of maximum slip. Based on these observations and the fact that there was to be no lubrication used, it was concluded that the relative performance of the material pairs could be based on their wear behavior in these slip regions.

Because of the sensitivity of polymer wear performance to temperature, it was necessary to consider the effect that these design changes would have on temperature. Since steel is a significantly better conductor of heat than polymers, it was anticipated that the plastic / plastic pairs would tend to run hotter. Since the general conditions of the application were similar to other applications in which plastic / plastic gear pairs were used, catastrophic degradation in wear performance due to temperature was not anticipated for the materials that were to be considered. However, it was felt that some

degradation might result and that it was necessary to include a temperature dependency in the model developed.

One way of treating wear in these slip regions was with the model for rolling wear and accounting for differences in sliding wear characteristics by means of the model's surface endurance limits for different amounts of slip. Another approach was to use a sliding wear model. A rolling action tends to moderate the severity of a sliding action. Intuitively, then, it was concluded that the sliding approach would tend to be more conservative and, as a result, preferred for a theoretical approach. Because of this and the fact that the formulations of the rolling wear model and Zero Wear Model for sliding Wear are so similar, it was decided to use the Zero Wear Model for sliding.

Even though the geometry was to remain constant, the amount of sliding experienced would tend to change because of differences in the contact areas obtained with different materials. With larger contact areas, there would be more sliding involved. However, the number of passes (used in the Zero Wear Model) would tend to remain constant since the sliding distance for a pass is the width of the contact. Therefore, it was assumed that the lifetime of a gear pair was proportional to the number of passes associated with the zero wear point (i.e., the zero wear lifetime in units of passes)

$$L = k_2 \times 10^3 \left(\frac{\Gamma_r \tau_y}{\tau_{\max}} \right)^9 \quad (5.37)$$

where k is independent of materials and L is the lifetime. The lifetime for a gear pair would be the smaller of the two individual lifetimes.

A temperature dependency was introduced into this relationship by considering τ_y , the shear yield stress, and E , Young's modulus, to be functions of temperature. For plastics, it was assumed that since both decrease with increasing temperature, the ratio, τ_y / E is a constant. Using this, the equations for contact stresses, and Eq. (5.37), the following relationship was obtained:

$$L(T) = L(T_0 \Phi(T)^{9/2}) \quad (5.38)$$

where

$$\Phi(T) = \frac{E(T)}{E(T_0)} \quad (5.39)$$

T_0 is a reference temperature. For a metal, Φ is 1. Equations (5.38) and (5.39) provided a means of analytically comparing the different pairs considered.

The use of these equations in the selection process can be illustrated by comparing the prime replacement candidates for this application. The prime candidates for replacing the steel / phenolic pair were nylon / phenolic, phenolic / phenolic, and nylon / nylon. Values for E , Φ , and τ_y for these two plastic are given in Table 5.2, as well as those for steel. Values for E were obtained from materials supplier information and $\tau_y(T_0)$ were determined from micro-hardness measurements using the relationship between micro-hardness and yield point given in Appendix IV. Room temperature was selected as T_0 . Available data for the coefficient of friction for these couples indicated that they were similar and in the 0.2–0.4 range.

For dissimilar pairs the smaller lifetime, which is the lifetime for the pair, is associated with the softer material. For the steel / phenolic pair, this the phenolic. However, as can be seen by analyzing the data in Table 5.2, nylon is harder at lower temperatures

Table 5.2 Elastic Properties of Nylon and Phenolic^a

Temperature (°F)	E (10^6 psi)		τ_y (psi)		Φ	
	Nylon	Phenolic	Nylon	Phenolic	Nylon	Phenolic
72	1.03	2.03	11,800	8000	1	1
100	0.83	1.95	9500	7700	0.806	0.960
125	0.67	1.85	7700	7300	0.656	0.911
150	0.54	1.75	6200	6900	0.524	0.862
175	0.43	1.65	4900	6500	0.417	0.813
200	0.33	1.59	2800	6300	0.320	0.783
225		1.53		6000		0.753
250		1.48		5800		0.729
300		1.41		5600		0.695
350		1.30		5100		0.640
400		1.10		4300		0.542

^aFor comparison, the properties of steel are: E (10^6 psi), 30; τ_y (psi), 80,000; and Φ , 1.

and phenolic is harder at higher temperatures. The transition occurs somewhere in the vicinity of 110°F.

Assuming all the pairs have the same value of Γ_r , Eqs. (5.38) and (5.39) were used to compute the lives of the candidate pairs relative to the steel / phenolic pair. These are shown in Fig. 5.8 as a function of operating temperature. Only a moderate temperature increase, < 100°F, was anticipated and later confirmed. This graph indicates that any of the pairs would be acceptable as a replacement, provided they had the same value of Γ_r as the steel / phenolic pair. However, since there tends to be two characteristic values for this factor, this may not be the case. Most steel / plastic combinations tend to have a value for Γ_r of 0.54. Since the specific pair was observed to have good wear characteristics, it was assumed that the value was likely 0.54. If a candidate pair had the lower characteristic value of 0.2 for Γ_r , this would result in a reduction of the computed values by a factor of approximately 10^{-4} , which implies a shorter life than that of the steel / phenolic combination. In which case, the pair would not be a satisfactory replacement. Since the values for Γ_r are strongly related to the tendency for adhesion, self-mated pairs tend to have the lower value; thus, the dissimilar pair of nylon and phenolic was selected as the replacement. Subsequent machine tests confirmed the selection. Because of the strong effect that the value of Γ_r has on life, it is likely that significant wear would have been observed in these tests if the value were 0.2 for this combination.

5.6. TYPE CARRIER BACKSTOP

This case study provides an illustration of the implementation of the Zero and Measurable Wear Models for impact wear, as well as the use of theoretical and analytical considerations to support a primarily experimental approach. It also illustrates a modeling approach to two-body wear. A photograph of a type carrier is shown in Fig. 5.9, along with a photograph showing the contact between the type and the backstop. The individual type elements, which are mounted on a common shaft, are held against the backstop by means of compressed springs.

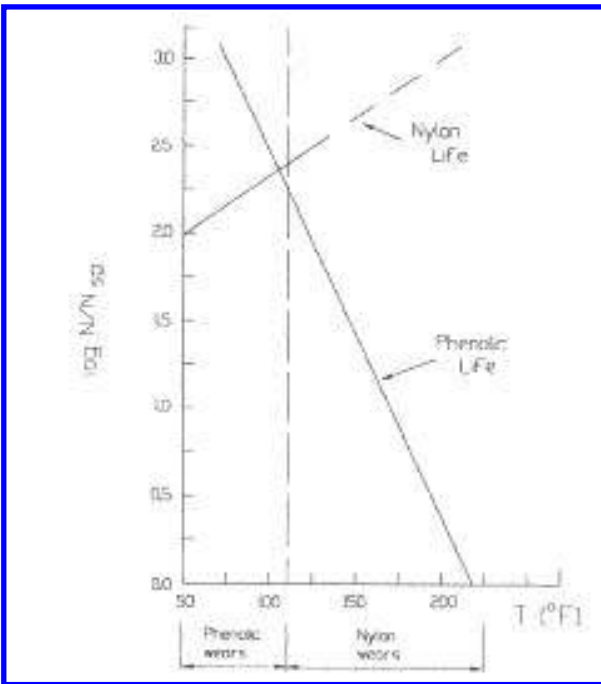


Figure 5.8 Wear lives of the phenolic and nylon gears as a function of temperature.

This type of carrier was used in the print cartridge of a high-speed impact line printer. The carrier rides on a rail. In the print area, a hammer hits the back of a selected type element, causing the type to go into free flight and ultimately impact the ribbon and paper stack. The type then rebounds from this impact and impacts the backstop of the carrier, ultimately coming to rest before the next print cycle. This case study was concerned with the wear between the type and the carrier at the backstop. Wear at this interface affected the position of the type relative to the hammer. This is important since it affected print quality. While the printer design allowed for some adjustment to account for changes in hammer locations, there was no compensation for changes in type location. Printing considerations resulted in a requirement that wear at this interface be equal to or less than 0.001 in. after 2×10^8 impacts or print cycles for the individual type elements.

While wear at this interface was of concern, it was not the only or primary aspect influencing the design of the interface. Because of experience with slower printers, type manufacturing, fatigue aspects, and type settling time were the primary factors influencing the design. Wear had to be controlled within the constraints associated with those concerns. As a consequence, the initial wear design approach consisted of selecting parameters to optimize wear behavior as much as possible and to monitor the wear produced during printer tests. End-of-life wear would be projected from these data by

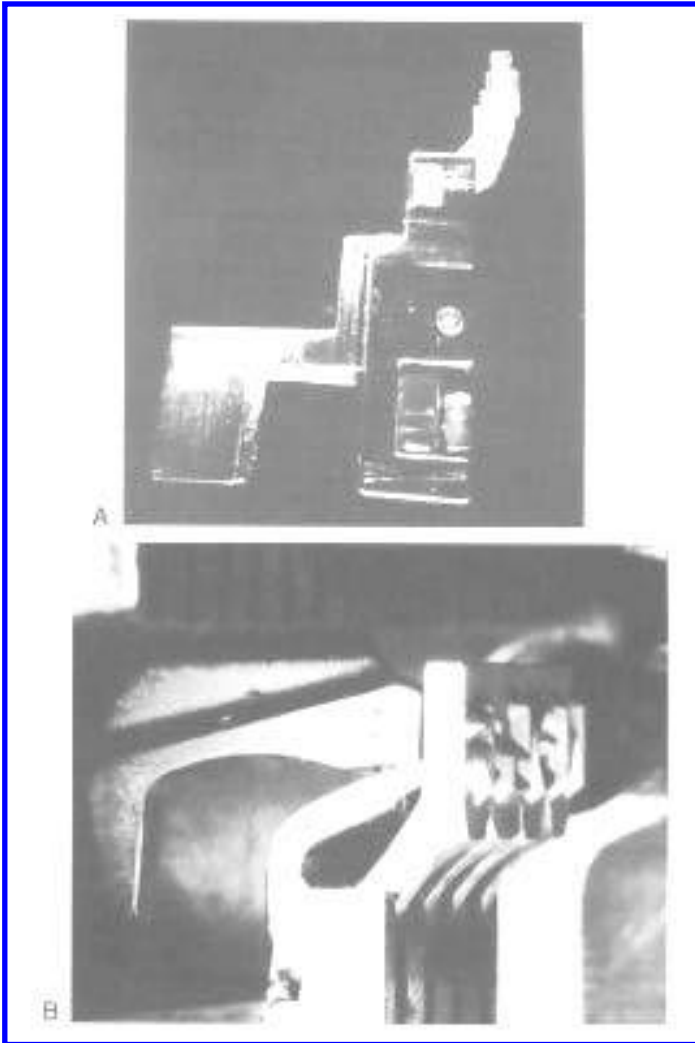


Figure 5.9 Photographs of the type carrier. “A” shows an assembled type carrier. “B” shows the type resting against the backstop as the hammer begins to strike at the top of the type.

using the conservative assumption that wear is proportional to the number of impacts. This was a reasonable strategy since a number of printer tests would be performed under a variety of conditions. This would allow the accumulation of a large number of print cycles at many individual sites. The thrust in optimizing wear behavior was to reduce the tendency towards adhesive wear and to reduce stress levels as much as possible. These

initial considerations resulted in the selection of hardened and dissimilar materials, insuring adequate lubrication for the interface, placing as large a radius as possible on the surface of the backstop, tumbling the type to round the edges, and specifying moderate surface roughnesses. The material for the type was M2 tool steel and that selected for the backstop was P5 mold steel. The maximum radius that could be used on the backstop was 0.25 in. The surface roughness on both members was specified to be an R_a of 15 μin .

These original selections of design parameters were found to be adequate. While wear was evident in most of the tests, it was generally too small to be measured, except at the end of the longest tests. Based on measurements taken after 10^7 impacts, the end-of-life wear was projected to be significantly less than 0.001 in., which was acceptable. However, near the end of the development of the printer, a change to the backstop was required. To decrease the settling time of the type, it was necessary to increase the height of the backstop. This resulted in the backstop engaging the type in a new location and implied a significant change in impact dynamics. Since either of these could effect wear, it was necessary to evaluate the new design and determine if it had adequate wear life.

Unfortunately, the initial wear design approach provided little information that could be used in an analytical approach to estimate the effect of these changes. There were no analytical models developed that related design parameters to wear or for the loads and motions at this interface. Observations made regarding the behavior or potential behavior of the carrier and type indicated a sufficiently complex wear situation that experimental verification for any model would be required. In addition to the primary impact, there were indications that fretting motions and secondary impacts were likely complications and their relative contributions were not known beforehand.

There were several reasons, which suggested such complications. One is that since the type had significant tangential velocity relative to both the hammer and the ribbon/paper stack, impact with these surfaces would tend to induce lateral vibrations or displacements of the type. Therefore, there was the potential for a fretting component during impact with the backstop. The likelihood of this was supported by wear scar measurements, which tended to indicate that scars on the backstop were wider than the type. There was also the possibility of induced secondary impacts on adjacent type, as a result of wave propagation in the backstop from the primary impact. There was some evidence of this from kinematic studies. Finally, there was the possibility that fretting motions could be induced by carrier instabilities during printing. There was evidence of this from some idling tests (i.e., running without printing) that had been performed as part of the overall development activity. Superficial wear marks could be visually discerned on the backstops of carriers used in those tests. Since the ratio of idle time to print time in these printers was extremely small, it was concluded that wear during idling was negligible and could be ignored. However, this did indicate that carrier motion could result in relative motion between the backstop and the type. Wear from this motion would be associated with the spring pre-loads and not the primary impacts.

Because of the lack of an established model for this situation and the time and resource constraints associated with the overall development effort, it was decided that the most expedient way of addressing the adequacy of the design was to develop an empirical wear relationship. This would then be used to project life and to compare that relationship to those predicted by various theoretical models. Correlation between the empirical relationship and the models would increase the confidence in the projection. At the same time, it would provide verification of a model for this wear situation that could be used in future design considerations.

The wear data needed to generate the empirical wear relationship were obtained from a printer test. By means of a special print pattern, it was possible to reach 10^8 impacts on a limited number of type. To develop the wear relationship, the test was stopped at two intermediate number of impacts and the type elements and backstops were measured for wear. A summary of the wear data is shown in Table 5.3. Because of the shape of the part and the magnitude of the wear, it was not possible to obtain sufficiently accurate wear depths on the type to establish a wear relationship. However, it was possible to conclude from the measurements and the appearances of the scars that the wear on the type did not exceed that on the backstop. To obtain a wear relationship for the backstop, the best fit of the individual measurements to the following expression was done:

$$h = CN^m \quad (5.40)$$

where h is the depth of wear and N is the number of impacts. This form was chosen because it generally provides a reasonable fit to wear data in a stable wear regime, as had been discussed previously. In this case, the best fit resulted in the following:

$$h = 2.3 \times 10^{-11} (\text{in./impact}^{0.8}) N^{0.8} \quad (5.41)$$

The expression for total wear at the interface, H , was

$$H \leq 4.6 \times 10^{-11} (\text{in./impact}^{0.8}) N^{0.8} \quad (5.42)$$

This resulted in a projection of 0.0002 in. of wear at life, which was acceptable.

Based on the operational characteristics associated with the type / backstop interface, it was decided that for modeling wear should be considered as resulting from two separate modes. The primary mode was considered to be an impact wear mode with some fretting. The secondary mode was a small-amplitude sliding wear mode that could be characterized as fretting and was associated with the pre-load of the springs. Since the wear at the interface could be characterized as mild, it was decided to model these two modes, using the formulations provided by the Zero and Measurable Wear Models for impact and sliding. These required the determination of contact stresses.

While there was the possibility of both primary and secondary impacts contributing to the wear, it was decided to consider only the effect of the initial impact. This was based

Table 5.3 Backstop Wear

Carrier	Type location	Wear depth ($\mu\text{in.}$)			
		5.5 cycles ($\times 10^7$)	8.4 cycles ($\times 10^7$)	9.7 cycles ($\times 10^7$)	10 cycles ($\times 10^7$)
2	1	70		120	100
	4	30		50	30
3	1	0		10	10
	2	20		20	60
4	2		30	60	60
	3		80	90	100
5	1			60	80
	3			80	60
	Average	30	55		62
	S.D.	29	55		33

on the observation that the Hertz impact theory shows that the peak contact stress would be proportional to $v^{1/2}$, where v is the impact velocity. As a result the impact zero wear lifetime would be proportional to $v^{-9/2}$, suggesting a sharp decrease in wear rate as velocity decreases. Consequently, only those secondary impacts with velocities close to the initial impact velocity needed to be considered and these could be counted as additional primary impacts. Impact load and stresses for the primary contact were determined analytically using a combination of Hertz impact theory and finite element analysis. The latter was used to determine contact time, which for the primary impact was found to be approximately 7 μ sec. Available data showed that the primary impact velocity was approximately 90 in. / sec, which, according to the analysis, would result in a peak load of 45 lb and a peak contact stress of 153 kpsi.

The relationship for the zero wear life for impact is

$$N'_0 = 2 \times 10^3 (1 + \beta)^{-1} \left(\frac{\Gamma'_I \sigma_y}{\sigma} \right)^9 \quad (5.43)$$

where N'_0 is the zero wear life in terms of the number of impacts; Γ'_I , the zero wear factor for impact; β , the surface damage contribution factor; σ_y , the compressive yield strength; σ , the contact pressure. Since both steels were hardened to Rc60–62, σ_y was approximately 300 kpsi for both materials. (See Appendix IV.) Both Γ'_I and β are empirical wear coefficients, which are material and impact conditions dependent, respectively. Since Γ'_I for most material systems has been found to be 1.1, this value was assumed for the lubricated type/backstop material system. β is a function of the amount of sliding and surface damage that occurs during the impact. For a normal impact without fretting, it is 0. If there is fretting, the value can be significantly larger (e.g., values greater than 10 have been observed), depending on the amount of fretting wear that is present. (Table 2.4.) Lubrication has been shown to be significant in these situations and tends to decrease the value of β . Under lubricated conditions, β tends to be less than 10 and can approach 0. Using a value for β of zero in Eq. (5.43), an upper limit of 2×10^6 impacts was obtained for N'_0 for both materials.

Analysis of the carrier design indicated that the pre-load of the springs produced a load of approximately 0.2 lb at the backstop interface. This corresponded to a contact stress of approximately 10 kpsi. This is equivalent to a maximum shear stress of approximately 5 kpsi for a coefficient of friction of 0.2, which is typical of boundary lubricated steel couples. For sliding, the zero wear relationships is

$$N''_0 = 2 \times 10^3 \epsilon^{-1} \left(\frac{\Gamma'_S \tau_y}{\tau} \right)^9 \quad (5.44)$$

where N''_0 is the number of print cycles a carrier experiences; ϵ , the number of passes associated with a print cycle; Γ'_S , the zero wear factor for sliding; τ_y , the yield point in shear; and τ , is the maximum shear stress. τ_y for both materials was estimated to be 150 kpsi, based on hardness. (See Appendix IV.) Assuming as a worst case the lower characteristic value for Γ'_S , 0.2, Eq. (5.44) reduces to the following.

$$N''_0 = 2 \times 10^{10} \epsilon^{-1} \quad (5.45)$$

Since there are four type elements in a carrier,

$$N''_0 > 0.25 N''_0 \quad (5.46)$$

Therefore, the number of impacts for zero wear based on sliding was

$$N'_0 \geq 5 \times 10^9 \varepsilon^{-1} \quad (5.47)$$

Since the fretting motions would be less than the length of the contact, L , ε can be expressed as

$$\varepsilon = \frac{2am}{L} \quad (5.48)$$

where m is the number of vibration cycles of amplitude a . L was the width of the type element, 0.045 in. Substituting these into Eq. (5.37), results in the following for N'_0 .

$$N'_0 = 1 \times 10^8 \frac{\text{in.}}{am} \quad (5.49)$$

It was considered to be virtually impossible to have a situation where the product of a and m exceeded 1 in. To do this would have either required a few cycles of very large amplitude or a very large number of cycles of small amplitude. Neither condition was considered to be realistic. Experience indicated that a few cycles of moderate to small amplitude (i.e., < 0.01 in.) motion might be possible. As a result, the zero wear lifetime based on the sliding mode was several orders of magnitude greater than that for the primary impact mode. Because of this large difference, it was concluded that the secondary mode is a negligible contributor to the wear and could be ignored.

Since the average depth of the wear scar at the zero wear life time is half the peak to valley roughness, the value estimated from the experimental wear relationship for the zero wear life time was approximately 19×10^6 impacts. While this was nine times larger than that estimated on a theoretical basis (2×10^6), the disagreement was not considered significant, since a 25% error in the estimation of the stress level could account for such a factor. The fact that the theoretical life was smaller tended to support the positions that fretting and secondary impacts are not major factors. However, because of the sensitivity to stress that is associated with this model and the likelihood of errors in the estimation of the stress, it was impossible to use these results to conclude that they were insignificant. For example, the experimental value could be obtained by a 50% reduction in stress and a value for β of 9, which would imply a strong contribution of fretting.

The next step of the modeling effort was to apply the impact wear model for measurable wear. This model, like the one for measurable sliding wear, provides differential equations for two different modes of wear, a constant energy mode and a variable energy mode. Basically, it is necessary to determine which mode is applicable by empirical methods. While this is the case, there are some trends in for impact wear. The variable energy mode for impact wear is typical for most systems and normal impact. Under compound impact conditions, which result in significant sliding, or under normal impact conditions, combined with fretting, the constant energy mode is likely. Since fretting was possible, it was decided to use both formulations and to see which provided better agreement with the experimental data.

Some solutions to these differential equations are available for simple geometries (Table 2.5), including those for a cylinder against a flat surface. The solutions provided are based on the assumption that only one surface is wearing. Because the depth of wear was small in comparison to the radius of the backstop, it was concluded that these solutions would be suitable for engineering approximations of the wear. Basically, this treated the wear of the type as the wear of a soft plane impacted by an unwearing cylinder and the wear of the backstop as the wear of a soft cylinder impacting an unwearing plane. The

Number of impacts	h/h_{10} Impact wear mode	
	Variable energy	Constant energy
10	1	1
100	2.3	6.5
1000	6.1	41
10,000	13.6	207

relative values of wear depth as a function of number of impacts, obtained using these relationships, are given in Table 5.4 for both the constant and variable energy wear modes. In Fig. 5.10 they are compared with Eq. (5.40). It can be seen that Eq. (5.40) provides a reasonable relationship for the two solutions. For the variable energy mode, n is approximately 0.4; for the constant energy mode, 0.75. The exponent for the constant energy mode agrees with the empirical value and implies that fretting was a significant factor in the wear at the interface. If fretting were not significant, the variable energy mode would have been expected. It can be seen that in this case the Measurable Wear Model provided a clearer indication of the significance of fretting than did the Zero Wear Model.

By combining the Zero and Measurable Wear Models, a theoretical expression for backstop wear was developed. This was done by using the theoretical zero wear lifetime and the specified roughness to determine C . This resulted in the following expression for backstop wear:

$$h = 2.8 \times 10^{-10} (\text{in./impact}^{0.75}) N^{0.75} \quad (5.50)$$

Using this relationship for both the type and the backstop, a projection of end-of-life wear was made. For the worst case, it was concluded that total wear would be less than or equal to 0.0009 in., which was acceptable.

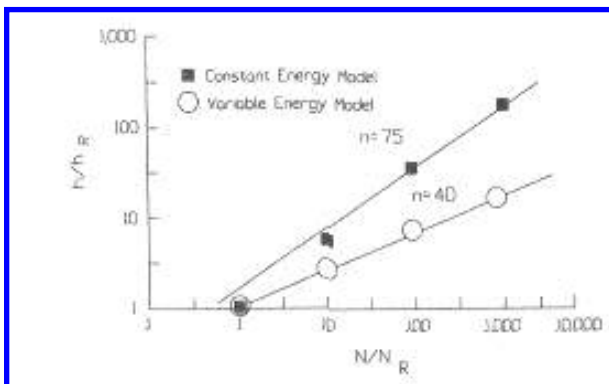


Figure 5.10 Approximation of the impact wear relationships by simple power relationship, $h = N^n$.

While higher than the experimental projection, this theoretical estimate provided support to the conclusion that the design change was acceptable. The modeling activity also provided further understanding of the wear situation and a basic set of relationship between design parameters and wear. It was concluded from the modeling that the wear is the result of the impact of the type against the backstop after printing and that fretting motions associated with that impact contribute to and modify the wear.

The wear scars that were developed in the test were carefully examined. The morphological characteristics of the wear scars were found to be similar to those typically observed in laboratory impact wear tests that allowed some fretting vibrations to occur. Wear at this interface resulted in a field problem when the printer was converted for use outside the USA. This is treated in Sec. 7.3.

5.7. THERMAL CONDUCTION MODULE

This case study provides an example of the integrated use of wear design in development. In this instance wear design was introduced very early in the development process. Initially, the approach was analytical and used to examine design feasibility and in the determination of the initial design. This was followed by empirical approaches, which were used to develop a database for specific material pairs and to verify satisfactory wear performance of the design.

The thermal conduction module was an electronic packaging structure for computer chips (4). A typical module is shown in Fig. 5.11. An essential function of this module was to conduct heat away from the semiconductor chip. This was accomplished by the design shown in Fig. 5.12. While the functioning of this module did not require relative motion between the surfaces, motion was possible as a result of mechanical vibrations, shocks, and thermal cycling. Sources for these might be fan motor vibrations, vibrations transmitted through the machine frame during shipping, shocks associated with bumps that

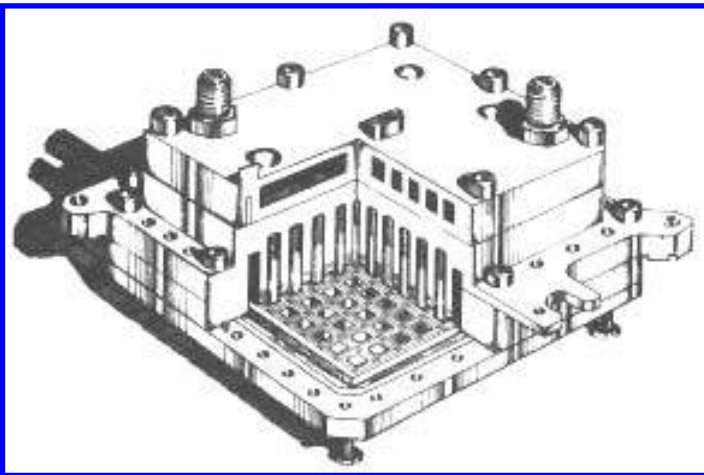


Figure 5.11 Thermal conduction module. (From Ref. 33.)

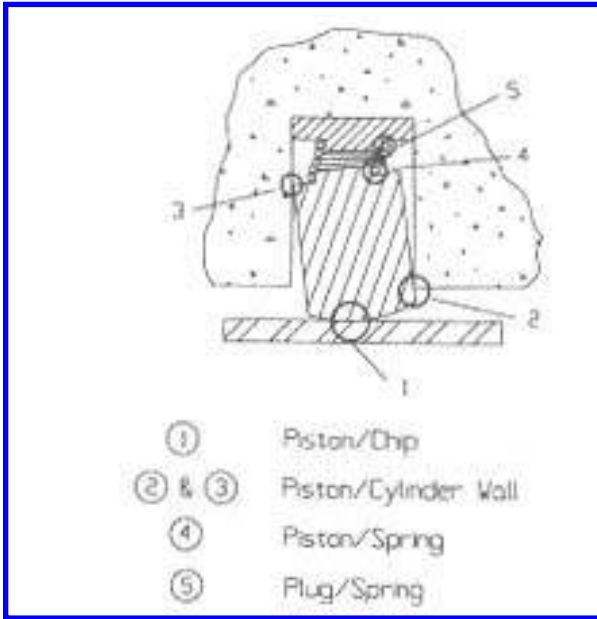


Figure 5.12 Potential wear sites in the thermal conduction module.

the machine may experience during shipping or relocation, and thermal expansions and contractions associated with power on / off cycles. These extraneous motions could cause wear at the interfaces involved with the conduction of heat away from the chip. This was a concern because of the potential effect that the wear might have on the thermal contact resistance of these interfaces, e.g., the effect of wear debris on conduction. Thermal analysis had indicated that, while there were several such interfaces involved, the primary one was that between the chip and the piston.

Packaging design considerations, such as the size and number of chips to be in the module, the amount of heat to be dissipated, allowed dimensions for the module, etc., had led to an overall design. This design provided nominal definitions for the sizes, shapes, spring loads, and materials to be used but variations or modifications were possible within the overall design concept. An initial development concern regarding the design was that its feasibility would be limited by the wear resulting from the extraneous motions. Since hardware was not immediately available, a two-phase approach to wear design was formulated. The first phase involved the analytical estimation of potential wear life and the effects that different modifications or options would have on wear life. This enabled design features, which would enhance wear performance to be included in early hardware. It also identified critical factors controlling the wear performance. Hence, it was possible to develop an evaluation strategy that was needed to insure that there would not be a wear problem. The second phase, which was primarily empirical, involved the implementation of that strategy.

The first step of the system analysis was the identification of potential wear points and the motions, which might occur at these points. After review of the design, several areas of potential wear were identified and these are shown in Fig. 5.12. These involve

contacts between the chip, piston, cylinder wall, and spring, where relative motion was considered likely. The contact between the insert and the cylinder wall was not considered as a wear point since this was to be designed as a press fit. Two contact conditions were possible between the piston and the cylinder wall. One is a cocked configuration (Fig. 5.12); the other is an axial aligned configuration in which line contact occurs. At all of the locations, relative motion from two sources was considered to be possible, temperature changes and mechanical excitation from either vibrations or shock. After reviewing the geometries, it was concluded that at each location these sources could cause relative sliding, but not necessarily pure sliding. At the contact points between the piston and the wall and between the piston and the chip, a rolling component might also be present if the piston rocks. It was also possible to have impact at these same locations if shock levels were sufficient to cause separation. The type of motion, its direction, and its magnitude at each location would depend on the nature and magnitude of the excitation, as well. Finally, it was also probable that with each type of excitation there would be a threshold level, below which it would not cause motion.

One approach in modeling the wear situation at each site was to determine separately the amount of wear produced by each independent source. With this approach, shock and vibration inputs at different locations and different directions would be considered as separate source. This would have involved determining the load and motion for each of these sources. This approach was considered to be impractical for design use in this case because of the number of unknowns and variations associated with the design and the number of possible motions that needed to be considered. A less precise but more practical approach was used, which was based on worst case considerations and tended to be conservative. It involved defining worst case loading conditions for each site and evaluating likely wear behavior on the basis of these. In implementing this strategy, it was decided initially to separate the consideration of any impact wear situations where separation might be possible from consideration of wear situations when separation did not occur. Reasons for this were:

- (1) Separation was considered to be likely only for very high shock loading and exposure to this was limited.
- (2) The possibility of significantly higher loads when separation occurs than when separation does not occur.
- (3) The possibility of conflicting design requirements for these two conditions (e.g., an increase in spring load would tend to decrease the tendency for separation but would increase sliding or rolling wear).

When separation did not occur, worst case wear conditions for each of the three sources were defined as sliding under the maximum normal load associated with that source, since sliding is a more aggressive motion than a rolling. Worst case conditions with separation were considered to be the impacts resulting from mechanical shocks.

An initial element for the wear design was establishing what amount of wear could be accepted as a design goal. The concern was that wear, by modification of the surface topography and the generation of debris, would adversely effect heat conduction across the interface. Since realistic design allows for some variations of initial surface topography and the real area of contact tends to be insensitive to small variations in roughness, it was concluded that some wear could be tolerated, provided it was confined to the asperities. The definition of "zero wear" describes such a condition. At the zero wear point, the average depth of wear is one half the average asperity height. With wear of this magnitude,

debris generation is usually not significant or a concern. Therefore, it was decided to accept the zero wear point as the acceptable amount of wear for the design and, as a consequence, the zero wear life as the wear life. An acceptable design would then be one for which the zero wear life exceeded the expected or required life at each wear point. The zero wear lifetimes of the various contact points in the module could be calculated from the relationships of the Zero Wear Models once the load (normal to the interface) and the contact geometries were determined.

Since sliding was assumed as the worst-case conditions, it was convenient to use the Zero Wear Model for sliding to determine the maximum amount of sliding that was associated with the zero wear condition, S_{\max} . This could then be compared to the amount of motion likely to result from the three sources. The zero wear equation, Equation (2.18), can be written in the following form:

$$S_{\max} = 2 \times 10^3 W \left(\frac{\Gamma_r \tau_y}{\tau_{\max}} \right)^9 \quad (5.51)$$

where W is the width of the area of contact in the direction of sliding.

When there was no separation, several sources for static and dynamic loads were identified. It was deduced that the static loads affected all the interfaces and resulted from the compression and diametrical interference of the spring. It was also deduced that the dynamic loads resulted from piston motions caused by vibrations and shocks. It was assumed that the spring would have a negligible effect on piston acceleration and that the acceleration would act through the center of mass of the piston. Product specifications allowed vibration levels up to 1.25 times gravity in the 5–500 Hz range and shock levels up to 500 Gs. These upper values for these accelerations were used to determine worst case loading under dynamic conditions. Only the static loads were used to estimate wear for thermal motions. For motions due to shock and vibration, static and dynamic loads needed to be combined but one or the other was found to predominate. Since the mass of the piston was 1 g, it was concluded that loading due to vibration was insignificant with respect to the static loads and that the static loads were insignificant to the maximum

Table 5.5 Thermal Conduction Module Worst-Case Loading

Interface	Motion condition			Contact geometry description
	Thermal (g)	Vibration (g)	Shock (g)	
Piston/chip	50	50	500	Sphere/plane
Piston/wall				
Cocked	20	20	250	Cylinder/plane without stress concentration
Aligned	0	0	0	
Piston/spring				
Lip	29	29	29	Parallel cylinders
Diameter	29	29	29	Cylinder/plane with stress concentration
Caps/spring				
Lip	29	29	29	Parallel cylinders
Diameter	29	29	29	Cylinder/plane with stress concentration

shock loads. A summary of the worst-case loads is given in Table 5.5. Also included in the table is the contact geometry used for the calculation of contact stress at the wear points. It can be seen that two potential wear points were identified for the spring/piston and spring / cap interfaces. One was where the spring contacted the lip of either the piston or the cap and the other was at the end of the wire, where there was the possibility of stress concentration. Both of these conditions are illustrated in Fig. 5.13.

Several of the interfaces were exposed to wear from thermal motion, vibration, and shock. While the resulting motions from each of the sources were likely not the same, some surface regions would experience some superposition of these motions. The wear situation for these regions is similar to sliding with a variable load, in which case a weighted average or equivalent stress is used for the zero wear calculations. Since the maximum loads associated with motions due to temperature excursions and vibrations were the same (i.e., those based on static considerations), it was possible to divide the situation into a combination of static and shock loads. Therefore, the following was used to determine the average stress to be used in determining the zero wear life:

$$\tau_{\max} = [\tau_{\max\text{static}}^9 (1 - \alpha) + \tau_{\max\text{shock}}^9 \alpha]^{1/9} \quad (5.52)$$

where α is the fraction of the total motion that was associated with shock.

The parameters of the proposed design are given in Table 5.6. It can be seen that except for silicon all the materials involved were typical engineering materials. However, the design of the thermal conduction module required the use of helium gas as coolant and no lubrication. Because of the uniqueness of this environment, there was no specific data available regarding wear or friction behavior and some assumptions had to be made to continue the analysis. Since helium is an inert gas, it was concluded that it could be considered as a very poor lubricant and data for unlubricated sliding could be used to estimate values for Γ_r , the zero wear factor, and μ , the coefficient of friction. Under these conditions, most couples tend to have the lower characteristic value of 0.2 for Γ_r and μ is greater than 0.5. However, existing data for anodized surfaces and plastics indicated that for couples involving these materials Γ_r was frequently 0.54 and μ , 0.2–0.3 without lubrication. (See Appendix II.)

Using these values, zero wear distance, S_{\max} , was computed for different values of α , the relative amount of shock motion, and the unspecified design parameters. A summary of these values for S_{\max} is given in Table 5.7. Estimates for the amount of motion associated with thermal cycling, vibration, and shock were done to see how adequate these lifetimes were. Mechanical analysis indicated that over the temperature range of an on / off

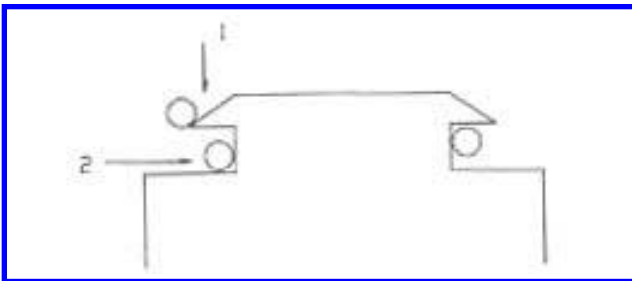


Figure 5.13 Wear points between the spring and the piston. “1” contact between wire and end of lip; “2” contact between end of wire and inner diameter of piston.

Table 5.6 Initial Design Parameters for the Thermal Conduction Module

Wall	<p>2024-T3 aluminum Diameter 0.2165 ± 0.0005 in. Roughness $10 \mu\text{in. CLA}$ Young's modulus 1×10^7 psi Poisson's ratio 0.33 Yield point in shear 20×10^3 psi</p>
Piston	<p>Anodized aluminum, maximum coating thickness 0.0001 in. Length 0.610 ± 0.010 in. Diameter 0.2145 ± 0.0005 in. End radius 5.512 ± 0.03 in. Roughness prior to anodization $10 \mu\text{in. CLA}$ Tip to spring recess 0.575 ± 0.010 in. Recess diameter 0.166 ± 0.004 in. Maximum diameter at lip 0.173 in. Maximum interference with spring 0.0095 in. Lip edge unspecified Material properties Young's modulus 1×10^7 psi Poisson's ratio 0.33 Estimated yield point in shear 65×10^3 psi (using data for 0.0002 to 0.0004 in coatings and the following relationship between shear and tensile yield points, $0.58 \sigma_y \approx \tau_y$)</p>
Chip	<p>Flat backside of Si chips Roughness $< 1 \mu\text{in. CLA}$ Material properties Young's modulus 1.6×10^7 psi Poisson's ratio 0.3 Yield point in shear 150×10^3 psi</p>
Spring	<p>302 SS, spring tempered Wire diameter 0.0120 ± 0.0005 in. Inside diameter of spring 0.173 ± 0.003 in. End condition unspecified Material properties Young's modulus 2.7×10^7 psi Poisson's ratio 0.3 Yield point in shear 87×10^3 psi</p>
Cap	<p>Unfilled polycarbonate Diameter press fit with wall Recess diameter 0.166 ± 0.004 in. Maximum diameter at lip 0.173 in. Lip edge unspecified Maximum interference with spring 0.0095 in. Material properties Young's modulus 3.4×10^5 psi Poisson's ratio 0.38 Yield point in shear 5.4×10^3 psi</p>
Gas	He ₂
Temperature	Maximum 85°C

Table 5.7 Motions Estimates for the Initial Design

Estimated worst case amounts of sliding

Thermal expansion	Chip/piston interface	< 10 in.
	Other interfaces	< 30 in.
Shock	All interfaces	< 4 in.
Vibration	All interfaces	< 10 ⁷ in.

Location	Edge radius (in.)	S _{max} (in.)		
		All thermal/vibration motion	All shock motion	One percent of total motion shock
Amount of sliding acceptable				
Piston/chip				
Piston				
(Γ _r = 0.2/μ = 0.5)		2.5 × 10 ⁹	4.6 × 10 ⁶	2.4 × 10 ⁸
(Γ _r = 0.54/μ = 0.2)		7.3 × 10 ¹⁶	1.3 × 10 ¹⁴	7 × 10 ¹⁵
Chip				
(0.2/0.5)		4.6 × 10 ¹²	8.5 × 10 ⁹	4.3 × 10 ¹¹
(0.54/0.2)		1.3 × 10 ²⁰	2.5 × 10 ¹⁷	1.3 × 10 ¹⁹
Piston/wall				
Piston				
(0.2/0.5)	0.050	2.2 × 10 ⁹⁸	5.5 × 10 ¹⁶	4.3 × 10 ⁹⁵
	0.010	2 × 10 ¹²	7.2 × 10 ⁷	3.9 × 10 ⁹
	0.001	2.1 × 10 ⁷	1 × 10 ³	4.1 × 10 ⁴
Cylinder				
(0.2/0.5)	0.050	9.9 × 10 ¹⁶	2.1 × 10 ¹²	1.9 × 10 ¹⁴
	0.010	7.8 × 10 ⁷	2.8 × 10 ³	1.5 × 10 ⁵
	0.001	7.9 × 10 ²	4.0 × 10 ⁻²	1.5
Piston/spring lip				
Piston				
(0.2/0.5)	0.050	1.5	1.5	1.5
	0.010	3.9 × 10 ⁻⁴	3.9 × 10 ⁻⁴	3.9 × 10 ⁻⁴
	0.001	1.5 × 10 ⁻⁷	1.5 × 10 ⁻⁷	1.5 × 10 ⁻⁷
(0.54/0.2)	0.050	8.5 × 10 ⁴	8.5 × 10 ⁴	8.5 × 10 ⁴
	0.010	2.2 × 10 ¹	2.2 × 10 ¹	2.2 × 10 ¹
	0.001	8.5 × 10 ⁻³	8.5 × 10 ⁻³	8.5 × 10 ⁻³
Spring				
(0.2/0.5)	0.050	2 × 10 ¹	2 × 10 ¹	2 × 10 ¹
	0.010	5.2 × 10 ⁻³	5.2 × 10 ⁻³	5.2 × 10 ⁻³
	0.001	2 × 10 ⁻⁶	2 × 10 ⁻⁶	2 × 10 ⁻⁶
(0.54/0.2)	0.050	1.1 × 10 ⁶	1.1 × 10 ⁶	1.1 × 10 ⁶
	0.010	3 × 10 ²	3 × 10 ²	3 × 10 ²
	0.001	1 × 10 ⁻¹	1 × 10 ⁻¹	1 × 10 ⁻¹
Diameter				
Piston				
(0.2/0.5)	0.050	7.2 × 10 ⁻¹	7.2 × 10 ⁻¹	7.2 × 10 ⁻¹
	0.010	2.6 × 10 ⁻¹	2.6 × 10 ⁻¹	2.6 × 10 ⁻¹
	0.001	1.1 × 10 ⁻⁴	1.1 × 10 ⁻⁴	1.1 × 10 ⁻⁴

(continued)

Table 5.7 (Continued)

Location	Edge radius (in.)	S_{\max} (in.)		
		All thermal/ vibration motion	All shock motion	One percent of total motion shock
(0.54/0.2)	0.050	2×10^7	2×10^7	2×10^7
	0.010	8.7×10^6	8.7×10^6	8.7×10^6
	0.001	2.9×10^3	2.9×10^3	2.9×10^3
Spring (0.2/0.5)	0.050	9.9	9.9	9.9
	0.010	3.6	3.6	3.6
	0.001	1.5×10^{-3}	1.5×10^{-3}	1.5×10^{-3}
(0.54/0.2)	0.050	2.9×10^8	2.9×10^8	2.9×10^8
	0.010	1×10^8	1×10^8	1×10^8
	0.001	4.4×10^4	4.4×10^4	4.4×10^4
Cap/spring lip				
Cap (0.2/0.5)	0.050	8.1×10^{-3}	8.1×10^{-3}	8.1×10^{-3}
	0.010	2.1×10^{-6}	2.1×10^{-6}	2.1×10^{-6}
	0.001	8×10^{-10}	8×10^{-10}	8×10^{-10}
(0.54/0.2)	0.050	4.6×10^2	4.6×10^2	4.6×10^2
	0.010	1×10^{-1}	1×10^{-1}	1×10^{-1}
	0.001	4.5×10^{-5}	4.5×10^{-5}	4.5×10^{-5}
Spring (0.2/0.5)	0.050	5.9×10^8	5.9×10^8	5.9×10^8
	0.010	1.5×10^5	1.5×10^5	1.5×10^5
	0.001	5.9×10^1	5.9×10^1	5.9×10^1
(0.54/0.2)	0.050	3.3×10^{13}	3.3×10^{13}	3.3×10^{13}
	0.010	8.5×10^9	8.5×10^9	8.5×10^9
	0.001	3.4×10^6	3.4×10^6	3.4×10^6
Diameter				
Cap (0.2/0.5)	0.050	1.5×10^{-3}	1.5×10^{-3}	1.5×10^{-3}
	0.010	2×10^{-5}	2×10^{-5}	2×10^{-5}
	0.001	7.6×10^{-8}	7.6×10^{-8}	7.6×10^{-8}
(0.54/0.2)	0.050	4.4×10^4	4.4×10^4	4.4×10^4
	0.010	5.8×10^2	5.8×10^2	5.8×10^2
	0.001	2.2	2.2	2.2
Spring (0.2/0.5)	0.050	1.1×10^8	1.1×10^8	1.1×10^8
	0.010	1.5×10^6	1.5×10^6	1.5×10^6
	0.001	5.6×10^3	5.6×10^3	5.6×10^3
(0.54/0.2)	0.050	3.2×10^{15}	3.2×10^{15}	3.2×10^{15}
	0.010	4.4×10^{13}	4.4×10^{13}	4.4×10^{13}
	0.001	1.6×10^{11}	1.6×10^{11}	1.6×10^{11}

cycle, that is, 20–85°C, the maximum amount of motion possible between the spring and the piston or the cap was 0.010 in. and between the chip and the piston, 0.004 in. Since the required number of on / off cycles was 2500, the potential motion caused by thermal cycling over life was estimated as 30 in. for the spring interfaces and 10 in. for piston

interfaces. Over the life of the component the number of significant shocks that were likely were considered to be less than 100. Considering the tolerances and the clearances involved with the design, maximum motion per shock would be 0.035 in. Total shock motion was therefore estimated to be < 4in. Prior experience indicated that standard design considerations would limit the amplitude of possible vibrations to a few thousands of an inch for the lower frequency and less for the higher frequencies. At best, there was the possibility that there could be zero motion. This experience indicated that an extremely worst-case assumption for vibration motion would be to assume continuous vibration at the maximum frequency allowed, 500 Hz, with an amplitude of 0.001 in. Since the required life was 10^4 hr, this amounts to an upper limit of vibration motion of 10^7 in. A similar estimate would result from an assumption of 0.010 in. amplitude at 60 Hz, which again was considered to be a worst-case assumption. These values are summarized in Table 5.7. As can be seen by comparing the values for allowed motion and expected motion, this analysis indicated some potential areas of concern.

The possibility of impact wear as a result of separation from severe mechanical shocks also needed to be considered. The Zero Wear Model for Impact Wear was used to evaluate the potential for impact wear. The zero wear lifetime for impact wear is given by

$$N_{\max} = \frac{2 \times 10^3}{1 + \beta} \left(\frac{\Gamma'_r \sigma_y}{\sigma_{\max}} \right)^9 \quad (5.53)$$

N_{\max} is the maximum number of impacts for zero wear; Γ'_r , the zero wear factor for impact wear and is typically 1.1; β , a factor related to the amount of slip associated with the impact; σ_y , the yield point in tension; σ_{\max} , the maximum tensile stress.

Mechanical evaluation of the design indicated that accelerations as low as 65 G could result in separation of the piston, which was well below the shock level the module was expected to withstand, namely a 500 G for 1 ms. With separation, impacts between the wall and the piston and between the piston and the chip would occur. Based on mechanical analysis and other design consideration, it was concluded that the maximum force associated with these impacts would be 5 lb.

β in Eq. (5.53) is used to account for sliding effects during impact, either fretting motions or slip in compound impacts. Consideration of the possible modes of separation suggested that two impact situations are likely. One involved a rotation of the piston and impact with the wall. The other was a near normal impact of the piston against the chip. Because of the spring and the nature of the impacts, both a wiping action (slip) and fretting were considered possible at these interfaces. Considering just the possibility of fretting, impact wear studies indicated a worst-case estimate for β would be 10 (Table 2.4, (5)). It was anticipated that, since β is zero for normal impacts without fretting, it would be small for the near normal impact conditions in these two situations. As a result, it was concluded that the value for fretting would provide a conservative estimate, covering both possibilities.

To confirm this estimate, these impacts were considered as a compound impact situation where the impact velocity was $V \sin \Theta$ and the tangential velocity was $V \cos \Theta$; where Θ was the angle of impact, as shown in Fig. 5.14. For such a condition, it can be shown that the slip factor, f , which is used to determine β , is given by

$$f = \frac{\cot \Theta}{\mu} \quad (5.54)$$

Considering the geometries involved, it was concluded that Θ was at least 88° . Using this value and the relationship between f and β , it was found that for values of μ up to 1, β was much less than 1 (Fig. 2.22).

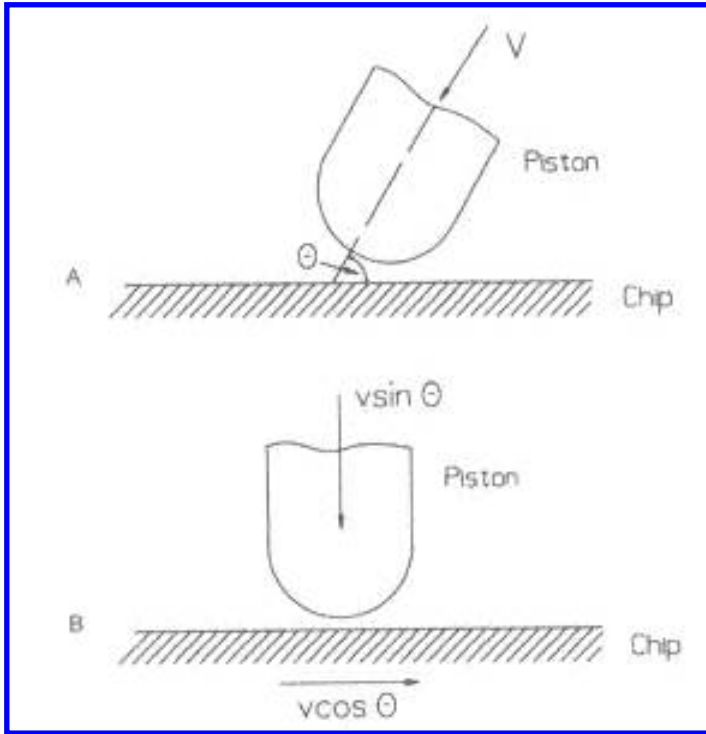


Figure 5.14 The impact between the piston and the chip as a compound impact. “A” shows the actual impact condition. “B” shows the equivalent compound impact condition used in the analysis.

A value of 1.1 was assumed for Γ'_p , since this is the value that has been found for most materials. Using these values and the geometries indicated in Table 5.7, the number of impacts allowed for zero wear was computed using Eq. (5.53). The number of impacts allowed for the piston/wall interfaces was greater than 10^9 for all edge conditions; for the piston/chip interface, it was approximately 10^{13} impacts. Since the anticipated number of shocks was a hundred or less, this was clearly a satisfactory condition. Because of the large zero wear lifetimes and the limited number of actual shocks in the application, it was concluded that the effect of separation on wear did not need to be given any further consideration. Because of this simplification, it was then possible to focus further design considerations simply on sliding wear issues.

The results of the sliding analysis, summarized in Table 5.7, indicated that with some refinements to the design, there would be minimal exposure to wear as a result of thermal and shock motions and that some amount of vibratory motion could also be tolerated. However, these results also indicated several areas of concerns and risk. These areas needed to be explored further by considering additional design change, verification of wear behavior assumptions, and improvements in the estimates of likely motions, before it could be concluded that wear would not be a limiting factor for the module and acceptable designs identified.

One of the concerns was associated with the chip/piston interface. While the zero wear lifetimes exceeded the estimates of possible motion, there was low confidence in

the values used for the key material parameters (i.e., Γ_r , μ , and τ_y). There was no wear or friction data available for silicon and τ_y was based on Moh's hardness value for silicon. The value for the anodized coating was based on data from 0.0002 to 0.0004 in. thick coatings used in wear tests. Thermal considerations indicated that the thickness of the anodized layer for the piston could not exceed 0.0001 in. There could be a substantial reduction of the effective hardness and τ_y of the anodized layer in this thickness range. It was estimated that τ_y could be as low as 25×10^3 psi. This would reduce the zero wear life of the pistons by a factor of 5×10^3 . To address these concerns, it was decided that it was necessary to do a simulative wear test so that actual values for these parameters and the wear characteristics of silicon be determined. It was not considered necessary at this point to do this for the other materials, since their values used were based on existing wear and friction data. However, the possibility of needing such tests for those materials was also recognized, since that data were for air, rather than helium.

Another concern was with the edges of the wall, piston lip, and the ends of the springs. The analysis indicated that these areas could be regions of high wear. It was concluded that it was necessary to minimize the sharpness of these edges as much as possible and to provide specifications for these edge conditions. For the contact between the piston and the wall, the analysis indicated that wear would be acceptable with these incorporated into the design. For the interfaces with the spring, the analysis indicated that, while necessary, these changes were not sufficient to insure adequate performance. In looking for other ways to improve the wear situation at this interface, it was decided to examine the effect that changes in the diametrical interference conditions might have on the wear, since this determines the load. It was found to be a substantial factor. Using nominal dimensions for the part, the load reduced to 3.4×10^3 lb from the 6.4×10^2 lb obtained for the maximum interference condition that had been assumed. This reduction resulted in a minimum of 6×10^3 increase in the zero wear lives. By combining changes in the interference conditions with edge condition changes, it was concluded that an acceptable wear condition would be likely for thermal motions and for some amount of vibration motion. Since vibratory motion at these interfaces was considered to be unlikely and that there were further design changes possible, this was considered to be a moderate risk.

Based on this analysis, there was confidence that with these changes there would be no problem with either thermal cycling or mechanical shock. However, there was a concern that vibrations could be a problem. Considering the large differences in some cases between allowed values of motion and the estimate of possible vibration motion, it was possible that it would be necessary to design so that any vibratory motion would be prevented. Consequently, it was concluded that it was necessary to investigate the susceptibility of the design to this type of motion. To do this, it was decided to do wear tests using assembled modules and standard shock and vibration stress tests. These tests would also provide information about wear points and material behavior that would help to refine and verify the models.

To simulate the wear situation between the piston and the chip, an oscillating ball-plane apparatus was modified to provide a 0.002 in. stroke in an He_2 atmosphere at the elevated temperatures required by the application (i.e., up to 70°C). Fixtures were developed so that actual pistons could be mounted in place of the ball and to accommodate a silicon chip as the plane. Because of the small stroke, it was not possible to measure the coefficient of friction with this apparatus. It was decided to use a load of 50 g for the initial tests with this apparatus, simulating the static load, and to examine the surfaces after 2 hr or 30 in. of sliding. Early vintage pistons and scrap silicon chips were available for this purpose. Based on the analysis, it was anticipated that only some slight burnishing would be

produced under these conditions. However, measurable wear scars were observed. The chips tended to experience the more severe. Wear scar depths on the chip ranged from 60 to 125 $\mu\text{in.}$, while wear depths on the pistons ranged from 20 to 50 $\mu\text{in.}$ Because of this result, considerable effort was expended in examining the specimens and the characteristics of the wear.

It was discovered that there were considerable variations in the topography and contour of the pistons and none were within specifications. Roughness ranged from 25 to 30 $\mu\text{in.}$ CLA and radii ranged from 0.8 to 2.5 in. It was also determined that the anodized layer tended to be thin (e.g., < 0.0001 in.) and non-uniform. SEM and EDX analysis was also used to characterize the debris and the morphology of the silicon wear scar. The debris consisted mainly of submicron flakes of silicon and the morphology suggested a delamination or fatigue process.

Using the zero wear equation (Eq. (5.51)), the measured values of the radii were used to estimate what value of the factor $(\Gamma_r \tau_y / \mu)$ would be consistent with a zero wear distance of several inches. These calculations indicated that this value was in the range of 5×10^3 psi. This was much lower than the values used in the analysis. For silicon, the worst-case estimate was 60×10^3 psi; for the anodized surface it was 26×10^3 psi. This result for the anodized surface was understandable in terms of the quality and thickness of the layer and the possibility of a significantly higher μ than assumed. For example, the deduced value is consistent with the assumption of an ineffective anodized layer for which τ_y would be 25 kpsi and m equal to 1. However, the value for silicon seemed extremely low and would reduce the estimated zero wear distance for vibration and thermal cycling to under 10^3 in. Because of the implications of this result, more tests were performed using different loads, sliding distance, and conditions to investigate the applicability of the Zero Wear Model to this interface and further investigate the wear behavior of silicon.

The first wear data from these tests were analyzed using the combined Zero and Measurable Wear Models. For wear of either the ball or the flat, the Measurable Wear Model results in the following type of wear relationship between wear depth, h , and the distance of sliding, S :

$$h = CS^m \quad (5.55)$$

Two exponents, m , were possible, approximately 0.5 and 0.25, depending on the nature of the wear (i.e., constant or variable energy). The appropriate one was determined from measurements made after 3 and 30 in. of sliding. These data for the silicon chip and the anodized piston, shown in Fig. 5.15, indicated better agreement with the exponent for the constant energy mode than with the variable. The constant, C , was determined from the zero wear condition (i.e., average depth of the wear scar is approximately the CLA roughness at the zero wear lifetime). This resulted in the following for C :

$$C = \frac{2\delta_0}{S_{\text{min}}^{0.5}} \quad (5.56)$$

δ_0 is the CLA (RMS) roughness of the rougher surface. Combining Eqs. (5.51), (5.55), (5.56), and the Hertz stress equation, the following relationship for $(\Gamma_r \tau_y / \mu)$ was obtained:

$$\frac{\Gamma_r \tau_y}{\mu} = 0.044 \frac{(\delta_0/h)^{0.2} P^{0.3} S^{0.1}}{K^{0.7} R^{0.7}} \quad (5.57)$$

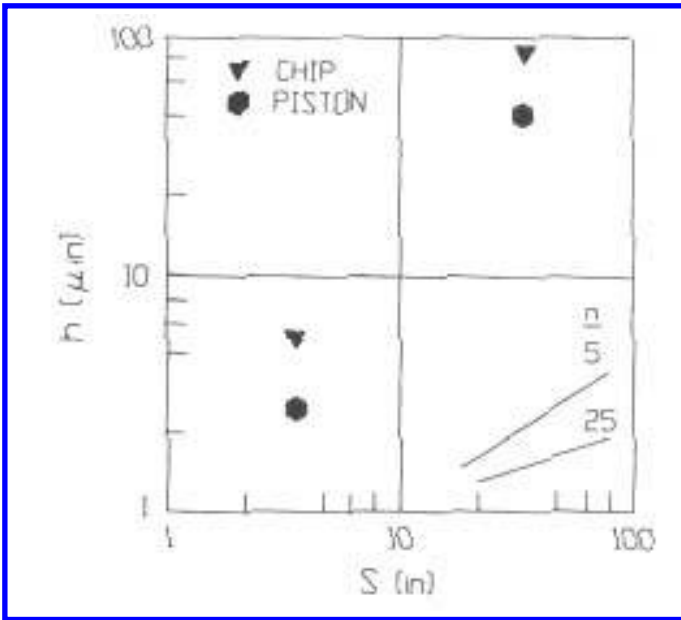


Figure 5.15 Wear test data for the chip / piston interface.

where R is the radius; P , the load; and

$$K = \frac{(1 - \nu_1^2)}{\pi E_1} + \frac{(1 - \nu_2^2)}{\pi E_2} \tag{5.58}$$

ν and E are Poisson’s ratio and Young’s modulus of the materials, respectively.

As discussed in Sec. 2.4, the use of the Zero Wear Model to determine C tends to over estimate the effect of roughness for larger values of surface roughness (greater than CLA 20 $\mu\text{in.}$). Since there were large variations in the surface roughness of the piston specimens, it was felt that it was necessary to improve this approximation. As described in Sec. 2.4, this can be done by replacing δ_0 , the CLA roughness, in Eq. (5.56) by $5.4 \delta_0^{0.3}$ for roughnesses above 10 $\mu\text{in.}$ (assumed δ_0 is in $\mu\text{in.}$) For roughness above the value, Eq. (5.57) becomes

$$\frac{\Gamma_r \tau_y}{\mu} = 0.044 \left\{ \frac{5.4 \delta_0^{0.33}}{h} \right\}^{0.2} \frac{\rho^{0.3} S^{0.1}}{K^{0.7} R^{0.7}} \quad \delta_0 (\mu\text{in.}) \geq 10 \mu\text{in.} \tag{5.59}$$

In the original analysis of this wear situation, another method was used to refine the effect if roughness. It is also based on the data shown in Fig. 2.18 and utilizes a method proposed in Ref. 34. In that reference, it is proposed that the following can be used to provide better agreement:

$$h = 2\eta \left[\frac{F(\delta_0)}{F(2)} \right]^n \left(\frac{L}{L_0} \right)^n \tag{5.60}$$

η is the ratio of the maximum wear depth of the scar to the average wear depth, h / hL is the amount of use and L_0 is the zero wear lifetime. The function, $F(\delta_0) / F(2)$, is obtained from the data shown in Fig. 2.18 and is the normalized wear depth raised to the 4.24 power. The behavior of this function is shown in Fig. 5.16. As can be seen, this function

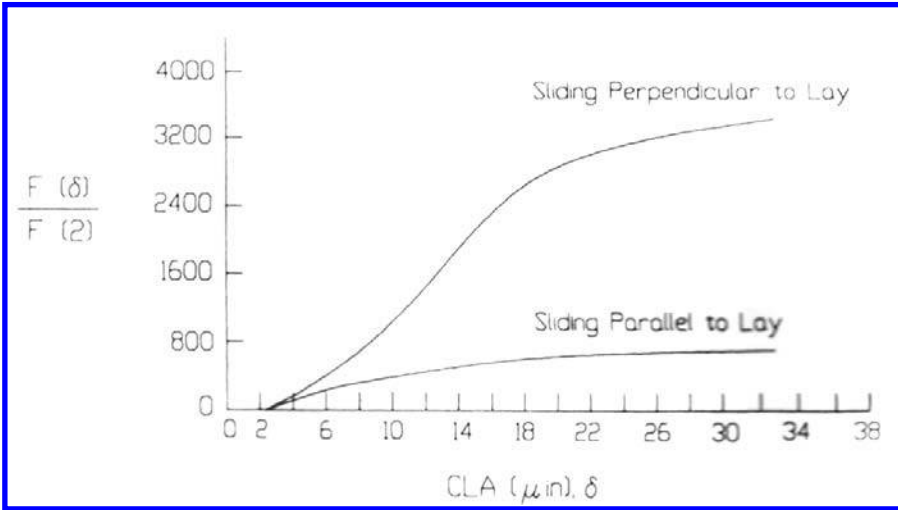


Figure 5.16 Roughness relationship for use with the Measurable Wear Model for sliding. (From Ref. 34.)

is different for sliding parallel and perpendicular to the lay. The form for this function for surfaces, which did not have exhibit lay parallel or perpendicular to the motion, was obtained by averaging the curves shown in Fig. 5.16. The resulting form is shown in Fig. 5.17.

Using this method, the expression for C becomes,

$$C = 4 \left(\left[\frac{F(\delta_0)}{F(2)} \right]^{0.5} / S_{\max}^{0.5} \right) \quad (5.61)$$

and Eq. (5.57) becomes

$$\frac{\Gamma_r \tau_y}{\mu} = \frac{0.0444(2/h)^{0.2} \left[\frac{F(\delta_0)}{F(2)} \right]^{0.1} P^{0.3} S^{0.1}}{K^{0.7} R^{0.7}} \quad (5.62)$$

By using Eqs. (5.58) and (5.62), the measured values of wear depth after known amounts of sliding were used to determine the value of the combined materials wear factor ($\Gamma_r \tau_y / \mu$). When this was done for the same material pairs, reasonably consistent values were obtained for this combined factor. Examples of this are shown in Table 5.8* (These values are approximately 1.6 times those obtained using Eq. (5.59) for the roughness correction.) These results supported the use of the Zero Wear Model in this situation. Also these further tests and more refined analysis confirmed the lower than assumed values of the combined material factors.

*The values in Table 5.8 are different than those in References 6 and 36 and are corrected for a computational error that did not significantly affect the results and did not alter the conclusions of the analysis.

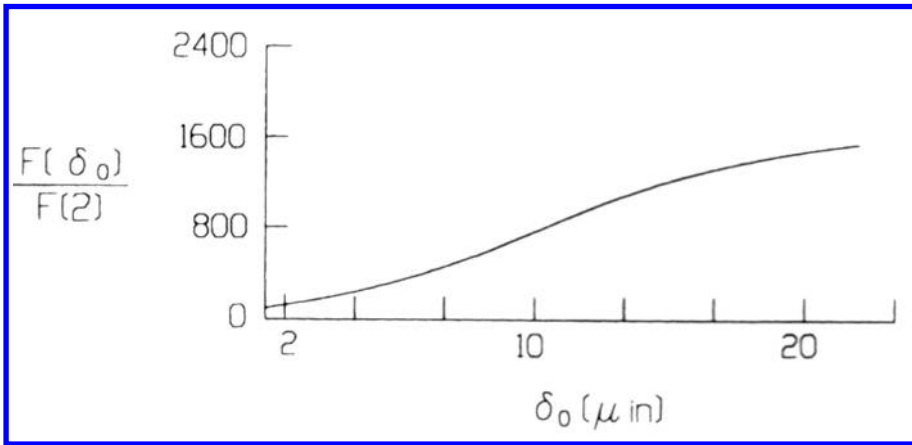


Figure 5.17 Approximation for the Measureable Wear Roughness Factor for surfaces which does not exhibit a lay. (See Fig. 5.16.)

In an attempt to improve the wear performance of this interface, the laboratory test was used to evaluate different anodized coatings for the piston, as well as the effects of different surface roughnesses and manufacturing processes. However, while improvements could be made, the effects were limited to less than a factor of 3 in the combined material factors. It was concluded that severe wear was likely if there was any sustained amount of vibratory motion.

Table 5.8 Combined Wear Factor for Silicon

Environment condition	Anodized coating	Piston radius (in.)	CLA roughness (μin.)	Test load (g)	Test duration (hr)	Γ_{rr_s}/μ (kpsi)
He ₂ , 70°C	Black	0.25	1	375	2	3.3
		0.25	1	30	2	2.9
					avg. S.D.	3.1
Air, 20°C	PTFE impregnated	0.20	30	50	2	0.3
						3.9
		0.15	25	50	2	4.5
		0.20	10	50	2	3.7
		0.17	30	50	0.2	3.8
			avg. S.D.	4.0		
He ₂ , 70°C	Clear	0.44	20	50	0.2	0.4
		0.44	30	50	0.2	2.4
		0.44	35	50	2	2.4
		0.10	5	50	2	3.0
		0.39	25	50	2	4.2
					avg. S.D.	3.6
					3.1	
					0.8	

Source: Ref. 6.

Two series of assembly tests were performed at the shock and vibration levels that the module must withstand. These involved several hours of exposure to vibrations as well as to multiple shocks. The tests utilized down-level pistons, similar to some of those used in the laboratory test. After the completion of the tests, the modules were disassembled and examined for wear and evidence of motion. None was found after careful and extensive examinations. This confirmed some of the more optimistic results from mechanical analysis, which indicated that motion was unlikely. A third test was also performed at levels higher than that required. The assembly was examined in a similar manner and evidence of motion was found at the chip / piston interface. Wear, which had the same characteristics as in the laboratory test, was found on a number of chips. The wear pattern suggested that the wear resulted from a rocking motion of the piston. Based on these assembly tests, it was concluded that there would be no motion due to vibration and therefore the concern with wear in the module was eliminated. This conclusion has been supported by field experience since that time.

From the laboratory tests, a working hypothesis for the low value of the combined material factor for the chips was formulated but not verified. It was proposed that there were two likely factors. One was that the surfaces of these chips were not as hard as assumed, probably as a result of surface films, and that the effective τ_y was significantly lower, possibly as low as 50 kpsi. The other was that the coefficient of friction was significantly higher than anticipated, likely in excess of 1. This hypothesis was consistent with the one proposed for the behavior of the anodized coatings. It was also consistent with the observation regarding the effects that lubrication and silicon surface conditions had on the wear behavior of these silicon chips. It was found that both lubrication and polishing to remove surface layers significantly reduced the wear on the chips. It was speculated that differences in the initial oxides and oxides formed on the surface of the silicon during processing were a factor in the behavior (6).

5.8. HAMMER PIVOT

This example is from a high-speed line printer, which utilized a pivoting hammer for printing (Fig. 5.18). The goal was to develop a model for the wear between the hammer and the pivot, which could be used to relate wear performance to specific design parameters, to assess design feasibility, and to reduce the amount of testing required to verify performance. The wear design in this case involved several elements, including model development, the consideration of alternative models, and the use of laboratory and robot testing to determine wear coefficients and to verify the model.

At the initiation of a print cycle, the hammer was pressed against a push rod by the return spring shown in Fig. 5.18. The hammer was then accelerated by the push rod, going into free flight when the push rod reaches its maximum displacement. After a period of free flight, the hammer impacted a structure composed of paper, ribbon, print band, and platen to accomplish the printing. The hammer then rebounded, assisted by the spring, and after a series of impacts against the push rod, it finally came to rest before the next print cycle began. Typical hammer displacement during this print cycle is shown in Fig. 5.19. While there are several wear points normally associated with these hammers, as well as several regions where fatigue was also a concern, this case study focuses on the wear between the bearing hole of the hammer and the surface of the shaft, which serves as the pivot. (Case studies described in Secs. 5.10 and 7.4 deal with wear of the push rod tip in this application.)

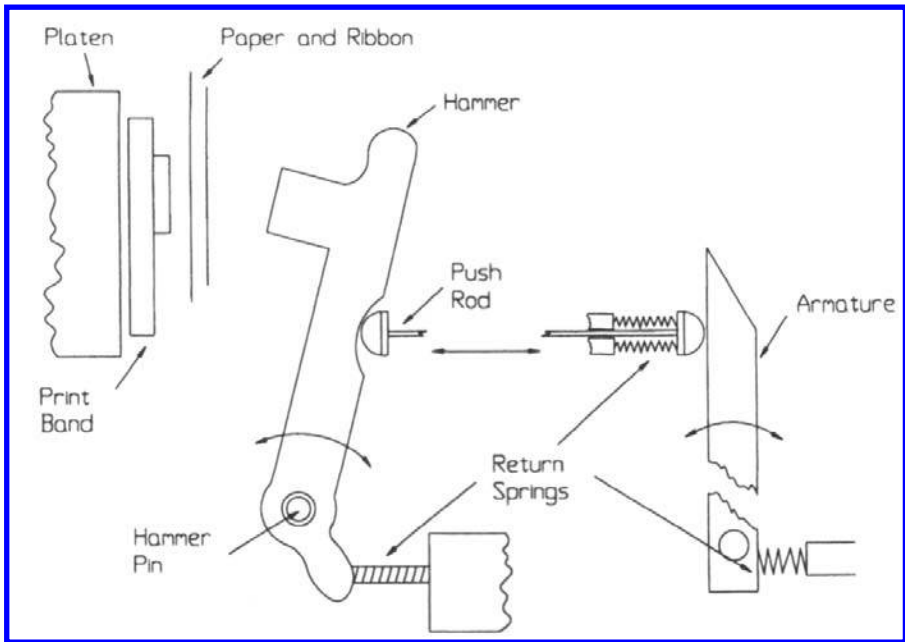


Figure 5.18 Design used for high-speed impact printing.

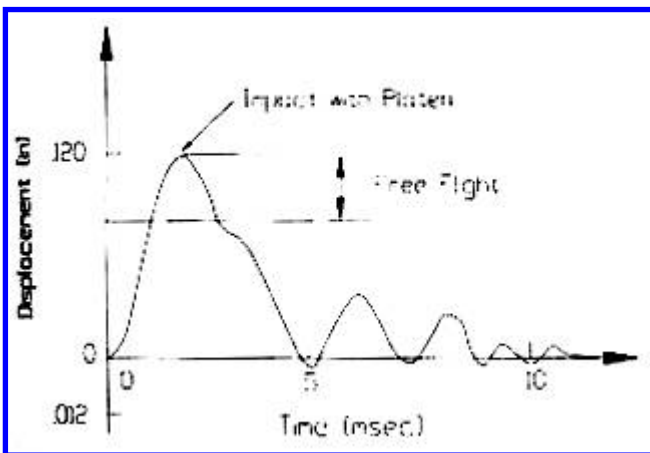


Figure 5.19 Displacement of the hammer face during a print cycle.

In addition to the force generated by the return spring, which existed for the entire print cycle, there were several sources for intermittent loads at this interface, as well. All were reaction forces associated with the different parts of the print cycle. Analysis and measurements provided estimates for these forces. The magnitude of the reaction force due to the spring was approximately 0.35 lb; push rod acceleration, 1 lb; free flight reaction, 0.07 lb; printing pulse, 10 lb; and return impacts, 1 lb. Because of the small angular rotation and the geometries involved, the lines of action of the reaction forces due to the spring, push rod acceleration, and the impacts were within 10° of each other. However, the reaction force associated with printing is in the opposite direction of the others. The line of action associated with the reaction force to the centripetal acceleration during free flight was approximately perpendicular to these. It was concluded from this information that there were potentially two predominate wear locations that were approximately diametrically opposed; one is associated with the non-printing portion of the cycle and the other is with the printing portion. This is illustrated in Fig. 5.20.

The dimensions of the hammer and the pin were: hole diameter, $4 (+0, -0.01)$ mm; hammer thickness, 1.55 ± 0.025 mm; pin diameter, $3.988 (+0, -0.01)$ mm. These were selected on the basis of printing, space, and fatigue requirements. Manufacturing and cost considerations resulted in the initial roughness specifications for the pin and the hole, which were $16 \mu\text{in. CLA}$ and $8 \mu\text{in. CLA}$, respectively. The small clearance between the hole and the pin and the tight tolerance on the parts were required because of the high sensitivity of print quality to positional variations in this region. These same requirements made the design very sensitive to the amount of wear that occurs at the interface between the hammer hole and the pivot pin. Total wear at the interface could not exceed 0.001 in. over the desired life of 2×10^9 print cycles.

Primarily to insure low and stable friction, the hammer–pivot interface was lubricated by a thin coating of oil that was applied to the pin during assembly. This film was then maintained by using oil-impregnated sintered blocks (e.g., bronze or iron) to support and hold the pin. These blocks served as oil reservoir as the oil would migrate

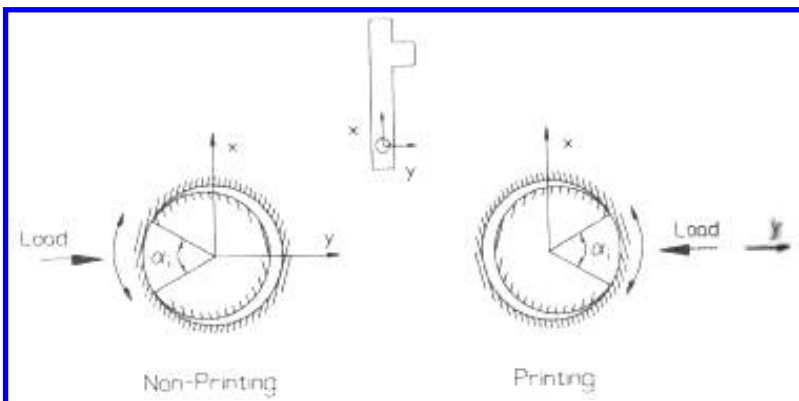


Figure 5.20 Contact between the pin and the hammer during the non-printing portion of the print cycle and during printing.

from the block and along the surface of the pin (Fig. 5.21). Oil also migrated along the hammer, providing lubrication to the other wear points.

Because of the geometry of this interface, journal-bearing models were initially considered as a way of simplifying the modeling portion of the wear design. However, because of the nature of the loading and motion in this application, it was concluded that these models were not applicable, since they typically assumed unidirectional journal rotation, not the oscillatory-bearing motion involved in this case. Also, the loading conditions assumed in these models were generally much simpler and not representative of the complex loading situation between the hammer and the pivot. Therefore, it was considered necessary to develop a model, which would take into account the unique features of this application.

The operation of the print hammer was reviewed. It was concluded that the predominant wear mode was sliding for the non-printing portion of the cycle. However, during the printing portion of the cycle, there was the possibility that impact motions could develop as printing takes place and the location of the contact region changed. While this was a likely possibility, it was not possible to confirm the nature or severity of such impacts. It was therefore considered that it was not useful to directly model this wear situation as either simple or compound impact wear. An alternative and somewhat conservative approach was then considered. Since the effect of these impacts, if they occurred, would be included in the pulse measurements used to determine the reaction load during printing, a sliding model using this load could be developed which would provide a worst-case estimate. This is because the severity of the wear in a compound impact wear situation approaches that for pure sliding as the amount of sliding increases. Hence, it was decided to model both wear situations as sliding wear. This resulted in some simplification, since the same model could be used for both contact situations.

Wear of both members needed to be considered. Since the amount of wear that was acceptable was small, the worn and unworn contact situations were similar. For this small amount of wear, the geometrical shape of the hammer and pin wear scars would also be

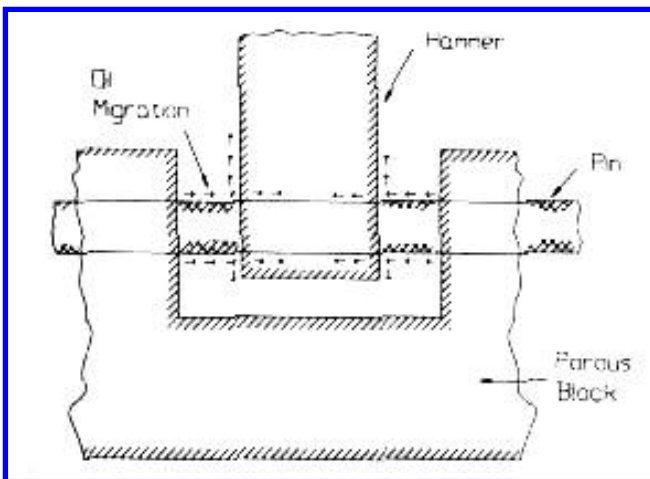


Figure 5.21 Lubrication of the hammer-pin interface. Arrows show the migration path of the oil from the impregnated sintered block used to hold the pins.

similar. As a result, two simplifying assumptions were used in the development of a model. One was to treat the wear of each member independently (i.e., only one member wearing at a time) and the second was that the same wear relationship could be applied to either member. With these two assumptions, it was only necessary to develop a relationship for one-body wear of the hammer and this could be used for the pin. The wear situation is illustrated in Fig. 5.22.

The general plan for the wear design approach was to model the wear situation and to use estimates of wear coefficients to determine feasibility and to identify areas of concern. Laboratory wear tests were planned to determine wear coefficients for different material pairs, which would be used to refine the projections of wear behavior and to select materials. Printer robot tests to verify the analysis were also planned. For the mild wear behavior and low wear that was required in this application, the normal approach would be to use the Zero and Measurable Wear Models as the basis of the analysis, subject to subsequent verification. An alternative approach was to use a linear wear model as the basis for the analysis. This is often the approach used to model the wear of journal bearings (e.g., the *PV* model—see Sections 2.2 and 2.8). Because of the journal-bearing characteristics of this application, it was decided to use both models in the initial phases of the wear design in an attempt to bracket wear behavior and to identify all the potentially significant design factors. Data from the same laboratory wear tests could be used to determine coefficients for both models. Ultimately, the printer robot tests could be used to determine the correct model.

Operationally, both contact situations were viewed as the same, namely as reciprocating sliding contact in which the load varied throughout the cycle. Figure 5.23 shows the variations in load over a cycle for both contact regions. The printing condition involved much less sliding and a heavier load than the non-printing condition. Both situations were modeled by assuming constant equivalent load for the entire cycle. The value of this equivalent load depended on the model. For the approach based on the Zero and Measurable Wear Models, the relation for the equivalent value was

$$P = \frac{\left(\sum P_j^3 \Theta_j\right)^{1.9}}{\sum \Theta_j} \quad (5.63)$$

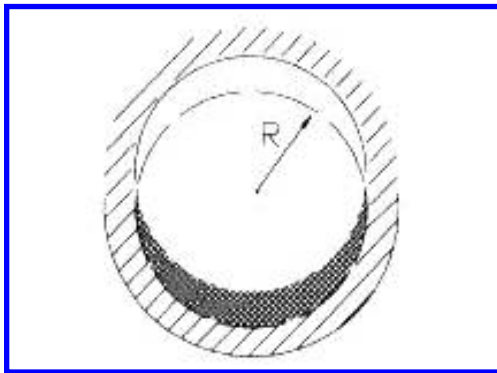


Figure 5.22 Wear scar geometry for the hammer-pin interface.

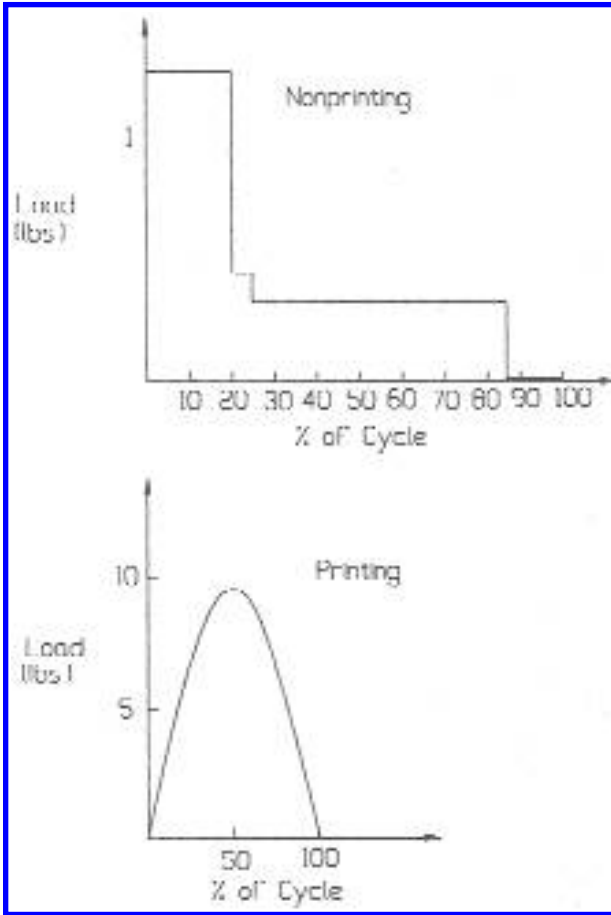


Figure 5.23 Loading during the printing and non-printing portions of the print cycle.

since stress is proportional to load in a conforming contact, Θ_j is the fraction of cycle at load P_j . For the approach based on the linear wear model

$$P = \frac{\sum P_j \Theta_j}{\sum \Theta_j} \quad (5.64)$$

since the volume of wear is proportional to the load. These expressions resulted in the following equivalent values for the non-printing region, 1.1 lb for Eq. (5.63) and 0.5 lb for Eq. (5.64); for the printing region, 8.3 and 6 lb, respectively.

Because the difference in the diameters was less than 0.5%, it was necessary to consider the contact as a conformal contact. The normal assumption for a conformal journal-bearing configuration is that contact occurs over half the circumference and to use the projected area of contact to determine stress. Implicit with this assumption is the fact that some wear will have to occur before this condition is achieved and for this to become a reasonable approximation. But for this application, the wear required for this would have been comparable to or in excess of the wear considered acceptable. Therefore,

a refinement of this assumption was considered necessary. It was proposed that the contact area be defined as the region over which asperity interactions occur. This area was estimated to be the region over which the separation of the two surfaces was less than the sum of the CLA values for these surfaces when the surface just touched. This concept is illustrated in Fig. 5.24, along with the arc, α , that was obtained for several different conditions. The contact stress was then based on the projected area subtended by this arc. (See Section 2.8).

The Zero and Measurable Wear Models were applied in the following manner. Since the contact only changes with wear in the direction of sliding, there was no need for distinction between the two equations for measurable wear. It was only necessary to consider one, namely

$$dQ = C dN \quad (5.65)$$

where Q is the area of the scar perpendicular to the sliding direction and N , the number of passes. In this case,

$$dQ = T dh \quad (5.66)$$

and, since the amplitude of the motion is less than the contact width,

$$dN = \frac{\theta}{\alpha} dL \quad (5.67)$$

h is the depth of wear scar; θ is the total angular rotation of the hammer; L , the number of print cycles, α is a function of h , as shown in Fig. 5.25. By consideration of the geometry

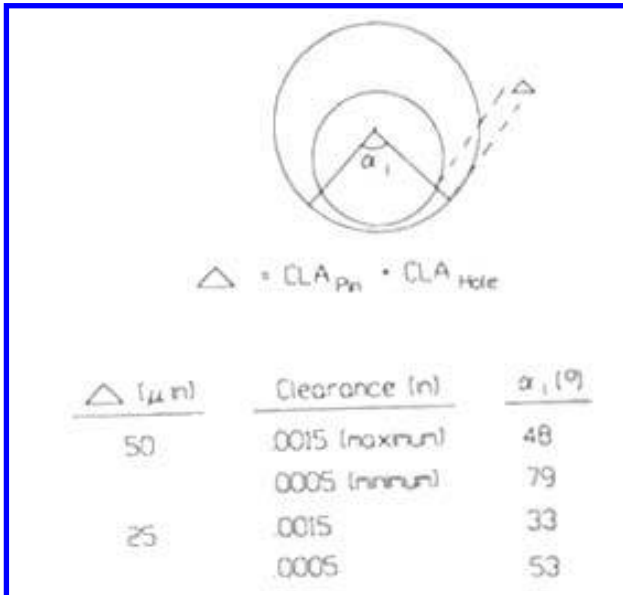


Figure 5.24 Determination of the contact area between the pin and the hammer.

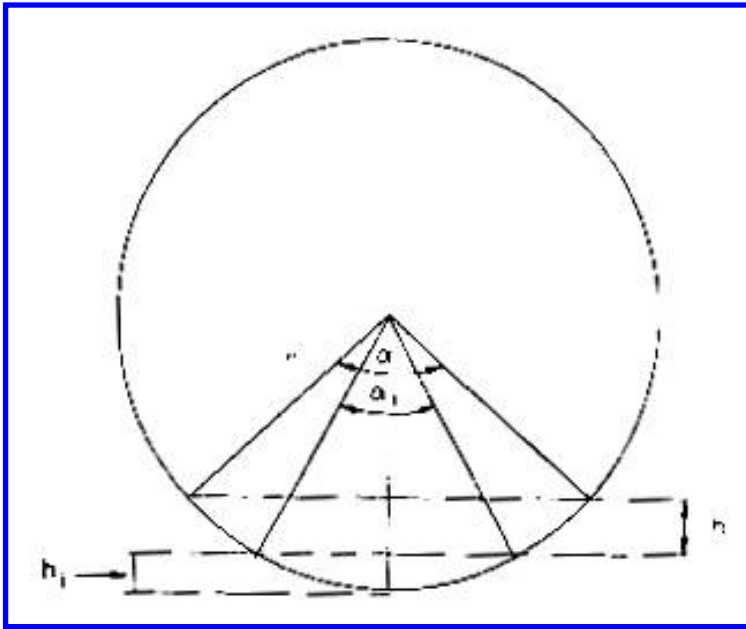


Figure 5.25 Wear scar geometry assumed in the analysis.

shown in this figure, the following relationship was obtained between α and h :

$$\alpha = 2 \cos^{-1} \left(1 - \frac{h_i}{r} - \frac{h}{r} \right) \tag{5.68}$$

where h_i is the initial cord height associated with the initial contact angle, α_i . The zero wear point was used to determine C , namely

$$h = \delta \quad \text{for } L = L_0 \tag{5.69}$$

δ is the CLA roughness and L_0 , the number of print cycles for zero wear.

The general relationship between h and L obtained from these equations was complex (Fig. 5.26), although it could be simplified for specific ranges of the variables involved. For the range of interest, it was found that this complex relationship could be reduced to a linear one and, in particular, it was found that for $h < 0.01$ in. ($L / L_0 < 1000$, and $\alpha_i < 10^\circ$), the relationship simplifies to

$$h = \delta \frac{L}{L_0} \tag{5.70}$$

The zero wear expression resulted in the following for L_0 :

$$L_0 = 1 \times 10^6 \left(\frac{\tau_y}{\delta} \right) \frac{[\Gamma_r \tau_y \sin(\alpha_i/2)]^4}{(KP)^2 (0.25 + \mu)^{1.5}} \tag{5.71}$$

where Γ_r is the zero wear factor; τ_y , the yield point in shear; μ , the coefficient of friction; P , the load; K , a stress concentration factor associated with the edges of the hole in the hammer.

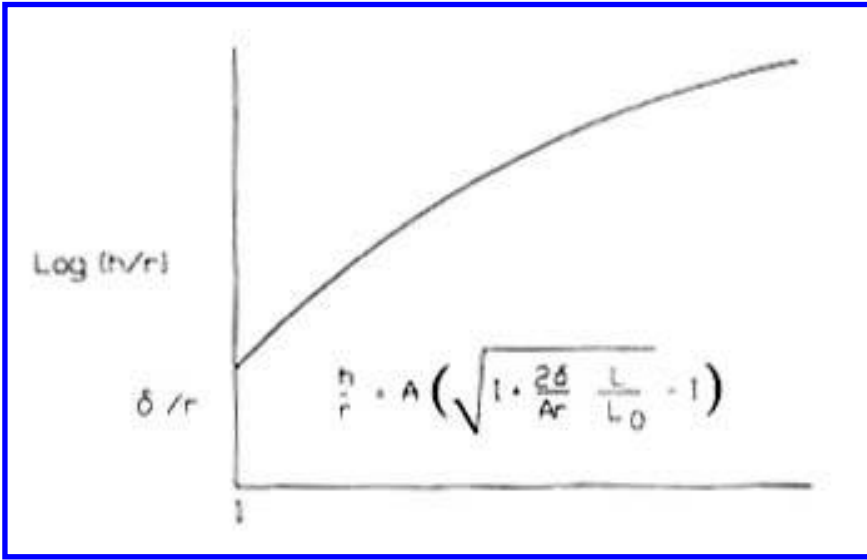


Figure 5.26 Wear curve based on the Zero and Measurable Wear Models for sliding.

The analysis, using a linear wear relationship, was less involved. In this case, the analysis was based on the following:

$$V = \mathbf{K}PS \quad (5.72)$$

where V is the wear volume; S , the distance of sliding; and \mathbf{K} , the wear factor. By considering the geometry, the following relationships for V and S were obtained:

$$V = hr \sin\left(\frac{\alpha}{2}\right) T \quad (5.73)$$

$$S = \left(\frac{\theta}{90}\right) \pi r L \quad (5.74)$$

Combining this relationship with Eq. (5.68) and using nominal values for α_1 and r , this resulted in the following approximate relationship:

$$h = 2\pi\mathbf{K} \left(\frac{\theta}{90}\right) \frac{PL}{T} \quad (5.75)$$

These relationships for h (Eqs. (5.70) and (5.75)) were used to evaluate the feasibility of the design. It was assumed that the allowed wear could be equally distributed on both members. As a result the feasibility estimate was based on a maximum wear depth of 0.0005 in. for 2×10^9 cycles. The approach was to use these equations and this life criterion to determine the minimum hardness that might be required and to compare this value with those of candidate materials. For the model based on the Zero and Measurable Wear Models, values for K and μ needed to be assumed. It was felt that a conservative estimate for K would be 3, since experience indicated that with proper edge conditioning this is an easily achievable value. A worst-case value used for μ was 0.3, since the contact was lubricated and μ is typically < 0.3 with lubrication. Using these values, Eqs. (5.70) and (5.71)

indicated that a minimum value of 75kpsi was required for τ_y , assuming the lower characteristic value for Γ_r , 0.20. This corresponds to a Vickers hardness of 350 kg / mm² (Rc 40). (See Appendix IV.) Since there was a wide selection of materials for this application with hardness above this value, the zero-measurable wear model indicated that the design was feasible.

The linear wear model resulted in a minimum value of 1×10^{-14} in.³ / lb in. (1.4×10^{-11} mm² / kg) for **K**. This was related to hardness by means of the model for adhesive wear which expresses **K** as

$$\mathbf{K} = \frac{K_p}{p} \quad (5.76)$$

where K_p is a probability factor associated with the material couple and lubrication and p is the hardness. For the best wear conditions, K_p is generally considered to be in the range of 10^{-6} – 10^{-7} . This implies a minimum hardness of 7000 kg / mm², which is well beyond the range of engineering materials. This model indicated that the design was not feasible.

Since one of the models indicated that the design was feasible, it was decided to proceed with the design and to optimize the selection of the materials, based on the linear wear model analysis. This meant using the hardest and most compatible materials considered practical, which were hardened 8620 steel for the hammer and a tungsten carbide pin. Both these materials generally exhibited good wear performance in other applications and were considered to be compatible. At the same time, because of the risk indicated by this analysis, considerations of alternative designs for printing began to be investigated. The laboratory-testing phase of the wear design was also initiated at this point.

The purpose of these tests was to determine the wear coefficients for different material couples. This required simulation of the application. In addition to using the materials in the same form and conditions as in the application, an important element to be considered in the simulation was the nature and relative amount of sliding between the two surfaces. To simulate this, it was considered necessary to use a test, which provides oscillatory motion for which the amplitude was less than the width of the contact. The loading condition was another factor to be considered for simulation. It was only considered necessary for this to be well within the elastic range of the materials, since this was or would be the condition in the application. These considerations ultimately led to the selection of a reciprocating ball–plane wear apparatus, which could provide an amplitude of 0.002 in., the use of specimen with a 0.25 in. radius, and two loads (0.55 and 1.1 lb) for the tests. For this radius and these loads, the diameter of the Hertz contact spot was > 0.003 in. and the maximum Hertz contact pressure was < 120 kpsi. These loads were comparable to average loads associated with the non-printing portion of the cycle.

Plane specimens of candidate materials for the hammer were obtained and spheres or spherical-ended rods were obtained for candidate pin materials. The roughness of these specimens was representative of those to be used in the application. A thin film of the lubricants considered for use in the application was applied to the plane specimen. Tests were conducted at a repetition rate of 145 cycle / min for 10^3 , 10^4 , 10^5 , 5×10^5 , and 10^6 cycles for each of the material combinations of interest. At the end of each test, the wear was measured by means of a profilometer.

For the coefficient of the linear wear model, the profilometer measurements were used to compute the volume of wear generated. This was then divided by the load and distance of sliding to provide a value for **K**. For the wear coefficient of the Zero Wear Model, the data were used to generate a wear curve, which was then used to obtain an estimate of

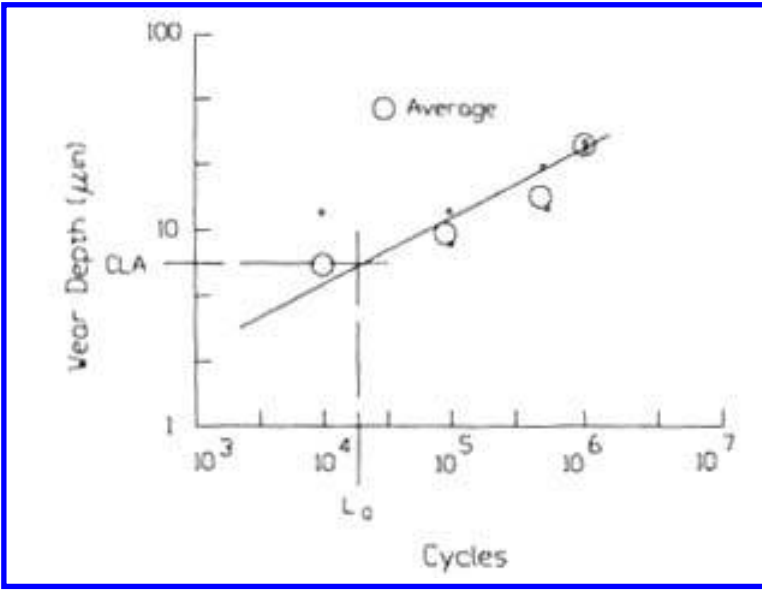


Figure 5.27 Method used to estimate the value of L_0 in the wear test.

the number of cycles for zero wear. This is illustrated in Fig. 5.27*. Using this estimate and Eq. (5.77), a value for the product, $\Gamma_r \tau_y$, was obtained*

$$\Gamma_r \tau_y = 0.062 \sigma_0 \left(\frac{L_0}{a} \right)^{1/9} \quad (5.77)$$

where σ_y and a are the Hertz contact pressure and the radius of the Hertz contact area in the test, respectively. L_0 is the estimated cycles for zero wear.

Values of \mathbf{K} and $(\Gamma_r \tau_y)$ for several of the materials tested are given in Table 5.9. These values were used to reevaluate the feasibility of the design using these materials. It can be seen that for all these material combinations, the zero-measurable wear model predicts satisfactory but not equivalent performance. The linear wear model predicts unsatisfactory performance for all the combinations. In addition, the wear factor for some combinations was lower than previously estimated.

The robot wear-testing portion of the wear design consisted of evaluating the wear at the hammer-pivot interface produced during printer robot tests designed to simulate typical printing situations. The robot and these tests were designed to evaluate many different aspects of the printer, including functional aspects. The results from two initial tests of this type were useful in determining which of the models were more appropriate and further tests confirmed the initial conclusions reached. Several robot tests were conducted.

The print energy was excessive in the first robot test and as a result the print reaction force was estimated to be 20 lb, rather than the 10 lb used in the analysis. The test was

* For lubricated conditions, the coefficient of friction is less than 0.3. As a consequence, the maximum shear stress is independent of the coefficient of friction, as is the zero wear equation.

stopped after 100×10^6 print cycles and the hammer–pivot area was examined for wear. While wear could be observed to occur on both the hammer and the pin, it was not possible to obtain quantitative data from the hammer. However, the wear could be measured on the pin with a profilometer. An average wear depth of $70 \mu\text{in.}$ was measured on the pin at the location associated with printing. While visual signs of wear were observed in the region associated with the non-printing portion of the cycle, the contour was not different than in the unworn region. These results did not appear to be consistent with estimates based on either model. For the conditions of the test, the linear model predicted $60 \mu\text{in.}$ for the non-printing region and $< 20 \mu\text{in.}$ in the print region. The “less than” symbol is used for the printing region because of the assumption to use a sliding wear model for what is likely an impact situation. The zero-measurable wear model predicted negligible wear for both regions, but indicated the print area as being the more severe.

In a second robot test, the hammer–pivot area was examined for wear more frequently and the test was carried out for 250×10^6 cycles. In this test, which was conducted with the proper print force, wear was also observed on both members and again it could only be measurable on the pin. The wear was negligible in the print location, while an average depth of $40 \mu\text{in.}$ was measured in the non-print region after 250×10^6 cycles. In addition, the profilometer measurements, particularly those made earlier in the test, indicated that the surface of the hole was crowned, rather than flat as the design specified. Examples of these profilometer traces are shown in Fig. 5.28. Cross-sections of hammers confirmed the crowning. Estimates, based on these measurements, indicated that the radius of this crown was of the order of 0.3 in.

The effect of this crown on the projections of the two models was evaluated. For the linear model, the crown would effect the relationship between wear depth and volume and result in a tendency to underestimate the wear depth before the wear scar was fully developed. The effect of the crown on the predictions of the zero-measurable wear model

Table 5.9 Experimental Wear Coefficients from Reciprocating Ball Plane Tests

Material	Counterface	Lubricated	$\Gamma_r \tau_y$ (kpsi)	K ($10^{-15} \text{ in.}^2/\text{lb}$)
Tungsten carbide	Steel	Yes	≈ 84	≈ 50
8620, hard	WC	Yes	63	64
8620, special heat treat	WC	Yes	61	116
Electroless Ni on hardened steel, heat treat	WC	Yes	59	118
Electroless Ni on hardened steel, modified heat treat	WC	Yes	60	111
High-density sintered steel, hard	WC	Yes	57	345
MoS ₂ conversion coating on hard steel	WC	No	≈ 20	640–4900
Theoretical range for $\Gamma_r \tau_y$ based on hardness				
Tungsten carbide	40–110 kpsi			
Hardened steel	30–81 kpsi			
Theoretical range for K based on hardness				
Tungsten carbide	$80\text{--}7500 \times 10^{-15} \text{ in.}^2/\text{lb}$			
Hardened steel	$100\text{--}10,000 \times 10^{-15} \text{ in.}^2/\text{lb}$			

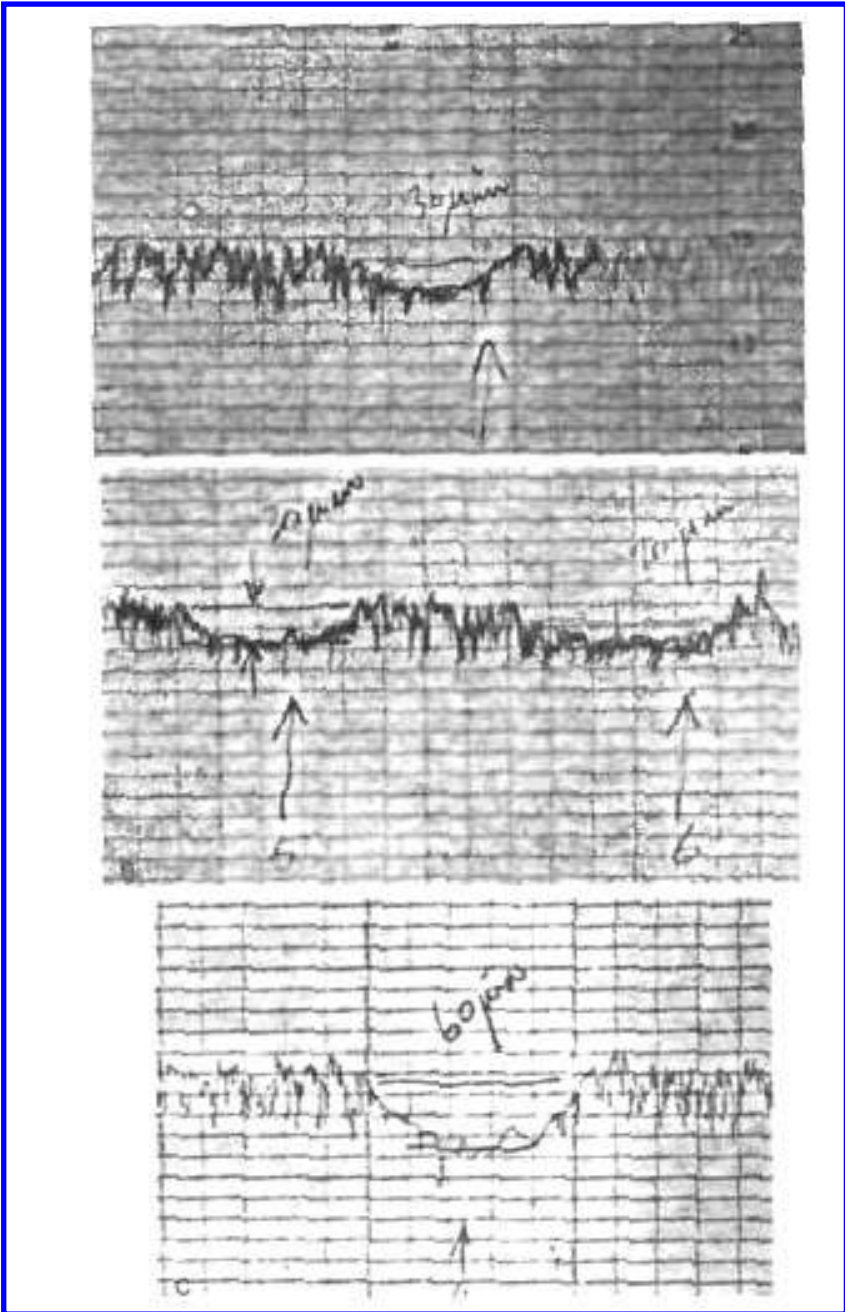


Figure 5.28 Profilometer traces of wear scars on the pin. There were multiple hammers on a single pin.

was much more pronounced because of the effect on stress. With a crown of the magnitude measured on the parts, the contact configuration changes from a conforming contact to a Hertzian point contact and resulted in a significant increase in stress. The effect of a crown on contact stress is shown in Fig. 5.29. An estimate of the effect of this on wear behavior was done by considering the effect on L_0 , which is proportional to stress to the 9th power, and using Eq. (5.70). Using these modified conditions, the models predicted the following wear depths for 250×10^6 cycles: linear model, 150 $\mu\text{in.}$ in the non-printing region and $< 25 \mu\text{in.}$ in the printing region; zero-measurable wear model, 40 $\mu\text{in.}$ and $< 0.013 \text{ in.}$, respectively.

Comparison of these theoretical values with the actual data of the second test indicated that there was better agreement with the zero-measurable wear model, assuming that in the print region the mode was primarily impact and little or no sliding occurred. As discussed earlier, this was considered a distinct possibility but that a sliding model was assumed as a worst-case estimate. This also provided an explanation for the wear in the first test. Estimates of the zero wear lifetimes, using the impact wear model, ranged from as low as 10^6 to as high as 200×10^6 print cycles for the conditions of the first test, depending on the amount of sliding or fretting present and the actual stress level. For the second test, these would increase by an order of magnitude. Since the data indicated a zero wear lifetime in the range of 30×10^6 cycles for the first test and greater than 250×10^6 in the second, it was concluded that the assumption of impact as the primary mode during printing was reasonable.

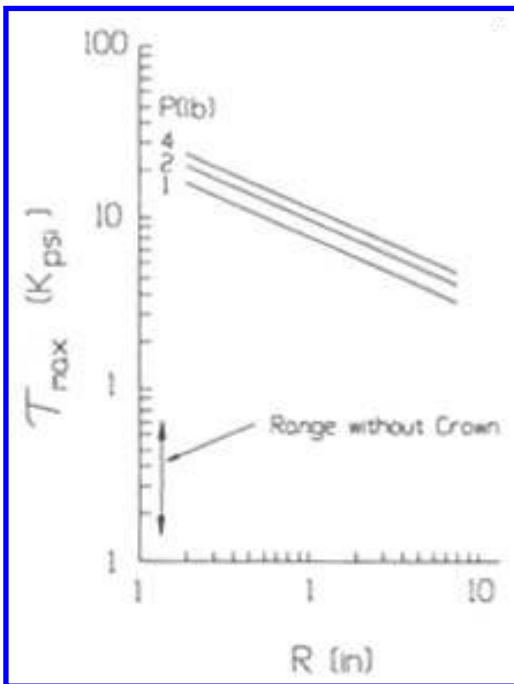


Figure 5.29 Stress as a function of the hammer crown radius.

Based on these considerations, it was concluded that the model based on the Zero and Measurable Wear Models was the correct one to use. This was verified in a third robot test. In this test, hammers with the correct hole profile were used and the wear was effectively reduced to 0. It was also concluded that for the print portion of the cycle the wear would be better described by the Zero and Measurable Wear Models for Impact rather than for sliding, since impact appeared to be the predominant mode during that portion of the cycle.

This model was also applied to another printer application involving a hammer-pivot. It was used to select materials and sizes for this design. With this application, initial tests also resulted in higher wear than predicted by the model. Using the model, it was deduced that the problem was related to lubrication (provided in a similar manner to that in the initial application). This was verified and modifications and controls were introduced to insure continuous lubrication. With the lubrication problem corrected, the wear was negligible, as predicted by the model.

5.9. BAND-PLATEN INTERFACE

In this case study, a wear design approach was used to identify and evaluate different design alternatives, as well as to select parameters. The wear design approach involved the use of both analytical and empirical modeling as well as elements of system analysis, database development, and verification.

One technology for impact printing involves the use of metallic bands with etched characters on their surfaces. Pulleys usually drive the band across a platen surface, which acts as a support during printing. In this type of printer, there is a print hammer for each print position and the paper and ribbon are located between the hammer and the band. The typical configuration of such a printer is shown in Fig. 5.30. Printing is accomplished

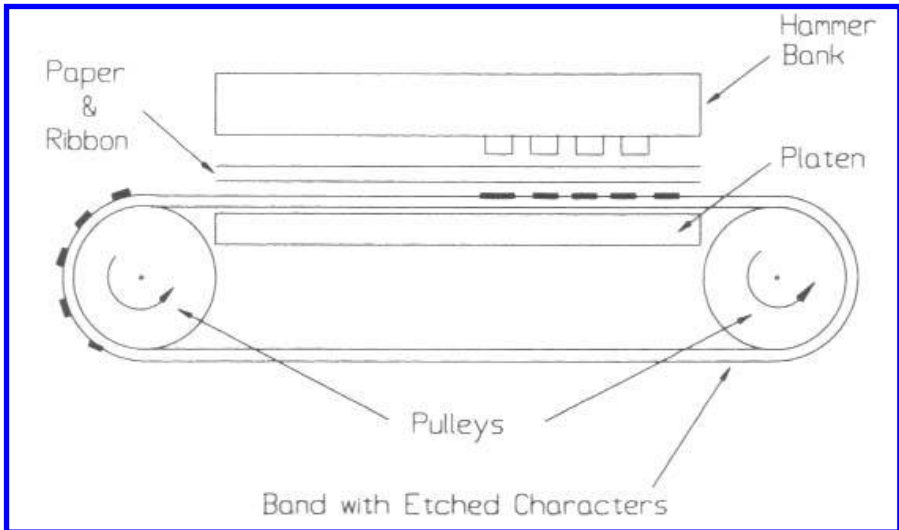


Figure 5.30 Configuration of a band printer.

by selective activation of the hammers to strike the appropriate character on the band as it passes the print position. Normally, these bands contain several sets of characters and a character set might contain more than one of a highly used character. One wear situation in this type of technology is that between the platen surface at a print position and the region on the back of the band, which is behind a character being printed. This is the wear situation addressed in this case study. A companion wear situation is the wear of the character face that occurs during the same period as a result of contact with the ribbon. This latter situation is considered in another case study (Sec. 5.11).

The general operational characteristics of this wear situation are as follows. The band is not in contact with but is moving across the surface of the platen, prior to printing. During printing, the hammer, through the intervening ribbon and paper layers, drives the region of the band behind the selected character against the surface of the platen. During the contact between the band and platen, the band continues to move without a reduction in speed. As the hammer rebounds, the band separates from the platen. Depending on the speed range of the printer and the type of printing, the peak values of the force pulses ranged from 20 to 40 lb and the contact times or pulse duration ranged from 10 to 200 or more μsec . Band speeds from under 100 to 1000 in. / sec were used. The usage conditions for the band and platen are significantly different in this type of printer. For the platen, the region associated with a print position would be struck a maximum of once per line of printing and experience contact with many different characters and regions of the belt. For the belt, however, an individual character may be used several times across a line or not at all. Also, it was possible that different new or used bands could be used in the same machine without changing the platen.

The development situation involved the extension of this printer technology from band speeds in the range of 100 in. / sec up to a 1000 in. /sec. Experiences with prior machine development programs indicated that wear at this interface had become more of a problem as the printer speeds increased (i.e., lines printed per minute) and the band speeds increased. In these earlier development programs, any wear design activity for this interface was more in the form of problem resolution than design development. Because of this prior history, it was decided to use a more formal and anticipatory wear design approach for the extension of this technology to these high band speeds, i.e., range of 1000 in. /sec. The goal of the wear design was to investigate the feasibility of these higher speed applications, to identify design alternatives to address any wear concerns, and to develop a design with adequate wear performance.

The approach was to develop an analytical expression relating wear to design parameters and verify it by using data from existing designs. Then with material wear coefficients obtained from laboratory wear tests, to use the relationship to evaluate the potential wear performance of different design concepts. Robot or machine tests would then be used to verify the wear performance of the selected design. These steps were followed. However, after initial robot tests at high speeds, it was concluded that the accuracy provided by the analytical model and laboratory tests was not sufficient to use this as the sole basis for design selection. An empirical approach, guided by the analytical relationships and using a high speed robot for wear tests, was adopted to establish the final design. Using this approach, an acceptable design utilizing an interposing strip of polymer was developed for these high band speed applications.

The wear design and problem solving activities associated with the prior applications provided significant information. Among this was information regarding the effects of lubrication and character size on wear and a description of the failure modes associated with the wear. The former is shown in [Fig. 5.31](#). The curves in this figure indicate a

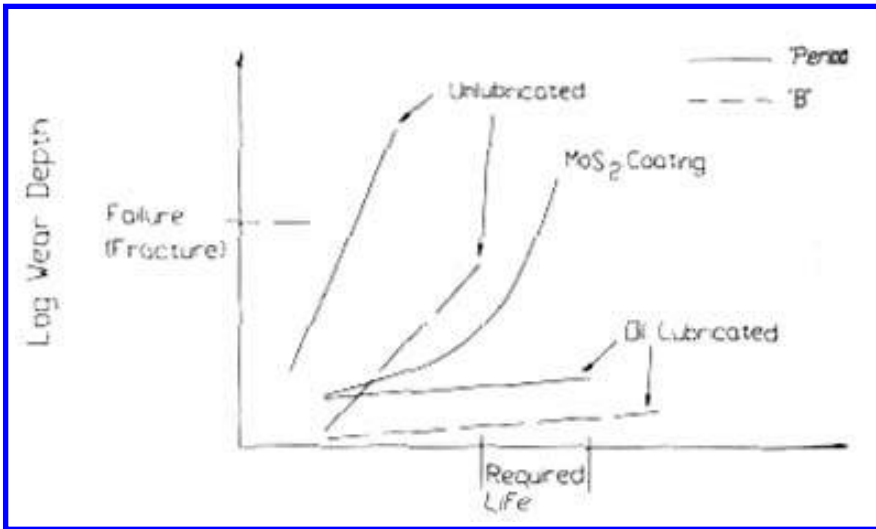


Figure 5.31 Band-platen interface wear behavior in prior applications.

transition in wear behavior when a lubricant was present and when it was not. A very high depth wear rate was obtained under unlubricated conditions; however, when the ink used in the ribbon was used as lubricant, a much lower wear rate results. Similar behavior was obtained initially with a thin plating of MoS₂ on the band. However, once this coating and the MoS₂ debris were worn away, the wear rate dramatically increased to that of an unlubricated system. A significant effect of character base area on wear was also found. The change in the depth of wear associated with particular characters was found to be much greater than would be anticipated by the ratios of the base areas of the characters. Curves obtained by the use of special print patterns are shown in Fig. 5.31 for the unlubricated wear associated with the “.” and “B” characters for one of the fonts. Because of the font design and the etching process used to manufacture the bands, the base area of these two characters differed by approximately a factor of 2. As can be inferred from the graphs, the difference between the depth rates of wear for these two characters was greater than two orders of magnitude.

Two modes of failure were identified in these earlier applications. The more severe and limiting one was associated with the fracture of the band. If the wear depth on the platen or on the back of the band was great enough, the flexing of the band around the character base would result in the initiation and propagation of cracks in the band. In some cases, these cracks would result in the character dropping out of the band; in others, complete fracture of the band would occur. The critical depth for this process to occur appeared to be in the range of 0.0005–0.001 in. This mode is illustrated for the case of band wear in Fig. 5.32. The second mode was associated with degradation in print quality as a result of a platen wear. For this to occur, the wear depth on the platen needs to exceed 0.001 in.

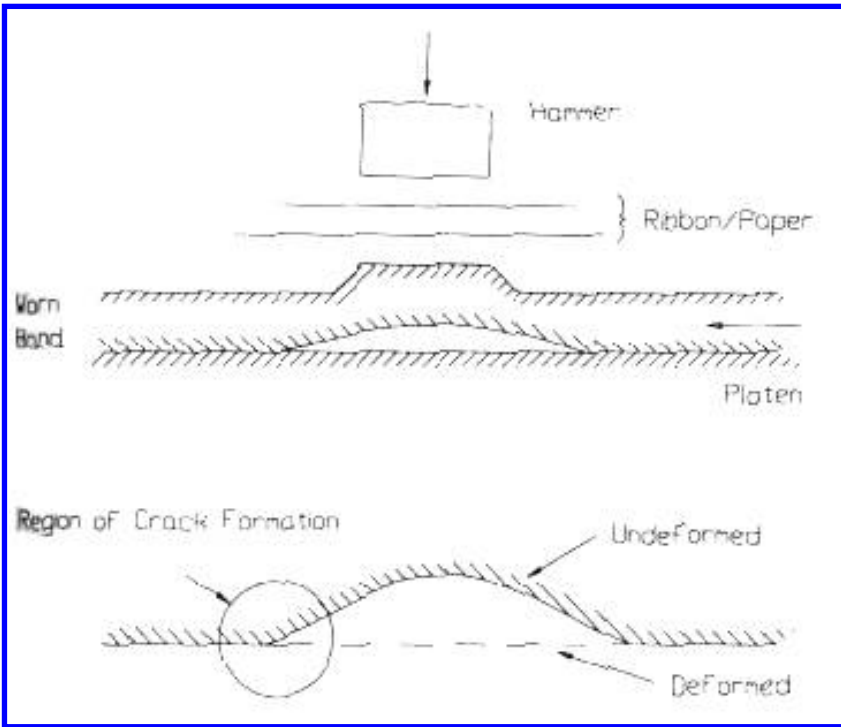


Figure 5.32 Failure mode associated with band-platen interface wear. “A” shows the condition prior to printing. As shown in “B”, flexure occurs at the edge of the wear scar during printing, leading to the formation of cracks in the band.

In the initial applications of this technology, adequate life was obtained by the use of lubrication and replaceable platen surfaces. In one application, the band had “windows” which allowed ink from the ribbon to migrate to the back of the band and provide lubrication. In another, a plated MoS_2 conversion coating was used to meet the life goals (7). For a third application, using a softer material for the platen and replacing the platen surface at half the machine life, eliminated the wear on the band. In this design, a platen was designed which provided two wear surfaces of a PTFE / Pb coated sintered bronze material (DU-bearing material) that could be interchanged.

Since sliding behavior tends to predominate when sliding is continuous during impact, it was decided to model the wear situation as sliding with a time-varying load, rather than as a compound impact. In addition to the theoretical consideration supporting this assumption, there was some empirical evidence supporting it as well. The morphology of wear scars in the prior low band speed applications had features suggestive of sliding. This trend would also become more valid as the band speed increased in this technology. It was also decided to use the Zero and Measurable Wear Models for sliding as the basis for the analysis. There were two reasons for the selection of these models. One was the general success with these models in analyzing low wear situations and the other was the strong sensitivity of the wear to character size, which suggested a stress rather than a load

dependency on wear. If these models did not result in good correlation with observed behavior, other models would then be considered.

In order to solve the measurable wear equations, analytical relationships describing features of wear scar geometry were needed. To obtain these, it was first necessary to identify the shape of the wear scars. The prior problem solving activities helped to do this. Profilometer traces of band and platen wear scars made during that time indicated that the shape was similar on both the band and the platen. These traces also indicated that the general features of the wear scar were similar to that which would be produced by a large radius sphere, oscillating parallel to the length of the band. In a plane perpendicular to band motion, the shape could be approximated by a chord section of a circle. Based on these observations, it was decided to approximate the cross-sectional wear scar areas, perpendicular to band motion, as a progression of chord sections of a constant radius circle for both the band and the platen (Fig. 5.33). Because of this, the wear relationship for band and platen wear would be the same. This implied also that the width of the wear scar (i.e., the chord length), Ω , would change with increasing wear. Therefore, both the variable and constant energy equations need to be considered.

The load was transmitted through the raised character to the interface. Since the contact was over the wide area subtended by the character (Fig. 5.34), it was concluded that this contact could be treated as a conformal contact. Since there were no pre-existing edges involved and the tendency is for wear to eliminate stress concentrations, it was also concluded that it was not necessary to consider a stress concentration factor, that is, the stress concentration factor was assumed to be 1. For analytic purposes, it was assumed that the area subtended by each character could be represented by a circle of radius, r . Initially (and in the zero wear region) r was determined from the base area of the character. With wear, r would increase because of band flexure (Fig. 5.34) and based on symmetry, r would be one half the cord length (i.e., $\Omega / 2$) in the measurable wear region.

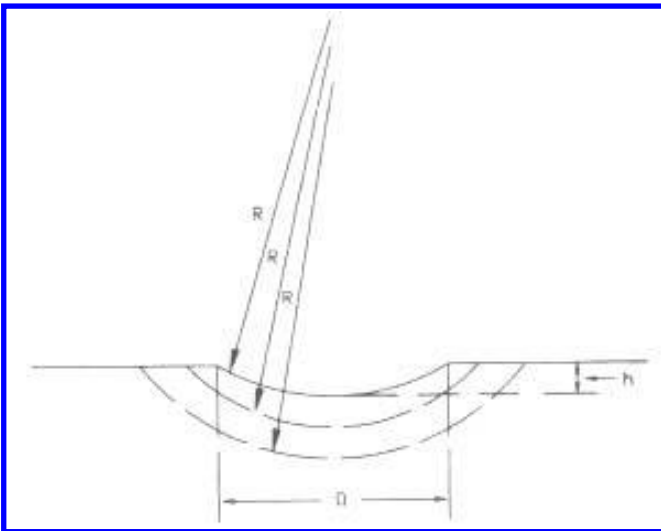


Figure 5.33 Wear scar profile used in the analysis.

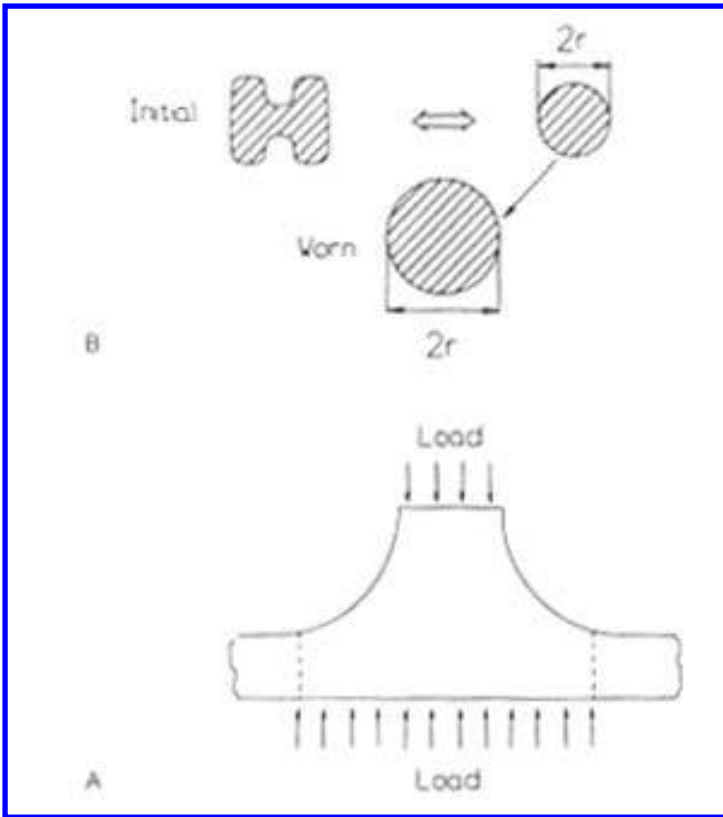


Figure 5.34 Contact and load distribution between the band and the platen during printing.

The load at this interface was in the form of a pulse. Therefore, a constant equivalent value, P_{avg} , was used in the zero wear equations, namely

$$P_{avg} = \frac{\left(\int_0^{T_c} P(t)^9 dt\right)^{1/9}}{T_c} \tag{5.78}$$

where P is the magnitude of the print force; T_c , the duration of the print force; t , the time. Since the print pulse could be approximated by a half sine wave of peak amplitude P_m ,

$$P_{avg} = 0.86P_m \tag{5.79}$$

For these conditions, the following expression for wear depth, h , was obtained for both band and platen wear:

$$h = \delta \frac{[(0.25 + \mu^2)^{4.5} P_m^9 v T_c]^n}{[1.4 \times 10^8 (\Gamma_r \tau_y)^9 r_i^{19}]^n} L^n \tag{5.80}$$

δ as twice the CLA roughness; μ , the coefficient of friction; v , the band speed; T_c , the duration of the print force; L , the number of print cycles or “hits” the location

experienced; Γ_r , the zero wear factor for sliding; τ_y , the yield point in shear of the material; r_i , the initial value of r ; and n , an exponent depending on the wear mode. n was 0.5 for the constant energy mode and 0.24 for the variable energy mode.

The next step in the wear design was to determine wear coefficients of different material systems, both those being considered for potential use and those used in prior applications. The latter was needed to verify Eq. (5.80). In selecting the test to determine these coefficients, it was desirable to simulate the application as much as possible. An apparatus that provided the same speed range and intermittent nature of the sliding as in the application was not available. What was available was a reciprocating ball-plane apparatus and a unidirectional ball-plane apparatus. The possibility of using the latter, which could provide the higher speeds, was eliminated because of the difficulty in obtaining suitable specimens, (i.e., those for the disk in this test configuration). It was concluded after some consideration that the reciprocating ball-plane apparatus, which provided speeds in the range of a few inches per second, could be used with some risk that it would not provide adequate simulation. This was based on two assumptions. One was that the primary effect of higher speeds in the printer would be to increase surface temperature. The second was that the effect would be minimal, since high temperatures were unlikely because of the intermittent nature and short duration of the contacts and the nature of the materials being considered. Only metals and high-temperature plastics were being considered and these materials generally provided stable wear performance over a wide temperature range. In addition, a temperature problem was not indicated in the initial applications of this technology and as it was decided to proceed with the risk, subject to later verification in the robot tests at high speed.

The distance of sliding during the contact tended to be less than the width of the contact (e.g., < 0.01 in. compared to 0.1 in.). Generally, a small amplitude would be used with the ball-plane apparatus to simulate such a condition. However, in this case, the motion in the application was unidirectional and repeated engagements were not over the same region of both surfaces. It was felt that the film formation characteristics of such a situation would be much different than those of a small-amplitude reciprocating test. It was decided that better simulation would be provided by a large-amplitude reciprocating sliding test. This was done by selecting a 1 in. amplitude and a repetition rate of 60 cycles / min, which provided an average speed of 2 in. / sec for the tests used to determine the wear coefficients.

Sliders with a 2 in. radius were used in these tests. To determine the wear coefficient, a load of 25 g was used in the large-amplitude tests. For the materials evaluated this resulted in a stress that was below their elastic limit, which was a requirement in the application. The contact stress in the test ranged from 1 to 55 kpsi, depending on the elastic moduli of the materials. Contact stresses in the application were estimated to be between 7 and 15 kpsi, depending on font size and print conditions. The compressive yield stress range for the materials considered was estimated to be between 10 and 300 kpsi.

In general, the materials were tested in both forms (i.e., as both the ball and the plane). This was done for two reasons. The primary one was that there was no clear indication, which test member provided the better simulation for either the band or the platen. Both the band and the platen could be thought of as experiencing rubbing over a much larger surface. The second reason was that, because of the tendency for the ball to wear in this test, it was sometimes necessary to use both materials as the slider to determine its wear coefficient. (Situations in which wear would only occur on the ball.)

Supplemental tests with several of the pairs were also performed because of the risk associated with the simulation in these tests. These tests were selected to investigate the sensitivity of the wear to motion conditions. In these supplemental tests, the test parameters were significantly different. The supplemental test conditions were: amplitude, 0.005 in.; load, 500 g; repetition rate, 170 cycles / min. The average speed in these tests was 0.03 in. / sec and the power dissipated at the interface was approximately half that of the larger amplitude test. Stress levels were still below the elastic limit of the materials.

It was necessary to determine the mode of wear (i.e., constant energy or variable energy), the combined wear coefficient, $(\Gamma_r \tau_y)$, and the coefficient of friction, μ . Therefore, wear curves were generated in the tests. The data were analyzed using the relationships for ball and for platen wear that were obtained by applying the Zero and Measurable Wear Models to those situations. (See Sec. 5.6; Appendix VI; 8.) For ball wear in the large- and small amplitude tests and platen wear in the small-amplitude test, these equations are

$$h = \delta \left(\frac{L}{L_0} \right)^n \quad (5.81)$$

$$L_0 = 2 \times 10^3 \frac{A}{D} \sigma_0^{-9} \left(\frac{\Gamma_r \tau_y}{\Phi} \right)^9 \quad (5.82)$$

For platen wear in the large-amplitude test,

$$L_0 = 2 \times 10^3 \sigma_0^{-9} \left(\frac{\Gamma_r \tau_y}{\Phi} \right)^9 \quad (5.83)$$

In both expressions for L_0

$$\Phi = \mu, \quad \mu \geq 0.31 \quad (5.84)$$

$$\Phi = 0.31, \quad \mu \leq 0.31 \quad (5.85)$$

h is the depth of wear; δ , twice the CLA roughness; A , the diameter of the Hertz contact circle; D , the amplitude of the test; σ_0 , Hertz contact pressure; and L , the number of cycles. In the tests, n had the following values:

Constant energy mode:

Ball wear $n = 0.5$

Plane wear $n = 0.67$

Variable energy mode:

Ball wear $n = 0.24$

Plane wear $n = 0.27$

Since the ball–platen apparatus provided the capability of measuring the friction force when large sliding amplitudes were used, it was possible to determine the coefficient of friction in the 1 in. amplitude tests.

The wear data from both types of tests were first analyzed to see which of the theoretical exponents provided the best fit. The theoretical value of n for that mode was used to determine values for $(\Gamma_r \tau_y / \Phi)$ from each of the data points and an average value was obtained. A typical wear curve is shown in Fig. 5.35. Values obtained from both the large- and small-amplitude tests are given in Table 5.10. It can be seen that while the

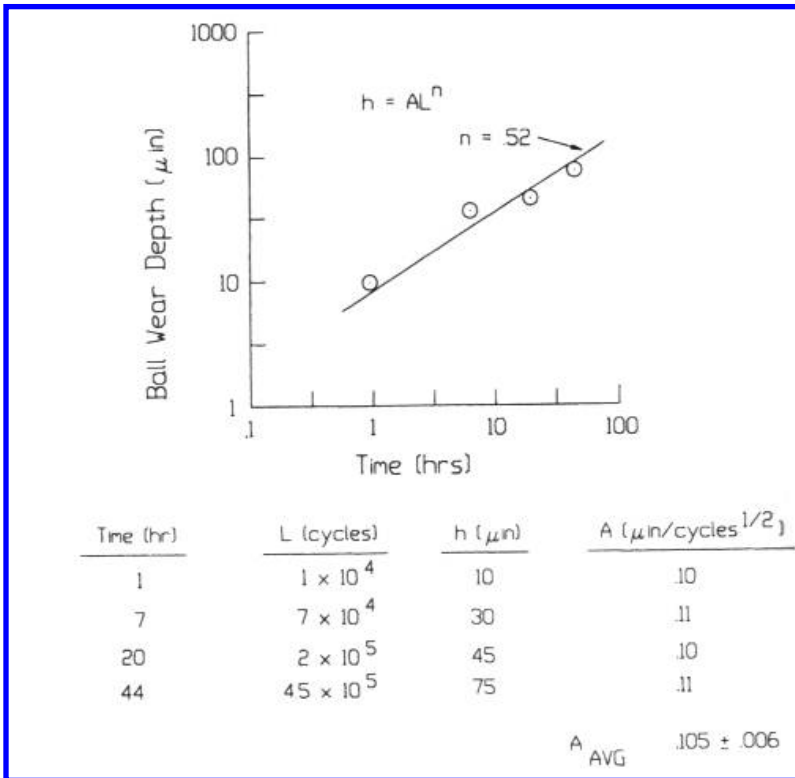


Figure 5.35 Analysis method used to determine n and $\Gamma_r \tau_y$ from wear tests. The data indicated a constant energy mode and as a result, the theoretical value of 0.5 for n was used to determine the value of A for each data point.

modes of wear for both types of tests were the same, there was a significant difference in the values for $(\Gamma_r \tau_y / \Phi)$. The values obtained from the small-amplitude tests were approximately twice those obtained from the large-amplitude tests. While the specific reasons for these differences were not determined, these results did suggest that the coefficients in the applications might be lower than those obtained in the tests. However, this was not found to be the case when these data were used to analyze the prior applications.

Using the wear coefficients determined in the large-amplitude tests, the accuracy of model was evaluated by comparing the amount of wear predicted to that found in several earlier applications of this technology. The operational parameters of these applications are listed in Table 5.11, along with the measured and projected wear. In general, there was good agreement between the theoretical estimates and actual behavior. It also can be seen that the model provided an explanation for the different relationships between wear depth and usage that were obtained in prior applications (i.e., with and without

Table 5.10 Values of the Combined Wear Coefficient, $\Gamma_r \tau_y/\phi$, and the Wear Mode Exponent, n , from the Large- and Small-Amplitude Tests

	n							
	Counterface material and test amplitude							
	Cr plating		Gin 6 SS		410 SS		7C27MO2 steel	
	Large	Small	Large	Small	Large	Small	Large	Small
420 SS	0.5	0.5						
7C27MO2 steel	0.5	0.5						
MoS ₂ coated 17-7pH steel	0.5	0.5						
Ni plating			0.5	0.5				
PTFE					0.24	0.24		
Vespel					0.24	0.24		
DU							0.24	0.24
	$\Gamma_r \tau_y/\phi$ (kpsi) and test amplitude							
	Counterface material and test amplitude							
	Cr plating		Gin 6 SS		410 SS		7C27MO2 steel	
	Large	Small	Large	Small	Large	Small	Large	Small
420 SS	24	58						
7C27MO2 steel	15	34						
MoS ₂ coated 17-7pH steel	19	39						
Ni plating			13	22				
PTFE					0.36	0.58		
Vespel					1.7	3.5		
DU							13	28

lubrication). Because of this good correlation, it was decided to use the model and the wear coefficients obtained from the large-amplitude tests to evaluate potential designs for the higher band speed applications (i.e., up to 1000 in. / sec).

The operational parameters for this higher speed application are given in Table 5.12 and the results of this analysis are given in Table 5.13. Band life in the intended application was required to be no less than 1 year and platen life to be 5 or more years. As can be seen from Table 5.13 none of the combinations tested were projected to satisfy both requirements simultaneously. It was also concluded from these estimates that without lubrication, it would be necessary to use a sacrificial platen surface to obtain the required band life. Since lubrication can significantly affect both the mode of wear and the Γ_r value, the analysis suggested that with a suitable lubricant both requirements might be simultaneously satisfied.

Based on this analysis, several design options were identified for investigation. One was obtain a wear resistant and lubricating composite for the platen or platen surface. A second was to use a design, which provided continuous lubrication to the interface, preferably using a dry or solid lubricant to minimize contamination of the print area

Table 5.11 Comparison Between Printer Data and Model Projections

	Printer Conditions					
	Printer A		Printer B		Printer C	
Band speed	72.5 in./sec		110 in./sec		364 in./sec	
Band material	17-7 pH steel with without a MoS ₂ conversion coating		7C27MO2 steel		410 SS	
Platen material	Cr plated hardened steel		DU material		Vespel	
Print force	30 lb		30 lb		20-30 lb	
Contact time	125 μs		125 μs		20-40 μs	
Hammer speed	72 in./s		80 in./s		300 in./s	
Average radius of contact area	0.03 in for MoS ₂ coated bands; 0.04 in for uncoated bands		0.04 in.		0.06 in.	
Printer	μ	δ (μin.)	Wearing member	Wear Depth (μin.)		Number of operations
				Model	Test	
A						
With MoS ₂ coated band	0.1	40	Band	81	50	1 × 10 ⁸ print cycles
Without MoS ₂	0.5	40	Band	15	20	4.24 × 10 ⁸ print cycles
B	0.2	50	Platen	5	15	2.7 × 10 ⁷ lines
C	0.3	80	Platen	1.7	1	2 × 10 ⁷ lines
<i>n</i> Values						
Printer				Model	Test	
A						
With MoS ₂				0.5	0.5	
Without character “.”				0.5	> 1 ^a	
“B”				0.5	0.6	
B					0.24	

^aAssociated with severe (catastrophic) wear behavior.

and to avoid surface tension problems*. A third possibility was to use a rotating, high-wearing platen, where the wear could be confined to the platen and distributed over a much larger area. A fourth was to use a replaceable interposer between the band and the platen, which would eliminate the wear on both the band and the platen. Since the model was approximate, a final possibility that was considered was the use of bands of 420 stainless steel and a chromium plated platen. While design consideration was being given to each of these options, it was decided to obtain results from a printing robot with a band speed of 1000 in. / sec and to compare predicted and actual performance for one of the combinations evaluated.

* In previous application, it was found that if a meniscus formed, the band would be pulled against the platen and drug would increase.

Table 5.12 Parameters of New Applications

Maximum print force	30 lb
Contact time	$\leq 30 \mu\text{sec}$
Maximum band speed	1000 in./sec
Font (average radius of support area, r_{avg})	0.043 in.
Usage	25×10^6 lines/month
Acceptable wear	≤ 0.0005 in.
Life	
Band	Minimum 1 year
Platen	Minimum 5 years

The operating parameters for the robot test are summarized in Table 5.14. For verification of the projections, tests were conducted using a band made of the 7C27MO2 stainless steel and a Cr plated platen. The model tended to underestimate the amount of wear found but was in reasonable agreement. For 1×10^6 impacts, the model predicted 300 $\mu\text{in.}$ on the band and 80 $\mu\text{in.}$ on the platen, compared to the average values measured of 800 and 110 $\mu\text{in.}$, respectively. While there was some agreement, the differences between theoretical and experimental values were considered to be significant. There were several possible reasons for the difference between these values, other than poor simulation in the ball-plane tests. The model indicated that the wear was very strongly influenced by the print force and the character area. At this stage in the development of the machine, there was considerable variability and uncertainty associated with both of these parameters, which were sufficient to account for the differences. Because of these considerations, it was decided that the printer robot would be used in further evaluation and development of the design options, rather than relying solely on the ability of the model to predict wear performance or to determine the specific reason for the difference. In effect, these robot tests replaced the reciprocating ball-plane tests in determining the wear coefficients. The dependencies on the other design parameters were still provided by the model.

In the robot wear test, wear was measured as a function of usage. In general, it was found that the data could be fit by exponential relationships and that the exponents of these relationships tended to be close to those of the model (Figs. 5.36–5.38).

With the robot tests, it was also possible to refine the failure criteria associated with this wear and to identify any other failure modes associated with the proposed design, such as those associated with lubricant build-up or the attachment of an interposer. It was

Table 5.13 Wear Life Projections

Materials		Projected Life	
Platen	Band	Platen	Band
Cr platen hard steel	420 SS	> 5 years	1–10 months
Cr platen hard steel	7C27MO2 steel	> 5 years	< 1 month
Vespel	Stainless steel	< 1 month	> 12 months
DU	Stainless steel	= 1 month	> 12 months
Cr plated hard steel with lubrication	Stainless steel	> 5 years	> 5 years

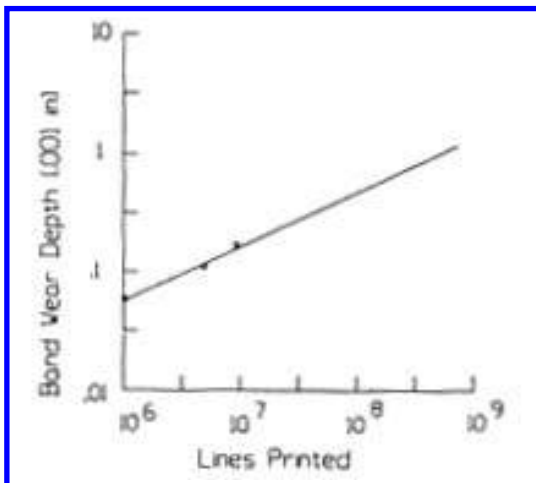
Table 5.14 Operating Parameters of Printing Wear Robot

Peak force	33–35 lb
Contact time	50–80 μ sec
Band speed	1000 in./sec

found that band fracture was ultimately the limiting factor. With metal platens, it was found that the acceptable amount of wear was 0.0005 in.; beyond this, cracks would tend to form in the band. With polymer platens or interposers, it was found that wear depths up to 0.001 in. could be tolerated before cracks were initiated. This was attributed to the lower stiffness of the polymer and the effect that this would have on band flexure.

The results of the robot wear test with the 7C27MO2 band and the Cr platen, when combined with the results of the laboratory comparison and the model, indicated that there was very little chance of obtaining adequate performance with a 420 stainless steel band and a Cr platen. As a result, this option was no longer considered. Several composite coatings, which appeared to have potential for these applications, were identified from vendor literature and evaluated. However, none were found to have adequate resistance in these robot tests and this option was eliminated from consideration. Robot tests with lubricants, polymer interposers, and plastic platens indicated that it was possible to obtain adequate wear performance with any of these. Examples of data obtained for these systems are shown in Figs. 5.36–5.38. Several of the materials considered for the interposer had coatings. With these transitions in wear behavior could be seen when these coatings were worn through. In these cases, the useful life was associated with the life of the coating.

The results of these tests and the analytical and empirical modeling were combined with other design considerations, such as human factors, cost, and space, to select a design. It was decided to use a replaceable 0.005 in. strip of Kapton F as an interposer. Kapton F consisted of a polyamide core, coated with PTFE. Several additional robot wear

**Figure 5.36** Wear curve for band wear in robot tests using lubrication.

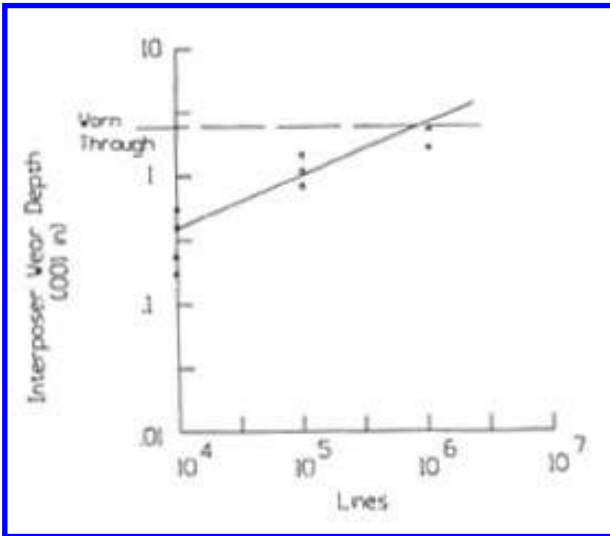


Figure 5.37 Wear curve for a Mylar D interposer in robot tests.

tests were performed to provide better characterization and wear relationship for this material. These data are shown in Fig. 5.39. This wear curve was used to determine the replacement intervals for the interposer.

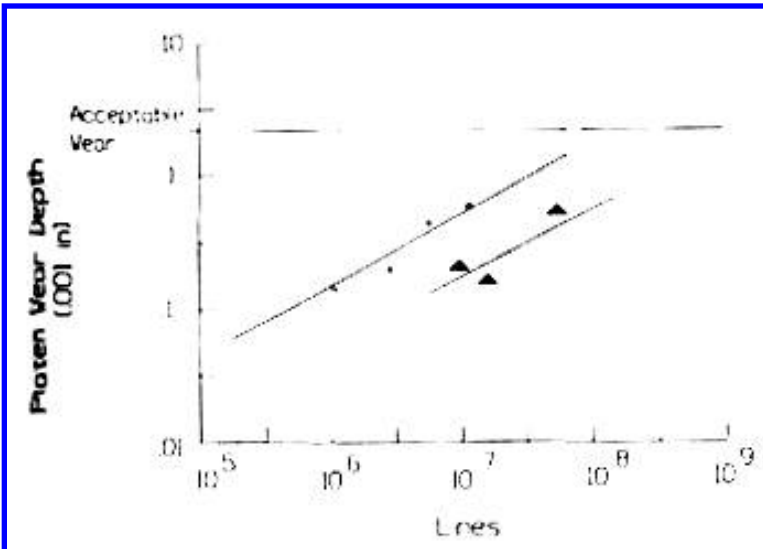


Figure 5.38 Wear curves for two filled polyimide platens in robot tests.

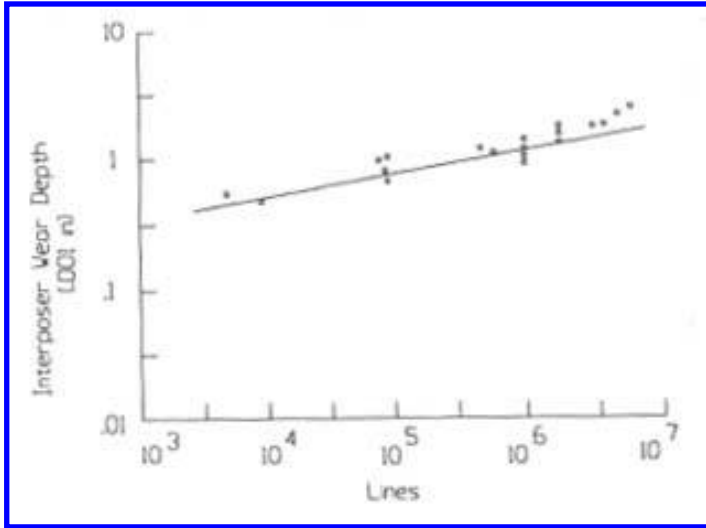


Figure 5.39 Wear curve for the Kapton F interposer.

5.10. PUSH ROD TIP

The significance of systems analysis in wear design is illustrated in this case study. In this case study, the wear relationship was initially developed using a description of the wear situation that was ultimately found to be inaccurate when the system was analyzed more rigorously. While providing some engineering information, the initial wear model resulted in a significant overestimate of the amount of wear and would have led to the rejection of the design. However, the wear, predicted by the final model, was found to be in very good agreement with available data and was acceptable in the application. This case study also illustrates the use of the impact wear model for elastomers.

This example is taken from the development of a high-speed impact printer. In this printer, push rods were used to transmit energy from relatively large electromagnets to relatively small print hammers. The general configuration of this type of design is shown in Fig. 5.40. (See Sec. 5.8 for additional information about this type of design.) At the start of a print cycle, all the elements are in contact. When the magnet is actuated, the moveable armature accelerates the push rod and the hammer. The motion of the armature stops at some point and the hammer and push rod go into free flight. These two also separate prior to printing. The rebound energy of the hammer and some return springs are used to restore all three elements to their initial positions, prior to the start of the next print cycle.

The use of this design concept in prior applications resulted in some significant wear problems between the tips of the push rods, the hammer and the armature surfaces. While these wear problems were successfully resolved, a wear design approach was not used. A cut-and-try material selection and development approach were used that resulted in the development of a unique elastomer tip for the push rod. This tip design is shown in Fig. 5.41 and utilized a 95 Shore A Durometer adiprene urethane. The intention for the new application was to use the same push rods; however, many of the design parameters associated with the new application and prior applications were different. Table 5.15

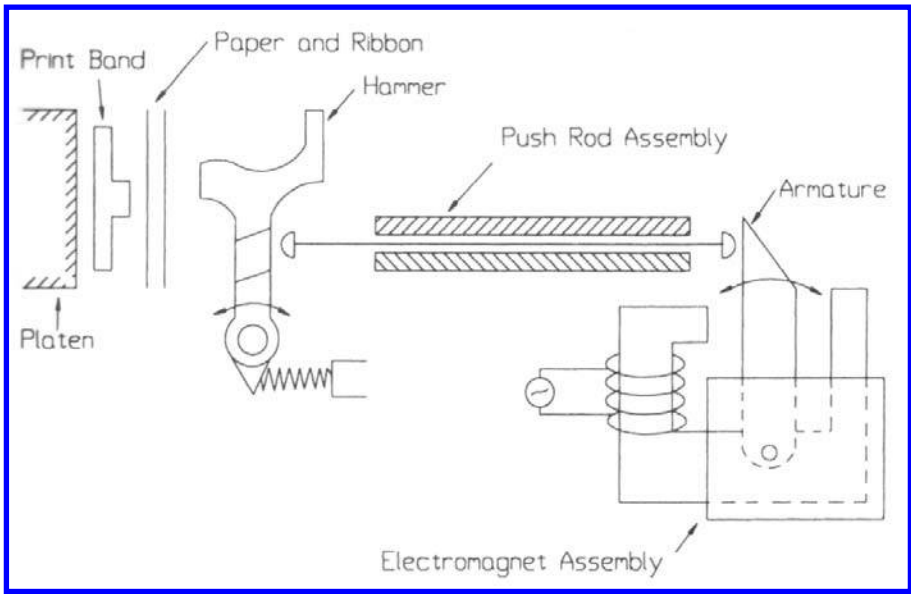


Figure 5.40 Impact printer design, involving the use of push rod to transmit energy from the magnet to the print hammer.

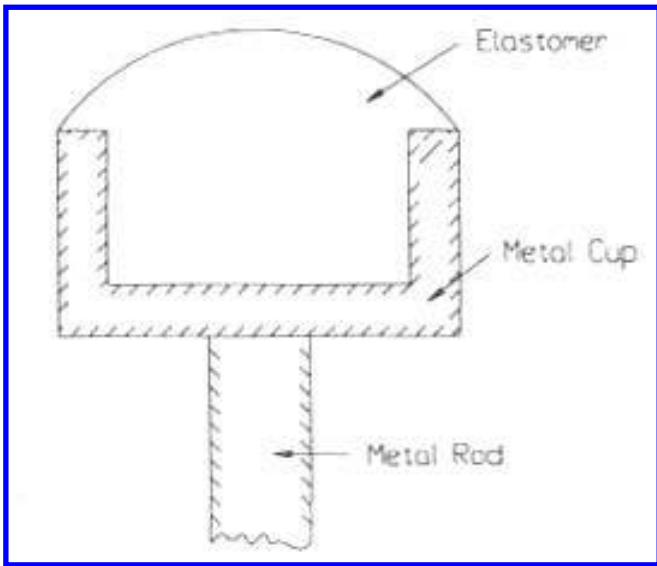


Figure 5.41 Push rod tip.

Table 5.15 Parameters of Push Rod Applications

Parameter	Prior application	New application
Backstop radius	1.0 in.	0.8 in.
Armature mass	2.7 g	4.2 g
Effective armature mass at push rod	1.0 g	1.7 g
Hammer mass	0.55 g	0.24 g
Effective hammer mass at push rod	2.5 g	1.2 g
Hammer velocity at printing	200 in./sec	323 in./sec
Armature return velocity at backstop	53 in./sec	86 in./sec
Hammer energy	65 kergs	80 kergs
Armature travel at tip	0.0394 in.	0.0445 in.
Distance between armature pivot and push rod location	1.42 in.	1.37 in.
Maximum repetition rate	2000 cyc/min	5000 cyc/min

provides a comparison of these parameters by listing nominal values for the proposed and the most similar prior application. The new application involved the transmission of higher energy, higher speed, and a longer life requirement, all of which implied a more severe wear concern. In addition, there were differences in the masses and dimensions of the hammers and armatures, which affect kinematics and, possibly, wear. To address the concerns in the new application, a wear design approach was followed to insure success and provide design flexibility. The focus was to develop a model for the wear of these tips that could be used for the early identification of any wear concerns for proposed printer designs and for the development of any needed design modifications.

The counterfaces for these tips were significantly harder than the urethane. The armature material was a soft iron, usually with a thin plating for corrosion protection and selected for its magnetic properties; the hammer surface was hardened steel with a thin plating for corrosion protection. As a result, wear was confined to the elastomer tips. Provided contact with the rim of the cup was avoided, this eliminated a fundamental wear concern with these devices, which was wear of these metal counterfaces. Wear of the metal counterfaces was undesirable, since it increased the probability of fatigue failures of these members. Since contact with the rim could occur as a result of tip wear, this concern provided a limit to the amount of wear acceptable for the tips. Based on the geometries involved, contact with the rim could occur with wear depths of greater than 0.010 in. Provided the rate of wear was small enough (e.g., < 0.001 in. / 10^6 print cycles), smaller amounts of tip wear were acceptable, since timing adjustments could be made to compensate for them. These tips were expected to have a minimum life of 2×10^9 print cycles.

The overall nature of the design suggested that very little sliding was involved. However, since the wear performance of elastomers tends to degrade rapidly with sliding, additional consideration was given to this aspect. While the nominal movement of the push rod was translation, both the hammer and the armature rotated. The general design was such that for the displacements involved, the contact between the tips and the hammer and armature surfaces was near normal, $> 75^\circ$. For such conditions, slip would not occur when the coefficients of friction are above 0.3, which is below the values normally associated with elastomers (e.g., > 0.5). Thus sliding was not considered to be possible in the application. This agreed with observations made in prior applications. These indicated that during the acceleration portion of the print cycle, the tendency was for the elastomer tip to deform and stick and for the rod to deflect. During the return portion of the cycles, it

was observed that impacts would occur. Negligible rotation would occur during the short duration of a typical impact. As a result, the tendency for sliding to occur was further reduced during this portion of the cycle. Therefore, it was decided to use the impact wear model for elastomers as the basis for the model and to assume a pure impact mode. (See Sec. 2.5.)

The basic relationship of the impact wear model for elastomers is

$$\mathbf{h} = \frac{\alpha_0 T \sigma_a \beta e^{-\beta/L}}{L^2} + \frac{\mathbf{h}_0 \sigma_a}{\sigma_f}, \quad \sigma_a \leq \sigma_f \quad (5.86)$$

where α_0 , \mathbf{h}_0 , β , and σ_f are material constants; σ_a is the contact stress; \mathbf{h} is wear depth per impact; L is the number of impacts. The first term of this expression is related to a deformation mode of wear, which results in the elastomer taking a permanent set without loss of material as a result of repeated load pulses. The second term is related to a surface fatigue mode, which results in loss of material as a result of these load cycles. σ_f is the flow stress of the elastomer. The model assumes that, if unconstrained, an elastomer will deform in such a manner that $\sigma_a \leq \sigma_f$. With elastomers, an over-stress condition can occur (i.e., $\sigma_a > \sigma_f$), if the contact area is constrained. When this occurs, catastrophic wear results and Eq. (5.86) no longer applies, \mathbf{h}_0 is the wear rate for the elastomer when σ_a equals σ_f . Since this elastomer used for the tips had been used in several other applications, values for these material constants were available (9). They were: α_0 , 0.008 kpsi⁻¹; $\beta < 10^6$ impacts; σ_f , 8.6 kpsi; \mathbf{h}_0 , 1.6×10^{-11} in. / impact. Additional data were also available for this material, such as the frequency dependency of its complex modulus (10).

Experience gained from the prior push rod applications indicated that three major load pulses of similar magnitude occurred during a print cycle. The first was associated with the initial acceleration portion of the cycle. The second was an impact in the return portion of the cycle, involving all three elements and prior to armature engagement of the backstop. The third was an impact involving all three when the armature hits the back-stop. This loading situation, along with the estimated value of these loads, is shown in Fig. 5.42. Wear behavior in prior applications appeared to be similar on both ends of the push rod. This description of the dynamics of the print cycle provided a simple explanation for that behavior. The major impacts always involved both ends. This observation was viewed as providing additional support to xthis model. Estimates for the forces involved at these three periods were based on different models. The value of the load, P for the first pulse, was estimated using an assumption of constant acceleration. With such an assumption, the force was related to the displacement during the acceleration portion of the cycle, s , the print or terminal velocity of the hammer, v , and the masses of the hammer, m_h , and push rod, m_{pr} , by the following equation:

$$P = \frac{m v^2}{2s} \quad (5.87)$$

For the armature end, m is $(m_h + m_{pr})$; for the hammer end, m_h . Since the mass of the push rod was small in comparison to the effective mass of the hammer, the forces at both ends were approximately the same.

The load was estimated for the second pulse by considering the impulse-momentum exchange between the coupled hammer-push rod and the armature. It can be shown that for such situation,

$$P = 1.57 \frac{m_a(m_h + m_{pr})}{m_a + m_h + m_{pr}} (1 + \varepsilon) v_h t_c^{-1} \quad (5.88)$$

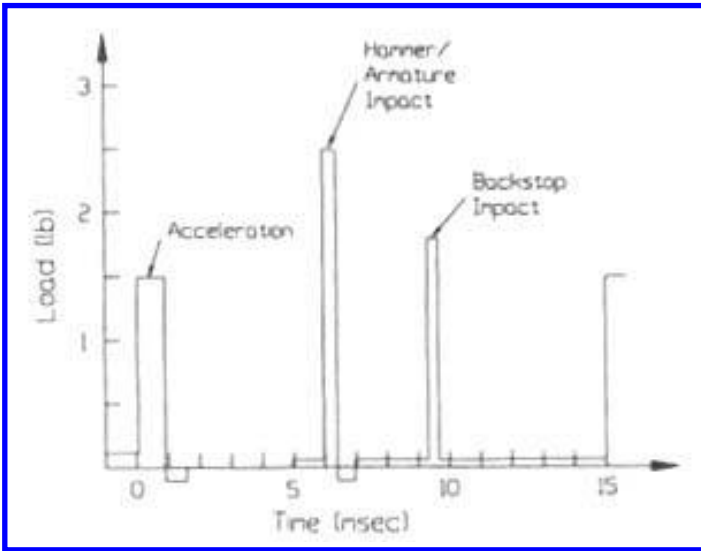


Figure 5.42 Push rod loading used in the initial analysis.

where the subscripts a, h, and pr stand for armature, hammer, and push rod, respectively; the remaining terms are m , element mass; v , impact velocity; ϵ , the coefficient of restitution, which was estimated to be 0.5; and t_c , duration of the impact; P , the peak load. Since the stiffness of the tips was significantly smaller than any of the other members involved, t_c was estimated from the second mode of vibration of the mass spring system shown in Fig. 5.43, where the stiffness of the spring was half the stiffness of a tip. The relationship for t_c was

$$t_c = \pi \left[S \frac{m_a(m_h + m_{pr})}{(m_a + m_h + m_{pr})E} \right]^{1/2} \quad (5.89)$$

where E is Young's modulus of the elastomer and is a function of frequency or t_c . As a result, an iterative technique was used to determine t_c , using available information regarding the frequency dependency for this urethane. S is a shape factor associated with the geometry of the tip and was determined experimentally from a compression test by means of the following relationship:

$$S = \frac{P'}{d'E'} \quad (5.90)$$

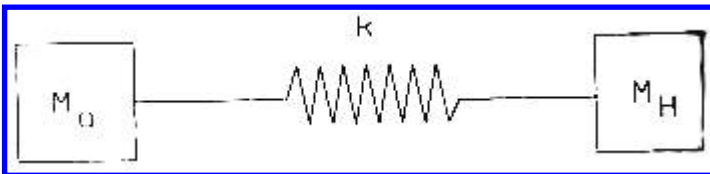


Figure 5.43 Mass-spring model used to estimate contact time for push rod impacts.

where d' was the compression measured under a load p' . E' is the modulus at the frequency of the test.

The estimate for the third pulse was based on force measurements at the backstop. These values were converted to force at the push rod tip by the ratio of the lever arms for the two sites (i.e., the distance from the armature pivot to the backstop contact region over the distance from the pivot to the push rod location).

Since the basic concept of the impact wear model for elastomers was that the wear resulted from stress cycling of the surface, the load pulse during the acceleration portion of the print cycle was considered to be an impact of long duration. Furthermore, since the magnitude of these load pulses was similar, it was decided to approximate the situation as three impacts where the maximum force was equal to the arithmetic average of the three forces.

The nature of the contact and observations made regarding the wear scars in the prior application indicated that flat spots develop on the tip. The following relationships were therefore used for the contact area, A_c , and the contact pressure, σ_a :

$$A_c = 2\pi r h \quad (5.91)$$

$$\sigma_a = \frac{P}{2\pi r h} \quad (5.92)$$

where r is the initial radius of the tip. Using these, integration of the rate equation for the wear (Eq. (5.86)), resulted in the following for values of $L > \beta$:

$$h = \left[\frac{P}{\pi r} \left(\alpha_0 T + \frac{h_0 L}{\sigma_f} \right) \right]^{1/2} \quad (5.93)$$

Since there were three impacts for each print cycle,

$$h = \left[\frac{P}{\pi r} \left(\alpha_0 T + \frac{3h_0 N}{\sigma_f} \right) \right]^{1/2} \quad (5.94)$$

where N is the number of print cycles.

For the estimated values of the forces this equation projected wear in excess of 0.0015 in. after 10^5 print cycles and in excess of 0.012 in. after 2×10^9 print cycles. The latter result was a concern, since the maximum allowable wear was 0.01 in. These projections indicated a marginal condition at best. When data started to become available from simulation tests, it appeared that the model tended to significantly overestimate the wear. For example, wear was found to be less than 0.001 in. for 10^6 print cycles. This level of agreement was not considered to be satisfactory since there were too many variables and factors involved to assume that the model would significantly over-estimate the long-term wear. Therefore, the model and the associated assumptions were reviewed to see if some modifications to the model could be made to improve the agreement. Out of this review came a concern with the model for print cycle dynamics. Impact-momentum modeling suggested that it would be highly unlikely that simultaneous impacts with the hammer and armature would occur. These analyses suggested that a series of less severe impacts between the push rod and hammer and between the push rod and armature would be more likely. As a result, a study was undertaken to determine print-cycle dynamics in this application.

A print hammer unit was instrumented so that the motions of the hammer, armature, and the ends of the push rod could be measured as a function of time. The results

of this study confirmed the suspicion that a series of milder impacts took place, each involving only two elements at a time. This is illustrated in Fig. 5.44, which shows how push rod velocity changes as a function of time. In this figure, changes in velocity indicate impacts either with the hammer or the armature. Impacts with the hammer increased the return speed of the push rod, while impacts with the armature decreased the return speed. Using the appropriate masses, the force associated with each of these impacts was determined in the same way as for the second pulse in the initial analysis. However, since the change in velocity was known for each impact, it was not necessary to assume a coefficient of restitution. The following expression for P was used:

$$P = m_{pr} \frac{\delta v}{t_c} \quad (5.95)$$

where δv is the change in push rod velocity. The measured velocity changes for the push rod and the computed forces are given in Table 5.16 for all of the impacts observed.

Because of the large range in the magnitude of the load pulses, it was necessary to modify the assumptions used in the wear analysis. In the previous analysis, there was little difference in the three values, so there was no need to determine an average or equivalent value. However, this is not the case with these series of impacts. For the deformation component, the wear approaches a limiting value for greater than 10^5 cycles. Since this asymptotic value is determined by the maximum stress for each cycle, it was concluded that for this mode the maximum load in the print cycle should be used rather than an average value. For the surface fatigue mode, each pulse would contribute to the wear. Because

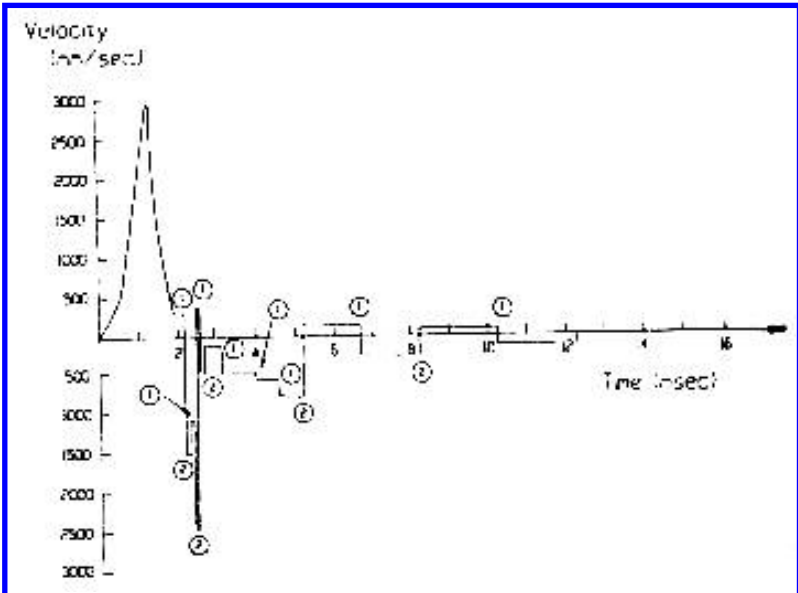


Figure 5.44 Measured push rod tip velocity during a print cycle. “1” indicates an impact between the hammer and the push rod. “2” indicates an impact with the armature.

Table 5.16 Impact History

Location	Impact number	δv (in./sec)	P (lb)
Hammer end	1	67	1.1
	2	38	0.6
	3	36	0.6
	4	10	0.2
	5	3	0.05
	6	5	0.08
	7	15	0.2
	8	6	0.08
Armature end	1	15	0.2
	2	101	1.6
	3	12	0.2
	4	31	0.5
	5	12	0.2
	6	2	0.03

of the linear dependency on load and stress of this mode, the wear situation could be approximated by a series of equal pulses whose magnitude was the arithmetic average of the individual pulses, as in the initial analysis. The important factor for this mode is the average load and the number of pulses per print cycle or the sum of the individual loads over a cycle.

With this modification, the wear was modeled in the same fashion as in initial analysis. The new analysis resulted in similar wear for both ends of the push rod, even though separate impacts were involved. This was because the maximum loads in the print cycle were approximately the same for both ends and the total load for the cycle was also similar. The total load for both ends was approximately 4.0 lb for a single print cycle, (when the initial acceleration pulse was included) and the maximum individual load was 1.1 lb for the hammer end, and 1.6 lb for the armature end. These new values also resulted in lower wear depths and an acceptable end of life condition. Wear curves for the initial and revised analyses are shown in Fig. 5.45 for comparison, along with actual data. The revised model predicts 0.010 in. of wear for 2×10^9 print cycles. However, since the model tended to overestimate the wear, this was considered acceptable. With a better understanding of the wear conditions, the agreement between the revised model and short-term data was sufficient to conclude that acceptable wear performance would be obtained in the new application. No special tests were performed to verify this. The examination of tips from printer qualification tests and field trials supported this conclusion.

Further discussion of the wear of these tips can be found in the Problem Solving section (7.4).

5.11. BAND-RIBBON INTERFACE

This case study involves the wear of two components at a common interface with each being worn by different mechanisms. It also involves a specific goal for the wear design to provide accurate and explicit wear relationships that could be combined with other design relationships to determine a total design.

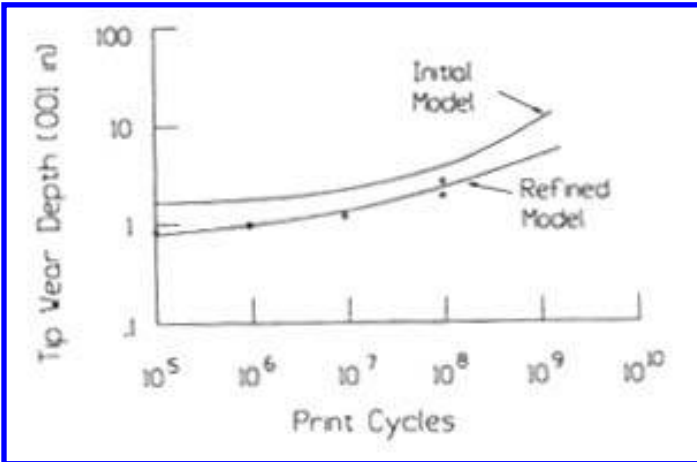


Figure 5.45 Push rod tip wear curves, compared with actual data.

In band printers (as described previously in Sec. 5.9) a ribbon, which is normally a woven nylon fabric containing a liquid ink, is driven against raised type on a moving band (Fig. 5.46). This printing action tends to cause wear on both the typeface and the ribbon. Wear of the type results in a reduction of the height of the etched characters, which can lead to degradation in print quality. One reason is that individual characters tend to wear at different rates. With large differences in the height of characters, it becomes impossible to time or adjust the machine to obtain good print quality for all characters. Also since the sides of the etched characters tend to be not straight (Fig. 5.47), the face area of the characters tends to increase with wear, changing the appearance of the printed character

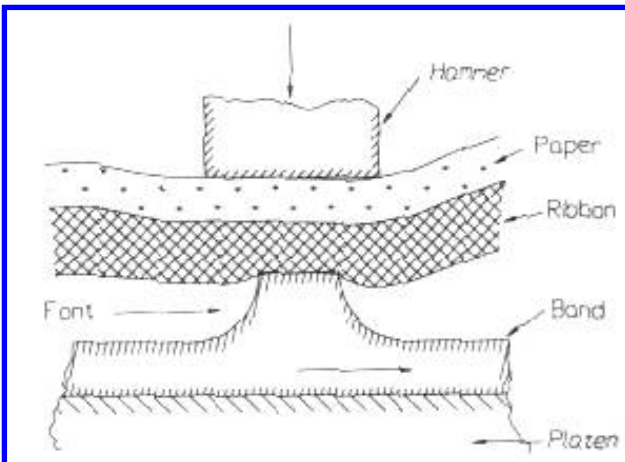


Figure 5.46 Wear situation between ribbon and front in a band printer.

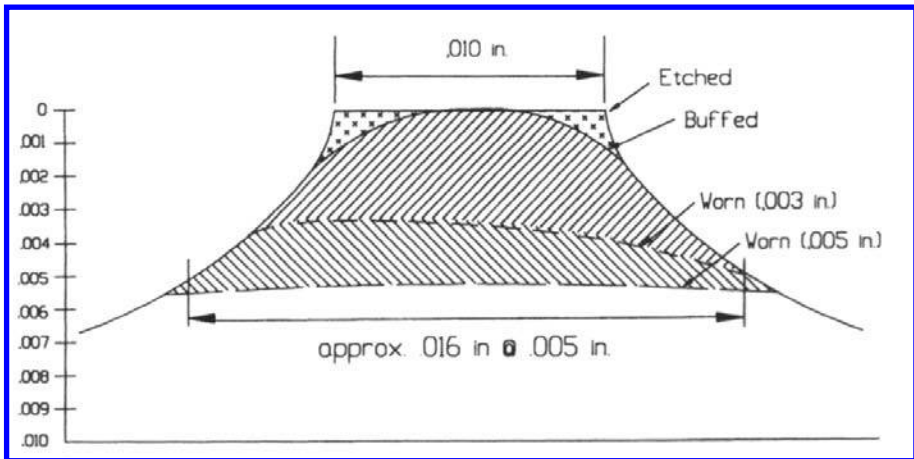


Figure 5.47 Cross-section of an “I”, showing the effects of buffing and wear on font profile.

and print density (i.e., the amount of ink transferred per unit area). Both effects result in (degraded print quality. Wear of the ribbon involves damage to the individual fibers and a distortion of the weave, which effects the mechanical characteristics of the fabric. Generally, the worn fabric becomes less stiff and deforms non-uniformly. With sufficient wear, these changes can result in a variety of unsatisfactory conditions, such as folds, ribbon jams, or shrinkage below the width required for printing, which cause failure. (The number of lines or characters printed required for these modes of failure is called their wear life. Some of these changes simply result in unacceptable printing (e.g., ink smudges or missing information), while others, such as jams, can also result in damage to other machine elements. Because of this, it is necessary to insure that the wear life of a ribbon is greater than its ink life. A ribbon ink life is the amount of usage required to reduce the amount of ink to that needed for acceptable printing. By satisfying this goal, a ribbon will be replaced prior to a wear failure.

In impact printing, ribbon and character properties are important factors in determining print quality. Because of this, ribbon development and band development are interrelated processes. They are also interrelated because of life concerns. Band design, involving character shape and material selection, affects not only the band life but also affects ribbon fabric life and ribbon ink life. Ribbon properties can also affect character wear and ink life determines a minimum requirement for fabric life. Hence, a design strategy, which involved the joint consideration of all three life requirements, that is, character life, fabric life, and ink life, was necessary for the development of a new, higher speed band printer. To support this strategy and reduce testing time, a wear design was developed which provided relationships for wear that could be used to analytically evaluate trade-offs in the design of each element and lead to the optimization of the individual lives. This approach led to the development of new character sets, a new fabric, and a new ink to meet the functional and reliability goals.

Type wear, fabric life, and ink life were common concerns in all types of impact printers and considerable background information and experience was available. For each concern, this consisted of data and observations from prior development programs and partially verified conceptual and analytical models. Because of the similarity in the state

of knowledge regarding these three concerns, the same general approach was used in each case. This was to refine or modify the preexisting models as necessary, to verify these models, to use laboratory tests to determine parameters for these models, to use these models and these tests to develop solutions, and to project performance, and to verify the projections in machine tests.

It was known from prior studies that type wear was caused by the ink in the ribbon, not by the fabric (11). Typically, the wear caused by un-inked fabrics was several orders of magnitude smaller than those resulting from ink-impregnated fabric. These studies had also shown that the wear was primarily abrasive in nature, resulting from submicron particles in the ink. There was also evidence that oxidative effects also influenced the wear. A standard wear test, ANSI /ASTM G56, had been developed to determine the abrasivity of ribbons. (See Sec. 9.2.12 in MWFT2E). A model for the abrasive wear of type, either by ribbon or paper, had been formulated and used successfully in several prior applications, including some slower speed band printers (12). Theoretical values of wear rates tended to be within a factor of 2 of the measured values, while theoretical and experimental relative wear rates for different values of the mechanical parameters of speed, mass, and character area were in much closer agreement (e.g., 10–20%). The basic relationship of this model was

$$V = \pi^{-1} \frac{K}{H_m} \nu t_c P_{\max} C(f) N \quad (5.96)$$

$$C(f) = \frac{f}{2}, \quad f < 2 \quad (5.97)$$

$$C(f) = 2 \left(1 - \frac{1}{f} \right), \quad f \geq 2 \quad (5.98)$$

where K is an abrasivity coefficient for the paper or ribbon; H_m , the hardness of the type face; ν , relative tangential speed; t_c , contact time; P_{\max} , peak force; f , the slip factor for compound impact; N , the number of times printed; V , wear volume; f is related to the amount of slip that occurs during impact and is given by

$$f = \frac{\pi m \nu}{\mu P_{\max} t_c} \quad (5.99)$$

where m is the mass of the impactor and μ is the coefficient of friction between the type and the paper or ribbon. Since character height was the significant engineering parameter and changes in character height were easily measured, Eq. (5.96) was used in the modified form

$$h = \pi^{-1} \frac{K}{H_m} \frac{\nu t_c P_{\max} C(f)}{A} N \quad (5.100)$$

where h is the change in character height and A is the area of the character face.

This model assumed that the wear of the typeface resulted from slip during printing and could be described by the following relationship for abrasive wear:

$$V = \frac{K}{H_m} P S \quad (5.101)$$

where S is the amount of sliding. The fact that slip occurred during printing was known for some time and was taken into account in the design of type fonts for printers. For

example, because of the slip, the character “T” was designed with a crossbar thicker than the stem to provide a printed image of uniform thickness. Since the structures involved in printing were not completely rigid in the direction of motion, slip velocity would not be constant over the entire period of contact. Some acceleration would take place during the contact time and tend to reduce the amount of slip. The method of analysis used to determine slip for compound impact wear was used in these situations. It was assumed that the primary mass to be accelerated or decelerated in printing was that of the impactor. This could either be a hammer or a type element, depending on the type of printer.

The ASTM test, G56, has been used to determine the abrasive coefficient for the ribbons. Values of K for ribbons were found to range from less than 10^{-6} to greater than 10^{-5} and to decrease as a result of use (i.e., a used ribbon was less abrasive than a new ribbon). Coefficients of friction between type and ribbon have been determined in sliding tests. While there seemed to be some effect of character shape, the coefficient was typical of what would be expected for lubricated sliding between nylon and steel (i.e., 0.2–0.3).

In reviewing this model for use in the wear design, it became apparent that its ability to evaluate the effects of material parameters on wear was relatively poor. The model tended to overestimate the amount of wear and there was up to a five-fold difference between the theoretical and experimental values for wear rate with some type materials and ribbons. The data also indicated considerable scatter regarding the effect of type hardness on wear rate. For example, wear rates for different materials of essentially the same hardness were found to differ by as much as a factor of 3. Two factors were thought to contribute to this. One was the oxidative or chemical component associated ribbon abrasivity and the other was a change in the abrasivity with use. Neither of these effects were taken into account by the model, but could be very significant in the development of a band / ribbon combination. Thus, it was decided to investigate these aspects before the model was used in the wear design.

It was proposed that the oxidative effect could be included in the model by combining the ratio of K / H_m into one factor \mathbf{K} , which was the abrasive wear coefficient for each type material / ribbon couple. \mathbf{K} could be determined by replacing the 52100 steel specimen in the ASTM test with a specimen of the type, or in this case, the band material. \mathbf{K} would be given by

$$\mathbf{K} = \frac{V}{PvT} \quad (5.102)$$

where v was the volume of wear measured in that test; P , the load used in the test; v , the velocity used in the test, T , the duration of the test. The effect of use on ribbon abrasivity could then be taken into account by using an average or effective value for K , based on determinations after different amounts of usage. With these modifications, Eq. (5.100) became

$$h = \pi^{-1} \mathbf{K}_{\text{avg}} \frac{v t_c P_{\text{max}} C(f)}{A} N \quad (5.103)$$

where \mathbf{K}_{avg} is an effective value for \mathbf{K} .

These modifications were investigated in two ways; both involved obtaining specimens of band materials for the ASTM type of test. Since there was considerable type wear rate data available from two different speed printers for two different band materials and the same ribbon, it was decided to determine \mathbf{K}_{avg} for these two pairs and to compare estimates obtained from Eq. (5.102) with average machine data. The second evaluation of

these modifications involved new and carefully controlled tests with the higher speed machine and using only one band material and one type of ribbon.

A value for K_{avg} for the first evaluation was determined by repetitive wear tests on the same specimen of an unused ribbon. It was found that the decrease in abrasivity could be approximated by

$$K_i = 0.64K_1 e^{0.44/i} \quad (5.104)$$

where i is the number of tests with the ribbon sample and K_1 is the value from the first test. Since in printing applications, the number of characters printed per unit area of ribbon was high (e.g., several hundred), Eq. (5.104) implied that for most of its life the ribbon's abrasivity would $0.64 K_1$. As a result, $0.64 K_1$ was used for K_{avg} . It was found that these modifications to Eq. (5.100) resulted in significant improvement in the agreement between theoretical wear rates and experimental ones. This is shown in Table 5.17.

In the second evaluation, printer tests were conducted using selected characters of known face area and ribbons inked with ink from the same batch and to the same ink weight. Four different ink formulations were used in these tests and one type of band material. The printer used for these tests was adjusted and monitored to insure consistent print conditions as well. Character height was measured as a function of usage and a single evaluation involved the use of several ribbons. An average wear rate was obtained from these individual measurements (Fig. 5.48). A different method was used to determine K_{avg} for the ribbons used in this evaluation. It was decided to measure K as a function of ink-life of the ribbon (Fig. 5.49). While all four inks exhibited linear relationships, the slopes were different and tended to be proportional to the abrasivity. Since the tests used to determine wear rate involved several ribbons, the average value that was determined from these curves was used for K_{avg} . The results of this study are shown in Tables 5.18 and 5.19. Because of the good agreement obtained, it was concluded that the modified model was adequate for the wear design.

It was concluded that the use of actual band material as wear specimens to obtain a wear coefficient was a major factor in the improvement in the model. However, since it was costly and difficult to obtain such specimens in the numbers required for developing ink, an alternative approach was needed. Wear volumes obtained for a number of candidate band materials and the 52100 steel specified in the ASTM tests are shown in Table 5.20. A comparison of these values suggested an alternative approach to guide development of ink, namely the use of two reference materials with different sensitivities to oxidative wear. With this approach, tests with the actual band material would only be required when values for K_{avg} were needed to estimate machine performance. 52100 steel and 420 SS were selected as the two reference materials. They were both easily obtainable as the spheres used in the test. While 52100 steel was considerably harder than

Table 5.17 Type Face Water Rates

Band speed	Band material	Depth wear rate h (10^{-3} in./ 10^8 hits)	
		Model	Printer test
70 in./sec	17-7pH/CH900 steel	20	22
	7C27MO2 steel	9	5
110 in./sec	17-7pH/CH900 steel	33	27
	7C27MO2 steel	15	10

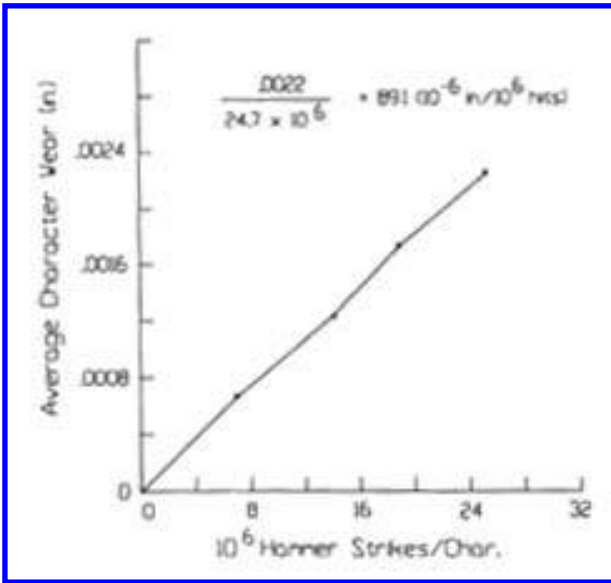


Figure 5.48 Wear curve for type face wear.

the 420 SS, the 420 SS seemed to be less affected by ink chemistry than the 52100. Also the 420 stainless steel was more representative of the materials being considered for the bands and very similar to the 7C27MO2 steel used in prior applications. This proved to be a very effective approach.

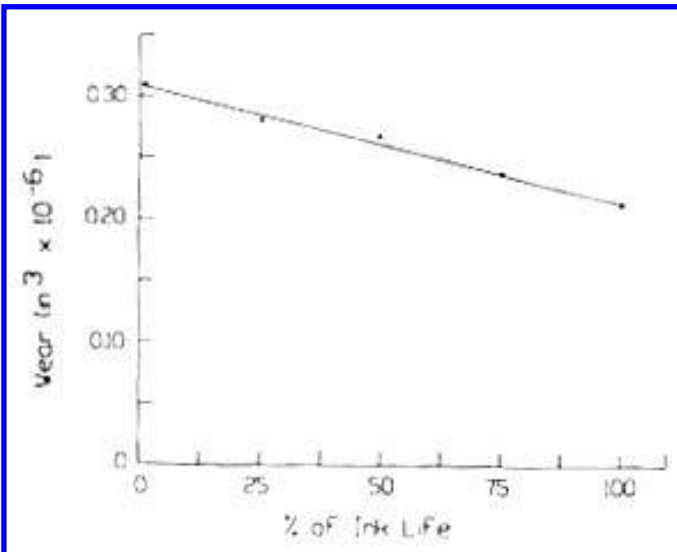


Figure 5.49 Results of drum wear tests to determine the effect of ribbon use on ribbon abrasivity.

Table 5.18 Wear Rates for the Letter O for Four Different Inks

Ink	Depth wear rate h (10^{-3} in./ 10^8 hits)	
	Model	Printer tests
A	8.41	8.91
B	6.06	5.22
C	1.22	1.40
D	0.66	0.45

Table 5.19 Type Wear Rates for Two Different Size Letters

Letter	Surface area (10^{-3} in. ²)	Depth wear rate h (10^{-3} in./ 10^8 hits)	
		Model	Printer test
O	1.457	6.06	5.22
I	0.912	9.69	7.38

A final step in the wear design approach was to verify performance in the machine. The agreement between the model and actual performance that was obtained is shown in Figs. 5.50 and 5.51.

Examinations of used ribbons from prior printers showed that the characteristics of fabric or ribbon wear were significantly different than type wear. The primary features of ribbon wear were large deformation of the individual fibers, deformation of the fiber bundles composing the weave, and rupture of individual fibers. These features can be seen

Table 5.20 Wear Volumes for Different Materials in the ASTM Test for Ribbon Abrasivity (ASTM G56)

Wear specimen	Hm (kg/mm ²)	Wear volume in 1 hr test (10^6 in. ³)										
		Ribbon										Paper ^a
		A	B	C	D	E	F	G	H	I	J	
52100	760	1.8	1.2	2.6	1.0	0.7	1.7	1.05	1.03	0.034	0.018	0.0003
7e27mo2	607	0.4	0.4	1.0	0.8	0.3	0.6					.0055
17-7pH/CH900	480	2.0	0.9	2.2	1.1	0.4	0.7					0.0115
416SS	480	0.9	0.8	1.3	0.7	0.5	0.6					0.0085
430SS	480	0.8	0.7	1.1	1.1	0.8	0.6					0.0085
420SS	607	0.2	0.4	0.4	0.3	0.1	0.1	0.31	0.15	0.040	0.018	0.0085
420SS	607	0.3	0.4	0.4	0.4	0.5	0.7					0.0075
422SS	607				0.5							

^aValues from a similar test using paper as the abrasive medium, showing the relative resistance of these materials to abrasion by small particles without oxidative effects.

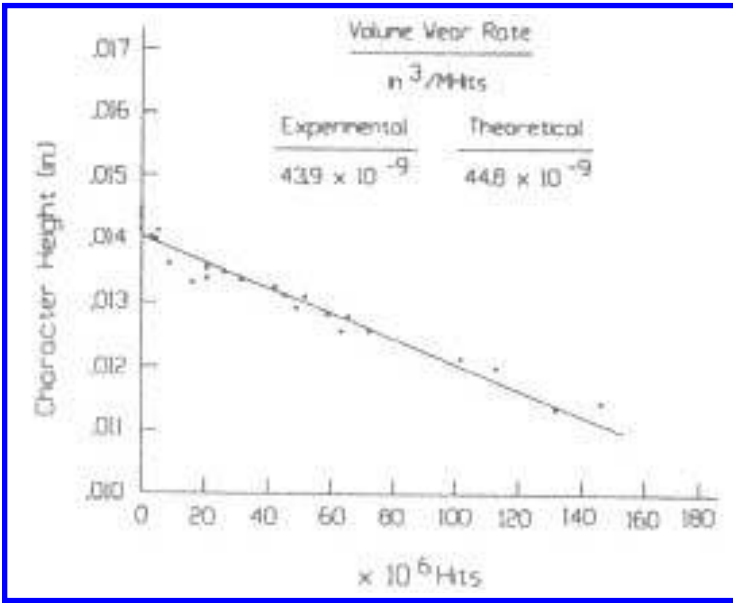


Figure 5.50 Wear curve for type face wear in a printer test.

in the micrographs shown in Figs. 5.52–5.55. Rupture of the fibers tends to occur in the later stages of life and after deformation. Near the end of life, broken fibers are predominant features of the wear pattern. There was no evidence of significant material loss being involved in the wear or any abrasion by the ink. From the morphology of the wear and from tests comparing inked with un-inked fabric, it had been concluded that the ink is a lubricant with respect to the fabric, tending to impart longer life to it. It had also been observed that the wear or damage on the type side was much more severe than on the paper side, as can be seen in the figures.

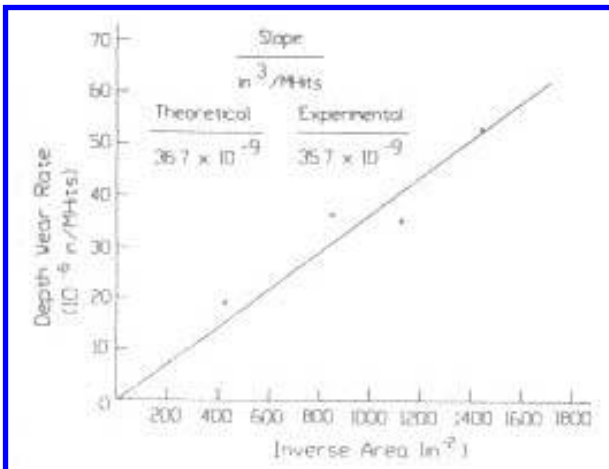


Figure 5.51 Depth wear rate as a function of type face area.

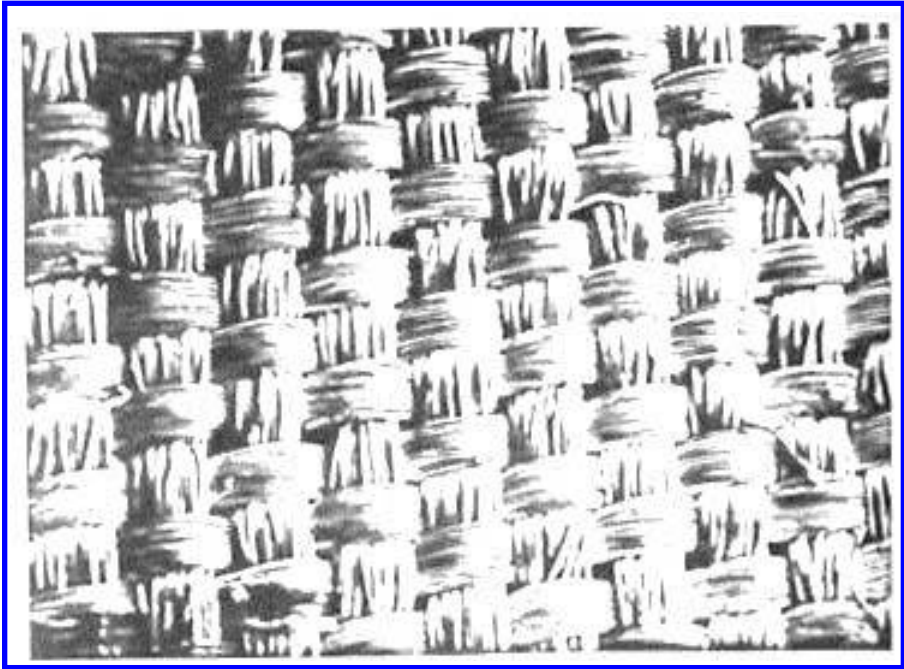


Figure 5.52 Unused ribbon.

Fabric life was defined as the amount of printing that could be done with a ribbon before a fold or a hole was produced in the ribbon. These conditions were determined by either inspection of the ribbon or the examination of print samples. For most situations, it had been found that folding was the more likely and limiting mode. While folding can be influenced by the design of the ribbon transport system, the state of damage to the ribbon when folding did occur was found to be similar in several printers. A typical end-of-life condition is shown in Fig. 5.55. Several parameters had been found to affect fabric life. Increases in print force, contact time, and tangential velocity appeared to reduce life, while the use of larger size fonts, rounded character edges, and smooth character surfaces tended to increase life.

A model, which was consistent with these observations, had been developed and had been used in the resolution of fabric life problems associated with edge and roughness conditions. This model provided the following relationship for fabric life, L_f :

$$L_f = \frac{1.6\Gamma A_t A_f}{k_r K_c P_{\max} V} \quad (5.105)$$

$$K_r = 1 + \frac{\Phi}{z_r} \quad (5.106)$$

$$K_c = 1 + \frac{z_e}{R} \quad (5.107)$$

where A_t is the average type face area; A_f , the surface area of the ribbon used; P_{\max} , the

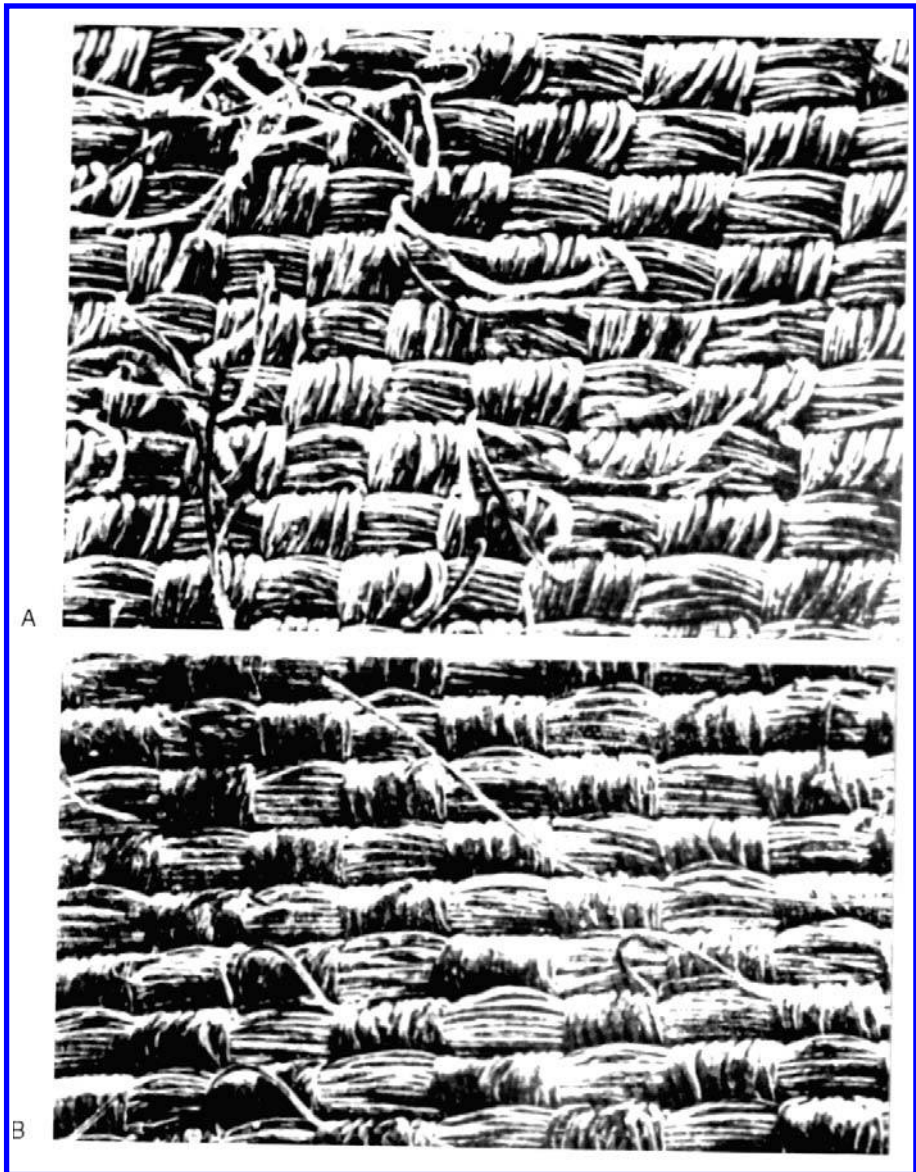


Figure 5.53 Used ribbon before end of life. “A”, band side; “B”, paper side.

maximum print force; v , the relative tangential speed between the type and the ribbon; Γ , a material life parameter for the ribbon; R , the radius of the leading edge of the character; Φ , a roughness parameter for the face of the character; α_f and α_e , experimental parameters found to be 4 $\mu\text{in.}$ and 0.02 in., respectively. For the surface profile shown in [Fig. 5.56](#),



Figure 5.54 Ribbon fiber damage. “A”, band side; “B”, paper side.



Figure 5.55 Ribbon wear at end of life. “A”, band side; “B”, paper side.

Φ was defined as

$$\Phi = 1.27\Omega_0 \left[\frac{\Omega}{\Omega_0} \left\{ 1 - \cos \left[\sin^{-1} \left(\frac{\Omega_0}{\Omega} \right) \right] \right\} - \sin^{-1} \left(\frac{\Omega_0}{\Omega} \right) \right] \quad (5.108)$$

This roughness parameter was developed to account for the blunting of asperities that processes, which were frequently used to finish type surfaces, such as buffing or

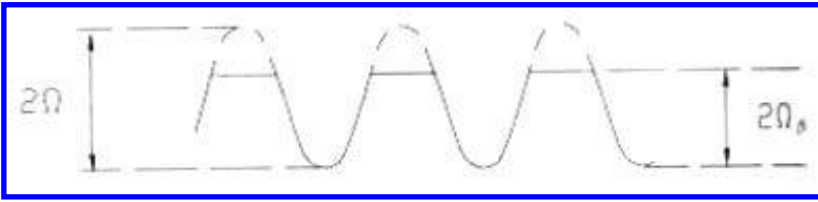


Figure 5.56 Surface profile used in the model for ribbon damage.

polishing, can produce. Φ can be approximated to within 30% for most surfaces by half the CLA value.

The model assumed that fabric life was directly related to the wear of the fibers. The hypothesis was that once these fibers wore to a characteristic amount, fracture of the fibers was likely to occur. This would result in degradation of the structural integrity, which allow folding to occur. It was inferred from the predominance of deformation features in the wear that the wear process could be viewed as a form of single-cycle deformation wear, where the deforming element was the type. Therefore, it was assumed that fiber wear volume was proportional to both load and sliding distance. Since many individual fibers were involved in a single printing action, it was assumed that the product of an average depth of wear for the fiber, h , and the face area of the character could approximate the wear volume. These two assumptions resulted in the following:

$$h = KPS \quad (5.109)$$

where K is a wear coefficient; P , the average pressure during the contact; and S is the amount of sliding in a print cycle. Since very little variation in the slip factor was found in analysis of type wear situations, it was assumed that S was proportional to vt_c . It was further assumed that the radius of the leading edge and surface roughness of the characters would effect the deformation of the fibers and the load distribution across the fibers. It was further assumed that two factors, K_e and K_r , could describe these effects. The relationships used for both of these are those given by Eqs. (5.106) and (5.107).

The forms used for these factors were selected because of their simplicity and the fact that they would approach values of 1 as the surface got smoother and the edges became more rounded. The selection of the radius as the parameter to be used for the one factor was based on general engineering concepts. It was felt that as the radius became larger there would be a more even distribution of the load across the fibers and that fiber displacements in the direction of motion would be less, because of the more favorable contact between the character profile and the fibers. These trends are also suggested by the behavior of the coefficient of friction between ribbon and sliders of different geometries. This is shown in Figure 5.57. Similar effects were postulated for surface roughness. Since asperity spacing of typical surfaces was often comparable to or larger than fiber diameters, asperity size and spacing could affect the load on the fibers and the tangential displacement of the fibers. Figure 5.58 illustrates this interaction. Because of these effects, wear would increase for surface conditions that resulted in greater penetration. It was decided to use the average asperity penetration that a surface could produce, Φ , as the parameter for this. Profilometer characterization of type surfaces indicated that these surfaces could be approximated by a sine wave prior to any post-forming buffing or polishing. The basic sine characteristic tended to remain after buffing or polishing. However, the tips of

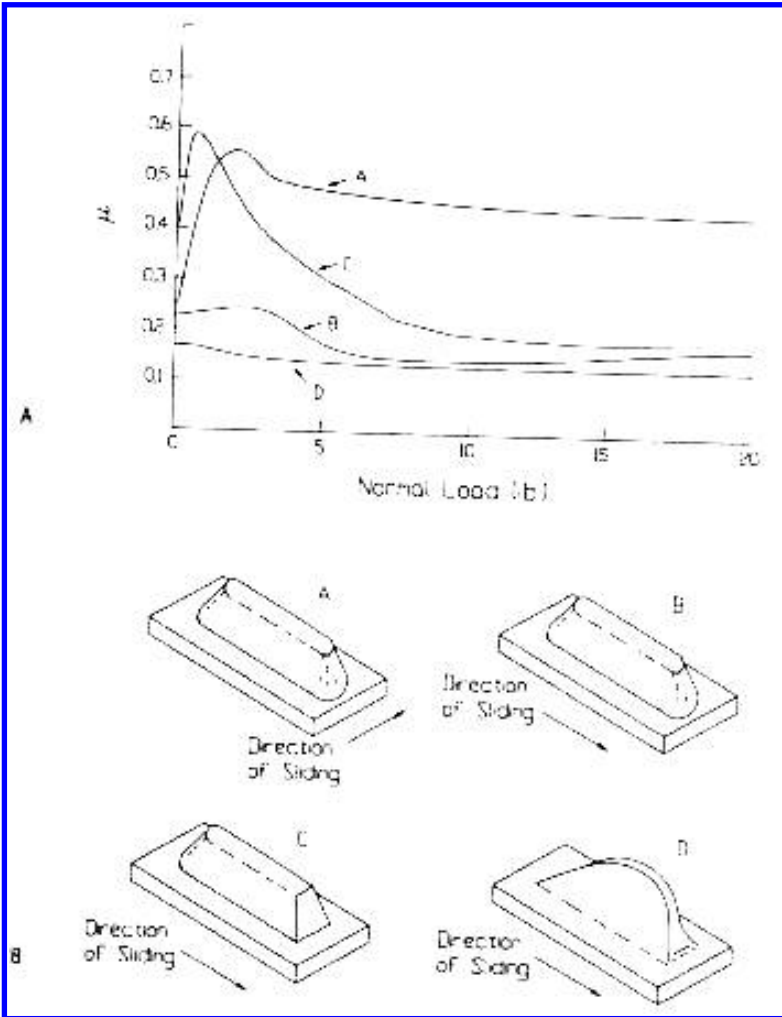


Figure 5.57 The effect of font shape on the coefficient of friction against a ribbon surface. “A” shows the friction behavior as a function of load. “B” shows the different shapes and sliding directions used for the four curves. (From Ref. 13.)

asperities tended to be flattened. This condition was modeled to obtain Φ for these surfaces and Eq. (5.108) resulted.

Approximating the print pulse by a half-sine wave, the following was obtained:

$$h = 0.64 K_c K_r \frac{P_{\max}}{A_t} \nu_c N \tag{5.110}$$

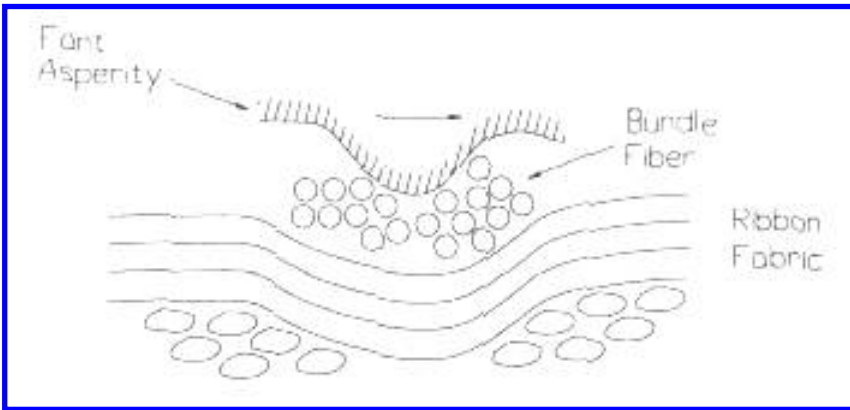


Figure 5.58 Asperity–fiber interaction.

wherein N is the number of print cycles per unit area of the ribbon and P_{\max} is the peak value of the force pulse. Since end of life occurs when h reaches a critical value, h_c ,

$$h_c = 0.64KK_cK_r \frac{P_{\max}}{A_t} \nu t_c \frac{L_f}{A_f} \quad (5.111)$$

To obtain Eq. (5.105), h_c/K were combined into a single empirical coefficient, Γ .

When this model was first developed, it was evaluated by extensive printer tests in which the ribbon was in the form of a narrow strip, moving between reels. These tests had focused on the effects of character parameters and the data obtained were used to determine a single set of values for the coefficients. A summary of that data is shown in Table 5.21. Limited data from a higher speed application were also available and this was examined for consistency with model. Reasonable agreement was obtained. (See Table 5.22.)

This model was also evaluated using sliding wear tests, performed with a reciprocating ball / plane apparatus. For these tests “.”s (periods) were cut from print bands and used as the ball specimen. A section of ribbon, backed by paper, was stretched across a steel platen. A normal force of 1000 g. and a 1 in. stroke were used. The test was stopped periodically and the ribbon surface examined for wear. The number of cycles required to produce damage that was characteristic of end of life was determined in this manner for each of the periods tested. When these data (Table 5.23) were analyzed using the model and the coefficient deduced from the printer tests, a correlation coefficient of 0.86 was obtained. Based on these evaluations, it was decided to use this model in the wear design.

In the new application, the ribbon was in the form of a wide sheet being moved and controlled by rollers above and below the print band. Band speeds were also considerably higher (up to five times those in prior printers). Because of these differences, it was decided to verify the model under these new conditions, as soon as possible. When a prototype printer became available, printer tests were performed at several band speeds. Much lower fabric life was obtained than anticipated (i.e., projected by the model). From failure analysis of these ribbon samples, it was recognized that the different form of the ribbon resulted in the lay of the warp (the higher fiber bundles) being perpendicular to the motion of the band. The warp was parallel to the band motion in prior applications. These two conditions are illustrated in Fig. 5.59. It was speculated that

Table 5.21 Ribbon Life Data from a Low Speed Printer

Band description			Printer condition	Ribbon life (10^6 characters)	
Face area (in. ²)	Φ (μ in.)	R (in.)		Typical	Range
Ribbon angle 2 50'					
0.0012	6	0.002		15	6-25
0.0014				18	10-28
0.0012	2	0.002		25	13-38
0.0014				30	15-45
0.0012	1	0.004		45	23-68
0.0014				54	27-81
0.0012	1	0.006		60	30-90
0.0014				72	36-108
Ribbon angle 2 10'					
0.0012	2	0.002		17	9-26
0.0014				20	10-30
0.0012	1	0.004		30	15-45
0.0014				36	18-54
0.0012	1	0.006		40	20-60
0.0014				48	24-72
Ribbon angle 2 10' reduced print force (10%)					
0.0012	1	0.006		44	22-66
0.0014	1	0.004		40	20-60

the new condition resulted in higher fiber deformation and a smaller value of r , because of an increased tendency to grab fibers in this orientation. To verify this, printer tests were performed with the fabric rotated. A significant improvement in fabric life was obtained. End-of-life values were close to those predicted using the original value for Γ (Fig. 5.60). It was concluded that the model was still valid and could be used in the wear design. Γ was now considered to be constant for a given fabric and orientation, which needed to be determined empirically.

Because folding was influenced by machine conditions, it was necessary to determine Γ for different ribbon materials in a printer test. This model provided the justification

Table 5.22 Ribbon Life Data from a Higher Speed Printer

Band description			Ribbon life (10^4 characters)	
Face area (in. ²)	Φ (μ in.)	R (in.)	Model	Range
0.0018	4	0.003	9.9	8.9
0.00177	4	0.004	12.8	> 8.9
0.00170	1	0.007	19.2	16.5
0.00169	4	0.004	12.1	> 7.5
0.00108	4	0.004	7.7	7.5

Table 5.23 Ribbon Life Obtained with a Reciprocating Ball/Plane Apparatus Using Periods “..” as the Slider

Description of period			
Diameter (in.)	Φ (μ in.)	R (in.)	Cycles to failure
0.034	1.1	0.4	> 1000
0.031	15.4	0.1	> 1000
0.028	16.5	0.14	> 1000
0.026	4	0.25	> 1000
0.030	0.4	0.005	> 1000
0.030	25.4	< 0.001	10–50
0.025	10.4	0.002	10–50
0.037	14.0	0.0005	< 10
0.023	9.5	0.005	100
0.032	2.1	0.004	500
0.031	4.1	0.005	200
0.034	10.8	0.002	50–200
0.030	14.3	0.008	200
0.025	4.5	> 0.010	200
0.041	12.0	0.010	1000
0.038	3.7	0.001	< 1

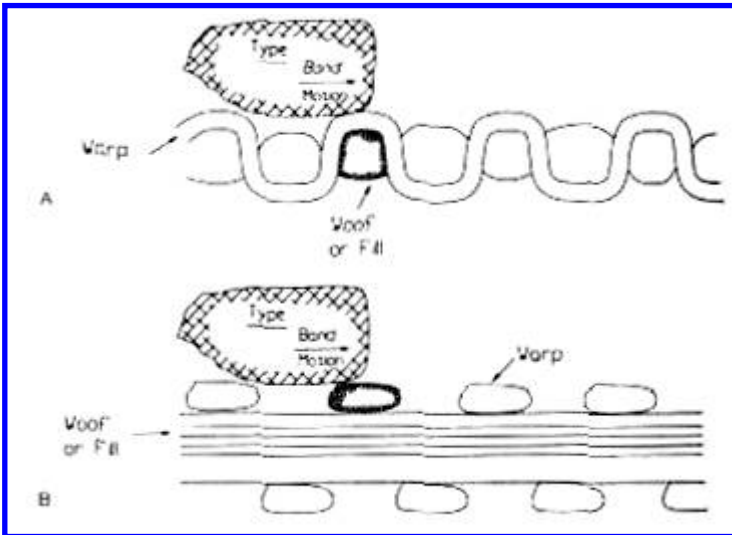


Figure 5.59 The effect of font / fabric interaction as a result of fabric orientation. “A” shows the condition in the prior application. “B” shows the condition in the new application.

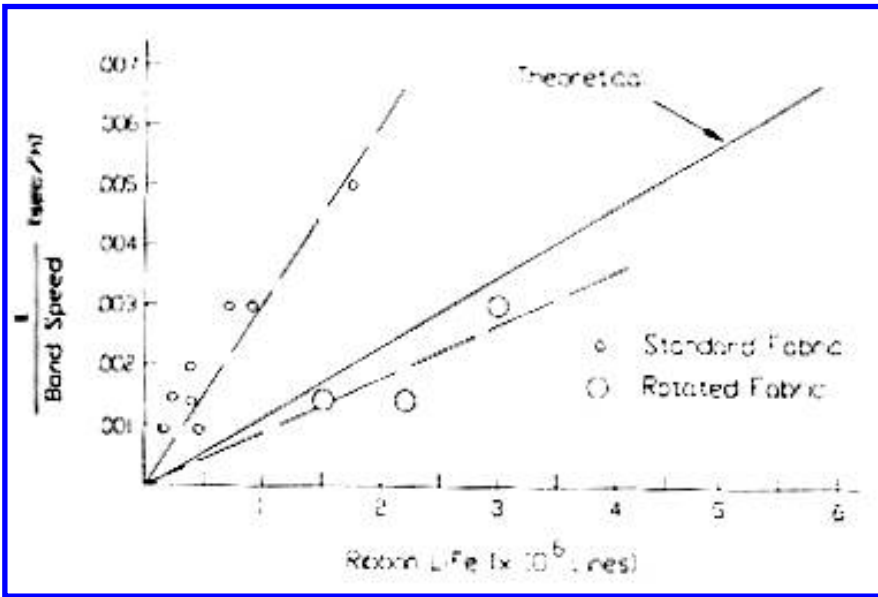


Figure 5.60 The effect of fabric orientation on ribbon fabric life.

for conducting these tests on small ribbon sections. This significantly reduced testing time and enabled the evaluation of different fabrics when only small samples were available. The background of the model used for ink-life was similar to the background for the models of type and fabric life. The model for ink-life provided the following relationship that was used in the wear design:

$$L_t = 20.63 \frac{A_f}{A_t} K^* \quad (5.112)$$

where K^* is an end-of-life ribbon-ink coefficient determined by a laboratory test. The relationships between K^* and various printing parameters, such as print force, were also available.

These models were used to assess the effect of changes in printing parameters, the evaluation of different design options, and to guide the development of the band and ribbon. This approach resulted in the development of a new band design, a new ink, and a new fabric, which provided the performance required. A verification test was performed for the final design of these two components.

5.12. MAGNETIC READ HEAD

This case study illustrates all the elements of wear design. In particular, the wear design involved some unique elements. These included the need to develop two models (one for the wear mechanism and the other for the device), the use of a wear test to evaluate design parameters other than material properties, and an extensive system analysis effort to characterize the field environment.

The basic features of the magnetic read head are shown in Fig. 5.61. It utilized a Hall Effect sensor, which was deposited on the interior surface of one of the pieces used to form the head. This piece was referred to as the substrate, while the other as the closure. The thin film was sensitive to mechanical damage and corrosion and would be destroyed if exposed to the atmosphere or rubbing. Therefore, the active element was located below

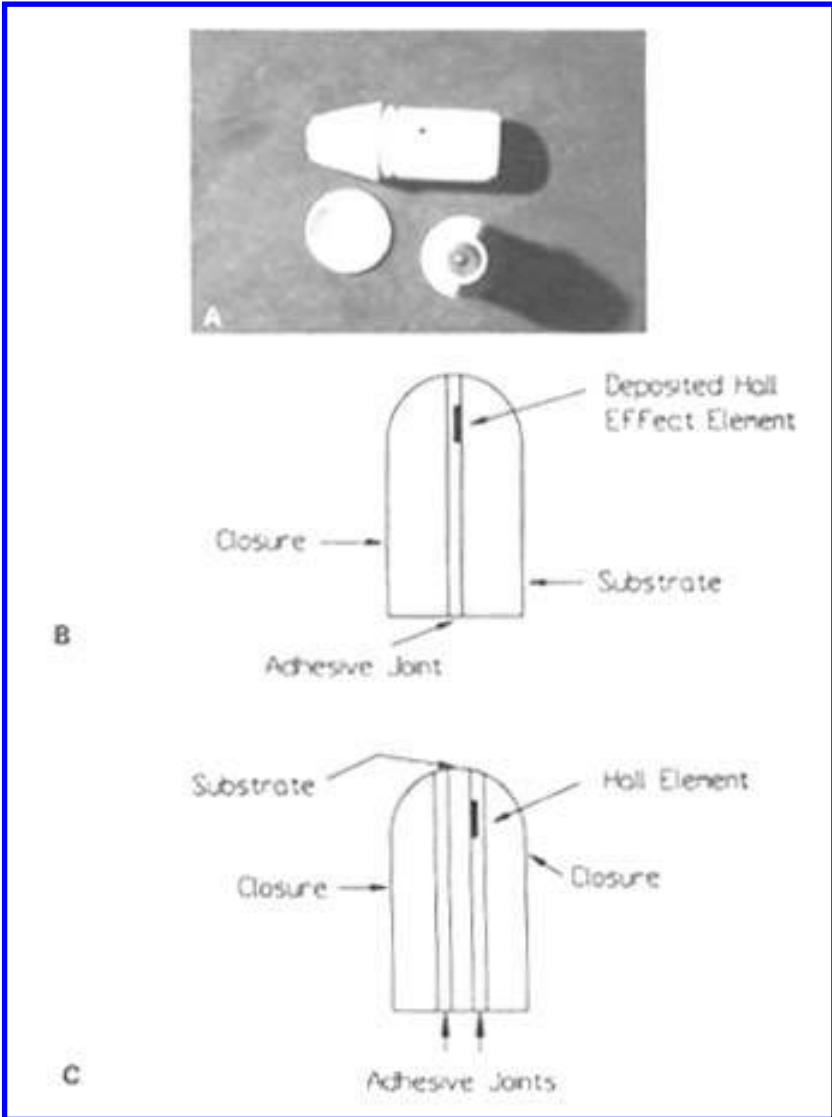


Figure 5.61 Photograph of a magnetic read head, “A”, “B”, and “C” show cross-sections of two designs for the active region. For the design in “B”, the closure and substrate material could be the same or different. “C” was called a sandwich design and the substrate and closure materials were different.

the surface. These heads were intended to read strips of magnetic tape that would be mounted on a variety of surfaces and objects (e.g., containers, documents, labels, tags, cards, etc.) that could be scanned with a hand held wand or pulled through a slot reader. In the former, the head was mounted in a gimbal and spring loaded to control the load and alignment. In the latter, guides and pressure pads were used to control the load and the alignment as the document was pulled through the slot reader. These devices were to be used in office, retail, and manufacturing applications in several different systems and expected to perform satisfactorily for tens of thousands of scans over several years of operation. An individual magnetic strip in these systems was expected to be read less than 100 times in its life.

Because silicon (Si) provided an appropriate substrate for the deposition and operation of the Hall element and was readily available, the first prototypes used Si as the substrate and closure material. During the functional evaluation and development of these devices, it was observed that the heads tended to wear sufficiently so that the element was damaged or destroyed. To improve this situation, it was decided to use a harder material for the closure. After some cut-and-try approaches, sapphire was selected as the closure material. With sapphire, wear behavior was satisfactory for much of the functional development of the head. Since these heads were to function in uncontrolled and possibly hostile environments, there was concern with the effect that contaminated surfaces would have on the head's ability to read the strip. These functional concerns led to the testing of heads on deliberately contaminated surfaces and surfaces that were exposed for prolonged periods in several industrial environments. Because of the severe wear observed in these tests, the wear life of these heads became a major concern. While it was obvious that the wear resistance of the heads needed to be improved, it was not known how much an improvement was needed. There was no experience with performance of these type of devices in these uncontrolled and potentially hostile environments. Moreover, most computers and computer peripherals were designed to operate in either a controlled environment, such as a computer room, or a relatively clean and air conditioned office environment. It was not known if the conditions of the tests were too severe, representative, or mild, compared to those of the intended applications. At this point in the development of these heads, a wear design approach was adopted. The specific and more immediate goal of the wear design was to develop an acceptable design for this application. A secondary goal was to establish the basis for a general methodology that could be used in the wear design of other devices intended for these environments.

While sliding abrasive wear was considered to be the probable wear mode, the first step was to determine the wear mode. This involved a review of the conditions of the prior tests, examination of worn heads, and laboratory wear tests. From these activities, it was concluded that the wear mode for clean and contaminated tape surfaces was abrasion. Wear scars from clean tape were highly polished and consistent with the wear that would be expected with fine (small) abrasive particles, such as the magnetic particles in the tape. By coating the tape with a variety of abrasives, wear scar morphology and wear rates similar to those observed in the contamination tests were obtainable in the laboratory tests. The next step was to develop a standard test that could be used to evaluate and select materials and designs to insure adequate performance in the field.

These preliminary tests had shown that there was a wide range in morphology and wear rate that could be achieved by using different amounts and types of abrasive. One way of selecting a standard test that could be related to field performance would have been to do field tests for several different environments that were representative of the application and to correlate these with a proposed laboratory test. However, there was

not time for such an approach, so an alternate approach was taken. This was to determine relationships for the abrasive wear coefficient in terms of the amount and type of abrasive on the surface. These relationships could then be used to relate the results of a standard test to field performance, if the description of the contamination in the field was known. Such a model was developed and verified (14). At the same time, contamination samples were obtained from the environments that were representative of the potential application. This was an extensive undertaking and involved sampling of a variety of different environments in five different industries (15). Ultimately, it was possible to develop a standard test to measure material properties, which was based simply on reproducibility, ease of implementation, and duration.

The next step in the wear design was to develop a model for the wear of the head, using abrasive wear concepts in addition to the effects of contamination. This model included the effects of size, structure, and load on head wear and life. Coefficients and relationships for this model were determined in laboratory tests. The overall model was verified in field tests prior to the selection of the final design. From this effort, a new head design was successfully developed and used. There were several additional benefits from this approach as well. The analytical nature of models developed enabled projections to be made for performance in the corrosive environments which is likely to be encountered in some of the installations. The standard test that was developed was used to evaluate manufacturing processes and also as a quality control tool. The basic approach was also applied to other devices operating in a contaminated environment.

The wear characteristics of magnetic tape are similar to those of paper and ribbon. While these materials can wear very hard materials, their wear resistance is poor. The amount of wear or damage that would occur to the tape was small in the application because of the low usage an individual strip received. The wear on the head was the result of contact with many individual strips. To simulate this aspect, it was decided to use the wear apparatus used in ASTM G56 for ribbon abrasiveness, which was available. (See Sec. 9.2.12 of MWFT2E). The tape replaced the ribbon and either material samples or actual heads were used as the wear specimens. Test parameters were modified to simulate the application. Drum speed of 36 cm / sec and a specimen speed of 0.25 mm / rev were selected. This combination resulted in adequate separation of the wear tracks at a sliding speed representative of the application. A test load of 50 g generally was used, since the nominal load in the application was 40 g.

Heads were used as the wear specimens in the initial series of tests to investigate the mode of wear. The surface of the tape was coated with a variety of abrasive materials, including AC Fine and AC Coarse Test Dusts (different size distributions of sand particles) and powdered alumina. It was found that wear morphology similar to those obtained in the functional tests could be obtained and that the abrasive action of even a small number of these particles significantly increased the wear. Typical results are shown in Figs. 5.62 and 5.63, along with the micrographs of the contaminated tape surfaces (Fig. 5.63). The effect of sliding distance and load on wear was also investigated to see if the typical linear wear relationship for abrasion

$$V = KPS \tag{5.113}$$

was followed. In this equation, V is the volume of wear; K , a wear coefficient dependent on both the abrasivity of the surface and the wear resistance of the abraded material; P , the load; and S is the distance of sliding. This was found to be the case (Figs. 5.64–5.66). It was concluded that the wear mode was abrasive and that Eq. (5.113) could be used.

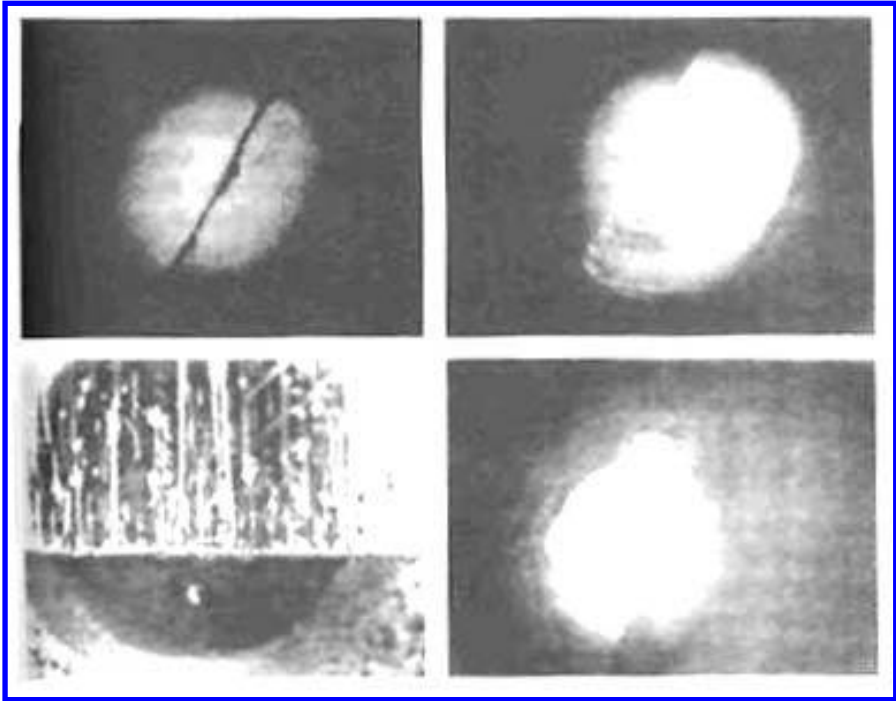


Figure 5.62 Heads worn in preliminary field tests. (From Ref. 14, reprinted with permission from Elsevier Sequoia S.A.)

The next step in establishing a model for this wear situation was to relate K to the amounts and types of abrasives on the tape surface.

The general wear situation was viewed as shown in Fig. 5.67. Part of the time the head would be in sliding contact with the tape surface; part of the time it would be sliding on the particles. As the amount of abrasives increased, there would be less and less contact with the tape and K would increase. At some point contact with the tape would be eliminated and K would no longer increase with additional amounts of abrasives. It was hypothesized, therefore, that the effective wear coefficient for the surface, K , could be defined in terms of the surface coverage of the abrasive by means of the following equation:

$$K = (1 - \delta)K' + \delta K'' \quad (5.114)$$

$$\delta = \frac{\alpha}{\alpha_0} \quad (5.115)$$

where K' is the coefficient for clean tape; K'' , the coefficient for a surface completely covered by the abrasive; α , the surface density of the abrasive (e.g., g / mm²); α_0 , the minimum surface density required for saturation (i.e., the point at which additional amounts of abrasive did not increase K). Test results provided support for this concept,

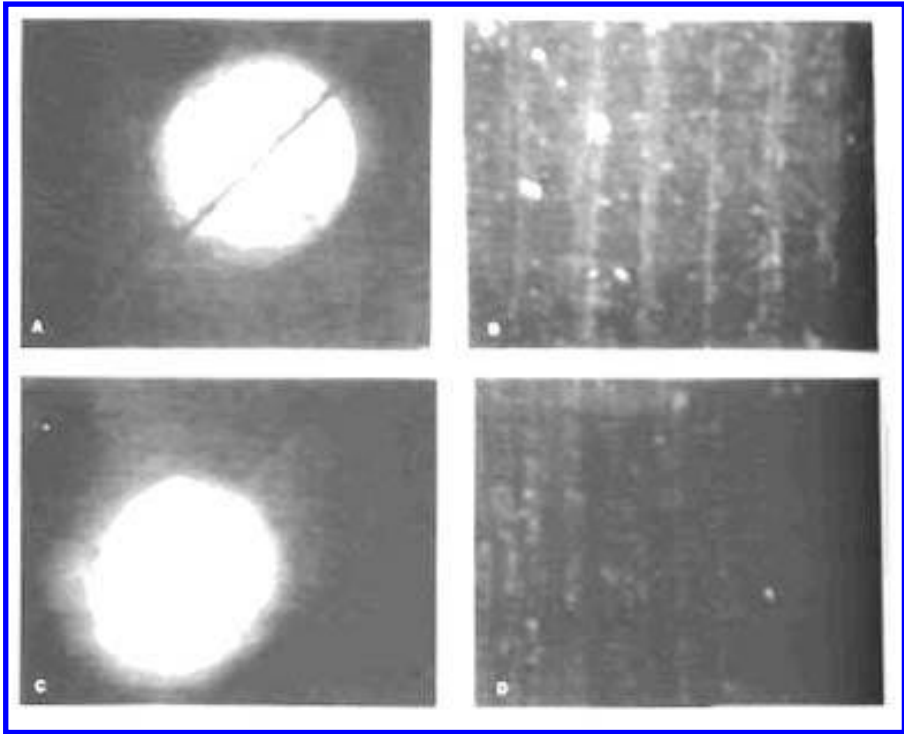


Figure 5.63 Heads worn in laboratory tests, using contaminated magnetic tape. “A” shows a head worn by the AC Fine Dust/Gelatin coating on magnetic tape, shown in “B”. “C” shows a head worn by magnetic tape, shown in “D”, which is coated with loose AC Fine Dust. (From Ref. 14, reprinted with permission from Elsevier Sequoia S.A.)

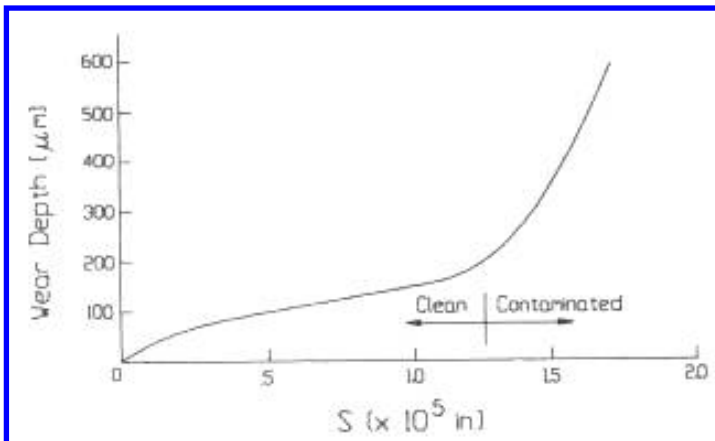


Figure 5.64 The effect of contamination on head wear. (From Ref. 14.)

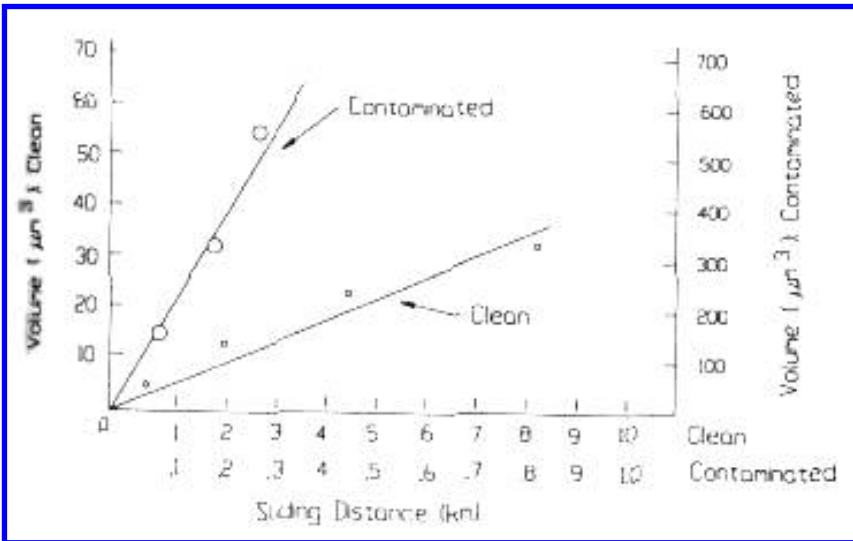


Figure 5.65 Wear volume as a function of sliding distance on clean and contaminated magnetic tape. (From Ref. 14.)

as shown in Fig. 5.68. α_0 is primarily related to the ability of the particles to prevent contact with the surface of type. Therefore, it was conjectured that its value could be a function of size and density of the abrasive. Tests were conducted with different size abrasives to investigate this possibility. The results of those test indicated that α_0 was

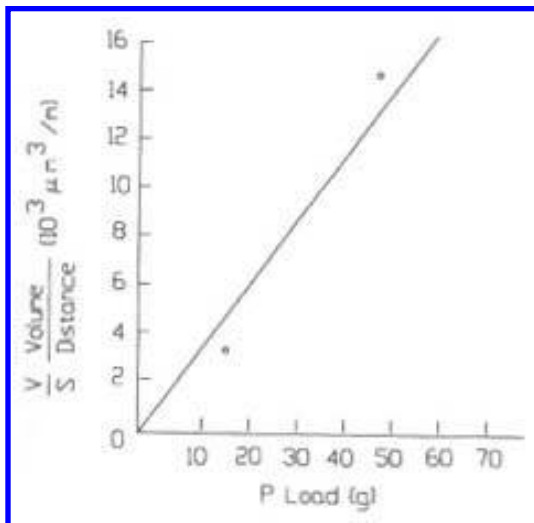


Figure 5.66 Wear volume as a function of load. (From Ref. 14.)

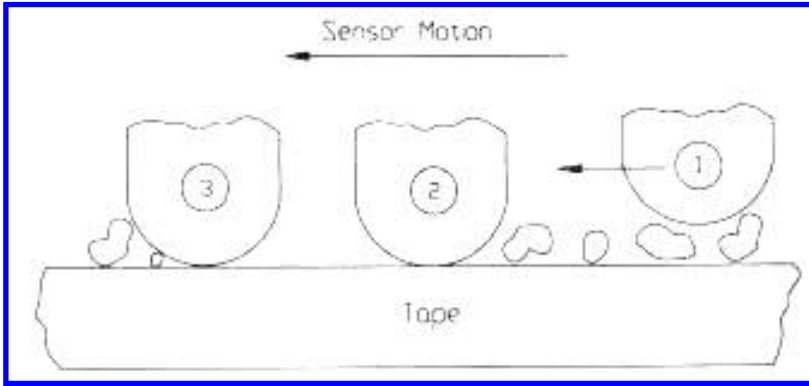


Figure 5.67 Contact conditions with contamination. (From Ref. 14.)

approximately

$$\tau_{\max} \propto (W/w)^{-1} \propto W^{-1} \quad (5.16)$$

$$W = (2rh_s)^{1/2} + h_s \cot \Phi \quad (5.17)$$

where D is the average particle size and ϕ is the ratio of the abrasive's density to that of SiO_2 .

From abrasive wear theory, it was known that K'' would depend on the shape, size, and hardness of the particle. While this was the case, it was not considered necessary to explicitly treat the effect of shape, since angular-shaped abrasives, which simulated most field abrasives, were used in the laboratory tests to determine the coefficients.

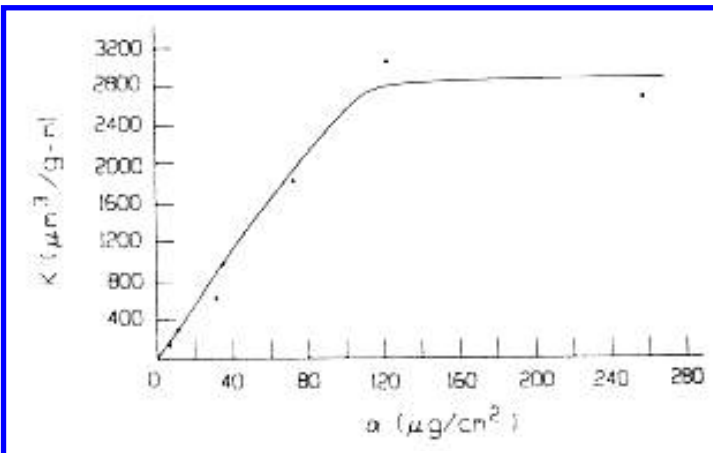


Figure 5.68 Abrasive wear coefficient as a function of the amount of contamination. (From Ref. 14.)

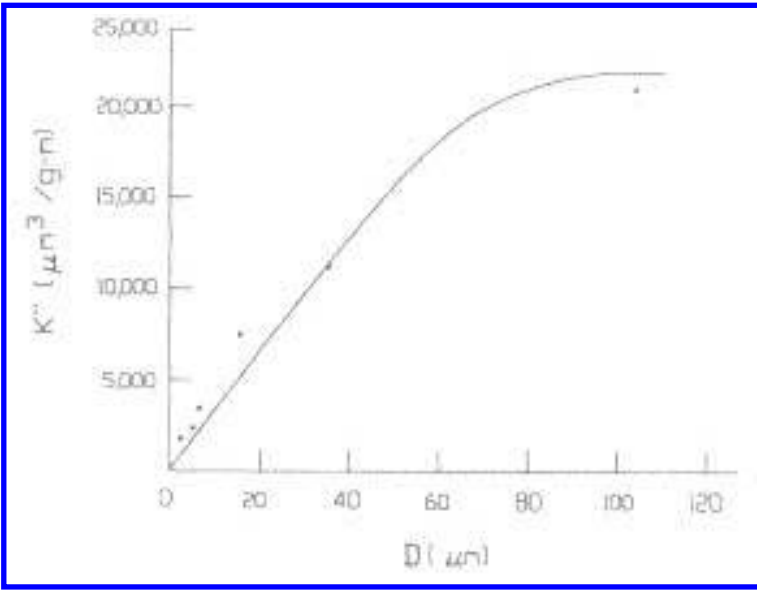


Figure 5.69 The effect of particle size when the abrasive is harder than the abraded surface. (From Ref. 14.)

Several general trends of abrasive wear were used to relate K'' to size and hardness. These were:

- (1) Only hard particles tend to act as abrasives against hard surfaces.
- (2) Abrasivity is proportional to particle size up to some limiting value, above which it is independent of size.
- (3) There is a transition in abrasivity when the hardness of the abraded surface approaches that of the abrasive; above and below this condition, abrasivity tends to be constant.

These concepts were evaluated in a series of tests and general agreement with them was found for this wear situation (Figs. 5.69 and 5.70). By implication, these concepts indicated that the effect of particles of the same size but different composition would be the same, provided they were both either harder or softer than the abraded surface. The following relationships were used to describe the effect of different particles on wear. For $H_{m,abrasive} / H_{m,abraded} \geq 1$,

$$K'' = K''_H, \quad D \geq D_0 \tag{5.118}$$

$$K'' = K''_H \frac{D}{D_0}, \quad D < D_0 \tag{5.119}$$

For $H_{m,abrasive} / H_{m,abraded} < 1$,

$$K'' = K''_S, \quad D \geq D'_0 \tag{5.120}$$

$$K'' = K''_S \frac{D}{D'_0}, \quad D < D'_0 \tag{5.121}$$

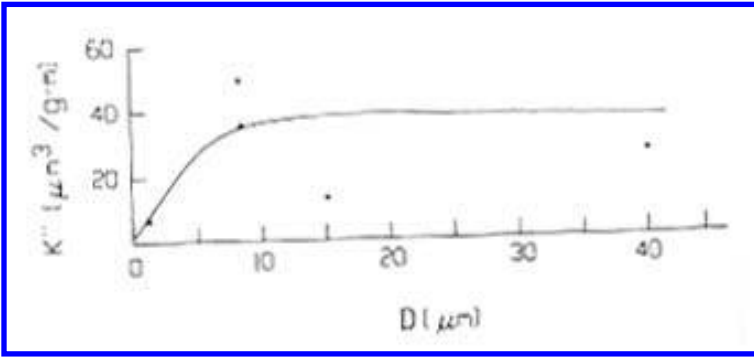


Figure 5.70 The effect of particle size when the abrasive is softer than the abraded surface. (From Ref. 14.)

where H_m is the hardness; D , the average size of the abrasive; D_0 and D'_0 , the transition sizes; and K is the maximum abrasivity for the two hardness conditions. Wear tests with a variety of abrasives and wear specimens were performed to determine values for D_0 and D'_0 . D_0 was found to be $80 \mu\text{m}$; D'_0 , $8 \mu\text{m}$. (Figs. 5.69 and 5.70). These tests also indicated that the ratio of K''_H / K''_S was approximately 50:1.

With these relationships, it was possible to establish equivalence of different states of contamination relative to a specific abraded material, to compare the relative abrasivity of different situations, and to use a limited number of standard test conditions to determine K for different materials. In fact, two such test conditions were used. One was for clean tape, which provided the value for K' and another for a saturated coating (i.e., $170 \mu\text{g} / \text{cm}^2$ of AC Fine Test Dust), which provided a value for K'' , relative to SiO_2 . D for this dust mixture was approximately $15 \mu\text{m}$. This test condition was chosen for several reasons. One was the use of a saturated condition tended to minimize scatter. A second was that AC Fine Test Dust was an easily available controlled test dust. The third was that AC Fine Test Dust was 90% SiO_2 with a particle size range 1– $80 \mu\text{m}$, which was representative of the majority of the contamination found in the field survey. Several methods had been explored to coat the tape and finally a convenient and repeatable technique was found. It consisted of spraying the dust in a gelatin mixture. Before this method was selected, numerous tests were performed to insure that the gelatin did not affect the abrasive action.

These two standard tests were used to determine values of K' and K'' for candidate materials. The field survey had shown that most of the abrasive contamination was similar in hardness to SiO_2 . Occasionally, harder abrasives were found and typically these were alumina. Therefore, most of the materials evaluated were harder than SiO_2 , because of the reduction in wear coefficient that occurs when the abraded surface is harder than the abrasive. Data for some of these materials are shown in Table 5.24. The standard tests were also used for the selection and evaluation of several design parameters, other than material selection.

To verify the model for K , three verification tests involving different abrasive conditions were performed. One was conducted at a test site. The second was in a dust chamber, which circulated AC Coarse Dust. The third test used a dust mixture that simulated a typical field condition and the drum apparatus. For each of these, the contamination on the surfaces of the tapes was characterized in terms of size, amount, and type

Table 5.24 Abrasive Wear Coefficients of Different Materials in the Standard Test

Material	Wear plane	Sliding direction	Wear coefficient ($\mu\text{m}^3/\text{g}\cdot\text{m}$)	
			K'	K''
Sapphire single crystal	(10 $\bar{1}0$)	[0100]		20.4
		[0001]		16.9
	(0001)	[$\bar{1}$ 120]	0.3	48.5
		[3300]	1.4	54.7
	(1120)	[0001]	0.03	3.6
	(1120)	[1100]		24.6
	(3032)	[1210]	0.003	64.0
		[2023]	0.3	86.5
		[0001]	0.002	39.7
	(0110)	[$\bar{2}$ 110]	0.002	30.4
Tungsten carbide			0.5	44.8
Ceramic (Al_2O_3)			0.06	20.7
Titanium carbide			17.5	30.4
Natural diamond			0.004	0.01
52100 steel (Rc 60-62)			30	8000
Silicon			=30	=8000

Source: Ref. 14.

and the model was used to determine a value for K for that situation. These values were compared to values for K determined from the wear relationship (Eq. (5.113)). Good agreement was found (Table 5.25).

Since the general wear patterns that were observed on the proposed head designs were more complex than the simple abrasion of a spherical surface, it was necessary to develop a model for the abrasive wear of the head. The general wear pattern that was observed is shown in Fig. 5.71. This pattern was indicated by theoretical considerations. (See Fig. 5.62.) Preferential wear would occur when one member was softer than the other. Local increased wear at the interfaces would result from chipping of the edges. It was observed that the combined effect (given by $h_0 + H_0$) tended to achieve a stable value with sliding (use) (Fig. 5.72). This behavior suggested that the magnitude of the step was controlled by abrasive size. With the development of this step, fewer particles would contribute to the wear in this region, since the tendency would be for particles smaller than the step to move through this region with little or no interference. It was therefore assumed that once this stable condition was achieved, the harder material would support the load. With this assumption, it can be shown that

$$H = (h_0 + H_0) + \left[\left(\frac{\varepsilon}{\pi R} \right) PKS \right]^{1/2} \quad (5.122)$$

ε is 1 for designs in which both halves are of the same hardness or have the same wear coefficient. It is 2 for those conditions in which there is a difference in hardness or wear coefficient. K is the abrasive wear coefficient for the harder material. Since the Hall element was located at some depth below the surface, the end-of-life condition was defined as H equal to \mathbf{H} , where \mathbf{H} was somewhat less than the depth of the element to insure continued corrosion protection. It was determined that approximately 50 μm . was required to maintain adequate corrosion protection.

Table 5.25 Theoretical and Experimental Values of the Abrasive Coefficient K for Several Different Tests

Test	K ($\mu\text{m}^3/\text{g}/\text{m}$)	
	Theoretical	Experimental
Factory environment ^a		
52100 steel		
Horizontal surface scanning	640	504
Vertical surface scanning	74	62
Si-sapphire		
Horizontal surface scanning	4	5
Vertical surface scanning	0.5	0.7
Dust chamber	14	11
Simulated factory environment ^b		
Sapphire-sapphire sensors		
Hand scanner	6	5
Slot reader	0.7	0.6

^aGlass particles and fibers were a major contaminant in this location.

^bDust mixture used to simulate factory environment: 90 wt% steel particles, mean size 39 μm ; 3 wt% SiO_2 , mean size 32 μm ; 3 wt% Al_2O_3 particles, mean size 48 μm ; 4 wt% calcite particles, mean size 19 μm .

Source: Ref. 14.

While $(h_0 + H_0)$ was independent of material properties within a design type, it was found to be dependent on other factors, such as the amount and size of the abrasives involved, the orientation of the gap or interface to the scanning direction, and the width of the adhesive joint or gap. Tests were done using a variety of abrasive conditions and sliding directions to evaluate the effects of these factors. The effect of sliding direction found in these tests for two types of design is shown in Fig. 5.73 (see p. 268). These tests were done not only to identify the existence of these effects, but also to provide the data required to develop an empirical model. It was found that when heads utilized the same material for the substrate and closure, values for h_0 tended to be influenced mainly by

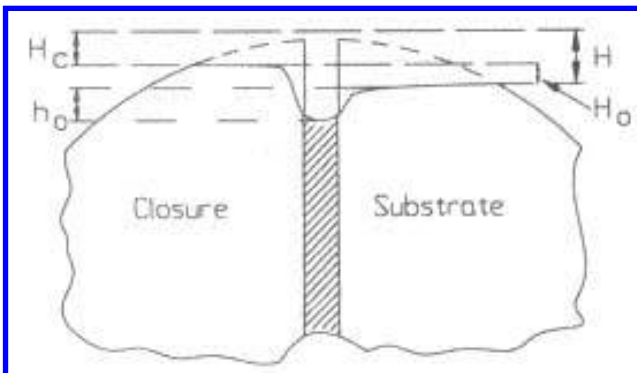


Figure 5.71 General Wear Scar Profile of a head. (From Ref. 14.)

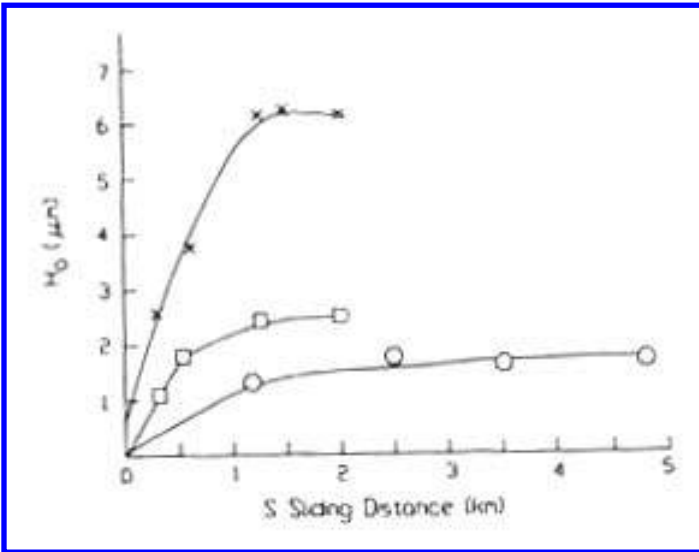


Figure 5.72 Behavior of H_0 for three different contamination conditions. (From Ref. 14.)

the width of the interface. For the gap used, finally selected h_0 was found to be $< 75 \mu\text{m}$ for all conditions. When there was a difference in hardness between the closure & substrate, h_0 tended to be small in comparison to H_0 and there was no need to differentiate between h_0 and H_0 . In these cases (i.e., different materials for each half), the value for H_0 was found to be significantly affected by orientation and abrasive size. Since a stable step implies that particles can pass over the surface of the softer member with very little interference, it was concluded that H_0 should be linear function of \mathbf{D} . It was also considered likely that the concentration of particles on the surface would modify the distribution of particles abrading the head, probably in a nonlinear manner. For example, with smaller concentrations, the larger particles might be displaced by the head rather than causing abrasion of the softer surface. Since a step was observed with clean tape, the following expression was proposed and found to provide an adequate agreement with the data:

$$H_0 = A + B \left(\frac{\alpha}{\alpha_0} \right)^n \mathbf{D} \quad (5.123)$$

where A is the value for clean tape; B , a function of sliding direction and design (e.g., sandwich or regular design); and n is a function of design. Values obtained for A , B , and n for several conditions are shown in Table 5.26. The agreement that was obtained using these values is shown in Fig. 5.74 (see p. 269).

This combined model was verified in two field trials in retail applications. Good agreement was found in both cases. In one test, wear was determined as a function of usage, using one design. Wear predictions were based on parameters determined in laboratory tests and characterization of the abrasive environment in the application. Table 5.27 shows the results of the contamination studies and the typical value of \mathbf{D} and α that was deduced for this evaluation. In Table 5.28, the projections of the model and the actual data are shown. In the second test, two designs were compared (i.e., a silicon/sapphire and a sapphire / sapphire design). The model indicated a minimum of $15\times$ improvement with sapphire / sapphire design; the data indicated a $28\times$ improvement.

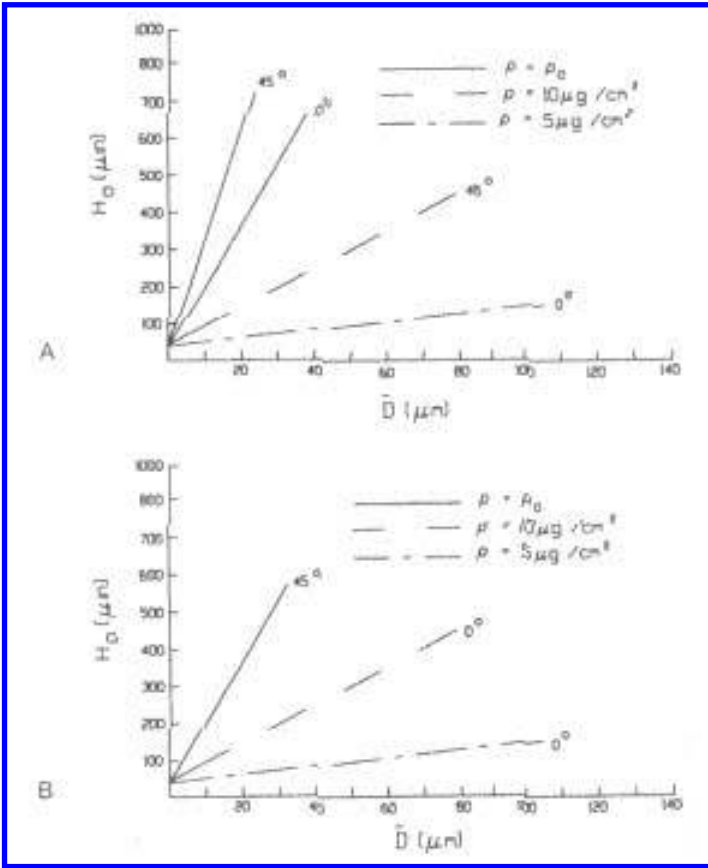


Figure 5.73 Behavior of H_0 as a function of the amount and size of the abrasives and orientation of the gap with respect to the sliding direction. “A” is for a sandwich design. In this design, the head consists of three elements, with the active element deposited on the middle element. “B” is for the standard design (two elements) with different materials for the closure and substrate.

These expressions were used to compare various designs and the effects that modifications of various parameters, such as sliding direction, radius, and material properties, might have. One conclusion that was reached was that the performance of designs using dissimilar materials would rapidly degrade in environments where large size abrasives would be present. The difference between these designs is shown in Fig. 5.75 (see p. 271). These relationships were also used with the field contamination data to project field performance for various designs in different environments and markets. This ultimately led to the selection of an all-sapphire design with an 0.1 in. radius. Field experience has confirmed the adequacy of the design.

The two standard tests developed in this wear design were also used to evaluate other components, such as magnetic write heads of the type shown in Fig. 5.76 (see p. 272). The model for K was also found useful in other applications involving hostile environments.

Table 5.26 *A*, *B*, and *n* Values for Different Designs

Design	Sliding orientation	<i>A</i> μm.	<i>B</i> μin/μm.	<i>n</i>
Standard design				
Homogeneous	All	75	0	—
Non-homogeneous	0°	50	9.7	0.29
	45°	50	16.7	0.29
Sandwich design	0°	50	16.3	0.60
	45°	50	30	0.60

5.13 EROSION APPLICATIONS

Wear design has been used for a variety of applications involving erosion. Several examples that illustrate a range of approaches can be found in the literature (16–20). In one, an analytical approach was applied to the design of gas turbines. The others used more empirical approaches and involved various forms of slurry erosion. In these case studies conceptual models were formulated and used in conjunction with laboratory or robot tests

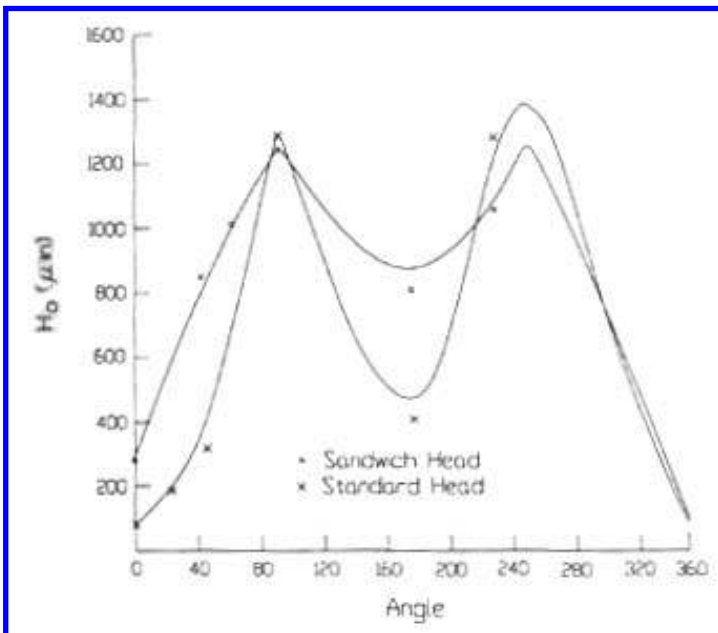


Figure 5.74 Comparison of model for H_0 and experimental data for the standard AC Fine / Gelatin mixture.

Table 5.27 Examples of Abrasive Particle Distributions from the First Test Site

Sample	Total sample (mg)	Abrasive particle type	Size (μm)	Percent of total sample
1	17	Quartz	21	21
		Feldspars	20	15
		Magnetic spheres and chips	10	Trace
2	6.1	Limestone ^a	10	10
		Quartz	33	8
3	0.1	Crushed brick	500	79
		Mineral grains	18	10
		Iron oxides	18	3
4	1.4	Titanium dioxide	1	44
		Limestone ^a	7	5
		Quartz	18	3
9	6.4	Limestone ^a	6	2
		Iron oxides	6	1
<i>Site values</i>				
Average of 10 samples			$\alpha = 9 \mu\text{g}/\text{cm}^2$	D = 61 μm
Weighted average (used to project field behavior)			$\alpha = 4 \mu\text{g}/\text{cm}^2$	D = 32 μm
Ranges				
All samples				$\alpha = 0.06 - 61 \mu\text{g}/\text{cm}^2$
				D = 1 - 436 μm
80% of samples				$\alpha = 0.3 - 14 \mu\text{g}/\text{cm}^2$
				D = 6 - 63 μm

^aOnly considered to be an abrasive for Si. Not considered in obtaining the average values.

to determine design parameters for several different applications. One was concerned with wear in pipelines, which handle slurries. Another was concerned with wear in pumps used in oil drilling and a third was concerned with wear problems in recirculating liquid systems, such as those used for cooling. In all of these cases, including the gas

Table 5.28 Field Test Results

Scanning amount (10^3 in.)	Wear depth ($\mu\text{in.}$)	
	Projected	Measured
7.5	475	400, 600
17.5	500	400, 500, 700
30.0	575	600, 650
50.0	650	600
55.0	660	800
60.0	680	500, 800
70.0	700	450
77.5	725	550
90.0	750	700, 750

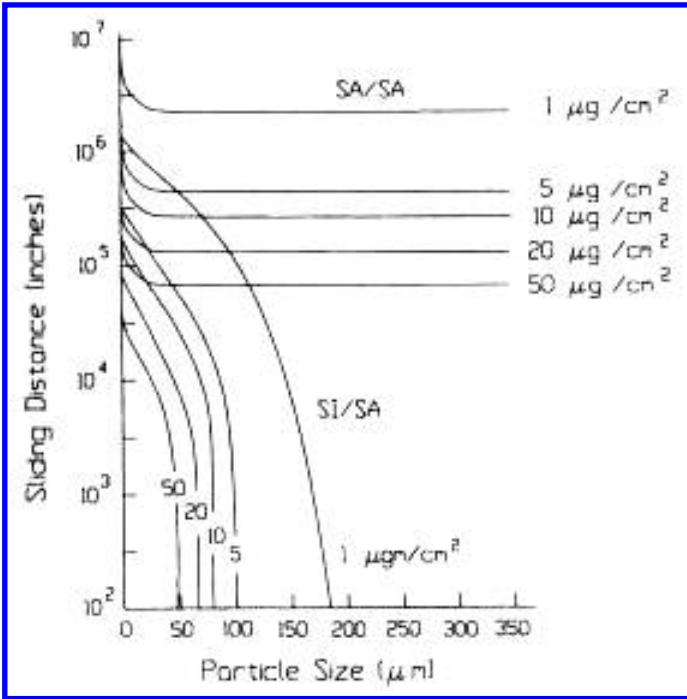


Figure 5.75 Theoretical wear behavior of an all-sapphire standard head and a standard head with a silicon substrate and sapphire closure. (From Ref. 14.)

turbine one, the wear design started with systems analysis, which provided an operational characterization or definition of the wear situation.

One example of the use of wear design in erosive situations involves the development of a turbine generator used in a coal gasification process for power generation (18). The wear design approach was used in the early stages of development. Part of the power generation process involved the passage of combusted coal gas through a gas turbine. System analysis indicated that in this region the stator and rotor blades would be exposed to erosion by coal ash and dolomite sulfur sorbent particles contained in the gas stream. It was concluded that the bulk of these particles would range in size from 1 to 12 μm, since the larger size particles, i.e., > 12 μm, tended to be eliminated by any of the gas cleaning processes being considered. It was also concluded that corrosion and deposition would modify the surfaces of the blades. The purpose of the initial wear design was to investigate feasibility and focused on the effects that various cleaning procedures would have on life. It was assumed that the wear behavior could be described by the general equations for erosion (Eqs. (2.163) and (2.164)), which combine the effects of ductile and brittle behavior. These are

$$e = \left[K_d v^n \cos^n \alpha \sin \left(\frac{\pi \alpha}{2\beta_0} \right) + K_b v^m \sin^m \alpha \right] \mathbf{M}, \quad \alpha \leq \beta_0 \tag{5.124}$$

$$e = (K_d v^n \cos^n \alpha + K_b v^m \sin^m \alpha) \mathbf{M}, \quad \alpha \geq \beta_0 \tag{5.125}$$

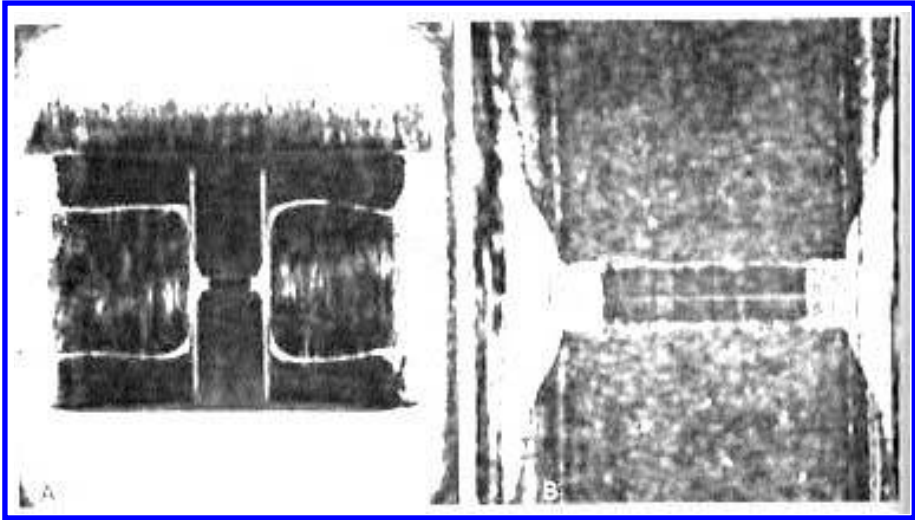


Figure 5.76 Magnetic write head worn with the AC Fine/Gelatin mixture. “A”, entire head; “B”, write area.

These equations involve several empirical coefficients that are material and environment dependent. At the time the design study was undertaken there was very little data and information available regarding the wear properties and wear coefficients for the super-alloy turbine materials being considered, particularly under the application conditions involved. However, for similar quantities and ranges of particle size, there were data for silicon carbide eroding a nickel–cobalt alloy of the type being considered in the application. There were also some data available comparing the erosiveness of coal ash and silicon carbide. These data indicated that coal ash had $1/25$ th the erosiveness of silicon carbide particles. Initial assumptions were that environmental effects would be small for the alloys used in turbine blade applications and that the wear resistance of these materials would be equal to or better than that of the nickel–cobalt alloy. With those assumptions, the silicon carbide data, scaled by $1/25$ th, were used to estimate the coefficients of the equations. It was recognized that there was considerable risk associated with these assumptions, so programs were initiated to determine the values of these coefficients for the materials and conditions involved.

As indicated by these equations, the erosion rate is also a function of particle velocity and impingement angle. In order to estimate the wear on the blades, it was necessary to determine the motion of the ash and dolomite particles through the turbine blades. Fluid flow as well as particle size and mass affect the motion of the particle. This was done by numerical simulation techniques used for particle deposition analysis (21,22). In these simulation techniques, the flow of the gas is assumed to be unaffected by the particles, while the motion of the particles is affected by the flow of the fluid (e.g., drag). The flow was considered to be inviscid and the particles were assumed to be spherical and only subjected to drag and inertial force. The effect of particle size and density on trajectory is shown in Figs. 5.77 and 5.78. It can be seen that small, light particles tend to impinge less and to have low, grazing angles of contact with the blades, while large, heavy particles tend to impinge more and to have higher contact angles.

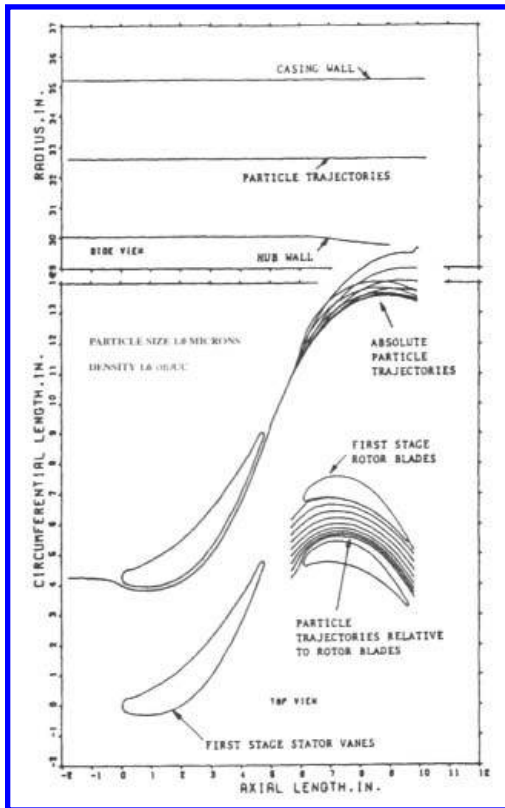


Figure 5.77 Trajectory of 1 μm particles through the stator and rotor passages. (From Ref. 35, reprinted with permission from ASTM.)

Design feasibility was investigated by combining these simulation techniques with Eqs. (5.124) and (5.125) and using the estimated values of the material coefficients to determine the effective wear rate for different conditions. A series of calculations were performed for several different particle distributions, which were representative of different cleaning processes (Fig. 5.79). The results of the calculations are illustrated in Figs. 5.80 and 5.81 for different regions of the blades. It was concluded that satisfactory blade life could be obtained by using a cleaning process to eliminate all particles above 6 μm and to reduce the particle concentration of 6 μm and smaller particles to less than 0.0046 g per standard cubic meter.

A different approach had been used for erosion problems in pipelines handling slurries (20). It is based on the use of two standard tests described in ASTM G75. (See Sec. 9.2.3. of MWFT2E). These tests were developed to provide simulation of the slurry erosion found in pipeline applications. Rankings obtained with this test have also been found to correlate with field performance. A significant portion of the development effort

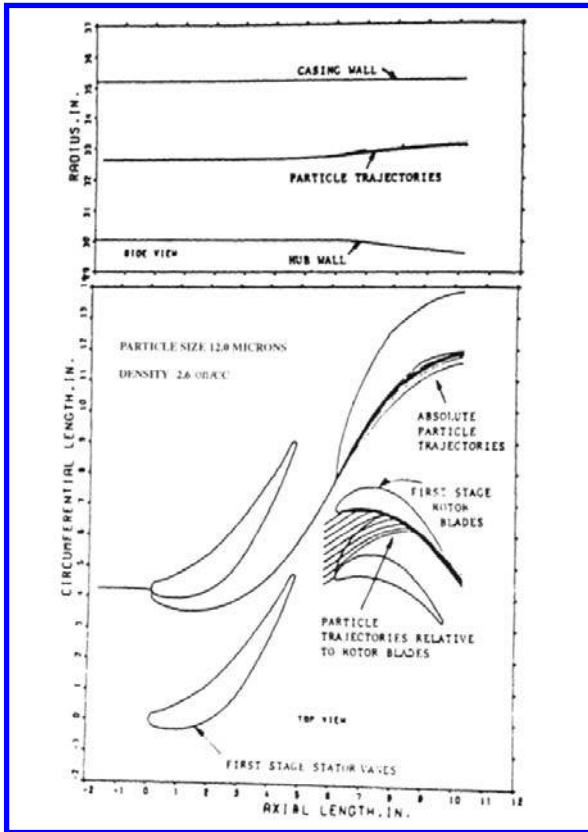


Figure 5.78 Trajectory of 2 μm particles through the stator and rotor passages. (From Ref. 35, reprinted with permission from ASTM.)

for these tests invoked the comparison of test results with observed field behavior in terms of wear scar morphology and relative wear rates. Two indices are obtained from these tests. One is the Miller number, which measures the abrasivity of a slurry; the other is the SAR number, which measures the relative abrasion resistance of materials to a slurry. A database has been developed that relates field performance for various components to these two indices. This was done by testing with slurries and materials, used in applications where performance was known or could be established, and determining their Miller and SAR numbers. The wear design method is used to obtain a sample of the slurry in the application and to determine its Miller number. The Miller number is then used to select from the database materials and component design, whose performance meets or exceeds the requirements for slurries with that of Miller number. If the material being considered is not in the database, the SAR number is used to determine its relative performance. This is done by determining the SAR number for the unevaluated material and the SAR number of a material in the database, using the slurry in the application. The ratio of the SAR

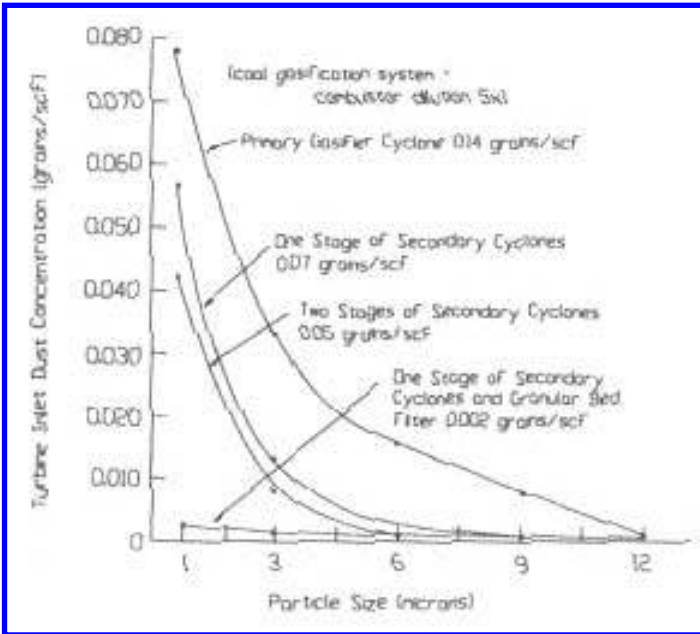


Figure 5.79 Inlet particle size distributions for different particle removal systems. (From Ref. 35.)

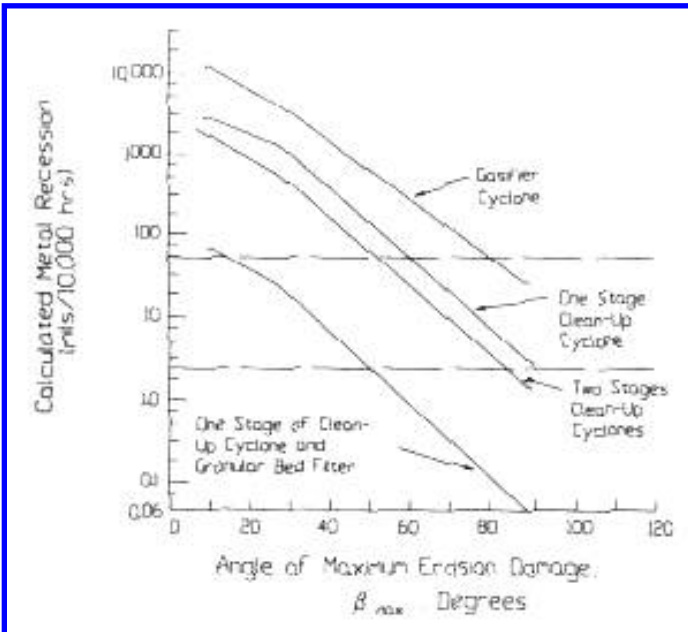


Figure 5.80 The effect of different cleaning procedures on the erosion of the trailing edge of the 1st stage vanes, predicted by the model. $0.1 \text{ in./} 10^4 \text{ hr}$ was considered to be the acceptable limit on erosion rate. (From Ref. 35.)

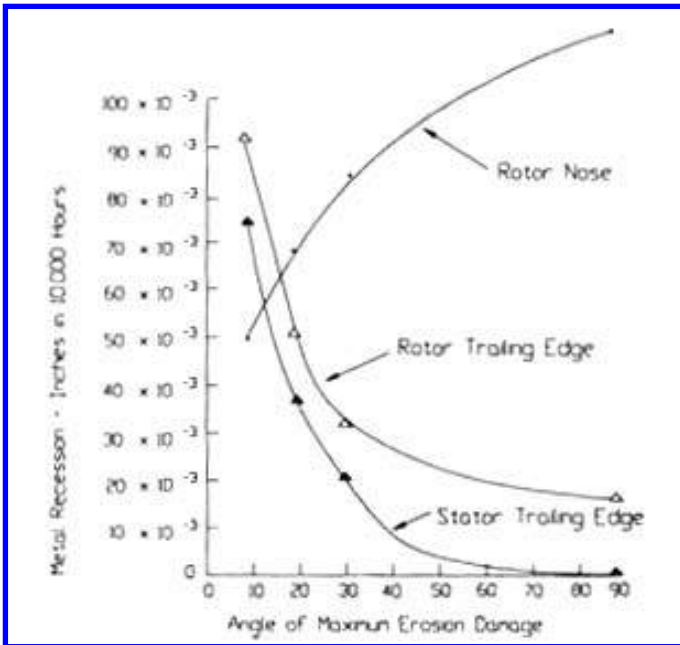


Figure 5.81 Theoretical erosion rates using the best cleaning procedure (i.e., a one-stage clean cyclone followed by filter bed). (From Ref. 35.)

numbers provides an estimate of the relative improvement or degradation in performance for the candidate material relative to that of the material in the database.

A robot test has been used as the basis for wear design in the development and selection of pumps and filters for recirculating fluid systems (17). Examination of used and failed pumps had indicated that the major cause of wear failures was abrasive contaminants entrained in the fluid. To evaluate the wear resistance of a pump, a robot test, simulating a recirculating system, was developed to provide design information. A schematic for this test is shown in Fig. 5.82. The pump was operated at its rated conditions in this test. The test consisted of incrementally introducing different size particles to the fluid and measuring the flow rate of the pump after a specific interval and comparing it with the rated value. The same amount of abrasive was added at each interval, but the size range increased. Different cuts of AC Test Dust, which is mainly sand particles (i.e., SiO_2), were used as the abrasives, since it was representative of the type of abrasives typically found in these systems. Survivability curves, Figs. 5.83 and 5.84, were developed for the pumps from these data. These curves were used to compare pump designs and to investigate the effect of different parameters, such as pressure, on wear resistance. By assuming that wear is proportional to the amount of abrasive passing through the pump, these same curves were used to project life (Fig. 5.85). These data also were combined with filtration data for filters to determine the life of different filter/pump systems (Fig. 5.86). Beta in this figure is the filtration ratio for the filter, which is used to describe the fraction of particles of a given size that the filter will allow to pass. A graph showing that relationship is shown

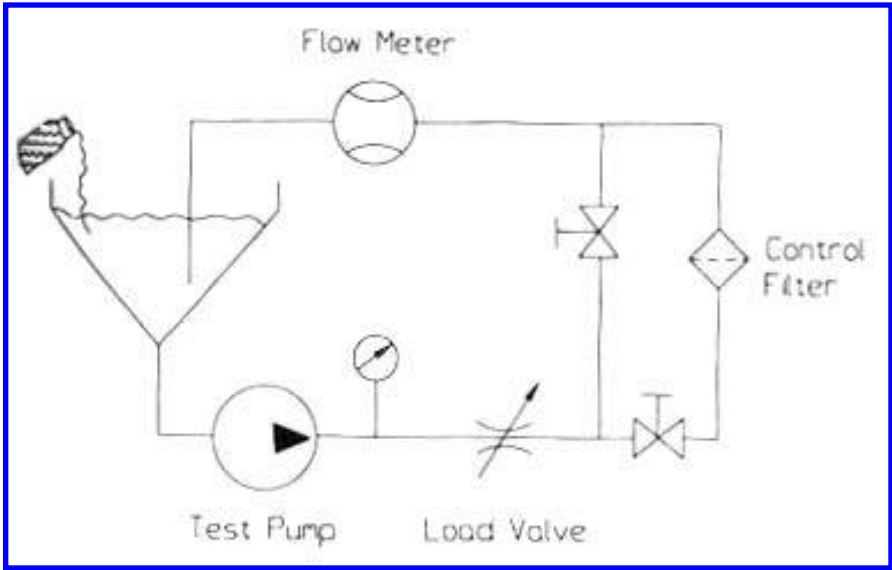


Figure 5.82 Schematic of robot test used to develop wear design information for pumps. (From Ref. 17.)

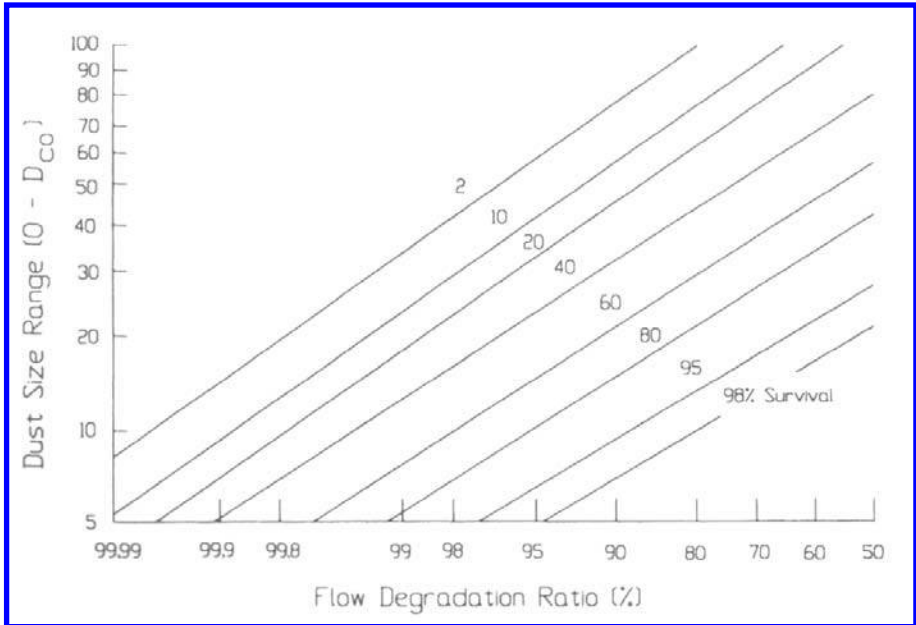


Figure 5.83 Survivability curve for all pumps tested. (From Ref. 17.)

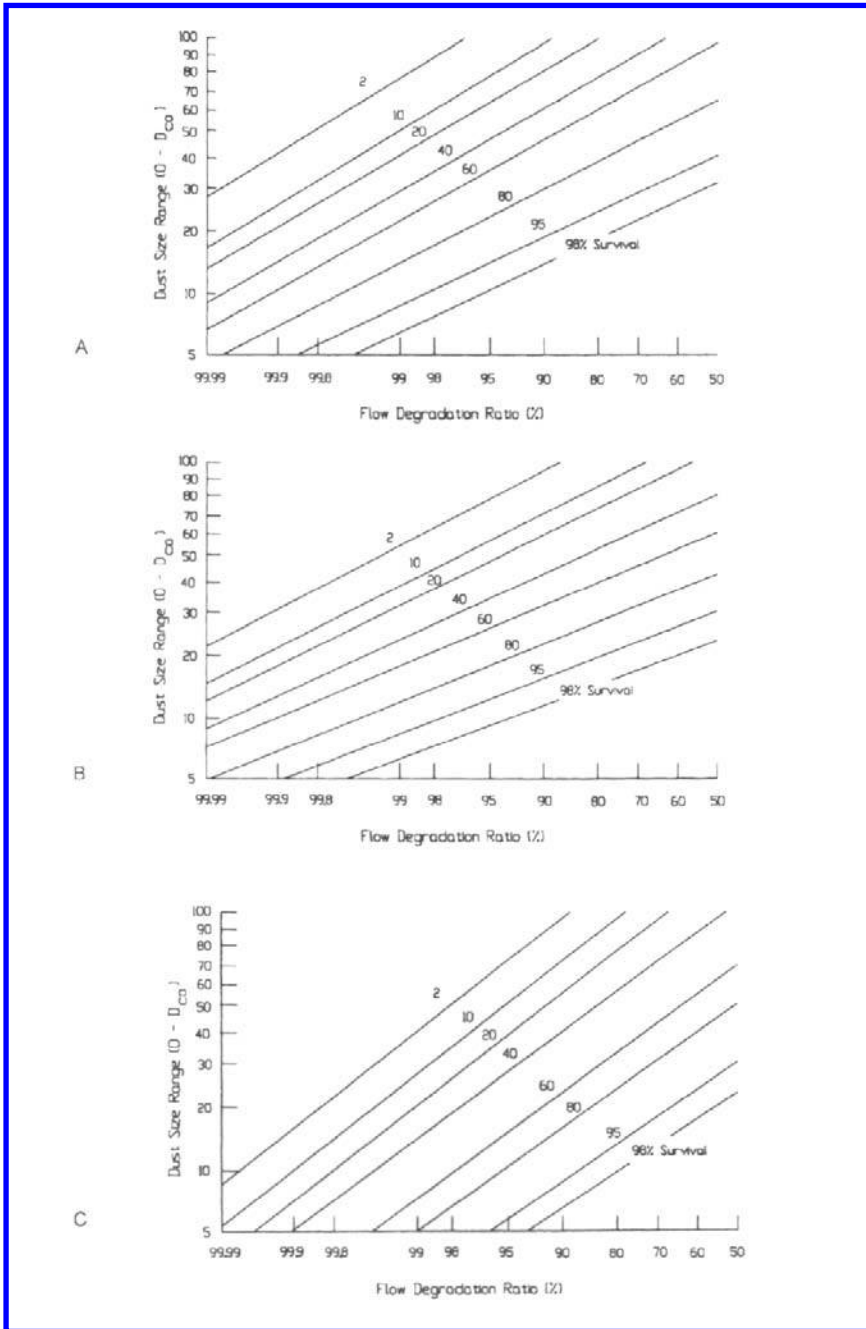


Figure 5.84 Survivability curves for different pump designs. “A”, gear pumps; “B”, piston pumps, and “C”, vane pumps. (From Ref. 17.)

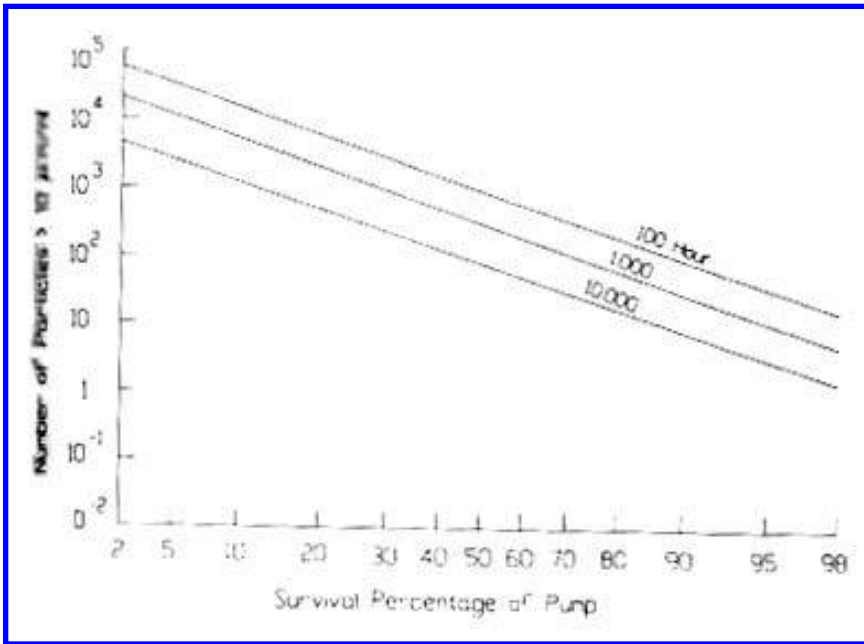


Figure 5.85 Projected pump life for different concentrations of particles. (From Ref. 17.)

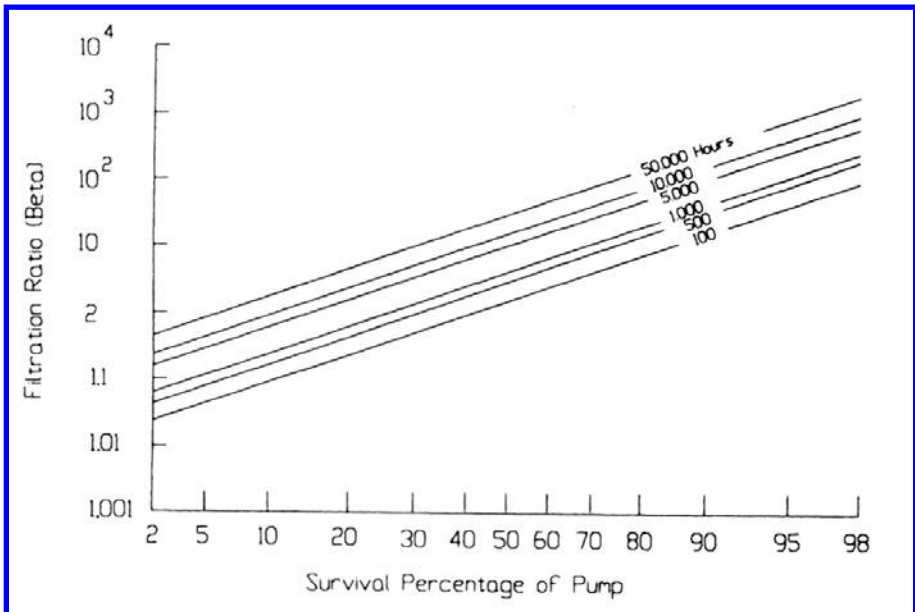


Figure 5.86 Relationship between pump life and filter characteristics. (From Ref. 17.)

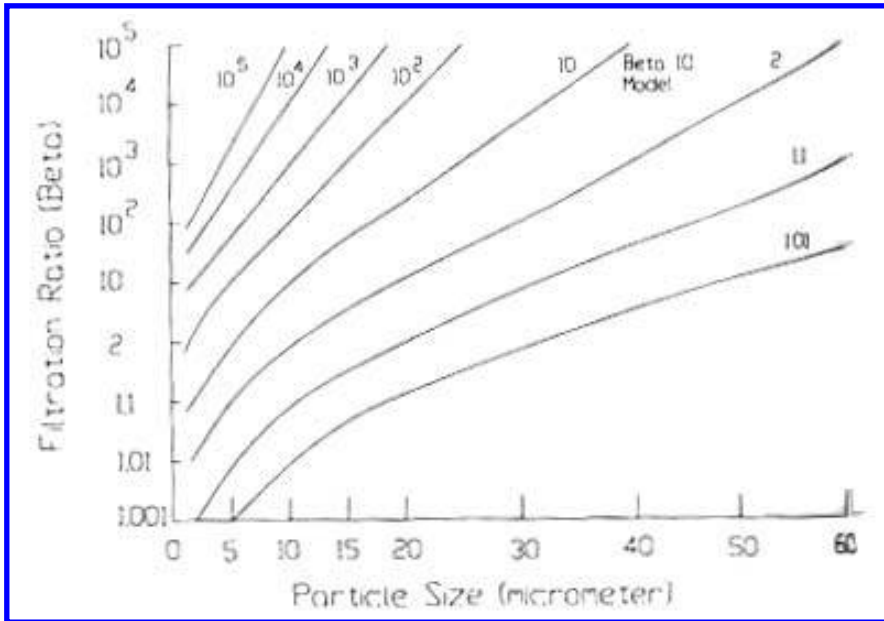


Figure 5.87 Beta 10 Filter Model for filtration ratios, β , which is the ratio of the particles “in” to the particles “out.”

in Fig. 5.87. By using this relationship and a characterization of the amount of contamination in the unfiltered fluid, the quantity and size distribution, of the particles passing through the pump can be determined. Using this information and the survivability curves, pump life can be determined for the particular pump/filter combination. Alternatively, a suitable combination of pump and filter can be identified for an application.

A wear design method has also been used in the development of drilling mud pumps that are used in oil drilling (16). In deep-well oil drilling, a recirculating system is used to pump a thick fluid, called drilling mud, down the hole and around the drill to prevent blowouts, to improve the drilling, and to lubricate and cool the drill bit. This mud consists of a mixture of oil and / or water, clays, inhibitors for chemical compatibility, and other fillers to increase its density. Even though the recirculation system contains a reconditioning and cleaning stage, the mud becomes contaminated with abrasives from the drilling. The pumps used in these installations tended to have a short service life (e.g., order of 100 hr), as a result of wear. The wear design approach used to develop a more wear resistant pump was empirical and consisted of system analysis, model development, database development, and verification.

The wear design started with the thorough examination of used and worn pumps to determine wear points in the pumps and to characterize the wear at those sites. The general design of these pumps is shown in Fig. 5.88. One of the wear sites that was identified was the interface between the piston and the cylinder. Wear was observed on the cylinder or liner, on the side of the piston, and on the end seals of the piston (Fig. 5.89). Several modes

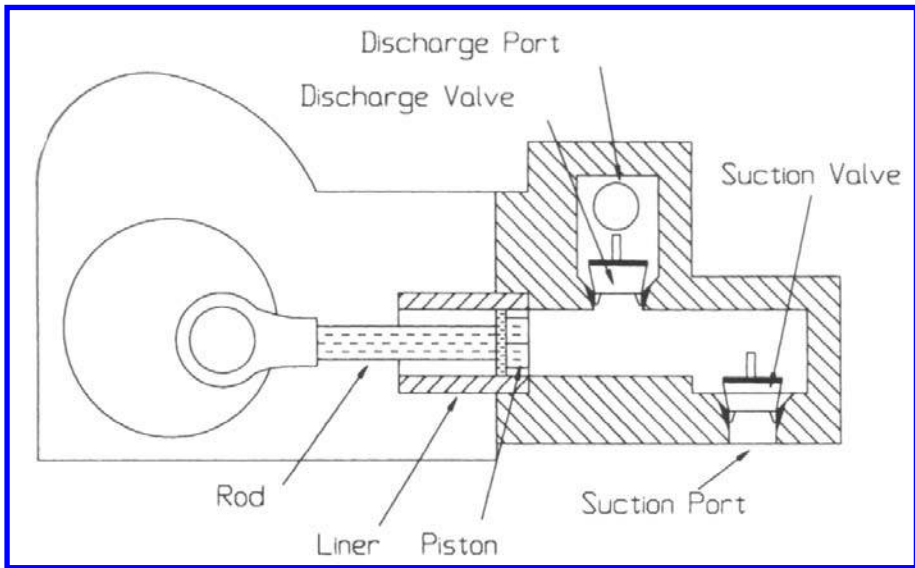


Figure 5.88 Beta filter models. (From Ref. (17).)

of wear were identified from the morphology of the wear scars. Erosive wear was identified as taking place on the sides of the piston and the liner. There was also some evidence of metal-to-metal sliding wear. Two modes of sliding wear were identified on the seal. The lip of the seal appeared to be worn by a deformation mode that involved extrusion and tearing. In other areas, the wear was representative of general sliding contact. From the distortion and surface morphology of the seals, which often suggested melting and softening of the elastomer seals, it was concluded that thermal effects contributed to seal wear. It also was observed that the seal did not contact the liner in the manner intended. This was thought to be the result of thermal expansion and mismatch. It was hypothesized that with wear and distortion, the seal surface tended to trap abrasive particles, which would then contribute to the wear of the liner. Examples of some of these features are shown in [Figs. \(5.90–5.94\)](#) (see pages 283, 284, 285).

These observations and speculations led to a conceptual wear model that was based on the hypothesis that high operating temperatures resulted in distortion of the seal and a high wear rate for the seal material. Because of this, the effectiveness of the seal rapidly degraded. This allowed particles to enter the interface between the liner walls and the pistons. These particles then eroded these surfaces. The high temperature, distortion, and wear of the seal material also enhanced entrapment of particles in the seal material, thereby causing abrasive wear of the liner. Based on this model, it was concluded that, by modifying the design to cool and flush the seal area, improved life could be obtained. To evaluate these types of changes and to select materials for an improved pump, it was decided to use a robot test. A specialized research test pump was built by modifying a 60-ton punch press. This test pump was designed so that a variety of prototype piston / liner designs could be evaluated and various parameters, such as temperature, could be measured. Samples of field mud were obtained and used as the slurry in these tests. Tests were

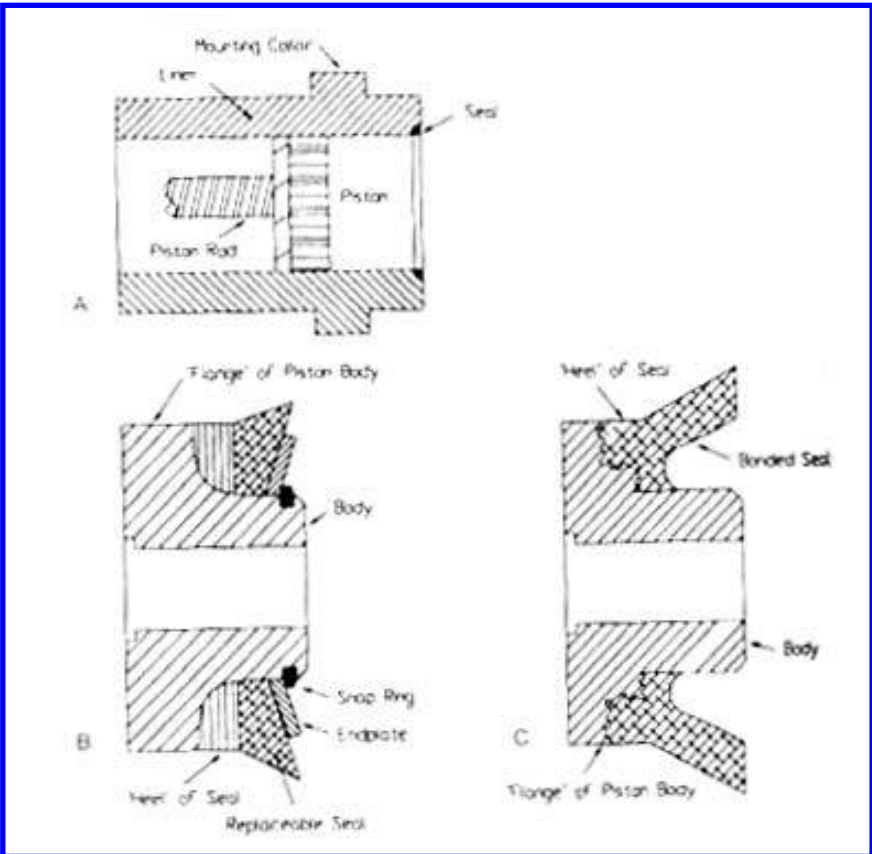


Figure 5.89 Details of the pumping cylinder. “A”, overview; “B” and “C” show details of the seal designs commonly used. (From Ref. 16.)

initially performed with existing designs to insure that the robot test simulated field performance. It was found that in the robot tests failure occurred in about one-third to one-fourth of the time to that found in the field, but the failure conditions were identical. It was therefore concluded that the test provided adequate simulation as well as some acceleration, which is always a desirable feature. These tests were then used to evaluate various proposed designs and materials.

In addition to these robot tests, laboratory type tests were performed to evaluate and study specific features of these designs, such as friction and extrusion tendencies. These tests were done utilizing prototype piston–liner assemblies.

These laboratory tests were used to develop and select a new design. To verify the performance of this new design, field tests were also performed. Figure 5.95 shows the comparative wear behavior that was observed in these tests for the standard and new designs.

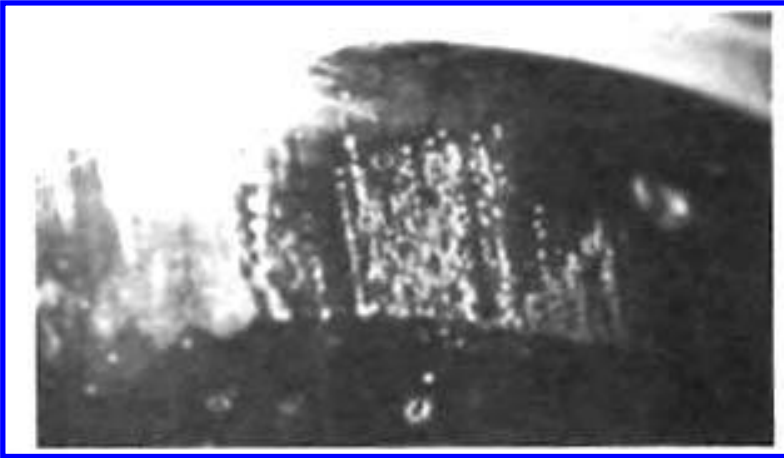


Figure 5.90 Oxidized adhered piston material on the surface of the cylinder. (From Ref. (16), reprinted with permission from ASME.)

5.14. ABRASION APPLICATIONS

A variety of approaches have been used in wear designs associated with several abrasion applications. The magnetic read head case study is one such example (Sec. 5.12) of an analytical approach. Similar approaches have been used for feed rolls in check sorting machines and type and wire wear in dot-matrix printers (23). Empirical approaches have also been used with success. The development of shredder hammers for sugar cane is one such example (24). A combination of laboratory and field tests was used to evaluate design alternatives so that engineering decisions involving cost and maintenance could be made. The development of improved paper slitters provides another example (25,26).

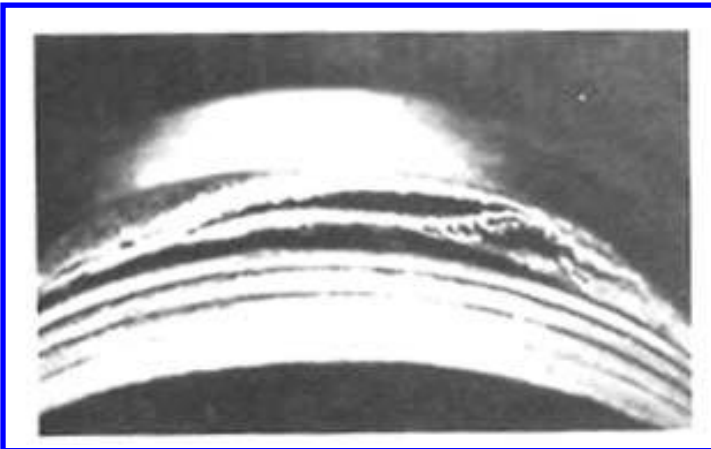


Figure 5.91 Damage to the heel region of the seal. (From Ref. 16, reprinted with permission from ASME.)



Figure 5.92 Examples of wear on the surfaces of the cylinder, “A”, and on the piston, “B” associated with seal leakage. (From Ref. 16, reprinted with permission from ASME.)

In this case, a laboratory test was developed and used to investigate the effect of various design parameters on slitter blade life and to determine the failure criteria for these blades. These last two examples of wear design are discussed in this section.

Shredders are used in the processing of sugar cane to facilitate the removal of the sugar. In these machines, pivoting hammers are mounted on a rotating wheel and used to crush sugar cane stalks (Fig. 5.96). These hammers consisted of a steel body and a replaceable tip. Since tip damage affects the ability of these hammers to effectively shred the cane, hammer replacement was often required and the maintenance costs were significant. Thus, it was desirable to increase hammer life. The system analysis involved both failure analysis and system characterization. From failure analysis, two failure modes were identified for the hammers. One was fracture of the tips. The other was wear of the tips. From the system analysis, it was determined that mixed with sugar cane was stones, rocks, tramp iron, and dirt that contained silica particles. Finally, it was known that sugar cane, itself, contained fine silica particles in their structure.

A phenomenological model was developed based on these observations. From the morphology of the worn surfaces and the general nature of the wear situation, it was concluded that the wear was the result of abrasion by the hard particles, particularly the silica and that the fracture was the result of impacts against larger stones, rocks, and iron particles. From the general nature of these two forms of damage, it was recognized that the engineering solution to extending hammer life might involve some trade-offs or compromises, particularly in terms of material selection. Wear life of the tips could be improved

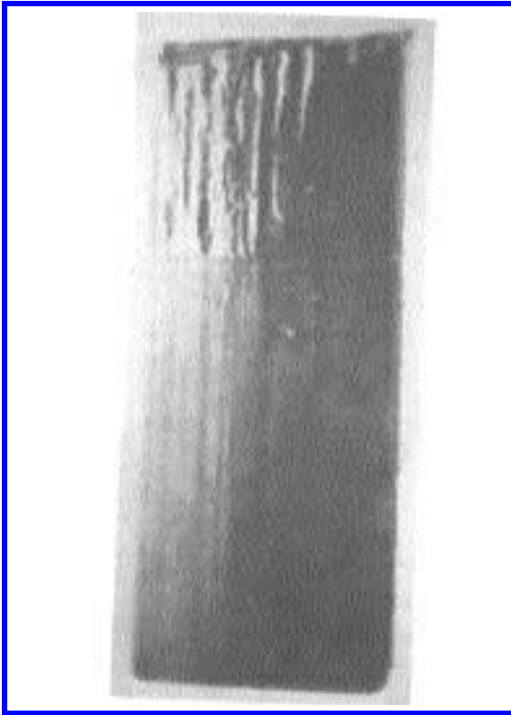


Figure 5.93 Melting of the seal surface. (From Ref. 16, reprinted with permission from ASME.)

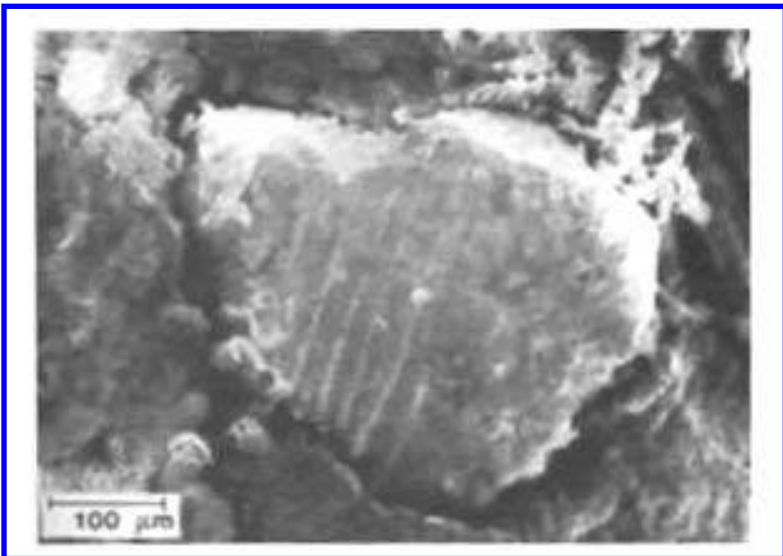


Figure 5.94 Trapped particle on the surface of the seal. (From Ref. 16, reprinted with permission from ASME.)

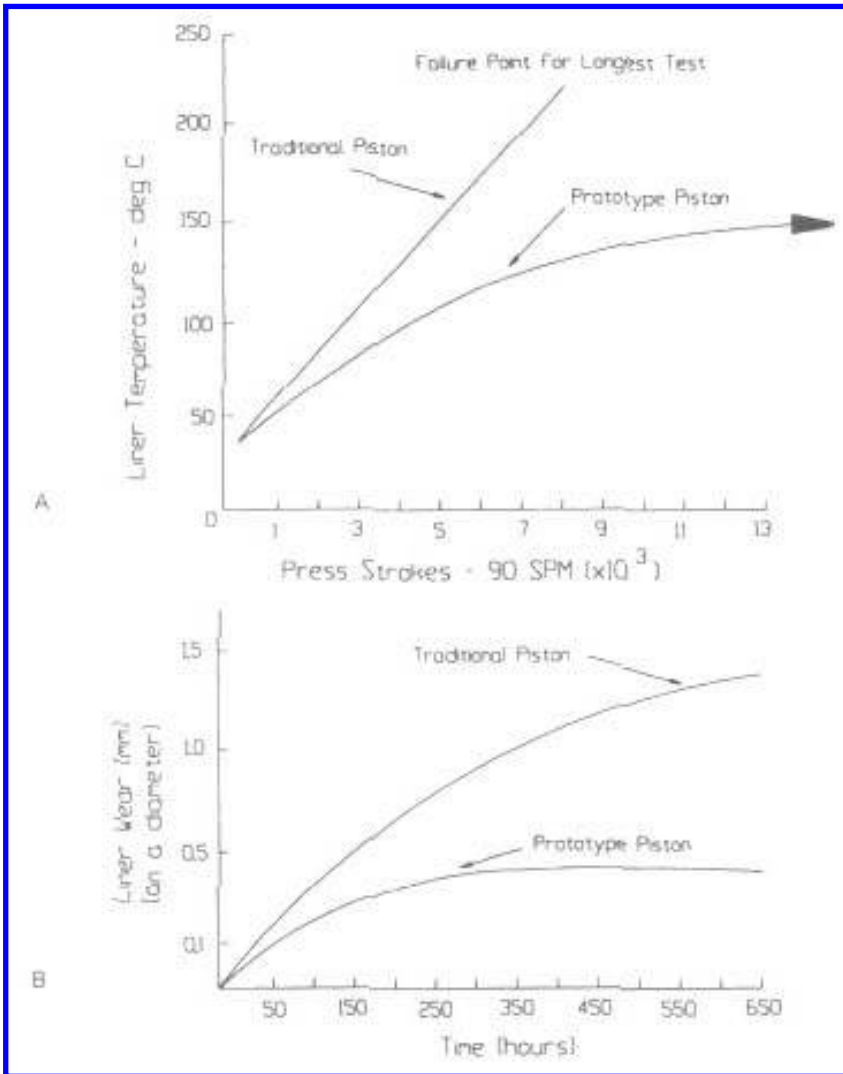


Figure 5.95 Comparisons of the standard and new designs. "A" shows the difference in liner temperature obtained in extrusion tests. "B" shows the difference in wear obtained in field tests. (From Ref. 16.)

by the use of hard materials to combat abrasive wear. However, these materials tend to be brittle and fracture life might be reduced. Ductile materials, which would increase fracture life, tend to be softer and would have poorer abrasion resistance. To identify the significance of various factors on these two modes of damage, it was decided to use two tests. One test was used to investigate fracture and another was primarily used to investigate wear (but fracture data were also obtained from this test).

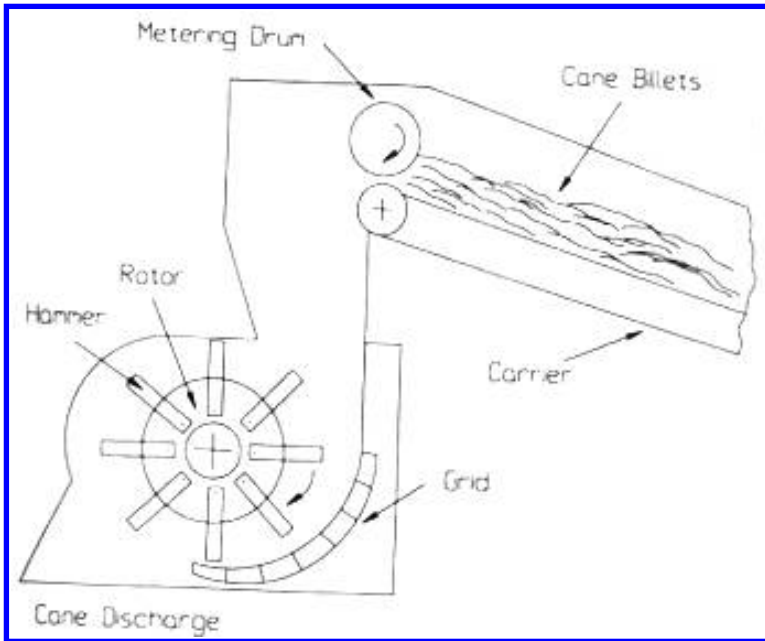


Figure 5.96 Sugar shredder hammer mill. (From Ref. 24.)

To study fracture, a robot was developed, which simulated the action of the shredder and stone. Rock and tramp iron could be introduced via a feed chute. This test was used to investigate the effect that different design aspects had on fracture, such as the shape of the tips, edge conditions, and method of attachment, as well as comparing of the materials. Some of the design features that were evaluated in this test are shown in Fig. 5.97. It was found that even with brittle materials design features could significantly reduce the tendency for fracture. The test was also used to evaluate the relative significance of rock, stone, and iron in causing fracture. It was found that the tramp iron was the major contributor to tip fracture. Because of the nature of the impacts involved, the rock and stone particles tended to be fractured by the hammer, while the tramp iron did not. The use of a magnet to remove the iron was identified as means of improving fracture life.

Wear was studied in field tests by utilizing specially fabricated tips and mounting them in a shredder. These tips were periodically inspected and measured for signs of wear and fracture. Wear rates of different materials were obtained. These provided a means of ranking and a basis for determining a maintenance schedule. Some of the materials evaluated are listed in Table 5.29. Some of the wear data obtained in these tests are shown in Table 5.30. It was found that if the hardness of the tip was greater than that of silica (approximate hardness, $H_v 700 \text{ kg} / \text{mm}^2$), a significant reduction in wear rate occurred (e.g., a factor of $115 \times - 1110 \times$). It was therefore concluded that tip hardness should exceed $1000 \text{ kg} / \text{mm}^2 H_v$ for long service life. The conclusions and data obtained in these two experimental studies were used to develop cost effective engineering improvements.

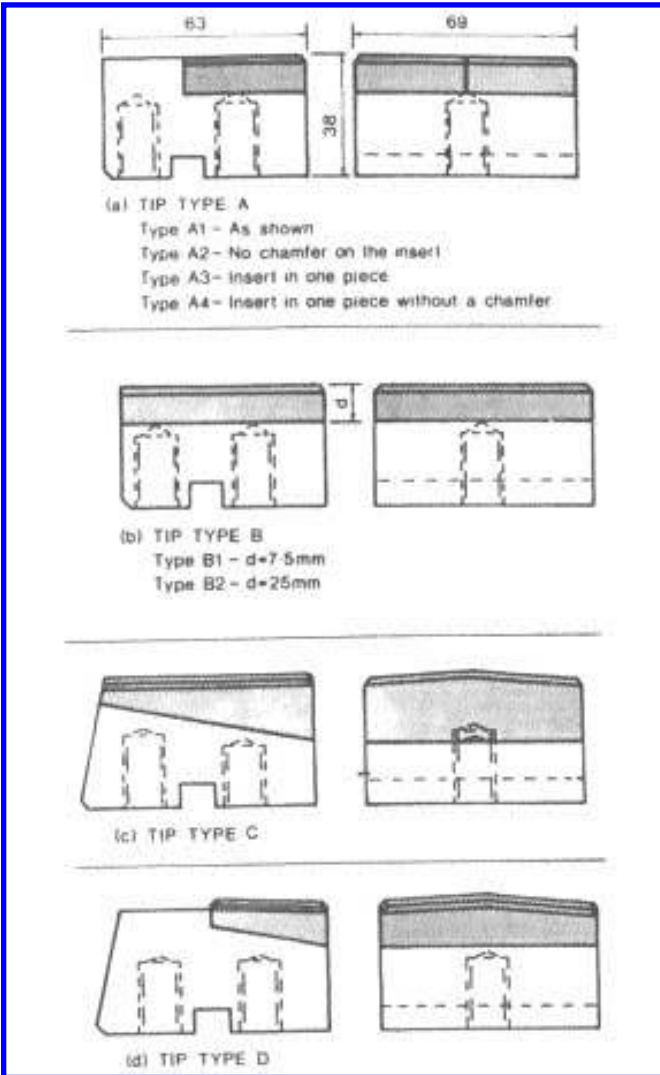


Figure 5.97 Design features evaluated in the shredder robot. (From Ref. 24, reprinted with permission from ASME.)

The design approach in the paper slitter application was also an empirical approach. In this case, it centered around the development of a laboratory wear test apparatus, which in turn simulated the wear that occurred in actual slitters. This apparatus was then used to study slitter wear and to investigate the effects that various design parameters had on wear and wear life.

Table 5.29 Materials Evaluated for Sugar Cane Shredder Hammers

Material		Hardness (Hv)
WC-Co		≈1100
Iron	15-3	560
		600
		790
		810
		860
	27% Cr	570
		750
	35% Cr	680
	4% Ni 2% Cr	725
		730
Hardfacing	23% Cr	
	26% Cr	

Source: Ref. 24.

In the initial phase of the wear design slitter conditions were studied. Also worn blades from paper mill slitters were examined to determine the wear mode(s). It was concluded from these that the blades that were worn as a result of three-body abrasion by the paper dust, it was found that the hard, angular particles, which are frequently contained in papers, tended to be exposed, making the dust abrasive. To simulate this situation in the laboratory, a small, multiple specimen slitter was built, which allowed the same adjustments as full-scale slitters. While the tester could slitter paper, slitting was not used to generate the wear. Rather a mechanism was developed which could feed paper dust to the blades. Periodically, the test was stopped and the

Table 5.30 Wear Losses From Tip Tests

Tip no	Cane crushed (ton)	No. of tips	No./type of failures	Averages mass loss (q)	Estimated volume losses		
					Base (mm ³)	Insert (mm ³)	at 40,000 tons (mm ³)
1	48,359	6	1 insert	44.0	3100	1400	1200
1F	30,167	6	0	37.5	600	2200	2900
2	30,167	6	3 insert	43.0	1000	1900	2500
2M	30,167	6	0	45.0	1900	2000	2700
3	30,167	6	0	77.0	1900	8300	11,000
3H	48,359	6	1 insert (?)	68.0	1500	7500	6200
4	30,167	6	0	92.0	1900	10,300	13,700
4H	48,359	6	1 insert. 1 braze	60.0	1500	6500	5300
6FH	33,949	6	6 base	28.5	500	3300	3900

Source: Ref. 24.

wear of the blades measured. Paper was slit at these times to determine the effect of the wear on slitting. The design of this apparatus is shown in Fig. 5.98. Several tests were performed with and without paper dust to insure that the blades wore in the same manner as in actual slitters. The morphology of the wear scars with paper dust had the same abrasive characteristics observed in the application. In addition, the geometry of the wear scars was similar. An idealized profile of a worn blade is shown in Fig. 5.99. A profilometer technique was developed to measure the profile and to determine both dimensions, a and b . Without the paper dust, the blades also wore but the morphology of the wear was entirely different and characteristic of dry, sliding wear between metals.

From prior studies of blade wear, it was known that wear life was not directly related to the volume of wear or either of the dimensions indicated. It had been proposed that a dimension (called the open cut distance) was the parameter that controlled life (Fig. 5.100). The open cut distance is the horizontal distance between the supporting point on the bottom blade and the cutting point on the top blade. This was calculated from the measured wear profile data. This hypothesis was investigated with this apparatus and found to be valid. The maximum open cut distance that could be tolerated was found to be a function of the paper being slit (Fig. 5.101). Typically, this dimension

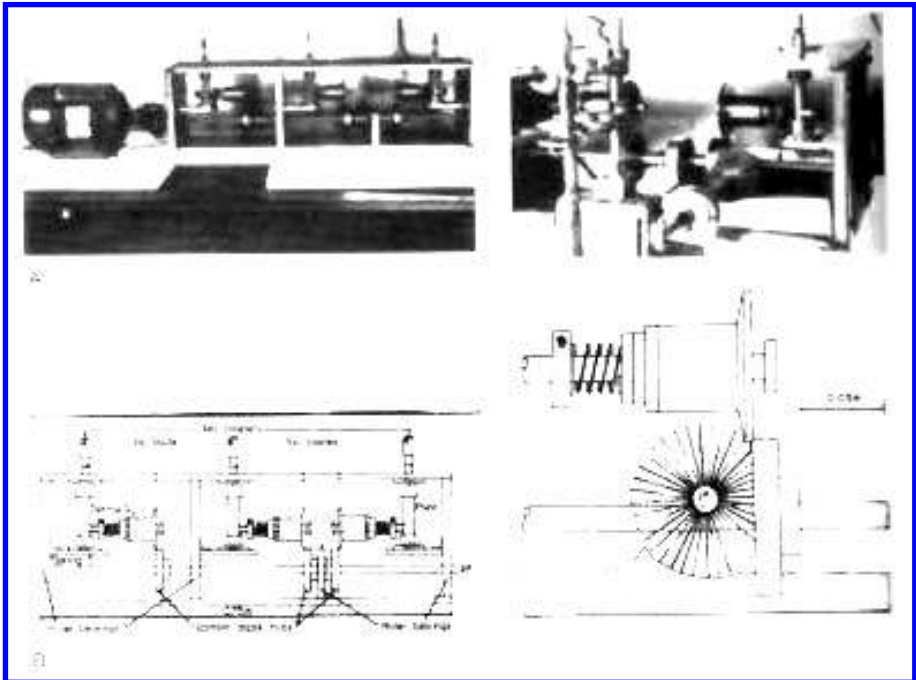


Figure 5.98 Apparatus designed to simulate the wear of slitter blades. “A” shows actual installation; “B” shows the method of introducing paper dust to the interface. (From Ref. 26, reprinted with permission from Butterworth Heinemann Ltd.)

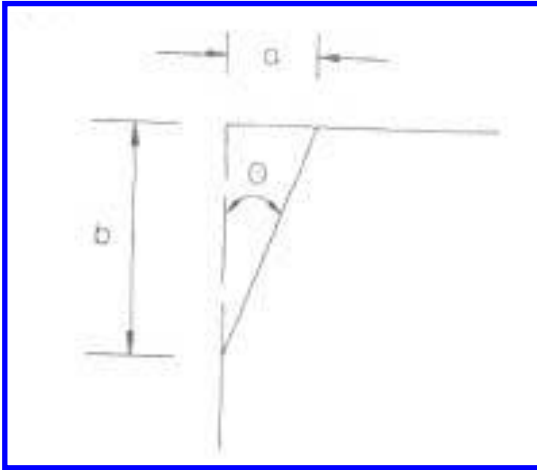


Figure 5.99 Profile of a worn blade. (From Ref. 26.)

was of the order of several 100 μm . Typical relationships between usage and the various wear measures are shown in Figs. 5.102–5.104 (see pages 292, 293).

This apparatus was used to investigate the effects that different design parameters, operator adjustments, and materials had on the open cut dimension and on life (Fig. 5.105—see p. 294). While these studies tended to confirm the selection of design settings that had evolved over the years, they also provided the basis to further enhance life.

While the implied relationship for wear life was nonlinear, it was found that the normal relationship for abrasive wear applied

$$V = K \frac{P}{H} S \quad (5.126)$$

where V is the volume of wear; P , the load; H , the hardness; S , sliding distance; and K , is an abrasive wear coefficient. This is shown in Fig. 5.106 (see p. 295). This observation was useful in the selection of materials and test conditions and the evaluation of test results. Profilometer data were used to compute V .

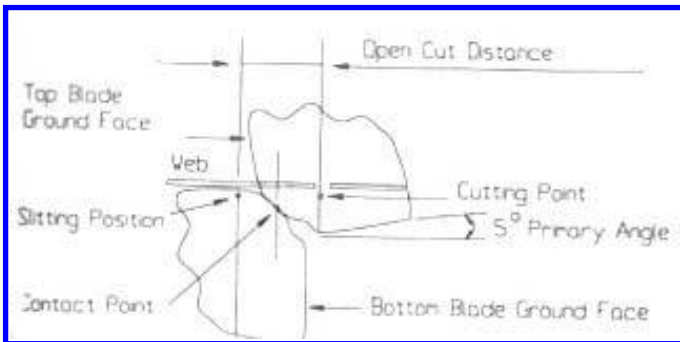


Figure 5.100 Open cut distance. (From Ref. 26.)

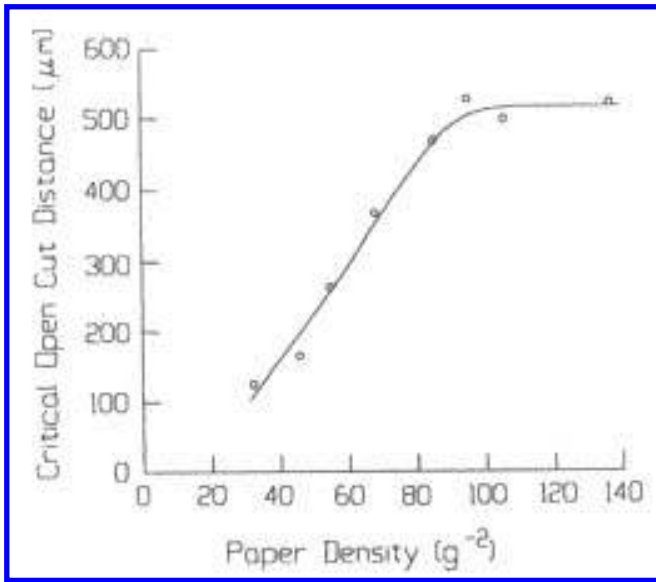


Figure 5.101 Relationship between open cut distance and paper density. (From Ref. 25.)

5.15. NUCLEAR VALUE

In this case study, three levels of wear tests were used to select materials for a check valve used in the cooling system of a nuclear plant (27). The information obtained from these different levels of testing was used to develop a phenomenological model for the wear behavior. Final selection of the materials was based on this model and data obtained in these tests. The specific material combination selected was not evaluated in these tests, but its selection was based on the extrapolation of this information.

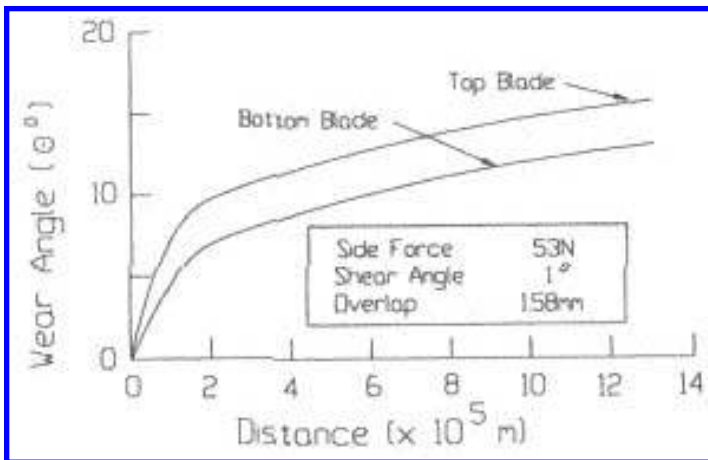


Figure 5.102 Wear curve for wear angel. (From Ref. 26.)

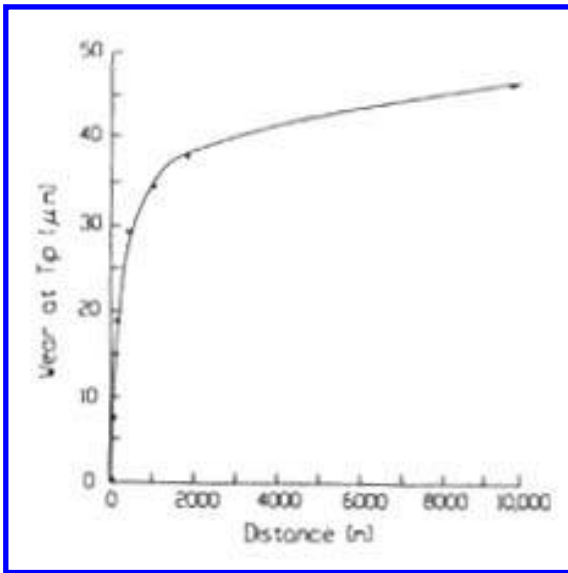


Figure 5.103 Wear curve for tip wear. (From Ref. 26.)

The design of the check valve is shown in Fig. 5.107. The intended use of the valve was to prevent back-flow in the cooling system during emergencies. These valves were designed for low usage but long installation life and to operate at 275°C and in water. The nominal diameter of the swing disk was 18 in. During service a major wear problem

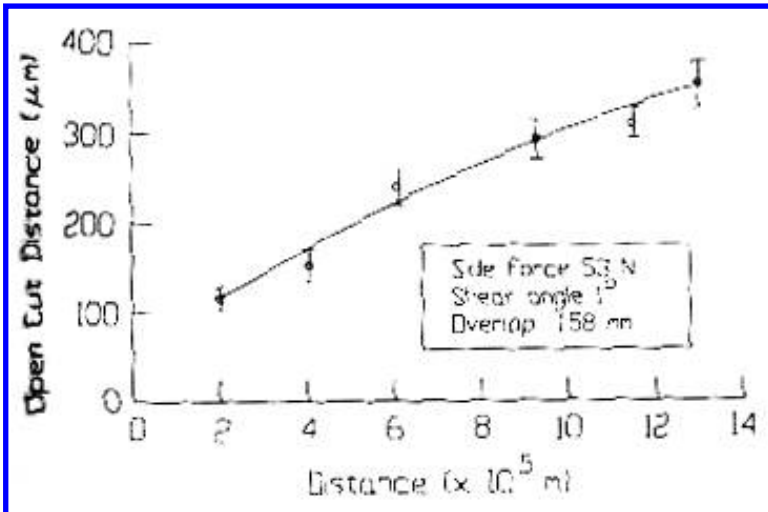


Figure 5.104 Wear curve for open cut distance. (From Ref. 26.)

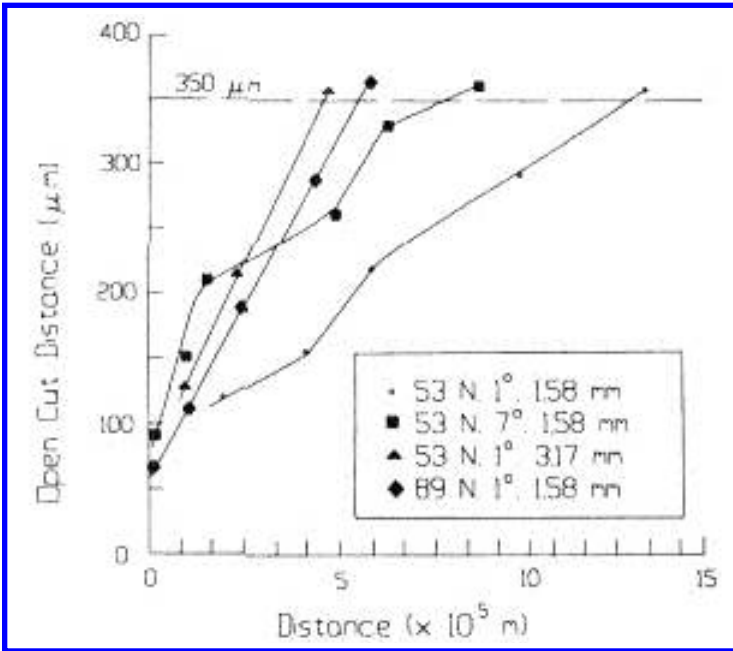


Figure 5.105 Variations in the wear curves for open cut distance. Failure occurred at 350 μm in all cases. Legend indicates side load, shear angle, and overlap. (From Ref. 25.)

was found, which resulted in the replacement of all these values in a nuclear installation. Severe wear was found on all the bushings and the bushing were worn through in some cases. Milder but noticeable wear was also found on the shafts. Some examples of this condition are shown in Fig. 5.108. After new valves were installed, wear of the valves was periodically measured and it was concluded that the valves had a service life of 7 years in the application. Since replacement of these valves was costly and undesirable, a program was undertaken to extend the life of the valves beyond 7 years.

The operation and operating environment of these valves were studied. It was found that these valves were used in regions of the cooling system that characteristically experienced perturbations in the flow. Hence, the valves tended to flutter continuously at about 0.5 Hz. As a result, the bearing would experience some 150,000 in. of sliding each year. This was considerably different (orders of magnitude larger) than what was anticipated because of the low use of the valve. Two ways of improving the life were considered. One way of extending the life of these valves was to modify the cooling system to eliminate the flow perturbations where these valves were used. This was considered to be impractical. A second way was to change materials. While there was no guarantee of success (i.e., identifying a material pair with better wear characteristics), this was the approach selected. Because of the uncertainty of identifying improved materials for this application, it was decided to use a less simulative but more implementable test that would allow a large number of candidates to be evaluated. The purpose of this test was to identify candidates for a second and more simulative test, which would be used to select materials for a field test. The intention was to make the final selection on the basis of the field test results.

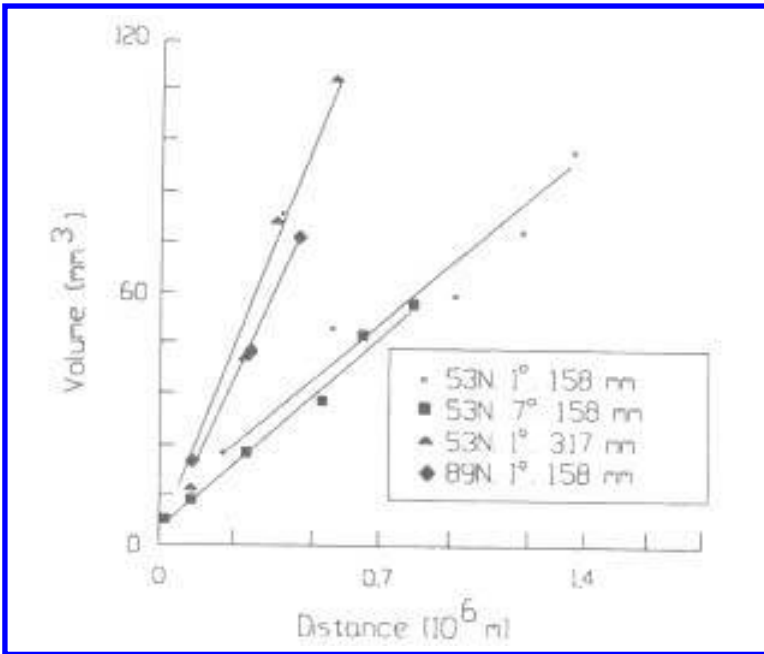


Figure 5.106 Wear curves relating volume to distance of sliding for several conditions of side load, shear angle, and overlap. (From Ref. 25.)

With this approach, it was possible to evaluate a large number of materials in an efficient manner. Candidate materials for the initial test were selected on the basis of their hardness (since wear tends to decrease with hardness), their compatibility with the water environment (since this was the fluid in which they were to operate), and good

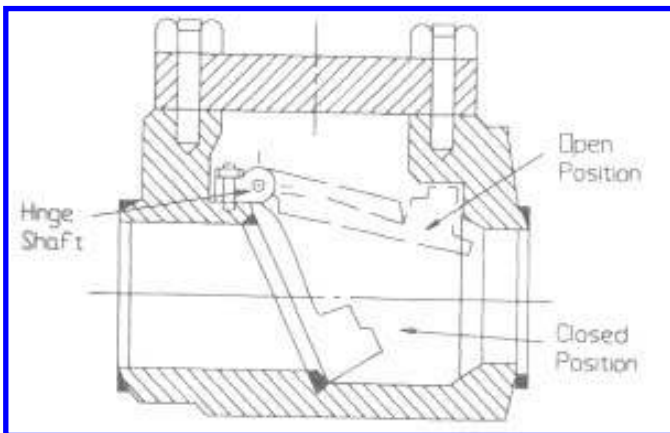


Figure 5.107 Check valve. (From Ref. 27.)

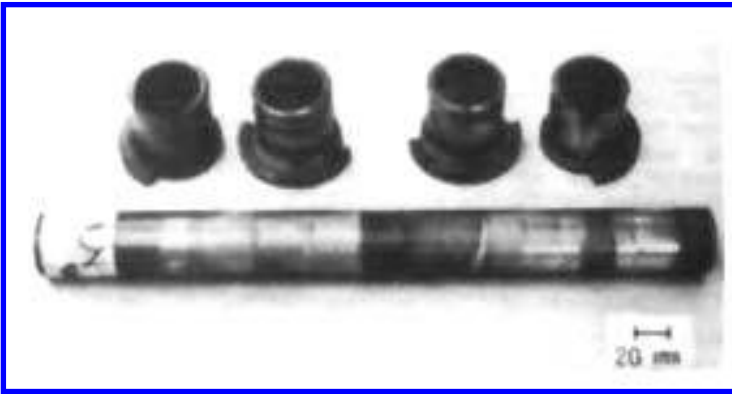


Figure 5.108 Worn bushings and shafts. (From Ref. 27, reprinted with permission from ASME.)

performance in similar applications. A list of some of the materials considered is shown in Table 5.31. The first two levels of tests involved the evaluation of the initial combination (i.e., the S-6 material for bushings and the HS-25 for the shaft), so that the relative improvement of a candidate pair could be estimated.

The first test used the geometry shown in Fig. 5.109. Tests were conducted in a 85°C water bath at speeds of 0.5 and 0.8 m / sec. This test provided something between 1st and 2nd degree simulation of the application. In addition to using this type of test for ranking purposes, it was also used for other purposes (see Sec. 8.1 of MWFT2E). Tests were conducted at a variety of loads and surface roughness to determine how sensitive the wear was to these parameters. Most tests were conducted for 10,000 m of sliding, which was estimated to be less than 10% of the amount of sliding that takes place in a year of service.

Table 5.31 Materials Considered for Nuclear Valve Application

	Test material properties and compositions								
	Shaft/plate materials		Pin material						
	HS25	N-60	S-6	S-1	N-45	N-41	T700	N-600	410
B					2.9	2.8			
C	0.1	Max 0.1	1.2	2.0	0.6	0.4		Max 0.1	0.12
Co	51		65	59	Max 0.2	Max 0.2			
Cr	20	17	27	24	14	13	15	17	12
Fe	2	61	Max 2	Max 2	4	4		61	88
Mn	1.5	8	Max 0.5	Max 0.5					8
Mo							32		
Ni	10.5	8.5			74	76	50	8.5	
N		1.2		1.2					
Si	0.2	4.0	1.2	1.2	4	4	3	4.0	
W	15		5						
HRC	26	30	45	54	55	47	45	95(HRB)	25
Condition	a	b	c	c	c	c	c	a	d

Conditions: a mill annealed; b cold reduced 30%; c as cast; d quenched and tempered. Additional materials: 1-borided coatings on HS-25 and S-6; aluminate diffusion coating on 410.

Source: Ref. 27.

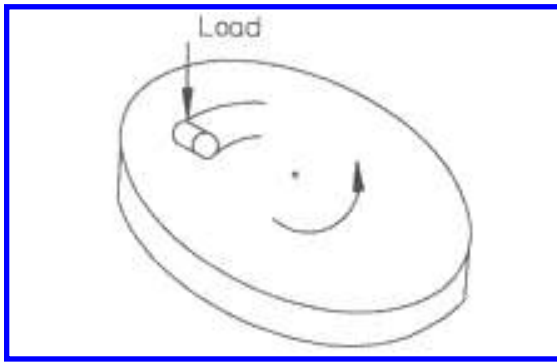


Figure 5.109 Configuration of the initial apparatus.

More lengthy tests, up to 150,000 m., were run on the more promising candidates. [Table 5.32](#) shows some of the wear data obtained in this first level of testing.

The second type of test used provided better simulation. It used the conforming configuration shown in [Fig. 5.110](#) and was conducted in a water environment with the components at 275°C. The radii of the shaft and conforming pin were nominally the same as those of the shaft and bushing in the application. The same load per unit length as in the application was used and the chemistry of the water was controlled to match that in the application. This test configuration did not simulate the reciprocating motion or the complete geometry of the application (i.e., a shaft in a bushing). As a result, the test provided 2nd degree simulation of the application. [Fig. 5.111](#) shows some of the wear curves obtained from those tests. From these type of data, two pairs of materials were selected for field evaluation. The material pairs were S-1 / borided HS-25 (shaft) and N-45 / borided borided HS-25 (shaft).

Field tests were conducted by building several valves using these material combinations and installing them in an operating system. The valves were removed and the wear measured after 1 year of service. The data are summarized in [Table 5.33](#). While these results indicated a significant reduction in wear, as predicted from the prior testing, the results were not entirely as expected. The fact that the S-1 material wore more than the N-45 was not indicated by the prior data. In addition, the data did not indicate the large shaft wear that occurred with N-45. To understand these differences, the wear scars were carefully studied and a model proposed for the behavior. This model centered on the lack of simulation in the second test regarding motion and overall geometry. It was proposed that in the application wear debris tends to be trapped in the bearing area and to act as an abrasive, thereby accelerating wear. However, in the test configuration, the debris tended to be removed from the contact region. It was also speculated that the alternating stress fields in the application could increase fatigue wear effects over that occurring in a unidirectional test. This could possibly result in a faster rate of debris generation, compounding the abrasive action. This led to the following model for the wear behavior. The S-1 debris, which contained carbides, was hard enough to cause abrasive wear of the parent material but not hard enough to abrade the borided surface. With the N-45, the wear debris contained borides, which abraded the borided surface of the shaft. Shaft wear debris then accelerated the wear on both members. Without the borided layer on the HS-25 material, there was evidence from the prior testing that wear debris from the N-45 would become imbedded in the surface

Table 5.32 Laboratory Wear Test Results

Pin material	Plate materials											
	HS-25 (CLA 9 μm)		HS-25 (CLA 1 μm) Borided HS-25 N-60									
Pin-on-plate test results: Pin wear ($\text{mm}^3/[\text{kg}\cdot 10^5\text{m}]$)												
S-6	33, 35		15, 45		5							
S-1			19		1							
N-45	20		30		3, 4							
N-41			81		3							
T-700	52											
Borided S-6	41, 43				10							
Aluminided 410	1535											
N-60					72							
Pin-on-plate test results: pin wear ($\text{mm}^3/[\text{kg}\cdot 10^5\text{m}]$)												
Test distance (10^3m)	Pin wear					Shaft wear (by location)						
	HS-25 shaft		Borided shaft			Borided		HS-25-1		HS-25-2		
	S-6	S6-1	S1-1	N-45	S-1	N-45	1	2	3	4	3	4
84.5	273			131	5.1	7.7	9	13	1	84		
107.7		350		245	20	65	26	48			187	1
84.1			28	349	75	145	36	78			263	4
192.3					113	427	52	770				

Source: Ref. 27.

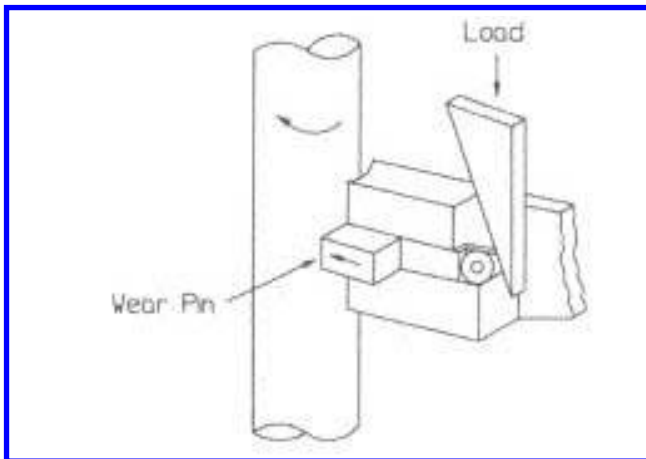


Figure 5.110 Configuration of the second apparatus, which provided better simulation. (From Ref. 27.)

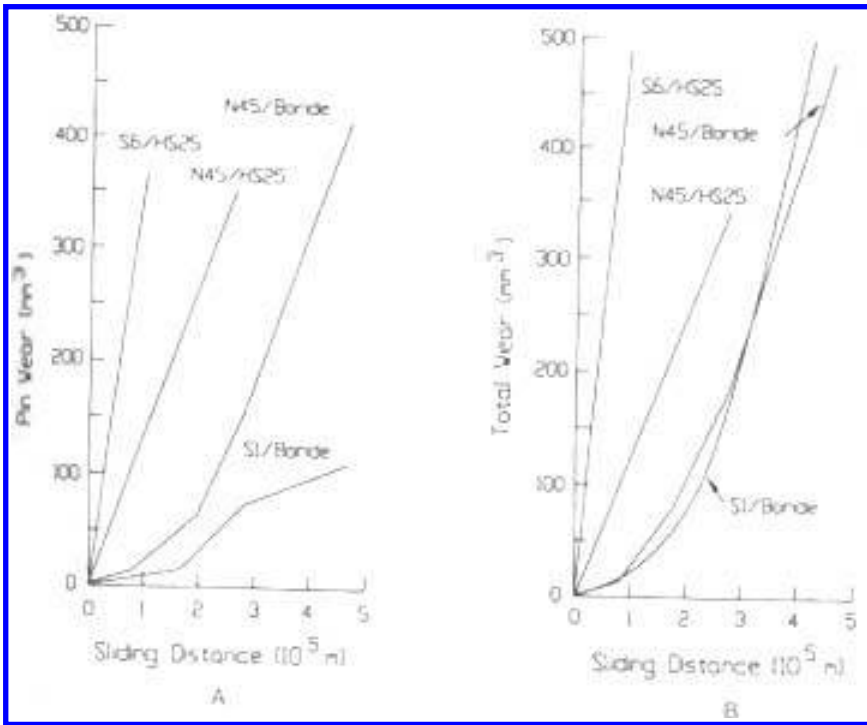


Figure 5.111 Wear results obtained with the second apparatus. “A” shows the pin wear, “B” shows system wear (i. E., pin wear plus shaft wear). (From Ref. 27.)

of the HS-25, improving the wear resistance of that surface. While no tests were done to verify this model, support for the various elements of the model was found in the published literature.

Because of its superior performance in the field tests, N-45 was selected as the bushing material. Uncoated HS-25 was selected as the shaft material because of the acceleration of wear by the borided coating debris that was deduced to occur with this

Table 5.33 *In-service Test Results*

Component	Position*	Wear depth (mm)
Bushing S-1	a	0.53
Bushing N-45	b	0.25
Bushing S-1	c	0.28
Bushing N-45	d	0.43
Shaft	a	0.01
Shaft	b	0.013
Shaft	c	0.025
Shaft	d	0.13

* Positions: a, right side of the valve disc; b, right side of the support trunnion; c, left side of the support trunnion; d, left side of the valve disc.
 Source: Ref. 27.

material. Using the wear data from the field test for the N-45, which is considered to be significantly higher than what which would occur without the borided layer, wear life of the bushing would be 11 years, compared to the 7 for the original material. Using data from the second test, it was estimated that wear rate for the unbored shaft would be 0.25 mm/year, which is approximately three times that for the original. In 11 years, shaft wear would be less than 3 mm, which was acceptable. Therefore, for this combination life was still determined by bushing wear and the new material pair was therefore expected to provide at least a 1.6 times improvement in life.

5.16. PLUG VALVE

Galling was the wear mode in this case study and an empirical approach was used to develop a number of general recommendations for applications where galling tends to be a concern. The test method that was used was similar to the ASTM method, G98, which was standardized some time later (Sec. 9.29 of MWFT2E).

The application, which initiated the wear design, was a plug valve used in a chemical piping system, similar to the plug valve shown in Fig. 5.112 (28). These valves had a tapered plug, which was lapped to fit the tapered body cavity of the valve. In order to prevent leaks tight tolerances, smooth finishes, and large apparent areas of contact are characteristics of these designs. These valves were stationary most of the time and only occasionally operated. With use these valves frequently developed leaks and became difficult to operate. In the extreme seizure would occur. When valves that exhibited these problems were disassembled and examined, localized regions of galling were observed (i.e., localized regions of material transfer and high plastic deformation). A study was initiated to determine better combinations of materials to minimize this tendency, the effects of various material properties on the tendency toward galling, the influence of load and pressure on galling, and the effect of surface roughness parameters on galling. To simulate the conditions of the applications, a tester was developed in which two flat rings were pressed together and rotated 90°. The samples were then separated and the surfaces examined for signs of galling. The apparatus developed is shown in Fig. 5.113, along with a picture

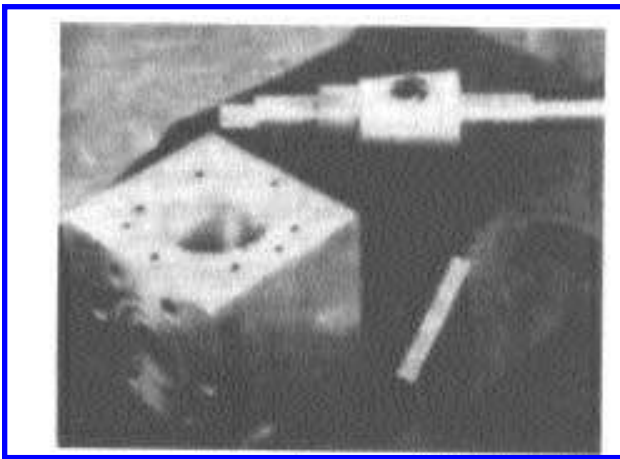


Figure 5.112 Plug valve. (From Ref. 28, reprinted with permission from ASME.)

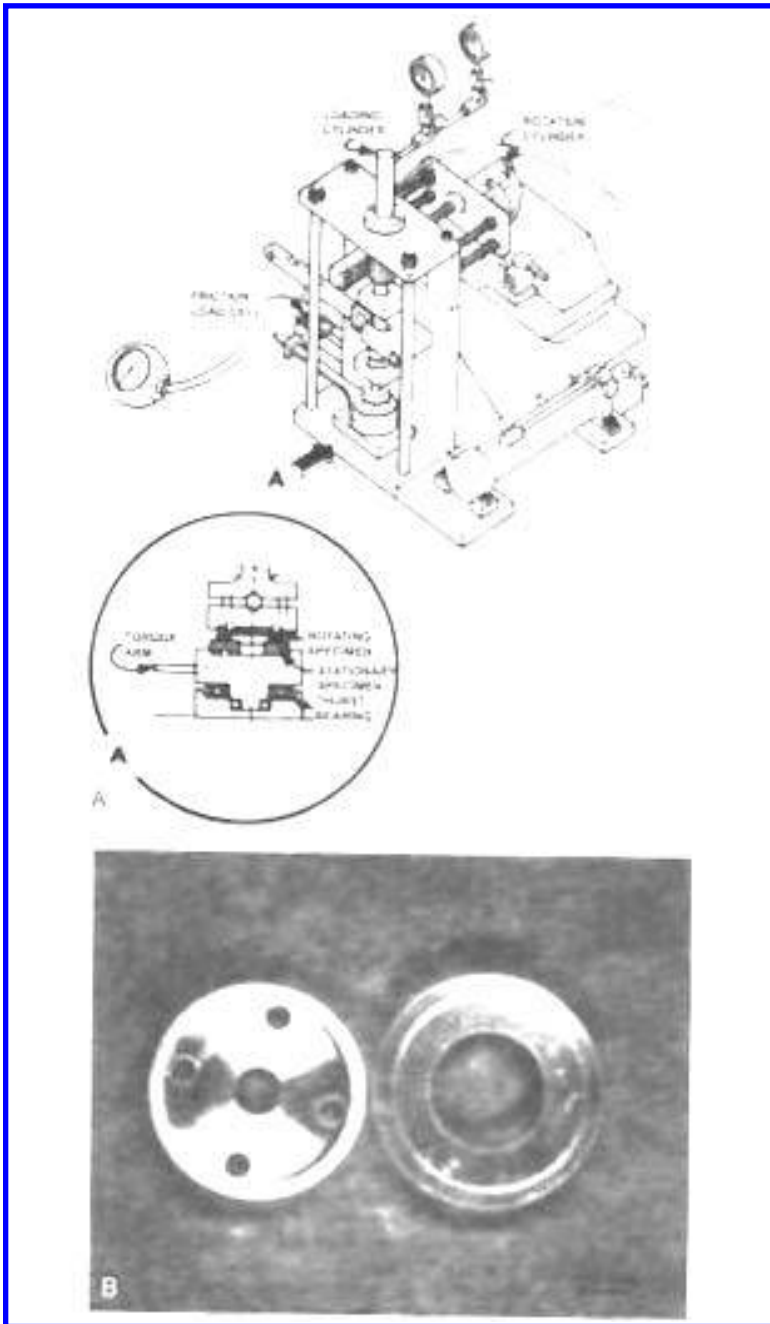


Figure 5.113 Apparatus used to evaluate galling, “A”, and tested specimens “B”. (From Ref. 28, reprinted with permission from ASME.)

of a specimen pair after a test. This tester provided the large conforming contact area, pressures, and typical motion of these valves.

Two methods were used to characterize the effect that the various parameters had on galling. In one method, the test was repeated with increasing loads to determine the critical pressure at which galling just occurs. The onset of galling was determined by carefully examining the surfaces for signs of transfer and deformation after each test; the higher the critical load, the lower the tendency for galling. In the second method, the area of the galled region was determined; a larger area indicated lower galling resistance. Some of the material rankings obtained with the first method are shown in Fig. 5.114. Some of the results related to surface roughness are shown in Fig. 5.115. The type of data obtained from the second method is illustrated in Fig. 5.116. It can be seen that either method provided a means of differentiating galling resistance of materials and the evaluating the effect of different conditions on galling resistance.

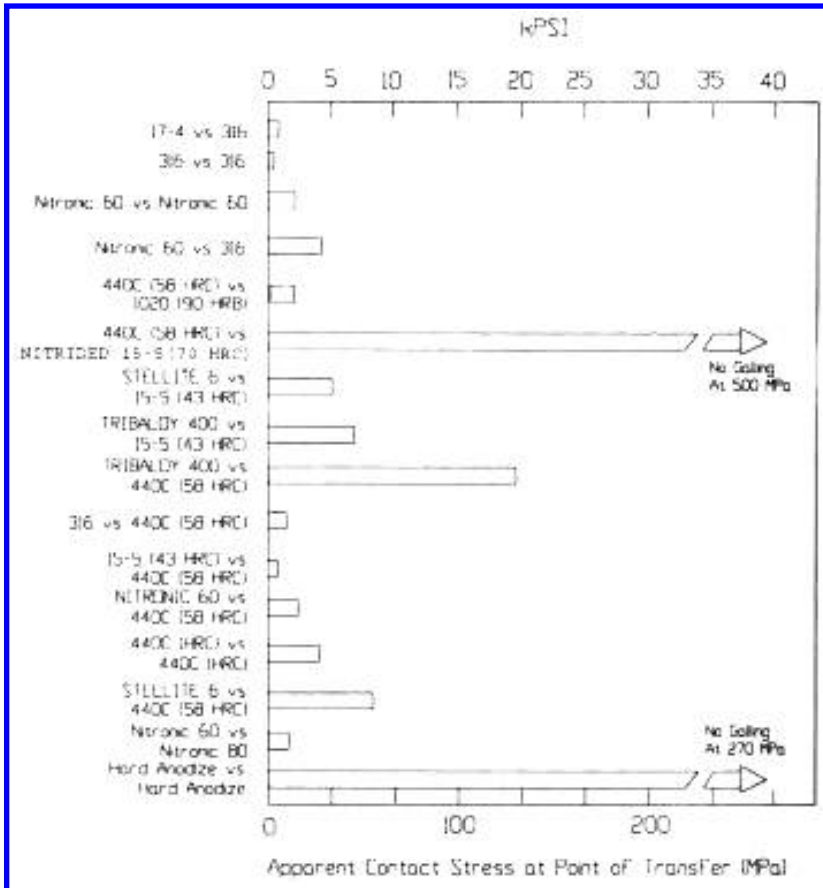


Figure 5.114 Threshold stresses for galling, based on optical examination. Hardness of the 316 specimens was Rb90; Tribaloy 400, Rc48; Stellite 6, Rc42; Nitronic 60, Bhn 200. (From Ref. 28.)

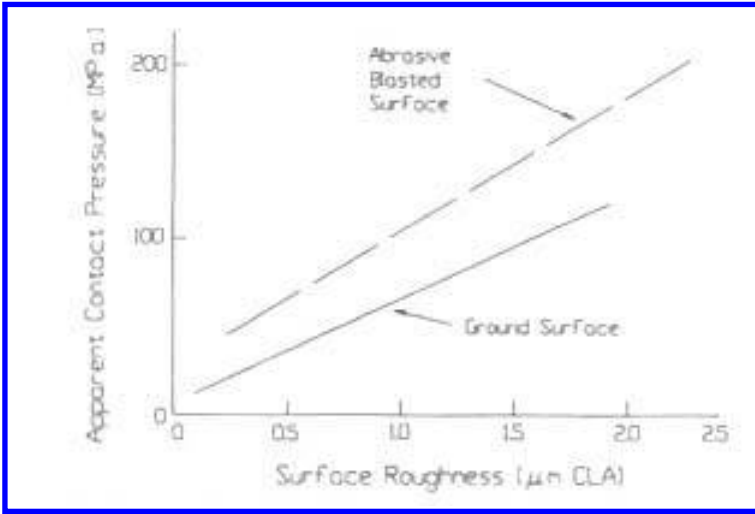


Figure 5.115 Effect of surface finish on galling. (From Ref. 28.)

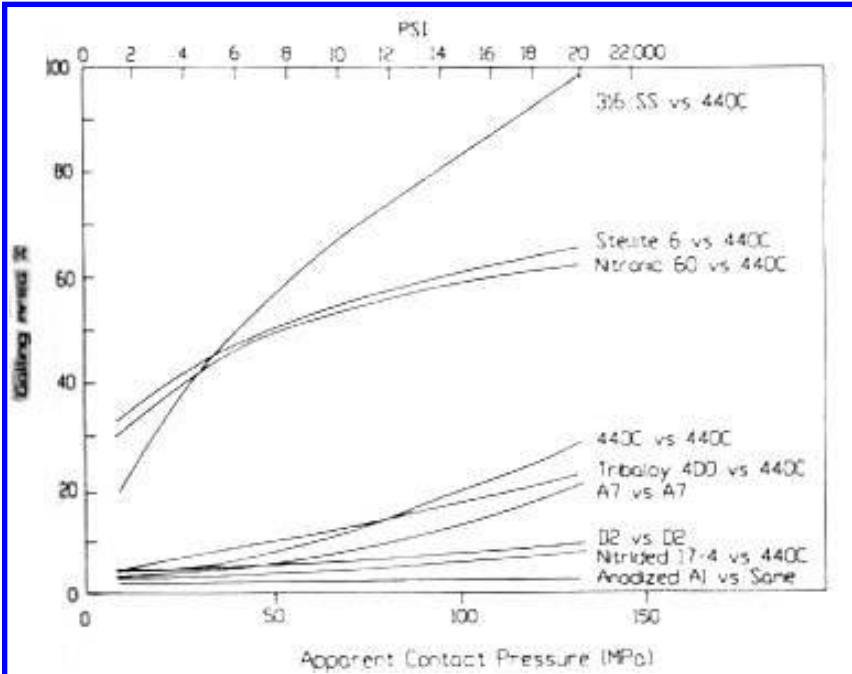


Figure 5.116 Galling area as a function of pressure. (From Ref. 28.)

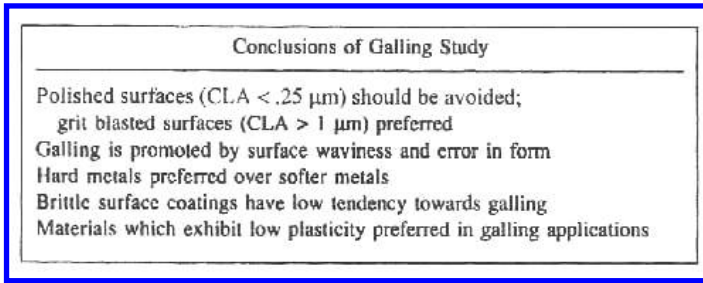


Figure 5.117 Design rules for applications prone to galling. (From Ref. 28.)

From the database that was developed, a more galling-resistant material pair and surface roughness conditions that reduces the tendency for galling were selected for this application, which resulted in improved valve performance. In addition, this information resulted in the formulation of several rules (or guides) for designing devices for which there was an exposure to galling. These design recommendations are shown in Fig. 5.117.

5.17. SCREWNUT–SPINDLE

This case study provides an example of a very systematic approach in the characterization of the wear situation and the development of a test to select materials for a specific application. It involves the development of an improved screwnut–spindle design for an airplane-landing flap (29). The initial design, shown in Fig. 5.118, needed to be replaced after every 3000 landings, because of wear between the nut and the spindle. The purpose of the redesign effort was to improve the life of this device by the use of different materials for the both the spindle and the nut. The approach taken was empirical. A simulative wear test was developed to evaluate different material pairs and used to select the most promising pair for increasing the wear life. Field tests were then performed using the new combination before a complete change over to the new design was implemented.

The starting point for the wear design was examination of the operating conditions and used parts. A very detailed characterization of the operating conditions was developed from these examinations, as well as a characterization of the wear mode. A summary of these characteristics is shown in Fig. 5.119. Fig. 120 (see p. 306) shows a photograph of a typical wear scar on the spindle. It was concluded from these that a compound mode of wear existed. The wear was a combination of abrasive wear, caused by contamination of the grease by dirt during landings and takeoffs, and lubricated sliding wear. Abrasive features of the wear can be seen in Fig. 5.120. Sliding wear features can also be seen. In addition features suggestive of adhesive wear (i.e., transfer) were often found on worn parts. It was decided to develop a simulative test, using a pin-on-ring apparatus (Fig. 5.121—see p. 306). In this apparatus, the spindle material was used for the ring and



Figure 5.118 Spindle and screwnut assembly. (From Ref. 29, reprinted with permission from ASME.)

I.	Type and Technical Function Screwspindle for operating landing flaps of aeroplane
II.	Operating variables Type or motion: intermittent, reciprocating sliding Number of individual operations: 3000 operations between overhauls Sliding distance s [measured along the spindle surface in one direction of movement]: 46 m per single operation Sliding speed v : 0.32 m/sec Load F_N increases with forward displacement from 0 to 4200 N at full displacement; decreases with reversal from a maximum of 1200 N at full displacement to zero. Temperature environment T : $-20^\circ\text{C} < T < +50^\circ\text{C}$
III.	Structure of the Tribosystem Material spindle: CrNiMo steel, comp (wt%): C: 0.30, Ni: 2.5, Cr: 0.7, Mo: 0.50, Mn: 0.65, Si: 0.25, Fe: balance Material screwnut: Copper-Aluminum comp (wt%): Al: 10.0, Fe: 50, Ni: 6.3, Mn: 10, Cu: balance Workshop finish spindle: Grinding; roughness perpendicular to grinding marks: rms = 0.4 μm Workshop finish screwnut: Grinding; roughness perpendicular to grinding marks: rms = 1.6 μm Lubricant: lithium grease "Aeroshell nr. 17" Contaminant: abrasive dust from runways Lubrication condition: mainly boundary Environment: air Contact area screwnut-spindle A : 1915 mm^2 (maximum average pressure p : 2.3×10^6 N/m^2) Contact area/wear track ratio ϵ : screwnut: 100%; spindle: 15%
IV.	Tribological characteristics Worn surface of screwnut: metallic bronze colored; scratches in direction of sliding Worn surface of spindle: differing from one location to another; scratched, lightly oxidized, and covered with transferred CuAl Wear depth after 3000 landings: screwnut: ≈ 1.3 mm; spindle: ≈ 0.13 μm

Figure 5.119 Characterization of the spindle–screwnut tribosystem. (From Ref. 29. Reprinted with permission from ASME.)

the nut material was used for the pin. A comparison of the test parameters and those of the application are shown in Table 5.34. The test conditions did not match the operating conditions in all cases, primarily because of limitation associated with the apparatus. For example, the large load and contact areas of the application could not be duplicated because of size limitations associated with the apparatus. However, it was determined that while there were differences, the morphology of the wear scars in the application and in the test was similar.

Because of the mixture of sliding and abrasive wear in the application, a key element to the simulation was the use of contaminated grease as a lubricant. The amount of Norwegian sand that was added to the grease to provide simulation was selected by a cut-and-try procedure. Tests were run without lubrication and severe transfer, uncharacteristic of the application resulted. With uncontaminated grease, significant transfer still

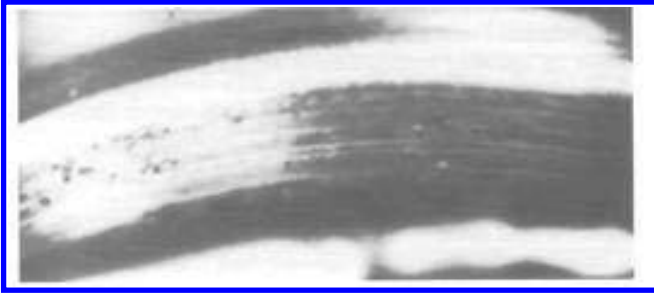


Figure 5.120 Wear scar on spindle, showing sliding and abrasive wear features. (From Ref. 29. Reprinted with permission from ASME.)

occurred and the abrasive features were absent. With the addition of the sand, abrasive features were introduced and transfer was further reduced. By trying several different ratios, it was concluded that the 7/4 ratio resulted in a morphology that was most similar to the morphology occurring in the application. The results of these tests are shown in Table 5.35. It was also found that with this ratio, the average wear factor for the original materials (i.e., wear, volume / load \times distance) was similar in the test and in the application.

Material candidates for the application were selected on the basis of availability, machinability, and cost. They included a variety of bearing materials, both metallic and polymer, for the nut and a variety of coated and uncoated steels for the spindle. Three filled fluorocarbons and electroless nickel coated steel combinations were identified as replacement candidates. Test results for these combinations and the original material pair are given in Table 5.36. It was anticipated that a 30-fold improvement in life might be achievable with these combinations. Partial results of field tests with these pairs have indicated that the actual improvement was greater than a factor of 10.

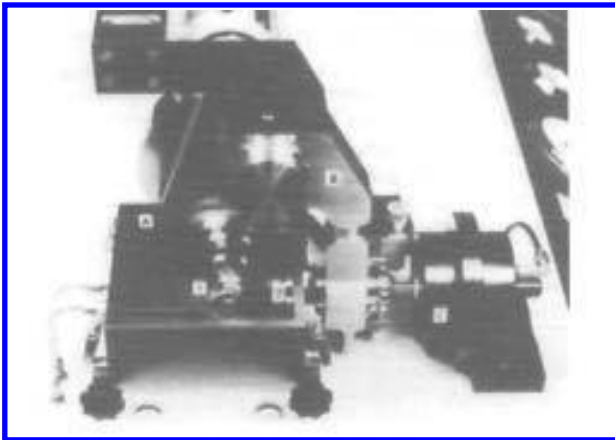


Figure 5.121 Pin-on-ring apparatus used to stimulate spindle/screw nut wear. (From Ref. 29, reprinted with permission from ASME.)

Table 5.34 Comparison of Operating Variables and System Structure in Practice and in the Laboratory

Item	Practice	Laboratory
Geometry	Screw-nut spindle	Pin-ring
Contact area	1915 mm ²	160 mm ²
Contact ratio	Screw-nut: 100% Spindle: 15%	Pin: 100% Ring 15%
Workshop finish	Screwnut: 1.6 μm rms Spindle: .4 μm rms	Pin: 1.6 μm rms Ring: .4 μm rms
Load	Variable; maximum 4400 N	Constant; 875 N
Contact pressure	Variable; maximum 2.3×10^6 N/m ²	Constant; 5.47×10^6 N/m ²
Type of motion	Intermittent; reciprocating sliding	Continuous sliding
Sliding speed	0.32 m/s	0.32 m/s
Total sliding distance	27,600 m	6192 m
Energy dissipated	3.03×10^7 Nm	0.6048×10^7 Nm
Lubricant	Grease "Aeroshell nr. 17"	Grease "Aeroshell nr. 17"
Contaminant	Dust from runways	"Norwegian sand"

Source: Ref. 29.

5.18. CARDAN JOINT

An empirical approach was used in this case study. The wear design started with an investigation of the application and determination of operating and environmental parameters. Two wear testers were then designed and built to simulate the wear condition of the application. One provided a constant load but could accommodate several specimens, facilitating the development of a database. The other tester provided dynamic loading conditions, more representative of the application but could only accommodate a single specimen. Tests with these apparatuses were used to investigate the effect of several

Table 5.35 Test Results for the Reference Couple, Cu10Al Bronze-CrNiMo Steel. Used to Establish Simulation

Condition	Wear depth (mm)			Transfer
	Pin	Ring	μ	
Dry; no abrasive	> 9.3		0.37	Heavy
Grease; no abrasive	0.1	< 0.01	0.03	Mild
Grease with abrasives;	1.8	0.10	0.14	Mild
7:1 grease to abrasive ratio	0.6	0.02	0.11	Medium
	0.2	0.06	0.08	None
	> 5.3	> 0.01	0.25	Heavy
	0.1	0.01	0.12	Mild
	5.5	0.01	0.23	Heavy
Grease with abrasives;	1.3	0.09	0.16	Mild
7:4 grease to abrasive ratio	3.0	0.19	0.18	Mild
	> 6.4	> 0.55	0.14	Mild
	1.3	0.14	0.16	Mild

Source: Ref. 29.

Table 5.36 Wear Test Results for Several Fluorocarbons against Nickel Coated Rings

Pin material	Wear depth (mm)		Transfer
	Pin	Ring	
Fluorocarbon A	0.1	0.01	None
	0.1	0.03	None
Fluorocarbon B	< 0.1	0.03	None
	0.1	0.02	None
Fluorocarbon D	0.1	0.01	None
	0.1	0.01	None
Original pair	3.0	0.24	Mild

Source: Ref. 29.

factors on wear and to evaluate materials for use in this application. Conceptual models were developed for the observed effects and related to the application. The data and information developed were used to improve the existing design.

This wear design approach was used to identify design improvement for a cardan joint to reduce maintenance (30). The cardan joint was used in roll-drive spindles used in a steel mill. The configuration of the spindles and the joints are shown in Fig. 5.122. During operation, reciprocating sliding occurred between the slipper pads, the joint head, and the wobbler causing wear. The joint was designed to accommodate replacement of the slipper pads. In an effort to confine the wear to these pads, copper alloys or polyimides were generally used for the pads and hardened steels for the joint head and

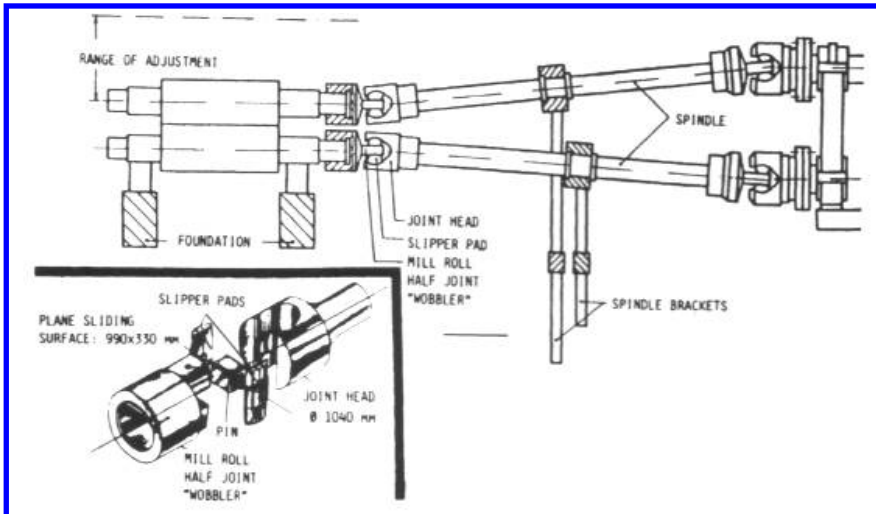


Figure 5.122 Steel mill roll-drive assembly and the cardan joint (inset). (From Ref. 30, reprinted with permission from ASME.)

wobbler. However wear, sufficient to require their replacement, frequently occurred on the counterfaces as well. The purpose of the wear design was to identify improvements to these designs that would extend life, particularly of the joint heads and wobblers, and result in significantly reduced maintenance costs.

From a study of the operating conditions, it was concluded that the interface conditions could nominally be described as a heavily loaded flat-on-flat contact with mixed or boundary lubrication. The load tended to fluctuate and that the reciprocating motion was sinusoidal. Abrasives from the steel mill environment were found to contaminate the lubricant and the interfaces. This tended to be particularly severe for the joints near the roll, since shielding could not be used in that location. It was decided to simulate these conditions in a wear tester and to use the tester to study the effects of different materials and other design parameters on wear. Among these were the effects of pressure, lubrication rate and type, and load fluctuation on wear. To provide adequate simulation, it was considered necessary to match the basic contact geometry, motion, pressure, lubrication, and contamination conditions in the application. Two testers were developed for this simulation. One was a multi-specimen tester that maintained a constant load. The other used a single specimen but had the capability of providing an oscillating load, which could be used to simulate the fluctuating load condition in the application. Both used the same type of specimens (Fig. 5.123). The simulation that these two testers provide is illustrated in Table 5.37. The table summarizes the conditions in the two testers and the application.

For metals, wear was measured in terms of weight loss. For plastics, because of their lower density, this was impractical. For these materials, the wear was measured in terms of changes in specimen thickness. Friction was also measured in many of the tests, as well as temperature of the specimens. Frequently, the state of the worn specimens was analyzed

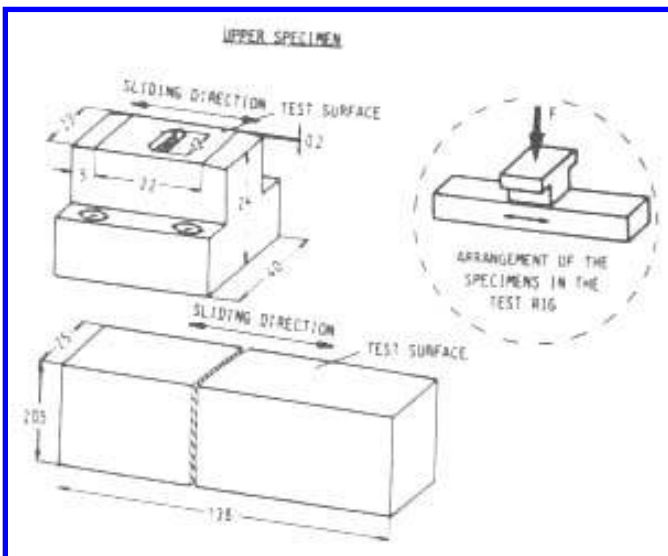


Figure 5.123 Wear specimens used to simulate cardan joint wear. (From Ref. 30, reprinted with permission from ASME.)

Table 5.37 Comparison of the Parameters of the Cardan Joint in the Mill Application with Those of the Wear Test Apparatus

Parameter	Application	Wear test apparatus	
		Test rig I	Test rig II
Number of test positions	—	4	1
Sliding surface area (mm ²)	< 10 ⁵		0–400
Compressive force (N)	0.001	Static: 4×10^3 -3×10^4	Static: 5×10^2 – 10^5 Dynamic: $F_{0\max} = 6 \times 10^4$ $F_{0\min} = 0.05 F_0$ 3–16
Frequency of oscillation (Hz)	12–16	—	3–16
Contact pressure (N/mm ²)	$p \geq 10$	Static: 10–75	Static: 1.3–250 Dynamic: $p_{0\max} = 150$
Speed (min ⁻¹)	45–100		30–70
Unidirectional stroke length (mm)	0–150		0–100
Rubbing speed (m/s)	$v_{\max} = 0.8$		$v_{\max} = 0.36$
Lubricant conditions	Mixed friction, continuous and discontinuous oil and grease lubrication. Dry operation is possible		
Contamination:	Scale, dust; addition of abrasive particles is possible		

Source: Ref. 30.

by other techniques, such as SEM examination and microhardness measurements, to gain a more complete understanding of the wear. These examinations were used in the development and verification of conceptual models for observed trends in wear behavior. Wear curves (i.e., wear vs. sliding distance) were obtained by intermediate measurements during tests of standard duration. Typical wear curves from these tests are shown in Fig. 5.124. The amount of wear at the end of these tests was used to evaluate the effects of various factors on the wear of the individual counterfaces and of the system.

Consideration was given only to those materials whose properties were consistent with the general requirements of the application. In effect, this limited the materials considered to those already in use or to materials whose manufacturing characteristics, corrosion resistance, mechanical strength, and thermal characteristics were similar. A list of some of the materials selected and evaluated is shown in Table 5.38. Wear results for several plastic / steel pairs are given in Fig. 5.125 (see p. 313). These data illustrates some of the factors, such as pressure and processing, which were considered in the wear design. From subsequent analysis of the worn specimens, it was concluded that the superior wear performance obtained with the carbon fiber-filled polyimide was the result of better thermal conductive and higher strength obtained with this fiber.

The effect of fluctuating load on wear was also investigated (Fig. 5.126—see p. 314). It was concluded that two effects were likely involved. One was an improvement in lubrication as the result of a pumping action caused by the load fluctuation. The other was the increase in wear associated with peak contact stress (load).

Another factor that was investigated was the relative hardness of the two counterfaces. This was considered to be an important factor, since it was desirable to have most of the wear to occur on the pad rather than the wobbler or head. Fig. 5.127 (see p. 315) shows such a comparison. As can be seen in this figure, an optimum condition was also

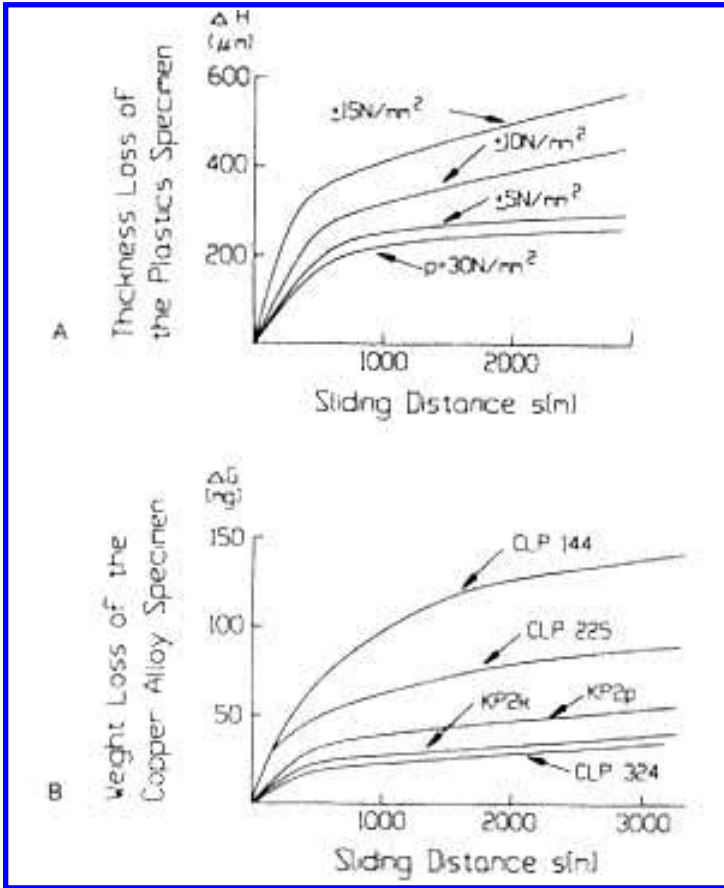


Figure 5.124 Wear curves obtained with Test Rig II. “A” shows the influence of dynamic load amplitude; “B” shows the influence of different lubricants. (From Ref. 30.)

found to exist with this variable, relative hardness. This was explained in terms of the interaction of three effects. One effect is the tendency for the steel to wear more as the hardness of the counterface increases. The second is the tendency for the adhesion effects to increase the wear of the copper alloy as its hardness is lowered. The third is an increase in abrasive wear of the steel as a result of copper alloy wear debris. SEM studies of the worn surfaces confirmed these effects.

Tests were also conducted to evaluate other effects. This included evaluating different greases and oils, different rates of lubrication, and the effect of contamination on wear. From the results of these tests design recommendations were developed, which resulted in improved performance. Some of the modifications were optimizing hardness differences, optimum metallurgical structure for copper alloys, use of carbon fiber reinforcement for polyimides, and replacement of polyimide pads with copper alloy pads when there is an exposure to contamination by hard particles.

Table 5.38 Materials Considered for the Cardan Joint and Their Properties

Material characteristics												
Composition												
Cu alloys DIN1700/06	Cu	Sn	Zn	Ni	Mn	Fe	Al	Pb	Mg	Hardness (HV10)		
CuAl10Ni	78.5	< 0.1	0.07	5.6	0.26	5.15	10.3	0.01	< 0.01	219		
CuSn12	87.6	11.2	0.07	0.66	< 0.01	0.2	0.01	0.16	< 0.01	97		
CuSn12Ni	86.0	11.8	0.05	1.4	< 0.01	0.28	0.01	0.4	< 0.01	106		
CuZn34Al2	60.8	0.28	32.7	0.8	2.1	1.0	2.0	0.28	< 0.01	154		
CuAl11Ni	77.9	0.1	< 0.07	6.2	0.31	5.1	10.3	0.02	< 0.01	234		
Steels ^a DIN1700/06	Cu	C	Si	Ni	Mn	P	Al	S	N	Cr	Mo	Y
34CrMo4	0.17	0.34	0.38	0.18	0.92	0.025	0.034	0.024	0.011	1.1	0.24	0.04
34CrNiMo6	0.15	0.35	0.30	1.43	0.60	0.021	0.033	0.029	0.006	1.6	0.21	< 0.01
46MnSi4	0.17	0.49	0.95	0.08	0.99	0.023	0.006	0.028	0.006	0.2	0.01	< 0.01
Plastics DIN7728					Density (mg/mm ³)	Tensile strength (N/mm ²)		Modulus (N/mm ²)		Thermal conductivity (W/K m)		
Molded polyamide + MoS ₂ (2%)					1.16	78		3200		0.24		
Molded polyamide					1.16	76		3200		0.24		
Extrude polyamide					1.14	80		3200		0.23		
Thermoset polyimide					1.64	40 ^b		13000		—		
Molded polyamide + glass fibers (20%)					1.23	190 ^b		15000		1.51		
Oils ^c DIN51502	Kinematic viscosity (mm ² /s)					Density (kg/m ³)	Flash point °C	NN mgKOH/g oil	SN mgKOH/g oil			
	50°C	100°C										
CLP 144	148.2	19.3				906	242	1.02	1.48			
CLP 225	242.7	26.5				912	248	0.88	1.21			
CLP 324	317.9	34.3				907	280	1.12	1.92			
Base oil												
Kinematic viscosity (mm ² /s)												
Greases ^d DIN51502	50°C	100°C	Flash point °C				Thickener		Timken-Test			
KP2k	92	15	220				Li-12-hydroxy-sterarat		5.0 + 0.5 mg wear at 43 lb			
KP2p	300	—	310				Organic polymer		Wear < 5 mg at 35 lb			

^aAll steel heat treated to 230 to 350 HV10.

^bFracture strength.

^cAll oils are mineral oils with additives for corrosion protection, resistance to aging, and extreme pressure.

^dGreases with extreme pressure additives and an operating temperature range of -20 °C to 140 °C.

Source: Ref. 30.

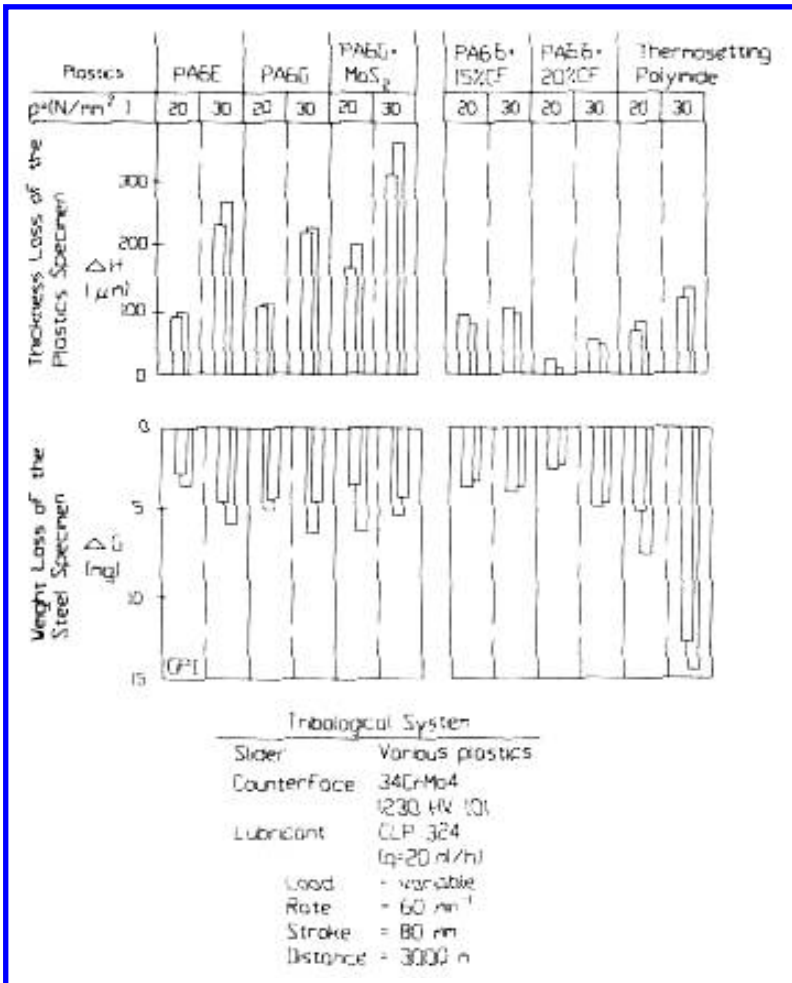


Figure 5.125 Wear of various plastic/steel couples. (From Ref. 30.)

5.19. ELECTROMAGNETIC CLUTCH

This case study provides an example of the use of mathematical simulation of coupled wear and functional behavior. In this wear design, mathematical models for both function and wear were used to investigate the effects of various design parameters on performance and life (31).

Electromagnetic clutches are frequently used in computer peripheral applications for the transmission of intermittent motions. Examples can be found in high-speed printers, where the paper motion is stopped for each line of print, and in tape drives, where the

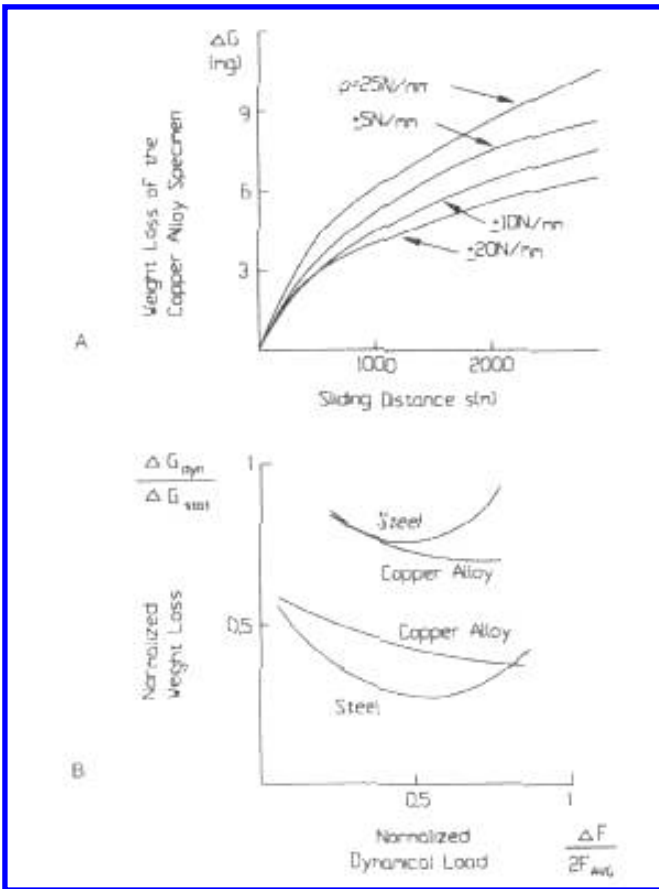


Figure 5.126 The influence of load fluctuations on the wear. “A” shows wear curves for a static load and different amplitude of fluctuating load. “B” shows the effect as a function of the ratio of the amplitude of the fluctuation to the average load. (From Ref. 30.)

tape is continually stopped and started. Transmission of torque and start / stop times is significant functional characteristics of these applications and long wear life is desirable. The design of a typical clutch used in these applications is shown in Fig. 5.128. An electric current is used to create a magnetic field, which is transmitted through the metal rings of the rotor and the metal plate of the armature. This causes the stationary armature to be pulled against the surface of the rotor, which is in motion. As a result of friction between the two surfaces, torque is transmitted across the interface, which causes the armature to accelerate until its speed matches that of the rotor. During this acceleration period, relative slip occurs between the two surfaces and results in wear. A similar situation occurs when these devices are used as brakes. However, in those cases, the armature is initially moving and the rotor is fixed. Slip occurs until the armature is stopped.

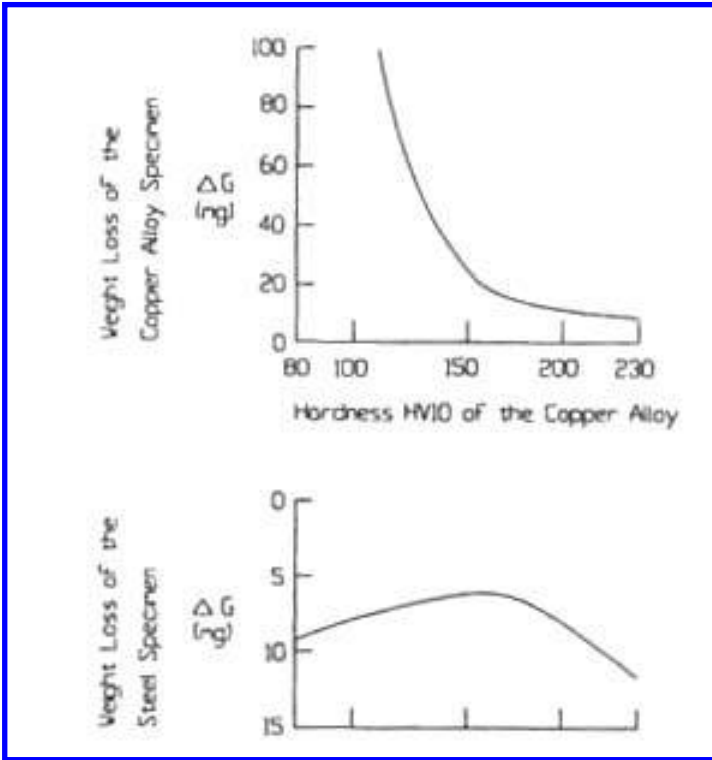


Figure 5.127 The effect of relative hardness on wear. The data are for Cu alloys of different hardness sliding against a 230 HV 10 steel counterface. A hardness differential of 80 HV 10 results in an optimum wear condition. (From Ref. 30. Reprinted with permission from ASME.)

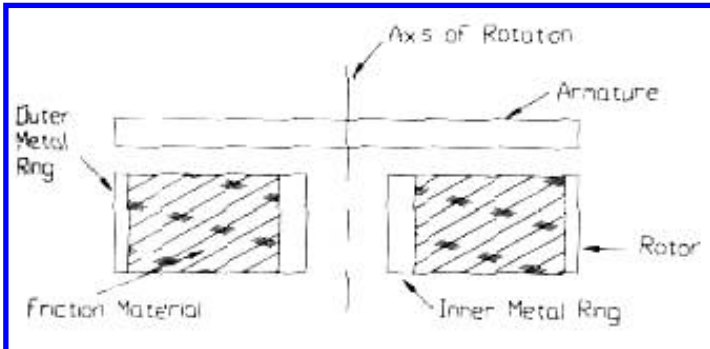


Figure 5.128 Disk clutch design. (From Ref. 31.)

An important design parameter for response time of these devices is the air gap between the rotor and the armature, when unactuated. Wear tends to increase this gap and results in degraded performance. For small amounts of wear, it is often possible to readjust the device to give the desired performance. However, after large amount of wear, it is necessary to replace the device.

Typically, a soft iron or similar material was used for the armature and the inner and outer rings of the rotor to avoid residual magnetism. The material, located between the rings of the rotor, was a filled plastic. While called a friction material, the main function of this material was to influence the wear life of the device. The coefficient of friction between this material and the armature tended to be much lower than between the rings and the armature. As a result, the torque was primarily transmitted through the ring-armature interfaces. Wear life, on the other hand, was known to be a function of both the friction material and the metals used for the rotor and armature. Since this was the case, one way of improving the wear resistance of these clutches was the use of hardened or harder steels as the ring and armature materials. In considering the use of these harder materials, two concerns were identified, which were both associated with the magnetic properties of these materials. One was the effect that these harder magnetic materials might have on functional performance (e.g., a possible reduction in torque because of poorer magnetic properties). The other one was residual magnetism causing the armature to remain in contact with the rotor when unactuated. Both of these could result in more slip at the interface, tending to increase wear. It was concluded that it was necessary to evaluate the effect of such a material change in context of the overall system, including performance aspects and material interactions. To investigate the feasibility of such changes, it was decided to analytically model the wear behavior of a clutch.

For the purposes of analysis, it was assumed that the design could be simplified to the one shown in Fig. 5.129 and that only wear of the rotor needed to be considered. It was also assumed that Zero and Measurable Wear Models for Sliding could be used to describe the wear of each material. For the contact geometry, these models provide the following expressions for the wear rate of each member:

$$W_{fm} = \left[\frac{(0.25 + \mu_{fm}^2)^{0.5}}{\Gamma_{Rfm} \tau_{yfm}} \right]^9 P_{fm}^9 \quad (5.127)$$

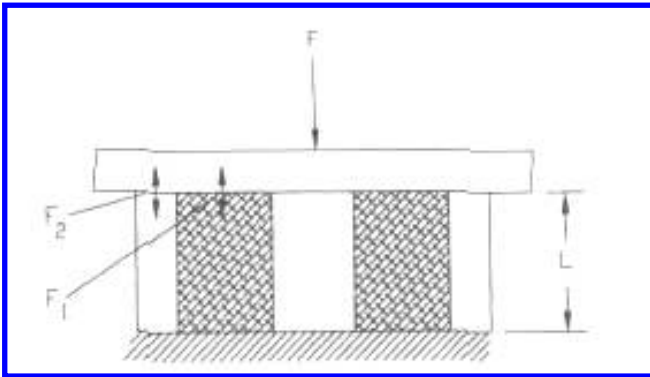


Figure 5.129 Model used for disk clutch. (From Ref. 31.)

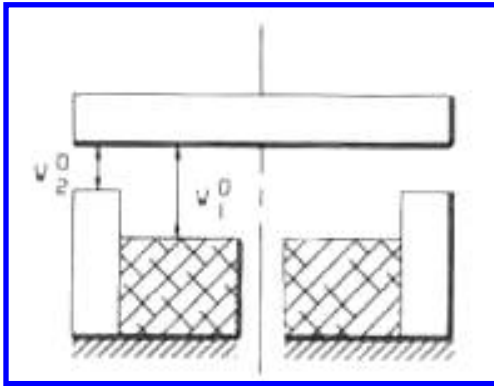


Figure 5.130 Unloaded clutch after initial wear. (From Ref. 31.)

$$W_r = \left[\frac{(0.25 + \mu_r^2)^{0.5}}{\Gamma_{Rr} \tau_{yr}} \right]^9 P_r^9 \tag{5.128}$$

where W is the depth wear rate; μ , the coefficient of friction; Γ_r , the zero wear factor; τ_y , the yield point in shear; and P is the contact pressure. The subscripts, fm and r, indicate the friction material and ring material, respectively. At any stage in the life of the clutch, it was assumed that the pressure on each member was different. It was concluded from examinations of worn rotors that the ring tends to protrude above the friction material

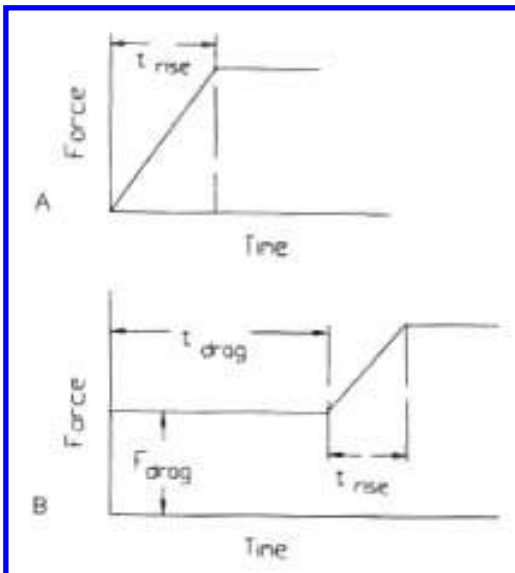


Figure 5.131 Clutch force-time profiles. “A” for the case where there is no residual magnetism present; “B”, when there is. (From Ref. 31.)

(Fig. 5.130). Assuming this to be the case and that uniform contact occurs when the armature is in contact, it can be shown that the pressure on the two members at any stage of the wear is as follows:

$$P_{fm} = \frac{FL + (W_r - W_{fm})E_r A_r E_{fm}}{E_{fm} A_{fm} + E_r A_r} \frac{E_{fm}}{L} \quad (5.129)$$

$$P_r = \frac{FL + (W_r - W_{fm})E_r A_r + (W_{fm} - W_r)E_r}{E_{fm} A_{fm} + E_r A_r} \frac{E_r}{L} \quad (5.130)$$

where P is the pressure on the member, F , the total load created by the magnetic field; W , the wear depth on each member; E , the modulus of each material; A , the areas of each member; and L is the thickness of the two members. Two functional forms that were based on magnetic theory and data for electromechanical devices were assumed for F . These are illustrated in Fig. 5.131. The amount of drag and the rise time were a function of assumed magnetic properties.

Using these basic relationships, a set of simultaneous differential and algebraic equations were developed which described both the functional and wear performance of the device (Fig. 5.132). These equations were solved numerically for several different

Operational equations

$$\frac{dP_2}{dt} = \frac{E_2}{E_1 A_1 + E_2 A_2} \frac{dF}{dT} + \left[k_1 c_1 \left(\frac{F - A_2 P_2}{A_1} \right)^9 - k_2 c_2 P_2^9 \right] \frac{E_1 E_2 A_1}{(E A_1 + E_2 A_2) L}$$

$$x_1 = R (\Theta_{in} - \Theta) = x_2$$

$$\dot{\Theta}_{in} = \frac{2 \pi RPM_{in}}{60}$$

$$\dot{\Theta} = \int \ddot{\Theta} dt$$

$$\dot{\Theta} = \frac{T}{J}$$

$$T = TP_1 + TP_2$$

$$TP_i = P_i \left(\frac{2}{3} \pi \mu_i \right) \left(\frac{OD_i}{2} \right)^3 - \left(\frac{ID_i}{2} \right)^3, \quad i = 1, 2$$

Wear equations

$$W = \int \dot{W} t \, dt$$

$$FWR_i = \frac{\Delta W_i}{\Delta \text{Cycles}} \quad i = 1, 2$$

$$\dot{W} = C P^9$$

$$C = B \left(\frac{\sqrt{25 + \mu^2}}{\gamma_r \tau_y} \right)^9$$

Figure 5.132 Equations used to describe the operation and wear behavior of the clutch. (From Ref. 31.)

Table 5.39 Parameter Values for Reference Clutch

$D_1 = 1.453$ in.	$B = 100,000$	$E_{fm} = 456,000$ psi
$D_2 = 1.672$ in.	$\mu_{fm} = 0.35$	$E_r = 30,000,000$ psi
$D_3 = 2.359$ in.	$\mu_r = 0.75$	slope = 25,000 lb/sec
$D_4 = 2.500$ in.	$\tau_{yfm} = 1,500$ psi	$t_{rise} = 0.002$ sec
$L = 0.5$ in.	$\tau_{yr} = 44,000$ psi	$t_{drag} = 0.0$ sec
$J = 0.0032$ in. lb sec ²	$\Gamma_{Rfm} = 0.54$	$F_{drag} = 0.0$ lb
$RPM_{in} = 760$	$\Gamma_{Rr} = 0.2$	

Source: Ref. 31

conditions to determine trends. One set of conditions, shown in Table 5.39, described a clutch for which there were functional data and as well as some limited wear data. These data were used as a reasonableness check on the model. The results of several of these numerical simulations are shown in Figs. 5.133–5.136. Since a scaling factor was used for wear in the calculation to conserve computer time, absolute time is not indicated on these graphs. It can be seen that after an initial period, the torque and wear rate tended to stabilize for all conditions considered. This behavior was also observed experimentally for this clutch. Additionally, there was good agreement between the torque and response time predicted by the model and those measured. The model also demonstrated the beneficial effect of the friction material on the overall wear behavior that had been found to be the case in practice. As a result, it was concluded that this model for clutch behavior

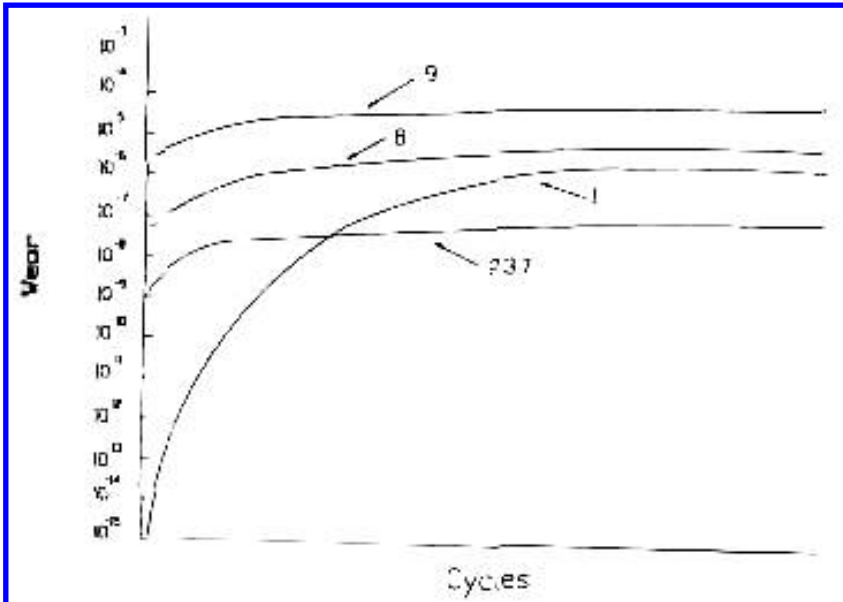


Figure 5.133 Friction material wear curves for different design conditions. (From Ref. 31.)

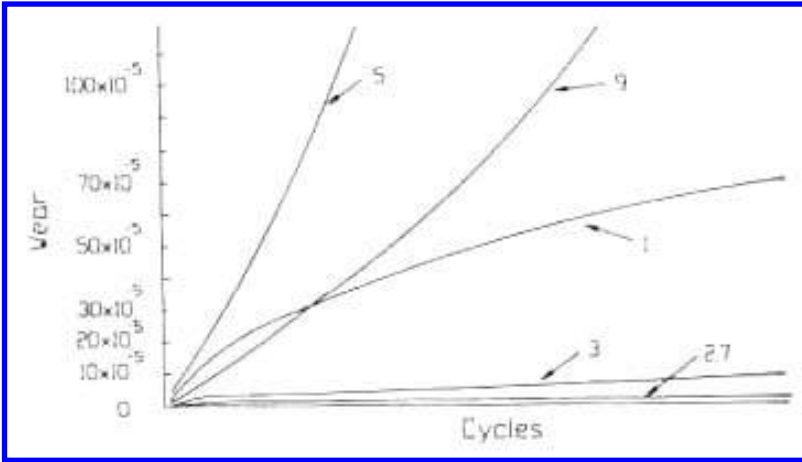


Figure 5.134 Ring wear curves for different design conditions. (From Ref. 31.)

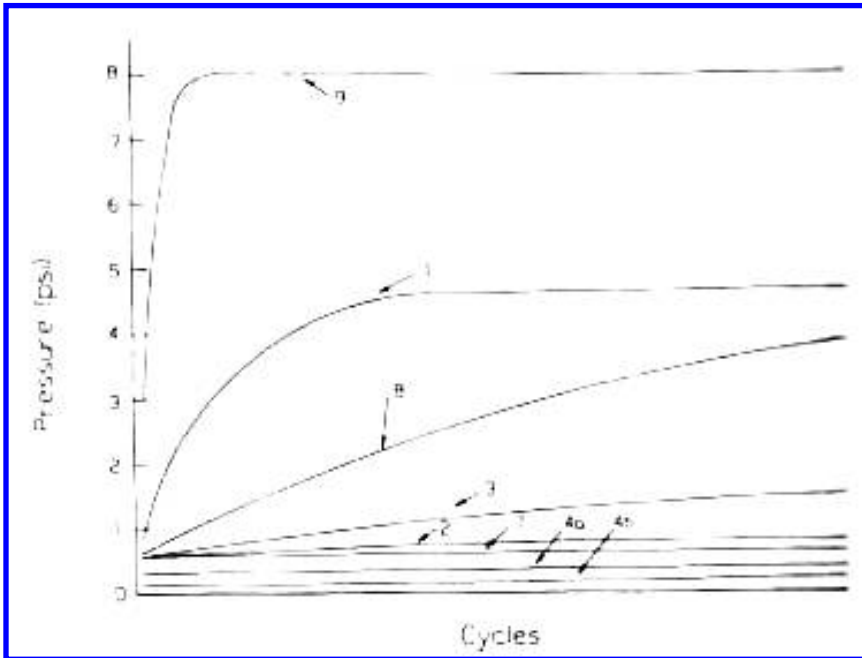


Figure 5.135 Pressure change on the friction material for different design conditions. (From Ref. 31.)

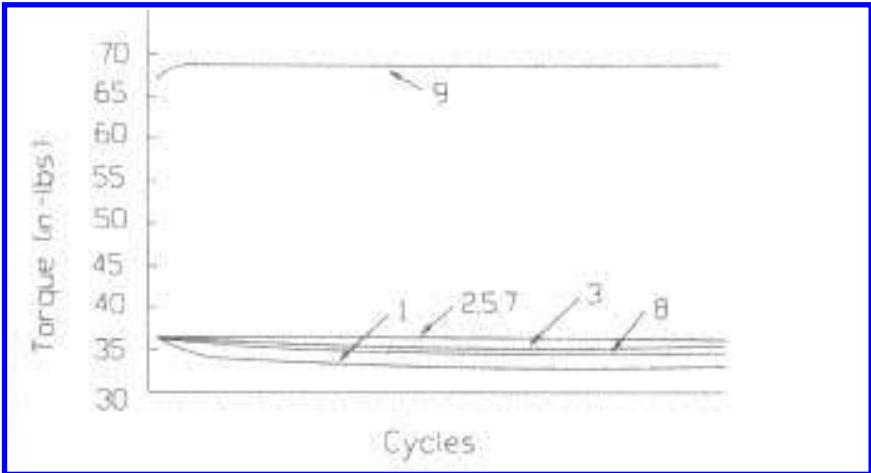


Figure 5.136 Changes in torque as a result of wear for different conditions. (From Ref. 31.)

Table 5.40 Simulation Results Obtained with the Clutch Model

Case	Long-term wear rate (normalized)		Wear depth (normalized)	
	Friction material	Ring	Friction material	Ring
Ref.	1	1	1	1
Increased residual magnetism by a harder ring	1.57×10^{-7}	4.6×10^{-2}	1.23×10^{-7}	3.0×10^{-2}
Increased ring hardness (simulation of the effect of work hardening)	1.05×10^{-4}	2.25×10^{-1}	4.07×10^{-1}	1.76×10^{-1}
Effect of drag with a hard ring:				
"a" $2 \times$ drag in "b"	a 8.9×10^{-11}	2.6×10^{-4}	1.55×10^{-10}	1.65×10^{-4}
	b 1.69×10^{-13}	5.07×10^{-7}	3.0×10^{-13}	3.21×10^{-7}
Removal of friction material		7.29		4.63
Removal of the ring material	1.92×10^6		3.4×10^6	
Hardening of the ring without drag	1.29×10^{-7}	4.35×10^{-2}	1.05×10^{-7}	2.86×10^{-2}
Decreasing the rate of buildup of magnetic force	1.49×10^{-1}	5.5×10^{-1}	5.56×10^{-2}	5.35×10^{-1}

Source: Ref. 31.

could be used to evaluate the feasibility of material changes to obtain improved wear performance.

From simulations of the wear and performance behavior for different design parameters, it was concluded that harder materials could be used for the rings and armature to obtain better wear life without the loss of functional performance. In fact, the analysis indicated that some improvement in functional performance was possible with harder materials. The model predicted more stable behavior and higher torque with harder materials.

REFERENCES

1. RG Bayer. *Wear Analysis for Engineers*. NY: HNB Publishing, 2002.
2. R Bayer, T Ku. *Handbook of Analytical Design for Wear*. New York: Plenum Press, 1964.
3. C Moyer, H Neifert. A First-order solution for the stress concentration present at the end of roller contact. *ASLE Trans* 6:324–326, 1963.
4. A Blodgett, D Barbour. Thermal conduction module: a high-performance multilayer ceramic package. *IBM J R&D* 26(1):30–36, 1982.
5. P Engel. Percussive impact wear. *Trib Intl* 1978; Jun:169–176.
6. R Bayer. Influence of oxygen on the wear of silicon. *Wear* 69:235–239, 1981.
7. R Bayer, A Trivedi. Molybdenum Disulfide Conversion Coating Metal Finishing 1977; Nov: 47–50, 1977.
8. R Bayer. Experimental verification of fatigue wear equation. *Wear* 11:700–706, 1968.
9. R Bayer. Impact wear of elastomers. *Wear* 112:105–120, 1986.
10. P Engel, E Sacher. A computer implementation of frequency-temperature superposition for dynamic mechanical transformations. *J Appl Polymer Sci* 19:791–799, 1975.
11. R Bayer. Wear by paper and ribbon. *Wear* 49:147–168, 1978.
12. P Engel, R Bayer. Abrasive impact wear of type. *J Lub Tech Trans ASME Series F* 98(2): 330–334, 1976.
13. R Bayer, J Sirico. Comments on the frictional behavior between a print character and a camon ribbon. *Wear* 11:78–83, 1968.
14. R Bayer. A model for wear in an abrasive environment as applied to a magnetic sensor. *Wear* 70:93–117, 1981.
15. R Bayer, R Ginsburg, R Lasky. Settable and Airborne Particles in Industrial Environments. *Proc 35th Mtg IEEE Holm Conf Electrical Contacts IEEE* 155–166, 1989.
16. E Lewis. Application of magnetization measurements to wear debris analysis. *Proc Intl Conf Wear Mater ASME* 791, 783–804, 1981.
17. E Fitch, R Tessmann. Controlling contaminant wear through filtration. *Wear* 34(3):319–330, 1975.
18. M Menguturk, E Sverdrup. Calculated Tolerance of a large electric utility gas turbine to erosion damage by coal ash particles. In: W Adler, ed. *Erosion: Prevention and Useful Applications*. STP 664. West Conshohocken, PA: ASTM, 1979, pp 193–226.
19. J Miller. *Chem Eng* 7/ 22/ 74, 103–106.
20. J Miller. The Miller Number—A New Slurry Rating Index. *AIME Paper No. 73-B-300*. SME Fall Mtg, Pittsburgh, Sept, 1973.
21. S Abuzeid, A Busnaina, G Ahmadi. Wall deposition of aerosol particles in a turbulent channel flow. *J Aerosol Sci* 22:43–62, 1991.
22. A Li, C Ahmadi. Dispersion and deposition of spherical particles from point sources in a turbulent channel flow. *Aerosol Sci Tech* 16:209–226, 1990.
23. R Bayer. Tribological approaches for elastomer applications in computers. In: R Denton, M Keshavan, eds. *Wear and Friction of Elastomers*. STP 1145. West Conshohocken, PA: ASTM, 1992, pp 114–126.
24. V Mason, C Perrott, I Sare. Wear resistant materials for sugar cane shredder hammers. *Proc Intl Conf Wear Mater. ASME* 343–350, 1979.
25. P Anstice, B McEnaney, P Thornton. Wear of paper slitting blades: the effect of slitter machine settings. *Trib Intl* 14(5):257–262, 1981.
26. P Anstice, B McEnaney, P Thornton. An apparatus for measuring wear of paper slitting blades. *Trib Intl* 14(5):251–256, 1981.
27. D Trimble, T Galimoto. Selection of a non-cobalt alloy for sliding-wear service in a nuclear valve. *proc intl conf wear mater. ASME* 219–228, 1981.
28. K Budinski. Incipient galling of metals. *Proc Intl Conf Wear Mater. ASME* 171–178, 1981.

29. A Begelinger, A Gee, W van Bethlehem, M van de Sluijs. Selection of materials for a screwnut–spindle combination-example of a selection procedure base on function-oriented tri-bometry. Proc Intl Conf Wear Mater. ASME 117–123, 1979.
30. H Krause, C Hammel. The wear behavior of copper alloy / sell and polyamide/steel sliding pairs for heavily loaded cardan joints. Proc Intl Conf Wear Mater. ASME 625–635, 1983.
31. R Kilburn. Reducing wear in an electro-magnetic clutch. ASME Paper No. 67-WAIDE-4, Pittsburgh, Nov, 1967.
32. R Bayer, J Wilson. Designing for wear characteristics of members in sliding mechanisms. Paper No. 71-DE-39. Design Eng Conf and Show 4 / 71. ASME, NY.
33. IBM J Res Develop 25(5): 1981.
34. R Bayer, J Sirico. The influence of surface roughness on wear. Wear 35:251–260, 1975.
35. M Menguturk, E Sverdrup. Calculated tolerance of a large electric utility gas turbine to erosion damage by coal ash particles. In: W Adler, ed. Erosion: Prevention and Useful Applications. STP 664. West Conshohocken, PA: ASTM, 1979, pp 193–226.
36. R Bayer. Mechanical wear prediction and prevention. Table C24, p. 462. Marcel Dekker, New York, NY.

6

Problem Solving Methodology

6.1. GENERAL

Problem solving is different than wear design. With wear design, the potential for wear is anticipated and the approach involves selecting or determining design parameters to obtain the desired wear life or performance. With problem solving, the wear problem is generally not anticipated and the focus is to identify measures to eliminate the problem. A common problem-solving situation is one in which there is some prior experience of good or acceptable wear behavior for a design or devices and unacceptable wear behavior is suddenly encountered. The presumption in these situations is that the difference in wear behavior can be traced to some specific difference with the prior situation, such as out-of-specification parts, improper adjustment, or a change in the wear environment. Once these differences are identified, corrective action can then be taken to eliminate the wear problem. When the basic wear conditions are the same in the two situations, these actions frequently involve quality control improvements or tolerance refinements. When there is a difference between the operating conditions of the two situations, more substantial changes are often required, such as material changes or modifications of the overall design. In this case, a wear design approach might be used to improve the wear performance.

While details of problem-solving approaches tend to vary with the nature of the application, there are some common elements and a general methodology can be identified. This methodology involves three major elements or activities—failure analysis, hypothesis development, and testing—which are similar to those elements identified in wear design. They are also elements of a wear analysis approach (1). Compared to a wear design methodology failure analysis replaces system analysis, hypothesis development replaces model development, and testing replaces data base development and verification. Because of the similarities in these elements, problem-solving activities can often become similar to a wear design approach, particularly when the difference in wear behavior can be traced to difference in operating or environmental conditions. Each of the three elements of the problem-solving methodology is discussed in greater length in the following sections. Also in this section several case studies are presented, which illustrate problem-solving approaches.

Additional examples of problem solving can be found in Ref. 1, as well as additional discussions of different aspects of problem solving. Additional information on techniques and methods used for the examination of wear scars can also be found in Ref. 2.

6.2. FAILURE ANALYSIS

Failure analysis is the starting point for all problem-solving approaches. Its purpose is to provide a basis for the development of working hypotheses for the wear, which are then used to identify possible corrective actions. To develop these hypotheses, three aspects need to be included in the failure analysis. One is an examination of the wear scars to characterize the wear, the second is an evaluation of the overall application to determine operating conditions, and the third is an evaluation to determine if parts were within specification. The sophistication and depth of these activities need not be the same. However, it is generally desirable to start each with techniques and methods that provide a general or macro-characterization, before proceeding to micro-characterization and more refined levels of analysis, which provide very specific details. This initial macro-phase would include determining the macro-features of the wear scars, nominal operating conditions, and determining if the parts conform to the specifications. There are both logical and practical reasons for proceeding in this manner. One is that the macro-level often provides a different perspective and different information than that which can be obtained from micro-techniques. This perspective is generally needed to provide overall guidance to any further analyses (e.g., selection of more sophisticated and refined techniques and the proper utilization of the information obtained from them). Also, in some cases, the information obtained from the macro-phase might be sufficient for engineering resolution of the problem. Since the techniques and methods used in the macro-phase are typically more easily done and less expensive than the more refined and sophisticated levels of analysis, this approach also tends to reduce the cost and effort associated with failure analyses.

The initial macro-phase should characterize the wear and should include unaided and low magnification optical examination of the wear scars, the worn parts, and the counterfaces involved. These techniques provide general information such as the location of the wear scar, overall dimensions of the scar, general nature of the wear, and features of the counterface that may be important. Various micro-techniques of surface and materials, analysis can then be used to supplement and complement these observations. Perhaps the most routinely used and useful micro-technique for engineering applications is scanning electron microscopy (SEM) analysis. SEM analysis provides a means of studying the morphology of wear scars and, because of the various measurements modes associated with most SEMS, some information about the composition of the surfaces, as well. Examinations by cross-sectioning, high magnification optical microscopy, Auger analysis, electron spectroscopy for chemical analysis (ESCA), and secondary ion mass spectroscopy (SIMS) are examples of other micro-techniques that might be used in the characterization of the wear. Generally, the selection of these techniques and the regions to be analyzed by them are guided by the results of the macro- and SEM analyses.

The same initial techniques of examination used for the characterization of the wear are also important in the characterization of the operating conditions. These techniques can often point to possible problems with alignment, lubricant supply, changes in the nature of the environment (e.g., contamination), and possible out-of-specification conditions that might contribute to or be primarily responsible for the unacceptable wear. In addition to these, other techniques are often required for characterization of operating conditions. A variety of experimental and analytical techniques may be required for the characterization of the operating conditions. These included measurement and analytical techniques to determine loads, velocities, environmental conditions, flow patterns, etc., as well as a variety of mathematical analytic techniques, such as mechanical static and kinematic analyses, finite element modeling (FEM) analysis, thermal analysis, and fluid

flow analysis. Many of these techniques and methods can be done with varying degrees of sophistication and rigor. When possible, it is often desirable to use the less rigorous forms in the first or macro-stage of the failure analysis and to use those results to determine the need for a more rigorous application of the technique.

For the characterization of the operating conditions, it may also be necessary to include the evaluation of performance characteristics and properties of other components or parts which have an influence on the operating conditions at the wear interface. An example of this would be the need to characterize the performance of an oil pump when variations in the amount of lubricant supplied to the wear interface might be responsible for the high wear.

Typical macro-phase examination techniques of parts are those used to determine nominal composition, surface measurements of hardness, surface roughness, and critical dimensions. These techniques can be augmented by more sophisticated techniques, such as metallurgical analysis techniques, more refined methods for determining composition, T_g (glass transition temperature) measurements, more complete roughness characterization, and SEM surface characterization, as required.

When performing a failure analysis, it is important to recognize that wear is a system property and the large number of factors that can influence wear behavior. In doing a failure analysis each of these factors should be considered, characterized, and evaluated for possible significance in the current situation. Considering the effect of these factors on the individual wear mechanisms and the contribution of that mechanism to the overall wear behavior can often do this. However, it should be kept in mind that there could be more than one mode of wear involved and that several factors could be responsible for the wear behavior. The operational classification of wear and its relationship to wear mechanisms (see Sec. 1.5 and Table 1.1) can also be useful in guiding the failure analysis and assessing the significance of various parameters and factors on wear behavior.

A technique that is very useful in failure analysis is the comparison of failed systems and parts to those exhibiting good wear behavior. The same methods of analyses should be used on each type and any differences that are observed should be evaluated as to its significance in the wear. Another approach that is often useful is to examine the data obtained and the observations made to see if they are consistent with the conception of how the device should operate and wear. If there are inconsistencies, they should be explored since the reasons for them may account for the unexpected wear behavior.

6.3. HYPOTHESIS DEVELOPMENT

The purpose of this element of the methodology for wear problem solving is the development of the theory or model upon which the solution is based. To do this, these models should provide a complete explanation for the unacceptable wear in the particular situation. It is generally necessary to include in these models aspects beyond those associated with physical wear mechanisms. In many engineering situations, the key elements of the model are often associated with these additional elements. Examples are the additional aspects that are often needed to provide the explanation for the exceptionally high loads that are responsible for the unexpected high wear or the reduced amount of lubrication that is the cause of the short wear life. Quantitative and analytical models, such as those used in wear design, can be used in establishing the solution. However, they generally are not necessary. Typically, qualitative and phenomenological models, which may be somewhat heuristic, are sufficient in many engineering situations.

These models evolve from the findings of the failure analysis and knowledge of wear and wear behavior. By considering this information, it is generally possible to propose one or more models for the wear behavior. These models are basically in the form of tentative or working hypotheses that need to be evaluated. While additional data from continued failure analysis activity can often be used to evaluate and eliminate some of the hypotheses, some amount of testing will be required to establish the final model. As a minimum, this would be a verification test of the solution. In many cases, however, simulative laboratory robot or machine tests might be required to evaluate these hypotheses prior to the identification of a solution.

Quantitative relationships for wear and wear behavior can often be helpful in these evaluations, since the comparison of the wear projected by these relationships and actual wear behavior can be used to test the validity of models and for the refinement of proposed models (1).

6.4. TESTING

The remaining element of the methodology is testing. Testing is always an element in problem solving. While this is the case it may be required and used for a variety of purposes. These include determination of the effect of various parameters on the wear behavior, selection of parameters values or materials for resolution, characterization of operating conditions, development and evaluation of models, as well as verification of the proposed solution. Not all problem-solving situations require testing for all of these purposes. However, testing to verify the proposed solution is always necessary and may simply take the form of monitoring wear performance of the device after the changes have been introduced. Wear tests used in problem solving can be of several types, namely, simulative laboratory, robot, field or machine tests. The type of test used tends to vary with the purpose of the test. Typically, simulative laboratory tests are used to evaluate the effect of different parameters on wear and to select materials and material conditions. Testing to evaluate the effects of parameters (e.g., load, surface roughness, and lubrication) and to select materials and processing parameters are examples of this. When it is difficult to provide adequate simulation in a laboratory test, robot or field tests may be used for these purposes as well; however, these type of tests tend to be more complex and difficult to control than laboratory tests. While this is the case, robot and field or machine tests are typically needed for the characterization of operating conditions and to evaluate models. Field or machine tests are required to verify the solution.

REFERENCES

1. RG Bayer. *Wear Analysis for Engineers*. New York: HNB Publishing, 2002.
2. P Blau ed. *Lubrication, and Wear Technology*, ASM Handbook. Vol. 18. Metal Parks, OH: ASM Intl, 1992

7

Problem Solving Case Studies

7.1. INTRODUCTION

In this section, several examples of problem solving approaches are used to illustrate the general features of the methodology. These examples involve unique wear situations. In the discussions of these case histories, emphasis is therefore placed on the more general aspects of the problem solving activities, rather than on the details of the individual activities used in establishing the solution.

7.2. CARD EDGE CONNECTOR FRETTING

This case study describes the problem solving approach used to resolve an unanticipated wear problem found in an application of a card edge connector system. The connector system was used to attach printed circuit cards to a printed circuit board, which formed part of a cage or rack assembly. In these applications, the cage was mounted to a machine frame. [Figure 7.1](#) shows an illustration of the connector system and the general configuration involved in these applications. The female portion of the connector system, which was soldered to the board using a pin-in-hole technology, consisted of one or two rows of opposing spring contacts in a plastic housing. These springs mated with contact pads along the edges of printed circuit cards. Inserting the cards into the slot and actuating a cam, which causes the springs to move out and contact the pads, makes the electrical contact. During this engagement, the springs slide across the pads, providing a wiping action of 0.01–0.020 in. to remove non-conducting material from the contact regions. This wiping action, which is designed into the contact system, results in wear of the contact system. Wear is a concern with these contact systems because of the possibility of wear-through of the noble metal platings, which are used to prevent oxidation of the underlying conductor, e.g., Cu. With wear-through non-noble underlayers are exposed and corrosion may take place, leading to increases in contact resistance and failure.

The pads for this connector system had Au surface layer, approximately 100–150 μm . thick, and 80–120 μm . Ni underlayer, on an electroplated Cu substrate. The springs had a 100–150 μm . Pd–Ni surface layer coated with a 10 μm . flash of Au, on a 75–100 μm . Ni underlayer over a Be–Cu substrate. The contact surface of the spring was spherical, with a nominal radius of 0.025 in. The normal forces exerted by the springs were nominally 175 g, with a tolerance range of 125–225 g. The pads were also coated with a thin coating of a polyolester lubricant.

During development of this contact system, insertion wear (i.e., the wear associated with actuation and deactuation) was a prime concern. Using basically empirical

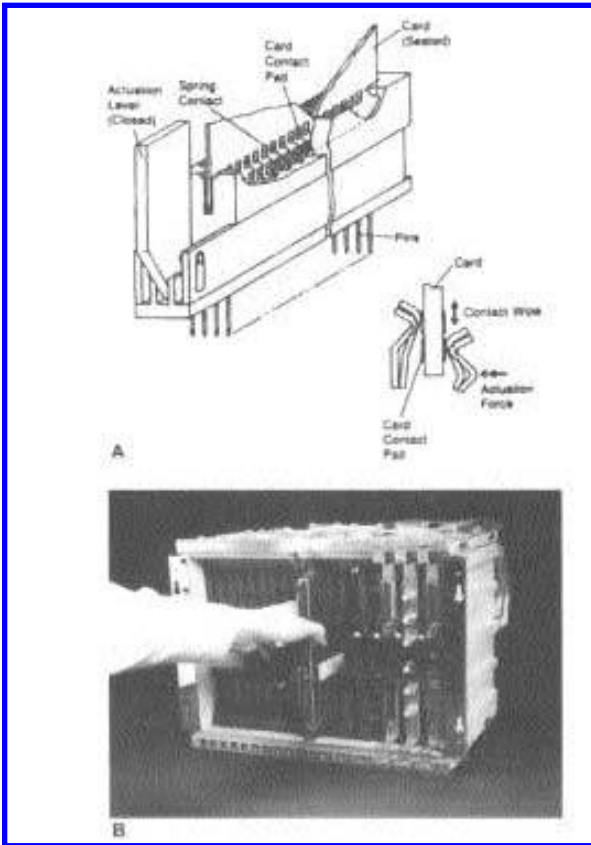


Figure 7.1 A card edge connector system is shown in “A” “B” shows a card assembly being plugged into a cage, which is then mounted in a machine frame or rack.

approaches, insertion wear behavior was investigated extensively and it was established that the wear life of the design was significantly greater than the 50-actuation / deactuation actuation cycles required. While not determined, it was estimated that the wear life for these contacts was in the range of 100–200 cycles. Trends in insertion wear behavior were also evaluated for a number of design parameters and used to select tolerance ranges. For example, the effects of load, spring roughness, plating parameters, spring radius, and lubrication on insertion wear were evaluated (1).

The potential for sliding motion and wear due to other sources, such as machine induced vibrations, was recognized. However it was felt that, because of the high retention forces developed by these connectors and the use of additional retention mechanisms, these types of motions would not be present in the applications or limited to a low number of cycles, such as in shock situations. Therefore, wear due to these motions was not a design factor and not characterized. Qualification tests of initial applications,

which involved shock and vibration testing, as well as thermal cycling, supported this position. No evidence of thermal or vibration motion was found at worst case excitation levels that were associated with field conditions. While some motion due to high shock level were observed, the number of these shocks expected in the field was small in comparison to the number of insertions the contacts were able to withstand. Hence, motions produced by mechanical shocks were not considered to be a factor in overall wear life.

While initially this design was evaluated and intensively studied for one application, the use of this contact system was extended to other application each of which were subjected to the same type of stress tests (e.g., shock and vibration) that were used for the original application. At the end of a series of these tests for one of these applications, an unacceptable wear condition was found. Exposed Ni and Cu were detected on a number of card pads during routine examination of the tested hardware. The resolution of this problem required several steps. Characterization of the observed wear, characterization of the hardware and components to verify that they were within specifications, determining which stress test or tests caused the wear, correlating test conditions to field conditions, simulative laboratory wear testing to characterize fretting wear behavior, and the evaluation of proposed fixes were required.

Characterization of the hardware indicated that the parts were within the specifications. This eliminated the hypothesis that the unsatisfactory wear resulted from an out-of-specification condition. Of the critical parameters measured, most were close to nominal. However, it was observed that the thickness of the Au and Ni layers on some of the cards tended to be near the lower limits of the specification.

Visual and low power optical examination of the cards involved in the qualification provided more significant information. Various patterns in the wear behavior were detected that were consistent with fretting wear due to vibration and shock motions. These examinations of pad wear patterns (Fig. 7.2) indicated the occurrence of three different types of motion during the course of the tests. The overall length and tear drop shape of the wear scar were characteristic of actuation and deactuation, while the chaotic wear paths on some pads were typical of motions that are induced by shock. The exaggerated spot at the end of some of the wear scars, which were not observed in prior applications, suggested the existence of small amplitude oscillatory motion or fretting. It was also observed that when this condition was found on a card, the severity of the wear in this region was not uniform across the pads; it varied but tended to follow some regular pattern over the card. More refined analysis techniques (e.g., such as SEM, EDX, metallography, and profilometer measurements of scar depth) indicated that Ni and Cu exposure and significant wear was confined to the fretting region at the end of the scar.

Springs were also examined for wear and exposure of sub-layers. However no significant wear was found on the springs, including those mated with severely worn pads. It was concluded that the problem was confined to the pad. This was consistent with data obtained in prior wear tests and evaluations done regarding insertion wear. In these tests, significant wear was also confined to the pads.

Based on the operational characteristics of the two wear situations, the insertion wear data base that had been developed for this contact system was not considered to be adequate to address fretting issues. Operationally, fretting involves a large number of small amplitude cycles and insertion wear involves a small number of large amplitude cycles. To extend this database to the fretting regime, it was decided to do simulative laboratory wear tests. In addition to simply obtaining data in the fretting region, one purpose of these tests was to verify that wear can be correlated to total amount of sliding

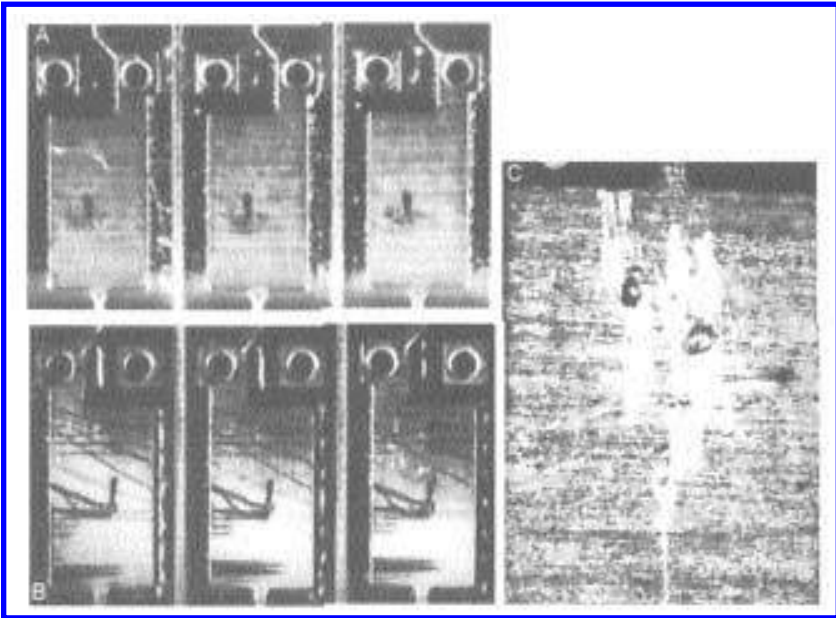


Figure 7.2 Tab wear scars, indicative of different types of motions. “A” shows the wear scars resulting from actuation and deactuation. “B” shows wear scars resulting from mechanical shocks to the cage. “C” shows wear scars caused by vibrations.

(i.e., the product of amplitude and the number of cycles). This correlation is suggested by the results of prior studies of fretting (2–4). This correlation was verified by comparing wear data from several tests using different amplitudes, number of cycles, and frequencies. It was therefore possible to characterize the wear behavior, using a single amplitude, and to generate master curves relating wear and total sliding. This is shown in Fig. 7.3. As a corollary, this correlation also allowed the use of total amount of sliding, as a measure of the severity of various vibration conditions.

Since the motion was not anticipated, it was considered necessary to understand the reason for the motion before solutions to the problem could be developed. It was also considered necessary to understand the significance of the magnitude of the wear in these qualification tests. These qualification tests were primarily stress tests designed to insure overall reliability and not to determine wear life. These issues were investigated by repeating some of the vibration tests to identify the causes of the motion and by conducting some simulated field tests, using prototype hardware, to establish correlation with the stress tests and to determine how realistic they were.

The hardware, which first showed the problem, had experienced a number of actuation / deactuation cycles, a series of mechanical shock and vibration tests intended to simulate operating and shipping environments, and a limited number of thermal cycles simulating shipping. Since the combined number of shocks and thermal cycles was much smaller than the number of insertion cycles required for wear-through of the Au, it was hypothesized that the major source of this type of motion was the mechanical vibration portion of the test sequence. Vibration tests were done to verify this and to separate and characterize the effects of operational and shipping environments. These tests demonstrated that both types of vibration tests resulted in motion and unacceptable wear.

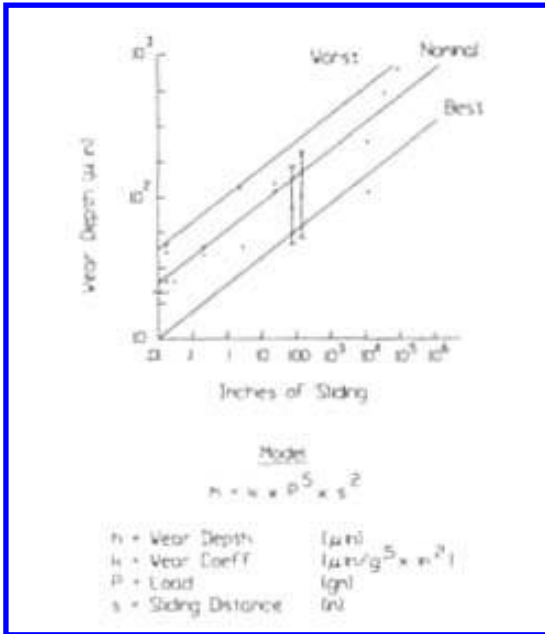


Figure 7.3 Master wear curve for contact wear and the corresponding analytical relationship. Worst case is for the poorest conditions allowed by the design. Best case is for the best conditions allowed the design.

However, differences in wear behavior were found for these two test conditions. Under simulated operational conditions, the amplitude of the motion was smaller, associated with resonance conditions in the application, and resulted from deflections. Card mass did not seem to be a factor. For shipping conditions, the amplitudes were larger and resulted from rigid body motion of the heavier cards. These two situations are illustrated in Fig. 7.4.

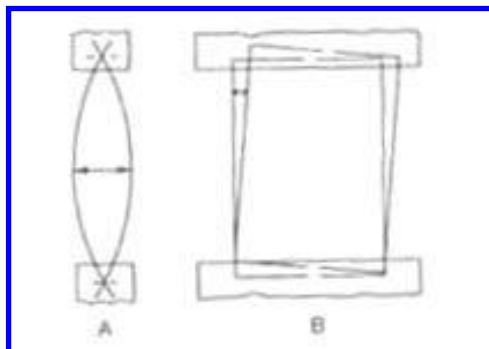


Figure 7.4 Types of card motion resulting from mechanical vibration. “A” illustrates a deflection mode. “B” rigid body motion.

Using data from these vibration tests and mechanical modeling, it was concluded that the motion under simulated operational conditions, was caused by a horizontal excitation to the base of the cage in which the cards were mounted. Under operating conditions, this type of excitation to the cage would be provided by vibrations transmitted through the machine frame. It was found that by inserting a slip pad between the base of the cage and the frame, the transmission of this mode of excitation could be reduced to the point where motion did not occur under the stress test conditions. This design modification resolved the problem for operational conditions.

Using similar techniques, it was concluded that the vibration motion under simulated shipping conditions was caused by the transmission of vertical vibrations through the machine frame. The stress tests used to simulate shipping provided vertical excitation at the base of the machine frame. Under random vibration conditions, this resulted in the transmission of mini-shocks to the cage holding the cards, causing the cards to move within the cage. While a similar mode of excitation was associated with operational vibration concerns, the levels in those tests were an order of magnitude lower than for shipping and were not sufficient to overcome the retention forces. With this understanding ways of reducing the transmission of these vibrations to the cage and providing better retention of the cards were explored. However, none were found that could be implemented within the constraints associated by the overall design of the machine. Since it was not possible to eliminate the motion, it was necessary to determine the total amount of motion that these contacts were likely to experience in the field so that this could be compared to the amount of motion required for exposure of Ni or Cu. If the former exceed the latter, ways of improving the wear resistance of the contact system had to be investigated.

One way to approach this was to establish a correlation between the accumulated motion produced in the stress test to the motion likely to be experienced in the field. This was done by comparing wear scars produced on prototype hardware in shipping and relocation experiments with those produced in stress tests and laboratory wear tests. Field tests demonstrated that the problem was real (i.e., significant wear and exposed Ni was produced in some cases) and that the total amount of motion produced in the stress test was representative of that possible in the field. It was concluded that the stress test could be used to verify the adequacy of proposed solutions. Using the master wear curve in conjunction with the results of the field tests, it was concluded that somewhere between 100 and 1000 in. of sliding distance should be anticipated. Therefore a design goal of 1000 in. of sliding was established for wear life.

Examination of the wear scars produced in the stress tests and those in the laboratory lead to the identification of an additional wear mode that had a significant effect on wear life under fretting conditions (5). As a result of repeated cycles of inelastic deformation of the Cu substrate, the Ni and Au layers buckle and produce high spots on the wear surface. At these high spots, the Au was more rapidly worn away, resulting in a localized exposure of the Ni. The end state of this process is shown in Fig. 7.5. Tests showed that this wear mechanism was dependent on load and number of cycles and with increased load, this mechanism was evident only after a few cycles of motion. In the load range of the contact system, however, several thousands of cycles were required. Since this mechanism was driven by substrate deformation, this mechanism was found to be more pronounced with thinner Au and Ni platings than with thicker platings. While this effect contributed to the severe wear initially observed with the thinner platings, it was found that the phenomena still occurred with platings of more nominal thicknesses. Consequently, the life requirement could not be met with the standard plating system.

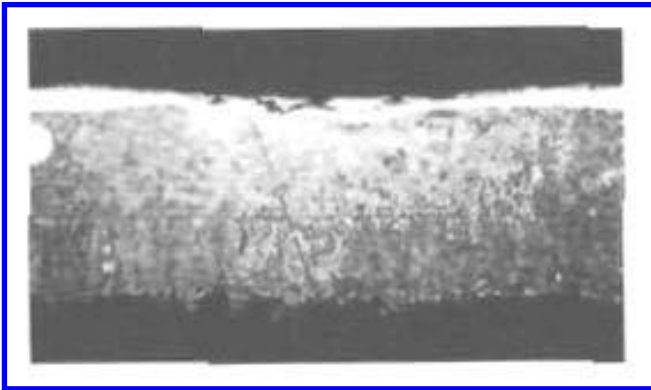


Figure 7.5 Cross-section view of a tab wear scar, showing the upsurgence and local exposure of underlying metallurgical layers. (From Ref. 5, reprinted by permission from Elsevier Sequoia S.A.)

It was determined experimentally, that a minimum combined thickness of 600 $\mu\text{in.}$ for the Ni and Au layers was required to eliminate the mechanism. With this mechanism eliminated, it was also found that a minimum thickness of approximately 250 $\mu\text{in.}$ of Au was required to obtain a lifetime of 1000 in. To provide a margin of safety, a new plating system of 300 $\mu\text{in.}$ Au over 300 $\mu\text{in.}$ Ni was proposed as a solution to the wear

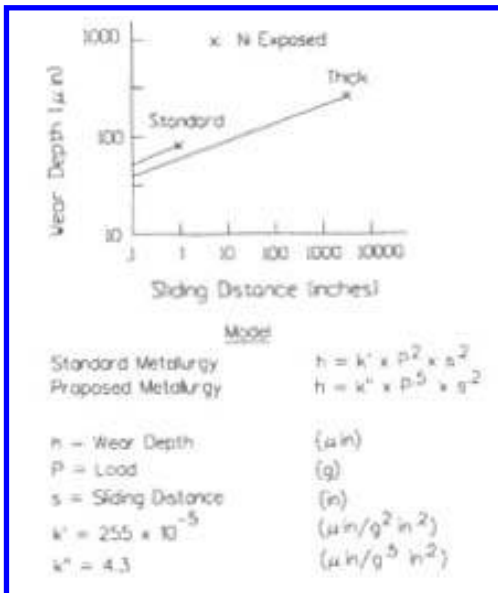


Figure 7.6 Wear curves for the standard and thick plating systems and the corresponding analytical relationships. (From Ref. 6.)

problem associated with shipping. Stress tests confirmed this as a solution to the problem.

Figure 7.6 compares the wear behavior of the original plating structure to the new. As indicated in this figure, the effect of load was different for the two systems. When the subsurface deformation mode was present, the sensitivity to load was much greater than when this mechanism was not present. In addition to the improvement in wear behavior, it was also found that the new system tended to reduce the amount of motion that would occur. For the excitation levels used in the stress test, the effect was negligible. While this was the case, some field tests showed that it could prevent motion under some conditions. An explanation for this serendipitous effect was developed.

Vibration tests had shown that threshold levels of excitation had to be exceeded for motion to occur and that these levels could be correlated with the coefficient of friction for the contact. In laboratory tests, it was found that plating thickness also influenced friction (6,7). As the platings became thicker and subsurface deformation decreased, the coefficient of friction tended to increase. Therefore, the excitation level need to cause motion in the application was found to be slightly higher with the new plating system than with the original. Since the excitation levels associated with shipping conditions were much higher than these threshold levels, motion could still occur with the recommended system but the number of situations in which motion was likely to be reduced.

A more complete description of the vibration and shock evaluations and procedures used in this case study can be found in Ref. 8.

7.3. EXCESSIVE CARRIER BACKSTOP WEAR

This case study discusses the resolution of a wear problem discovered in printers used in Europe and involves the same carrier backstop whose wear design was described in Sec. 5.6. As discussed in that section, a design was developed which would limit the combined wear at the backstop–type interface to be less than 0.0009 in. over the lifetime of the printer. Measurements of the wear at this interface on printers made and used in the US indicated that total wear was in the range of 0.0006 in. after 60% of life. This was in good agreement with the prediction and met the performance requirements for the printer. However, with printers manufactured and used in Europe, print quality problems were encountered that could be traced to excess wear at this interface. Measurements of backstops and type elements used for less than 20% of the design life indicated that combined wear was often in the range of 0.01–0.02 in. Accounting for the difference in usage, these data indicated that wear rate in machines used in the European market was one to two orders of magnitude higher than in the US and that predicted for the design.

Backstops and types obtained from both markets were examined, compared, and characterized as part of the failure analysis activity. On type carriers obtained from Europe, the wear at high usage and low usage positions were similar and wear scars on the backstop tended to be noticeably larger than the width of the type element. This was different than what was found on those from the US. On US parts, there was a significant difference between high and low usage characters and the width of the wear scars on the backstop were not significantly different than the width of the type. These latter features are the same as those observed during verification testing during development and point to the predominance of impact wear. The former features (wider wear scars) suggest fretting wear as the predominant mode, which had often been observed during development when there was a problem with lubrication. However, oil was visible on the European parts as

well as on the US parts. Before a series of working hypothesis were developed, it was considered necessary to examine other aspects, which could potentially explain these observations.

There were several general differences between the machines used in the US and those used in Europe, which potentially could be factors in the wear performance. Different manufacturing sites were used. Alternate materials, allowed by the design, were more likely to be used for the European machines because of availability considerations. Also, the European machines were modified to accommodate the electrical system used in Europe (e.g., 50 cycles vs. 60 cycles). Therefore, the hardware used in the European machines was extensively characterized and compared to those used in the US machines. The European hardware was found to be within specifications and, except for the lubricant used, it was determined that the critical materials were the same in both types of machines. The same general type of oil was used in both markets but obtained from different suppliers. The two oils were considered to be nominally equivalent but this was not verified for this application. Some differences in the nominal properties of the two hardware sets were found but none were sufficient to account for the large difference in wear behavior. Potential differences in machine assembly procedures and adjustment procedures were also investigated. Again, none were found that were considered probable explanations for the observed differences. Finally, field tests showed no difference in wear behavior between cartridges and carriers manufactured in Europe and the US.

Based on these failure analysis activities, it was concluded that the most probable explanation for the wear was related to lubrication and was machine oriented (European vs. US). Differences in lubrication in this type of wear situation were known to result in orders of magnitude differences in wear rates. The general features of the wear were also consistent with a lubrication problem and the lubricants were not identical. This prompted a more thorough comparison of the lubrication systems in the two machine groups. This resulted in the discovery that the clock motor used to operate the pump had not been converted to a 50 cycle one. As a result, the oil supply rate would be decreased by 1 / 6 in the European machines, which supported the hypothesis. Since both quantity and oil type can affect wear, it was necessary to investigate both aspects. To do this, it was decided

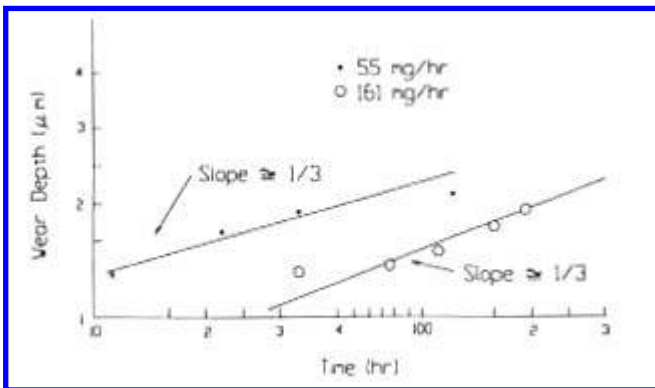


Figure 7.7 Wear curves from printer tests. (From Ref. 9.)

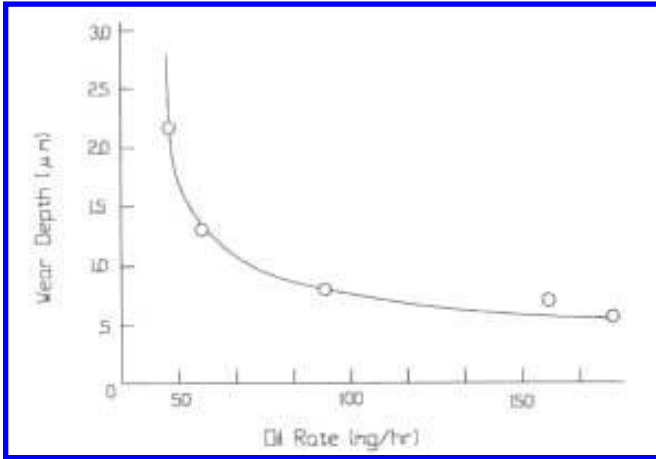


Figure 7.8 Wear depth as a function of oil rate. (From Ref. 9.)

to use machine tests, similar to those used during development to evaluate wear. The oil supply system was altered so that oil could be supplied at different rates and tests were to be conducted with both types of oils.

When these tests were done, the wear behavior with the two oils was found to be identical; however, wear behavior was found to be very sensitive to oil supply rate. [Figure 7.7](#) shows the results obtained with some lengthy initial tests. The print pattern used in these tests involved printing at only one of the five types in the carrier. The average value of all four positions is shown in the [Fig. 7.7](#). A larger number of shorter tests, using

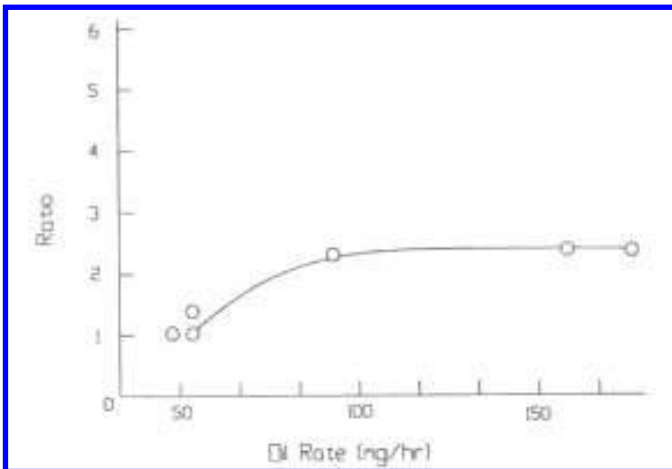


Figure 7.9 Ratio of wear depth at used positions to wear depth at unused positions. (From Ref. 9.)

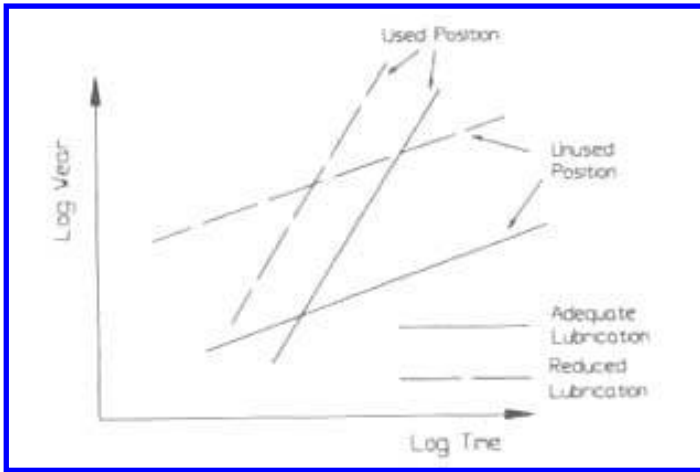


Figure 7.10 Trends predicted by wear models.

intermediate supply rates, were also performed and the results of those tests are shown in Fig. 7.8. The relative magnitude of the wear at the used and unused positions was found to change as a function of oil supply rate (Fig. 7.9).

During this phase of the investigation, pump performance was also evaluated in a separate test and some significant observations were made. It was discovered that the pump had a tendency to hang-up and to entrap air, both of which would reduce the amount of lubricant supplied to the interface.

The data regarding the effect of supply rate on wear, the observations regarding pump performance, and the use of a 60-cycle motor with a 50-cycle supply provided a reasonable explanation of the high wear in the European machines. The pump was designed to provide 90 mg / hr. The closeness of this value to the knee of the curve in Fig. 7.8 had not been suspected. The use of the 60-cycle motor would put the nominal supply rate at the knee of the curve, which is approximately 70 mg / hr, making the European machines more sensitive to pump performance. The data were also analyzed for consistency with the models used in the wear design. It was found that the wear behavior could be explained by typical variations in the parameters of these models that are associated with lubrication (9). The trends of the models for both used and unused position are illustrated in Fig. 7.10.

Therefore, it was concluded that a modified pump and the use of a proper motor should correct the problem. With the implementation of these recommendations, the wear problem in the European machines was eliminated.

7.4. PUSH ROD TIP FAILURE

Push rod tip wear in a high-speed impact printer was also discussed in Sec. 5.10. The wear design approach involved the development of a model for tip wear that was found to be in good agreement with the results of machine tests. The formulation and verification of the model was done early in the development cycle. As the design of the printer was modified during development, this model was used to evaluate the effects of the changes on tip wear.

Mechanical analysis indicated that these changes would result in only slight variations in the contact conditions (e.g., a $< 10\%$ change in contact forces and contact times). Since contact stress tends to remain constant for a broad range of conditions, the model indicated that wear behavior would be insensitive to such changes. It was therefore concluded that the changes that were introduced would have negligible effects on tip wear. This assessment was supported by experience involving the successful use of these tips in prior applications; the conditions were different but the wear behavior was similar. As a result, no specific tests were performed to evaluate the effects of such changes. However, tips were routinely inspected during the course of normal development testing, particularly when print quality degraded during the tests. During the last phase of development of the printer, severely worn push rod tips were found in the investigation of a print quality problem. A significant number of push rods with as little as 4×10^6 operations but more typically in the $10\text{--}30 \times 10^6$ operations range were found to have large sections of the elastomer tips worn off. This behavior was significantly different than expected (i.e., only a few thousandths of inch of wear after 10^9 operations, which was the required life). A problem solving effort was initiated to determine the cause of the failures and to establish corrective measures.

Similar experiences had occurred with prior applications, where the poor wear resistance was traced to quality problems in the manufacturing of the tips, such as bubbles, improper cure, and improper formulation. Here a similar quality control problem

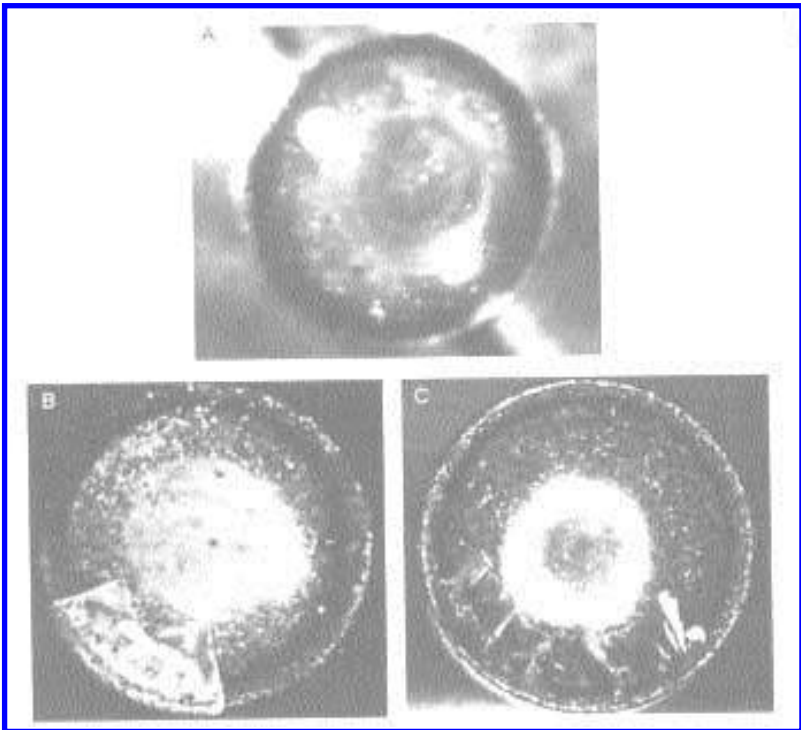


Figure 7.11 Used push rod tips. “A” shows the normal wear condition. “B” and “C” show examples of abnormal wear.

was initially suspected. Therefore, one of the initial actions of the failure analysis was the physical, chemical, and dimensional characterization of tips to insure that they were within specifications. Another action was the examination of a large number of used tips so that the wear behavior could be characterized. Initially this consisted of low power optical examination and in later stages SEM examinations. A wide range of wear conditions was found in these examinations. Some tips showed no loss of materials and a central wear scar consistent with the model. In some of these, subsurface cracks near the rim of the cap could be detected; in others, loose flaps of elastomer, still attached to the center of the tip, were observed. When material loss was observed, the morphology of the surface indicated tearing and fracture. Some of these conditions are shown in Fig. 7.11.

From these examinations, it was concluded that two distinct wear mechanisms were involved. One was the impact wear mechanism, which results in a central scar and was considered in the model used for the wear design. This had been the typical pattern seen in prior tests. The amount of wear, observed in this region in the more recent tests, was consistent with the model and acceptable. The second mechanism, which leads to the catastrophic loss of material, involved the initiation of cracks near the rim and the propagation of these cracks inward and upward to form loose particles. This fatigue fracture mode is illustrated in Fig. 7.12. The geometry of the tip suggests that the region near the rim is likely to be a region of higher strain when the elastomer is under load, providing a site for fatigue crack initiation. Since this mode of failure had not occurred in earlier tests, two reasons for this change in behavior were considered possible. One was that design changes resulted in higher strains in this region, which were sufficient to initiate cracks. However, it was unknown if any of the changes were sufficient to cause this or not. The second possible factor was quality problems with the tips in current use, as had been the case with earlier applications. For example, defects in this region could act as initiation sites or improper cure or formulation could result in lower resistance to crack initiation. While several quality problems were found, it was not possible to explain all failures in this manner. Tips from lots that were within specifications exhibited this mechanism, while some tips from lots that had quality problems did not. To investigate the relative contribution of design changes and quality aspects, it was decided to perform printer tests, using tips from different vintage lots and using different levels of design.

The results from these tests were analyzed using Weibull statistics. Some of the results obtained from these tests are shown in Fig. 7.13. As can be seen in this figure, there was a considerable range in performance. While both quality and design conditions were found to be significant factors, the predominant factor identified was design changes. Using tips from different lots, this was confirmed in laboratory impact wear tests. The test configuration is shown in Fig. 7.14. The impact region was varied in these tests and the number of cycles to initiate cracks was determined. It was found that, while tip conditions did influence the results, the strongest effect was associated with the location of the impact, i.e., the contact angle (θ). The dependency on contact angle found is shown in Fig. 7.15.

With these two results a detailed study of the design changes that were involved was conducted. Using theoretical and experimental analytic techniques, it was possible to demonstrate that two design changes caused a slight shift in the location the contact zone (Fig. 7.16). This, in turn, caused changes in the loading conditions involving both the location, magnitude, and type of loads involved. Values for these parameters for the original design and the modified design are shown in Table 7.1. Finite element modeling

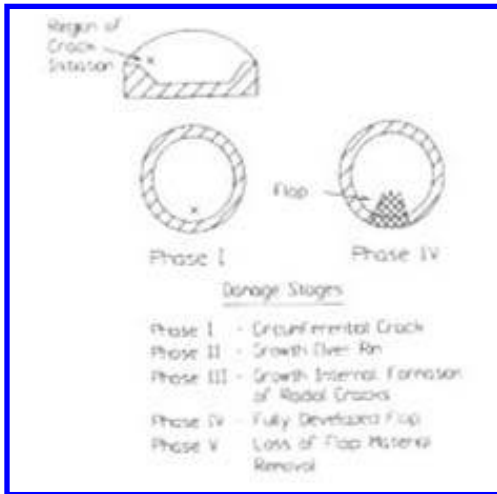


Figure 7.12 Stages of tip fracture.

showed that these changes were sufficient to cause a significant increase in local strain near the rim of the cap. In addition, the finite element modeling was also able to explain the major trends observed in the tests. The FEM was able to explain such effects as the problem at the armature end being more severe than the hammer end, location of failure in the tip, and the beneficial effect of lubrication on life, which were observed in the machine tests.

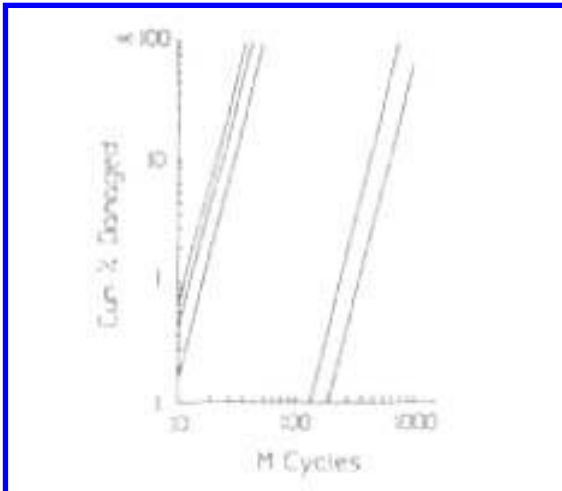


Figure 7.13 Tip failure curves. The two clusters of curves represent data obtained with different design levels of the printer. Variations within the clusters are the result of materials and processing differences.

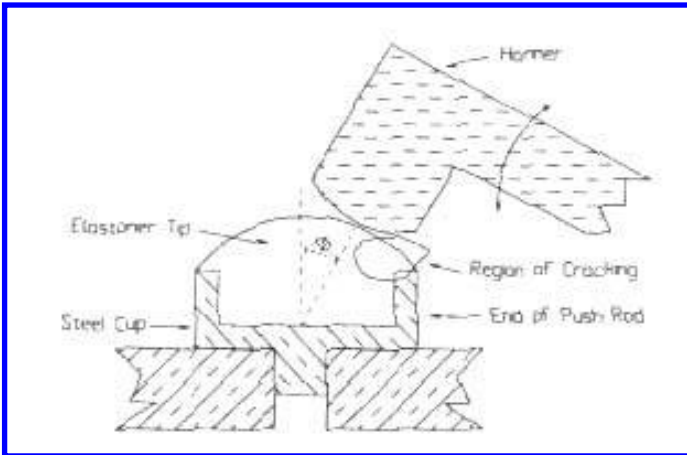


Figure 7.14 Test configuration used to investigate tip fracture. Φ is the contact angle. (From Ref. 10.)

As a result of these findings, the design was modified to reestablish the original contact zones. In addition, improved quality and manufacturing procedures were established to maintain consistent and required properties. With these in place, the problem was eliminated.

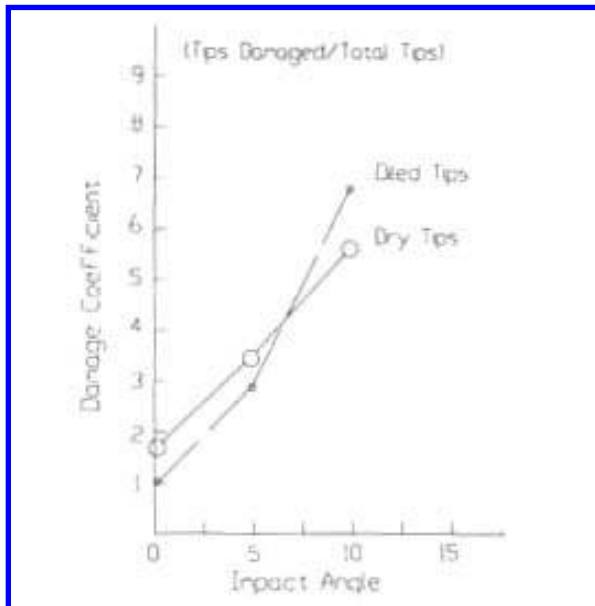


Figure 7.15 The effect of contact location on tip fracture.

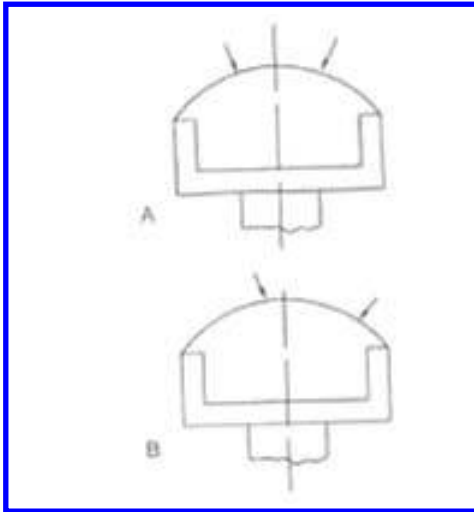


Figure 7.16 Contact zones for different design levels. “A” shows the region for the older design level in which fracture did not occur. “B” shows the region for the design level which resulted in fracture. Contact region is between arrows.

Table 7.1 The Effect of the Design Change on Push Rod Tip Loading

	Initial design	Modified design
Impact forces		
First impact F_x	0.64 lb	0.66 lb
F_y	7.31	8.29
F_y/F_x	11.44	12.64
Second impact F_x	0.24	0.31
F_y	5.59	4.44
F_y/F_x	23.20	14.51
Third impact F_x	-0.011	0.097
F_y	3.34	3.58
F_y/F_x	-312.15	37.06
Impact angles		
At rest	-3.8°	1.8°
Sealed	3.0	6.8
First bounce		
Contact	10.8	11.1
Maximum	9.3	8.9
Second bounce		
Contact	3.3	7.0
Maximum	3.3	5.7
Third bounce		
Maximum	0.8	3.5
Maximum shear stress	460-590 psi	500-870 psi

7.5. SEPARATOR ROLL

Separator rolls are used in checking sorting machines to control the separation between checks, allowing them to be sorted into different bins. The basic design and function of the separator is shown in Fig. 7.17. The separator rolls need to have low inertia and consisted of an aluminum hub with an elastomer layer on the outer rim. The separator roll stops checks that are fed into them, holds them for a certain period, and then accelerates a check into the processing stream. Both the terminal speed and the acceleration of these checks are high. In the machine involved with this case study, the velocity of the checks was in the range of 60 mph and the accelerations were in the range of several hundred G's. Slip under these high accelerations was a concern in these mechanisms, since this would result in wear of the elastomer coating. In earlier machines, a rubber coating was developed which gave satisfactory performance in these applications. In the new application, the same material was used but to compensate for the higher accelerations of the new application, traction was increased by increasing the number and width of rollers used, thereby keeping the load per unit length comparable with that in the earlier applications. Therefore, a wear problem in the new application was not expected. However, once the machine reached the state of development that permitted a significant amount of usage to occur, a major wear problem was identified. With only a moderate amount of usage most rollers had flat spots and regions where there were a significant loss of material and, in some cases there were regions where the elastomer layer was completely gone.

Based on past history, the initial speculation was that the new operating conditions caused increased slip and/or higher temperature in the elastomer, which resulted in a significant increase in abrasive wear caused by the checks. The failure analysis did not confirm those suspicions. Physical and chemical examination of used rollers did not indicate any significant temperature rise that could account for a transition in wear behavior or even a significant degradation in wear resistance. Furthermore, thermal measurements

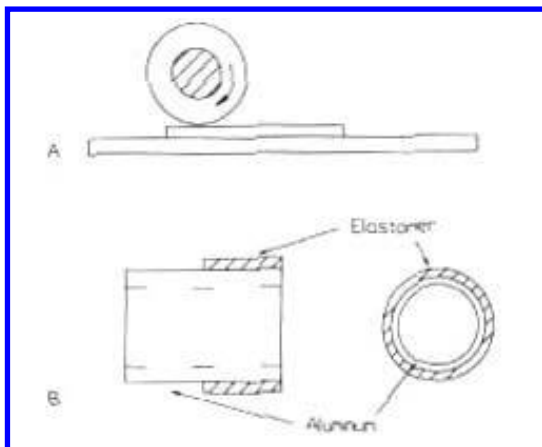


Figure 7.17 The configuration of the check separator mechanism is shown in "A". "B" shows design details of the roller. Nominal dimensions of the roller are hub-length, 1 in.; diameter, 1 in.; wall thickness, 0.03 in.; elastomer length, 0.5 in.; thickness, 0.03 in.

made during the operation of the separator indicated only a slight temperature rise, which provided support to this position. Since the elastomer used had good temperature resistance, temperature rise was, therefore, discounted as being a primary factor in the poor wear performance. Also, studies of the morphology of the wear scars indicated that abrasive wear was not the primary factor.

The surface morphology of the worn rollers was studied, primarily using low power optical microscopy, but supplemented with some SEM analysis. Three morphological patterns were found to occur on most rollers examined (Fig. 7.18). One was a relatively smooth surface, indicative of a mild wear process. Another was a rough surface, which suggested the formation of large wear particles. Frequently with this morphology, a wave-like pattern could be also be observed on the surface. The third morphology was still rougher and suggested the loss of large chunks of the elastomer as a result of

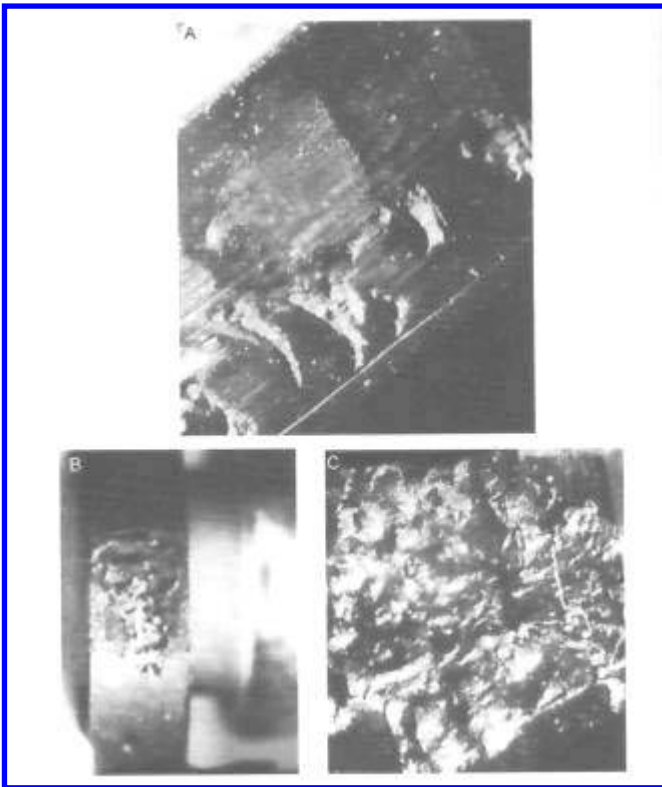


Figure 7.18 Morphology of used rollers. Different regions of the elastomer surface shown in “A” indicate the existence of smooth and rough wear models. “B” shows an example of a more severely worn surface. “C” is a higher magnification of the morphology in the rough regions.

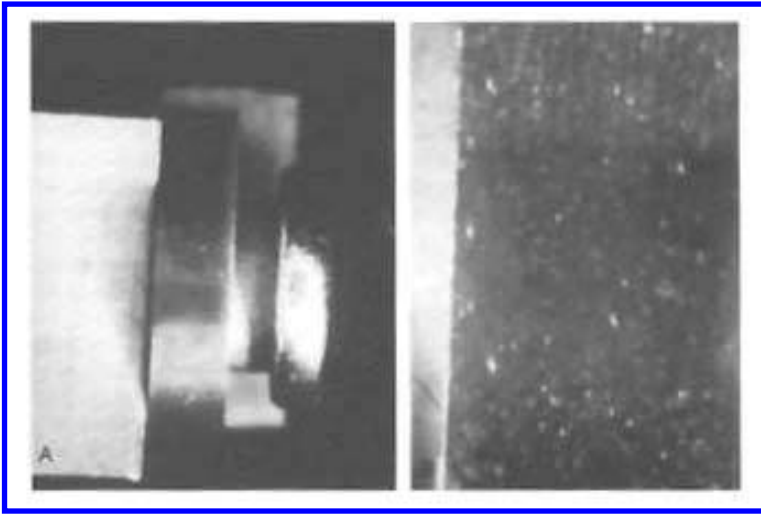


Figure 7.19 Two different magnifications of the morphology of wear scars produced in the drum tests. “A” provides an overview of the wear specimens used and the general geometry of the wear scar.

debonding at the interface. The wear in the smooth regions tended to be negligible compared to the wear in the rougher regions and was the only type that was characteristic of abrasive wear by paper (11,12). This was confirmed in abrasive wear tests against papers (10,12). Figure 7.19 shows a typical wear surface produced in those tests.

The interaction of the rollers and the checks were also studied with high-speed video techniques. Some slip was observed to occur and it was more pronounced during acceleration of the checks than during deceleration of the checks. Estimates indicated that total slip time for one check was of the order of 1 msec. However, the more pronounced feature that was observed was the engagement of the leading edge of the check with the roller. The check edge produced a noticeable amount of deformation in the elastomer. It was hypothesized that the high strains associated with this engagement could cause a fatigue wear process to occur, which could account for the moderately rough wear regions. To investigate this, a special sliding wear test was developed to simulate this behavior (Fig. 7.20) (10,12). It was found that the moderately rough wear scar morphology could be produced by this test but not by one using a flat, smooth platen.

From these studies, it was concluded that there were three failure mechanisms involved: interface delamination, surface fatigue from check edge contact, and paper abrasion. It was also concluded that the first two were the ones primarily responsible for the functional failures observed, since the dimensional changes associated with paper abrasion were not sufficient to cause a functional failure.

The interface problem was the easiest to solve. Enhancements were made to the bonding process and found to be satisfactory. A materials solution was sought for the fatigue wear. Three tests were used to compare materials: a friction test, an abrasive wear test against paper, and a sliding wear test against the grooved steel platen. Prototype rollers were used in these tests. The results of some of these tests are shown in Table 7.2. Criteria for selection was that the coefficient of friction and abrasive wear resistance

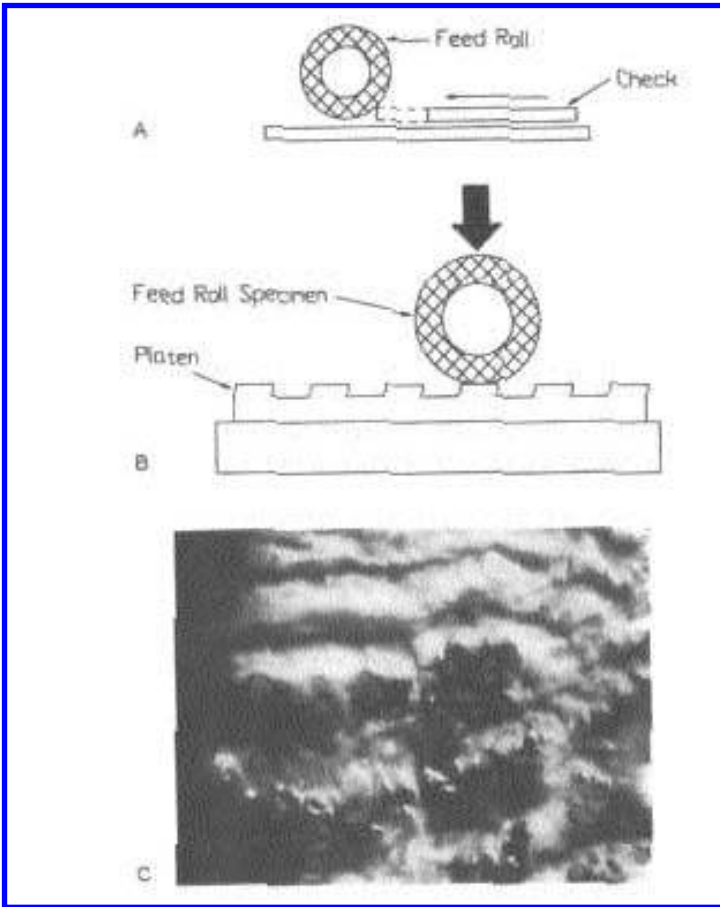


Figure 7.20 Contact between the check edge and roller, “A”, and the test used to simulate the wear situation, “B”. & “C” shows the morphology of the wear scar produced in these tests. (From Ref. 10, reprinted by permission from ASTM.)

Table 7.2 Friction and Wear Properties Determined for Candidate Feed Roll Material

Characteristic	Material			
	NBR 50 Shore A	Millable gum urethane	Modified NBR 60 Shore A	Hardened EPDM 60 Shore A
Abrasive wear resistance (depth of wear in drum test; mm)	0.066	0.053	0.058	0.051
Tear resistance	Poor	Good	Good	Very good
Coefficient of friction	1.22	1.03	0.86	0.72

Source: Ref. 12.

should be similar to or better than that of the original material and that the resistance to fatigue wear should be significantly better. This led to the selection of the millable gum urethane for this application.

In addition to selecting a new material, it was also decided to increase the thickness of the elastomer layer as much as possible. This was on the basis that fatigue wear life would be extended by decreasing the strain level and strain should decrease with increasing thickness. Simple stress and wear modeling indicated that fatigue wear life should be proportional to approximately the fourth or fifth power of the thickness. It was also decided to increase the roll diameter as much as possible, since this would also tend to reduce strain in the elastomer.

The amount of wear associated with abrasion over the desired lifetime was also estimated (10). This was based on a linear model for abrasive wear, the wear data obtained in the tests, and an estimate of the amount of slip obtained from the video studies. For both the original material and the new material, the amount of wear estimated was lower than that associated with a functional failure.

Subsequent machine evaluations with new rollers, which incorporated these changes, indicated that the problem was solved by these changes. Field experience later confirmed this.

7.6. MOTOR BRUSH LIFE

This case study concerns wear in an electric motor used to transport paper through a high-speed impact printer. The problem was discovered during the course of a wear design program to optimize the selection of brush material for the motor. These printer applications required special motors, which could stop and start paper very quickly at a high repetition rate. For example, these motors were required to provide accelerations in the range of 100G, hundreds of times a minute. In this particular case, the application involved more than 1000 acceleration / deceleration cycles per minute. While there was general information and data regarding brush wear behavior, there was a lack of relevant wear data because of the unique requirements of these applications. Therefore, a wear design approach had been initiated to select a brush material that would meet printer life requirements. The basic approach of the wear design was to develop a laboratory test that simulated the conditions of the application and that could be used to rank materials and to evaluate the effects of various parameters on brush wear behavior. General information about brush wear indicated that transfer films on the commutator surface played an important role in wear and that wear behavior could be affected by mechanical and electrical factors, as well as environmental conditions. A wear apparatus, which would allow the effects of these different elements to be studied, was built (Fig. 7.21). To verify that the apparatus simulated the application, wear rates obtained with the apparatus were to be compared with those measured in printer tests. In doing this, a greater than an order of magnitude difference in wear rate was observed between two motors, which were nominally the same and operated under the same nominal conditions. Extrapolation of data from the better performing motor indicated that life would be acceptable, while that from the poorer performing motor indicated a wear problem, significantly shorter life than required. A problem solving activity was initiated to determine the reason for this difference in behavior.

The problem solving activity started with the examination of worn parts. Initially this was limited to examination of the worn brushes, since examination of the commutators required interruption of printer tests. Morphology and composition of the brushes from the two motors were similar for both sets of brushes. The wear scar morphology

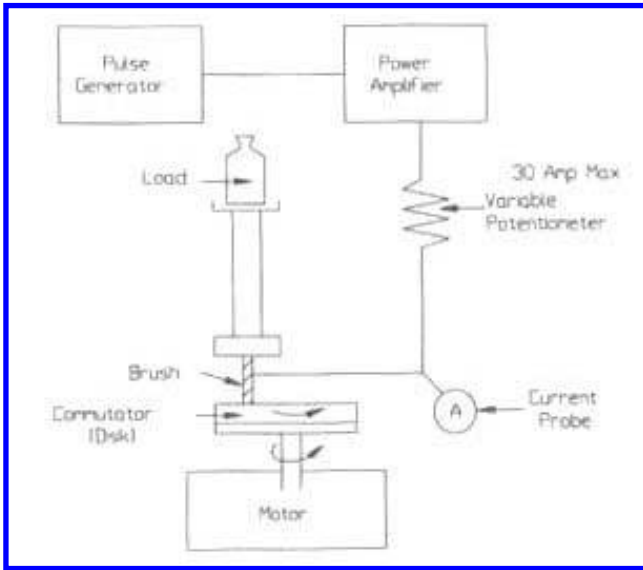


Figure 7.21 Apparatus used to simulate brush wear.

on these brushes was compared to those obtained in the laboratory tests and no significant difference was observed (Fig. 7.22). Test histories of both motors were reviewed for possible differences in operating conditions. Again no differences that appeared significant were found. Experience with the laboratory wear apparatus and test were reviewed for some insight into the problem. In doing this review, it was observed that mechanical instability in earlier levels of the test apparatus had resulted in much higher wear rates than obtained with the final design of the apparatus. The wear rates differed by one to two orders of magnitude. It was also observed that the wear rate from the better performing motor was in general agreement with the wear rates obtained when the mechanical instabilities were eliminated from the apparatus. Since the source of much of the instabilities in the test apparatus was associated with the bearing system, it was speculated that there might be some differences between the bearing systems of the two motors that could lead to differences in their mechanical stability.

In investigating this possibility, a difference in shaft run-out was found between the two motors. In the better performing motor, concentricity was found to be < 0.0002 in, while in the poorer it was approximately 0.0005 in. Since the wear rate associated with the better motor was consistent with the life requirements, it was concluded that the concentricity observed for this motor should be a requirement of the motor. With this as a goal, the entire bearing system was reviewed and several changes were made to insure that this new requirement would be consistently met.

The laboratory wear studies had shown that the major effect of mechanical instability on wear was as a result of the sparking that occurred in this case. Mechanical vibration was found to induce sparking, and sparking was found to affect the nature of the transfer film that was formed. Examples of the films produced in the laboratory tests on the wear

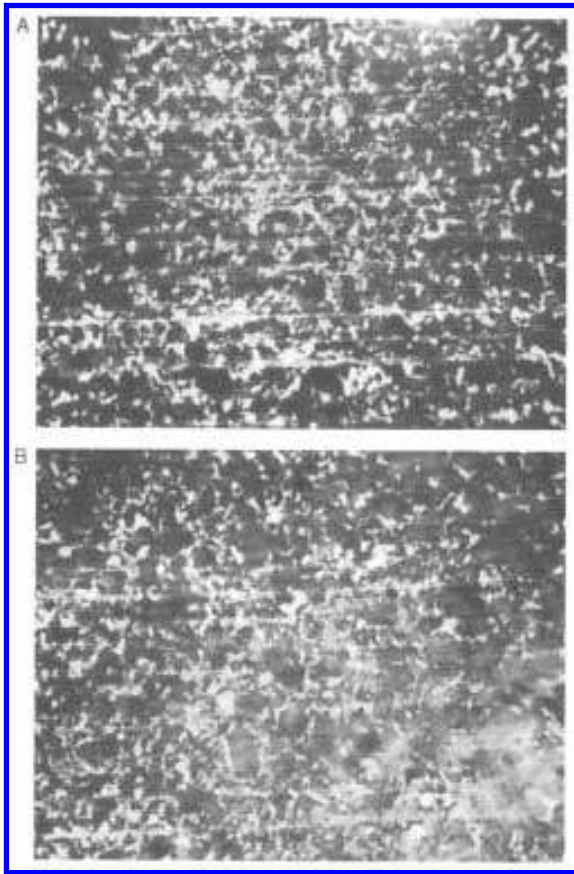


Figure 7.22 Micrographs of worn brush surfaces. “A” is the surface of a machine worn brush. “B” is the surface of the same type of brush worn in the test.

surface without current and with sparking are shown in Fig. 7.23. A much thicker film tends to be formed with sparking than without.

It was found that wear rates obtained with the final apparatus (vibration eliminated) were representative of those found in motors with good concentricity (Table 7.3). From this and morphological comparisons, it was concluded that the apparatus provided adequate simulation. This apparatus was then used to evaluate the effects of several factors

Motor test at constant speed without current	5.67×10^{-12} in./in-g
Wear test at constant speed with current	15.2×10^{-12} in./in-g
Motor test with current and non-constant speed	12.4×10^{-12} in./in-g

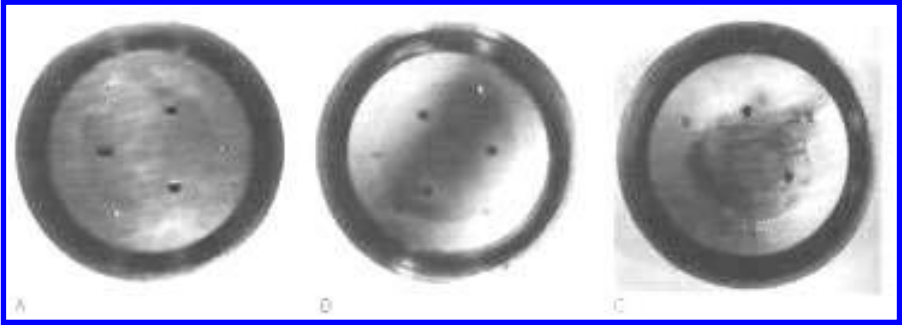


Figure 7.23 Examples of films formed on the Cu disks in the wear tests. “A” and “B” show the films formed with and without current, but without sparking, and “C” with sparking.

on wear, such as load, temperature, speed, and current pulse parameters. From these, it was concluded that after an initial break-in period, wear volume was proportional to distance of sliding and load. Except for the nature of the current pulse the effect of the other parameters did not appear to be significant in the range of interest. The graph in Fig. 7.24 shows the nature of the dependency on peak current that was typically found. Tests with different brush materials showed that there could be considerable difference in wear performance. Examples of this are shown in Table 7.4.

Based on these studies, it was possible to project life in the application and to select a material whose projected life met the life requirements of the printer. Wear measurements for motors used in printer test, which contained the improved bearing system and the selected material, confirmed these projections. Ultimately these were also verified by field performance.

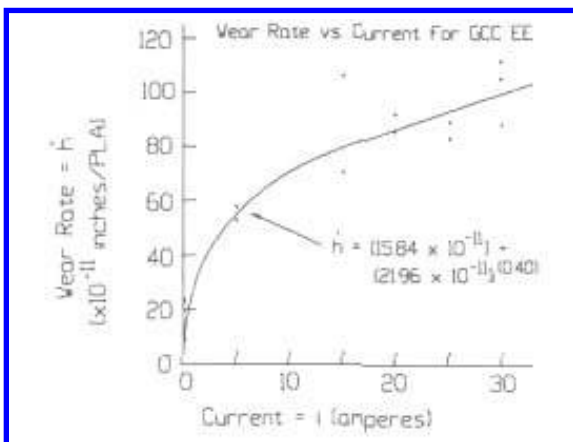


Figure 7.24 The effect of current on wear rate.

Table 7.4 Wear Rates for Different Brush Materials

Current (amps)	Wear rate (in./pulse g in. ³)								
	Metal graphite (type)						Natural graphite (type)		Electrolytic graphite (type)
	1	2	3	4	5	6	1	2	
0	3.9 ^a	15.8 ^a					2.4 ^a		
5	8.8	56.5	2.5	4.0	4.6	4.1	2.6	2.0	3.6
15	9.9	89.0							
20	11.0	90.0							
25	10.9	87.0							
30	10.5	103.6							

^a(m./g in.²)

7.7. MEMORY DISK DRIVE FAILURES

Disk drives are prone to failure as a result of abrasive wear by contamination of the head / disk interface. A situation involving such a wear concern provides an interesting case study (13). The initial steps of the problem solving approach, which was the identification of the problem as one resulting from contamination, are not discussed in the reference. However, it can be presumed that this likely consisted of the examination of used hardware, comparing failed units with unfailed operating units and relating the observations to wear behavior. Principal techniques were likely to be low power optical techniques, SEM microscopy, and EDX analysis. Subsequent steps, involving the resolution of the problem, are discussed in the reference.

Initial characterization of the morphology and composition of the contamination indicated that the source of contamination was likely internal to the machine, rather than from outside the machine. Air sampling techniques were used to collect particles circulating inside the machines. Table 7.5 shows the composition and size range of the particles found. The machine was reviewed for possible wear interfaces that would produce wear particles with these compositions. It was found that the band-stepper drive had such an interface. The band of this unit was stainless steel and it contacted an aluminum capstan (Fig. 7.25). Since the nominal operation of the unit did not involve sliding, it was speculated that the wear was caused by incidental fretting motion between the band and the capstan. Machines were then examined for evidence of fretting at this

Table 7.5 Distribution of Airborne Particles

Particle size (µm)	Elemental composition
0.15	Fe, Cr
0.15	Fe, Cr, Al, S
0.5	Fe, Cr, Al, S, Si
0.5	Fe, Cr, Al, S
1.5	Fe, Cr, Al, S
1.5	Fe, Cr, Al, S, Si
> 1.5	Fe, Cr, Ni, Al, Si, S

Source: Ref. 13.

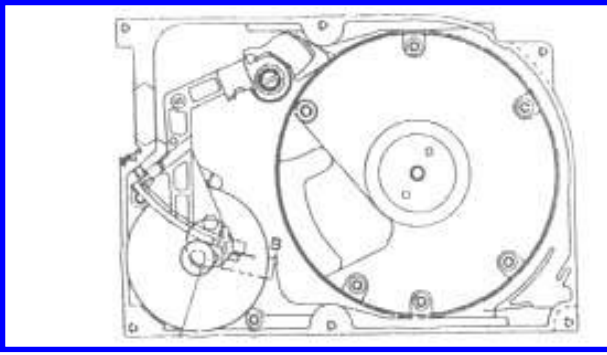


Figure 7.25 Band-stepper drive. (From Ref. 13, reprinted by permission from ASME.)

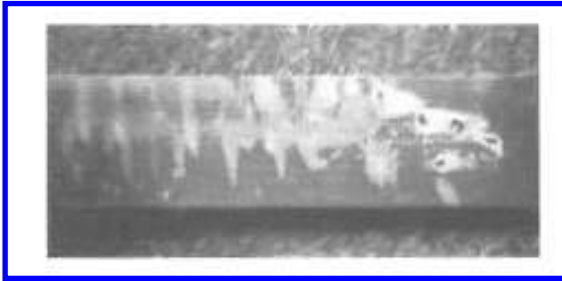


Figure 7.26 Fretting scars on the band. (From Ref. 13, reprinted by permission from ASME.)

interface. Evidence of fretting wear was found in several cases (Fig. 7.26). In other units operated for similar amounts of time, there was no indication of fretting. To verify that fretting at this interface was the source of the contamination, units of both types were run to collect air samples. In those units, which exhibited signs of fretting, the Fe–Cr–Al particles were found, while in those units, which did not exhibit signs of fretting, the particles were not found.

The next step in the problem solving activity was to determine the causes of the fretting wear. It was concluded that poor assembly and adjustment procedures allowed significant fretting motions to occur in some units. There was also some evidence found that contamination of these components during assembly or prior to assembly caused increased wear. Enhancing cleanliness and workmanship during assembly eliminated the failures.

7.8. EROSION IN FANS AND BLOWERS

Fans and blowers are used in many stages of steel production to move hot air, generally containing high levels of particulates and gaseous contaminants, at high speeds. Erosion of blades and other surfaces in these applications is common and often results in the need for frequent replacement or repair. Sometimes this is required after as little as several

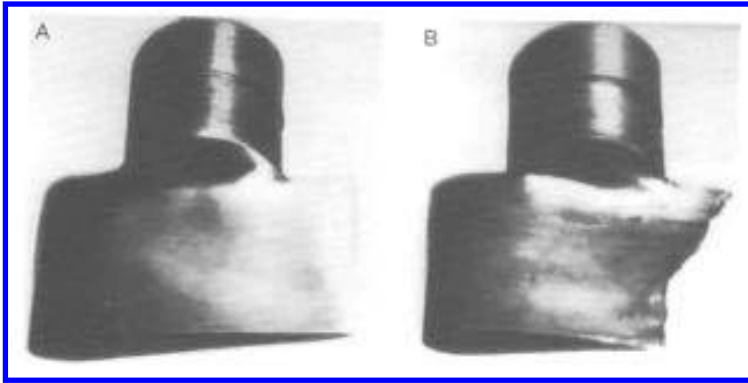


Figure 7.27 “A” shows an example of new inlet vane. “B” shows one after 1 $\frac{1}{2}$ years of service. (From Ref. 14, reprinted by permission from Elsevier Sequoia S.A.)

months of usage. An example is shown in Fig. 7.27. This case study describes an approach that was developed to resolve erosion problems in these applications (14). The basic premise of the approach is that the severe erosion in these applications is the result of turbulence in the air stream. In streamline flow, the particles tend to move parallel to the surfaces, while in turbulent flow the particles tend to impinge and cause erosion.

The general approach is this. After identifying the existence of an erosion problem, the flow characteristics and patterns in the devices are determined and examined for turbulence. Once these regions of turbulence are identified and the causes for the turbulence are established, ways of modifying the design to eliminate or significantly reduce the turbulence are investigated. If possible, the design is modified to reduce the turbulence and the improvement evaluated. If the life is still not adequate or if it was not practical to modify the design, hardfacing techniques for the critical areas are then investigated as a means to improve life.

In one application design changes were sufficient. Field trials showed that the design changes, which were introduced to eliminate turbulence, resulted in a > 10 -fold improvement in life. In the second application, design changes resulted in a significant improvement; however, it was not adequate. In this case, a hardfacing technique was used to further increase the life. The hardfacing increases the hardness from 200 Bhn to Rc68 in the critical regions. In the third application, it was not practical to modify the design to eliminate the turbulence. Therefore, the critical surfaces were hardfaced to give a moderate fourfold improvement. Assuming that the hardness of abrasive is greater than the surface, this fourfold improvement is approximately what would be projected by the change in hardness of the surfaces. By comparing the first case with the third, it can be inferred that for this type of wear problem, it was more effective to modify the design to eliminate turbulence than to change materials.

7.9. HYDRAULIC STRUCTURE WEAR

Water velocities in hydraulic structures, such as conduits, pipes and valves, often can be high enough to cause cavitation. Since cavitation can cause wear, replacement and repair of these structures because of wear is often a concern in these applications. This case study discusses a methodology that was developed to address this type of problem. It illustrates

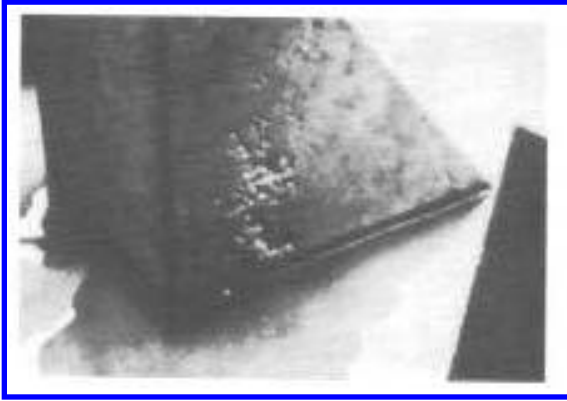


Figure 7.28 Cavitation damage on the side of a concrete baffle block. (From Ref. 15, reprinted by permission from ASME.)

the major aspects of problem solving, namely failure analysis, hypothesis development, and testing (15,16).

Cavitation is not the only source of wear or damage in these structures. Erosion, structural or material flaws, unusual one-time events, and fatigue are other sources of wear or damage to these structures. Figures (7.28–7.31) show examples of the damage from cavitation and other sources in these situations. In some cases, initial cavitation damage can lead to other failure modes, such as providing sites for damage due to freezing and thawing. Consequently, the first task of the failure analysis is to determine whether cavitation is involved in the damage and what roll it plays. This involves the examination of the damage and the characterization of the operating conditions. Several features are important in deciding whether or not cavitation is involved and how significant it might be. These are: flow velocity, upstream conditions affecting the flow, location of the damage, flow passage shape, similar damage in other locations, texture of damage, and presence of catastrophic damage. With all of these, the question asked is: “Is the observation consistent with cavitation behavior?”

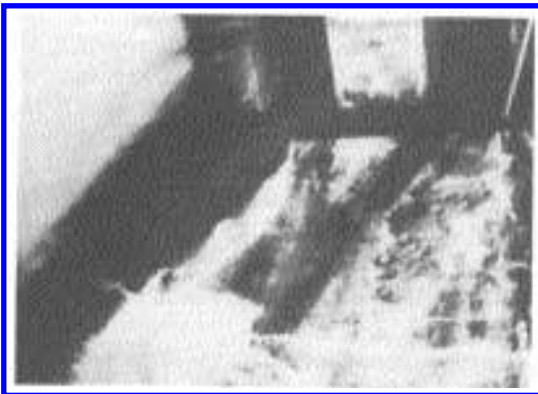


Figure 7.29 Cavitation damage on a chute floor downstream from a high pressure slide gate. (From Ref. 15, reprinted by permission from ASME.)



Figure 7.30 Abrasion damage on a stainless steel butterfly valve. (From Ref. 15, reprinted by permission from ASME.)

The results of the failure analysis can be augmented with the results from a variety of laboratory tests to develop a model for the damage. These same tests also can be used to verify the model and to identify solutions. The laboratory tests that are used to address these problems tend to fall into three categories. One involves the use of a scale model to determine what flow condition is required for cavitation. Another is the use of flow tests to evaluate the effects of local shapes and contours on cavitation. The third is cavitation wear tests, which provide information about how the individual materials wear in a cavitation field and a means of ranking materials.

The final phase of the method is to use the accumulated information to determine the most appropriate means of solving or alleviating the problem. This might involve a design

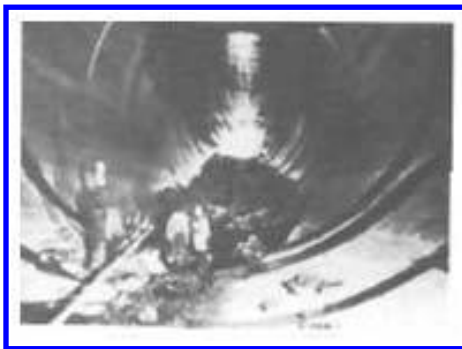


Figure 7.31 Catastrophic damage in a concrete-lined spillway tunnel that was initiated by cavitation. (From Ref. 15, reprinted by permission from ASME.)

change to reduce or eliminate the tendency for cavitation, a material change to provide more resistance to cavitation damage, and the development of maintenance schedule to minimize the effect of such damage [Table 7.5](#).

7.10. TEETER BEARING WEAR

This case study illustrates a primarily analytical method for developing solutions to a wear problem. In this case it involved the wear of a teeter bearing of a wind turbine generator. The bearing system consisted of a journal bearing or bushing and a thrust bearing. Both bearings were subjected to high and variable loads and small amplitude oscillatory motions. The design had gone through several iterations to improve wear and corrosion life. The current design provided adequate corrosion life but the wear life was still unacceptable. In under one year of operation, significant wear of the bearing surfaces occurred and the shafts were scored, requiring replacement of these three components. The target for the design was to have several years of operation before the bearings or the shaft had to be replaced. Both wear situations involved common elements and the same basic approach was applied to both situations, that is, wear of the bushing and the thrust bearing. For illustrative purposes, the discussion will focus on the bushing wear problem. A sketch of the bearing system is shown in [Fig. 7.32](#). Worn bearings and a shaft are shown in [Fig. 7.33](#).

The materials used in the design, which were acceptable from a corrosion standpoint, were a soft steel shaft and a special bearing material. The bearing material consisted of a bronze alloy substrate with trepanned holes. These holes were filled and the surface coated with an epoxy composite. Nominal parameters of the design and operating conditions are shown in [Table 7.6](#). The loading and amplitude of motion at these

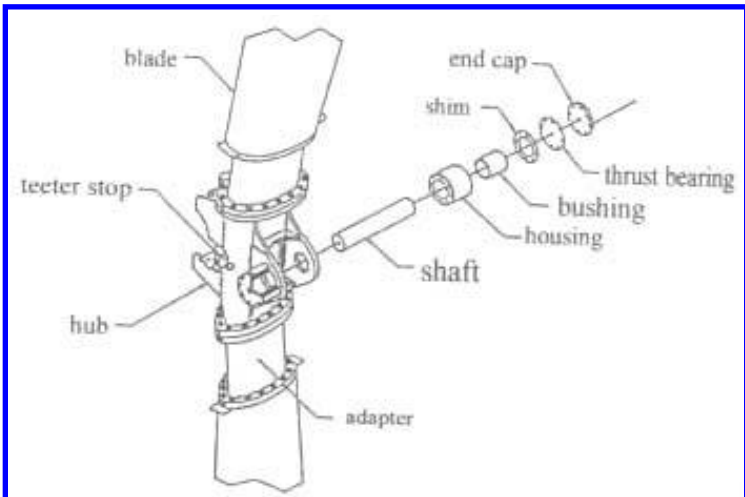


Figure 7.32 Schematic of a teeter bearing system for a wind turbine generator.

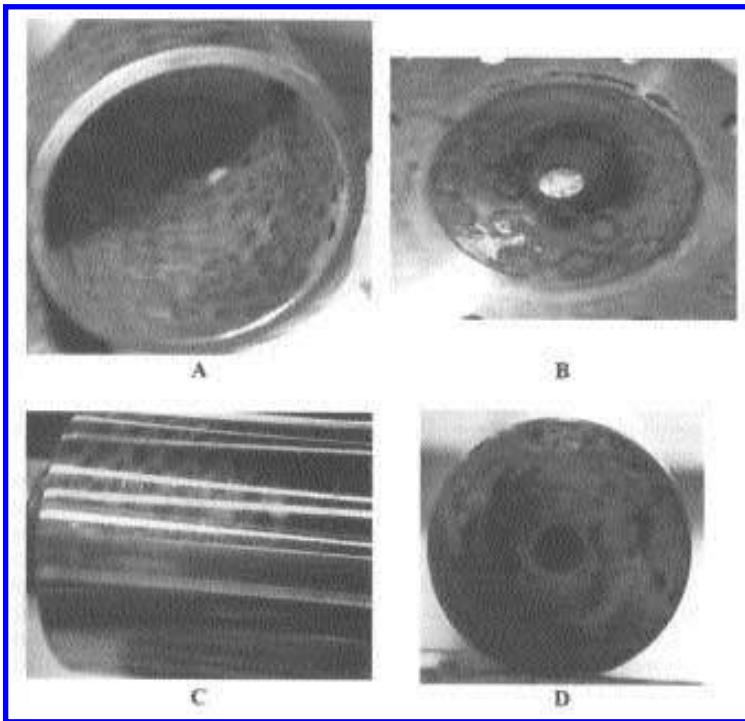


Figure 7.33 Used components of the teeter bearing system. “A” shows a worn bushing. “B” shows a worn thrust bearing. “C” shows a worn shaft. “D” as worn shaft thrust face

Table 7.6 Teeter Bearing Design Parameters^a

Shaft diameter	5.498–5.500 in.
Shaft roughness	63–15 μin. CLA
Shaft material	4000 series steel, Bhn 300 min
Bushing length	5.50 in.
Bushing diameter	5.507–5.509 in.
Bearing diameter	5.450 in. outside 1 in. inside
Bushing and bearing material	Coating: 0.007 in epoxy; substrate: bronze, Bhn 190, with trepanned holes filled with epoxy ^b
Lubrication	None
Loading	Variable bending moments
Motion	Small amplitude oscillations
Use	2/3 time
Environment	Exposed to dust and climatic conditions

^aSee Fig. 7.34 for illustration of bearing system.

^bSee Fig. 7.35 for illustration of substrate.

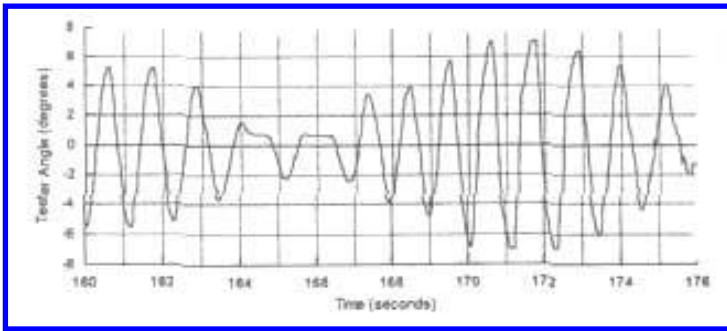


Figure 7.34 Example of teeter bearing motion based on simulation of wind conditions.

interfaces were the result of wind conditions, which fluctuate. Typical characteristics of the oscillatory motion and loading variation are illustrated in Figs. 7.34 and 7.35.

The initial steps in developing a solution to this problem consisted of modeling the design concept and the examination of worn parts. As a part of this initial activity, the operation of the teeter assembly was reviewed, as well as operational and environmental conditions. The purpose of the initial models was to see what the wear life could be under ideal conditions. Therefore, ideal contact conditions were assumed for both bearing situations, that is, perfect alignment and conforming contact. For the bushing, this meant that the area of contact was the length of the bearing times the diameter of the bearing. This

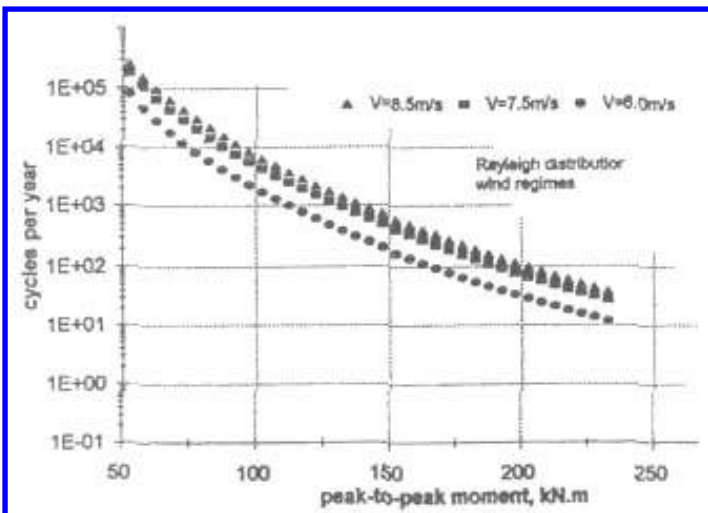


Figure 7.35 Example of the variation in loading conditions on a teeter bearing based on simulation of wind conditions.

wear situation was modeled using the K factor or linear wear model and the Zero and Measurable Wear model as applied to bearings. (See Sec. 2.8.) The first step in the analysis was to develop an equivalent load, \bar{P} , and equivalent amplitude, \bar{a} for use with these models. These were defined by the following equations:

$$\overline{P^n a} = \bar{P}^n \bar{a} \tag{7.1}$$

$$\bar{a} = 2 \int_0^{a_m} ap(a) da \tag{7.2}$$

$$\bar{P}^n = \frac{\int_0^{a_m} P(a)^n ap(a) da}{\bar{a}} \tag{7.3}$$

In these equations P is load, a is amplitude of the oscillation, $p(a)$ is a distribution function for the amplitude, $P(a)$ is the relationship between load and amplitude, and n is the exponent of the load in the wear equations. a_m is the maximum amplitude. The relationships for these distribution functions were obtained from simulations of turbine operation. From these same simulations, it was concluded that the nominal frequency of oscillation was 1 Hz. Table 7.7 shows the effective values of load and amplitude that were determined for the bushing and the thrust bearing for the different models.

Assuming that the wear factor for the bearing material was in the range of that reported for the best bearing materials, 1×10^{-10} in.³ min / ft lb hr, it was estimated that the life of the coating would be several years for either situation. If a nominal value, which was more representative of typical wearing combinations, was assumed, the life of the coating was still estimated to exceed one year. The Zero Wear Model indicated that zero wear lifetimes were even much longer under the ideal contact conditions assumed. Both of the models indicated that wear on the rod should be negligible after several years of operation. Examination of worn parts indicated that these ideal assumptions were not valid and that the wear was more severe than projected by these models.

The bearings and shaft with the equivalent of a third of a year of normal operation without lubrication were examined, using visual and low power optica microscopy. Several observations were made, while there was no sign of corrosion or significant abrasive wear due to contamination, there was significant wear on both the bearing surfaces and the rod. On the bearing surfaces, the coating had been worn through and wear had progressed into the substrate. Wear on the shaft consisted mainly of severe scratches corresponding to the regions where the coating on the bushing was worn off. While transfer and build-up of material was evident (primarily organic, likely consisting of epoxy debris), there was no indication of the formation of a stable and uniform transfer film or tribofilm formation

Table 7.7 Equivalent Loads and Amplitudes

	Model	n	Equivalent load \bar{P} (lbs.)	Equivalent amplitude \bar{a} (")
Bushing	Zero wear	9	8.4×10^3	5.5
	Measurable wear	4.5	6.7×10^3	5.5
	Linear	1	5.0×10^3	5.5
Bearing	Zero wear	9	5.7×10^3	2.7
	Measurable wear	4.5	5.7×10^3	2.7
	Linear	1	5.6×10^3	2.7

being a factor in the wear behavior. It was also found that the assumptions of conformity and alignment assumed for the modeling were not true. There was evidence of significant axial misalignment on both bearing surfaces and that contact only occurred over a small portion of the diameter of the bushing. On the parts examined, the wear scar on the bushing was tapered with the maximum arc of the contact region being in the range of 60° . In addition to these examinations the dimensions of the worn parts were measured and found to be within the specifications. However, it was noted that the roughness of the shaft was higher than that recommended by the bearing supplier. The supplier recommend a shaft roughness between 65 and 32 μin . approximately half of what was specified, 125–63 μin .

A review of the loading conditions on the teeter bearing verified that misalignment was intrinsic to the situation as a result of moment loading on the bearing and the clearances in the bearing. It was concluded from this review that the clearance between the shaft and the bushing was the primary method for controlling this.

Based on these findings, it was concluded that the primary cause of the wear problem was contact conditions (roughness, conformity, and alignment) and not material selection. Consequently, it was therefore decided to model the effect of these mechanical parameters on wear before looking for alternative materials. At this point, it was decided to model the effects of these parameters using the Zero and Measurable Wear relationships. This was decided for two reasons. One was that the effect of these parameters is more significant in the Zero and Measurable Wear formulation than in the linear wear formulation; the second was that the generally good agreement between these models and wear behavior in engineering situations. If the resulting model did not provide a good agreement with the observed behavior, alternative models would be investigated, including the ones based on the linear wear relationship.

After reviewing the practical consideration associated with the design, it was decided to initially limit the modeling to three effects, roughness, axial alignment (clearance), and lubrication. The first was to investigate the change in shaft roughness, as suggested by the supplier. The second was to determine how much misalignment could be allowed for acceptable wear. The third, the effect of lubrication, was also included in this modeling activity because of the significant effect that lubrication has on wear behavior and the fact that it was possible to lubricate these surfaces with grease. The initial design did not include the use of grease because of the difficulties associated with relubrication. In this situation, the use of grease could also prevent the formation of transfer films that might occur with the special bearing material used.

For the bearing material two phases of wear were modeled. The first phase of wear was when the wear of the bushing material was confined to the epoxy layer; the second phase was when the wear extended into the substrate. For simplicity in modeling the second phase, it was assumed that the properties (yield stress) of the metal substrate controlled the wear and the effect of the epoxy was that of a lubricant. A more realistic assumption, discussed at the end of this section, could be used but was found to be unnecessary. In this modeling, it was assumed that the shaft did not wear. The assumed progression of bushing wear when there is misalignment is shown in Fig. 7.36. This figure illustrates the transition of wear from phase 1 to phase 2. These five wear situations were modeled using the Zero and Measurable Wear formulations for bearing wear described in Sec. 2.8. In this, the shape of the wear scar was based on the shape of the initial contact area, as illustrated in Fig. 7.37. It was also assumed that in the second phase, the wear rate was uniform across the surface. Equation (7.4) is the general form of the equation for maximum wear depth obtained for the last four situations. This form also applies to the initial situation if there is plastic deformation of the epoxy layer, as was predicted to occur with

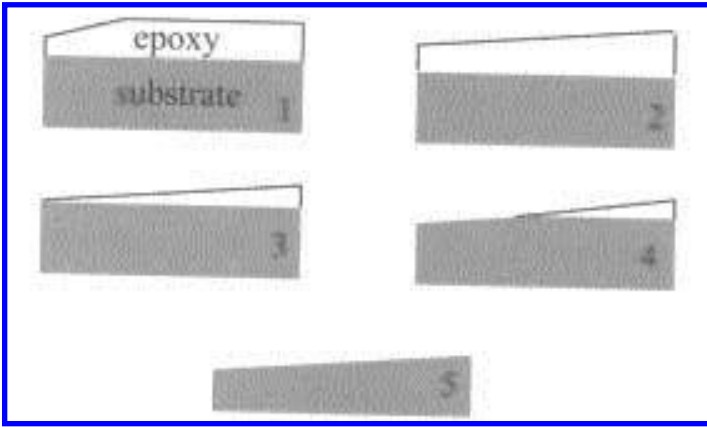


Figure 7.36 Stage of bushing wear: 1, initial deformation; 2, wear limited to epoxy layer; 3, wear-through of epoxy layer; 4, combined wear of substrate and layer; and 5, wear of substrate.

some alignment conditions. If there is none, the relationship for the first situation is Eq. (7.5). In these, equation H is the maximum depth of wear; L is the number of oscillations; α is the angle of misalignment; δ_0 is the CLA roughness of the shaft. L and H_j are the number of cycles at the end of the previous period and the wear depth at the end of that period, respectively. If there is an initial plastic deformation, H_j is the depth of the deformation and L_j is 0 for the initial stage. σ_i is the initial contact pressure and W_i is the initial width of the contact. The exponent, n , varies with the wear mode assumed (constant energy or variable energy) and whether the wear scar is longer (trapezoidal) or shorter (triangular) than the bushing.

$$H = \frac{2\delta_0 \bar{a}^n \tan^{9n} \alpha \bar{P}^{9n} (0.25 + \mu^2)^{9n/2}}{(4 \times 10^3)^n D^{5n} H_j^{1.5n} (\Gamma_r \tau_y)^{9n}} (L - L_j)^n \tag{7.4}$$

$$H = \frac{2\delta_0 \bar{a}^n D^n \sigma_i^{9n} (0.25 + \mu^2)^{9n/2}}{(2 \times 10^3)^n (90^\circ W_i)^n (\Gamma_r \tau_y)^{9n}} L^n \tag{7.5}$$

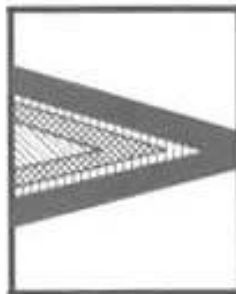


Figure 7.37 Progression of wear scar shapes on bushing when there is misalignment.

The unworn contact area was initially determined using the approximation method described in Sec. 2.8. Using these areas to determine contact stresses, it was found that for the clearances allowed by the design initial plastic deformation of the epoxy layer was likely. In this case, the contact area would be determined by the hardness of the epoxy and the contact pressure would be the flow pressure (hardness) of the epoxy and not by this approximation. The flow pressure of the epoxy was estimated to be in the range of 4 kpsi. For reduced clearances, plastic deformation would not occur and the contact pressure was determined using the approximation. For misaligned conditions resulting in plastic deformation, Eq. (7.4) was used for wear in the initial region with L_i equal to 0 and H_i equal to the maximum depth of the deformation. For conditions in which there was no plastic deformation, Eq. (7.5) was used for the initial region.

Progressive wear on the shaft was not a concern but scoring was. It was hypothesized that this would only occur after the epoxy film was worn through and metal-to-metal contact would occur. Since the shaft was harder than the substrate, it was further hypothesized that minimum number of cycles required for scoring would be the zero wear lifetime of the shaft, based on the maximum metal-to-metal contact pressure. This was affected by two factors: One was the relative amount of the two types of contact in the contact area, metal-to-metal and metal-to-epoxy; the other was the relative wear resistance of the epoxy and the bronze substrate. The model assumed that the wear rate of the bearing was uniform. These meant that the wear rates of the bronze substrate and the epoxy-filled hole were the same. Since the epoxy is softer than the bronze, this implies that the average pressure in the metal-to-metal region, the contact pressure is higher. This condition resulted in the following approximate relationship for contact pressures, where σ_m represents the metal-to-metal contact pressure and σ_e , the metal-to-epoxy contact pressure. In this equation Γ_{rm} is the zero wear factor for metal-to-metal contact, Γ_{re} is the zero wear factor for metal-to-epoxy contact, τ_m is the shear yield stress for the metal, and τ_e is the shear yield of the epoxy

$$\sigma_m \gg \frac{\Gamma_{rm} \tau_m}{\Gamma_{re} \tau_e} \sigma_e \quad (7.6)$$

Taking into account the relative contact area of these two types of contact, the following relationship can be obtained between σ , the average contact pressure, and σ_m :

$$\sigma_m = \sigma \left[\kappa + \frac{(1 - \kappa)}{\beta} \right]^{-1} \quad (7.7)$$

In this equation, β is the ratio of σ_m to σ_e Eq. (7.6) and κ is the fraction of the total area of contact that is metal-to-metal. Using this relationship, it was estimated that the initial metal-to-metal contact pressure was in the range of $6 \times$ time the average pressure. This was assumed to be the maximum, since stress level decreases with wear.

Table 7.8 summarizes the nominal results obtained from this modeling activity. It can be seen that there is an agreement between this model and observed behavior. Based on this analysis, it was decided to use the smoother surface finish recommended by the supplier, reduce the clearance by 60%, and to lubricate. These improvements were estimated, resulting in a minimum of $5 \times$ improvement in life. The problem was resolved by these actions. While a material change was not implemented, this modeling activity was also used to investigate possible material changes, such as a harder shaft and other bearing materials.

Table 7.8 Summary of Modeling Results for Bushing and Shaft

Clearance (in.)	Bushing		
	Initial wear rate (in./cycle)	Wear rate after 0.014 in. of wear (in./cycle)	Time for coating wear-through (years)
> 0.0010	9×10^{-7}	Rough and unlubricated $4 \times 10^{-9} - 3 \times 10^{-6}$	0.0004
> 0.0005	9×10^{-10}	$8 \times 10^{-11} - 6 \times 10^{-8}$	0.37
> 0.0010	9×10^{-7}	Rough and lubricated 4×10^{-9}	0.0004
> 0.0005	9×10^{-10}	8×10^{-11}	0.37
> 0.0010	3×10^{-7}	Smooth and lubricated 1×10^{-9}	0.001
> 0.0005	3×10^{-10}	2×10^{-11}	1.3
	Shaft		
	Clearance (in.)	Minimum time for scoring (years)	
		Rough and unlubricated	
	> 0.0010	0.001	
	> 0.0005	0.4	
		Rough and lubricated	
	> 0.0010	0.75	
	> 0.0005	36	
		Smooth and lubricated	
	> 0.0010	0.75	
	> 0.0005	37	

The modeling assumption that the properties of the metal substrate dominate the wear situation in the second phase could be made more realistic by considering the increase in pressure at the metal-to-metal contact, as done for determining the zero wear life of the shaft. Increasing the equivalent load used in Eq. (7.4) by the same multiplier used for the shaft could do this. This would make the analysis more complex, since this ratio would change as the amount of metal exposed increases. However, it would asymptotically approach a limiting value. The significance of this refinement on the results of the modeling was investigated and found not to be significant in terms of the design consideration.

REFERENCES

1. E Hsue, R Bayer. Tribological properties of edge card connector spring/tab interface. IEEE Trans CHMT 12(2):206–241, 1989.
2. A Wayson. A study of fretting on steel. Wear 7:435–450, 1964.
3. R Bayer, J Sirico. Wear of electrical contacts due to small-amplitude motion. IBM J R&D 15(2):103–107, 1971.
4. W Campbell. Boundary lubrication. In: F Ling, E Klaus, R Fein, eds. Boundary Lubrication. New York, NY: ASME, 1969, pp 87–118.

5. R Bayer, E Hsue, J Turner. A motion-induced sub-surface deformation wear mechanism. *Wear* 154:193–204, 1992.
6. R Bayer. A general model for sliding wear in electrical contacts. *Proceedings of the International Conference on Wear of Materials*, New York: Elsevier Science Publishing Co. 1993, pp 913–918.
7. P Engel, E Hsue, R Bayer. Hardness, friction and wear of multiplied electrical contacts. *Proceedings of the International Conference on Wear of Materials*, New York: Elsevier Science Publishing Co. 1993, pp 538–551.
8. RG Bayer, J Gregory. An engineering approach to vibration induced wear concerns of electrical contact systems. *EEP. Advances in Electronic Packaging*. 4–1. ASME, 1993, p 525.
9. R Bayer. The influence of lubrication rate on wear behavior. *Wear* 35:35–40, 1975.
10. R Bayer. Tribological approaches for elastomer applications in computers. In: R Denton, M Keshavan, eds. *Wear and Friction of Elastomers*. STP 1145, ASTM, 1992, pp 114–126.
11. R Bayer. Aspects of paper abrasivity. *Wear* 100:517–532, 1984.
12. N Payne, R Bayer. Friction and wear tests for elastomers. *Wear* 150:67–77, 1991.
13. R Reinisch. Fretting wear in magnetic memory disk drives. *Proceedings of the International Conference on Wear of Materials*, West Conshocken, PA: ASME, 1991, pp 581–584.
14. S Srivastava, S Mehra. Tribological design considerations in fans and blowers. *Wear* 25(2): 245–254, 1973.
15. D Colgate. Cavitation Damage in Hydraulic Structures. *Proceedings of the International Conference on Wear of Materials*. ASME, 1977, pp 433–438.
16. J Graham, T Rutenbeek. Repair of cavitation damaged concrete: a discussion of bureau of reclamation techniques and experiences. *International Conference on Wear of Materials*. ASME, 1977, pp 439–445.

Appendix

APPENDIX I

VALUES OF m AND n FOR USE WITH THE HERTZ CONTACT STRESS EQUATIONS

$\cos \Theta$	m	n
1.0	39.93	0.1263
0.9995	23.35	0.1651
0.9990	18.54	0.1854
0.9985	15.85	0.2005
0.9980	14.25	0.2114
0.9975	13.15	0.2201
0.9970	12.33	0.2273
0.9965	11.58	0.2345
0.9960	11.03	0.2404
0.9955	10.53	0.2460
0.9950	10.15	0.2506
0.9900	7.772	0.2866
0.9800	5.937	0.3284
0.9700	5.057	0.3563
0.9600	4.508	0.3780
0.9500	4.118	0.3961
0.9400	3.823	0.4118
0.9299	3.586	0.4258
0.9198	3.393	0.4380
0.9099	3.231	0.4500
0.9000	3.092	0.4607
0.8901	2.972	0.4708
0.8799	2.862	0.4805
0.8701	2.767	0.4895
0.8599	2.679	0.4983
0.8499	2.599	0.5067
0.8401	2.529	0.5146
0.8300	2.463	0.5224
0.8200	2.401	0.5299

(Continued)

$\cos \Theta$	m	n
0.8113	2.352	0.5363
0.8011	2.297	0.5436
0.7493	2.070	0.5780
0.6997	1.904	0.6082
0.6503	1.772	0.6365
0.5999	1.660	0.6642
0.5505	1.568	0.6906
0.4999	1.486	0.7171
0.4501	1.415	0.7432
0.4003	1.351	0.7692
0.3502	1.294	0.7955
0.2998	1.241	0.8225
0.2503	1.194	0.8495
0.1998	1.150	0.8778
0.1502	1.109	0.9063
0.1001	1.070	0.9363
0.0500	1.034	0.9674
0.0000	1.000	1.0000

APPENDIX II

ZERO WEAR FACTORS AND COEFFICIENTS OF FRICTION FOR SLIDING

Material pairs		Lubricant							
						μ			
		None	A	B	C	None	A	B	C
<i>Aluminum alloys</i>									
Al 43	Brass 65/35		0.54	0.2	0.2	1.12	0.23	0.25	0.2
	302 SS	0.2	0.54	0.54	0.54	1.67	0.24	0.24	0.18
	52100	0.2	0.54	0.54	0.54	1.42	0.12	0.22	0.25
Al 112	Brass 65/35	0.2	0.2	0.2	0.2	0.92	0.23	0.25	0.28
	302 SS	0.2	0.54	0.54	0.54	1.16	0.20	0.14	0.13
	52100	0.2	0.54	0.2	0.2	1.08	0.25	0.15	0.19
Al 195	Brass 65/35	0.2	0.2	0.2	0.2	0.94	0.17	0.25	0.24
	302 SS	0.2	0.54	0.54	0.54	1.17	0.15	0.14	0.20
	52100	0.2	0.54	0.54	0.54	1.07	0.17	0.13	0.19
Al 220	Brass 65/35	0.2	0.2	0.2	0.2	0.95	0.26	0.27	0.25
	302 SS	0.2	0.2	0.54	0.2	0.92	0.14	0.17	0.25
	52100	0.2	0.54	0.2	0.2	0.79	0.25	0.23	0.24

(Continued)

Appendix II (Continued)

Material pairs		Lubricant							
		$\bar{\gamma}_r$				μ			
		None	A	B	C	None	A	B	C
Al 355	Brass 65/35	0.2	0.2	0.2	0.2	1.11	0.22	0.24	0.25
	302 SS	0.2	0.54	0.54	0.54	1.11	0.17	0.20	0.18
	52100	0.2	0.54	0.54	0.2	1.21	0.13	0.20	0.24
Al 356	Brass 65/35	0.2	0.54	0.54	0.2	1.12	0.24	0.25	0.25
	302 SS	0.2	0.54	0.54	0.54	1.78	0.18	0.21	0.18
	52100	0.2	0.54	0.54	0.54	1.40	0.22	0.17	0.23
<i>Copper alloys</i>									
Be-Cu	Brass 65/35	0.2	0.2	0.2	0.2	0.80	0.25	0.23	0.13
	302 SS	0.2	0.54	0.2	0.54	0.92	0.22	0.12	0.16
	52100	0.2	0.54	0.2	0.54	0.78	0.29	0.15	0.29
Brass 65/35	Al 43	0.2	0.54	0.2	0.2	1.12	0.23	0.25	0.2
	Al 112	0.2	0.2	0.2	0.2	0.92	0.23	0.25	0.28
	Al 195	0.2	0.2	0.2	0.2	0.94	0.17	0.25	0.24
	Al 220	0.2	0.2	0.2	0.2	0.95	0.26	0.27	0.25
	Al 355	0.2	0.2	0.2	0.2	1.11	0.22	0.24	0.25
	Al 356	0.2	0.54	0.54	0.2	1.12	0.24	0.25	0.25
	Be-Cu	0.2	0.2	0.2	0.2	0.80	0.25	0.23	0.13
	Copper nickel (30% Ni)	0.2	0.54	0.54	0.54	0.90	0.25	0.19	0.24
	Phosphor Bronze	0.2	0.2	0.54	0.54	0.79	0.26	0.21	0.26
	Invar 36, free cutting	0.2	0.2	0.54	0.2	0.76	0.26	0.20	0.23
	HyMu 80	0.2	0.2	0.54	0.2	0.81	0.25	0.21	0.23
	Monel C	0.2	0.54	0.54	0.2	0.85	0.22	0.22	0.28
		0.2	0.2	0.54	0.2	0.70	0.22	0.19	0.18
	302 SS	0.2	0.2	0.54	0.2	0.77	0.22	0.19	0.22
	321 SS	0.2	0.2	0.54	0.2	0.78	0.23	0.13	0.23
	347 SS	0.2	0.2	0.2	0.2	0.82	0.19	0.23	0.22
	410 SS	0.2	0.2	0.2	0.2	0.67	0.23	0.17	0.21
	416 EZ SS	0.2	0.2	0.2	0.2	0.66	0.18	0.18	0.18
	440C SS	0.2	0.2	0.54	0.2	0.72	0.18	0.16	0.18
	1018	0.2	0.2	0.54	0.2	0.60	0.24	0.20	0.28
	1045	0.2	0.2	0.2	0.2	0.66	0.20	0.12	0.25
	1055	0.2	0.2	0.2	0.2	0.69	0.20	0.22	0.23
	1060	0.2	0.2	0.2	0.2	0.72	0.22	0.23	0.29
1085	0.2	0.2	0.54	0.2	0.68	0.20	0.20	0.22	
4140 LL	0.2	0.2	0.2	0.2	0.73	0.22	0.24	0.24	
4150	0.2	0.2	0.54	0.2	0.67	0.25	0.19	0.23	
4620	0.2	0.2	0.2	0.2	0.74	0.26	0.27	0.23	
5130 LL	0.2	0.2	0.54	0.2	0.62	0.26	0.20	0.21	
8214	0.2	0.2	0.54	0.2	0.69	0.22	0.20	0.21	
8620	0.2	0.2	0.54	0.2	0.69	0.21	0.17	0.20	
52100	0.2	0.2	0.54	0.2	0.82	0.26	0.20	0.21	
Carpenter 11	0.2	0.2	0.54	0.2	0.74	0.22	0.19	0.19	

(Continued)

Appendix II (Continued)

Material pairs		Lubricant							
		$\dot{\gamma}_r$				μ			
		None	A	B	C	None	A	B	C
	Hampden steel	0.2	0.2	0.2	0.2	0.73	0.17	0.24	0.21
	HYCC steel #1	0.2	0.2	0.2	0.2	0.73	0.21	0.23	0.19
	HYCC steel #2	0.2	0.2	0.54	0.2	0.68	0.18	0.21	0.23
	Nitralloy G	0.2	0.2	0.54	0.2	0.67	0.20	0.17	0.22
	Rexalloy	0.2	0.2	0.2	0.2	0.68	0.15	0.17	0.26
	Star zenith red wear	0.2	0.2	0.2	0.2	0.72	0.22	0.15	0.17
Sintered brass, 7.5 g/cm ² min	52100	0.54	0.54	0.54	0.54	0.37	0.33	0.20	0.31
Sintered bronze, 6.5 g/cm ² min	52100	0.2	0.2	0.2	0.2	0.26	0.23	0.11	0.18
Sintered bronze, 7 g/cm ² min	52100	0.2	0.2	0.2	0.2	0.31	0.17	0.23	0.25
Sintered bronze, 7.3 g/cm ² min	1117		0.2				0.20		
	4140		0.2				0.21		
	8620		0.2				0.26		
Copper nickel (30%)	Brass 65/35	0.2	0.54	0.54	0.54	0.90	0.25	0.19	0.24
	302 SS	0.2	0.54	0.54	0.54	1.17	0.14	0.17	0.19
Phosphor bronze	Brass 65/35	0.2	0.2	0.54	0.54	0.79	0.26	0.21	0.26
	302 SS	0.2	0.2	0.2	0.2	0.74	0.15	0.17	0.15
	52100	0.2	0.2	0.54	0.54	0.67	0.19	0.16	0.18
<i>Iron</i>									
Sintered iron, 7.0 g/cm ² min	52100	0.54	0.54	0.54	0.54	0.45	0.23	0.24	0.24
Sintered iron, 7.3 g/cm ² min	52100	0.54	0.54	0.54	0.54	0.40	0.26	0.23	0.26
Sintered iron, 7.5 g/cm ² min	52100	0.2	0.2	0.54	0.54	0.38	0.21	0.23	0.24
Sintered iron copper (15%), 7.1 g/cm ² min	52100	0.2	0.2	0.54	0.54	0.47	0.20	0.19	0.19
Sintered iron-copper, (20% Cu), 6 g/cm ² min	52100	0.2	0.2	0.54	0.54	0.43	0.21	0.26	0.27
<i>Nickel alloys</i>									
Invar 36, free cutting	Brass 65/35	0.2	0.2	0.54	0.2	0.76	0.26	0.20	0.23
	302 SS	0.2	0.2	0.2	0.2	1.33	0.16	0.19	0.20
	52100	0.2	0.2	0.2	0.2	1.28	0.24	0.18	0.26
HyMu 80	Brass 65/35	0.2	0.2	0.54	0.2	0.81	0.25	0.21	0.23
	302 SS	0.2	0.2	0.2	0.2	1.18	0.16	0.17	0.18

(Continued)

Appendix II (Continued)

Material pairs		Lubricant							
		γ_r				μ			
		None	A	B	C	None	A	B	C
Monel C	52100	0.2	0.2	0.54	0.2	1.00	0.16	0.13	0.16
	Brass 65/35	0.2	0.54	0.54	0.2	0.85	0.22	0.22	0.28
	302 SS	0.2	0.2	0.2	0.2	0.99	0.15	0.15	0.14
	52100	0.2	0.2	0.54	0.2	0.73	0.12	0.14	0.17
<i>Plastics</i>									
Delrin	302 SS	0.54	0.54	0.54	0.54	0.36	0.15	0.18	0.17
Nylatron G	302 SS	0.54	0.54	0.54	0.54	0.57	0.22	0.24	0.22
Nylatron GS	302 SS	0.54	0.54	0.54	0.54	0.60	0.24	0.24	0.24
Polyethylene, 0.93 s.g.	320 SS	0.54	0.54	0.54	0.54	0.31	0.22	0.26	0.20
Polyethylene, 0.94 s.g.	320 SS	0.54	0.54	0.54	0.54	0.40	0.24	0.30	0.26
Polyethylene, 91 s.g.	320 SS	0.54	0.54	0.54	0.54	0.26	0.17	0.17	0.13
Teflon	302 SS	0.54	0.54	0.54	0.54	0.09	0.15	0.11	0.12
Zytel 101	302 SS	0.54	0.54	0.54	0.54	0.60	0.27	0.27	0.23
<i>Stainless steels</i>									
302 SS	AL 43	0.2	0.54	0.54	0.54	1.67	0.24	0.24	0.18
	Al 112	0.2	0.54	0.54	0.54	1.16	0.20	0.14	0.13
	Al 195	0.2	0.54	0.54	0.54	1.17	0.15	0.14	0.20
	Al 220	0.2	0.2	0.54	0.2	0.92	0.14	0.17	0.25
	Al 355	0.2	0.54	0.54	0.54	1.11	0.17	0.20	0.18
	Al 356	0.2	0.54	0.54	0.54	1.78	0.18	0.21	0.18
	Be-Cu	0.2	0.54	0.2	0.54	0.92	0.22	0.12	0.16
	Brass 65/35	0.2	0.2	0.54	0.2	0.70	0.22	0.19	0.18
	Copper Nickel (30% Ni)	0.2	0.54	0.54	0.54	1.17	0.14	0.17	0.19
	Phosphor Bronze	0.2	0.2	0.2	0.2	0.74	0.15	0.17	0.15
	Invar 36, free cutting	0.2	0.2	0.2	0.2	1.33	0.16	0.19	0.20
	HyMu 80	0.2	0.2	0.2	0.2	1.18	0.16	0.17	0.18
	Monel C	0.2	0.2	0.2	0.2	0.99	0.15	0.15	0.14
	Delrin	0.54	0.54	0.54	0.54	0.36	0.15	0.18	0.17
	Nylatron G	0.54	0.54	0.54	0.54	0.57	0.22	0.24	0.22
	Nylatron GS	0.54	0.54	0.54	0.54	0.60	0.24	0.24	0.24
	Polyethylene, 0.93 s.g.	0.54	0.54	0.54	0.54	0.31	0.22	0.26	0.20
	Polyethylene, 0.94 s.g.	0.54	0.54	0.54	0.54	0.40	0.24	0.30	0.26
	Polyethylene, 91 s.g.	0.54	0.54	0.54	0.54	0.26	0.17	0.17	0.13
	Teflon	0.54	0.54	0.54	0.54	0.09	0.15	0.11	0.12
	Zytel 101	0.54	0.54	0.54	0.54	0.60	0.27	0.27	0.23
	302 SS	0.2	0.2	0.2	0.2	1.02	0.16	0.15	0.17
303 EZ SS	0.2	0.54	0.54	0.2	0.86	0.16	0.15	0.14	
321 SS	0.2	0.54	0.54	0.54	1.47	0.15	0.14	0.17	

(Continued)

Appendix II (Continued)

Material pairs		Lubricant							
		γ_r				μ			
		None	A	B	C	None	A	B	C
	347 SS	0.2	0.54	0.54	0.54	1.33	0.15	0.15	0.16
	410 SS	0.2	0.54	0.54	0.2	1.00	0.16	0.14	0.16
	416 EZ SS	0.2	0.54	0.54	0.2	0.87	0.14	0.15	0.21
	440C SS	0.2	0.54	0.2	0.54	0.90	0.13	0.15	0.15
	1018	0.2	0.54	0.54	0.54	0.80	0.14	0.165	0.18
	1045	0.2	0.2	0.54	0.54	0.71	0.16	0.14	0.15
	1055	0.2	0.2	0.54	0.2	0.90	0.17	0.16	0.13
	1060	0.2	0.54	0.2	0.2	0.88	0.16	0.15	0.16
	1085	0.2	0.2	0.54	0.2	1.03	0.18	0.15	0.16
	4140 LL	0.2	0.54	0.54	0.2	0.78	0.14	0.14	0.15
		0.2	0.2	0.2	0.2	0.73	0.22	0.24	0.24
	4150	0.2	0.2	0.2	0.2	0.67	0.15	0.15	0.23
	4150	0.2	0.54	0.2	0.2	0.90	0.17	0.15	0.20
	4620	0.2	0.2	0.54	0.2	0.96	0.18	0.15	0.17
	5130 LL	0.2	0.2	0.2	0.2	0.84	0.16	0.14	0.17
	8214	0.2	0.54	0.54	0.2	0.86	0.16	0.15	0.19
	8620	0.2	0.2	0.2	0.2	0.83	0.21	0.15	0.19
	52100	0.2	0.2	0.2	0.2	1.00	0.19	0.16	0.21
	Carpenter 11	0.2	0.54	0.2	0.2	0.84	0.16	0.14	0.13
	Hampden steel	0.2	0.54	0.54	0.54	0.79	0.16	0.13	0.14
	HYCC steel #1	0.54	0.54	0.54	0.54	0.89	0.14	0.14	0.16
	HYCC steel #2	0.2	0.2	0.54	0.2	1.00	0.17	0.15	0.16
	Ketos	0.2	0.54			0.95	0.16		
	Nitralloy G	0.2	0.54	0.54	0.54	0.83	0.14	0.14	0.16
	Rexalloy	0.2	0.54	0.54	0.54	1.03	0.15	0.15	0.15
	Star zenith	0.2	0.54	0.54	0.54	0.93	0.15	0.14	0.15
	red wear								
303 EZ SS	Brass 65/35	0.2	0.2	0.54	0.2	0.77	0.22	0.19	0.22
	302 SS	0.2	0.54	0.54	0.2	0.86	0.16	0.15	0.14
	52100	0.2	0.2	0.2	0.2	0.79	0.21	0.19	0.32
Sintered 316 SS, 7 g/cm ² min	52100	0.2	0.54	0.54	0.2	0.34	0.15	0.15	0.14
	4140		0.54				0.21		
321 SS	Brass 65/35	0.2	0.2	0.54	0.2	0.78	0.23	0.13	0.23
	302 SS	0.2	0.54	0.54	0.54	1.47	0.15	0.14	0.17
	52100	0.2	0.54	0.54	0.2	1.16	0.17	0.13	0.18
347 SS	Brass 65/35	0.2	0.2	0.2	0.2	0.82	0.19	0.23	0.22
	302 SS	0.2	0.54	0.54	0.54	1.33	0.15	0.15	0.16
	52100	0.2	0.2	0.2	0.2	1.15	0.16	0.15	0.12
410 SS	Brass 65/35	0.2	0.2	0.2	0.2	0.67	0.23	0.17	0.21
	302 SS	0.2	0.54	0.54	0.2	1.00	0.16	0.14	0.16
	52100	0.2	0.54	0.54	0.2	0.85	0.15	0.15	0.20
416 EZ SS	Brass 65/35	0.2	0.2	0.2	0.2	0.66	0.18	0.18	0.18
	302 SS	0.2	0.54	0.54	0.2	0.87	0.14	0.15	0.21
	52100	0.2	0.2	0.54	0.2	0.97	0.13	0.15	0.23

(Continued)

Appendix II (Continued)

Material pairs		Lubricant							
		γ_r				μ			
		None	A	B	C	None	A	B	C
440C SS	Brass 65/35	0.2	0.2	0.54	0.2	0.72	0.18	0.16	0.18
	302 SS	0.2	0.54	0.2	0.54	0.90	0.13	0.15	0.15
	52100	0.2	0.2	0.2	0.2	0.66	0.18	0.13	0.17
<i>Steel</i>									
1018	Brass 65/35	0.2	0.2	0.54	0.2	0.60	0.24	0.20	0.28
	302 SS	0.2	0.54	0.54	0.54	0.80	0.14	0.165	0.18
	52100	0.2	0.54	0.54	0.2	0.80	0.18	0.21	0.26
1045	Brass 65/35	0.2	0.2	0.2	0.2	0.66	0.20	0.12	0.25
	302 SS	0.2	0.2	0.54	0.54	0.71	0.16	0.14	0.15
	52100	0.2	0.54	0.2	0.2	0.67	0.15	0.17	0.28
1055	Brass 65/35	0.2	0.2	0.2	0.2	0.69	0.20	0.22	0.23
	302 SS	0.2	0.2	0.54	0.2	0.90	0.17	0.16	0.13
	52100	0.2	0.2	0.2	0.2	0.74	0.18	0.14	0.23
1060	Brass 65/35	0.2	0.2	0.2	0.2	0.72	0.22	0.23	0.29
	302 SS	0.2	0.54	0.2	0.2	0.88	0.16	0.15	0.16
	52100	0.2	0.2	0.2	0.2	0.73	0.14	0.21	0.31
1085	Brass 65/35	0.2	0.2	0.54	0.2	0.68	0.20	0.20	0.22
	302 SS	0.2	0.2	0.54	0.2	1.03	0.18	0.15	0.16
	52100	0.2	0.2	0.54	0.2	0.81	0.2	0.14	0.22
1117	Sintered 316 SS, 7 g/cm ² min		0.2				0.20		
4140	Sintered bronze, 7.3 g/cm ² min		0.2				0.21		
	Sintered 316 SS, 7 g/cm ² min		0.54				0.21		
4140 LL	Brass 65/35	0.2	0.2	0.2	0.2	0.73	0.22	0.24	0.24
	302 SS	0.2	0.54	0.54	0.2	0.78	0.14	0.14	0.15
	52100	0.2	0.2	0.2	0.2	0.57	0.21	0.17	0.26
4150	Brass 65/35	0.2	0.2	0.54	0.2	0.67	0.25	0.19	0.23
	302 SS	0.2	0.54	0.2	0.2	0.90	0.17	0.15	0.20
	52100	0.2	0.2	0.2	0.2	0.67	0.15	0.15	0.23
4620	Brass 65/35	0.2	0.2	0.2	0.2	0.74	0.26	0.27	0.23
	302 SS	0.2	0.2	0.54	0.2	0.96	0.18	0.15	0.17
	52100	0.2	0.54	0.54	0.2	0.79	0.19	0.15	0.27
5130 LL	Brass 65/35	0.2	0.2	0.54	0.2	0.62	0.26	0.20	0.21
	302 SS	0.2	0.2	0.2	0.2	0.84	0.16	0.14	0.17
	52100	0.2	0.2	0.2	0.2	0.62	0.16	0.16	0.21
8214	Brass 65/35	0.2	0.2	0.54	0.2	0.69	0.22	0.20	0.21
	302 SS	0.2	0.54	0.54	0.2	0.86	0.16	0.15	0.19
	52100	0.2	0.2	0.54	0.54	0.71	0.17	0.19	0.20
8620	Brass 65/35	0.2	0.2	0.54	0.2	0.69	0.21	0.17	0.20
	Sintered bronze, 7.3 g/cm ² min		0.2			0.26			
	302 SS	0.2	0.2	0.2	0.2	0.83	0.21	0.15	0.19
	52100	0.2	0.2	0.2	0.54	0.70	0.22	0.17	0.25

(Continued)

Appendix II (Continued)

Material pairs		Lubricant							
		γ_r				μ			
		None	A	B	C	None	A	B	C
52100	Al 43	0.2	0.54	0.54	0.54	1.42	0.12	0.22	0.25
	Al 112	0.2	0.54	0.2	0.2	1.08	0.25	0.15	0.19
	Al 195	0.2	0.54	0.54	0.54	1.07	0.17	0.13	0.19
	Al 220	0.2	0.54	0.2	0.2	0.79	0.25	0.23	0.24
	Al 355	0.2	0.54	0.54	0.2	1.21	0.13	0.20	0.24
	Al 356	0.2	0.54	0.54	0.54	1.40	0.22	0.17	0.23
	Be-Cu	0.2	0.54	0.2	0.54	0.78	0.29	0.15	0.29
	Brass 65/35	0.2	0.2	0.54	0.2	0.82	0.26	0.20	0.21
	Sintered brass, 7.5 g/cm ² min	0.54	0.54	0.54	0.54	0.37	0.33	0.20	0.31
	Sintered bronze, 6.5 g/cm ² min	0.2	0.2	0.2	0.2	0.26	0.23	0.11	0.18
	Sintered bronze, 7 g/cm ² min	0.2	0.2	0.2	0.2	0.31	0.17	0.23	0.25
	Phosphor bronze	0.2	0.2	0.54	0.54	0.67	0.19	0.16	0.18
	Sintered iron, 7.0 g/cm ² min	0.54	0.54	0.54	0.54	0.45	0.23	0.24	0.24
	Sintered iron, 7.3 g/cm ² min	0.54	0.54	0.54	0.54	0.40	0.26	0.23	0.26
	Sintered iron, 7.5 g/cm ² min	0.2	0.2	0.54	0.54	0.38	0.21	0.23	0.24
	Sintered iron, Copper (15% Cu), 7.1 g/cm ² min	0.2	0.2	0.54	0.54	0.47	0.20	0.19	0.19
	Sintered iron, Copper (20% Cu), 6 g/cm ² min	0.2	0.2	0.54	0.54	0.43	0.21	0.26	0.27
	Invar 36, free cutting	0.2	0.2	0.2	0.2	1.28	0.24	0.18	0.26
	HyMu 80	0.2	0.2	0.54	0.2	1.00	0.16	0.13	0.16
	Monel C	0.2	0.2	0.54	0.2	0.73	0.12	0.14	0.17
	302 SS	0.2	0.2	0.2	0.2	1.00	0.19	0.16	0.21
		0.2	0.2	0.2	0.2	1.02	0.16	0.15	0.17
		0.2	0.2	0.54	0.2	0.70	0.22	0.19	0.18
	303 EZ SS	0.2	0.2	0.2	0.2	0.79	0.21	0.19	0.32
		0.2	0.54	0.54	0.2	0.86	0.16	0.15	0.14
		0.2	0.2	0.54	0.2	0.77	0.22	0.19	0.22
	Sintered 316 SS, 7 g/cm ² min	0.2	0.54	0.54	0.2	0.34	0.15	0.15	0.14
	321 SS	0.2	0.54	0.54	0.2	1.16	0.17	0.13	0.18
	347 SS	0.2	0.2	0.2	0.2	1.15	0.16	0.15	0.12
	410 SS	0.2	0.54	0.54	0.2	0.85	0.15	0.15	0.20

(Continued)

Appendix II (Continued)

Material pairs		Lubricant							
		γ_r				μ			
		None	A	B	C	None	A	B	C
	416 EZ SS	0.2	0.2	0.54	0.2	0.97	0.13	0.15	0.23
	440C SS	0.2	0.2	0.2	0.2	0.66	0.18	0.13	0.17
	1018	0.2	0.54	0.54	0.2	0.80	0.18	0.21	0.26
	1045	0.2	0.54	0.2	0.2	0.67	0.15	0.17	0.28
	1055	0.2	0.2	0.2	0.2	0.74	0.18	0.14	0.23
	1060	0.2	0.2	0.2	0.2	0.73	0.14	0.21	0.31
	1085	0.2	0.2	0.54	0.2	0.81	0.2	0.14	0.22
	4140 LL	0.2	0.2	0.2	0.2	0.57	0.21	0.17	0.26
	4150	0.2	0.2	0.2	0.2	0.67	0.15	0.15	0.23
	4620	0.2	0.54	0.54	0.2	0.79	0.19	0.15	0.27
	5130 LL	0.2	0.2	0.2	0.2	0.62	0.16	0.16	0.21
	8214	0.2	0.2	0.54	0.54	0.71	0.17	0.19	0.20
	8620	0.2	0.2	0.2	0.54	0.70	0.22	0.17	0.25
	52100	0.2	0.2	0.54	0.2	0.60	0.21	0.16	0.21
	Carpenter 11	0.2	0.54	0.54	0.54	0.78	0.18	0.16	0.21
	Hampden steel	0.54	0.54	0.54	0.54	0.15	0.13	0.12	0.11
	HYCC steel #1	0.2	0.54	0.54	0.2	0.62	0.13	0.11	0.15
	HYCC steel #2	0.2	0.2	0.2	0.2	0.64	0.16	0.17	0.32
	Ketos	0.2	0.54	0.54	0.2	0.67	0.18	0.15	0.31
	Nitralloy G	0.2	0.2	0.2	0.2	0.63	0.13	0.13	0.11
	Rexalloy	0.2	0.54	0.2	0.2	0.73	0.13	0.13	0.14
	Star zenith	0.2	0.54	0.2	0.54	0.63	0.12	0.12	0.16
	red wear								
	Sintered steel, 6.2 g/cm ² min	0.2	0.54	0.54	0.54	0.50	0.25	0.16	0.23
	Sintered steel, 7 g/cm ² min	0.2	0.54	0.54	0.54	0.33	0.21	0.20	0.25
Carpenter 11	Brass 65/35	0.2	0.2	0.54	0.2	0.74	0.22	0.19	0.19
	302 SS	0.2	0.54	0.2	0.2	0.84	0.16	0.14	0.13
	52100	0.2	0.54	0.54	0.54	0.78	0.18	0.16	0.21
Hampden steel	Brass 65/35	0.2	0.2	0.2	0.2	0.73	0.17	0.24	0.21
	302 SS	0.2	0.54	0.54	0.54	0.79	0.16	0.13	0.14
	52100	0.54	0.54	0.54	0.54	0.15	0.13	0.12	0.11
HYCC steel #1	Brass 65/35	0.2	0.2	0.2	0.2	0.73	0.21	0.23	0.19
	302 SS	0.54	0.54	0.54	0.54	0.89	0.14	0.14	0.16
	52100	0.2	0.54	0.54	0.2	0.62	0.13	0.11	0.15
HYCC steel #2	Brass 65/35	0.2	0.2	0.54	0.2	0.68	0.18	0.21	0.23
	302 SS	0.2	0.2	0.54	0.2	1.00	0.17	0.15	0.16
	52100	0.2	0.2	0.2	0.2	0.64	0.16	0.17	0.32
Ketos	302 SS	0.2	0.54			0.95	0.16		
	52100	0.2	0.54	0.54	0.2	0.67	0.18	0.15	0.31
Nitralloy G	Brass 65/35	0.2	0.2	0.54	0.2	0.67	0.20	0.17	0.22
	302 SS	0.2	0.54	0.54	0.54	0.83	0.14	0.14	0.16
	52100	0.2	0.2	0.2	0.2	0.63	0.13	0.13	0.11

(Continued)

Appendix II (Continued)

Material pairs		Lubricant							
		γ_i				μ			
		None	A	B	C	None	A	B	C
Rexalloy	Brass 65/35	0.2	0.2	0.2	0.2	0.68	0.15	0.17	0.26
	302 SS	0.2	0.54	0.54	0.54	1.03	0.15	0.15	0.15
	52100	0.2	0.54	0.2	0.2	0.73	0.13	0.13	0.14
Star zenith red wear	Brass 65/35	0.2	0.2	0.2	0.2	0.72	0.22	0.15	0.17
	302 SS	0.2	0.54	0.54	0.54	0.93	0.15	0.14	0.15
	52100	0.2	0.54	0.2	0.54	0.63	0.12	0.12	0.16
Sintered steel, 6.2 g/cm ² min	52100	0.2	0.54	0.54	0.54	0.50	0.25	0.16	0.23
Sintered steel, 7 g/cm ² min ^a	52100	0.2	0.54	0.54	0.54	0.33	0.21	0.20	0.25

Lubricant properties

Oil A: Paraffin oil with anti-oxidation and anti-corrosion additives; neutralization number, 0.5; viscosity, 35 centistokes at 100°F; viscosity index, 102.

Oil B: Napthenic oil with anti-oxidation and tackiness additives; neutralization number, 0.08; viscosity, 80 centistokes at 100°F; viscosity index, 67.

Oil C: Paraffin oil with viscosity index improver and anti-wear additives; neutralization number, 0.20; viscosity, 15 centistokes at 100°F; viscosity index, 188.

Sources

1. R Bayer, T Ku. Handbook of Analytical Design for Wear. New York: Plenum Press, 1964.
2. RG Bayer, WC Clinton, CW Nelson, RA Schumecher. Handbook of Metal Wear Properties. IBM TR01.17.142.678, Endicott NY: IBM Corp. 1962.

APPENDIX III

WEAR AND FRICTION DATA

Wear Factors and Friction Coefficients

Materials			K'		
Wearing	Counterface	Lubricant	10^{-10} in. ³	10^{-10}	μ
			min/ft lb h	mm ³ /mm N	
ABS	Steel	None	3500	690	0.35
ABS with PTFE	Steel	None	300	59	0.16
ABS with PTFE, glass	Steel	None	75	15	0.20
Acetal	Steel	None	65	13	0.21
Acetal with PTFE	Steel	None	13-40	2.6-7.9	0.018-0.12

(Continued)

Appendix III (Continued)

Wearing	Materials		K'		
	Counterface	Lubricant	10^{-10} in. ³ min/ft lb h	10^{-10} mm ³ /mm N	μ
Acetal, with PTFE, glass	Steel	None	40–200	7.9–39.5	0.028–0.14
Alpha Molykote M1	4037	None	4400	867	
Alpha Molykote T1	1137	None	1100	217	
Al 24	416 SS, RB 100	None	2200	434	
	RC 55	None	8200	1620	
	RB 100	Petroleum oil A	33	6.5	
		Petroleum oil, B	13	2.6	
		Petroleum oil, C	16	3.2	
	440 SS, RC 53	Petroleum oil A	1700	335	
		Silicone oil	2500	493	
Al2014, with 5% SiC	Steel	None	10,000	2000	
Al2014, with 20% SiC	Steel	None	2500	500	
Al 24 anodized	416 SS, RB 100	Petroleum oil C	15	3	
Anodized Aluminum	Anodized Aluminum	None	14,000	2758	0.72
Aluminum	Steel	Petroleum oil	340	67	0.47
Bronze, RB 65		None	5080	1000	
Aluminum Bronze, RB 90	Steel	None	15,200	3000	0.46
Aluminum Oxide	Aluminum Oxide	None	0.04–30,500	0.8–6000	0.3–1.0
Al–Si,	Steel	None	2500	500	
Al–Si, with graphite	Steel	None	250	50	
Al–Sn	4140, RC 25	None	4100	808	0.33
		Petroleum oil	28,000	5516	0.41
Arguto K	1137	None	0.9	0.18	
Arguto MP	1137	None	1.4	0.28	
Babbitt	Steel	None	1400–12,000	280–2400	
		Petroleum oil	1–10,000	0.2–2000	
3abbitt Pb base	4140	None	5700	11,230	0.34
		Petroleum oil	33	6.5	0.17
Babbitt Sn base	4140	None	1400	276	0.34
		Petroleum oil	980	1193	0.36
Be–Cu	Stainless Steel	None	4–400	0.79–79	
		Petroleum oil	1–500	0.2–99	
Be–Cu, RC 40	Hard steel	None		100	

(Continued)

Appendix III (Continued)

Wearing	Materials		K'		
	Counterface	Lubricant	10^{-10} ; in. ³ min/ft lb h	10^{-10} mm ³ /mm N	μ
Boron Carbide	Boron Carbide, RC 84, with PTFE, graphite	None	7.2	1.4	0.21
	300SS	None	100	20	0.30
	Stellite	None	40	8	0.70
Brass, clock	416 SS, RB 100	Petroleum oil, A	800	15.8	
Brass, 1/2 HD clock	416 SS, RB 100	None	150	30	
		Petroleum oil, C	140	28	
Brass, Pb	52100, RC 60	None	1800	354	
Brass, yellow	52100, RC 60	Petroleum oil	580	114	0.37
Bronze	Steel	None	50-3300	9.9-650	
		Petroleum oil	0.1-3500	0.02-690	
Bronze, HV 80	440C SS	None	15,200	3000	
Bronze, HV 48	Steel	None	10,200	2000	
Bronze, Al	416 SS, RB 100	Petroleum oil, A	320	63	
	4140, RC 50	None	3100	611	0.53
Bronze, Pb	4140, RC 25	None	2200	434	0.37
		Petroleum oil	1400	276	0.36
Bronze, Pb-Sn, HB 48	Steel	None	10,200	2000	0.18
Bronze, graphited	4140	None	600	118	0.35
Bronze, P	Stainless steel	Petroleum oil	15-500	3-99	
	4140, RC 50	None	3100	611	0.53
Bronze, porous (sintered bronze)	416 SS, RB 100	Petroleum oil, C	2.3	0.45	
Cadmium, HV 21	Steel	None	5080	1000	
Cd-Ni, HB 35	Steel	None	1000	200	
Carboly	Carboly	None	< 5	< 1	0.2
	Cobalt	None	< 7	< 1.4	0.45
Carbon, RC 59	Cast iron	None		60	0.15
Carbon, shore 95, with Cu	Steel	None	51	10	0.16
Carbon Graphite	Steel	None	75	15	
Carbon Graphite, shore 85	Steel	None	150	30	

(Continued)

Appendix III (Continued)

Materials			K''		μ
Wearing	Counterface	Lubricant	10^{-10} in. ³ min/ft lb h	10^{-10} mm ³ /mm N	
Carbon Graphite, shore 70, with babbitt	Steel	None	100	20	
Carbon Graphite, shore 90, with resin	Steel	None	31	6	0.16
Carbon Graphite, Shore 90, with Ag	Steel	None	20	4	
Cast iron	Steel	None	30-40,000	6-7900	0.45
		Petroleum oil	30-15,000	6-3000	0.40
	Cast iron	None	1000-67,000	197-13,200	0.45
		Petroleum oil	24,000-79,000	4730-15,600	0.40
Cu, HV 42 Copper alloy DU	Steel	None	15,200	3000	
	Stainless steel 1137	Petroleum oil	7	1.4	
Iron, sintered	Steel	None	7.1	1.4	
		Petroleum oil	300-10,000	59-1970	0.4
	Cast iron	None	25-250	4.9-50	0.20
		Petroleum oil	1000-67,000	197-13,200	0.45
Maple, oil impregnated	4140, RC 25	None	20	3.9	0.12
		Petroleum oil	11	2.2	0.12
	Meehanite	None	350-550	67-108	0.40
		Petroleum oil	350-550	67-108	0.40
Melamine	416 SS, RB 100	None	300-1000	59-197	0.4
		Petroleum oil	300-1000	59-197	0.4
	52100, RC 60	Petroleum oil, C	4	0.79	
		None	3800	749	0.55
Monel	416 SS, RB 100	Petroleum oil	3300	650	0.55
		Petroleum oil, A	2	0.39	
	Stainless Steel	None	96	19	
Nylon Nylon, with graphite	Stainless Steel	Petroleum oil, B	63	12.5	
Nylon 6/12	Steel	None	190	37.5	0.31
Nylon 6/12, with PTFE	Steel	None	16	3.2	0.19
Nylon 6/12, with PTFE, glass	Steel	None	9-16	1.8-3.2	0.19-0.24
Nylon 6	Steel	None	200	40	0.26
Nylon 6, with PTFE	Steel	None	15-50	3-10	0.08-0.10
Nylon 6, with PTFE, glass	Steel	None	10-17	2-3.3	0.20-0.25

(Continued)

Appendix III (Continued)

Wearing	Materials		K'		
	Counterface	Lubricant	10^{-10} in. ³ min/ft lb h	10^{-10} mm ³ /mm N	μ
Nylon 6/10	Steel	None	180	36	0.31
Nylon 6/10, with PTFE	Steel	None	15	3	0.20
Nylon 6/10, with PTFE, glass	Steel	None	9-15	1.8-3	0.24-0.31
Nylon 6/6	Steel	None	200	40	0.28
Nylon 6/6, with PTFE	Steel	None	12-60	2.4-12	0.18-0.20
Nylon 6/6, with PTFE, glass	Steel	None	6-16	1.2-3.2	0.14-0.26
Nylon, amorphous	Steel	None	600	118	0.32
Nylon, amorphous, with PTFE, glass	Steel	None	22	4.3	0.26
Oilite, bronze	Soft steel	None	14,000	2760	0.45
		Petroleum oil	13,000	2560	0.40
	Cr-plated steel	None	230	46	0.35
Oilite, iron	416 SS, RB 100	Petroleum oil	180	36	0.30
		Petroleum oil, C	0.41	0.08	
Oilite, super	416 SS, RB 100	Petroleum oil, C	1.6	0.32	
PEEK, with carbon, PTFE	Steel	None	10-20	2-3.9	0.15
PEK, with glass	Steel	None	100	20	0.36
PEK, with carbon	Steel	None	58	11	0.14
Phenolic, fabric	Steel	None	2000	394	0.21
Phenolic, nylon	Steel	None	300	59	0.48
Phenolic, asbestos	Steel	None	1500	296	0.41
Phenolic bearing, fabric	Steel	None	35-300	6.9-59	0.10-0.18
Phenolic bearing, metallic	Steel	None	25	4.9	0.10
Phenolic, with graphite	416 SS, RB 100	None	8	1.6	
Polycarbonate	Steel	None	2500	493	0.38
Polycarbonate with PTFE	Steel	None	70-125	14-25	0.08-0.14
Polycarbonate with PTFE, glass	Steel	None	30-40	6-8	0.22
Polyester	Steel	None	210	42	0.25
Polyester, with PTFE	Steel	None	9-15	1.8-3	0.13-0.17
Polyester, with PTFE, glass	Steel	None	12-20	2.4-3.9	0.12-0.21
Polyester elastomer	Steel	None	1000	197	0.59

(Continued)

Appendix III (Continued)

Wearing	Materials		K'		
	Counterface	Lubricant	10^{-10} in. ³ min/ft lb h	10^{-10} mm ³ /mm N	μ
Polyester elastomer, with PTFE	Steel	None	40	7.9	0.25
Polyester elastomer, with PTFE, glass	Steel	None	25	4.9	0.20
Polyester elastomer, with PTFE, silicone	Steel	None	5	0.99	0.21
Polyether-sulfone	Steel	None	60	12	0.20
Polyether-sulfone, with carbon, PTFE	Steel	None	2-60	0.39-12	0.17-.20
Polyimide, with graphite	Steel	None	30	6	
Polyimide, filled (Vespel SP21)	Steel	None	33	6.5	
Polyphenylene oxide	Steel	None	3050	600	0.39
Polyphenylene oxide, with glass	Steel	None	255	50	0.27
Polyphenylene Oxide, with PTFE	Steel	None	100	20	0.16
Polyphenylene Sulfide, with carbon	Steel	None	150	30	0.20
Polyphenylene Sulfide, with glass	Steel	None	255	50	0.29
Polyphenylene Sulfide, with PTFE	Steel	None	51	10	0.10
Polyphenylene Sulfide	Steel	None	510	100	0.24
Polypropylene, with PTFE	Steel	None	35.5	7	0.11
Polysulfone	Steel	None	1500	296	0.37
Polysulfone, with PTFE	Steel	None	46	9.1	0.14
Polysulfone, with PTFE, glass	Steel	None	60	12	0.20
PPS	Steel	None	540	107	0.24
PPS, with PTFE	Steel	None	40-55	7.9-11	0.10
PPS, with PTFE, glass	Steel	None	100	20	0.17
PPS, with carbon, PTFE	Steel	None	25-35	4.9-6.9	0.10-0.18

(Continued)

Appendix III (Continued)					
Materials			K'		
Wearing	Counterface	Lubricant	10^{-10} in. ³ min/ft lb h	10^{-10} mm ³ /mm N	μ
PTFE and graphite coating	Boron carbide	None	9.6	1.9	0.17
	Stellite J, RC56	None	19	3.7	0.16
	347 SS, RB85	None	380	74.9	0.14
	PTFE and graphite coating	None	1200	237	0.21
Rulon A	1137	None	27	5.3	
Silver, HV 34	Silver	None	508,000	100,000	
304 SS, RB 82	Tool steel	None	100	20	
304 SS	304 SS, RB 85	None	1300	256	0.56
	PTFE and graphite coating	None	0.46	0.091	0.22
	Boron carbide	None	1800	355	0.51
	Stellite J, RC56	None	5600	1103	0.50
310 SS, RB 79	Tool steel	None	255	50	
416 SS	PTFE and graphite coating	None	2.4	4.7	0.18
	Boron carbide	None	680	134	0.34
	Stellite J, RC 56	None	27,000	5319	0.51
440C SS, RC 58	Steel	None	200	40	
Mild steel, RB 79	Steel	None	355,000	70,000	
Steel, soft	Steel	Petroleum oil	0.5–28,000	0.099–5520	
	Stainless steel	Petroleum oil	0.5–28,000	0.099–5520	
1040, RB 79	Steel	None	254,000	50,000	
52100, RC 62	52100, RC 62	None	5080	1000	
		Petroleum oil	1.0–150	0.2–30	
Sialon	Hard steel	None	150–203,000	30–40,000	0.4–0.6
Silicon–Carbide	Hard steel	Petroleum oil	0.025–0.25	0.005–0.0.5	0.02–0.1
	Ceramic	None	5.6–101,500	1.1–20,000	0.25–1.0
Silicon–Nitride	Ceramic	Petroleum oil	0.10–510	0.02–100	0.02–0.1
	Ceramic	None	0.02–5585	0.004–1100	0.45–0.9
Stellite, RC 54	Carburized 4620	None	355	70	
Stellite, RC 40	Carburized 4620	None	410	80	
Stellite, RC 39	Carburized 4620	None	100	20	

(Continued)

Appendix III (Continued)

Wearing	Materials		K'		
	Counterface	Lubricant	10^{-10} in. ³ min/ft lb h	10^{-10} mm ³ /mm N	μ
Stellite J	PTFE and graphite coating	None	26	5.1	0.20
	Boron-carbide	None	31	6.1	0.39
	347 SS, RB 85	None	50	10	0.33
	304 SS, RB 85	None	79	15.6	0.30
	Stellite J, RC 56	None	490	96.5	0.32
Styrene	Steel	None	3000	591	0.32
Styrene, with PTFE	Steel	None	175	34.5	0.14
Styrene, with silicone	Steel	None	37	7.3	0.08
Teflon	4140	None	13,000	2561	0.17
		Petroleum oil	13,000	2561	0.17
Teflon, with 50% glass	4140	None	38	7.5	0.28
		Petroleum oil	116	22.9	0.31
Titanium	Titanium, RC 56	None	8100	1596	0.45
	Titanium, RC 49	None	255,000	50,250	0.77
	Gear steel, RC 56	Petroleum oil	95,000	18,720	0.78
		Petroleum oil	8900	1753	0.48
D2 Tool steel, RC 55	Steel	None	205	40	
H11 Tool steel, RC 55	Steel	None	10,150	2000	
M2 Tool steel, RC 66	Steel	None	150	30	
Tribaloy T-400, RC 60	Carburized 4620	None	510	100	
Tribaloy T-700, RC 50	Carburized 4620	None	100	200	
Tribaloy T-800, RC 62	Carburized 4620	None	510	100	
Tungsten carbide, HV 1500	Tungsten carbide	None	10	2	
Urethane, thermoplastic	Steel	None	340	67	0.37
Urethane, thermoplastic, with PTFE	Steel	None	60	12	0.32

(Continued)

Appendix III (Continued)

Materials			K'		
Wearing	Counterface	Lubricant	10^{-10} in. ³	10^{-10}	μ
			min/ft lb h	mm ³ /mm N	
Urethane, thermoplastic, with PTFE, glass	Steel	None	30-35	6-7	0.25
	Steel	None	33	6.5	
Vespel SP21	Ceramic	None	4.4-13,200	0.86-2600	0.5
Zirconium oxide	4140	None	20,000	3940	0.5
Zinc		Petroleum oil	15,000	2955	0.30

Designation	Description
	Petroleum lubricants
A	Highly refined white petroleum oil, 100 SUS at 100°F
B	Paraffinic petroleum oil, 110 SUS at 100°F
C	Naphthenic petroleum oil, 85 SUS at 100°F

WEAR FACTOR AND P-V LIMITS FOR PLASTICS AND OTHER MATERIALS

Material	P - V Limit (lb ft/in. ² min)			K'^a (10^{-10} in. ³ min/ft lb h)
	Velocity			
	10 (ft/min)	100 (ft/min)	1000 (ft/min)	
ABS	18000	4000	2000	300
ABS, 15% PTFE filled		4000		300
Acetal	4000	3500	2500	50-65
Acetal, carbon filled		20,000		40
Acetal, PTFE filled		12,600		20
Acetal, 20% PTFE filled	> 40,000	12,500	5500	17-19
Acetal, silicone filled		9100		25
Acetal, 30% glass, 15% PTFE filled	12,500	12,000	8000	200
Epoxy, glass filled		50,000		
Fluorocarbon		1800		2500
Fluorocarbon, filled		30,000		1-20
Nylon, graphite filled		4000		50
Nylon 6, 30% glass, 15% PTFE filled	17,500	20,000	13,000	17
Nylon 6/10, 30% glass, 15% PTFE filled	20,000	15,000	12,000	15
Nylon 6/6	3000	2500	2500	200

(Continued)

Appendix III (Continued)

Material	<i>P-V</i> Limit (lb ft/in. ² min)			<i>K</i> ⁷⁰ (10 ⁻¹⁰ in. ³ min/ft lb h)
	Velocity			
	10 (ft/min)	100 (ft/min)	1000 (ft/min)	
Nylon 6/6, carbon filled		25,000		40
Nylon 6/6, glass filled		10,000		40
Nylon 6/6, 20% PTFE filled	> 40,000	27,500	8000	12
Nylon 6/6, PTFE filled		17,500		10
Nylon 6/6, 30% glass, 15% PTFE filled	17,500	20,000	13,000	16
Nylon 6/6, silicone filled		6000		40
PEEK, 30% carbon filled				60
PEEK, 5% carbon, 15% PTFE filled		40,000		60
Phenolic	5000	5000		250–2000
Phenolic, cotton filled		15,000		
Phenolic, wood filled		45,000		
Phenolic, PTFE filled		40,000		10
Polyamide		4000		190
Polyamide, graphite filled		4000		15
Polyamide-imide		100,000		
Polyamide-imide, PTFE, graphite filled		50,000		
Polycarbonate	750–850	300–500		2400–2500
Polycarbonate, carbon filled		8600		100
Polycarbonate, PTFE filled		20,000		100
Polycarbonate, PTFE, glass fiber filled		30,000		29
Polycarbonate, 30% glass, 15% PTFE filled	27,500	30,000	13,000	30
Polyester				210
Polyester, PTFE filled		15,400		15
Polyester, 30% glass, 15% PTFE filled	> 40,000	30,000	5500	20
Polyester, carbon filled		22,000		25
Polyester (linear aromatic), graphite filled		50,000		
Polyethylene (UHMW)		3000		
Polyethylene (UHMW), glass filled		5500		
Polyimide		100,000		150
Polyimide, graphite filled		100,000		25
Polyimide, filled (Vespel SP21)		500,000		33
Polyphenylene oxide		490		3000
Polyphenylene sulfide		3000–100,000		500
Polyphenylene sulfide, carbon filled		20,000		150
Polyphenylene sulfide, PTFE, carbon fibers filled		100,000		
Polyphenylene sulfide, glass filled		16,000		250
Polypropylene, PTFE filled		5100		36
Polypropylene, 30% glass, 15% PTFE filled	14,000	12,000	7500	36
Polysulfone	5000	5000	3000	1500
Polysulfone, carbon filled		8600		100
Polysulfone, 30% glass, 15% PTFE filled	20,000	35,000	15,000	70

(Continued)

Appendix III (Continued)

Material	<i>P-V</i> Limit (lb ft/in. ² min)			<i>K</i> ^{1/3} (10 ⁻¹⁰ in. ³ min/ft lb h)
	Velocity			
	10 (ft/min)	100 (ft/min)	1000 (ft/min)	
Polyurethane	2000	1500	< 1500	350
Polyurethane, 30% glass, 15% PTFE filled	7500	10,000	5000	35
PPS, 30% glass, 15% PTFE filled	27,000	30,000	> 30,000	110
PTFE		1500		20,000
PTFE, fabric reinforced		35,000		2
PTFE, glass filled		15,000		5
PTFE, glass fiber filled	10,000	10,000	10,000	6
PTFE, graphite filled		16,000		3
PTFE, graphite fiber filled			30,000	
Styrene acrylonitrile, 30% glass, 15% PTFE filled	17,500	10,000	10,000	65
Non-plastic bearing materials				
Sintered iron, oiled filled		30,000		25–250
Sintered bronze, oiled filled		35,000–50,000		2
DU		50,000		7
Wood, oil impregnated		12,000		20

^a10⁻¹⁰ in.³ min/ft lb h = 0.2 × 10⁻⁷ mm³/mN.

Sources:

1. (A Computerized Tribology Information System); 1992: U.S. Secretary of Commerce.
2. B Bhushan, B Gupta. Handbook of tribology, New York, NY: McGraw-Hill, Inc., 1991.
3. M Wolverton, J Theberge. Wear behavior of plastics on plastics: machine design, Cleveland, OH: Penton Publishing Co., February 12, 1981, 79–83.
4. M Wolverton, J Theberge. How plastics composites wear against metals: machine design, Cleveland, OH: Penton Publishing Co., February 6, 1986, 67–71.
5. LNP Bulletin LNP Corporation, Malvern, PA, 254–278.
6. FP Curry. Wear rates of polymers, IBM TR82.0032. IBM General Products Division, Tucson, AZ, 1982.
7. KJ Mack. Evaluation of self-lubricating plastics for bearings, IBM TR07.199. IBM Systems Development Division, Rochester, MN, 1967.
8. J Martin, CW Anderson. Filled and unfilled nylon 66—wear life comparison, IBM TR07.590. IBM General Systems Division, Rochester, MN, 1976.
9. J McGrew, G Hahn, R Lee, W MacFarland, R Thompson. Synthesis of strength distributions as a function of wear. GE Report RADC-TR-67-557, 1967.

APPENDIX IV

APPROXIMATE RELATIONSHIP BETWEEN VICKERS HARNDNESS AND YIELD POINT IN SHEAR

Vickers hardness (kg/mm ²)	Shear yield stress ^{a,b} (kpsi)
1	0.100
1.5	0.140
2	0.175
3	0.250
4	0.325
5	0.390
6	0.470
7	0.550
8	0.625
9	0.700
10	0.790
12.5	1.000
15	1.200
20	1.800
30	3.000
40	4.400
50	6.000
60	7.700
70	9.400
80	11.000
90	13.000
100	15.000
125	20.000
150	25.000
200	36.000
250	49.000
300	60.000
350	72.000
400	85.000
450	95.000
500	110.000
600	130.000
700	150.000
800	180.000
900	200.000
1000	220.000

^aapproximately 0.5 × tensile yield stress.
^b1 kpsi ≈ 6.9 Mpa.
Source: R Bayer, T Ku. Handbook of Analytical Design for Wear. New York: Plenum Press, 1964.

APPENDIX V

GALLING THRESHOLD STRESS

Material Pair		Threshold Stress		
		MPa	Kpsi	
Silicon bronze (Rb 94)	Silicon bronze (Rb 94)	28	4	
	304 SS (Rb 77)	300	44	
1020 (Rb 90)	440C SS (Rc 58)	14	2	
1034 (Rc 45)	1034 (Rc 45)	14	2	
	Nitronic 32 (Rb 94)	14	2	
4337 (Rc 48)	Nitronic 60 (Rb 94)	>350	>51	
4337 (Rc 51)	4337 (Rc 45)	14	2	
	Nitronic 60 (Rb 94)	>350	>51	
201 SS (Rb 94)	201 SS (Rb 94)	105	15	
	304 SS (Rb 77)	14	2	
	630 SS [17-4Ph] (Rc 41)	14	2	
	S24100 (Rc 21)	284	41	
	Nitronic 32 (Rb 98)	250	36	
	Waukesha 88 (Rb 77)	>350	>51	
301 SS (Rb 87)	416 SS (Rc 37)	21	3	
	440C (Rc 56)	21	3	
	Nitronic 60 (Rb 94)	>350	>51	
303 SS (Rb 81)	303 SS (Rb 81)	14	2	
	304 SS (Rb 77)	14	2	
	316 SS (Rb 81)	21	3	
	410 SS (Rc 38)	28	4	
	416 SS (Rc 37)	60	8	
	430 SS (Rb 84)	14	2	
	440C SS (Rc 56)	35	5	
	630 SS [17-4Ph] (Rc 45)	21	3	
	Nitronic 32 (Rb 99)	>350	>51	
	Nitronic 60 (Rb 94)	>350	>51	
	303 SS (Rb 85)	138	20	
	303 SS (Rb 89)	Waukesha 88 (Rb 77)	>350	>51
	304 SS (Rb 77)	Silicon Bronze (Rb 94)	300	44
201 SS (Rb 94)		14	2	
303 SS(Rb 81)		14	2	
304 SS (Rb 77)		14	2	
316 SS (Rb 81)		14	2	
410 SS (Rc 38)		21	3	
416 SS (Rc 37)		165	24	
430 SS (Rb 84)		14	2	
440C SS (Rc 56)		21	2	
630 SS [17-4Ph] (Rc 33)		14	2	
630 SS [17-4Ph] (Rc 45)		14	2	
630 SS [17-4Ph] (Rc 47)		14	2	

(Continued)

Appendix V (Continued)

Material Pair	Threshold Stress		
	MPa	Kpsi	
	Nitronic 32 (Rb 99)	210	30
	Nitronic 32 (Rc 43)	90	13
	Nitronic 50 (Rb 94)	28	4
	Nitronic 60 (Rb 94)	>350	>51
304 SS (Rb 86)	304 SS (Rb 86)	55	8
	304 SS (Rc 27)	28	4
	440C (Rc 55)	28	4
	S20910 (Rb 97)	69	10
	S2410 (Rc 23)	>104	>15
	Custom 450 (Rc 43)	21	3
	Custom 455(Rc 48)	124	18
	Nitronic 30 (Rb 96)	41	6
304 SS (Rc 27)	304 SS (Rb 86)	28	4
	304 SS (Rc 27)	17	2.5
316 SS (Rb 77)	Stellite 6B (Rc 45)	240	35
316 SS (Rb 81)	303 SS (Rb 81)	21	3
	304 SS (Rb 77)	14	2
	316 SS (Rb 81)	14	2
	316 SS (Rc 27)	55	8
	410 SS (Rc 38)	14	2
	416 SS (Rc 37)	290	42
	430 SS (Rb 84)	14	2
	440C SS (Rc 56)	14-255	2-37
	630 SS [17-4Ph] (Rc 45)	14	2
	Nitronic 32 (Rb 99)	21	3
	Nitronic 60 (Rb 94)	260	38
316 SS (Rb 83)	316 SS (Rb 83)	48	7
316 SS (Rb 90)	440C SS (Rc 58)	7	1
	Nitronic 60 (Rb 92)	35	5
316 SS (Rb 94)	Waukesha 88 (Rb 77)	>350	>51
316 SS (Rc 27)	316 SS (Rc 27)	35	5
	329 SS (Rc 27)	14	2
329 SS (Rc 25)	316 SS (Rc 27)	14	2
	329 SS (Rc 25)	7	1
410 SS (Rb 87)	410 SS (Rb 87)	7	1
410 SS (Rc 32)	416 SS (Rc 38)	28	4
	420 SS (Rc 50)	21	3
410 SS (Rc 34)	416 SS (Rc 40)	28	4
	420 SS (Rc 48)	21	3
410 SS (Rc 38)	303 SS (Rb 81)	28	4
	304 SS (Rb 77)	14	2
	316 SS (Rb 81)	14	2
	410 SS (Rc 38)	21	3
	416 SS (Rc 37)	28	4
	430 SS (Rb 84)	21	3
	440C SS (Rc 56)	21	3

(Continued)

Appendix V (Continued)

Material Pair		Threshold Stress	
		MPa	Kpsi
	630 SS [17-4Ph] (Rc 45)	21	3
	Nitronic 32 (Rb 99)	320	46
	Nitronic 60 (Rb 94)	>350	>51
410 SS (Rc 43)	410 SS (Rc 43)	21	3
	440C (Rc 55)	35	5
416 SS (Rb 83)	416 SS (Rc 32)	76	11
416 SS (Rb 95)	416 SS (Rb 95)	21	3
416 SS (Rc 32)	416 SS (Rb 83)	76	11
	416 SS (Rc 32)	42	6
416 SS (Rc 34)	430 SS (Rb 90)	21	3
416 SS (Rc 37)	301 SS (Rb 87)	21	3
	303 SS (Rb 81)	60	9
	304 SS (Rb 77)	165	24
	316 SS (Rb 81)	290	42
	410 SS (Rc 38)	28	4
	416 SS (Rc 37)	90	13
	430 SS (Rb 84)	21	3
	440 SS (Rc 55)	159	23
	440C SS (Rc 56)	145	21
	630 SS [17-4Ph] (Rc 45)	14	2
	20Cr-80Ni (Rb 89)	50	7
	Nitronic 32 (Rb 99)	310	45
	Nitronic 60 (Rb 94)	>350	>51
416 SS (Rc 37)	410 SS (Rc 32)	28	4
	416 SS (Rc 37)	62	9
416 SS (Rc 40)	410 SS (Rc 34)	28	4
420 SS (Rc 49)	410 SS (Rc 32)	21	3
	420 SS (Rc 49)	55	8
	Nitronic 60 (Rb 96)	>345	>50
420 SS (Rc 55)	420 SS (Rc 55)	125	18
430 SS (Rb 84)	303 SS (Rb 81)	14	2
	304 SS (Rb 77)	14	2
	316 SS (Rb 81)	14	2
	410 SS (Rc 38)	21	3
	416 SS (Rc 37)	21	3
	430 SS (Rb 84)	14	2
	440C SS(Rc 56)	14	2
	630 SS [17-4Ph] (Rc 45)	21	3
	Nitronic 32 (Rb 99)	21	3
	Nitronic 60 (Rb 94)	250	36
430 SS (Rb 90)	416 SS (Rc 34)	21	3
430 SS (Rb 98)	430 SS (Rb 98)	10	1.5
430F SS (Rb 92)	430F SS (Rb 92)	14	2
430C SS (Rc 56)	301 SS (Rb 87)	21	3
	303 SS (Rb 81)	35	5

(Continued)

Appendix V (Continued)

Material Pair	Threshold Stress		
	MPa	Kpsi	
	304 SS (Rb 77)	21	3
	304 SS (Rb 86)	28	4
	316 SS (Rb 81)	250	36
	410 SS (Rc 38)	21	3
	410 SS (Rc 43)	35	5
	416 SS (Rc 37)	145	21
	430 SS (Rb 84)	14	2
	440C SS (Rc 56)	75	11
	440C SS (Rc 59)	80	12
	630 SS [17-4Ph] (Rc 45)	21-76	3-11
	Nitronic 32 (Rb 99)	>350	>51
	Nitronic 60 (Rb 94)	>350	>51
440C SS (Rc 58)	1020 (Rb 90)	14	2
	316 SS (Rb 90)	7	1
	440C SS (Rc 58)	35-75	5-11
	17-5PH (Rc 43)	7	1
	17-5PH nitrided (Rc 70)	>500	>73
	S30430 (Rb 74)	83	12
	Nitronic 60 (Rb 92)	14	2
	Stellite 6 (Rc 42)	55	8
	Tribaloy 400 (Rc 48)	140	20
630 SS [17-4Ph] (Rc 33)	304 SS (Rb 77)	14	2
	630 SS [17-4Ph] (Rc 34)	35	5
	Nitronic 60 (Rb 96)	>350	>51
630 SS [17-4Ph] (Rc 36)	Nitronic 60 (Rb 94)	>350	>51
630 SS [17-4Ph] (Rc 38)	S13800 (Rc 46)	14	2
	S24100 (Rc 23)	76	11
	Custom 455 (Rc 48)	55	8
630 SS [17-4Ph] (Rc 41)	201 SS (Rb 94)	14	2
	S17700 (Rc 41)	21	3
	Nitronic 32 (Rb 94)	75	11
	Nitronic 32 (Rb 43)	21	3
630 SS [17-4Ph] (Rc 43)	631 SS (Rc 43)	21	3
630 SS [17-4Ph] (Rc 44)	Waukesha 88 (Rb 77)	>350	>51
630 SS [17-4Ph] (Rc 45)	303 SS (Rb 81)	14	2
	304 SS (Rb 77)	14	2
	316 SS (Rb 81)	14	2
	410 SS (Rc 38)	21	3
	416 SS (Rc 37)	14	2
	430 SS (Rb 84)	21	3
	440C SS (Rc 56)	21	3
	630 SS [17-4Ph] (Rc 45)	14	2
	S13800 (Rc 46)	62	9
	S17700 (Rc 44)	14	2
	Custom 450 (Rc 48)	76	11
	Nitronic 32 (Rb 99)	>350	>51

(Continued)

Appendix V (Continued)

Material Pair	Threshold Stress		
	MPa	Kpsi	
630 SS [17-4Ph] (Rc 47)	Nitronic 60 (Rb 94)	>350	>51
	304 SS (Rb 77)	14	2
	630 SS [17-4Ph] (Rc 47)	69	10
631 SS (Rc 43)	631 SS (Rc 47)	14	2
	630 SS [17-4Ph] (Rc 43)	21	3
17-5Ph (Rc 43)	440C SS (Rc 58)	7	1
	Stellite 6 (Rc 42)	35	5
	Tribaloy 400 (Rc 48)	48	7
17-5Ph nitrided (Rc 70)	440C SS (Rc 58)	>500	>73
660 SS (Rc 28)	660 SS (Rc 28)	21	3
	Nitronic 60 (Rb 94)	>350	>51
N08020 (Rb 87)	N08020 (Rb 87)	14	2
	Nitronic 60 (Rb 92)	48	7
S13800 (Rc 46)	630 SS [17-4Ph] (Rc 38)	14	2
	630 SS [17-4Ph] (Rc 45)	62	9
	S13800 (Rc 46)	21	3
S17700 (Rc 41)	Nitronic 60 (Rb 96)	>345	>50
	630 SS [17-4Ph] (Rc 41)	21	3
S17700 (Rc 44)	630 SS [17-4Ph] (Rc 44)	14	2
S18200 (Rb 98)	S1820 (Rb 98)	35	5
S20900 (Rb 96)	S20900 (Rb 96)	48	7
S20910 (Rb 95)	S24100 (Rc 43)	90	13
	Nitronic 60 (Rb 96)	>345	>50
S20910 (Rb 97)	S20910 (Rb 97)	35	5
	304 SS (Rb 86)	69	10
S20910 (Rc 34)	S24100 (Rc 23)	55	8
S24100 (Rc 21)	201 SS (Rb 94)	284	36
S24100 (Rc 23)	304 SS (Rb 86)	>104	>15
	630 SS [17-4Ph] (Rc 39)	76	11
S24100 (Rc 43)	S20910 (Rc 34)	55	8
	S24100 (Rb 23)	97	14
	S20910 (Rb 95)	90	13
S30430 (Rb 74)	S30430 (Rb 74)	35	5
	440C SS (Rc 55)	83	12
S66286 (Rc 30)	S66286 (Rc 30)	14	2
20 Cr-80Ni (Rb 89)	416 SS (Rc 37)	50	7
	Nitronic 60 (Rb 94)	250	36
Ti-6Al-4V (Rc 36)	Waukesha 88 (Rb 77)	>350	>51
	Nitronic 60 (Rb 94)	>350	>51
Custom 450 (Rc 29)	Custom 450 (Rc 29)	69	11
	Nitronic 30 (Rb 96)	55	88
Custom 450 (Rc 33)	Custom 450 (Rc 33)	14	2
Custom 450 (Rc 38)	Custom 450 (Rc 38)	17	2.5
Custom 450 (Rc 43)	304 SS (Rb 86)	21	3
	Custom 450 (Rc 43)	55	8

(Continued)

Appendix V (Continued)

Material Pair		Threshold Stress	
		MPa	Kpsi
	Nitronic 30 (Rb 96)	62	9
Custom 450 (Rc 48)	630 SS [17-4Ph] (Rc 45)	76	11
Custom 455 (Rc 36)	Custom 455 (Rc 36)	28	4
Custom 455 (Rc 43)	Custom 455 (Rc 43)	59	8.5
Custom 455 (Rc 48)	304 SS (Rb 86)	124	18
	630 SS [17-4Ph] (Rc 38)	55	8
	Custom 455 (Rc-48)	90	13
Gall Tough (Rb 95)	Gall Tough (Rb 95)	104	15
Hard Anodized	Hard Anodized	>270	>39
Nitronic 30 (Rb 96)	304 SS (Rb 86)	41	6
	Custom 450 (Rc 29)	55	8
	Custom 450 (Rc 43)	62	9
	Nitronic 30 (Rb 96)	166	24
	Nitronic 30 (Rc 35)	104	15
Nitronic 30 (Rc 35)	Nitronic 30 (Rb 96)	104	15
	Nitronic 30 (Rc 35)	62	9
Nitronic 32 (Rb 94)	1034 (Rb 94)	14	2
	630 SS [17-4Ph] (Rc 41)	75	11
	Nitronic 32 (Rc 43)	235	34
	304 SS (Rb 77)	50	7
Nitronic 32 (Rb 98)	201 SS (Rb 94)	250	36
	303 SS (Rb 81)	>350	>51
	304 SS (Rb 77)	210	30
	316 SS (Rb 81)	21	3
	410 SS (Rc 38)	315	46
	416 SS (Rc 37)	310	45
	430 SS (Rb 84)	55	8
	440C SS (Rc 56)	>350	>51
	630 SS [17-4Ph] (Rc 45)	>350	>51
	Nitronic 32 (Rb 99)	210	30
	Nitronic 50 (Rc 34)	55	8
	Nitronic 60 (Rb 94)	>350	>51
Nitronic 32 (Rc 43)	304 SS (Rb 77)	90	13
	630 SS [17-4Ph] (Rc 41)	21	3
	Nitronic 32 (Rb 43)	235	34
	Nitronic 50 (Rb 94)	90	13
Nitronic 50 (Rb 94)	304 SS (Rb 77)	28	4
	Nitronic 32 (Rc 43)	90	13
	Nitronic 50 (Rb 94)	14	2
	Nitronic 60 (Rb 94)	>350	>51
Nitronic 50 (Rc 34)	Nitronic 32 (Rb 99)	55	8
Nitronic 60 (Rb 92)	316 SS (Rb 90)	35	5
	440C (Rc 58)	14	2
	N08020 (Rb 87)	48	7
	Nitronic 60 (Rb 92)	14-104	2-15

(Continued)

Appendix V (Continued)

Material Pair		Threshold Stress	
		MPa	Kpsi
Nitronic 60 (Rb 94)	4337 (Rc 48)	>350	>51
	4337 (Rc 51)	>350	>51
	301 SS (169)	>350	>51
	303 SS (Rb 81)	>350	>51
	304 SS (Rb 77)	>350	>51
	316 SS (Rb 81)	260	38
	410 SS (Rc 38)	>350	>51
	416 SS (Rc 37)	>350	>51
	420 SS (Rc 48)	>350	>51
	430 SS (Rb 84)	250	36
	440C SS (Rc 56)	>350	>51
	630 SS [17-4Ph] (Rc 36)	>350	>51
	630 SS [17-4Ph] (Rc 45)	>350	>51
	660 SS (Rc 28)	>350	>51
	20Cr-80Ni (Rb 89)	250	36
	Ti-6Al-4V (Rc 36)	>350	>51
	Nitronic 32 (Rb 99)	>350	>51
	Nitronic 50 (Rb 94)	>350	>51
	Nitronic 60 (Rb 94)	>350	>51
	Stellite 6B (Rc 45)	>350	>51
Nitronic 60 (Rb 96)	301 SS (Rb 87)	>345	>50
	420 SS (Rc 50)	>345	>50
	630 SS [17-4Ph] (Rc 33)	>350	>51
	S13800 (Rc 44)	>345	>50
	S20910 (Rb 95)	>345	>50
Stellite 6 (Rc 42)	440C SS (Rc 58)	55	8
	15-5Ph (Rc 43)	35	5
Stellite 6B (Rc 45)	304 SS (Rb 77)	240	35
	316 SS (Rb 77)	25	3.5
	Nitronic 60 (Rb 94)	>350	>51
	Stellite 6B (Rc 45)	>350	>51
	Tribaloy 400 (Rc 54)	>350	>51
Tribaloy 700 (Rc 47)	Tribaloy 700 (Rc 47)	>350	>51
	Tribaloy 700 (Rc 47)	185	27
Tribaloy 400 (Rc 48)	440C SS (Rc 58)	140	20
	15-5 Ph (Rc 43)	48	7
Tribaloy 400 (Rc 54)	Tribaloy 400 (Rc 54)	>350	>51
Tribaloy 700 (Rc 47)	Tribaloy 700 (Rc 47)	185	27
Waukesha 88 (Rb 77)	201 SS (Rb 94)	>350	>51
	303 SS (Rb 89)	>350	>51
	316 SS (Rb 94)	>350	>51
	630 SS [17-4Ph] (Rc 44)	>350	>51
	20Cr-80Ni (Rb 89)	>350	>51

Sources:

1. J Magee. Wear of Stainless Steels. In: P Blau, Ed., Friction, Lubrication and Wear Technology, ASM Handbook. Vol. 18. Materials Park, OH: ASM International, 1992, 710-724.
2. B Bhushan, B Gupta. Metals and Ceramics, Handbook of Tribology. Chapter 4. New York: McGraw-Hill, 4.2-4.84, 1991.
3. K Budinski. Incipient Galling of Metals, Proc Intl Conf Wear Materials ASME 171-178, 1981.

APPENDIX VI

WEAR RELATIONSHIP FOR SLIDING WEAR BASED ON THE ZERO AND MEASURABLE WEAR MODELS FOR SLIDING

Allowable Load Relations

Nomenclature

E	Young's modulus, psi
K	stress concentration factor
L	length of contact in cases involving cylinders and planes, in.
L'	width of contact in cases of flat-on-flat conforming geometry, in.
n_0	frequency of oscillation, oscillations/min
n_r	angular velocity of a shaft, rpm
P	normal force between two contacting surfaces, lb
P_0	allowable load, lb
R	principal radius of curvature, in.
x	operation time, hr/month
y	machine life, months
z	total linear travel for one oscillation cycle, in./cycle
α	angle of contact in a shaft-in-hole conforming geometry, deg.
γ_r	zero wear factor for sliding
μ	coefficient of friction
ν	Poisson's ratio
τ_y	shear yield stress
ϕ	total angular travel for one oscillation cycle, deg./cycle

Note: Subscripts 1 and 2 of these variables apply to Body 1 and Body 2, as shown in the sketches and equations.

(Continued)

Appendix VI (Continued)

Area Contact

<p>Case 1.1—Cylinder in Hole Rotating cylinder; fixed partial hole; $R_1 = R_2 = R$</p>	<p>Case 1.2—Cylinder in Hole Rotating cylinder; fixed full hole; $R_1 = R_2 = R$</p>	<p>Case 1.3—Cylinder in Hole Fixed cylinder; rotating hole; $R_1 = R_2 = R$</p>
<p>$\alpha \leq 180^\circ$</p> <p>$L = \text{Lesser of } L_1 \text{ and } L_2$</p>	<p>$\alpha = 180^\circ$</p> <p>$L = \text{Lesser of } L_1 \text{ and } L_2$</p>	<p>$\alpha = 180^\circ$</p> <p>$L = \text{Lesser of } L_1 \text{ and } L_2$</p>

$$B1 = 1.535 \alpha^{1/9} \left(\frac{RL(\sin \alpha/2)}{K} \right) \left(\frac{\gamma_A \tau_{ys}}{\sqrt{0.25 + \mu^2}} \right) \left(\frac{1}{xy \nu_e} \right)^{1/9}$$

$$B2 = 2.953 \left(\frac{RL(\sin \alpha/2)}{K} \right) \left(\frac{\gamma_A \tau_{ys}}{\sqrt{0.25 + \mu^2}} \right) \left(\frac{1}{xy \nu_e} \right)^{1/9}$$

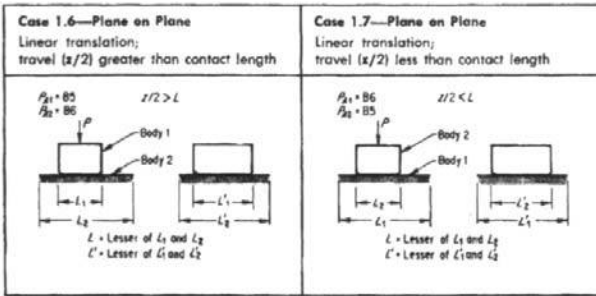
<p>Case 1.4—Cylinder in Hole Linear oscillation; either member fixed; travel $(x/2)$ greater than contact length; $R_1 = R_2 = R$</p>	<p>Case 1.5—Cylinder in Hole Linear oscillation; either member fixed; travel $(x/2)$ less than contact length; $R_1 = R_2 = R$</p>
<p>$x/2 > L_1$</p> <p>$L = \text{Lesser of } L_1 \text{ and } L_2$</p>	<p>$x/2 < L_1$</p> <p>$L = \text{Lesser of } L_1 \text{ and } L_2$</p>

$$B3 = 2.953 L^{1/9} \left(\frac{R}{K} \right) \left(\frac{\gamma_A \tau_{ys}}{\sqrt{0.25 + \mu^2}} \right) \left(\frac{1}{xy \nu_e} \right)^{1/9}$$

$$B4 = 2.734 \frac{RL}{K} \left(\frac{\gamma_A \tau_{ys}}{\sqrt{0.25 + \mu^2}} \right) \left(\frac{1}{xy \nu_e} \right)^{1/9}$$

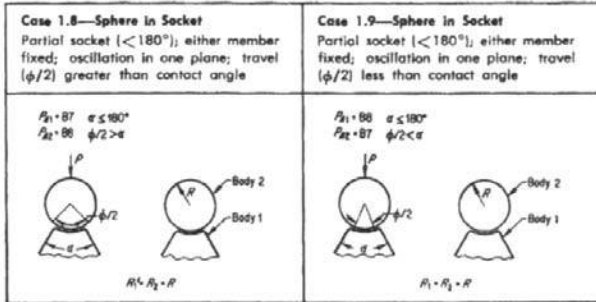
(Continued)

Appendix VI (Continued)



$$B5 = 1.476 L^{1/9} \left(\frac{L'}{K} \right) \left(\frac{\gamma_A \tau_{ps}}{\sqrt{0.25 + \mu^2}} \right) \left(\frac{1}{xy n_o} \right)^{1/9}$$

$$B6 = 1.367 \frac{LL'}{K} \left(\frac{\gamma_A \tau_{ps}}{\sqrt{0.25 + \mu^2}} \right) \left(\frac{1}{xy n_o} \right)^{1/9}$$



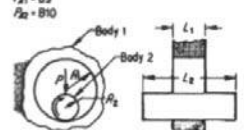
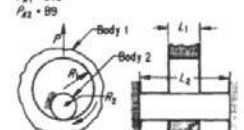
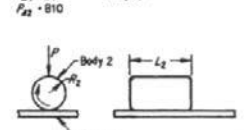
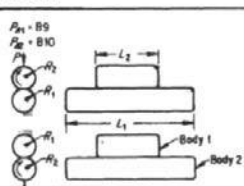
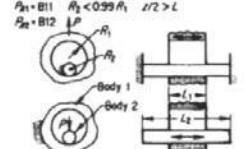
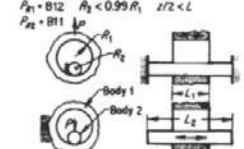
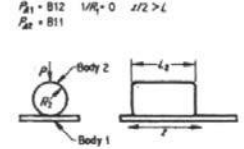
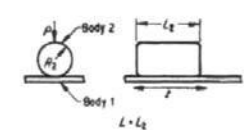
$$B7 = 4.638 \alpha^{1/9} \left(\frac{R^2 \sin^2 \alpha/2}{K} \right) \left(\frac{\gamma_A \tau_{ps}}{\sqrt{0.25 + \mu^2}} \right) \left(\frac{1}{xy n_o} \right)^{1/9}$$

$$B8 = 4.294 \left(\frac{R^2 \sin^2 \alpha/2}{K} \right) \left(\frac{\gamma_A \tau_{ps}}{\sqrt{0.25 + \mu^2}} \right) \left(\frac{1}{xy n_o} \right)^{1/9}$$

(Continued)

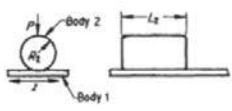
Appendix VI (Continued)

Line Contact

<p>Case 2.1—Cylinder in Hole Rotating cylinder; fixed hole; $R_2 < 0.99 R_1$</p>	<p>Case 2.2—Cylinder in Hole Rotating hole; fixed cylinder; $R_2 < 0.99 R_1$</p>	<p>Case 2.3—Cylinder on Plane Rotating cylinder; fixed plane</p>
<p>$\bar{P}_1 = B9$ $\bar{P}_2 = B10$</p>  <p>$L = \text{Lesser of } L_1 \text{ and } L_2$</p>	<p>$\bar{P}_1 = B10$ $\bar{P}_2 = B9$</p>  <p>$L = \text{Lesser of } L_1 \text{ and } L_2$</p>	<p>$\bar{P}_1 = B9$ $1/R_1 = 0$ $\bar{P}_2 = B10$</p> 
<p>Case 2.4—Cylinder on Cylinder One cylinder fixed; one rotating (Note: Reverse sign of R_1 in B9 and B10)</p> <p>$\bar{P}_1 = B9$ $\bar{P}_2 = B10$</p>  <p>$L = \text{Lesser of } L_1 \text{ and } L_2$</p>	$B9 = 32.07 \left(\frac{1 - \nu_1^2}{E_1} + \frac{1 - \nu_2^2}{E_2} \right)^{0.64}$ $\left(\frac{L}{R_2^{1/4}} \left[\frac{1}{1/R_2 - 1/R_1} \right]^{1/4} \right) \left(\frac{7.8 \tau_{y1}}{K(1 + \mu)} \right)^{0.64} \left(\frac{1}{xy n_0} \right)^{1/4}$ $B10 = 27.39 \left(\frac{1 - \nu_1^2}{E_1} + \frac{1 - \nu_2^2}{E_2} \right) \left(\frac{L}{1/R_2 - 1/R_1} \right)$ $\left(\frac{7.8 \tau_{y2}}{K(1 + \mu)} \right)^2 \left(\frac{1}{xy n_0} \right)^{1/8}$	
<p>Case 2.5—Cylinder in Hole Linear oscillation; either member fixed; travel $(x/2)$ greater than contact length</p>	<p>Case 2.6—Cylinder in Hole Linear oscillation; either member fixed; travel $(x/2)$ less than contact length</p>	<p>Case 2.7—Cylinder on Plane Linear oscillation parallel to cylinder axis; either member fixed; travel $(x/2)$ greater than contact length</p>
<p>$\bar{P}_1 = B11$ $R_2 < 0.99 R_1$ $x/2 > L$ $\bar{P}_2 = B12$</p>  <p>$L = L_1$</p>	<p>$\bar{P}_1 = B12$ $R_2 < 0.99 R_1$ $x/2 < L$ $\bar{P}_2 = B11$</p>  <p>$L = L_1$</p>	<p>$\bar{P}_1 = B12$ $1/R_1 = 0$ $x/2 > L$ $\bar{P}_2 = B11$</p>  <p>$L = L_2$</p>
<p>$B11 = 6.848 \left(\frac{1 - \nu_1^2}{E_1} + \frac{1 - \nu_2^2}{E_2} \right) \left(\frac{1}{0.25 + \mu^3} \right)$</p> $\left(L \right)^{11/9} \left(\frac{1}{1/R_2 - 1/R_1} \right) \left(\frac{7.8 \tau_{y1}}{K} \right)^2 \left(\frac{1}{xy n_0} \right)^{2/9}$ <p>$B12 = 5.870 \left(\frac{1 - \nu_1^2}{E_1} + \frac{1 - \nu_2^2}{E_2} \right) \left(\frac{1}{0.25 + \mu^3} \right)$</p> $\left(\frac{L}{1/R_2 - 1/R_1} \right) \left(\frac{7.8 \tau_{y2}}{K} \right)^2 \left(\frac{1}{xy n_0} \right)^{8/9}$ <p>Case 2.8—Cylinder on Plane Linear oscillation parallel to cylinder axis; either member fixed; travel $(x/2)$ less than contact length</p> <p>$\bar{P}_1 = B11$ $1/R_1 = 0$ $x/2 < L$ $\bar{P}_2 = B12$</p>  <p>$L = L_2$</p>		

(Continued)

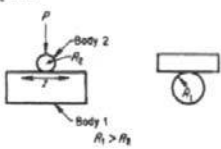
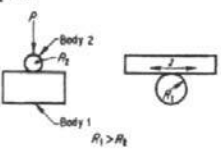
Appendix VI (Continued)

<p>Case 2.9—Cylinder on Plane Linear oscillation perpendicular to cylinder axis; either member fixed</p> <p>$\beta_{13} \cdot B13$ $\beta_{14} \cdot B14$</p> 	$B13 = 23.48 \left(\frac{\gamma_R \nu_{y1}}{(1 + \mu)} \right)^2 \left(\frac{L_2 R_1}{K^2} \right) \left(\frac{1 - \nu_1^2}{E_1} + \frac{1 - \nu_2^2}{E_2} \right) \left(\frac{1}{x y z n_o} \right)^{5/9}$ $B14 = 50.86 \left(\frac{\gamma_R \nu_{y2}}{(1 + \mu)} \right)^{5/4} \left(\frac{L_2^4 R_1^3}{K^9} \right)^{1/4} \left(\frac{1 - \nu_1^2}{E_1} + \frac{1 - \nu_2^2}{E_2} \right)^{5/4} \left(\frac{1}{x y z n_o} \right)^{1/2}$
---	---

(Continued)

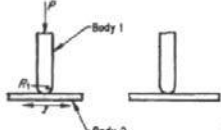
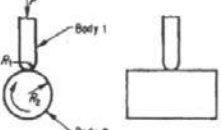
Appendix VI (Continued)

Point Contact

<p>Case 3.1—Crossed Cylinders Unequal cylinder diameters; linear oscillation parallel to axis of larger diameter cylinder</p>	<p>Case 3.2—Crossed Cylinders Unequal cylinder diameters; linear oscillation parallel to axis of smaller diameter cylinder</p>
<p>$\beta_1 \cdot B15$ $\beta_2 \cdot B16$</p>  <p>Body 2 Body 1 $R_1 > R_2$</p>	<p>$\beta_1 \cdot B16$ $\beta_2 \cdot B15$</p>  <p>Body 2 Body 1 $R_1 > R_2$</p>

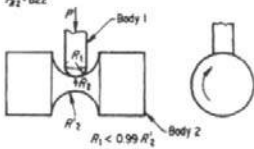
β = the greater of μ or 0.31
 $\cos \theta = \frac{R_1 - R_2}{R_1 + R_2}$

$B15 = 52.60 \left(\frac{\gamma N \gamma y_1}{\beta} \right)^3 \left(\frac{m^2 n^2 R_1^2 R_2^2}{(R_1 + R_2)^2} \right) \left(\frac{1 - \nu_1^2}{E_1} + \frac{1 - \nu_2^2}{E_2} \right)^2 \left(\frac{1}{xy n_0} \right)^{1/3}$
 $B16 = 153.4 \left(\frac{\gamma N \gamma y_2}{\beta} \right)^{27/8} \left(m^{27/8} n^{15/4} \right)^{5/8} \left(\frac{R_1 R_2}{R_1 + R_2} \right)^{15/8} \left(\frac{1 - \nu_1^2}{E_1} + \frac{1 - \nu_2^2}{E_2} \right)^{15/8} \left(\frac{1}{xy n_0} \right)^{5/8}$

<p>Case 3.3—Sphere on Plane Linear oscillation; either member fixed</p>	<p>Case 3.4—Sphere on Cylinder Rotating cylinder; fixed sphere</p>
<p>$\beta_1 \cdot B17$ $\beta_2 \cdot B18$</p>  <p>Body 1 Body 2</p>	<p>$\beta_1 \cdot B19$ $\beta_2 \cdot B20$</p>  <p>Body 1 Body 2</p>

β = the greater of μ or 0.31
 $\cos \theta = \frac{R_1}{2R_2 + R_1}$

$B17 = 29.57 \left(\frac{\gamma N \gamma y_1}{\beta} \right)^{27/8} (R_1)^{15/8} \left(\frac{1 - \nu_1^2}{E_1} + \frac{1 - \nu_2^2}{E_2} \right)^{15/8} \left(\frac{1}{xy z n_0} \right)^{5/8}$
 $B18 = 13.20 \left(\frac{\gamma N \gamma y_2}{\beta} \right)^3 (R_1)^2 \left(\frac{1 - \nu_1^2}{E_1} + \frac{1 - \nu_2^2}{E_2} \right)^2 \left(\frac{1}{xy n_0} \right)^{1/3}$
 $B19 = 76.99 \left(\frac{\gamma N \gamma y_1}{\beta} \right)^{27/8} \left(m^{27/8} n^{15/4} \right) R_2^2 \left(\frac{R_1}{2R_2 + R_1} \right)^{15/8} \left(\frac{1 - \nu_1^2}{E_1} + \frac{1 - \nu_2^2}{E_2} \right)^{15/8} \left(\frac{1}{xy n_r} \right)^{5/8}$
 $B20 = 66.53 \left(\frac{\gamma N \gamma y_2}{\beta} \right)^3 (mn)^3 \left(\frac{R_1 R_2}{2R_2 + R_1} \right)^3 \left(\frac{1 - \nu_1^2}{E_1} + \frac{1 - \nu_2^2}{E_2} \right)^3 \left(\frac{1}{xy n_r} \right)^{1/3}$

<p>Case 3.5—Sphere on Cylinder Rotating grooved cylinder; fixed sphere</p> <p>$\beta_1 \cdot B21$ $\beta_2 \cdot B22$</p>  <p>Body 1 Body 2 $R_1 < 0.99 R_1'$</p>

$B21 = 77.03 \left(\frac{\gamma N \gamma y_1}{\beta} \right)^{27/8} \left(m^{27/8} n^{15/4} \right) (R_2)^2$
 $\left(\frac{R_1 R_2'}{2R_2 R_2' + R_1 R_1' - R_1 R_2} \right)^{15/8} \left(\frac{1 - \nu_1^2}{E_1} + \frac{1 - \nu_2^2}{E_2} \right)^{15/8} \left(\frac{1}{xy n_r} \right)^{5/8}$
 $B22 = 66.56 \left(\frac{\gamma N \gamma y_2}{\beta} \right)^3 (mn)^2 \left(\frac{R_1 R_2 R_2'}{2R_2 R_2' + R_1 R_1' - R_1 R_2} \right)^2$
 $\left(\frac{1 - \nu_1^2}{E_1} + \frac{1 - \nu_2^2}{E_2} \right)^3 \left(\frac{1}{xy n_r} \right)^{1/3}$
 β = the greater of μ or 0.31
 $\cos \theta = \frac{R_1 (R_1 + R_2)}{2R_2 R_2' + R_1 R_1' - R_1 R_2}$

(Continued)

APPENDIX VI (Continued)

**WEAR EQUATIONS BASED ON THE MEASURABLE-WEAR
RELATIONSHIPS FOR SLIDING****Wear depth \propto operationsⁿ**

Situation		Wearing Member	n	
Geometry	Motion		Constant Energy	Variable Energy
Cylinder-in-hole	Rotation, cylinder	Cylinder	1	1
		Hole	0.67	0.67
	Rotation, hole	Cylinder	0.67	0.67
		Hole	1	1
	Angular oscillation, cylinder	Cylinder	0.67	0.67
		Hole	0.67	0.67
	Angular oscillation, hole	Cylinder	0.67	0.67
		Hole	0.67	0.67
	Linear oscillation, cylinder	Hole	0.67	0.27
		Cylinder	0.67	0.27
	Linear oscillation, cylinder	Hole	0.67	0.27
		Cylinder	0.67	0.27
Cylinder-on-flat	Rotation, cylinder	Cylinder	1	1
		Flat	0.67	0.67
	Angular oscillation, cylinder	Cylinder	0.67	0.67
		Flat	0.67	0.67
	Linear oscillation, perpendicular to axis	Cylinder	0.67	0.67
		Flat	1	1
	Linear oscillation, parallel to axis	Cylinder	0.67	0.27
Flat		0.67	0.27	
Parallel cylinders	Rotation	Moving	1	1
		Stationary	0.5	0.5
	Angular oscillation	Moving	0.5	0.5
		Stationary	0.5	0.5
	Linear oscillation	Moving	0.67	0.27
		Stationary	0.67	0.27
Crossed-cylinders	Rotation	Moving	0.5	0.27
		Stationary	0.5	0.27
	Angular oscillation	Moving	0.5	0.27
		Stationary	0.5	0.27
	Linear oscillation	Moving	0.67	0.27
		Stationary	0.5	0.24

(Continued)

Appendix VI (Continued)

Geometry	Situation		<i>n</i>	
	Motion	Wearing Member	Constant Energy	Variable Energy
Sphere-on-flat	Translation	Sphere	0.5	0.24
		Flat	0.67	0.27
Flat-on-flat	Translation	Larger	1	1
		Smaller	1	1
Journal bearing, aligned	Angular oscillation and rotation	Bearing	0.67	0.67
Journal bearing, misaligned	Angular oscillation and rotation	Bearing	0.4	0.14

Metric of operations: distance, cycle, Designing for Zero Wear, revolution, oscillation, or time.

Sources:

1. R Bayer, A Shalkey, A Wayson. Machine Design, 1/9/69, 142-151. Cleveland, OH: Penton Publishing Co., 1969.
2. R Bayer, A Wayson. Designing for Measurable Wear. Machine Design, 8/7/69, 118-127. Cleveland, OH: Penton Publishing Co., 1969.

APPENDIX VII

MODEL FOR THE EFFECT OF FLUID LUBRICATION ON ZERO WEAR FACTORS

Fatigue mechanisms can be the dominant wear mechanism in sliding and rolling situations. For both types of motion and under boundary lubrication conditions, it has been found that the number of unit operations required for a specified initial level of wear to occur can be related to the ninth power of the ratio of the yield point in shear to the maximum shear stress (1-4). One way of expressing this is

$$\eta \tau_m^9 = \eta_0 (\gamma \tau_\gamma)^9 \quad (\text{A.1})$$

where η is the number of unit operations. η_0 is a reference number of operations, τ_m is the maximum shear stress. τ_γ is the yield point in shear. and γ (zero wear factor) is the ratio of the maximum shear stress to the yield point in shear for η_0 operations.

In the case of rolling, the unit operation is a revolution. During it single revolution, the surface experiences one loading cycle. For sliding the corresponding unit is a pass, where it pass is defined its it distance of sliding equal to the length of the contact in the direction of sliding. The surface also experiences a single load cycle in a pass. The wear criterion for rolling is the formation of surface spalls. For sliding, the criterion is an average scar depth equal to the surface roughness. In the case of rolling, 10^8 revolutions is normally used for η_0 . For sliding, 2×10^3 passes is used. For pure rolling, γ is nominally independent of materials and lubricants and is approximately 0.8. When slip occurs, γ becomes smaller. In the case of sliding, γ is dependent on materials and lubricant and smaller than that for rolling. It tends to be bivalued, being approximately 0.54 for some materials and lubricant combinations and 0.20 for others. Combinations with higher value are generally referred to its good wearing combinations; with lower value as poor wear combinations.

Since Eq. (A. 1) applies to both rolling and sliding it is also applicable to situations where the motion is a mixture of rolling and sliding. γ for these conditions can be obtained from the values for pure rolling and sliding, provided they are based on the same value for η_0 and the same level of damage. Equivalent values may be obtained by adjusting the values associated with sliding to the level of damage and unit operating conditions used for rolling. The nominal depth of wear in the case of rolling is in the range of 2.5–25 μm : while that for sliding is in the range of 0.25 μm . Consequently, they differ by a factor somewhere between one and two orders of magnitude. For the geometry of typical rolling elements, it can be shown that wear depth for sliding is typically proportional to $(1/\gamma)^{4.5-6}$. Therefore, if κ is the ratio of the characteristic wear depths, γ for sliding should be increased by a factor of $\kappa^{\approx 0.2}$. An order of magnitude difference in wear is therefore equivalent to approximately a factor of $1.6 \times$ for γ . The equivalent value of γ for sliding at 10^8 unit operation is $0.3 \times$ at 2×10^3 . Using the conditions for pure rolling as the reference, the nominal values for sliding become 0.26 and 0.1, assuming a value of 10 for κ .

The primary reason for the two values of γ in the case of sliding is differences in the tendency for adhesion and adhesive wear (3). Combinations that tend to have a lower tendency towards adhesive wear have the higher value. Surface shear and slip tend to enhance adhesion and, therefore, the tendency for adhesive wear. Therefore, as slip decreases, the distinction in γ values for these two types of combinations should decrease.

The following relationship is proposed for this:

$$\gamma_{sp} = \frac{\gamma_{sg}}{1.7p_s + 1} \quad (\text{A.2})$$

Where γ_{sg} is the adjusted value of γ for good sliding combinations, γ_{sp} is the adjusted value γ for poor sliding combinations, and p_s is the slide ratio, defined as the slip for a single loading cycle per unit length at the interface. For pure sliding p_s is 1; for pure rolling, p_s is 0.

Using the same reference conditions, the value for γ for rolling with sliding under boundary lubrication is given by

$$\Gamma_b = \left[\frac{p_s}{\gamma_s^9} + \frac{(1-p_s)}{\gamma_r^9} \right]^{-1/9} \quad (\text{A.3})$$

where s and r refer to sliding and pure rolling, γ_s is γ_{sg} for good combinations and $[\gamma_{sg}/(1.7 p_s + 1)]$ for poor combinations.

Boundary lubricant is characterized by stable friction and wear behavior as a function of relative velocity between the surfaces. In this region of lubrication, there is asperity contact and interaction over the entire contact region. As the relative velocity increases, the elastohydrodynamic film increases reducing asperity interaction and improving friction and wear behavior. This tends to be significant when film thickness exceeds 2.5 nm (0.1 μin). Eventually, these films will increase to such a thickness that asperity contact will be completely eliminated, but stress cycling, of the Surface will still occur. As a result of the reduced asperity interaction, the γ values will increase to a maximum value, which is independent of materials, lubricant, and type of motion. The γ values for intermediate conditions of lubrication are given by

$$\Gamma = \left[\frac{p_a}{\Gamma_b^9} + \frac{(1-p_a)}{\Gamma_m^9} \right]^{-1/9} \quad (\text{A.4})$$

where Γ_m is the maximum value, associated with complete separation and p_a is the fraction of the contact area involving asperity interaction.

By observing, that the surfaces of a rolling bearing the experience a unit operation or loading cycle each time a rolling element passes over a spot, Eq. (A.1) can be used to determine bearing life. If Θ is the number of times the outer race experiences contact in a single revolution of the inner race, Eq. (A.1) becomes

$$L = \frac{10^8}{\Theta} \left[\frac{\Gamma \tau_y}{\tau_m} \right]^9 \quad (\text{A.5})$$

when Eq. (A.4) is used for γ and 10^8 is used for η_0 . L is the number of inner race revolutions.

By substituting appropriate geometrical relationships and contact stress relationships into Eq. (A.5) it is possible to obtain equations of the same form as the Lundberg–Palmgren equation for rolling bearing life,

$$L = \left(\frac{C_1}{P} \right)^n \quad (\text{A.6})$$

where L is the number of inner race revolutions, C_1 is a factor independent of the load but dependent on geometry and materials, and P is the load. n is 3.0 for ball bearings, when the normal Hertz stress relationship is used for point contact. However, it is 4.5 for roller bearing when the Hertz relationship for parallel cylinders is used. not the empirical value of 3.3. It is generally accepted that this is because the actual contact conditions are different than those assumed for the parallel cylinder relationships and closer to those associated with point contact. Possible explanations for this are curvature of the surfaces or the importance of edge conditions.

Equation (A.5) can be modified to the following form:

$$L = \left(\frac{C_2}{P} \right)^n \tau_y^9 \Gamma^9 \quad (\text{A.7})$$

Where C_2 is solely dependent on geometry.

It can be shown that the slip ratio for rolling bearing is

$$p_s = \frac{2\varepsilon}{Z \left(1 - \frac{d \cos \alpha}{d_m} \right)} \quad (\text{A.8})$$

Where ε is the slip the race experiences per unit length in a revolution, Z is the number of elements, d is the diameter of rolling element, d_m is the pitch diameter of the bearing, and α is the contact angle of bearing. The slip that occurs in bearings is dependent on bearing size and loading conditions and can range over several orders of magnitude, as shown by Fig. A. 1 and the following Eq. (A.5):

$$\varepsilon = 25.2 \times 10^{-3} \left(\frac{P}{C} \right)^{0.46} \frac{(OD[1 + 10 \sin \alpha])^{0.8}}{D} \quad (\text{A.9})$$

Where OD is the outside diameter of the bearing and D is the diameter of the outer race in millimeters. P is the load and C is the dynamic load rating of the bearing.

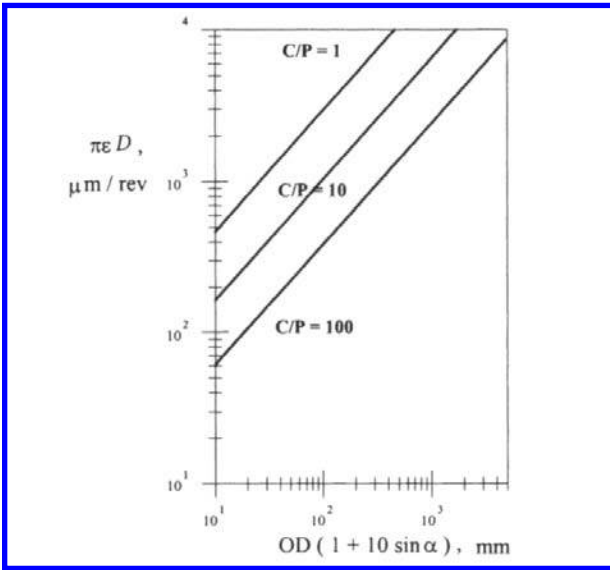


Figure A.1 Slip per revolution for different size bearings. D is the diameter of the outer race. (From Ref. 5.)

The slip ratio values, p_s , for rolling bearings can range over several orders of magnitude as a result. Estimates indicate that p_s can range from a high in the range of 10^{-2} to less than 10^{-4} .

Studies have indicated that the relationship between p_a and the lubrication thickness parameter, Λ , is approximately of the form

$$p_a = (\exp(-1.81\Lambda^{1.25}))^s \tag{A.10}$$

where s is close to 1 (6).

$$\Lambda \gg \frac{h}{(\sigma_1^2 + \sigma_2^2)^{1/2}}$$

where h is the thickness of the EHD film in the center of the contact. The σ s are either the AA (arithmetic average) or the RMS (root mean square average) values for the surface roughness of the two surfaces.

This model was evaluated by comparing lives predicted by Eq. (A.5) with those obtained using the Dynamic Load Rating Model for several ball and roller bearing examples. Regression analysis techniques were used to determine values for Γ_m , γ_{sg} , κ , and s , which gave good agreement, assuming a value of 1.25 for Λ and γ_r of 0.80. The former value is the one normally assumed for conditions used to determine the dynamic load rating. C (7). Since the elemental model is not a statistical model, as the Dynamic Load

* Λ is the ratio of the EHD film thickness to the composite surface roughness

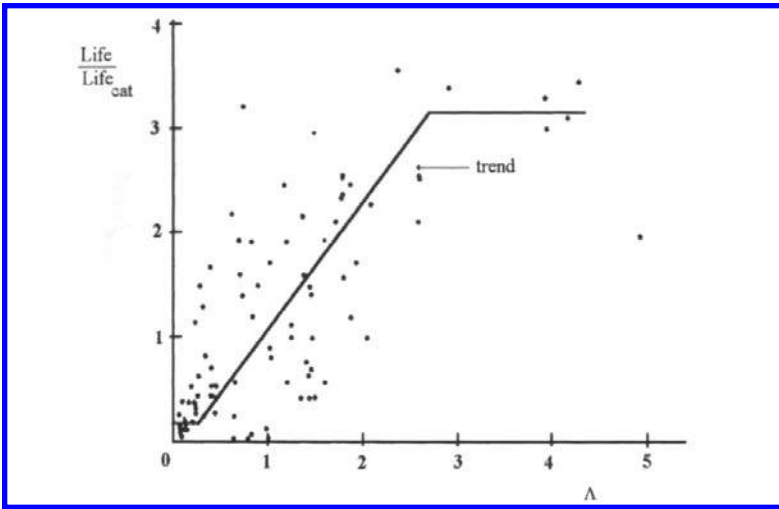


Figure A.2 Ratio of observed life to catalog life reported by different investigators as a function of the lubrication parameter, Λ . The line indicates the generally accepted trend. (From Ref. 8.)

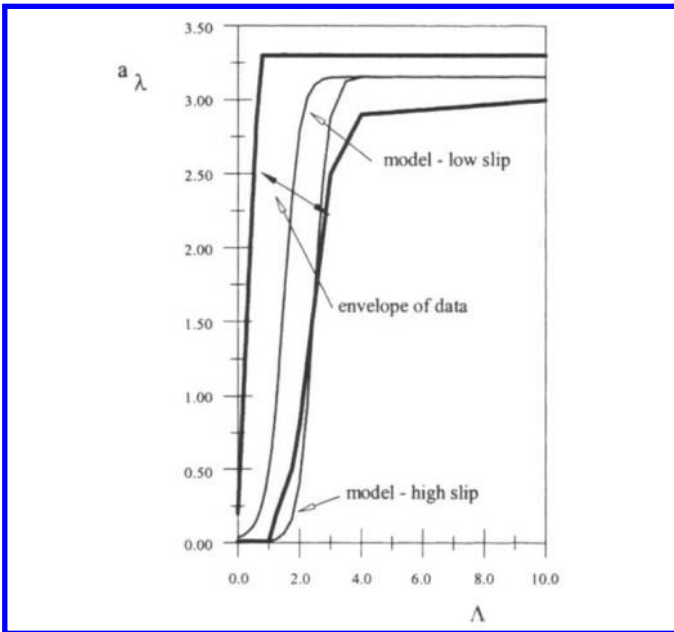


Figure A.3 Comparison of experimental values for a_λ and $(\Gamma / \Gamma_r)^9$. The experimental envelope is based on the data shown in Fig. A. 2 $(\Gamma / \Gamma_r)^9$ values are based on a Λ of 1.25 for the reference condition and γ_{sg} of $(0.40 / 1.7 p_s + 1)$ and Γ_m of 1.30.

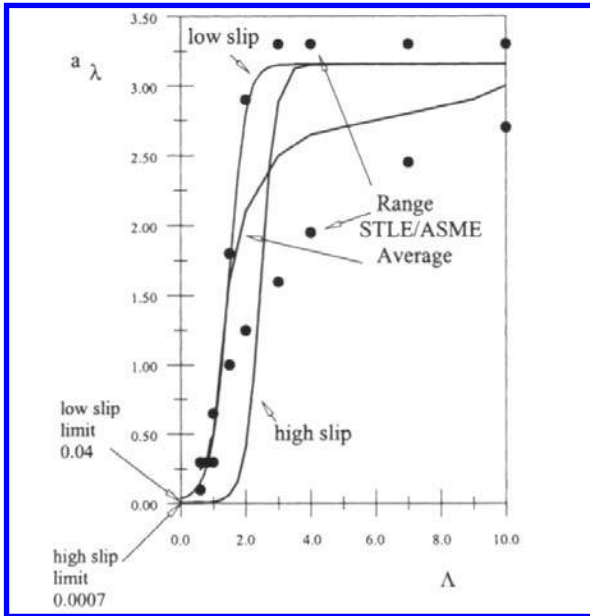


Figure A.4 Comparison of a_λ values base on $(\Gamma / \Gamma_r)^9$ and those recommended by STLE and ASME. The STLE / ASME curve is based on the average of two curves represented by the points. $(\Gamma / \Gamma_r)^9$ values are based on a Λ of 1.25 for the reference condition and γ_{sg} of $(0.40 / 1.7 p_s + 1)$ and Γ_m of 1.30. (From Refs. 9, 10.)

Rating Model is, comparisons were made with L_{50} values[†]. It was concluded that a good agreement could be obtained with the following set of values, which are consistent with the hypotheses of the model: s equal to 1.5, γ_{sg} of 0.40, Γ_m of 1.30, and κ from 50 to 100.

Another regression analysis was also performed, involving the effect that Λ has on bearing life. The influence of Λ on bearing life is shown in Fig. A.2. In this figure, the observed ratio of actual bearing life to L_{10}^* life or catalog life is plotted as a function of Λ for different types of bearings and loading conditions. It was concluded that the general trend as well as the scatter can be explained by the elemental model. It was found that it good agreement between these data and the model could be obtained by assuming different slip conditions and values for s , γ_{sg} , Γ_m and κ similar to those obtained in the previous analysis. This agreement is illustrated in Fig. A.3.

Because of the form of Eq. (A.7), the $(\Gamma / \Gamma_r)^9$ can be used as a life adjustment factor for lubrication. a_λ (9,10). Γ_r refers to the value of Γ associated with the reference conditions associated with the tests used to determine the Dynamic Loading Rating. The normally assumed condition for these tests is negligible slip and a value of 1.25 for Λ . This corresponds to a value of 1.14 for Γ_r . This life adjustment factor is in good

[†] Lifetime for 50% survival.

* Lifetime for 90% survival.

agreement with the factor recommended by STLE and ASME-bearing groups for Λ values above 0.6 (9,10). This is shown in [Fig. A4](#).

REFERENCES

1. E Buckingham, G Talbourdet. Roll test on endurance limits of materials. American Society of Metals, Jan. 1950.
2. R Bayer, W Clinton, C Nelson, R Schumacher Engineering model for wear. *Wear* 5:378-391, 1962
3. RG Bawr. Mechanical Wear Prediction and Prevention, Section C. . NY: Marcel Dekker, 1994.
4. P Engel, C Adams. Rolling wear study of misaligned cylindrical contacts. Proc Intl Wear Mater Conf ASME, 1979, pp 181-191.
5. MB Peterson, WO Winner, eds. Fig. 21 Wear Control Handbook. NY ASME, 1980, p 720.
6. LB Sibley. Rolling Bearing. In: MB Petersen, WO Winner, eds. Wear control Handbook. Park Ridge, IL: ASME, 1980, pp 699-726.
7. Ev Zaretsky, ed. Life Factors for Rolling Bearings, STLE, 1992, 200.
8. TE Tallian. Rolling Bearing Life Modifying Factors for Film Thickness, Surface Roughness and Friction; *Journal of Lubrication Technology*. ASME Transactions, Lubrication Technology 103. 1981, pp 509-520.
9. E Bamberger, T Harris, W Kacmarsky, C Moyer, R Parker, J Sherlock. E Zaretsky eds. Life Adjustment Factors for Ball Roller Bearings, NY: ASME. 1971.
10. EV Zaretsky, ed Life Factors for Rolling Bearings, Park Ridge. IL: STLE, 1992.

Glossary of Wear Mechanisms, Related Terms, and Phenomena

- Abrasion:** A process in which hard particles or protuberances are forced against and moving along a solid surface. (See abrasive wear.)
- Abrasion–corrosion:** A synergistic process involving both abrasive wear and corrosion, in which each of these processes is affected by the simultaneous action of the other.
- Abrasion erosion:** Erosive wear caused by the relative motion of solid particles, which are entrained in a fluid, moving nearly parallel to a solid surface.
- Abrasive wear:** Wear by displacement of material caused by hard particles or hard protuberances or wear due to hard particles or protuberances forced against and moving along a solid surface.
- Adhesive wear:** Wear by transference of material from one surface to another during relative motion due to a process of solid-phase welding or wear due to localized bonding between contacting solid surfaces leading to material transfer between two surfaces or loss from either surface. (Note: Sometimes used as a synonym for dry (unlubricated) sliding wear.)
- Anti-wear Number (AWN):** The base-10 log of the inverse of the wear coefficient.
- Asperity:** A protuberance in the small-scale topographical irregularities of a solid surface.
- Atomic wear:** Wear between two contacting surfaces in relative motion attributed to migration of individual atoms from one surface to the other.
- Beilby layer:** An altered surface layer formed on a surface as a result of wear.
- Boundary lubricant:** A lubricant that provides boundary lubrication.
- Boundary lubrication:** A condition of lubrication in which the friction and wear behavior are determined by the properties of the surfaces and by the properties of fluid lubricants other than their bulk viscosity.
- Break-in:** See run-in.
- Brinelling:** Indentation of the surface of a solid body by repeated local impact or impacts, or static overload or damage to a solid bearing surface characterized by one or more plastically formed indentations brought about by overload.
- Brittle erosion behavior:** Erosion behavior having characteristic properties that can be associated with brittle fracture of the exposed surface, such as little or no plastic flow and the formation of intersecting cracks that create erosion fragments.
- Brittle fracture:** A form of wear in rolling, sliding, and impact contacts, characterize by the formation of tensile cracks in a single loading cycle.

- Burnish (ing):** To alter the original manufactured surface of a sliding or rolling surface to a more polished condition or to apply a substance to a surface by rubbing.
- Catastrophic wear:** Rapidly occurring or accelerating surface damage, deterioration, or change of shape caused by wear to such a degree that the service life of a part is appreciably shortened or its function destroyed.
- Cavitation erosion:** Progressive loss of original material from a solid surface due to continued exposure to cavitation or wear of a solid body moving relative to a liquid in a region of collapsing vapor bubbles that cause local high-impact pressures or temperatures.
- Checking:** See craze cracking.
- Chemical wear:** See corrosive wear.
- Coefficient of friction:** Ratio of the force required to initiate or maintain motion between two bodies, F , and the force pressing these bodies together, N , F/N .
- Compound impact wear:** Impact wear when there is a component of relative velocity parallel to the interface between the impacting bodies.
- Coulomb friction:** A term used to indicate that the frictional force is proportional to the normal load.
- Corrosive wear:** A wear process in which chemical or electrochemical reaction with the environment predominates. (Also called chemical wear.)
- Craze cracking:** Irregular surface cracking associated with thermal cycling. (Also called checking.)
- Deformation wear:** Sliding wear involving plastic deformation of the wearing surface or in impact wear of elastomers, the initial stage of wear not involving material loss but progressive deformation, generally approaching an asymptotic limit.
- Delamination wear:** A wear process in which thin layers of material are formed and removed from the wear surface or a wear process involving the nucleation and propagation of cracks so as to form lamellar wear particles.
- Diffuse wear:** Wear processes involving diffusion of elements from one body into the other, such as those often occurring in high-speed cutting tool wear, generally requires high temperatures.
- Diamond film:** A carbon-composed crystalline film that has the characteristics of diamond.
- Diamondlike Film:** A hard, non-crystalline carbon film.
- DLC:** Diamondlike carbon coatings.
- Droplet erosion:** Erosive wear caused by the impingement of liquid droplets on a solid surface.
- Dry-film lubrication:** Lubrication resulting from the application of a thin film of a solid to a surface.
- Dry sliding wear:** Sliding wear in which there is no intentional lubricant or moisture introduced into the contact area.
- Dynamic friction:** See kinetic friction.
- Ductile erosion behavior:** Erosion behavior having characteristic properties that can be associated with ductile fracture of the exposed solid surface, such as considerable plastic deformation preceding or accompanying material loss from the surface which can occur by gouging or tearing or by eventual embrittlement through work hardening that leads to crack formation.
- Electrical discharge wear:** Material removal as a result of electrical discharge.

- Electrical pitting:** The formation of surface cavities by removal of metal as a result of an electrical discharge across an interface.
- Elastohydrodynamic lubrication:** A form of fluid lubrication in which the friction and film thickness is a function of the deformation of the surfaces and the viscous properties of the fluid lubricant.
- EP lubricant:** See extreme-pressure lubricant.
- Erosion:** Loss of material from a solid surface due to relative motion in contact with a fluid that contains solid particles or progressive loss of original material from a solid surface due to mechanical interaction between that surface and a fluid, multi-component fluid, and impinging liquid, or solid particles.
- Erosive wear:** See erosion.
- Erosion-corrosion:** A conjoint action involving corrosion and erosion in the presence of a corrosive substance.
- Extreme-pressure lubricant (EP lubricant):** A lubricant that imparts increased load-carrying capacity to a rubbing surface under severe operating conditions.
- False Brinelling:** Damage to a solid bearing surface characterized by indentations not caused by plastic deformation resulting from overload, but thought to be due to other causes such as fretting or fretting corrosion or local spots appearing when the protective film on a metal is broken continually by repeated impacts.
- Fatigue wear:** Removal of particles detached by fatigue arising from cyclic stress variations or wear of a solid surface caused by fracture arising from material fatigue.
- Ferrography:** Characterization of magnetic wear debris from oil samples.
- Flash temperature:** The maximum local temperature generated at some point in a sliding contact.
- Flow cavitation:** Cavitation caused by a decrease in static pressure induced by changes in the velocity of a flowing liquid.
- Fluid erosion:** See liquid impingement erosion.
- Fluid friction:** Frictional resistance due to the viscous or rheological flow of fluids.
- Fluid lubrication:** A form of lubrication with a fluid in which the friction and thickness of the film is a function of the viscosity of the fluid. (See elastohydrodynamic and hydrodynamic lubrication.)
- Fracture:** See brittle fracture.
- Fretting:** Wear phenomena occurring between two surfaces having oscillatory relative motion of small amplitude. (Note: Term also can mean small-amplitude oscillatory motion.)
- Fretting corrosion:** A form of fretting in which chemical reaction predominates.
- Fretting fatigue:** The progressive damage to a solid surface that arises from fretting and leads to the formation of fatigue cracks.
- Fretting wear:** See fretting.
- Friction:** The tangential force between two bodies that opposes relative motion between these bodies.
- Friction coefficient:** See coefficient of friction.
- Friction polymer:** An organic deposit that is produced when certain metals are rubbed together in the presence of organic liquids or gases.
- Full-film lubrication:** Fluid lubrication when the surfaces are completely separated by the fluid film.
- Galling:** A severe form of scuffing associated with gross damage to the surface or failure or a form of surface damage arising between sliding solids, distinguished

by macroscopic, usually localized roughening and creation of protrusions above the original surface, often includes plastic flow or material transfer or both or a severe form of adhesive wear.

Gouging abrasion: A form of high-stress abrasion in which easily observable grooves or gouges are created on the surface.

Heat checking: A process in which fine cracks are formed on the surface of a body in sliding contact due to the buildup of excessive frictional heat.

High-stress abrasion: A form of abrasion in which relatively large cutting force is imposed on the particles or protuberance causing the abrasion, and that produces significant cutting and deformation in the wearing surface.

Hydrodynamic lubrication: A form of fluid lubrication in which the friction and film thickness is a function of the viscous properties of the fluid lubricant.

Impact wear: Wear of a solid surface resulting from repeated collisions between that surface and another solid body.

Impingement corrosion: A form of erosion-corrosion generally associated with the impingement of a high-velocity flowing liquid containing air bubbles against a solid surface.

Incubation period: An initial amount of wearing action that is needed for the occurrence of some wear mechanisms or for these mechanisms to become detectable.

IRG Transition Diagram: See transition diagram.

Kinetic friction: Friction associated with sustained motion.

Lapping: A surface finishing process involving motion against an abrasive embedded in a soft metal or rubbing two surfaces together with or without abrasives, for the purpose of obtaining extreme dimensional accuracy or superior surface finish.

Limiting PV: The value of the PV Factor above which severe wear results. Typically use to characterize the wear behavior of plastics and other bearing materials.

Liquid impact erosion: See erosion.

Liquid impingement erosion: See erosion.

Low-stress abrasion: A form of abrasion in which relatively low contact pressure on the abrading particles or protuberances cause only fine scratches and microscopic cutting chips to be produced.

Lubricant: Any substance interposed between two surfaces in relative motion for the purpose of reducing the friction or wear between them.

Lubrication: The reduction of wear or friction by the use of a lubricant.

Lubricated impact wear: Impact wear with lubrication.

Lubricated rolling wear: Rolling wear with lubrication.

Lubricated sliding wear: Sliding wear with lubrication.

Measurable-wear: In the context of the Zero and Measurable Wear Models for sliding and impact, it describes a state of wear in which the wear exceeds the magnitude of the surface roughness.

Mechanical wear: Removal of material due to mechanical processes under conditions of sliding, rolling, or repeated impacts; includes adhesive wear, abrasive wear, and fatigue wear but not corrosive wear and thermal wear.

Metallic wear: Typically, wear due to rubbing or sliding contact between metallic materials that exhibits the characteristics of severe wear, such as, significant plastic deformation, material transfer, and indications that cold welding of asperities possibly has taken place as part of the wear process.

- Mild wear:** A form of wear characterized by the removal of material in very small fragments.
- Mixed lubrication:** A condition of lubrication in which the friction and wear behavior are determined by the properties of the surfaces and by the viscous and non-viscous properties of fluid lubricants.
- Oxidative wear:** A corrosive wear process in which chemical reaction with oxygen or oxidizing environments predominates.
- Peening wear:** Removal of material from a solid surface caused by repeated impacts on very small areas.
- Pitting:** A form of wear involving the separation of particles from a surface in the form of flakes, resulting from repeated stress cycling, generally less extensive than spalling.
- Plowing:** The formation of grooves by plastic deformation of the softer of two surfaces in relative motion.
- Polishing wear:** An extremely mild form of wear, which may involve extremely fine-scale abrasion, plastics smearing of micro-asperities, and/or tribochemical material removal.
- PV Factor:** Product of pressure and velocity. (See Limiting PV.)
- Quasi-hydrodynamic lubrication:** See mixed lubrication.
- Ratcheting:** A sliding wear process involving progressive deformation, ultimately leading to the formation of loose fragments.
- Rehbinder Effect:** Modification of the mechanical properties at or near the surface of a solid, attributed to interaction with a surface-active substance or surfactant.
- Repeated-cycle deformation wear:** Mechanical wear mechanisms requiring repeated cycles of mechanical deformation or engagement.
- Ridging (wear):** A deep form of scratching in parallel ridges usually caused by plastic flow.
- Rolling-contact fatigue:** Wear to a solid surface that results from the repeated stressing of a solid surface due to rolling contact between that surface and another solid surface or surfaces, generally resulting in the formation of sub-surface cracks, material pitting, and spallation. (Note: Often used as a synonym for rolling-contact wear.) See rolling-contact wear.
- Rolling-contact wear:** Wear due to the relative motion between non-conforming solid bodies whose surface velocities in the nominal contact location are identical in magnitude, direction, and sense; most common form is rolling-contact fatigue.
- Run-in:** An initial transition process occurring in newly established wearing contacts. (As a verb, run in, refers to an initial operation designed to improve wear and friction performance of a device.)
- Scoring:** The formation of severe scratches in the direction of sliding or a severe form of wear characterized by the formation of extensive grooves and scratches in the direction of sliding. (Note: Sometimes also called scuffing in USA.) See scuffing and scratching.
- Scouring abrasion:** See abrasion.
- Scratch:** A groove produced in a solid surface by the cutting and plowing action of a sharp particle or protuberance moving along that surface.
- Scratching:** The formation of fine scratches in the direction of sliding; a mild form of scoring.

- Scuffing:** Localized damage caused by the occurrence of solid-phase welding between sliding surfaces, without local surface melting or a mild degree of galling that results from the welding of asperities due to frictional heat or a form of wear occurring in inadequately lubricated tribosystems which is characterized by macroscopically observable changes in surface texture, with features related to the direction of relative motion. (Note: Sometimes also called scoring in USA.) See scoring.
- Selective transfer:** A wear process involving the transfer and attachment of a specific species from one surface to the mating surface during sliding.
- Self-lubricating material:** Any solid material that shows low friction without application of a lubricant.
- Severe wear:** A form of wear characterized by removal of material in relatively large fragments.
- Shelling:** A term used in railway engineering to describe an advanced phase of spalling.
- Single-cycle deformation wear:** Mechanical wear mechanisms requiring only a single cycle of contact or engagement.
- Sliding wear:** Wear due to relative sliding between two bodies in contact.
- Slurry abrasion:** Three-body abrasive wear involving a slurry.
- Slurry erosion:** Erosion produced by the movement of a slurry past a solid surface.
- Smearing:** Mechanical removal of material from a surface, usually involving plastic shear deformation, and redeposition of the material as a thin layer on one or both surfaces.
- Solid impingement erosion:** Progressive loss of original material from a solid surface due to continued exposure to impacts by solid particles.
- Solid lubricant:** Any solid used as a powder or thin film on a surface to reduce friction and wear.
- Solid particle erosion:** See solid impingement erosion.
- Sommerfeld Number:** A dimensionless number that is used to characterize the state of lubrication of a bearing. (See Stribeck curve.)
- Spalling:** A form of wear involving the separation of particles from a surface in the form of flakes as a result of repeated stressing, generally more extensive than pitting or a form of wear involving the separation of macroscopic particles from a surface in the form of flakes or chips, usually associated with rolling but may also result from impact.
- Specific wear rate:** Wear volume divided by load and distance of sliding. (See wear factor.)
- Static friction:** Friction associated with the initiation of motion.
- Stick-slip:** A relaxation oscillation in friction, which is generally characterized by a sharp decrease, followed by a more gradual increase in the force of friction. It generally causes jerky-type motion and squeaking.
- Stiction:** Term used to signify the condition in which the frictional resistance is sufficient to prevent macroscopic sliding.
- Stress fracture:** See brittle fracture.
- Stribeck curve:** A graph showing the relationship between the coefficient of friction for a journal bearing and the dimensionless Sommerfeld Number. There is a general correlation between this number and the different forms of lubrication with a liquid, boundary, mixed, and fluid. (See Sommerfeld Number.)
- Surface distress:** In bearings and gears damage to the contacting surfaces that occurs through intermittent solid contact involving some degree of sliding and surface fatigue.

- Traction:** The transmission of tangential stress across an interface.
- Traction coefficient:** Ratio of the traction force to the normal force pressing the surfaces together.
- Traction Force:** The tangential force transmitted across an interface.
- Transfer film:** A tribofilm composed wear debris from the counterface.
- Tribochemistry:** Chemistry dealing with interacting surfaces in relative motion.
- Tribofilm wear:** Wear processes that are controlled by the formation of tribofilms, such as transfer and third-body films.
- Tribosystem:** All those elements that affect friction and wear behavior.
- Thermal wear:** Removal of material due to softening, melting, or evaporation during sliding, rolling, or impact.
- Thermoelastic instability:** Sharp variation of local surface temperatures with passing of asperities leading to stationary or slowly moving hot spots of significant magnitude, resulting in local expansion and elevation of the surface.
- Third body:** A solid interposed between two contacting surfaces.
- Third-body film:** A tribofilm containing wear debris from the surface, generally a mixture of wear debris from both surfaces.
- Three-body abrasion:** Abrasive wear when the abrasive particles are free to move.
- Two-body abrasion:** Abrasive wear from protuberances or attached abrasive particles.
- Transfer:** The process by which material from one sliding surface becomes attached to another surface, possibly as the result of interfacial adhesion.
- Transition diagram:** A form of wear map, involving two or more experimental or operating parameters, which is used to indicate boundaries between different regimes of wear or surface damage or effectiveness of lubrication, such as the *IRG Transition Diagrams*.
- Vibratory cavitation:** Cavitation caused by the pressure fluctuations within a liquid, induced by the vibrations of a solid surface immersed in the liquid.
- Wear:** Damage to a solid surface, generally involving or leading to progressive loss of material, that is due to the relative motion between that surface and a contacting substance or substances.
- Wear coefficient:** Normally defined as the non-dimensional coefficient, k , in the following equation, $V = KPS / 3p$, where V is the volume of wear, P is the load, S is the distance of sliding, and p is hardness. Less specific, it is the dimensionless form of a wear factor obtained dividing it by the hardness of the wearing material.
- Wear curve:** Plot of wear as a function of usage, e.g., wear depth vs. sliding distance and wear volume vs. time.
- Wear factor:** Constant in a linear wear equation, $V = KPS$, where V is the volume of wear, P is the load, and S is the sliding distance. Wear volume divided by load and sliding distance. (Note: An alternative definition is based on the differential form of this equation, $\Delta V = KP\Delta S$, where ΔV is the incremental increase in wear volume over an incremental amount of sliding, ΔS .)
- Wear-in:** (See run-in.)
- Wear map:** A graphical characterization of wear behavior in terms of independent operational parameters of the tribosystem, such as speed and load. Various forms of wear maps are used to identify ranges and combinations of operational parameters for different wear mechanisms, same wear rates, and acceptable operating conditions. (See transition diagram.)

Wedge formation: In sliding metals, the formation of a wedge or wedges of plastically sheared metal in local regions of interaction between sliding surfaces.

Zero-wear: In the context of the Zero and Measurable Wear Models for sliding and impact, it describes a state of wear in which the wear or damage is less than the magnitude of the surface roughness.